THE JOURNAL OF
PHYSICAL CHEMISTRY

VOLUME 70, NUMBER 12 DECEMBER 15, 1966

The Isotopic Discrimination of Some Solutes in Liquid Ammonia

by Arlen Viste and Henry Taube[1]

George Herbert Jones Laboratory, The University of Chicago, Chicago, Illinois *(Received July 26, 1966)*

The nitrogen isotopic discrimination of some salts and metals, studied in liquid ammonia solution at −50°, decreases in magnitude in the order Pb^{2+}, Ca^{2+}, Li^+, Ag^+, Na^+, Li, K^+, Na, K. The isotopic discrimination appears to provide qualitative information about the strength of the cation–solvent interaction in liquid ammonia.

Introduction

Dissolving an anhydrous salt in water brings about a small change in the ratio of the activity of $H_2{}^{18}O$ to that of $H_2{}^{16}O$. This isotopic discrimination effect has been studied for a number of salts by Feder and Taube.[2-4]

Study of the isotopic discrimination of solutes in a nonaqueous solvent offers an opportunity to gain perspective on the isotopic fractionation method as well as on the results in aqueous solution. An important question about the method is whether the principal contribution to the observed fractionation comes from nearest-neighbor interactions of the ions with the solvent molecules, or whether on the other hand there is a major contribution from a long-range disruption of solvent structure.

The purpose of the present study was to extend isotopic fractionation studies to liquid ammonia (involving $^{15}NH_3$ and $^{14}NH_3$) to determine whether the fractionation results still show a reasonable correlation with other information about the strength of the cation–solvent interaction. Two points are of interest. One is that the vapor–liquid fractionation for bulk liquid ammonia even at −50° is substantially smaller than for bulk water at room temperature[5,6] even though the effects brought about by cation–solvent interactions are probably greater at lower temperatures as Feder has pointed out. Secondly, it seems interesting to compare the behavior of metal–ammonia solutions with that of ordinary salts in liquid ammonia.

Experimental Section

Reagents. Anhydrous ammonia was condensed into a glass tube on a vacuum line, dried by condensing onto potassium metal, and distilled into a small stainless steel cylinder on the line for storage. The cylinder could be removed from the line and weighed. All the ammonia in storage was used in running a reference and in running the corresponding solution. Lithium metal was supplied by Lithium Corporation of America, potassium metal by Fisher, and silver iodide by Mallinckrodt or by Matheson Coleman and Bell. It was also prepared from Goldsmith silver nitrate and Baker and Adamson potassium iodide. Mallinc-

(1) Department of Chemistry, Stanford University, Stanford, Calif.
(2) H. M. Feder, Ph.D. Thesis, University of Chicago, 1954.
(3) H. M. Feder and H. Taube, *J. Chem. Phys.*, **20**, 1335 (1952).
(4) H. Taube, *J. Phys. Chem.*, **58**, 523 (1954).
(5) H. G. Thode, *J. Am. Chem. Soc.*, **62**, 581 (1940).
(6) M. H. Wahl and H. C. Urey, *J. Chem. Phys.*, **3**, 411 (1935).

krodt $Ca(NO_3)_2 \cdot 4H_2O$ was dehydrated on a vacuum line for several days and finally heated in a tube furnace ($T \gtrsim 200°$ in the center of the furnace). Chemicals not otherwise specified were reagent grade materials.

Apparatus. The parameter to be measured experimentally is the enrichment factor $\alpha = 10^3(R_0 - R)/R_0$, where R_0 denotes the number ratio of $^{15}NH_3$ to $^{14}NH_3$ in the NH_3 vapor in equilibrium with a sample of pure NH_3, and R is the same ratio for vapor in equilibrium with a liquid ammonia solution made from this same ammonia. The equilibrations were carried out at $-50 \pm 0.6°$. Each vapor sample was oxidized completely to N_2 by circulation over CuO at about 625°. Though the $^{14}N^{15}N/^{14}N^{14}N$ isotope ratio is twice the $^{15}NH_3/^{14}NH_3$ isotope ratio in the NH_3 sample from which the N_2 was formed, the respective $^{14}N^{15}N/^{14}N^{14}N$ isotope ratios can be taken as R_0 and R, since the proportionality factors cancel in α. The isotope ratios of the nitrogen samples were measured mass spectrometrically by Professor John P. Hunt (Department of Chemistry, Washington State University, Pullman, Wash.).

In carrying out the equilibration and sampling, the glass vessel containing the solution and vapor was immersed in a thermostating bath. About 20–50 g of ammonia was used in the vessel of volume 350–400 cc. Solution and vapor were stirred (sealed magnetic stirrer) for 1 hr or more. A sample of ammonia vapor was then slowly withdrawn into the vacuum line through two sintered glass frits in series, usually over a period of 4–25 min. The volume of ammonia vapor removed was usually in the range of one to five times the volume of vapor in the thermostated vessel. After oxidation of the ammonia vapor sample over cupric oxide at about 625°, the resulting N_2 sample was freed of water by prolonged circulation through a trap cooled with liquid nitrogen. (In a few instances, the nitrogen samples were further circulated through magnesium perchlorate.) Oxidation of the ammonia sample to N_2 appeared to be quantitative to within 1 or 2%. Part of the nitrogen sample was then admitted to an evacuated gas sample bulb fitted with a high-vacuum stopcock and $\overline{\S}$ $^{14}/_{35}$ male joint.

Isotope ratios were read in respective pairs: each solution sample with its reference sample from vapor in equilibrium with pure liquid ammonia. Precision (machine reproducibility) in each isotope ratio is estimated to be 0.03 to 0.04%. Since α involves the difference between the two isotope ratios, the precision in it is presumably somewhat lower, perhaps ±0.5 part per thousand. In three instances, the presence of air or other impurities was noted by Professor Hunt in the course of the isotopic analyses; these three results have accordingly been discarded.

The sampling of vapor from a liquid ammonia solution was always carried out *after* obtaining the corresponding reference sample from vapor in equilibrium with pure liquid ammonia, so that the same ammonia

Table I: Values of α and $(\alpha - am)$ for the Liquid Ammonia Solutions Studied

Solute	Concn, m	α	$(\alpha - am)$[a]
$LiNO_3$	1.99	2.2	0.7
	3.08	3.6	1.2
	4.94	3.4	−0.4
	4.99	3.4	−0.5
	5.01	3.7	−0.2
$NaNO_3$	1.96	1.1	0.3
	3.00	1.5	0.2
	3.02	1.8	0.5
	5.02	2.0	−0.1
	5.04	1.7	−0.4
NaI	2.98	1.1	0.0
	3.02	1.1	0.0
NaSCN	4.58	1.5	0.2
	4.78	2.0	0.6
	8.79	2.2	−0.4
	8.87	2.6	0.0
KI	4.99	1.1	0.4
	4.99	1.0	0.3
	5.02	0.0	−0.7
AgI	5.74	2.5	0.0
	5.76	2.6	0.0
$Ca(NO_3)_2$	3.99	4.8	0.2
	4.03	4.5	−0.2
$Pb(NO_3)_2$	0.90	1.8	0.1
	0.904	1.7	−0.1
Li	4.59	1.0	−0.2
	4.86	0.0	−1.3
	12.04	2.9	−0.3
	12.04	3.3	0.1
	12.28	4.8	1.5
	12.69	3.0	−0.4
	13.90	3.3	−0.4
Na	5.17	−0.3	−0.4
	5.39	−0.3	−0.4
	10.9[b]	0.7	0.5
	10.9[b]	0.0	−0.2
K	4.63	−1.0	−0.5
	5.68	−1.0	−0.4
	10.22	−0.7	0.4
	10.35	−1.1	0.0

[a] Values of a shown in Table II. [b] Saturated solution.

was used in both cases. The ammonia was transferred into the small stainless steel cylinder by distillation for storage between the two equilibrations.

Results

Table I reports $\alpha = 10^3 (R_0 - R)/R_0$ and $(\alpha - am)$ for solutions of specified molal concentration. The parameter a is defined by the relation $\alpha = am$, and was calculated for each solute by a least-squares analysis of the data. The m denotes molal concentration. Table II reports a and the average deviation $\langle|\alpha - am|\rangle$ for each solute.

Table II: a and $\langle|\alpha - am|\rangle$ for Solutes in Liquid Ammonia

Solute	a	$\langle\|\alpha - am\|\rangle$
$LiNO_3$	0.77	0.6
$NaNO_3$	0.42	0.3
NaI	0.37	0.0
NaSCN	0.29	0.3
KI	0.14	0.5
AgI	0.44	0.0
$Ca(NO_3)_2$	1.16	0.2
$Pb(NO_3)_2$	1.94	0.1
Li	0.26	0.6
Na	0.02	0.3
K	−0.11	0.3

Discussion

Feder[7] has shown that for the general case in aqueous solution

$$\alpha = 10^3 \sum_s \frac{n_s m_s (K_s - 1)}{55.51}$$

where the sum is over all species s in solution of molality m_s and containing n_s equivalent water molecules. K_s refers to the equilibrium

$$H_2{}^{18}O(l) + H_2{}^{16}O(s) \overset{K_s}{\rightleftarrows} H_2{}^{16}O(l) + H_2{}^{18}O(s)$$

with l referring to bulk solvent and s to species s. The obvious extension to liquid ammonia solutions gives

$$\alpha = 10^3 \sum_s \frac{n_s m_s (K_s - 1)}{58.72} = \sum_s n_s m_s (K_s - 1) M$$

where M is the molecular weight of the solvent. The equilibrium in this case is

$$^{15}NH_3(l) + {}^{14}NH_3(s) \overset{K_s}{\rightleftarrows} {}^{14}NH_3(l) + {}^{15}NH_3(s)$$

If the fractionation originates entirely in the first solvation shell of the cation, this reduces to

$$\alpha = n_c m_c (K_c - 1) M$$

In this case, α should be linear in the molality of the salt. The linearity of α *vs.* m_c in most of Feder's data and the reasonable trends of $n(K_c - 1)$ in his work are at least encouraging, even though not conclusive. Taube[4] has also pointed out a reasonable correlation between the effect of a cation in promoting acidity and in producing isotopic discrimination.

In discussing the data on isotopic fractionation in solutions of electrolytes and metals in liquid ammonia, trends in a, from the equation $\alpha = am$, will be considered. If the data are analyzed from the point of view that the isotopic fractionation originates in the first solvation shell of a single predominant cationic species, then

$$a = \frac{10^3}{58.72} n_s (K_s - 1)$$

In such a case, one can obtain K', the equilibrium constant for the exchange reaction

$$^{15}NH_3(g) + {}^{14}NH_3(s) = {}^{14}NH_3(g) + {}^{15}NH_3(s)$$

(where $NH_3(s)$ refers to a molecule of NH_3 coordinated in the cationic species) from a and the known vapor–liquid isotopic equilibrium constant, if n_s (the number of NH_3 molecules coordinated in the cationic species) is known. In general, n_s is not known with confidence. However, in Table III are listed the values of $10^3 n_s(K_s - 1)$ and $10^3(K' - 1)$ obtained for what we believe are reasonable values of n_s.

Table III: $10^3 n_s(K_s - 1)$ and $10^3(K' - 1)$ for Solutes in Liquid Ammonia

Solute	$10^3 n_s(K_s - 1)$	$10^3(K_s' - 1)$[a] $n_s = 2$	$n_s = 4$	$n_s = 6$
$LiNO_3$	45.2		14.7	
$NaNO_3$	24.7		9.6	7.5
NaI	21.7		8.8	7.0
NaSCN	17.0		7.6	6.2
KI	8.2		5.4	4.8
AgI	25.8	16.3	9.8	7.7
$Ca(NO_3)_2$	68.1		20.4	14.8
$Pb(NO_3)_2$	113.9		31.9	22.4
Li	15.3		7.2	
Na	1.2		3.7	3.6
K	−6.5		1.8	2.3

[a] K' refers to the equilibrium, $^{15}NH_3(g) + {}^{14}NH_3(s) = {}^{14}NH_3(g) + {}^{15}NH_3(s)$, where $NH_3(s)$ refers to NH_3 coordinated to the cation. K_s refers to the equilibrium, $^{15}NH_3(l) + {}^{14}NH_3(s) = {}^{14}NH_3(l) + {}^{15}NH_3(s)$. If K refers to the vapor–liquid equilibrium, $^{15}NH_3(g) + {}^{14}NH_3(l) = {}^{14}NH_3(g) + {}^{15}NH_3(l)$, then $K' = K_s K$. $K \approx 1.0034$ at $-50°$.[5]

(7) Reference 2, p 9.

For these values of n_s, $(K' - 1)$ appears to decrease in the order

$$Pb^{2+} > Ca^{2+} \gtrsim Li^+ \gtrsim Ag^+ \sim Na^+ \gtrsim Li > K^+ > Na > K$$

$n_s(K_s - 1)$ also decreases in approximately the same order.

If $(K' - 1)$, or perhaps $n_s(K_s - 1)$, is regarded as a parameter related to the strength of the cation–solvent interaction, this order of decreasing $(K' - 1)$ appears qualitatively reasonable. For the four d^0 ions in the series, $(K' - 1)$ is observed to decrease with decreasing charge and increasing cationic radius. d^{10} ions may be considered to form bonds of greater covalent character than comparable d^0 ions.

The three sodium salts show much the same value of a. In aqueous solution too,[2] changing the identity of the anions affects the values of α very little. However, for each alkali element studied, the solution of the metal shows a value of a much lower than that of the corresponding salt (the order Li > Na > K is, however, preserved for the metals). The fractionation measurements for the metals were made in the metallic range of metal–ammonia solutions. The effective charge on the cation is expected to be higher in salt solutions than in the metallic range of metal–ammonia solutions, where some shielding of the cation by the conduction band electrons can probably take place, reducing the effective charge on the metal species somewhat. It is, of course, not surprising that the electrons in concentrated metal solution do not act simply like anions.

In aqueous solution, Ishimori[8] has measured the equilibrium constant for the exchange reaction

$$M(^{14}NH_3)_n + {}^{15}NH_3(aq) \overset{K_1}{\rightleftharpoons} M(^{14}NH_3)_{n-1}(^{15}NH_3) + {}^{14}NH_3(aq)$$

at 30° for M = Cu^{2+}, Zn^{2+}, Cd^{2+}, Ag^+, and Ni^{2+} by an ion-exchange technique. Of these five ions, only Ag^+ has been studied in liquid ammonia. If it is assumed that in aqueous solution K' may be obtained from K_1/n *via* the equilibrium

$$^{15}NH_3(g) + {}^{14}NH_3(aq) = {}^{14}NH_3(g) + {}^{15}NH_3(aq)$$

with equilibrium constant 1.005 at 25°,[9] and if in addition $n_s = 2$ for Ag^+ in liquid ammonia solution at −50°, then $(K' - 1) = 0.014$ in aqueous solution at 25–30°, and $(K' - 1) = 0.016$ in liquid ammonia at −50°. Although $(K' - 1)$ might have been expected to be somewhat larger than this at the lower temperature, in view of the rather substantial changes of conditions of solvent and temperature, probably only order of magnitude agreement can be expected.

Hunt and co-workers[10] have studied the isotopic discrimination of Cr^{3+} by a direct exchange determination. For the exchange reaction

$$Cr(^{14}NH_3)_6^{3+} + {}^{15}NH_3 \rightleftharpoons Cr(^{14}NH_3)_5(^{15}NH_3)^{3+} + {}^{14}NH_3$$

they find $K_{eq} = 6.100$ at 20°. This gives $10^3 n_s(K_s - 1) = 100$ at 20° for Cr^{3+}, with $n_s = 6$. This value of $10^3 n_s(K_s - 1)$ at 20° is nearly as large as the value 114 which we have found for Pb^{2+} at −50°; one would of course expect that Cr^{3+} would have a larger value at the lower temperature, but even making allowance for this, the effect of Pb^{2+} relative to Cr^{3+} is, in view of the lower charge and larger radius of Pb^{2+}, surprisingly large. The explanation may be that Pb^{2+} has an unsymmetrical coordination sphere and that it interacts very strongly with a small number of molecules at short distances. Just as acidity is increased by a reduction in coordination number, it is reasonable that the isotopic fractionation effect would be increased, the benefit to the intensity factor more than offsetting the loss because of reduction in the number of molecules interacting. A similar explanation may also apply to Ca^{2+} compared to Pb^{2+}, where the larger ion has a larger effect.

If the magnitude of the isotopic discrimination effect, as represented by $a = \alpha/m$, is regarded as an indication of the strength of the cation–solvent interaction (this could only be expected to hold at constant n_s), then the concentration dependence of a should, in principle, provide some clue as to the range of the interaction. If the fractionation is due to interactions primarily within the nearest-neighbor shell of solvent molecules around the cation, then α *vs.* m should remain linear until an appreciable number of solvent molecules are affected by more than one cation, *i.e.*, until sharing of solvent molecules between two cations begins to take place. Ordinarily, this is not expected to occur much before the mole ratio of solvent to salt approaches the coordination number of the cation. On the other hand, if the isotopic discrimination effect receives substantial contributions from long-range alteration of solvent structure, solvent molecules will begin to be affected by more than one cation (or perhaps anion) at a lower concentration, and deviations from linearity should ensue.[2]

The pertinent data on linearity or nonlinearity of α *vs.* m in liquid ammonia solutions are shown in Table

(8) T. Ishimori, *Bull. Chem. Soc. Japan*, **33**, 520 (1960).

(9) I. Kirshenbaum, J. S. Smith, T. Crowell, J. Graff, and R. McKee, *J. Chem. Phys.*, **15**, 440 (1947).

(10) T. W. Swaddle, L. F. Coleman, and J. P. Hunt, *Inorg. Chem.*, **2**, 950 (1963).

I. The imprecision in α due to instrumental precision in the isotope ratios is thought to be about ± 0.5.

Variation of α with molal concentration is not, strictly speaking, distinguishable from a linear dependence of α on m, since the average deviations from linearity, $\langle|\alpha - am|\rangle$, are of about the same magnitude as the imprecision expected from the mass spectrometric analyses. There are, however, some indications that α/m may decrease slightly with concentration for salts and either remain constant or increase slightly with concentration for metal–ammonia solutions. If real, these trends may suggest some distortion of solvent structure beyond the nearest-neighbor shell of ammonia molecules in salt solutions. A greater increase of α/m with concentration in the case of the metals might be explained either by less distortion of the solvent structure by the metal, due to a lower effective charge on M^+ in $M–NH_3$ solutions than in MX–ammonia solutions, or by an increasingly strong interaction between the metal and the surrounding NH_3 molecules with increasing concentration in the metallic region, in line with the discussion by LePoutre and Patterson.[11]

Improvement in the instrumental precision by an order of magnitude would be needed in order to settle the question of linearity with any degree of confidence. If the observed isotopic discrimination is contributed to appreciably by alterations of solvent structure beyond the first coordination sphere of the cation, however, it appears that the variability introduced by such contributions is not so large as to bring about gross changes from a reasonable order of increase of α/m among cations.

Acknowledgments. We wish to express our deep appreciation to Professor John P. Hunt, who performed the mass spectrometric determination of isotope ratios for the nitrogen samples. Fellowship support for A. V. by the National Science Foundation is gratefully acknowledged. This research was supported by the U. S. Atomic Energy Commission.

(11) G. LePoutre and A. Patterson, Jr., *Bull. Soc. Chim. France*, 989 (1961).

The Kinetics of Carbon Dioxide and Carbon Formation from Carbon Monoxide[1a]

by Stephen A. Pursley,

Department of Mechanical Engineering, Purdue University, Lafayette, Indiana

Richard A. Matula,[1b] and Otto W. Witzell[1c]

School of Engineering, Mechanical Engineering Department, University of California, Santa Barbara, California
(Received August 3, 1965)

The initial kinetics of the reaction $2CO \rightarrow CO_2 + C$ have been investigated in Vycor vessels in the temperature range from 740 to 860° and in the pressure range from 25 to 945 mm. The rate has been shown to be extremely slow and the reaction is essentially zero order and heterogeneous with an activation energy of 35 kcal/mole.

Introduction

The reaction $2CO \rightarrow CO_2 + C$ was first encountered by Bell[2] in his work involving the reactions occurring in blast furnaces. Boudouard[3a] and Cleminson and Briscoe[3b] catalyzed the same reaction in an effort to determine the equilibrium composition of the CO–CO_2–C system. It has been known for some time[4] that the commercially significant $CO_2 + C \rightarrow 2CO$ reaction is strongly retarded by carbon monoxide. Strickland-Constable,[5] Reif,[6] Kawana,[7] Ergun,[8] and Blackwood and Ingeme[9] have attributed this retardation to a first-order $CO + (CO) \rightarrow CO_2 + C$ reaction.

Reif[10] undertook a kinetic study of the $2CO \rightarrow CO_2 + C$ reaction in an attempt to characterize the CO retardation. The reaction, when carried out on degassed high-temperature coke, was shown to follow first-order kinetics with CO adsorption as the rate-determining step. Brandner and Urey[11] and Hayakawa,[12] in their work on the isotopic exchange between CO and CO_2, briefly investigated the $2CO \rightarrow CO_2 + C$ reaction in quartz vessels to determine if its rate influenced the exchange rate. The present investigation was conducted in order to determine the initial kinetics in CO pyrolysis.

Experimental Section

A static reaction vessel having 394 cc volume was constructed from Corning Code 7900 glass. The vessel had a surface to volume ratio of 0.90 cm^{-1}. The temperature of the reactor vessel during a given experiment was maintained at ±1°. Prior to installation in the furnace, the vessel was cleaned with reagent grade nitric acid and distilled water. The reactant gas (CP CO) was passed through a gas purification train before being admitted to the reactor vessel. Gas chromatography techniques were used for the quantitative analysis.

Preliminary experiments conducted without cleaning the reactor vessel between successive points indicated that a slow continual carbon buildup on the walls of the reactor was retarding the reaction. In order to eliminate this problem, a cleaning technique was developed which allowed the carbon to be removed from the vessel by introducing oxygen between subsequent runs. This procedure allowed reproducible and consistent kinetic data to be obtained.

(1) (a) This research is based on the Ph.D. dissertation of S. A. Pursley, Purdue University, 1965. (b) Department of Mechanical Engineering, University of Michigan, Ann Arbor, Mich. (c) Dean of the Graduate School, Drexel Institute of Technology, Philadelphia, Pa.

(2) I. L. Bell, *J. Chem. Soc.*, **22**, 203 (1869).

(3) (a) O. Boudouard, *Ann. Chim. Phys.*, **24**, 5 (1901); (b) J. Cleminson and H. V. A. Briscoe, *J. Chem. Soc.*, 1926, 2148 (1926).

(4) J. Gadsby, F. J. Long, P. Sleightholm, and K. W. Sykes, *Proc. Roy. Soc.* (London), **A193**, 357 (1948).

(5) R. F. Strickland-Constable, *J. Chim. Phys.*, **47**, 356 (1950).

(6) A. E. Reif, *J. Phys. Chem.*, **56**, 785 (1952).

(7) Y. Kawana, *Bull. Chem. Soc. Japan*, **26**, 507 (1953).

(8) S. Ergun, *J. Phys. Chem.*, **60**, 480 (1956).

(9) J. D. Blackwood and A. J. Ingeme, *Australian J. Chem.*, **13**, 194 (1960).

(10) A. E. Reif, *J. Phys. Chem.*, **56**, 778 (1952).

(11) J. D. Brandner and H. C. Urey, *J. Chem. Phys.*, **13**, 351 (1945).

(12) T. Hayakawa, *Bull. Chem. Soc. Japan*, **26**, 165 (1953).

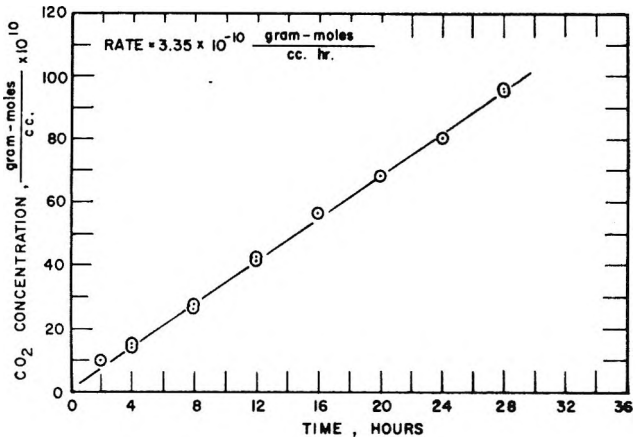

Figure 1. Plot of CO_2 concentration *vs.* time (T = 819°, P = 761 mm).

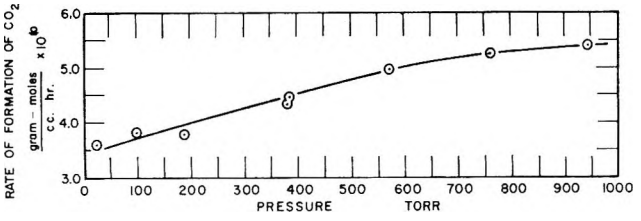

Figure 2. Variation in the rate as a function of pressure (T = 858).

Results

Figure 1 is a typical curve showing the experimentally determined CO_2 concentration as a function of time. Initial normalized rates, R_{CO_2}, obtained by multiplying the experimental slopes by the reciprocal of the vessel S/V ratio are listed in Table I. The variation of the rate of formation of CO_2, (R_{CO_2}) (S/V), at 858° in a vessel with S/V = 0.90 cm^{-1} as a function of initial CO pressure is given in Figure 2. At 858° it is seen that the rate increases slightly as the initial CO pressure is increased from 45 to 760 mm. However, at initial pressures greater than 760 mm, the rate is essentially independent of pressure. The data in Table I indicate that at temperatures lower than 858° the rate is essentially independent of initial CO pressures exceeding 0.5 atm. Further experiments with a vessel having an S/V ratio of 8.5 cm^{-1} indicated that within 10% the rate was linearly dependent on the S/V ratio. The reaction was, therefore, assumed to be heterogeneous.

It may be assumed that the rate is essentially independent of the initial CO concentration. Hence, R_{CO_2} can be equated to the zero-order rate constant K. Figure 3 is an Arrhenius plot of the temperature variation of the zero-order rate constant, as determined from the data in Table I. A least-mean-squares line resulted in an activation energy of 34.9 kcal/mole. The experimental zero-order rate expression for the formation of CO_2 is

$$R_{CO_2} = K = 9.9 \times 10^{-7} \exp(-34.9/R_u T) \text{ moles/cm}^2 \text{ sec} \quad (1)$$

Table I: Initial Rates of Carbon Dioxide Formation

T, °C	P_0, mm	R_{CO_2}, moles/cm² hr × 10¹⁰
742	762	1.03
779	760	2.03
781	382	2.00
819	761	3.72
820	382	3.74
858	945	5.99

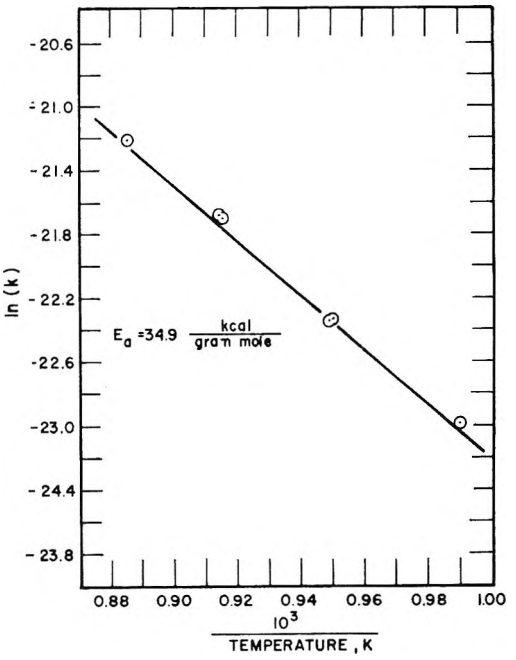

Figure 3. Arrhenius plot for the zero-order rate constant.

Discussion

The following equations are proposed to account for the initial kinetics of the over-all reaction $2CO \rightarrow CO_2 + C$

$$CO \underset{k_2}{\overset{k_1}{\rightleftharpoons}} (CO) \quad (2)$$

$$(CO) + (CO) \xrightarrow{k_3} (CO_2) + C \quad (3)$$

$$(CO_2) \underset{k_5}{\overset{k_4}{\rightleftharpoons}} CO_2 \quad (4)$$

where (CO) and (CO_2) refer to chemisorbed carbon monoxide and carbon dioxide, respectively. It is well known that CO, as well as CO_2, is chemisorbed on glass at the temperatures of interest in this investigation. Hayakawa[12] has reported isotherms for CO and CO_2 on quartz at 900°. These were low-pressure isotherms, up to 16 mm, but these results showed that CO was much more strongly adsorbed than CO_2 in separate isotherms.

Although adsorption as well as desorption are found to be rate controlling in many surface reactions, rates for adsorption and desorption processes are usually orders of magnitude higher than those encountered in this work. It appears reasonable, therefore, that the over-all rate is controlled by reaction 3 involving a Langmuir–Hinshelwood mechanism. Under this assumption, the rate is conveniently expressed as

$$R_{CO_2} = k_3\theta_{CO}^2 \qquad (5)$$

where θ_{CO} is the fractional surface coverage of adsorbed CO. Equation 5 expresses the results consistent with those found experimentally. The reaction is zero order at high pressures, while at lower pressures, the rate decreases with decreasing pressure, which is characteristic of chemisorption isotherm behavior. The retardation found in the preliminary experiments was apparently due to carbon deposition on the surface resulting in a decrease in the number of active reaction sites. It is not reasonable to attribute this retardation to CO_2 adsorption. The quantity of CO_2 adsorbed was very small compared to the quantity of CO. Furthermore, the introduction of oxygen into the system should not have an appreciable effect on adsorbed CO_2.

A theoretical estimate of the rate constant can be calculated by invoking the absolute rate theory which has been detailed by Glasstone, Laidler, and Eyring.[13] If the experimental activation energy is used in the formulation, the value of the theoretical rate constant is dependent on the choice of the number of active sites per square centimeter and the transmission coefficient. In order for the experimental and theoretical rate constants to agree, both the transmission coefficient and the number of active sites per square centimeter must be small. The choice of the number of sites per square centimeter is dependent on the total number of sites per square centimeter and an estimate of the maximum distance between nearest neighbors which would allow a reaction to proceed.

One class of reactions which have small transmission coefficients is nonadiabatic reactions. Although the form of the condensed carbon is not known, it is reasonable to assume that the carbon exists initially as condensed atomic carbon. Both CO and CO_2 have singlet ground states; however, atomic carbon has a triplet ground state. Hence, the reaction would be accompanied by a change of multiplicity. Under these circumstances, a transmission coefficient of the order of 10^{-3} to 10^{-5} would not be unreasonable.

Another possible cause for the low experimental rate is that the rate of the reaction is controlled by a surface diffusion process which may be very slow.

The experimental results may be summarized as follows. The reaction $2CO \rightarrow CO_2 + C$ has been shown to be heterogeneous when the reaction is allowed to proceed in Corning Code 7900 glass reactors. The initial rate of production of CO_2 is linearily dependent on the reactor S/V ratio. The zero-order rate constant has an activation energy of 34.9 kcal/mole and a frequency factor of 9.9×10^{-7} mole/cm² sec. The reaction has also been shown to be essentially zero order at high pressures, while at lower pressures the rate decreases with decreasing pressure. The above result is characteristic of chemisorption isotherm behavior.

(13) S. Glasstone, K. J. Laidler, and H. Eyring, "The Theory of Rate Processes," McGraw-Hill Book Co., Inc., New York, N. Y., 1941, pp 377–382.

Indicator Acid–Base Equilibria in Three Aqueous–Nonaqueous Solvent Mixtures[1]

by K. A. Boni and H. A. Strobel

Department of Chemistry, Duke University, Durham, North Carolina *(Received February 14, 1966)*

Using spectrophotometric procedures, the dissociation constant for the acid form of *p*-nitroaniline has been determined in dilute hydrochloric and perchloric acid solutions in acetic acid–water mixtures, and the apparent dissociation constants of *m*-nitroaniline in dioxane–water and of *o*-nitroaniline in formic acid–water mixtures have been determined, again for dilute HCl or $HClO_4$. Salt and medium effects were also measured for *p*-nitroaniline in acetic acid–water media. The process that brings about a minimum in indicator pK_a (or maximum in Hammett H_0 function) in several aqueous–nonaqueous mixtures is examined in terms of a model based on the relative basicity and molar volume of the solvent added to water.

It has been known for some time that measures of acidity such as the Hammett H_0 function[2] or indicator dissociation constants show marked maxima in mixtures of water with certain other solvents.[3]

Though the Hammett acidity function has in general been shown not to be a quantitative measure of acidity in mixed solvents because of the inconstancy of the indicator activity coefficient ratio,[4–7] such maxima may still be examined by following the behavior of the indicator dissociation constants.

In connection with recent ion-exchange studies of the selectivity coefficient maxima for the Na–H system in aqueous–nonaqueous mixtures,[8] dissociation constants have been determined for appropriate nitroaniline indicators in water–formic acid, water–acetic acid, and water–dioxane mixtures. These new data have prompted further examination of the indicator dissociation constant maxima (or pK_a minima) and of the role of solvents in the production of such indicator behavior.

Experimental Section

Materials. Eastman Kodak White Label *o*-, *m*-, and *p*-nitroaniline were recrystallized twice from alcohol after treating with Norit. The melting points (uncorrected) of the purified compounds were 71.5–72.0, 112.0–112.25, and 147.0–147.5°, respectively. The preparation of solvents and salts has been described elsewhere.[8]

pK_a Measurements. Absorption curves were determined with a Cary 14 spectrophotometer. A Beckman DU was used to measure absorbances at chosen wavelengths in 1-cm cells at 28 ± 2°. The DU wavelength scale was calibrated against the mercury spectrum; its photometric response was also found in agreement with literature values.[9]

The absorbance of indicator solutions in mixtures of water with dioxane and acetic acid was always measured at or near λ_{max}, the wavelength of maximum absorption. When no strong acid was added, an indicator was considered to be completely in the basic (neutral) form, since even in acetic acid–water mixtures the values of the molar absorptivity (extinction coefficient) at that wavelength, ϵ_{max}, were higher than in water. As

(1) Based in part on a dissertation submitted by K. A. Boni to the Graduate School of Duke University in partial fulfillment of the requirements for the Ph.D. degree, June 1962.

(2) L. P. Hammett and A. J. Deyrup, *J. Am. Chem. Soc.*, **54**, 2721 (1932).

(3) M. A. Paul and F. A. Long, *Chem. Rev.*, **57**, 1 (1957).

(4) B. Gutbezhal and E. Grunwald, *J. Am. Chem. Soc.*, **75**, 559, 565 (1953).

(5) (a) K. Schwabe, *Abhandl. Saechs. Akad. Wiss. Leipzig, Mathnaturw. Kl.*, **46**, 1 (1959); (b) K. Schwabe, *Oesterr. Chemiker-Z.*, **65**, 339 (1964).

(6) C. L. deLigny, H. Loriaux, and A. Ruiter, *Rec. Trav. Chim.*, **80**, 725 (1961).

(7) (a) D. Rosenthal, H. B. Hetzer, and R. G. Bates, *J. Am. Chem. Soc.*, **86**, 549 (1964); (b) R. G. Bates, *Kagaku To Kogyo* (Tokyo), **18**, 680 (1965).

(8) K. A. Boni and H. A. Strobel, to be published.

(9) National Bureau of Standards Circular 484, U. S. Government Printing Office, Washington, D. C., 1944.

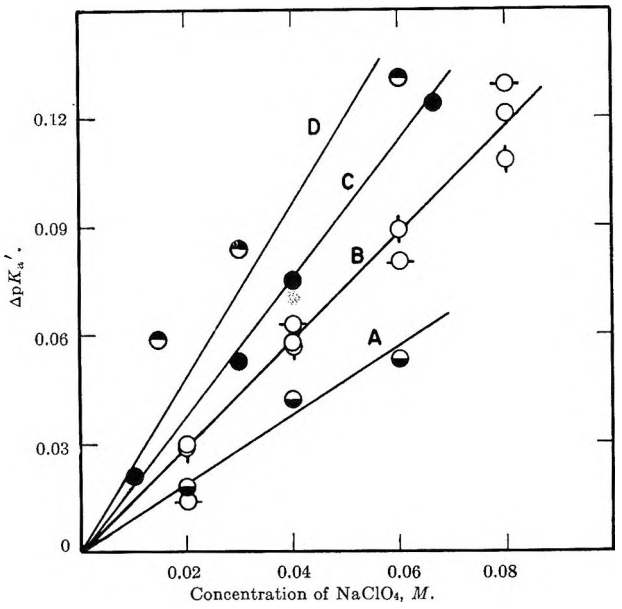

Figure 1. Salt effect for $NaClO_4$ in $HClO_4$ solutions in acetic acid–water mixtures. Curve A: 0.06 *M* $MClO_4$ in 73 mole % H_2O. Curve B: ○, 0.03 *M* $HClO_4$; ◑, 0.06 *M* $HClO_4$; ⊖, 0.09 *M* $HClO_4$ in 44 mole % H_2O. Curve C: 0.045 *M* $HClO_4$ in 34 mole % H_2O. Curve D: 0.015 *M* $HClO_4$ in 22 mole % H_2O.

discussed below, had the indicator been partly protonated, ϵ_{max} should have been lower. Values of λ_{max} and ϵ_{max} are given as a function of solvent composition in Table I. In formic acid–water media protonation was extensive, and determinations were made at the wavelength of maximum absorbance of the neutral species in pure water.

The absorption characteristics of the indicators are in general agreement with earlier values. The values for *p*-nitroaniline in water agree with the data of Salomaa[10] and Braude and Stern,[11] but are lower than the values 1.37×10^4 and 385 mμ reported by Schwarzenbach and Stensby.[12] The ϵ_{max} of *o*-nitroaniline in water is in agreement with the value given by Noyce and Castelfranco.[13] The wavelengths of maximum absorption of *m*-nitroaniline in different dioxane–water mixtures agree within experimental error with those of Braude and Stern but the present molar absorptivities are 4–5% smaller. Since their values for *p*-nitroaniline were duplicated in this laboratory, it is possible that their *m*-nitroaniline may have been slightly impure.

Table I: Indicator Absorption Characteristics

	p-Nitroaniline		*m*-Nitroaniline[a]	
	acetic acid–water		dioxane–water	
Mole % H_2O	λ_{max}, mμ	$\epsilon_{max} \times 10^{-4}$	λ_{max}, mμ	$\epsilon_{max} \times 10^{-3}$
22.4	368	1.32	...	...
44.0	372	1.34	378	1.50
62.6	378	1.34_2	378	1.44
80.9	380	1.34	374	1.34
90.0	381	1.31	369	1.32
100.0	378	1.30_5	357	1.38

[a] Interpolated at mole percentages indicated.

In mixtures of water with acetic or formic acids when a strong acid was also present, the indicator absorption spectrum changed slowly for a day or more. A study of this effect for *p*-nitroaniline in acetic acid–water–$HClO_4$ solutions showed that λ_{max} shifted to shorter wavelengths. A new species seemed to be forming, possibly the acetanilide of the indicator. Under similar conditions in formic acid–water media, Stewart and Mathews[14] proposed the formation of formanilide. To minimize the error from this source, measurements were made as soon as indicator was added.

The dissociation of the protonated form of indicator B, according to the equation $BH^+ \rightleftarrows B + H^+$, was followed by determination of pK_a values as a function of solvent composition. In solvent s

$$pK_a = -\log c_{H^+} + \log \frac{c_{BH^+}}{c_B} - \log {}_s\left(\frac{y_{H^+} y_B}{y_{BH^+}}\right) \quad (1)$$

where y_i is an activity coefficient on the molar scale referred to infinite dilution in solvent s. The ratio c_{BH^+}/c_B, which appears in the second term in the equation, is the usual indicator ratio *I* and was calculated from the expression $(\epsilon_B - \epsilon)/(\epsilon - \epsilon_{BH^+})$ where ϵ is the molar absorptivity of a particular solution and the other absorptivities are for the species indicated, all being obtained at the same wavelength.[3] The absorptivity ϵ_{BH^+} was assumed to be nearly zero for the three indicators since it has been shown that the spectrum of their protonated forms closely approaches that of nitrobenzene, which is essentially nonabsorbing at about 400 mμ.[15]

Apparent dissociation constants pK_a' were calculated using the first two terms of eq 1. For *p*-nitroaniline sufficient data were available in acetic–acid water mixtures to determine true dissociation constants. In each solvent mixture studied, apparent dissociation constants extrapolated linearly with concentration of strong acid. At zero strong acid concentration, since

(10) P. Salomaa, *Acta Chem. Scand.*, 11, 125 (1957).

(11) E. A. Braude and E. S. Stern, *J. Chem. Soc.*, 1971, 1976 (1948).

(12) G. Schwarzenbach and P. Stensby, *Helv. Chim. Acta*, 42, 2342 (1959).

(13) D. S. Noyce and P. Castelfranco, *J. Am. Chem. Soc.*, 73, 4482 (1951).

(14) R. Stewart and T. Mathews, *Can. J. Chem.*, 38, 602 (1960).

(15) L. Dede and A. Rosenburg, *Chem. Ber.*, 67, 147 (1934).

Table II: Apparent Dissociation Constants of *p*-Nitroaniline and H_0 Values in Acetic Acid–Water Mixtures

	p-Nitroaniline (2.98×10^{-5} *M*; measurements at 380 mμ)								
	0.0312 *M* HCl			0.624 *M* HCl			0.0936 *M* HCl		
N_{H_2O}	I	H_0	pK_a'	I	H_0	pK_a'	I	H_0	pK_a'
0.22	0.123[a]	0.62[a]	...	0.270	0.31[a]	...	0.379[a]	0.078[a]	...
0.44	0.574	1.23	1.26	1.330	0.87	1.33	0.099[a]	0.72[a]	...
							1.95	0.70	1.32
0.63	0.232	1.63	0.87	0.494	1.30	0.90	0.734	1.12	0.90
0.73	0.154	1.80	0.69	0.331	1.47	0.72	0.469	1.32	0.70
0.81	0.144	1.83	0.66	0.292	1.52	0.67	0.432	1.34	0.66
0.90	0.147	1.82	0.67	0.318	1.49	0.71	0.434	1.35	0.66
1.00	0.306	1.50	0.99	0.601	1.21	0.98	0.861	1.07	0.96

[a] *o*-Nitroaniline used (5.88×10^{-5} *M*; measurements at 412 mμ).

the indicator concentration was about 10^{-5} *M*, the last term of eq 1 became negligible, and pK_a was obtained.

Salt Effect. The salt or concentration effect on indicator dissociation may be conveniently separated from the medium effect. The salt effect $s\overline{BH^+}$ is the value of the activity coefficient ratio of eq 1 referred to infinite dilution in each solvent mixture. Then

$$pK_a' - pK_a = \Delta pK_a = -\log s\overline{BH^+} \quad (2)$$

Medium Effect. The medium effect on indicator dissociation in BH^+ is the set of activity coefficients relating the activity of species at infinite dilution in water to those at infinite dilution in the medium in question. For the dissociation of the acid form of indicator in solvents

$$pK_a - p({}_wK_a) = -\log m\overline{BH^+} \quad (3)$$

where the subscript w indicates the dissociation constant at infinite dilution in water.

In turn, one can calculate the standard free energy of transfer

$$\Delta G^\circ_{tr} = \Delta G^\circ_s - \Delta G^\circ_w =$$
$$RT \ln ({}_wK_a/K_a) = 2.303RT\,[pK_a - p({}_wK_a)] \quad (4)$$

Hammett Acidity Function. Values of the Hammett acidity function H_0 were calculated from

$$H_0 = p({}_wK_a) - \log I \quad (5)$$

The p_wK_a values used were the best values of Paul and Long,[3] 0.99 for *p*-, 2.50 for *m*-, and −0.29 for *o*-nitroaniline.

Results

The apparent dissociation constants for the indicators studied in the three mixed solvents are given in Tables II and III. Calculated H_0 values are also listed. Investigations were generally limited to solutions of ionic strength below 0.1 *M* and mixtures of dielectric constant greater than 20 to minimize departures from ideality. Only the three mixtures richest in dioxane had dielectric constants below 20 and must be regarded as yielding uncertain results for this reason. The standard deviation in pK_a' and H_0 is believed to be 0.02 unit. The values are least reliable when based on extreme values of I.

Table III: Apparent Dissociation Constants and H_0 Values

N_{H_2O}	I	H_0	pK_a'
A. 0.060 *M* $HClO_4$ in Dioxane–Water Mixtures			
m-Nitroaniline (2.07×10^{-4} *M*; measurements at λ_{max})			
0.32	1.13	2.45	1.28
0.46	0.60	2.72	1.00
0.62	0.49	2.81	0.91
0.70	0.53	2.78	0.95
0.86	1.58	2.30	1.42
B. 0.060 *M* HCl in Formic Acid–Water Mixtures			
o-Nitroaniline (5.88×10^{-5} *M*; measurements at 412 mμ)[a]			
0.15	12.8	−1.40	2.33
0.31	3.87	−0.88	1.81
0.51	0.78	−0.18	1.11
0.75	0.087	0.68	0.16
0.91	0.056	0.96	−0.02

[a] $A_B = 0.263$ in water in 1-cm cell.

In acetic acid–water mixtures, pK_a' values were found for both HCl and $HClO_4$ solutions. For 0.03 and 0.06 *M* $HClO_4$, the pK_a' values averaged 0.01–0.02 unit larger than those for HCl, and for 0.09 *M* $HClO_4$, they were 0.04 unit larger. These differences are believed to arise from the activity differences attributable to the anions.

In addition to the results reported in Table III, three

formic acid–water determinations were made with no strong acid present. These data together with H_0 values for the system found by Stewart and Mathews[14] appear as curve C in Figure 2. The agreement is good except at the highest water content, where the spectrophotometric error is appreciable.

The salt effect was also investigated for *p*-nitroaniline in acetic acid–water mixtures by adding sodium perchlorate to perchloric acid solutions. Four representative sets of data showing the change in pK_a', $\Delta pK_a'$, on addition of salt, are graphed in Figure 1 as a function of salt concentration. An independent check on these values was obtained by establishing that conductometric determinations of perchloric acid in the presence of sodium perchlorate agreed with determinations of the acid by indicator measurements.

As Figure 1 shows, the effect of sodium perchlorate on the acid dissociation of *p*-nitroaniline in acetic acid–water mixtures appears linear up to at least an ionic strength of 0.2 *M* based on the extensive data in 44 mole % water. The following measure of the change in salt effect with solvent composition was obtained.

Mole % H_2O	100	73	63	44	34
$\Delta pK_a'/C_{HClO_4}$	0.18[3]	0.95	1.2	1.5	1.9

The quantity $\Delta pK_a'/C_{HClO_4}$, which is equivalent to σ in the treatment of the salt effect on H_0 by Paul and Long,[3] increases nearly linearly with the mole % of acetic acid from the value they give for pure water, 0.18, to about 1.9 at 66 mole % acetic acid.

The extrapolation of apparent dissociation constants of *p*-nitroaniline in HCl, $HClO_4$, and $NaClO_4$–$HClO_4$ solutions in acetic acid–water mixtures to zero concentration of strong acid yielded the averaged pK_a values listed in Table IV. Also given are data for the medium effect for *p*-nitroaniline in this solvent system and free energies of transfer from the standard state in solvent s to the aqueous standard state w based on eq 3.

Table IV: Dissociation Constants, Medium Effect, and Free Energies of Transfer for *p*-Nitroaniline in Acetic Acid–Water Mixtures

N_{H_2O}	pK_a	Log $m\overline{BH^+}$	$\Delta G°_{tr}$, cal/mole
0.34	1.54	−0.54	−740
0.44	1.23	−0.23	−320
0.63	0.82	0.18	250
0.73	0.66	0.34	470
0.81	0.66	0.34	470
0.90	0.66	0.34	470
1.00	1.00[a]	0.00	0

[a] pwK_a.

Discussion

Hammett H_0 Results. Either ΔH_0 or ΔpK_a may serve as an index of the medium effect on indicator dissociation. This may be seen by combining eq 3–5 to obtain at zero ionic strength

$$\Delta pK_a = -\log m\overline{BH^+} = -\Delta H_0$$

or at finite concentrations of strong acid

$$\Delta pK_a' = -\Delta H_0$$

Since many indicator data have been reported for mixed solvent systems as H_0 values, the present results are graphed in Figure 2 as H_0–solvent composition curves. For purposes of comparison, H_0 plots also offer the advantage of beginning from a common value in water. A low maximum in H_0 (or minimum in pK_a) may be seen for the acetic acid–water system; a high maximum in dioxane–water; and an almost linear decrease from the value in pure water for formic acid–water mixtures. Where two different indicators were used as in acetic acid–water and formic acid–water, the H_0 values are seen to overlap satisfactorily. The addition of a more acidic cosolvent to water is seen eventually to cause H_0 to decrease in each system studied, though in the case of dioxane only after a concentration of 40 mole % has been reached. The results observed for dioxane–water mixtures are comparable to those of Braude and Stern in this medium for 0.1 *M* HCl solutions.[11]

Initially, acetic acid–water mixtures appear more basic than water; only when they contain more than 50 mole % acetic acid is the medium more acidic than water. An H_0 maximum of the same magnitude at the same composition has been reported by Noyce and Castelfranco[13] for 1 *M* H_2SO_4 and can be observed in the data of Schwarzenbach and Stensby,[12] Wiburg and Evans,[16] and Zajac and Nowicki[17] for other strong acids in acetic acid–water media. The latter three pairs of investigators did not call attention to their maxima, however.

In formic acid–water media by contrast, apparently because of self-ionization, H_0 falls rapidly when water is diluted by formic acid as shown in curve C of Figure 2. It is of interest that the H_0 results for 0.06 *M* HCl in the medium (curve D) parallel the first curve and are

(16) K. B. Wiburg and R. J. Evans, *J. Am. Chem. Soc.*, 80, 3019 (1958).

(17) W. W. Zajac, Jr., and R. B. Nowicki, *J. Phys. Chem.*, 69, 2649 (1965).

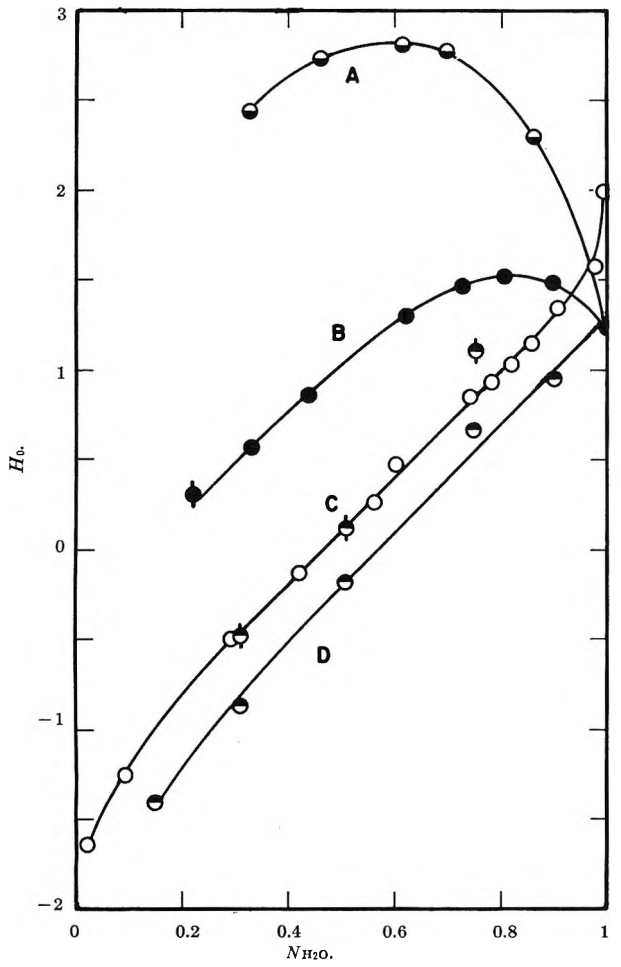

Figure 2. H_4 *vs.* mole fraction of water. Curve A: 0.06 *M* $HClO_4$ in dioxane–water mixtures. Curve B: 0.06 *M* $HClO_4$ in acetic acid–water mixtures; ◖, *o*-nitroaniline; ●, *p*-nitroaniline. Curve C: formic acid–water mixtures, *o*- and *p*-nitroaniline: ◖, this work; ○, Stewart and Mathews;[14] Curve D: 0.06 *M* HCl in formic acid–water mixtures.

displaced downward from it by only 0.30 H_0 unit on the average. If H_0 is taken as a valid acidity measure in this system, the shift indicates an acidity level in 0.06 *M* HCl consistently twice that provided by self-ionization. The marked difference in the behavior of formic and acetic acids in mixtures with water will be considered further below in the context of factors responsible for the production of maxima in H_0 or minima in pK_a.

The Minimum in pK_a. A qualitative relationship has been observed between pK_a minima in aqueous–nonaqueous mixtures and maxima in selectivity coefficient in the Na–H ion exchange in the same media.[8] Whenever a solvent mixture yields a maximum in the ion-exchange selectivity coefficient curve, a minimum is found in the pK_a curve; where no maximum is observed, the pK_a curve varies more or less monotonically with solvent composition. This relation is believed a consequence of the strong influence of the proton–metal ion exchanges in mixed solvents.[18]

As a result of this finding, it is of interest to examine the reasons for existence of such minima in pK_a. Some physical properties of solvents whose mixtures with water yield pK_a minima are collected in Table V[19–22] to guide the consideration.

Table V: Properties of Solvents and Their Mixtures with Water

Added solvent	Soln N_{H_2O} at pK_a min	Solvent[a] pK_{SH^+}	Solvent molar volume, ml	Soln $\frac{d\,pK_a}{d\,N_{H_2O}}$[b]	Solvent dipole moment,[21] D.
Ethanol	0.30[11]	0.869[c]	59	3.5	1.7
Methanol	0.40[10]	0.644[c]	41	2.0	1.7
Acetone	0.55[11]	−4.5[d]	74	5.6	2.8
Dioxane	0.60[8]	−4.4[3]	86	7.5	0.3
Acetic acid	0.82[8]	−6.3[3]	58	3.0	1.7

[a] pK for the dissociation of protonated solvent SH^+ into solvent and proton, relative to acid–base couple H_3O^+–H_2O, which is given a value of unity. [b] At $N_{H_2O} = 1$. [c] Calculated from relative basicities in acetic acid determined by Kolthoff and Bruckenstein.[22] [d] Average of values of Campbell and Edward[19] and Nagakura, *et al.*[20]

The table reveals a rough correlation between the basic strength of the cosolvent and the mole fraction of water at which a minimum in pK_a occurs. The evidence suggests that the more basic the added solvent, the more abundant it must be before pK_a reaches a minimum in the mixture. Note that the dissociation constant of the protonated cosolvent pK_{SH^+}, relative to that of H_3O^+ as one, is taken as a measure of its basic strength. In view of the poor reliability of the pK_{SH^+} data for the weaker bases, probably the correlation is as strong as could be expected. These data are based on indicator measurements in strongly acidic media where results are difficult to interpret. The problem is illustrated by acetone: its pK_{SH^+} as listed is an average of the values −7.2 determined by

(18) R. G. Fessler and H. A. Strobel, *J. Phys. Chem.*, **67**, 2562 (1963).

(19) H. J. Campbell and J. T. Edward, *Can. J. Chem.*, **38**, 2109 (1960).

(20) S. Nagakura, A. Minijishi, and K. Stanfield, *J. Am. Chem. Soc.*, **79**, 1033 (1957).

(21) C. P. Smyth, "Dielectric Behavior and Structure," McGraw-Hill Book Co., Inc., New York, N. Y., 1955.

(22) I. M. Kolthoff and S. Bruckenstein, *J. Am. Chem. Soc.*, **78**, 1, 10 (1956).

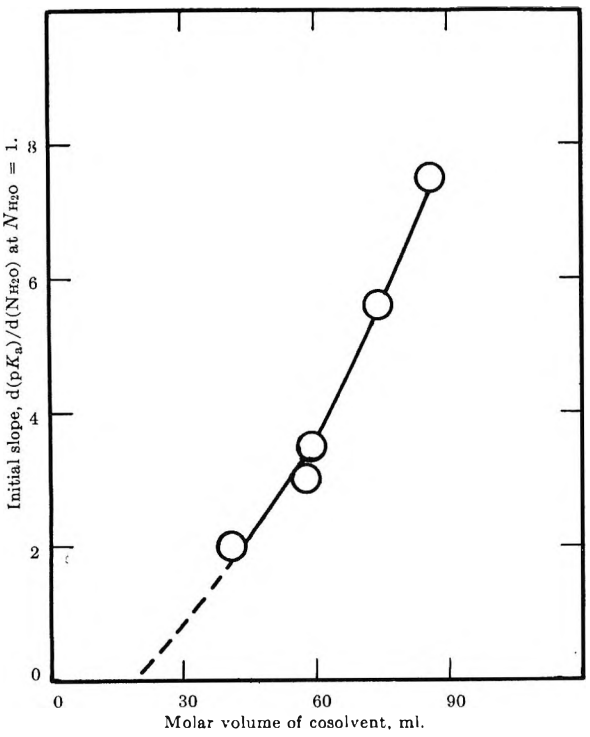

Figure 3. Correlation of initial rate of increase in dissociation constant with molar volume of cosolvent.

Campbell and Edward[19] and −1.8 found by Nagakura, *et al.*[20]

A second correlation is that the initial slope of the pK_a–solvent composition curve, $(d\,pK_a/d\,N_{H_2O})N_{H_2O} = 1$, varies nearly linearly with the molar volume of the cosolvent. This relation is shown in Figure 3. Interestingly, the curve might extrapolate to zero at 18 ml, the molar volume of water.

The two correlations suggest the following model for the occurrence of a minimum in pK_a (or a maximum in H_0) as water is mixed with a solvent which is less basic, but not as acidic, as formic acid. The dissociation of protonated indicator appears to go through a minimum as a result of two successive effects: (1) the added solvent causes an alteration of water structure that leads to greater binding of protons by water and greater dissociation of indicator; and (2) as molecules of the cosolvent begin to predominate, the increasing localization of protons near more weakly basic molecules leads to looser proton binding and less dissociation of the indicator.

The addition of molecules of a nonaqueous solvent to water involves both an initial net formation of structure[23-25] and a dilution effect which is, at least eventually, structure-breaking. Since larger nonelectrolyte molecules reduce the entropy more,[26] the initial stabilization of structure appears a function of molecular volume. Larger nonelectrolyte molecules should also lead to more extensive structure breaking as they become more abundant.

A reversal of the trend toward lower values of pK_a will occur, if at all, only as more weakly basic molecules become an appreciable fraction of the total and the proton binding must again loosen. Earlier, Braude and Stern[11] attributed H_0 maxima chiefly to structure breaking and identified the maximum with the appearance of monomeric water. It seems unlikely, however, that the maximum in H_0 or minimum in pK_a can be located so precisely in terms of structure. There is also no evident correlation of molecular dipole moment of the cosolvent with the rate of decrease in pK_a in Table IV, such as might be the case if preferential solvation were strongly involved.

To the extent the model is valid, pK_a minima for suitable indicators should occur rather generally when weakly acidic organic liquids ($pK_a > 5$) of sufficient solubility are added to water. Recently, for example, such minima (or H_0 maxima) have also been reported for mixtures of ethylene glycol–water[27] and tetrahydrofuran–water.[28]

The upper limit for cosolvent acidity for the appearance of a pK_a minimum is based on the evidence that formic acid–water mixtures show no minimum. Any cooperative solvent effects leading to a basicity greater than that of water would very likely be swamped by the intrinsic acidity of formic acid or stronger acids.

In the case of formic acid it should be noted that such cooperative solvent effects ought to be negligible. These effects, and H_0 maxima, have been reported only in mixtures of distinctly organic cosolvents with water, and formic acid is essentially inorganic. This suggests that such cooperative effects may be traced at least in part to hydrophobic structure reinforcement in water. Wells'[29] recent proposal that in methanol–water and 2-propanol–water mixtures the decrease in proton activity on addition of alcohol can be attributed to the formation of a solvated nonaqueous species more basic than water is not fundamentally at variance with this idea.

(23) E. M. Arnett and D. R. McKelvey, *J. Am. Chem. Soc.*, **87**, 1393 (1965).

(24) A. Ben-Naim, *J. Phys. Chem.*, **69**, 1922 (1965).

(25) F. Franks and D. J. G. Ives, *Quart. Rev.* (London), **20**, 1 (1966).

(26) R. A. Robinson and R. H. Stokes, "Electrolyte Solutions," 2nd ed, Butterworth Scientific Publications, London, 1959.

(27) C. Kalidas and S. R. Palit, *J. Chem. Soc.*, 3998 (1961).

(28) F. Brycman-Hauptschein and B. Tremillon, *Bull. Soc. Chim. France*, 1837 (1965).

(29) C. F. Wells, *Trans. Faraday Soc.*, **61**, 2194 (1965).

Acknowledgment. The authors express their appreciation to the U. S. Atomic Energy Commission for support of this research under Contract AT-(40-1)-2002.

Potentiometric Titrations of Polyelectrolytes with Separation of Phases

by A. Shatkay[1] and I. Michaeli

Polymer Department, Weizmann Institute of Science, Rehovoth, Israel *(Received March 4, 1966)*

A general equation has been developed to describe the potentiometric titration of a polydisperse system undergoing a phase separation, with a varying chemical potential of the precipitate. It includes two correction terms to the equation of Linderstrøm-Lang derived for a monodisperse system with a constant chemical potential of the precipitate. Experimental data are presented for a 0.01 monomolar solution of poly(DEAEM·HCl) in a 0.1 *M* solution of NaCl. The polymer in the precipitate was found to be virtually unionized. The results are discussed in terms of the above theory, and the correction terms to the Linderstrøm-Lang equation are shown to be negligible in the above system.

Introduction

Potentiometric titrations of polyelectrolytes have been extensively investigated, and comprehensive up-to-date reviews are available listing the relevant references.[2-3] In general, however, they deal with titrations of one phase only; if during the titration a phase separation (*e.g.*, precipitation) occurs, there is a tendency to regard such an occurrence as a complication which should be avoided, and not as a source of new information. This approach has been recently upheld by Steinhardt and Beychok[4] on the grounds that the precipitate interacts with the solvent and that it is not homogeneous enough to justify an exact thermodynamic treatment.

The only attempt known to us to investigate a potentiometric titration in conditions of phase separation is that of Linderstrøm-Lang and Grönwall.[5-7] Linderstrøm-Lang's treatment applies to a system fulfilling the following requirements: (a) it is monodisperse; (b) the chemical potential of the precipitate must remain constant during the titration; and (c) the salt concentration must be such that the activity coefficients of all the species of the polyelectrolyte remain practically constant. When these requirements are fulfilled, the following equation should hold

$$P = -\frac{1}{1 - \bar{\alpha}^*} \frac{\mathrm{d} \log C_p}{\mathrm{d\,pH}} \qquad (1)$$

where P is the degree of polymerization, $1 - \bar{\alpha}^*$ is the average degree of protonation in solution [*i.e.*, $P(1 - \bar{\alpha}^*)$ is the average number of protons on a macro-

(1) A part of a thesis submitted by A. Shatkay to the Weizmann Institute of Science in partial fulfillment of the requirements for the Ph.D. degree. The thesis was carried out under the direction of Professor A. Katchalsky.

(2) C. Tanford, "Physical Chemistry of Macromolecules," John Wiley and Sons, Inc., New York, N. Y., 1963, Chapter 8.

(3) J. T. Edsall and J. Wyman, "Biophysical Chemistry," Academic Press, Inc., New York, N. Y., 1958, Chapters 8, 9, and 11.

(4) J. Steinhardt and S. Beychok, "Interactions of Proteins with Hydrogen Ions and Other Small Ions and Molecules," in "The Proteins," H. Neurath, Ed., Academic Press, New York, N. Y., 1964, Chapter 8.

(5) K. Linderstrøm-Lang, *Arch. Biochem.*, 11, 191 (1946).

(6) A. Grönwall, *Compt. Rend. Trav. Lab. Carlsberg, Ser. Chim.*, 24, 185 (1942).

(7) K. Linderstrøm-Lang and S. O. Nielsen, "Acid-Base Equilibria of Proteins," in "Electrophoresis," M. Bier, Ed., Academic Press, New York, N. Y., 1959.

molecule in the liquid phase], and C_p is the concentration of the macromolecules in solution.

We have found in the literature no experiments demonstrating directly the validity of eq 1; in the investigation of Grönwall[6] C_p and pH were determined but $\bar{\alpha}^*$ was not, so that eq 1 could not be tested directly. An attempt was made to test eq 1 indirectly[5,6] by introducing an additional assumption which makes the determination of $\bar{\alpha}^*$ unnecessary. According to the authors, however, the results were found to be inconclusive. It is possible that the behavior of the experimental system investigated by the above authors could not be described by eq 1, since this system did not fulfill some of Linderstrøm-Lang's conditions cited above.

It appears, therefore, that it is important to evaluate the potentiometric-titration behavior of systems which may not obey the requirements listed above. It would also be of interest to investigate a system which does comply with the above requirements, and thus can be described by the simple equation (1).

In the present paper we shall both generalize eq 1 [dispensing with the requirements (a) and (b) above] and describe an experimental system obeying the simple eq 1 to a good approximation.

Theoretical

Following Linderstrøm-Lang we consider a solution of a monodisperse polymer, the macromolecules carrying i protons. The concentration of the chains with i protons on them is

$$C_i = a_0 a_H{}^i K_i / f_i \tag{2}$$

where a_i denotes the activity of macromolecules carrying i protons (including $i = 0$), a_H denotes the activity of the protons, and K is the association constant.

The total concentration of macromolecules in the solution is

$$C_p = \Sigma_i C_i = a_0 \Sigma_i a_H{}^i K_i / f_i \tag{3}$$

We abandon now the treatment of Linderstrøm-Lang, and differentiate eq 3 with respect to a_H (at constant temperature and pressure) without assuming that a_0 is constant.

$$\frac{dC_p}{da_H} = a_0 \Sigma_i i a_H{}^{i-1} K_i / f_i - a_0 \Sigma_i \frac{K_i}{f_i} a_H{}^i \frac{d \ln f_i}{da_H} + \frac{da_0}{da_H} \Sigma_i a_H{}^i K_i / f_i \tag{4}$$

If f_i are constant (according to the requirement (c) above which can easily be satisfied), the second term on the right-hand side of eq 4 equals zero. On rearrangement and on the introduction of the following three equalities

$$\text{pH} \equiv -\log a_H$$

$$P(1 - \bar{\alpha}^*) \equiv [\Sigma_i i C_i]/\Sigma_i C_i$$

$$d\mu_i \equiv RT \, d \ln a_i$$

eq 4 yields

$$P = -\frac{1}{1 - \bar{\alpha}^*} \frac{d \log C_p}{d \text{ pH}} - \frac{1}{1 - \bar{\alpha}^*} \frac{d\mu_0}{d\mu_H} \tag{5}$$

For a polydisperse system eq 5 is valid for each degree of polymerization P_k. As a rule $\bar{\alpha}^*$ is practically independent of the degree of polymerization, and we may write

$$\frac{\Sigma_k dC_{p,k}}{d \ln a_H} = (1 - \bar{\alpha}^*)\Sigma_k P_k C_{p,k} + \Sigma_k C_{p,k} \frac{d \ln a_{0,k}}{d \ln a_H} \tag{6}$$

Dividing both sides of eq 6 by $\Sigma_k C_{p,k}$ and introducing the number averages $\langle P \rangle$ and $\langle d\mu_0/d\mu_H \rangle$ we obtain

$$d \ln C_p / d \ln a_H = (1 - \bar{\alpha}^*)\langle P \rangle + \langle d\mu_0/d\mu_H \rangle \tag{7}$$

With the introduction of the monomolar concentration $C_m = \langle P \rangle C_p$, eq 7 may be readily transformed into

$$\langle P \rangle = \frac{1}{1 - \bar{\alpha}^*} \left(-\frac{d \log C_m}{d \text{ pH}} + \frac{d \log \langle P \rangle}{d \text{ pH}} - \left\langle \frac{d\mu_0}{d\mu_H} \right\rangle \right) \tag{8}$$

It should be noted that $\langle P \rangle$ refers to the average degree of polymerization of the polymer remaining *in solution*.

Comparison with eq 1 shows that eq 8 includes correction terms for polydispersity and for the change in the chemical potential of the polymer during titration.

Experimental Section

The experimental system chosen consisted of aqueous solutions of poly(diethylaminoethylmethacrylate hydrochloride). The polymer was synthesized from DEAEM monomer supplied by Monomer-Polymer-Laboratories according to the following procedure of S. Marian (to be published).

The monomer was distilled at a pressure of 25 mm between 108 and 109°. A 100-ml sample of the monomer was added to 1200 ml of dry benzene. Dry gaseous HCl was passed through the solution with cooling and stirring. DEAEM·HCl monomer precipitated and subsequently dissolved in an excess of HCl. On addition of 2 l. of dry ether, the quaternized monomer precipitated. The precipitate was washed with dry ether and dried *in vacuo* at room temperature. The

monomer is a white crystalline powder soluble in water, alcohol, and acetone. It does not polymerize in the cold. The N to Cl^- ratio on analysis is 1.00.

The polymerization was carried out in aqueous solution (approximately 400 g of the monomer per liter) at 40° with potassium persulfate (0.55 g/l.) as initiator. After 5 hr an equal volume of methanol was added. The resulting solution was divided into lots of 250 ml, and each lot was poured into 1 l. of acetone. Poly(DEAEM·HCl) precipitated. After drying *in vacuo* at room temperature to a constant weight, analysis yields an N to Cl^- ratio of 1.00 and shows the water content to be 8.8%.

In order to obtain the values of C_m, $\bar{\alpha}^*$, and pH corresponding to each point on the two-phase titration curve, the following procedure was adopted. For each point on the titration curve a separate sample was prepared. To each sample that contained n_m monomoles of the polymer, n_w moles of water, and n_{NaCl} moles of salt, n_{NaOH} moles of base were added so that the concentration of all the components fit the desired point on the titration curve. At sufficiently high degrees of neutralization of the total polymer (α), a precipitate appeared.

The pH *of the solution* in equilibrium with the precipitate was measured with a "Radiometer" PHM-4d meter using glass electrode G-202-B and calomel electrode K-401. The calibration was made with five different buffer solutions. The pH measurements were found to be accurate to ±0.01 pH unit. For the evaluation of μ_{HCl} and μ_{NaCl}, the same apparatus was employed with electrodes of Ag–AgCl for Cl^- and Beckman's 78178-v sodium electrode for Na^+.

After the potentiometric measurements, the solution and the precipitate were centrifuged for 1 hr at 10,000 rpm. Most of the supernatant liquid was withdrawn and analyzed for the concentrations of N, Cl^-, and Na^+. To the precipitate and the remaining solution H_2SO_4 was added to dissolve the precipitate, and this part was also analyzed for N, Cl^-, and Na^+ to confirm the analysis of the supernatant liquid.

The analysis for N was carried out by a semimicro Kjeldahl method; the results were accurate within ±1%. Chloride was determined with the aid of an Amino-Cotlove chloride titrator, also with an accuracy of ±1%. Sodium was determined with the aid of the Jouan flame photometer with an accuracy of ±5%.

The precipitation, the potentiometric titrations, and the separation of the supernatant liquid were carried out at the constant temperature of 25 ± 1°.

$\langle P \rangle_n$ was evaluated by the osmotic method of Alexandrowicz.[8] $\langle P \rangle_w$ was evaluated by the light-scattering method in excess of salt with double extrapolation to zero values of angle and polymer concentration.[9]

Results and Discussion

The general relationships which apply to a potentiometric titration during phase separation are fully expressed by eq 8. In addition to the term $\langle d\mu_0/d\mu_H \rangle$ present in any usual potentiometric titration of a solution at constant polymer concentration, eq 8 includes also the term d log C_m/d pH for the change in polymer concentration, and the term d log $\langle P \rangle$/d pH for the change in the mean degree of polymerization. The last two terms are given by directly measurable quantities, while the term $\langle d\mu_0/d\mu_H \rangle$ will be transformed into an expression whose terms may be readily evaluated.

For the thermodynamic evaluation of the experimental results, it is necessary to ascertain that the titration during the separation of phases is reversible. It was confirmed that in a solution of 0.01 monomolar poly(DEAEM·HCl) in a 0.2 *M* solution of NaCl the titration was reversible. In addition, the pH at various points of the titration curve was found to remain constant for 24 hr within the experimental error.

To evaluate the term $\langle d\mu_0/d\mu_H \rangle$ we proceed as follows. For a monodisperse polymer system where μ_0 is a function of only r_p and μ_{HCl} (T, pressure, and n_{water} being constant), it is obvious that for a constant n_p in the (two-phase) system

$$\frac{d\mu_0}{d\mu_{HCl}} = \left(\frac{\partial \mu_0}{\partial \mu_{HCl}}\right)_{n_p} \tag{9}$$

and we have the following cross relation

$$\left(\frac{\partial \mu_0}{\partial \mu_{HCl}}\right)_{n_p} = -\left(\frac{\partial n_{HCl}}{\partial n_p}\right)_{\mu_{HCl}} \tag{10}$$

In a system undergoing precipitation, the right-hand side of eq 10 may be interpreted as the ratio of HCl to polymer in the precipitate, as addition of these components in this ratio does not change the chemical potentials of the system (the water in the precipitate being neglected). This means that the right-hand side of eq 10 is identical with $-P(1 - \bar{\alpha}_{ppt})$. Thus at a constant μ_{Cl^-} in the solution, eq 9 yields

$$\frac{d\mu_0}{d\mu_H} = -(1 - \bar{\alpha}_{ppt})P \tag{11}$$

In a polydisperse system, the above conclusions apply to each species of a given degree of polymerization P_k with a concentration C_k. Writing eq 11 for P_k and

(8) Z. Alexandrowicz, *J. Polymer Sci.*, **40**, 113 (1959).

(9) A. Shatkay, Ph.D. Thesis, Weizmann Institute of Science, Rehovoth, Israel, 1965.

introducing the fraction $\theta_k = C_k/\Sigma_k C_k$, we get for the correction term in eq 8

$$\left\langle \frac{d\mu_0}{d\mu_H} \right\rangle = \Sigma\theta_k \frac{d\mu_{0,k}}{d\mu_H} = -(1 - \bar{\alpha}_{ppt})\langle P \rangle \quad (12)$$

Equation 12 shows that $\langle d\mu_0/d\mu_H \rangle$ is small if the precipitate is sufficiently deprotonized.

Two independent series of experiments were performed to determine the degree of protonation of the precipitate. In one of them direct measurements of the quantity of HCl on the precipitate were carried out; it was found that the Cl^- to N ratio in the precipitate is generally below 0.03. The amount of Na found on the precipitate is of the same order. Thus the precipitate is free from HCl within the bounds of our experimental error.

In another set of experiments, the quantity of Cl^- in the supernatant liquid was measured to detect any loss due to HCl being kept on the precipitate. The results of this set of experiments again indicate that the degree of protonation of the precipitate is less than 1%; *i.e.*, it is within the limits of our experimental error. It appears, therefore, that $\bar{\alpha}_{ppt} > 0.99$. The number-average degree of polymerization of the poly(DEAEM·HCl) used was 1100 on the basis of osmotic measurements. By introducing these values of $\langle P \rangle_n$ and $\bar{\alpha}_{ppt}$ into eq 12, $\langle d\mu_0/d\mu_H \rangle$ is found to be less than 11.

The value of $\langle d\mu_0/d\mu_H \rangle$ has been estimated also by using another procedure. For a system consisting of a monodisperse polyelectrolyte, salt, HCl, and water, at constant temperature and pressure when n_p and n_w are kept constant, it is possible to write

$$\frac{d\mu_{0,k}}{d\mu_H} = \left(\frac{\partial\mu_{0,k}}{\partial n_{HCl}}\right)_{n_{NaCl}} \frac{dn_{HCl}}{d\mu_H} + \left(\frac{\partial\mu_{0,k}}{\partial n_{NaCl}}\right)_{n_{HCl}} \frac{dn_{NaCl}}{d\mu_H} \quad (13)$$

The partial derivatives on the right-hand side of eq 13 may be substituted according to Maxwell's relations, so that

$$\frac{d\mu_{k,0}}{d\mu_H} = \left(\frac{\partial\mu_{HCl}}{\partial n_{k,0}}\right)_{n_{HCl},n_w,n_{NaCl}} \frac{dn_{HCl}}{d\mu_H} + \left(\frac{\partial\mu_{NaCl}}{\partial n_{k,0}}\right)_{n_{HCl},n_w,n_{NaCl}} \frac{dn_{NaCl}}{d\mu_H} \quad (14)$$

It can be easily shown by using eq 14 that in a polydisperse system

$$\left\langle \frac{d\mu_0}{d\mu_H} \right\rangle = \frac{dn_{HCl}}{d\mu_H}\left(\frac{\partial\mu_{HCl}}{\partial n_0}\right)_{n_{HCl},n_w,n_{NaCl}} + \frac{dn_{NaCl}}{d\mu_H}\left(\frac{\partial\mu_{NaCl}}{\partial n_0}\right)_{n_{HCl},n_w,n_{NaCl}} \quad (15)$$

The partial derivatives in eq 15 were evaluated from emf measurements at different values of n_0. Two sets of experiments were performed. In one set, solid polymer (deprotonized) was added directly to the system. In the other set of experiments, μ_{HCl} and μ_{NaCl} were determined in a series of two-phase systems prepared as follows: solutions of fully protonized polymer at different concentrations were prepared and NaOH and NaCl were added to obtain the required constant final values of n_w, n_{HCl}, and n_{NaCl}. The results obtained by these two methods are less conclusive than those obtained by eq 12, mainly because of experimental difficulties in making Δn_0 big enough to get significant changes in the measured emf values. The results, however, were in line with the more exact data obtained by the use of eq 12. We may therefore assume that $\langle d\mu_0/d\mu_H \rangle < 11$, and for a $\langle P \rangle = 1100$, the term including $\langle d\mu_0/d\mu_H \rangle$ in eq 8 may be neglected practically within the whole range of $\bar{\alpha}^*$.

As the precipitate is practically stripped of protons, the degree of deprotonation of the polymer in solution, $\bar{\alpha}^*$, has been calculated by the expression

$$\bar{\alpha}^* = \frac{n_b - n_{p(ppt)}}{n_{p(soln)}} \quad (16)$$

where n_b is the amount of base added, and $n_{p(ppt)}$ and $n_{p(soln)}$ are the amount of polymer in the precipitate and in the solution phase, respectively. The values of $\bar{\alpha}^*$ thus obtained are presented in Figure 1 where α is the ratio of the base added to the initial amount of hydrochloride in solution.

When $\bar{\alpha}^*$ approaches 1 the denominator in eq 16 is small and the numerator is a difference between two relatively large numbers, so that the values of $\bar{\alpha}^*$ obtained through eq 16 become inaccurate. Therefore, for $\bar{\alpha}^* > 0.6$ we use values of $\bar{\alpha}^*$ obtained by interpolation of the experimental results between $\bar{\alpha}^* = 0.6$ and 1, as given in Figure 1.

In order to evaluate the term d log $\langle P \rangle$/d pH, we have measured $\langle P \rangle$ in the solution phase at three degrees of neutralization: the first one before precipitation, the second one at the beginning of precipitation, and the third one when most of the polymer was precipitated. The value of $\langle P \rangle$ was measured by light scattering, thus yielding the weight average instead of the number average which appears in eq 8. As we are interested only in d log $\langle P \rangle$, the difference between $\langle P \rangle_w$ and $\langle P \rangle_n$ is immaterial as long as we neglect (to first approximation) the change in their ratio. The results of the light-scattering experiments show that $\langle P \rangle_w$ in solution decreases from 3500 at $\alpha = 0.39$ (immediately before the precipitation) to 2300 at $\alpha = 0.45$ (at the

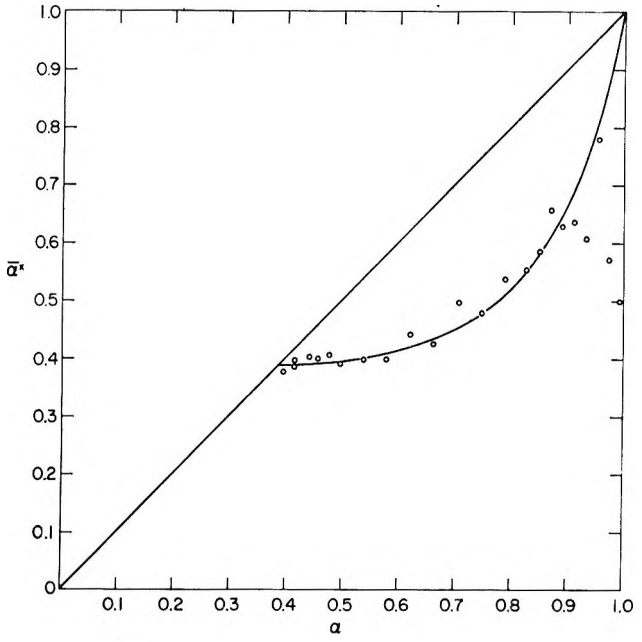

Figure 1. $\bar{\alpha}^*$ as a function of α during the titration of a 0.01 monomolar solution of poly(DEAEM·HCl) in a 0.1 M solution of NaCl.

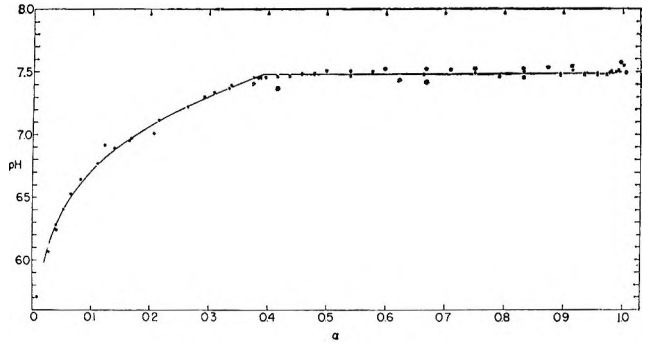

Figure 2. Titration of 2.43×10^{-4} monomole of poly(DEAEM·HCl) in 25 ml of a 0.1 M solution of NaCl: ———, calculated titration curve; dots, experimental results.

beginning of the precipitation), and to 2100 at $\alpha = 0.91$ (when most of the polymer precipitated out of the solution). Thus $[1/(1 - \bar{\alpha}^*)][\Delta \log P/\Delta \mathrm{pH}]$ is -30 for the change of the concentration C_m from 9.4×10^{-3} to 7.9×10^{-3} monomolar, and is -2 for the subsequent change from 7.9×10^{-3} to 2.8×10^{-3} monomolar. It appears, therefore, that the correction term in eq 8 due to polydispersity is negligible for our system even for the larger value of -30. Moreover, this value obtained at the beginning of the precipitation may be due to the preferential precipitation of the cross-linked chains so that the lower value of -2 is nearer the correct value.

The above considerations show that we are justified

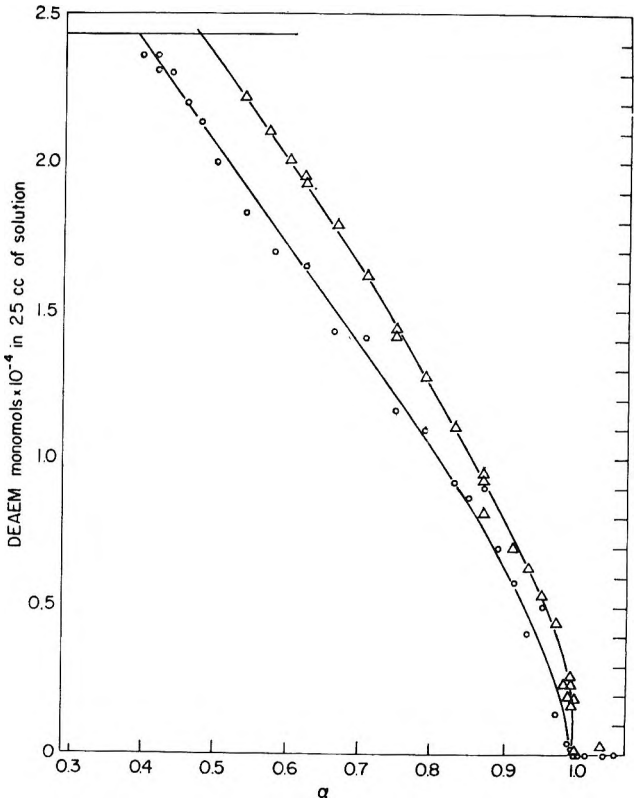

Figure 3. Stability of poly(DEAEM) during titration of 2.43×10^{-4} monomole of poly(DEAEM·HCl) in 25 ml of solution; ○, in a 0.1 M solution of NaCl; △, without addition of salt.

in applying the simple equation (eq 1) of Linderstrøm-Lang to the system under investigation.

The dependence of pH on the amount of base added is given in Figure 2. As could be expected, the potentiometric behavior of poly(DEAEM·HCl) up to the precipitation point can be adequately described by the empirically modified Henderson–Hasselbach equation[10]

$$\mathrm{pH} = \mathrm{p}K + n \log \frac{1 - \alpha}{\alpha} \qquad (17)$$

with $\mathrm{p}K = 7.68$ and $n = 1.02$.

Figure 3 represents the relationship between C_m and the amount of base added. According to Figure 3, precipitation starts at $\alpha = 0.391$ so that eq 17 yields for the precipitation point the pH of 7.48. To describe the rest of the titration curve, we write eq 1 in the integral form

$$\mathrm{pH} - \mathrm{pH}_{(\mathrm{ppt\ pt.})} = -\frac{1}{\langle P' \rangle} \int_{C_{m(\mathrm{ppt\ pt})}}^{C_m} \frac{1}{1 - \bar{\alpha}^*} \, \mathrm{d} \log C_m \qquad (18)$$

(10) A. Katchalsky and P. Spitnik, *J. Polymer Sci.*, **2**, 432 (1947).

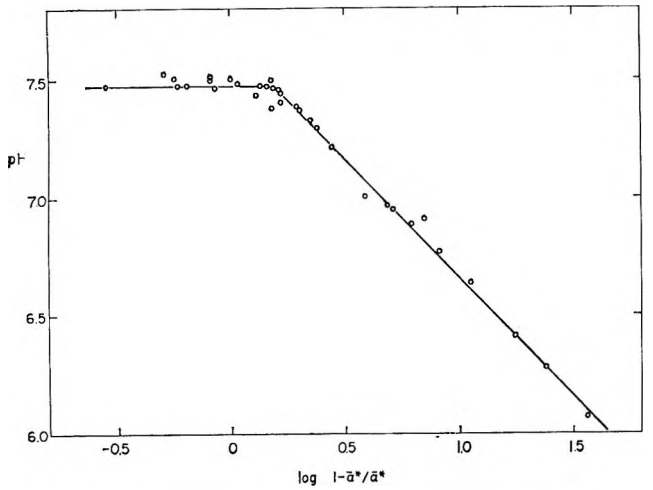

Figure 4. pH as a function of log $[(1 - \alpha^*)/\alpha^*]$: ———, calculated by eq 17 and 18; ○, experimental results.

where $1/\langle P \rangle$ has been taken out of the integral, as in our system $\langle P \rangle$ is constant.

It should be noted that eq 18 is valid in the two-phase region independently of the relationship between pH and $\bar{\alpha}^*$. The latter relationship is a characteristic of each polymer, and the specific values of $\bar{\alpha}^*$ and pH at a given point of the titration will determine the solubility (C_m) of the polymer in question at this point according to eq 18.

The $\bar{\alpha}^*$ to pH relationship is represented in Figure 4. It will be observed that the experimental curve of pH *vs.* log $[(1 - \bar{\alpha}^*)/\bar{\alpha}^*]$ has a critical transition at $\bar{\alpha}^* = 0.39$ similar to those observed in some polyacids:[11-14] at higher degrees of ionization the curve obeys the modified Henderson–Hesselbach equation (eq 17) while after a critical $\bar{\alpha}^*$ there is a significant deviation from eq 17 and a high buffering region appears. However, as noted above, eq 18 is independent of the validity of eq 17.

Figure 4 compares the experimental data with a theoretical line where pH has been calculated with the aid of eq 17 for the one-phase region and eq 18 for the two-phase region, using the experimental C_m and $\bar{\alpha}^*$ data with $\langle P \rangle = 1100$.

Integration according to eq 18 predicts that pH will increase by 0.002 unit from the precipitation point at $\alpha = 0.39$ to $\alpha = 0.935$, and by 0.006 unit to $\alpha = 0.99$. However, upon further increase of α the pH will increase noticeably by 0.014 unit from $\alpha = 0.990$ to $\alpha = 0.995$.

The theoretical results are given by the line in Figure 2. For pH values below 7.48 the curve was calculated according to eq 17, while for the values of pH above 7.48 the equation employed was eq 18.

It should be noted that the term $\langle P \rangle(1 - \bar{\alpha}^*)$ is very large for the major part of the two-phase titration, so all one can tell for this region is that the pH will remain virtually constant. However, in accordance with eq 18, the experimental pH in our system increases steeply from $\alpha = 0.99$ to the equivalence point.

Acknowledgment. We are greatly indebted to Professor A. Katchalsky for his interest and advice. We wish to express our thanks also to S. Marian, who instructed us in the polymerization techniques, and to A. Litan for his many helpful suggestions.

(11) A. Wada, *Mol. Phys.*, **3**, 409 (1960).

(12) M. Nagasawa and A. Holtzer, *J. Am. Chem. Soc.*, **86**, 538 (1964).

(13) J. C. Leyte and M. Mandel, *J. Polymer Sci.*, **A2**, 1879 (1964).

(14) I. Michaeli, International Symposium on Macromolecular Chemistry, Prague, 1965.

The Adsorption of Polystyrene–Poly(methyl methacrylate) Mixtures at a Solid–Liquid Interface[1]

by Curt Thies

The National Cash Register Company, Dayton, Ohio 45409 *(Received March 17, 1966)*

The adsorption of polystyrene (PS) and poly(methyl methacrylate) (PMMA) mixtures on finely divided silica from dilute trichloroethylene solutions at 25° has been studied in order to establish the competitive adsorption behavior of these polymers. It has been shown that under equilibrium conditions, reached within 2–4 hr, PS is not adsorbed unless the available PMMA is unable to saturate the adsorbent surface. If PS is first equilibrated on the silica surface and excess PMMA is added later in a second step, complete PS displacement occurs within 2–4 hr. Within limits of the experimental technique used, the rate and extent of displacement are essentially independent of the time the PS is equilibrated on the surface and the PS surface coverage. Polymer–polymer incompatibility was found to have little effect on the adsorbance and/or adsorbed structure of either polymer. Infrared bound fraction data establish that simultaneous adsorption of PS and PMMA on silica induces relatively small changes in the average number of segments of either polymer that are attached to the adsorbing surface. However, these results may be uniquely applicable to dynamic systems involving small adsorbent particles such as employed in this study.

Introduction

The absorption of polymers at solid–liquid interfaces has been studied extensively and is the subject of several recent reviews.[2–4] Past studies have led to the conclusion that polymers adsorbed at such interfaces have a looped or coiled structure in which only a fraction of their segments are attached directly to the interface. Many such structures are possible, ranging from ones which yield a relatively flat and compressed adsorbed polymer layer to ones which give adsorbed layers highly extended away from the interface. Thus, efforts have been made to measure directly the structure of adsorbed polymers.[3–7] Of particular interest is an infrared method first reported by Fontana and Thomas.[8] This utilizes the fact that various molecular groups possess a characteristic infrared band which appears at a certain frequency when the group is unadsorbed and then shifts slightly to a new frequency when the group is bound or attached to an interface. If only a fraction of a polymer's segments are attached, this fraction can be determined by resolving the infrared peaks due to the adsorbed and unadsorbed segments. From these peaks, the concentrations of free and bound segments can be determined, and the infrared bound fraction, p, can be calculated. Hence, p represents the average fraction of groups that are bound directly to the interface.

By combining bound fraction data with isotherm data, considerable insight into polymer adsorption phenomena can be gained. The purpose of this study is to utilize these tools to explore the competitive ad-

(1) Portions of this paper were presented at the 149th National Meeting of the American Chemical Society, Polymer Division, Detroit, Mich., April 1965, and the 13th Canadian High Polymer Forum, Ottawa, Canada, Sept 1965.

(2) R. E. Hughes and C. A. von Frankenberg, *Ann. Rev. Phys. Chem.*, 14, 290 (1963).

(3) F. Rowland, R. Bulas, E. Rothstein, and F. R. Eirich, *Ind. Eng. Chem.*, 57, No. 9, 46 (1965).

(4) F. R. Eirich, *Consig. Naz. Ric.* (Rome), 1963.

(5) R. R. Stromberg, D. J. Tutas, and E. Passaglia, *J. Phys. Chem.*, 69, 3955 (1965).

(6) R. R. Stromberg, E. Passaglia, and D. J. Tutas, *J. Res. Natl. Bur. Std.*, 67A, 431 (1963).

(7) M. Gottlieb, *J. Phys. Chem.*, 64, 427 (1960).

(8) B. J. Fontana and J. R. Thomas, *ibid.*, 65, 480 (1961).

sorption behavior of polystyrene (PS)–poly(methyl methacrylate) (PMMA) mixtures and determine whether polymer incompatibility effects alter the adsorbance or adsorbed structure of either polymer when they are simultaneously adsorbed on silica. Equilibrium and reversibility of the adsorption processes occurring in such systems also were investigated.

Experimental Section

Materials. A series of PMMA and PS polymers was prepared by azobisisobutyronitrile initiated polymerization of freshly distilled monomers at 55° in sealed glass ampoules. Except for PS-1, which was carried to approximately 90% conversion, all polymerizations were carried to about 20% conversion. Each polymer was repeatedly reprecipitated from benzene into methanol and then freeze-dried from benzene. Characterization data are given in Table I. Number average molecular weights ($\bar{M}_n$) were determined in toluene at 37° using a Mechrolab Model 502 membrane osmometer (F and M Mechrolab Division, Hewlett-Packard Corp., Mountain View, Calif.). Intrinsic viscosity measurements were made in benzene at 30 ± 0.05° using a Cannon–Ubbelohde viscometer. Viscosity average molecular weights ($\bar{M}_v$) were calculated from the equation $[\eta] = KM^a$, where $[\eta]$ represents the intrinsic viscosity, M the molecular weight, and K and a appropriate constants. The K and a values used for PS were those of Ewart and Tingey[9] while values reported by Stanley[10] were used for PMMA.

Table I: Characterization of Polymers Used for Adsorption Studies

Sample	Polymerization method	$\bar{M}_n \times 10^{-5}$	$\bar{M}_v \times 10^{-5}$
PMMA-1	Bulk	8.22	19.0
PMMA-5	Solution[a]	3.20	3.68
PS-1	Bulk	1.05	2.46
PS-2	Solution[a]	0.36	0.39

[a] Toluene/monomer ratio was 1:1 by volume.

The adsorbent for all experiments was Cab-O-Sil M-5 (Cabot Corporation, Boston, Mass.). This is a finely divided silica powder having a manufacturer's specified surface area (nitrogen adsorption) of 175–200 m²/g. It was heated at 110° for 48–72 hr, cooled, and stored in a desiccator until used. Most experiments were run using a single lot of Cab-O-Sil in order to avoid lot-to-lot variations in adsorption behavior. Only the rate of adsorption plot for PS-1 shown in Figure 2 was obtained using a second lot.

The solvent for all experiments was Chromatoquality trichloroethylene (C_2CHCl_3) (Matheson Coleman and Bell, Norwood, Ohio). It was used as received.

Adsorption Isotherms. Adsorption isotherms for the individual polymers were constructed at 25 ± 1° by agitating 25-ml sealed glass ampoules containing a known weight of adsorbent, w (grams), and 15 ml of polymer solution of initial concentration, c_0 (grams/100 ml), on an Eberbach laboratory shaker at 170 1.5-in. strokes/min (Eberbach, Ann Arbor, Mich.). The shaker was enclosed in order to prevent photoinitiated decomposition of C_2HCl_3 during prolonged agitation periods. All ampoules were flushed with nitrogen before sealing. After known agitation periods, the suspension was centrifuged, and the concentration of unadsorbed polymer remaining in the supernatant, c_s (grams/100 ml), was determined by infrared analysis. The characteristic band of PS at 697 cm^{-1} and the band for PMMA at 1720 cm^{-1} were utilized for these analyses. Polymer adsorbances are reported as weight of polymer adsorbed per unit weight of adsorbent, x/m (milligrams per gram). The absence of surface-active impurities was confirmed by varying the ratio of adsorbent to volume of solution used in carrying out the adsorption experiment.[11]

Adsorption isotherms for PS–PMMA mixtures were obtained in a manner similar to that used for the individual polymers. In this case, initial concentrations of both polymers were fixed while the amount of adsorbent added was varied. Mixture isotherms are plotted as values of c_s for both polymers *vs.* w. Since neither PS or PMMA has infrared bands which overlap the other's characteristic infrared band, the concentrations of both in binary mixtures were readily determined by infrared analysis.

PS Displacement. PS was adsorbed from C_2HCl_3 on silica and equilibrated for a known time. Excess PMMA then was added to the system and the c_s values for both polymers were determined by infrared analysis after known displacement periods. In all cases, the PS was added to the silica first as 10 ml of solution and 5 ml of PMMA solution was added later. Most runs were made as outlined for construction of adsorption isotherms. When PS was equilibrated on the surface for 3 min before PMMA addition, the samples were agitated vigorously by hand rather than on the mechani-

(9) R. H. Ewart and H. C. Tingey in "Styrene, Its Polymers, Copolymers and Derivatives," R. H. Boundy and R. F. Boyer, Ed., Reinhold Publishing Co., New York, N. Y., 1952, p 334.

(10) E. L. Stanley in "Analytical Chemistry of Polymers," Part I, G. M. Kline, Ed., Interscience Publishers, Inc., New York, N. Y., 1959, p 14.

(11) R. Perkel and R. Ullman, *J. Polymer Sci.*, 54, 127 (1961).

cal shaker. Displacement times < 0.3 hr could not be examined, since this much time was required to separate the adsorbent from the supernatant.

Infrared Bound Fractions. The average fraction of segments on an adsorbed polymer chain which are bound to the surface (p) was calculated for each polymer from a shift in its characteristic infrared band which occurs upon adsorption. The bands used were (a) the carbonyl stretching frequency of PMMA which shifts from 1720 to 1703 cm^{-1}, and (b) the out-of-plane C–C ring vibration of PS which shifts from 697 to 701 cm^{-1}. The procedure[8,12] involved adsorbing the polymer(s) on silica and forming a uniform suspension. This was transferred to a demountable fixed-thickness cell which was placed in the sample beam of the infrared spectrophotometer (Perkin-Elmer 337). A variable cell containing a known concentration of unadsorbed polymer was placed in the reference beam and adjusted by trial and error until the concentration of free polymer segments was exactly compensated. The fraction of bound segments, p, was calculated from the known concentration of adsorbed polymer, c_a, and the measured concentration of bound segments, c_b. Stable suspensions necessary for determining infrared p values were formed using a ratio of 0.15 g of silica to 5 ml of C_2HCl_2. In order to minimize errors arising from nonuniform suspensions, each reported bound fraction value represents an average of two to four infrared scans on the same sample. The measurement error associated with these repeated scans was estimated by calculating the standard deviation, σ, as suggested by Wilson.[13] Based on nine samples (32 observations), $\sigma = \pm 0.025$ for PS-1; based on ten samples (24 observations), $\sigma = \pm 0.013$ for PMMA-5. These values of σ reflect scatter in p associated with transferring uniform, stable suspensions into the infrared cell and recording the spectra.

Results and Discussion

Equilibrium adsorption isotherms for each PS and PMMA polymer studied are shown in Figure 1. Included are representative infrared bound fraction values for PS-1 and PMMA-5 obtained from samples agitated >24 hr. The isotherms are typical for polymers, and have a steep rise in x/m at low values of c_s followed by a long plateau region in which x/m is almost independent of c_s. The values of p for PMMA-5 vary somewhat with surface coverage, particularly at x/m = 65 mg/g, where p appears to increase rather sharply from approximately 0.29 to 0.35. The high values of p reported here are similar to those observed previously when two bulk polymerized PMMA polymers were adsorbed on silica from chloroform.[12] This implies that PMMA is adsorbed from both solvents by silica

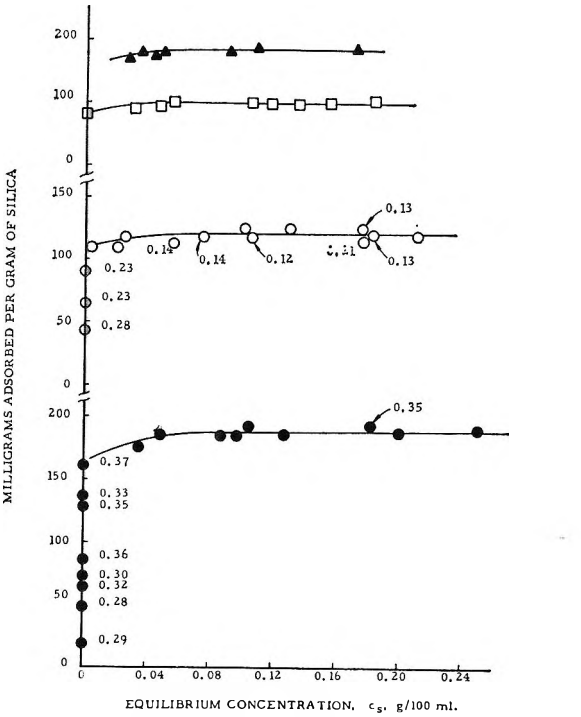

Figure 1. Equilibrium adsorption isotherms on silica from C_2HCl_3 at 25°. The numbers on the graph are the values of p, the bound fraction, at that point: ●, PMMA-5; ○, PS-1; ▲, PMMA-1; □, PS-2.

to form a highly compressed adsorbed polymer layer. In contrast to PMMA-5, bound fraction values for PS-1 were both lower and more variable. The trend toward lower values of p at higher surface coverages indicates that a more extended adsorbed structure is formed as the surface fills with adsorbed PS-1, and is consistent with previous observations.[5,12]

Rate of adsorption curves given in Figure 2 show that PMMA-5 and PS-1 reach their equilibrium adsorbance values within 1.5 and 0.5 hr, respectively, when suspensions are agitated on the mechanical shaker. PS-1 samples agitated by vigorous hand shaking reached essentially equilibrium adsorbances in 3 min, demonstrating that the rate of adsorption increases with agitation as La Mer and Healy reported.[14]

The question of the extent to which the bound fraction data represent equilibrium values was examined by determining p as a function of agitation time. Representative data for PS-1 and PMMA-5 mixtures are shown in Table II together with data obtained for a

(12) C. Thies, P. Peyser, and R. Ullman, Proceedings of the 4th International Congress on Surface Activity, Brussels, in press.

(13) E. B. Wilson, Jr., "An Introduction to Scientific Research," McGraw-Hill Book Co., New York, N. Y., 1952, p 245.

(14) V. K. La Mer and T. W. Healy, *Rev. Pure Appl. Chem.* (Australia), 13, 112 (1963).

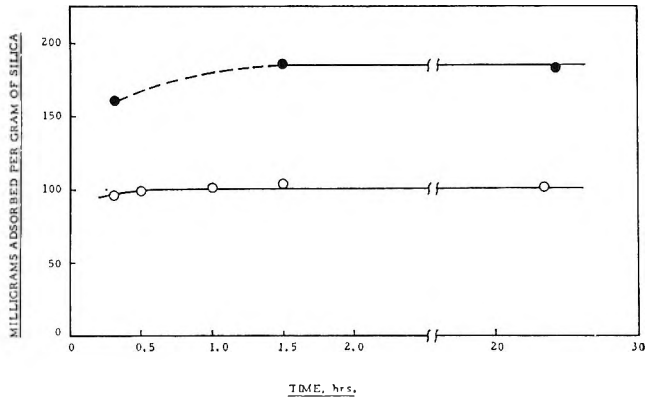

Figure 2. Rate of polymer adsorption on silica from C_2HCl_3 at 25° when suspensions are agitated on a mechanical shaker: ●, PMMA-5; ○, PS-1.

series of experiments in which PS-1 was adsorbed alone. The mixture results indicate that values of p for both polymers scatter in a random manner when samples are agitated 24 to 192 hr. As a rule, similar data were obtained when these polymers were adsorbed alone and agitated up to 400 hr. The only significant time-dependent effect on p observed throughout this study was that for the series of PS-1 samples included in Table II. Major alterations in x/m or c_s did not accompany this change. The explanation may lie in the relatively high value of c_s (0.175–0.211 g/100 ml) here, relative to that of most systems examined. As the equilibrium concentration of unadsorbed polymer increases, it is possible that one may encounter relatively slow adsorption–displacement phenomena involving various molecular species which differ grossly in size. More extensive studies involving systems with high values of c_s are needed.

Table II: Effect of Agitation Time on Infrared Bound Fractions

Agitation time, hr	$(x/m)_{PMMA}$, mg/g	p_{PMMA}	$(x/m)_{PS}$, mg/g	$(c_s)_{PS}$, g/100 ml	p_{PS}
		PS-1–PMMA-5 Mixture[a]			
24.8	38.0	0.29	98.3	0.029	0.19
98.5	38.0	0.29	93.4	0.047	0.17
169.8	38.0	0.34	87.8	0.052	0.14
45.7	36.0	0.34	102.6	0.101	0.15
160.3	36.0	0.30	98.9	0.107	0.15
47.5	36.0	0.25	45.0	0	0.16
162.5	36.0	0.32	45.0	0	0.21
94.0	63.6	0.37	91.2	0.108	0.18
191.8	65.6	0.37	92.5	0.101	0.19
		PS-1			
18.0	...	...	118.6	0.211	0.24
44.7	...	...	125.3	0.176	0.21
166.0	...	...	123.2	0.175	0.13
184.9	...	...	121.1	0.181	0.13

[a] For PMMA-5, c_s = 0 in all cases.

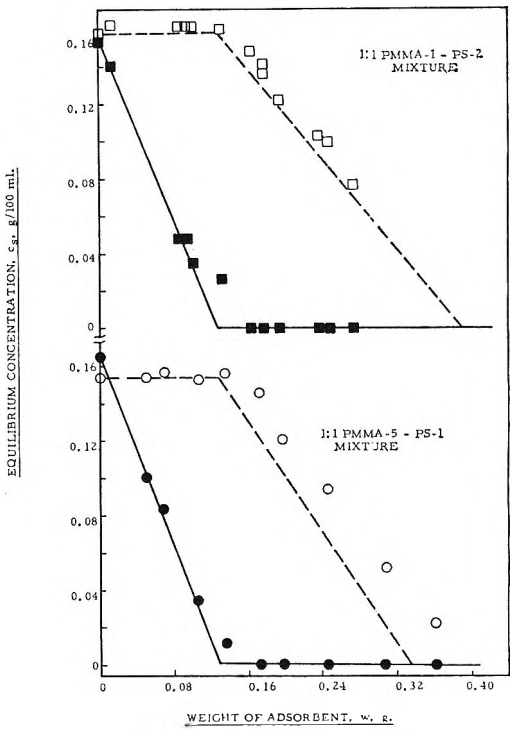

Figure 3. Equilibrium adsorption isotherms for 1:1 (by weight) PMMA–PS mixtures. The solid and dashed curves represent PMMA and PS isotherms calculated assuming complete PMMA adsorption occurs before PS is adsorbed. Experimental points shown represent: ●, PMMA-5; ○, PS-1; ■, PMMA-1; □, PS-2.

Equilibrium adsorption isotherms for 1:1 (by weight) PS–PMMA mixtures are presented in Figures 3 and 4. The solid curves shown represent the calculated relationship between the c_s values for PMMA and weight of adsorbent, while the dashed lines represent the same relationship for PS. These calculations involved two basic assumptions. (1) PMMA is completely adsorbed before any PS adsorbs and PS has no influence on the adsorbance of PMMA. (2) PS adsorbs once PMMA adsorption is complete and the presence of PMMA on the surface has no effect on the adsorbance of PS.

Since the plateau region of each of the isotherms in Figure 1 extends to low values of c_s, the relation between c_s and w for each polymer was calculated using its appropriate adsorbance at surface saturation, $(x/m)^s$.

As shown by the experimental points, PS adsorption does not occur until complete removal of PMMA from solution. The adsorbance of PMMA is unaffected by the presence of PS in the system, except at low values

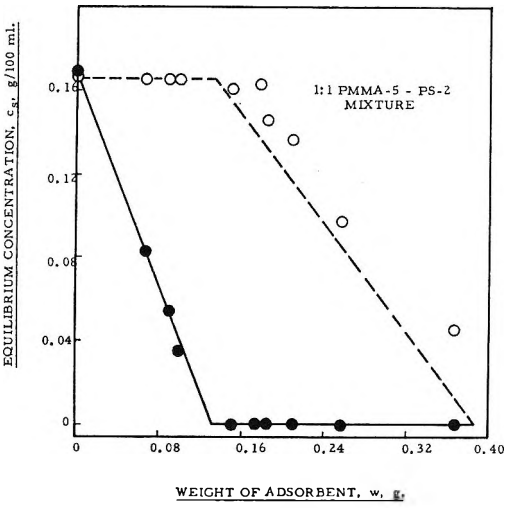

Figure 4. Equilibrium adsorption isotherms for a 1:1 (by weight) PMMA–PS mixture. The solid and dashed curves represent PMMA and PS isotherms calculated assuming that complete PMMA adsorption occurs before PS is adsorbed. Experimental points shown represent: ●, PMMA-5; ○, PS-2.

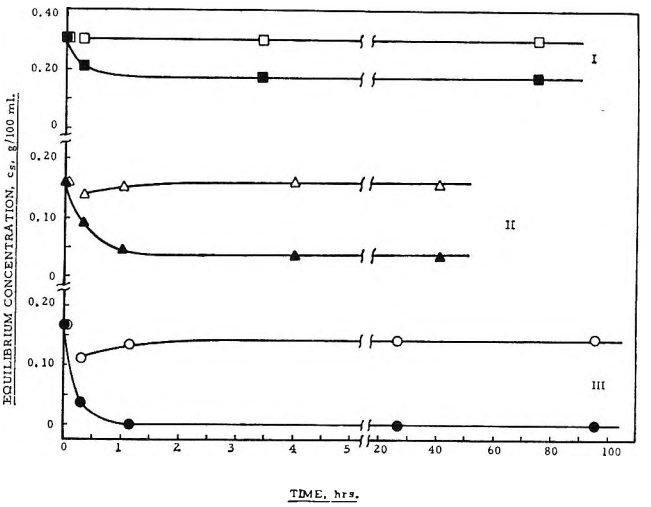

Figure 5. Rate of adsorption of 1:1 (by weight) PS–PMMA mixtures on silica from C_2HCl_3 at 25°. Curves I and II designate cases where PS is not adsorbed at equilibrium; curve III is a case where it is. Experimental points shown represent: □, △, ○, PS-1 c_s values; ■, ▲, ●, PMMA-5 c_s values.

of c_s for PMMA. These deviations are well beyond the small error introduced in the calculated isotherms when $(x/m)^s$ for PMMA was assumed to extend to $c_s = 0$. Once PMMA adsorption is complete, PS adsorption begins immediately. The measured values of c_s for PS are somewhat greater than the calculated ones, but in all cases, the adsorbance of PS is nearly independent of PMMA surface coverage. These results demonstrate that at equilibrium PMMA is preferentially adsorbed on silica from C_2HCl_3 containing PS–PMMA mixtures. This reflects PMMA's stronger interaction with the silica surface arising from its more polar character and greater hydrogen bonding ability. Related to this finding is Fontana's[15] observation that the ester segments in an alkyl methacrylate–polyglycol methacrylate copolymer tend to be excluded from the silica surface while the polyglycol ether segments are preferentially adsorbed.

Rate of adsorption curves for several 1:1 (by weight) PS–PMMA mixtures are plotted in Figure 5. These show that equilibrium adsorbances in such systems are reached quickly. This is true whether PS is (curve III) or is not (curves I and II) adsorbed at equilibrium. Values of c_s for PMMA decrease uniformly with agitation time until their equilibrium levels are reached. In contrast, the first experimental values for PS on curves II and III suggest that c_s for PS may increase with agitation time. Such a trend implies that some PS is adsorbed initially when PS–PMMA mixtures are added to silica and then is completely displaced from the interface by excess PMMA in the system. This would be reasonable, since the rate data of Figure 2 indicate that PS-1 is adsorbed more rapidly than PMMA-5. However, more complete rate curves are needed to confirm this observation. They were not obtained since the procedure utilized to isolate the supernatant polymer solution from the silica required approximately 0.3 hr.

The displacement of PS by PMMA was examined more fully by first adsorbing varying amounts of PS-1 on silica from C_2HCl_3 and then adding excess PMMA to the system. Values of c_s for both polymers were measured as a function of time. The amount of PMMA added was calculated to give an equilibrium PMMA c_s value of 0.128 g/100 ml, if complete PS displacement occurred. Results are given in Figure 6. The dashed lines represent the unadsorbed PS concentrations, c_s, if PS displacement is complete. The $(x/m)^0$ values shown on the graph are the PS-1 adsorbances before addition of PMMA-5. The experimental points represent c_s values measured as a function of displacement time. The solid and open experimental points are c_s values obtained for samples equilibrated on the silica surface 3 min and 22 hr, respectively, before excess PMMA was added. The 3-min samples were shaken by hand, but control experiments established that they essentially reached their equilibrium adsorbances within this time.

The data of Figure 6 establish that PMMA rapidly and completely displaces PS from silica under all conditions examined. The extent and rate of displacement

(15) B. J. Fontana, *J. Phys. Chem.*, **67**, 2360 (1963).

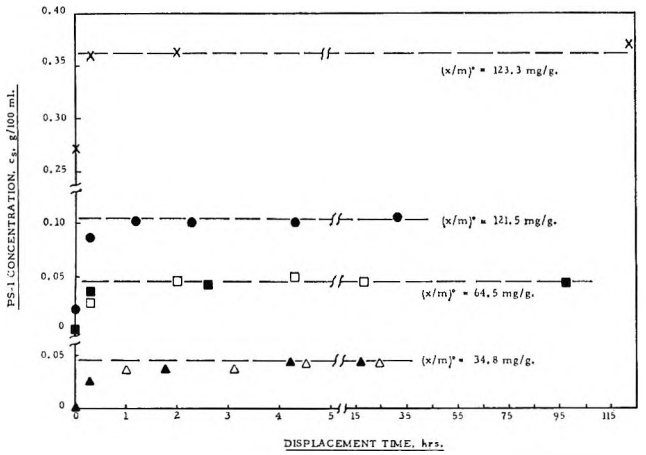

Figure 6. Rate of PS displacement from silica at 25° by excess PMMA. Dashed curves represent unadsorbed PS-1 concentrations, c_3, calculated for complete PS displacement. $(x/m)^0$ values on the graph are PS-1 absorbances before displacement. Experimental points shown represent: ▲, ■, ●, ×, PS-1 equilibrated on the surface 3 min before displacement; △, □, PS-1 equilibrated on the surface 22 hr before displacement.

are essentially independent of PS surface coverage or length of time the PS was equilibrated on the surface before being displaced. Marked changes in the conformation of an adsorbed polymer molecule can occur as a function of these parameters. The fact that no major effects are observed demonstrates that any changes which do occur have little effect upon the displacement process, within limits of the experimental technique used. A trend toward longer displacement times at lower PS surface coverages suggests that PMMA has more difficulty displacing PS under these conditions. This is consistent with the increased values of p for PS-1 at lower surface coverages (see Figure 1), since a greater number of polymer–surface attachments must be ruptured in order to effect displacement. However, the concentration changes involved are so small that more complete displacement rate data are required to confirm this trend.

The complete displacement of PS by PMMA observed throughout this study demonstrates the reversibility of the PS adsorption process and is consistent with previous observations that preferential adsorption of more surface-active molecules can effect polymer displacement.[16,17] Eirich[4] and others[18,19] have stressed that polymer adsorption is reversible under suitable conditions, showing that no irreversible polymer–surface bonds are formed. The comparatively rapid rate of PS displacement shows that PMMA molecules have the ability to rupture quickly and irreversibly all PS–surface bonds. This establishes that multiple surface attachments characteristic of adsorbed polymers do not necessarily limit the extent of polymer displacement or cause it to be extremely slow, especially when molecular species which have a stronger affinity for the adsorbing surface are present.

Significantly, PMMA rapidly displaces PS from silica even though PS and PMMA are incompatible polymers. Dobry and Boyer–Kawenoki established that they are incompatible in benzene,[20] while several qualitative experiments in this study established that they also are incompatible in C_2CHCl_3. Except at low concentrations, these incompatible polymers form two liquid phases with the solute in each phase consisting of a preponderance of one polymer component and a small proportion of the other. Such incompatibility arises because polymers characteristically have small, but positive, heats of mixing accompanied by negligible entropies of mixing.[21] All solutions used for the mixture adsorption experiments had initial PS and PMMA concentrations well below the critical point of phase separation and hence were homogeneous. However, the concentration of PS segments in an adsorbed layer could be much greater than that in the original bulk solution, depending on the thickness of this layer and the distribution of segments in it. The concentration could be so great that most PMMA molecules would be excluded from the adsorbed layer due to incompatibility with the "PS-rich" environment. The fact that PMMA rapidly and completely displaces PS from silica in all cases examined establishes that PMMA readily penetrates the adsorbed PS layer. Polymer–polymer incompatibility effects do not seem to affect the displacement process. Additional evidence that polymer–polymer incompatibility effects are small is provided by the data in Figures 3 and 4, which show that PS's adsorbance is nearly independent of the amount of PMMA adsorbed on the surface. Interactions between PS and PMMA responsible for incompatibility are not sufficiently strong to exclude PS from the surface totally or markedly reduce its adsorbance.

Another measure of the interactions between PS and PMMA is gained by determining values of p for both polymers when simultaneously adsorbed on silica. Such data are presented in Table III, where most of the

(16) J. Koral, R. Ullman, and F. R. Eirich, *J. Phys. Chem.*, **62**, 541 (1958).

(17) S. Ellerstein and R. Ullman, *J. Polymer Sci.*, **55**, 123 (1961).

(18) A. Silberberg, *J. Phys. Chem.*, **66**, 1872 (1962).

(19) R. R. Stromberg, W. H. Grant, and E. Passaglia, *J. Res. Natl. Bur. Std.*, **68A**, 391 (1964).

(20) A. Dobry and F. Boyer-Kawenoki, *J. Polymer Sci.*, **2**, 90 (1947).

(21) P. J. Flory, "Principles of Polymer Chemistry," Cornell University Press, Ithaca, N. Y., 1953, Chapter XIII.

reported values of p represent averages of two to four determinations. The average errors given are mean deviations of p from the reported mean values. Comparisons of the values of p shown here with those reported in Figure 1 for cases where the individual polymers are adsorbed alone establish the following points.

Table III: Infrared Bound Fraction Values, p, for PS-PMMA Mixtures[a]

PMMA-5		PS-1		
Adsorbance, mg/g[b]	p	Adsorbance, mg/g[b]	c_s, g/100 ml	p
36.0	0.29 ± 0.035	36.0	0	0.19 ± 0.025
37.5	0.29 ± 0.023	73.0	0.040	0.18 ± 0.020
37.0	0.32 ± 0.017	81.5	0.11	0.14 ± 0.010
66.8	0.37 ± 0.025	45.6	0	0.16 ± 0.025
65.3	0.38 ± 0.010	52.3	0.040	0.18 ± 0.025
64.6	0.37 ± 0.0050	60.0	0.11	0.19 ± 0.025
67.5	0.40 ± 0.0050	49.9	0.18	0.12 ± 0.0050
104.0	0.37	29.9	0.237	0.13
156.3	0.33	4.0	0.433	...

[a] For PMMA-5, $c_s = 0$ in all cases. [b] Based on total weight of silica in system.

1. Average values of p for PMMA-5 are relatively unaffected by the simultaneous adsorption of PS-1 and PMMA-5. Only at a PMMA-5 adsorbance of approximately 65 mg/g does the presence of PS-1 cause an obvious change from p = 0.30–0.32 to 0.37–0.40. Variations in PS-1 concentration at constant PMMA-5 adsorbance have no significant effect on the value of p for PMMA-5 over the range of PS-1 concentrations examined.

2. Average values of p for PS-1 vary from 0.12 to 0.19 when it is simultaneously adsorbed with PMMA-5. For those mixtures having a PS-1 c_s value >0, this range of p values approaches that observed when PS-1 is adsorbed alone and having $c_s > 0$. Values of p for two mixtures where $c_s = 0$ are somewhat below those observed when equivalent amounts of PS-1 are adsorbed alone.

The relatively small changes in values of p for both polymers when simultaneously adsorbed on silica are undoubtedly due in part to the increased amounts of polymer adsorbed. For a given PS or PMMA adsorbance, the total weight of adsorbed polymer is greater in the mixture system than when either polymer is adsorbed alone. Since p for both polymers varies with surface coverage as seen in Figure 1, one would anticipate slight changes in the measured values of p. In general, it appears that PS cannot compete with PMMA for available surface sites and must occupy only those adsorption sites that the PMMA molecules are unable to fill. However, the PS does not undergo marked structural rearrangements in order to fill these sites. The PS and PMMA molecules occupy similar numbers of sites when adsorbed simultaneously as when adsorbed individually.

In conclusion, it should be noted that this study was carried out under dynamic conditions and involved a very finely divided silica as adsorbent. Hence, the results obtained may be uniquely applicable to such systems. The adsorbent, Cab-O-Sil M-5, is reported to have an average particle size range of 0.015–0.020 μ and is formed by a pyrogenic process.[22] Fully dispersed particles of this size approach the root-mean-square end-to-end dimensions of random polymer coils in solution. Assuming the silica actually was well dispersed to give this particle size range, the possibility exists that one or perhaps a few adsorbed polymer molecules effectively saturate the surface of each small adsorbent particle. Bridging of several particles might occur as La Mer and Healy have discussed,[14] but still comparatively few molecules would be required to saturate the available surface area on a given particle or aggregate of particles. Alternatively, the PS and PMMA could be fractionated in such a manner that certain adsorbent particles adsorb only PS molecules and others only PMMA molecules. In both cases, a pronounced effect on the adsorbance and/or adsorbed structure of either polymer arising from polymer–polymer incompatibility might not be observed, since each polymer molecule is being adsorbed in an environment virtually unchanged from that encountered in systems where it is the only polymeric adsorbate present. Unfortunately, it is not known whether Cab-O-Sil ever is completely dispersed into independent particles of 0.015–0.020-μ diameter, since electron photomicrographs consistently yield aggregates of 50–100 individual particles[22] which conceivably could be chemically fused together. In any case, additional studies involving adsorbents which are known to be essentially infinite planar surfaces should give more insight into this question. Both the small adsorbent particle size and dynamic nature of these experiments must be recognized when attempts are made to compare the results of this

(22) Technical Bulletin Describing Cab-O-Sil M-5, Cabot Corporation, Boston, Mass.

(23) See ref 2 for a recent review of these theories. More recent contributions include: C. A. J. Hoeve, E. A. DiMarzio, and P. Peyser, *J. Chem. Phys.*, **42**, 2558 (1965); R. J. Roe, *ibid.*, **43**, 1591 (1965); E. A. DiMarzio and F. L. McCrackin, *ibid.*, **43**, 539 (1965); C. A. J. Hoeve, *ibid.*, **44**, 1505 (1966).

study with theoretical treatments based on infinite adsorbing planar surfaces and static systems.[23]

Acknowledgment. The author gratefully acknowledges Mr. J. A. Herbig's encouragement of this work as well as many stimulating discussions with Dr. Hans F. Huber.

Partial Molal Volume Changes during Micellization and Solution of Nonionic Surfactants and Perfluorocarboxylates Using a Magnetic Density Balance

by L. Benjamin

Miami Valley Laboratories, the Procter & Gamble Co., Cincinnati, Ohio *(Received March 24, 1966)*

A simple magnetic density balance is described for obtaining partial molal volume data at 25° for various nonionic surfactants and perfluorocarboxylates. The data show that the standard volume change of micellization per mole, ΔV°_m, is always positive and becomes increasingly so the longer the alkyl chain length of the dimethylalkylamine oxides (DC_nAO). For these compounds ΔV°_m approaches zero at $\sim C_6$ chain length below which micelles do not form. It is inferred that a part of the alkyl chain near the head group retains its hydration in the micellar state. Solution of the fluorinated molecules studied is attended by more contraction than with their hydrogen counterparts and this leads to larger positive ΔV°_m values.

Aqueous solutions of compounds partially or totally hydrophobic in character often exhibit unusual thermodynamic properties associated with ordering of water molecules around the solute. Thus the unfavorable positive free energy of solution of, for example, hydrocarbons has favorable enthalpy contributions (hydrogen bond formation) but overriding negative entropy contributions from the resulting water structure. Although such unusual properties had been recognized for some time previously,[1] the classification of various solutes as structure makers and structure breakers in aqueous solution was first generalized by Frank and Evans.[2] More recently, considerable interest has developed in entropic contributions arising from the breakdown of such water structure during hydrophobic bonding—the nonspecific interaction accompanying the transfer of hydrophobic groups from an aqueous to a less aqueous environment.[3-12] Volume changes associated with this process, all positive in nature, have been discussed.[3,13-18]

(1) J. A. V. Butler, *Trans. Faraday Soc.*, **33**, 229 (1937).

(2) H. S. Frank and M. W. Evans, *J. Chem. Phys.*, **13**, 507 (1945).

(3) W. Kauzmann, *Advan. Protein Chem.*, **14**, 1 (1959).

(4) I. M. Klotz and S. W. Luborsky, *J. Am. Chem. Soc.*, **81**, 5119 (1959).

(5) H. A. Scheraga, G. Némethy, and I. Z. Steinberg, *J. Biol. Chem.*, **237**, 2506 (1962).

(6) G. Némethy and H. A. Scheraga, *J. Phys. Chem.*, **66**, 1773 (1962).

(7) E. D. Goddard, C. A. J. Hoeve, and G. C. Benson, *ibid.*, **61**, 593 (1957).

(8) H. Schneider, G. C. Kresheck, and H. A. Scheraga, *ibid.*, **69**, 1310 (1965).

(9) W. P. Jencks, *Federation Proc.*, **24**, Suppl. 15, S-50 (1965).

(10) C. Tanford, *J. Am. Chem. Soc.*, **84**, 4240 (1962).

(11) L. Benjamin, *J. Phys. Chem.*, **68**, 3575 (1964).

(12) G. C. Kresheck and L. Benjamin, *ibid.*, **68**, 2476 (1964).

The present study is of the partial molal volumes of surfactants and other compounds in aqueous solution and how these values change during micellization where hydrophobic bonding is involved,[11] particularly as a function of surfactant alkyl chain length. Data were obtained with a simple magnetic density balance.

Experimental Procedure

Magnetic Density Balance. Volume changes occurring on micellization are small and require the detection of density changes of the order of 1 in 10^5. This was achieved using the apparatus shown in Figure 1 drawn roughly to scale. As in other magnetic density balances,[19-23] a glass float (volume ~6 ml) containing a soft iron core is just buoyant in the solution studied at the given temperature and floats against a stop. Thus the float is immersed at all times, eliminating effects due to the air–solution interface. In the conventional procedure the float is attracted by the field of a small solenoid, S_1, and the current, i_0, which just fails to cause the float to move away from the stop, is determined by extrapolation of the measured float velocity as a function of current i. It can then be shown that $i_0^2 \propto \rho$[23] where ρ is the solution density. In the present instrument another solenoid has been added, S_2, in which a constant current (i_c = 0.1 amp) is passed in the reverse direction to the current i flowing in S_1. This has the effect of producing a stationary position of the float at a distance x_0 above S_1. Mechanical movement of the float allows it to oscillate about x_0, but at a sufficient height x_e above S_1 the float escapes from the magnetic field. Thus at x_0 and x_e for a given solution of density ρ and a fixed value of i, the force (F) on the float is zero. The magnetic field H_x at a point distant x along the axis of a "point" solenoid, or single wire carrying current i, is $(2\pi d^2 i)/[(x^2 + d^2)^{3/2}]$, where d is the solenoid radius.[24] In the present apparatus if l is the separation of S_1 and S_2, $F = k_0 H_x(dH_x/dx) + k_2\rho$, or

$$F/k_1 = i^2\left(\frac{x}{(x^2 + d^2)^4}\right) - i\left(\frac{i_c[(x + l)(x^2 + d^2) + x((x + l)^2 + d^2)]}{[(x^2 + d^2)((x + l)^2 + d^2)]^{5/2}}\right) + \frac{i_c^2(x + l)}{((x + l)^2 + d^2)^4} + K\rho \quad (1)$$

that is

$$F/k_1 = i^2 f_1(x) + i i_c f_2(x) + [i_c^2 f_3(x) + K\rho] \quad (2)$$

In general for a given x value there are thus two i values at which F is zero, corresponding to either the float equilibrium or escape. At a particular i value

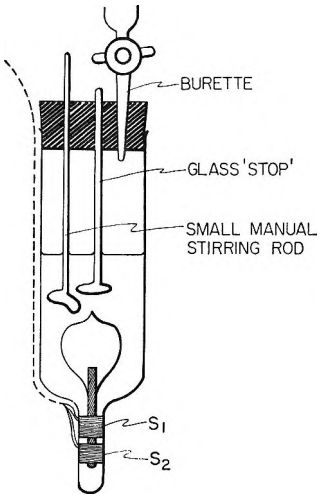

Figure 1. Magnetic density balance.

(i_0), however, the quadratic equations, eq 1 and 2, have a singular solution for $F = 0$, and the positions of equilibrium and escape are coincidental at x_{0e}. In this case

$$i_0 = -i_c f_2(x_{0e})/2f_1(x_{0e}) \quad (3)$$

and

$$K\rho = i_0^2\left[f_1(x_{0e}) - \frac{4(f_1(x_{0e}))^2 f_3(x_{0e})}{[f_2(x_{0e})]^2}\right] \quad (4)$$

Thus ρ is seen to be proportional to i_0 when the float is at position x_{0e}.

It is worth pointing out that the dimensions and construction of the balance are not critical. A number of balances have been made in which the float size, number of turns in the coils S_1 and S_2, etc., have been varied, giving different sensitivity, range of density, and ease of operation. For a sensitivity of about 1 part in 10^5 required in these studies, the coils contain

(13) G. Némethy and H. A. Scheraga, *J. Chem Phys.*, **36**, 3401 (1962).
(14) K. Shinoda and T. Soda, *J. Phys. Chem.*, **67**, 2072 (1963).
(15) W. L. Masterton, *J. Chem. Phys.*, **22**, 1830 (1954).
(16) F. Franks and H. T. Smith, *J. Phys. Chem.*, **68**, 3581 (1964).
(17) H. Lal, *J. Colloid Sci.*, **8**, 414 (1953).
(18) D. N. Glew, *J. Phys. Chem.*, **66**, 605 (1962).
(19) A. B. Lamb and R. E. Lee, *J. Am. Chem. Soc.*, **35**, 1666 (1913).
(20) D. A. MacInnes, M. O. Dayhoff, and B. R. Ray, *Rev. Sci. Instr.*, **22**, 642 (1951).
(21) W. Geffcken, C. Beckmann, and A. Kruis, *Z. Physik. Chem.*, **B20**, 398 (1933).
(22) J. W. Beams and A. M. Clarke, *Rev. Sci. Instr.*, **33**, 750 (1962).
(23) A. R. Richards, *Ind. Eng. Chem., Anal. Ed.*, **14**, 595 (1942).
(24) S. G. Starling, "Electricity and Magnetism," 7th ed, Longmans Publishing Co., 1941, p 228.

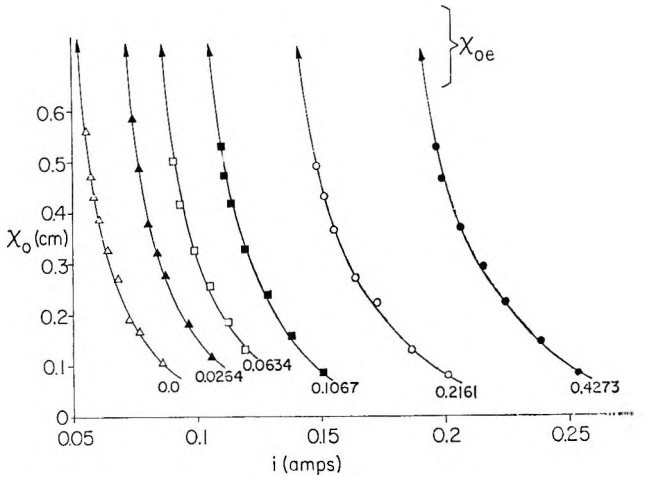

Figure 2. Float position *vs.* current for NaCl solutions of concentrations (% w/w) shown.

approximately 30 turns wound on a 1-cm diameter. The float can contain a little mercury to aid in correcting for buoyancy while the final adjustment is conveniently made by grinding away some of the glass stem. A cathetometer measures the float position to within 0.05 mm and a potentiometer is used to determine i. Either a constant current device or a reliable storage battery can be used to maintain i_c.

Experimental Method. The use of eq 4 is illustrated by the curves shown in Figure 2 where x_0 *vs.* i curves for various solutions are almost parallel, especially at high x_0 values where x_{0e} is approached. Because of the steepness of the curves in this region, values of i corresponding to x_0 values somewhat lower than x_{0e} still satisfy eq 4 and show ρ to be proportional to i^2 as in other magnetic density balances. Examples of this are shown in Figure 3 for NaCl solutions using three x positions for estimating i values (an arbitrary zero for the x scale has been chosen). The balance sensitivity is seen to vary slightly with the x value chosen and the latter should be as close to x_{0e} as possible for eq 4 to be most applicable. The applicability of eq 4 in this way is also seen in Figure 4, where the buoyancy of the float in water is varied by adding platinum wire to the float. Calibration of the float at a given temperature is achieved by measuring the slope in Figure 4. This calibration gives density variations for NaCl solutions in agreement with literature values. The addition of platinum also adjusts the buoyancy of the float for using it in the required density range. The reproducible departure from linearity of the curve in Figure 4 indicates that i values less than 50–60 ma should not be used. Data for protein solutions obtained with a similar balance agree well with those determined pycnometrically.[25]

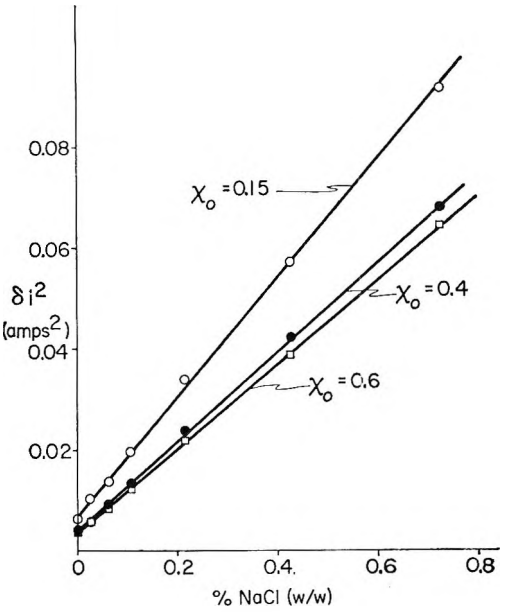

Figure 3. Changes in (current)^2 *vs.* NaCl concentration for various float positions as shown.

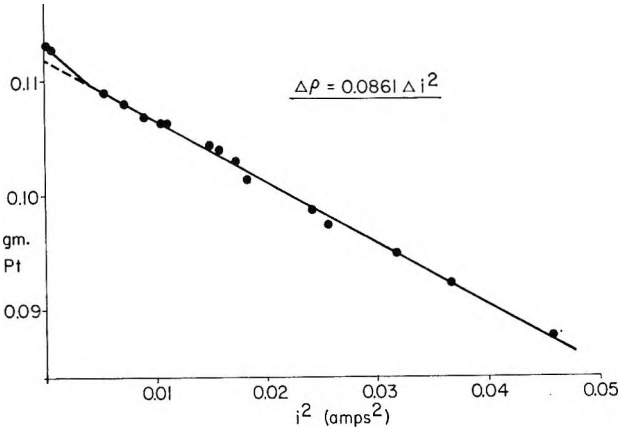

Figure 4. Float calibration showing change in (current)^2 *vs.* weight Pt added to float for a fixed x_0 position.

A typical run involves measuring a series of curves as in Figure 2 for water and solutions prepared in the cell by adding a strong solution from a buret and manually stirring (Figure 1). Because of the parallel nature of the curves only three or four points about the chosen x_0 need be obtained and the method is thus rapid. The cell is thermostated at 30.00 ± 0.02°. Results typical of surfactant solutions are shown in Figure 5. The partial molal volume, $\bar{V}_2$, is derived from such data using eq 5.

(25) W. L. Gagen, *Biochemistry*, 5, 2553 (1966).

$$\bar{V}_2 = \frac{M_2}{\rho}\left(1 - \frac{(100 - c)}{\rho}\frac{d\rho}{dc}\right) \quad (5)$$

where c is the weight per cent concentration and M_2 the solute molecular weight. An abrupt change in $\bar{V}_2$ occurs on micellization as can be seen from the change in slope for dimethyldecylamine oxide ($DC_{10}AO$) at the critical micelle concentration (cmc). The cmc for dimethylhexadecylammoniopropane sulfonate (DC_{16}-APS) is too low to be discernible by such measurements. An abrupt, small, apparent density change is often measured at extremely low concentrations, as in Figure 5, and then ρ changes smoothly at a normal rate. This is probably due to adsorption of the surfactant on the glass float requiring a modification of Archimedes' principle, *i.e.*, the displacing body is now the float plus that amount of the adsorbed layer unable to exert buoyancy due to kinetic motion.

Crystal Densities. Certain of the dry solutes were powdered in an agate ball mill (in a drybox in the case of the amine oxides) and pressed at 2000 psi into 1.3-cm diameter disks approximately 1 mm thick. This was achieved using a process in which the powder is subjected to a vacuum as normally employed for preparing KBr powder disks for infrared spectroscopy. Disks were then weighed and measured to obtain densities of the solid solute. Values obtained in this way may be a little lower than the true densities because of remaining voids in the pellets. For instance, a value was obtained of 2.663 g/ml for KBr compared to the reported value of 2.75.[26] Molal volumes in the crystalline state, V_M, are readily derived from such data.

Materials. Deionized water was used and the amine oxides (DC_nAO) were prepared in the manner previously described.[27] The preparation of the dimethylalkylphosphine oxides (DC_nPO) has also been described[28] and their purity was assessed as >99% using gas chromatography techniques. Various preparations of dimethylalkylammoniopropane sulfonates (DC_nAPS) were used as indicated elsewhere and purities of the samples were estimated as being 99% or better.[29] The perfluorocarboxylates were prepared by neutralizing the acids (perfluorobutyric and perfluorocaproic from the Minnesota Mining and Manufacturing Co., and trifluoroacetic and perfluorooctanoic acid from Matheson Coleman and Bell) with sodium or potassium hydroxide. The perfluorooctanoic acid was recrystallized from benzene and the trifluoroacetic acid was distilled prior to neutralization. The sodium perfluorobutyrate was recrystallized from dioxane solution and gently heated to remove the solvent, although nmr spectral data indicated that about 0.2% (w/w) dioxane remained in the sample. Fluorine magnetic resonance spectra showed that the trifluoroacetate and *n*-perfluorobutyrate contained no detectable amount of fluorine-containing unidentified impurity, while ~5% of a fluorinated impurity (probably branched chain) was present in the *n*-perfluorocaproate and somewhat greater than 10% of such impurity was present in the *n*-perfluorooctanoate. The sample of sodium *n*-butyrate used was obtained from best grade Matheson Coleman and Bell reagent which was recrystallized from slightly aqueous ethanol. No hydrogen-containing impurities were detectable from the proton nmr spectrum. All samples were vacuum dried over P_2O_5 prior to use.

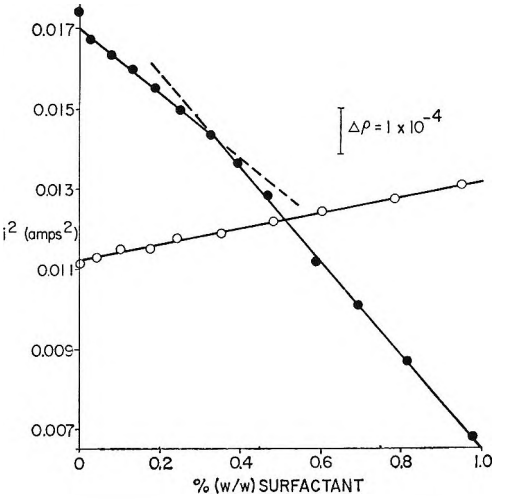

Figure 5. Density (proportional to i^2) changes of solutions as a function of concentration: ●, dimethyldecylamine oxide; ○, dimethylhexadecylammoniopropane sulfonate.

Results and Discussion

Data of the type shown in Figure 5 give the partial molal volumes shown in Table I for monomer (at infinite dilution) and micellar species (just above the cmc). Also included are the molal volumes, V_M, and cmc values as determined where possible from density–concentration plots similar to those in Figure 5. These cmc values are in agreement with data obtained by other methods (light scattering,[27,29] calorimetry,[11,30] vapor pressure lowering, and surface tension) for these surfactants. In some cases monomer or micelle data

(26) "Handbook of Chemistry and Physics," 43rd ed, Chemical Rubber Publishing Co., Cleveland, Ohio, 1961.
(27) K. W. Herrmann, *J. Phys. Chem.*, **66**, 295 (1962).
(28) R. G. Laughlin, *J. Org. Chem.*, **30**, 1322 (1965).
(29) K. W. Herrmann, *J. Colloid Sci.*, in press.
(30) L. Benjamin, unpublished data.

Table I: Partial Molal Volumes of Crystal, Monomer, and Micelle Species of Surfactants (ml/mole)

Surfactant	V_M (25°)	$\bar{V}^\circ_2$ monomer (30°)	$\bar{V}_2$ micelle (30°)	Cmc, % w/w
DC_nAO, n = 1	68.3	72.2 ± 0.5		...
7	170.5	171.2 ± 1		...
8	181.4	183.9 ± 1	179.4 ± 3	2.4
9		204.0 ± 1	205.2 ± 2	1.1
10	205.9	216.5 ± 1	222.8 ± 1	0.33
11	222.4	231.7 ± 2	241.1 ± 1	0.13
12	233.2	242 ± 5	255.0 ± 1	0.045
DC_nPO, n = 8	194.7	202.7 ± 0.5	207.1 ± 2	0.8
10	224.6	238.1 ± 1	240.9 ± 0.5	0.07
12	253.1	...	273.0 ± 2	
DC_nAPS, n = 8	243.5	246.0 ± 1		
10	273.3	279.0 ± 1	282.9 ± 1	1.1
12	305.9	316.3 ± 1	321.0 ± 1	0.12
16	371.3		386.0 ± 0.5	
CF_3COONa		32.5 ± 2		
C_3F_7COONa	115.5	72.2 ± 5		
$C_5F_{11}COOK$	171.7	126.3 ± 8		
$C_7F_{15}COOK$		140.0 ± 10		
C_3H_7COONa	82.3	59.9 ± 4		

were not obtained because the cmc values were too low or too high, respectively. The estimated errors in $\bar{V}^\circ_2$ are largely dependent on the particular range of monomer concentration, *i.e.*, the cmc value.

Using conventional standard states for the micellization process,[11] the standard molal volume change of micellization, ΔV°_m, is given by

$$\Delta V^\circ_m = \bar{V}_2 \text{ (just above cmc)} - \bar{V}^\circ_2 \text{ (at infinite dilution)} \quad (6)$$

and the data in Table I show that this is always positive. Furthermore, all literature data for surfactant solutions support this conclusion as can be seen from Table II. These values are either as reported or have been calculated from published data where indicated. It has been shown for sodium dodecyl sulfate that the positive ΔV°_m value agrees with that calculated from the increase in cmc with increasing pressure.[31]

A thermodynamic process analogous to micellization is the reverse of solution of a liquid phase,[11] *i.e.*, where aggregation numbers approach infinity. Thus V_M (liq) − $\bar{V}^\circ_2$ values (standard molal volume change of solution, ΔV°_S) for alcohols, ethylene glycol, and glycerol are also positive when H_2O is the solvent.[32] These ΔV°_S values increase with the degree of branching as can be seen from Table III. The data show that branching of the chain increases V_M values and also increases $\bar{V}^\circ_2$ in the case of propanol. Lowering of $\bar{V}^\circ_2$ values results from branching with butanol. The agreement between the two sets of data for 1-butanol is excellent and indicates that ΔV^c_S does not vary from 20 to 30°. It may also be noted from Table III that, whereas ΔV°_S increases by 1.4 ml/mole from methanol to ethanol and from ethanol to 1-propanol, no further increase is observed from 1-propanol to 1-butanol. It has previously been shown[11] that the standard entropy and enthalpy of solution also tend to show leveling off tendencies with increasing chain length near 1-butanol and such an effect has been held to be consistent with curling of hydrocarbon chains in solution for chain lengths greater than C_4–C_5.

Returning to the data in Table I, the ΔV°_m values for the amine oxides are found to increase for longer chain lengths and approach a zero value near the C_6–C_7 members. This is evident from Figure 6, where V_M data are also seen to approach $\bar{V}^\circ_2$ values near these chain lengths. Transfer of nonpolar molecules such as hydrocarbons from aqueous to nonaqueous environments has been known to occur with an increase in volume due, presumably, to the contraction associated with the water structure surrounding the nonpolar group, the so-called "iceberg" region.[2] Such volume increases associated with hydrophobic bonding are consistent with the data in Figure 6 since ΔV°_m is zero at just the chain length below which micelles do not form, even though some trimers, tetramers, etc., may be present at shorter chain lengths.

(31) E. Hutchinson, V. E. Sheaffer, and F. Tokiwa, *J. Phys. Chem.*, **68**, 2818 (1964).

(32) K. Nakanishi, *Bull. Chem. Soc. Japan*, **33**, 793 (1960).

Table II: Partial Molal Volumes of Monomeric and Micellar Surfactant Species at 25° Except Where Specified in Superscripts

Surfactant	$\bar{V}^\circ_2$ monomer, ml/mole	$\bar{V}_2$ micelle, ml/mole	Ref
Glucosyltoluene	213[d]		
Glucosylethylbenzene	198[d]		31
Glucosylpropylbenzene	226[d]	232[d]	
Glucosylbutylbenzene	240.5[d]	249.5[d]	
Sodium dodecyl sulfate	236.6[23]	248.7[23]	*f*
Sodium decyl sulfate		219.5	*e*
Sodium tetradecyl sulfate	265.7[26]	281.6[26]	14
Dodecylammonium chloride		241[30]	*f*
Dodecyltrimethylammonium chloride		293[23]	*f*
Tetradecyltrimethylammonium chloride		320[23]	*f*
Dodecyl sulfonic acid	228	239	14
Sodium dodecyl sulfonate	228.7[31.5]	238.7[31.5]	14
Sodium tetradecyl sulfonate	265.8[39.5]	277.3[39.5]	14
Potassium laurate	202.4	217.7	17
	192.9[0.2]	211.2[0.2]	17
Butyric acid	81.1[0]	~87.0[0]	Estd from
	85.6[35]	~90.4[35]	*g*
Igepal CO-710[a]		621.5	
Surfonic N-95[b]		582.4	*i*
Triton X-100[c]		581.7	
Sodium butylbenzene sulfonate	168	179	14, *h*
Sodium octylbenzene sulfonate	223	239	

[a] Polyoxyethylated nonylphenol, av no. of EO groups = 10.3. [b] Polyoxyethylated nonylphenol, av no. of EO groups = 9.5. [c] Polyoxyethylated octylphenol, av no. of EO groups = 9.7. [d] $\bar{V}_2$ values are concentration dependent. Also the $\bar{V}^\circ_2$ values for glucosyltoluene and glucosylethylbenzene may have been switched in the source publication. [e] E. Hutchinson and C. S. Mosher, *J. Colloid Sci.*, **11**, 352 (1956). [f] P. Mukerjee, *J. Phys. Chem.*, **66**, 1733 (1962). [g] J. Grindley and C. R. Bury, *J. Chem. Soc.*, 679 (1929). [h] R. G. Paquette, E. C. Lingafelter, and H. V. Tartar, *J. Am. Chem. Soc.*, **65**, 686 (1943). [i] C. W. Dwiggins, Jr., R. J. Bolen, and H. N. Dunning, *J. Phys. Chem.*, **64**, 1175 (1960).

Table III: Partial Molal Volumes of Alcohols (ml/mole)

Alcohol	V_M	$\bar{V}^\circ_2$	ΔV°_B	T, °C
Methanol	40.25[d]	37.75	2.5[a]	15
Ethanol	58.05[d]	54.15	3.9[a]	15
1-Propanol	74.37[d]	69.07	5.3[a]	15
2-Propanol	76.14[d]	70.04	6.1[a]	15
1-Butanol	91.53[d]	86.2[b]	5.33	20
	92.35[d]	87.02[c]	5.33	30
2-Butanol	91.73[e]	84.93	6.8[a]	20
2-Methyl-2-propanol	93.98[e]	85.98	8.0[a]	20
Ethylene glycol	55.64[e]	54.44	1.2[a]	20
Glycerol	73.09[e]	70.29	2.8[a]	20

[a] Ref 32. [b] Estimated from data in ref 32. [c] W. H. Pasfield, *J. Phys. Chem.*, **69**, 2406 (1965). [d] From data in "International Critical Tables," McGraw-Hill Book Co., New York, N. Y., 1928. [e] From data in ref 26.

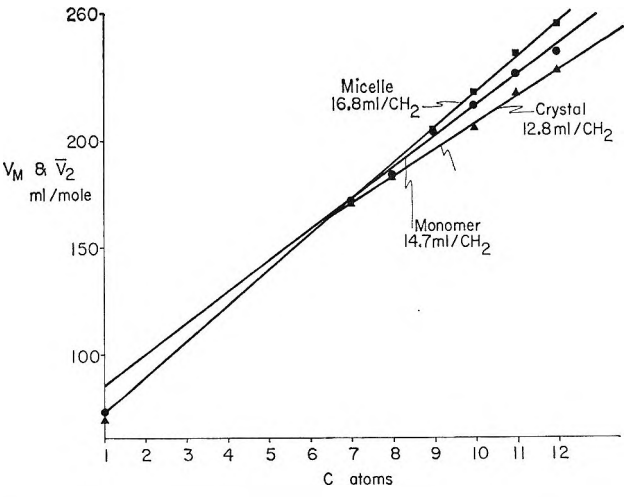

Figure 6. ▲, crystal molar volumes (25°) and partial molal volumes of ■, micelle and ●, monomer species (30°) of dimethylalkylamine oxides as a function of alkyl chain length.

The data in Table IV illustrate the disappearance of micelles at short chain lengths. That ΔV°_m is zero near C_6 chain length and increases for longer chains suggests that some portion, approximately four to six carbon atoms in length, of the chain next to the head group remains almost unchanged in the micellization

process and contributes little to the volume change associated with the release of "iceberg" water. Nmr data for sodium alkylsulfate solutions support this conclusion.[33] Such a process is not unreasonable for strongly polar surfactants such as the amine oxides (dipole moment ~4.8 D.) which would tend to resist packing and retain maximum hydration. Heat capacity data also support this conclusion.[30] For a given chain length above C_{10} the cmc of a surfactant is generally higher the more polar the head group (*cf.*, *e.g.*, Table I for C_{10} species) and the chain length below which micelles do not form decreases the less polar the head group becomes. Thus ionic, zwitterionic, and very polar nonionic surfactants require long chain lengths (C_6–C_8) for micelle formation, while weakly polar nonionic surfactants (*e.g.*, the phosphine oxides), carboxylic acids, amines, alcohols, etc., form micelles or separate as liquid phases even with short chain length species ($>C_4$). Aggregation numbers of five to ten would seem to be a reasonable requisite for micellization in such a discussion since the cooperative, and therefore critical, nature of the aggregation process decreases markedly in this region.[11] An increase in ΔV°_m with chain length is also observed (see Table II) for the glucosylalkylbenzenes, the sodium alkylsulfates, and the sodium alkylbenzene sulfonates.

Table IV: Critical Micelle Concentrations and Aggregation Numbers for Amine Oxides Near 25°

Chain length	Cmc, % w/w	n[27]
C_6	estd ~30	
C_7	~10	
C_8	2.4	15
C_9	1.1	
C_{10}	0.33	32
C_{11}	0.13	
C_{12}	0.045	76

Interpretations of ΔV°_m data as outlined above, only in terms of the positive volume change associated with hydrophobic bonding, may be oversimplified for a number of reasons. First, one must consider volume changes which might occur due to decreased hydration of the head group and possible electrostriction effects. If the above interpretation is correct and the head group and adjacent alkyl chain remain essentially unchanged during micellization, such hydration changes should not be an important factor. Secondly, the interior of micelles is under pressure due to the electrostatic forces at the surface.[34] Although this excess pressure is difficult to estimate in absolute terms for the amine oxides (treating the dipole as two separated charges), calculations based on estimated micelle diameters and aggregation numbers (n) show that this pressure is approximately the same for the C_8 and C_{12} species. Thus volume changes due to compression should be roughly equivalent and not affect differences in ΔV°_m with chain length. Thirdly, the question arises of how efficiently molecules constrained to a spherical micelle configuration can pack together. The increment in $\bar{V}_2$ per CH_2 group in the micellar state is 16–17 ml/mole (*cf.* Table I), which is in agreement with values for liquid hydrocarbons.[26,35,36] A liquidlike hydrocarbon interior for the micelles is therefore strongly indicated. This is supported by heat capacity measurements[30] and by the observations that $\bar{V}_2$ values for molecules solubilized in micelles are close to their liquid V_M values.[37] Thus any inefficient packing leading to voids, say, between head groups, even if it exists, does not appear to change as chain length and micelle size increase.

Figure 7 shows a similar increment in $\bar{V}_2$ per CH_2 group for the carboxylates, differences between the sodium and potassium salts being equal to the predicted values at infinite dilution, namely 10.2 ml/mole.[38] The increase in $\bar{V}_2$ for the micellized carboxylates between 20 and 90° can be seen from the data in Figure 7 to be ~5%, which compares with similar increases in micellar $\bar{V}_2$ values of 3% for sodium dodecyl sulfonate between 40 and 70° (see footnote *f* of Table II), 4% for butyric acid between 0 and 35° (Table II), 3% for sodium tetradecyl sulfate between 25 and 45°,[14] and 3% for potassium laurate between 0 and 25° (Table II). These increases in molar volume are similar to those of comparable liquid hydrocarbons[35,36] and again support the idea of a liquid hydrocarbon interior for the micelle. It is also worth noting, from the data in Table II, that an ethylene oxide group in the micellar surface has a partial molal volume of 48.9 ml/mole—a reasonable value, close to that of three CH_2 groups.

It is difficult to interpret differences in $\bar{V}_2$ (solution) and the crystal V_M values because the latter depend on the lattice structure and can show alternation with chain length, some of which is even carried over into

(33) J. Clifford, *Trans. Faraday Soc.*, **61**, 1276 (1965).

(34) A. E. Alexander and P. Johnson, "Colloid Science," Vol. I, Clarendon Press, Oxford, 1949, p 87.

(35) F. Krafft, *Ber.*, **15**, 1687 (1882).

(36) A. K. Doolittle, *J. Chem. Eng. Data*, **9**, 275 (1964).

(37) W. D. Harkins, R. W. Mattoon, and M. L. Corrin, *J. Colloid Sci.*, **1**, 105 (1946).

(38) H. S. Harned and B. B. Owen, "Physical Chemistry of Electrolytic Solutions," 3rd ed, Reinhold Publishing Corp., New York, N. Y., 1958, p 361.

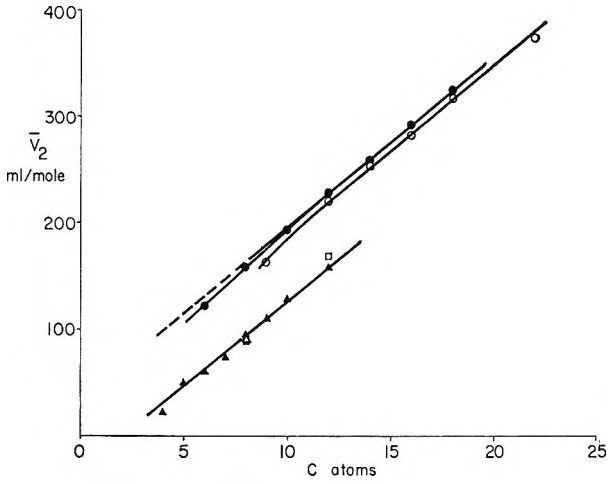

Figure 7. Micellar partial molal volumes of *n*-alkanoates. ▲, sodium salts at 20°, estimated from data in K. Hess, W. Philippoff, and H. Kiessig, *Kolloid-Z.*, **88**, 40 (1939); ○, sodium salts at 90°, estimated from data in "International Critical Tables," McGraw-Hill Book Co., New York, N. Y., 1928; ●, potassium salts at 90°, estimated from data in above ref; □, potassium laurate at 25°;[17] △, potassium octanoate at 25°, D. G. Davies and C. R. Bury, *J. Chem. Soc.*, 2263 (1930); ■, sodium octanoate at 18° (using data in footnote *d* of Table III). The low temperature data have been displaced downward by 50 ml/mole.

the liquid state V_M values at the melting point.[39] In the present study, V_M crystal values vary approximately linearly with chain length when this is greater than C_7. Such linear variation does not extrapolate for DC_nAO data to the value for trimethylamine oxide (C_1), however (*cf.* Figure 6), and this may be due to changes in crystal structure between C_1 and C_7 members. Likewise, $\bar{V}^\circ_2$ values do not increase with chain length as rapidly at longer ($>C_7$) chain lengths as in the shorter (C_1–C_7) chain length region and this may result from curling of the longer hydrocarbon chains, as deduced previously from entropy data.[11] The higher values of $\bar{V}^\circ_2$ and $\bar{V}_2$ (micelle) compared to V_M (crystal) are consistent with a partial melting process since the increase in volume for homologous series of paraffins, alcohols, and carboxylic acids during fusion is of the order of 10–20%.[39]

Fluorinated Molecules. Thermodynamic data for fluorocarbon surfactants are scarce. Values of $\bar{V}_2$ for monomer and micellar perfluorooctanoic acid were found by Shinoda and Soda to be 206 and 227.5 ml/mole at 30°, respectively.[14] The value of $\bar{V}^\circ_2$ in Table I for the potassium salt of this acid is much lower than expected from the above value and from extrapolation of the data for shorter chain lengths (Table I). This may result from the presence of branched-chain isomers in the sample used, as inferred from the nmr spectrum (see earlier).

A larger decrease in volume is associated with the solution of fluorinated molecules than with their hydrogen counterparts as can be seen from the butyrate data (Table I). This in turn is reflected in higher ΔV°_m values for fluorocarbon surfactants.[14] Higher compressibilities of fluorinated chains may explain these effects since heat capacity studies[30] do not show fluorinated molecules to order more water in the "iceberg" sense than their hydrogen analogs. The increment in $\bar{V}^\circ_2$ (monomer) is approximately 21 ml/mole of CF_2 from C_1 to C_5 (allowing for $\bar{V}^\circ_2(K^+ - Na^+)$ = 10.2 ml/mole[38]).

Acknowledgments. The author wishes to thank Mrs. Ruth Callahan for synthesizing many of the surfactants used and Mr. N. E. Gilman for his invaluable experimental assistance.

(39) H. Sackmann and F. Sauerwald, *Z. Physik. Chem.* (Leipzig), **195**, 295 (1950).

The Acid Ionization Constant of HOCl from 5 to 35°

by J. Carrell Morris

Division of Engineering and Applied Physics, Harvard University, Cambridge, Massachusetts
(Received April 11, 1966)

Acid dissociation constants for hypochlorous acid, HOCl, relative to the second ionization constant for H_3PO_4 have been determined by a spectrophotometric technique with a precision of 0.005 unit in pK_a at temperatures from 4 to 34°. Values of pK_a have been evaluated from the data. The results, considered accurate to 0.01 unit, are: 7.825 (0°), 7.754 (5°), 7.690 (10°), 7.633 (15°), 7.582 (20°), 7.537 (25°), 7.497 (30°), and 7.463 (35°).

The acidity constant of HOCl has been a subject for much investigation, partly because of its close connection with the chemical and biological reactivity of dilute solutions of chlorine or hypochlorite. Accurate determination has presented difficulties, however, because of its instability, its great reactivity, and its weakness as an acid.

The earliest investigation appears to have been that of Sand,[1] who determined the acidity relative to that of CO_2 by measurement of the solubility of CO_2 in solutions of NaOCl and obtained a value, 3.7×10^{-8}, not greatly different from more recent determinations.

Other determinations have been based on conductance measurements,[2] measurement of vapor pressures of HOCl from hypochlorite solutions,[3] kinetics of decomposition of hypochlorite solutions as a function of pH,[4] and potentiometric titrations of hypochlorite solutions using a "chlorine" indicator electrode.[5]

Since the development of the glass electrode, potentiometric measurements on partially neutralized solutions of HOCl or NaOCl with the glass electrode as pH indicator have become the preferred method for determination of this constant.[6]

Most of these potentiometric investigations have given reasonably consistent results. In some of them, notably those of Ingham and Morrison, Hagisawa, Asmussen and Muus, and Caramazza, corrections to zero ionic strength have been made; corrections for other earlier studies were made by Ingham and Morrison, and still others provide data from which correction can be made.

A summary of the more concordant measurements with the glass electrode, together with some of the more precise results by other methods is given in Table I. Even these presumably best figures leave uncertainties of about 0.05 in pK. Moreover, except for the value at 0° derived from the conductance measurements of Shilov and Kanyaev, none of the values can be regarded as thermodynamic ones because of the problem of liquid-junction potential.

In an endeavor to obtain more reliable values for the acid ionization constant of HOCl by a method that would yield thermodynamic results, an adaptation of the indicator method based on the ultraviolet absorption bands of HOCl and OCl^- has been used; the

(1) J. Sand, *Z. Physik. Chem.*, **48**, 610 (1904). Sand's value needs to be corrected for salting out of CO_2, for ionic strength effect, and, by use of a more accurate value, for the acidity of CO_2, but these corrections nearly cancel and leave the value essentially unchanged.

(2) W. A. Noyes and T. A. Wilson, *J. Am. Chem. Soc.*, **44**, 1630 (1922); E. A. Shilov and N. P. Kanyaev, *Zh. Fiz. Khim.*, **5**, 654 (1934).

(3) F. G. Soper, *J. Chem. Soc.*, **125**, 2227 (1924).

(4) F. Giordani, *Gazz. Chim. Ital.*, **54**, 844 (1924); J. M. Gallart, *Anales Soc. Espan. Fis. Quim.*, **31**, 422 (1933); R. M. Chapin, *J. Am. Chem. Soc.*, **56**, 2211 (1934); K. M. Markuze, *Rekonstruktsiya Tekstil. Prom. Za*, **14** (5), 43 (1935); A. Skrabal and A. Berger, *Monatsh. Chem.*, **70**, 168 (1937); A. Skrabal and R. Skrabal, *ibid.*, **71**, 251 (1938); M. W. Lister, *Can. J. Chem.*, **30**, 879 (1952).

(5) A. Rius and V. Arnal, *Anales Soc. Espan. Fis. Quim.*, **31**, 495 (1933).

(6) F. H. Yorston, *Pulp Paper Can.*, **31**, 374 (1931); G. F. Davidson, *Shirley Inst. Mem.*, **12**, 1 (1933); *J. Textile Inst.*, **24**, 186 (1933); H. T. S. Britton and E. N. Dodd, *Trans. Faraday Soc.*, **29**, 537 (1933); J. W. Ingham and J. Morrison, *J. Chem. Soc.*, 1200 (1933); E. A. Shilov and J. V. Gladtchikova, *J. Am. Chem. Soc.*, **60**, 490 (1938); M. Kiese and A. B. Hastings, *J. Biol. Chem.*, **132**, 267 (1940); H. Hagisawa, *Bull. Inst. Phys. Chem Res.* (Tokyo), **19**, 1220 (1940); G. Holst, *Svensk Kem. Tidskr.*, **52**, 258 (1940); J. Høye, *Kgl. Norske Videnskab. Selskabs Forch.*, **14**, 1 (1941); *ibid.*, **16**, 8 (1943); R. W. Asmussen and L. T. Muus, *Trans. Danish Acad. Tech. Sci.*, No. 1, 3 (1946); E. A. Shilov, A. I. Slyadnov, and G. V. Kupinskaya. *Zh. Obshchei Khim.*, **22**, 1497 (1952); I. E. Flis, *Zh. Priklad. Khim.*, **31**, 1194 (1958); I. E. Flis and M. K. Bynyaeva, *Tr. Leningrad. Tekhnol. Inst. im V. M. Molotova*, No. 7, 70 (1959); R. Caramazza, *Gazz. Chim. Ital.*, **87**, 1507 (1959).

Table I: Some Reported Ionization Constants for HOCl

Temp, °C	pK'	Approx ionic strength	pK	Source
0	...	10^{-4}	7.72	Shilov and Kanyaev
	...	...	7.82	Caramazza
0.6	...	...	7.66	Asmussen and Muus
5	7.55	0.03	7.63[a]	Kiese and Hastings
10	...	...	7.72	Caramazza
15	7.49	0.02–0.2	7.58[b]	Britton and Dodd
	...	...	7.65	Caramazza
18	7.43	0.05	7.53	Ingham and Morrison
18–20	7.43	0.05	7.53[b]	Davidson
20	7.50	0.015	7.56[a]	Shilov and Gladtchikova
	...	...	7.55	Asmussen and Muus
	7.48	0.013	7.51	Shilov, Slyadnov, and Kupinskaya
25	7.25	0.1–1.0	7.55[c]	Skrabal and Berger
	...	...	7.53	Hagisawa
	...	...	7.53	Caramazza
35	...	...	7.50	Caramazza
45	...	...	7.46	Caramazza

[a] Obtained from reported pK' values by the formula $pK = pK' + 0.5\sqrt{\mu} - 0.3\mu$. [b] See Ingham and Morrison. [c] Obtained from reported pK' by the formula $pK = pK' - 2.0 \log f$ with $f = 0.7$.

method yields directly the acid ionization of HOCl relative to the accurately known second ionization of phosphoric acid without need of pH measurements. Results with a precision of 0.005 pK unit, considered accurate within 0.01 pK unit at temperatures from 5 to 35°, have been obtained.

Principle of the Method

When HOCl is added to a solution of $H_2PO_4^-$ and HPO_4^{2-}, reaction occurs in accord with the equation

$$HPO_4^{2-} + HOCl = H_2PO_4^- + OCl^- \quad (1)$$

At equilibrium the expression

$$\log K_a - \log K_2 = \log (m_{OCl^-} m_{H_2PO_4^-} / m_{HOCl} m_{HPO_4^{2-}}) + \log (\gamma_{OCl^-} \gamma_{H_2PO_4^-} / \gamma_{HOCl} \gamma_{HPO_4^{2-}}) \quad (2)$$

holds, where K_a and K_b are the acid ionization constants of HOCl and $H_2PO_4^-$, the quantities m are the molalities of the designated species at equilibrium, and the quantities γ are the corresponding activity coefficients on the molal scale.

The first term on the right of eq 2, which contains the experimental quantities, may be designated as $\log K_c$. In terms of the measured initial millimoles of $H_2PO_4^-$, HPO_4^{2-}, and HOCl—M_1, M_2, and M_a—and the spectrophotometrically determined equilibrium fractions of HOCl and OCl^-—F_a and F_b

$$\log K_c = \log [F_b(M_1 + F_b M_a)/F_a(M_2 - F_b M_a)] \quad (3)$$

for the remaining units cancel in the ratios.

Bates[7] has reported values of the function

$$\log f_r = \log (\gamma_{H_2PO_4^-} \gamma_{X^-} / \gamma_{HPO_4^{2-}}) \quad (4)$$

at 25° for equal molalities of $H_2PO_4^-$ and HPO_4^{2-}, and for X^- representing chloride, bromide, or iodide. The same function, where X^- is chloride, can be obtained from the data given by Bates and Acree[8] for other temperatures.

The second term on the right of eq 2 can then be written

$$\log (\gamma_{OCl^-} \gamma_{H_2PO_4^-} / \gamma_{HOCl} \gamma_{HPO_4^{2-}}) = \log f_r + \log (\gamma_{OCl^-} / \gamma_{X^-} \gamma_{HOCl}) \quad (5)$$

The data of Bates are applicable provided $M_1 + F_b M_a = M_2 - F_b M_a$.

Substitution into eq 2 gives the expression

$$\log K_a - \log K_2 = \log K_c + \log f_r + \log (\gamma_{OCl^-} / \gamma_{X^-} \gamma_{HOCl}) \quad (6)$$

This may also be written in the form

$$pK_a - pK_2 = pK_c - \log f_r - \log (\gamma_{OCl^-} / \gamma_{X^-} \gamma_{HOCl}) \quad (7)$$

and abbreviated to

$$\Delta pK = \Delta pK' - \log (\gamma_{OCl^-} / \gamma_{X^-} \gamma_{HOCl}) \quad (8)$$

The last term of this equation, the only undetermined one, should be a slowly varying linear function of ionic strength becoming zero at zero ionic strength. Evaluation of pK_c and $\log f_r$ for several ionic concentrations and extrapolation of their differences, $\Delta pK'$, to zero ionic strength will give a true thermodynamic value for ΔpK.

Experimental Section

Preparation of Solutions. Redistilled and decarbonated water with a resistivity of 0.5–1 megohm was used in the preparation of all reagent and reaction solutions.

Stock solutions of HOCl, 0.05–0.1 M, were prepared by overnight treatment of chlorine water with Ag_2O or yellow HgO followed by distillation under reduced pressure at 30–35°. The stock solutions, tested for freedom from Cl^- with $AgNO_3$ and from strong acid or base by pH measurement, were collected in Pyrex "actinic glass" flasks and stored at 7°. Losses

(7) R. G. Bates, *J. Res. Natl. Bur. Std.*, **39**, 411 (1947).

(8) R. G. Bates and S. F. Acree, *ibid.*, **30**, 129 (1943); **34**, 373 (1945).

in titer, less than 1%/week, appeared to be due only to volatilization of HOCl during removal of portions of the solution. Fresh stock solutions were prepared weekly or more often.

Potassium dihydrogen phosphate and disodium hydrogen phosphate were pH standard reagents obtained from the National Bureau of Standards. They were dried and stored in accordance with instructions. Stock solutions of the individual phosphates, about 0.2 wt *M*, were prepared and dispensed on a weight basis for some of the experiments, primarily those at 25°. The solid phosphates were weighed directly for each experiment in the remaining studies.

Spectrophotometric Equipment and Operation. A Beckman Model DU spectrophotometer was used for the absorption measurements. The 1-cm cell compartment was modified with jacketing for circulation of water from a thermostat, the whole being heavily lagged with asbestos. Provision was made for passage of dry nitrogen through the cell compartment to prevent fogging of the cells at low temperatures and for reading the temperature of the cell compartment to 0.1°.

Operation of the spectrophotometer was checked by measuring the absorbance of solutions containing 0.1000 g of potassium acid phthalate/l.[9] The mean value found for the absorbance maximum at 281 mμ was $A = 6.30 \pm 0.03$; that for the minimum at 264 mμ (nearer 265 mμ with this instrument) was $A = 4.15 \pm 0.02$.

Matched silica cells (1-cm) were used throughout. Cell blanks were determined for each experiment with blank solutions appropriate to the experiment. Cells were cleaned with 6 *M* HCl whenever significant changes in the blank values occurred (0.010–0.015 near 235 mμ and 0.002 or less near 290 mμ).

Absorbance measurements were made traversing the spectrum from shorter to longer wavelengths and then retraversing in the opposite direction. The absorbance readings agreed within 0.002 in almost all instances.

Absorption Data for HOCl and OCl^-. Absorption spectra for HOCl and OCl^- in the ultraviolet region are shown in Figure 1. Spectrophotometric determinations of these substances were based on absorption measurements at wavelengths near the maximum exhibited by HOCl at 235 mμ with a molar absorptivity equal to about 100 cm^{-1} and near the maximum for OCl^- at 292 mμ with a molar absorptivity equal to about 350 cm^{-1}.

To obtain the precise values of the absorptivities needed for analytical purposes, absorption measurements were made on a series of solutions of HOCl and

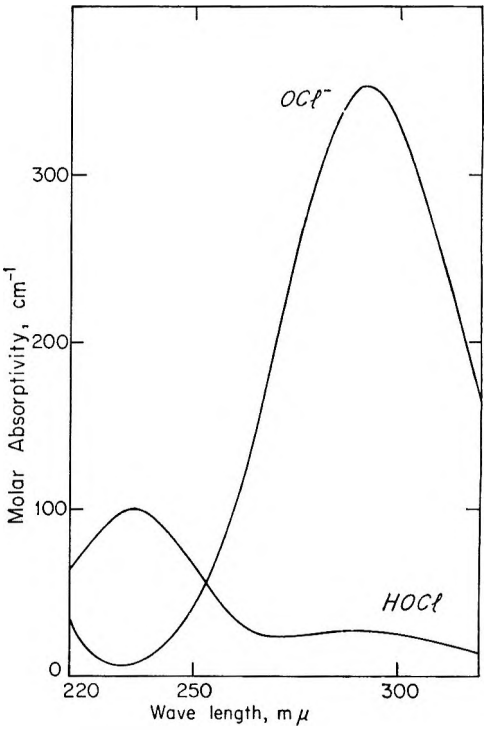

Figure 1. Ultraviolet absorption spectra for HOCl and OCl^- at 25°.

of OCl^- at 5-mμ intervals from 225 to 245 mμ and from 280 to 300 mμ. For measurements on HOCl, portions of standard stock HOCl solutions were diluted to 5–10 m*M* with either redistilled water or 10^{-4} *M* $HClO_4$; when pure water was used as diluent, corrections to observed absorption values were made for the 0.1% or so ionized to OCl^-. Solutions for measurement of OCl^- absorption were obtained by diluting stock HOCl to 1–3 m*M* with 0.005 *M* CO_2-free NaOH; the blanks for these measurements were 0.002 *M* NaOH. Concentrations of hypochlorite in the working solutions were confirmed by titration of suitable portions with 0.01 *N* thiosulfate following addition of acetic acid and KI. The concentrations of HOCl and OCl^- were chosen to give absorbance readings at their absorption maxima between 0.4 and 1.0.

Measurements were made at three temperatures—4, 25, and 34°. In each instance flasks containing the appropriate diluent and the stock HOCl solution were placed in a water thermostat at the temperature of the experiment for several hours prior to preparation of the working solutions. Absorptivities at 4° were so little different from those at 25° that it was deemed unnecessary to calibrate further at intermediate tempera-

(9) G. W. Ewing and T. Parsons, Jr., *Anal. Chem.*, **20**, 423 (1948).

tures. Values at 10 and 16° were derived by interpolation of those at 4 and 25°.

Molar absorptivities obtained from these measurements and used in the later computations are shown in Table II. Those at 25° have been computed from measurements on eight solutions; the values at 4 and 35° are based on triplicate measurements. It had originally been planned to use five wavelengths centered on 235 mμ as well as five centered on 290 mμ for the analytical determinations; however, measurements at 245 mμ and particularly at 225 mμ were appreciably more erratic than those at the other wavelengths and so these were eliminated.

Table II: Molar Absorptivities for HOCl and OCl^-

Wavelength, mμ	Molar absorptivity 4°	10°	16°	25°	34°
	a. Hypochlorous Acid				
230	93.8	93.7	93.6	93.3	92.8
235	99.9	99.8	99.8	99.6	99.3
240	96.9	96.8	96.7	96.5	95.8
280	26.0	26.0	26.0	26.1	25.9
285	26.6	26.6	26.6	26.5	26.5
290	27.1	27.0	27.0	26.9	26.7
295	26.8	26.8	26.7	26.6	26.5
300	25.7	25.7	25.6	25.4	25.3
	b. Hypochlorite Ion				
230	7.2	7.2	7.2	7.2	7.2
235	7.8	7.8	7.8	7.8	8.0
240	13.9	13.9	13.9	13.9	13.6
280	303.6	302.2	300.8	298.0	297.0
285	335.1	334.2	333.8	332.6	330.8
290	349.7	349.9	350.0	350.4	349.2
295	345.1	346.1	347.1	349.2	348.1
300	325.2	326.7	328.3	331.4	330.9

The eight sets of measurements on solutions of HOCl gave an average deviation in absorptivity of 1.8% in the 235-mμ region; the measurements on the OCl^- solutions near 290 mμ had an average deviation of 1.3%. These deviations, however, included errors in the titrimetric determination of HOCl as well as errors in spectrophotometric readings. When adjustments were made in the titrimetric molarities to give a constant absorptivity at 235 mμ, the deviations at 230 and 240 mμ were reduced to 0.8%; similarly, when molarities for the OCl^- solutions were based on the absorbance at 290 mμ, the average deviations at the adjacent wavelengths were reduced to 0.5%. It appears that titrimetric errors were of the order of 1%, about twice as great as absorptiometric errors near 290 mμ and of the same order as absorptiometric errors near 235 mμ.

Experimental Procedure. An accurately known amount of KH_2PO_4, approximately 5 mmoles, was dispensed into a weighed volumetric flask, an accurately known quantity of Na_2HPO_4 equal to the KH_2PO_4 plus twice the expected amount of reaction 1 was added to it, the flask was about two-thirds filled with redistilled water, and then the flask and contents were placed in a thermostated water bath at the experimental temperature. After a suitable time a measured volume of standardized stock HOCl sufficient to give a total hypochlorite concentration 5–10 m*M* was added, the flask was filled to the mark with water previously brought to the experimental temperature, and the flask plus contents was reweighed. After thorough mixing, a suitable aliquot was withdrawn for titrimetric analysis of total hypochlorite, and the flask was then replaced in the thermostated bath for 0.5 hr before a portion of solution was dispensed into the absorption cell for spectrophotometric measurements.

Absorbance measurements were made in the same manner as described for determination of the absorptivities of HOCl and OCl^- at 5-mμ intervals between 225 and 245 mμ and between 280 and 300 mμ, scanning first in one direction and then in reverse against blank equimolar phosphate mixtures of the same ionic strength. The temperature in the cell compartment was recorded at the end of the absorbance measurements.

Generally, three experiments were performed for each set of conditions. The first was usually an exploratory run, for it was found that previous values for K_a were not precise enough to permit accurate evaluation of the extent of reaction 1 and hence of the required amount of Na_2HPO_4 to yield equimolar $H_2PO_4^-$ and HPO_4^{2-} in the equilibrated solution. The experience of the first run was used for modification of the amount of Na_2HPO_4 in subsequent experiments. As data accumulated, better predictions could be made for the initial runs and then only duplicate experiments were carried out. No results have been included in the final tabulation in which the equilibrium phosphate ratio differed from unity more than 4%, even though data from experiments in which the ratio was as much as 10% off indicated that the activity factor was not sensitive to this parameter.

Calculations

Computation of pK_c. The experiments gave three sets of data: absorbance values near 235 mμ due mainly to HOCl, absorbance values near 290 mμ due mainly to OCl^-, and analytical determinations of the sum of HOCl and OCl^-. Any pair of these three can

be used for determination of the individual concentrations of HOCl and OCl^-. The usual technique making use of the two absorbance values takes no account of the analytical determination; since in the present experiments the analysis had the same order of precision as the absorbance measurements, it was desired to include it to make the results as reliable as possible.

The following procedure was used. From the equations, $A = a_1c_1 + a_2c_2$ and $C = c_1 + c_2$, where A is the measured absorbance at some wavelength and C is the analytical molarity, the equation

$$F_1 = c_1/C = (a' - a_2)/(a_1 - a_2) \qquad (9)$$

is easily derived, a' being A/C, a_1 the absorptivity of the principal absorbing species, and a_2 that of the other species. With the aid of this equation, F_b, the fractions of OCl^-, were computed for the five wavelengths near 290 mμ and F_a, the fractions of HOCl, for the three wavelengths near 235 mμ.

Because of experimental errors, the mean values of F_a and F_b computed in this way for each experiment did not sum exactly to unity. The deviations, however, were small, a maximum of 0.011 for experiments at 25°, and a mean of 0.011 over-all. The greatest deviations, 0.03, were at 4°. Adjustments were applied to the F_a and F_b values to make their sum unity based on the judgment that the error in the analytical concentration was twice as great as that in the mean of the five absorbance measurements near 290 mμ and half as great as the mean of the three absorbance measurements near 235 mμ.[10] A typical computation is shown in Table III.

The error in K_c computed from the corrected experimental data is 1.3–1.5 times the error in the F_b value, which is estimated to have a mean error about 0.7% at 25° and 1% at other temperatures. Accordingly, the expected mean error of pK_c is about 0.004 at 25° and 0.006 at other temperatures.

Evaluation of Log F_r. Bates[7] developed his values for log f_r at 25° from measurements with series of solutions having fixed values for the molal ratio, m_x/μ, m_x being the molality of Cl^-, Br^-, or I^-. The data of these experiments pertain to a nearly constant value of m_x, about 1.8 mm, with variable μ.

Accordingly, detailed plots of log f_r against m_x/μ, similar to those shown in Bates' Figure 2 were constructed for each value of μ and for all three halide ions; then values for log f_r corresponding to $m_x = 1.8$ mm were taken with a precision of 0.0002 log unit from the straight lines of best fit through the points on each plot. At the low halide ion concentration of concern the values differed only slightly from the limiting log f_r^0 values corresponding to zero halide—the difference being about 0.0004 for the Cl^- series up to a mean of about 0.001 for the I^- series. Consequently, variations in log f_r over the concentration range of 1.4–2.0 mM OCl^- for the individual experiments at 25° were insignificant compared with Bates' assigned accuracy of 0.002 unit for log f_r in the Cl^- series and 0.003 unit in the Br^- and I^- series.

Table III: Typical Determination of pK_c[a]

Wavelength, mμ	Measd absorbance	Apparent absorptivity, a'	$a' - a_2$	$a - a_2$	F_a	F_b
230	0.451	72.9	65.7	86.1	0.7624	
235	0.479	77.4	69.6	91.8	0.7576	
240	0.475	77.7	62.9	82.6	0.7621	
280	0.557	90.0	63.9	272.0		0.2350
285	0.610	98.5	72.0	306.1		0.2353
290	0.636	102.7	75.8	323.5		0.2344
295	0.633	102.3	75.6	322.6		0.2344
300	0.602	97.3	71.8	306.0		0.2348
				Means	0.7607	0.2348

[a] Run 11, 25°, 0.05 ionic strength. Solution: 25.35 g of 0.2000 m (0.1947 wt M) KH_2PO_4, 35.25 g of 0.2000 m (0.1945 wt M) Na_2HPO_4, 49.93 ml of 0.0622 M HOCl diluted to 500 ml or 499.75 g. Molarity of HOCl: by analysis, 0.00616; by calculation, 0.00622; average, 0.00619. Corrected: molarity = 0.00618; $F_a = 0.7645$; $F_b = 0.2355$; $M_a = (0.00618)(500) = 3.090$; $F_bM_a = (3.090)(0.2355) = 0.728$; $M_1 = (25.35)(0.1947) = 4.936$; $M_2 = (35.25)(0.1945) = 6.465$. $K_c = (0.2355)(4.936 + 0.729)/(0.7645)(6.465 - 0.728) = 0.3041$; $pK_c = 0.517$.

The values of log f_r thus obtained were plotted as a function of μ for each of the three series in enough detail that log f_r appropriate to the ionic strength of each experiment could be obtained with a precision of 0.001 unit.

At temperatures other than 25°, similar data are available only for the Cl^- series, from the paper of Bates and Acree.[8] Evaluation could be based on their formula

$$\log f_r = \frac{2A\sqrt{\mu}}{1 + Ba^\circ\sqrt{\mu}} + \beta\mu \qquad (10)$$

for they found that β alone depended on the contribution of m_{Cl} to the ionic strength and that its variation was linear with m_x/μ. Thus, correction could be made with the substitution $\beta\mu = \beta_0\mu + km_x$, with k found to be 0.24 at all temperatures. The actual corrections for the chloride contribution to μ amounted to about

(10) If $\Delta = F_a + F_b - 1$, the corrections to be applied are: $F_b = F_b(\text{uncor}) - [R_2/(2R_1 + R_2)]\Delta$, $F_a = F_a(\text{uncor}) - [2R_1/(2R_1 + R_2)]\Delta$, and $M_a = M_a(\text{uncor})[1 - \Delta/(2R_1 + 0.5R_2 - \Delta)]$. Here $R_1 = F_a(\text{uncor}) + [a_2/(a_1 - a_2)]_{235}$ and $R_2 = F_b(\text{uncor}) + [a_2/(a_1 - a_2)]_{290}$.

0.0004 unit, in agreement with the previously noted value for the 25° data.

Computations based on eq 10 were made at 5, 10, 15, and 35° with the values for the parameters given by Bates and Acree and for the molal ionic strength of each of the present experiments. Correction to the experimental temperatures near 4, 10, 16, and 34° was slight; for log f_r, values at constant ionic strength change only about 2×10^{-4}/deg.

Results

Data for the experiments at 25° and values of log K_c and $\Delta pK'$ computed from them are presented in Table IV. The three sets of $\Delta pK'$ are based on log f_r values for chloride, bromide, and iodide systems as designated. Replicate values at each ionic strength exhibit a range less than 0.01 unit; moreover, the $\Delta pK'$ based on log f_r for the iodide system vary only slightly with ionic strength, the total range for the nine experiments being 0.013 unit.

Table IV: Values of pK_c and $\Delta pK'$ at 25°

a. Experimental Data and Evaluation of pK_c[a]

Soln vol, ml	Initial mmoles of HPO_4^{2-}, M_2	Initial mmoles of HOCl, M_a	Equil fraction for OCl^-, F_b	Equil phosphate ratio	pK_c
100	5.237	0.919	0.1790	0.994	0.659
100	5.237	0.915	0.1803	0.994	0.655
200	5.653	1.887	0.2018	0.991	0.594
200	5.653	1.869	0.2036	0.992	0.589
200	5.778	2.232	0.2038	0.987	0.586
250	5.811	2.229	0.2090	0.989	0.573
250	5.731	2.036	0.2102	0.989	0.570
500	6.465	3.090	0.2355	1.013	0.517
500	6.465	3.095	0.2344	1.014	0.520

b. Evaluation of $\Delta pK'$

pK_c	Ionic strength, μ	Log f_r Cl	Log f_r Br	Log f_r I	$\Delta pK'$ Cl	$\Delta pK'$ Br	$\Delta pK'$ I
0.659	0.206	0.290	0.299	0.306	0.369	0.360	0.353
0.655	0.206	0.290	0.299	0.306	0.365	0.356	0.349
0.594	0.108	0.233	0.238	0.243	0.361	0.356	0.351
0.589	0.108	0.233	0.238	0.243	0.356	0.351	0.346
0.586	0.110	0.235	0.239	0.244	0.351	0.347	0.342
0.573	0.088	0.216	0.221	0.225	0.357	0.352	0.348
0.570	0.087	0.215	0.220	0.224	0.355	0.350	0.346
0.517	0.047	0.172	0.175	0.177	0.345	0.342	0.340
0.520	0.047	0.172	0.175	0.177	0.348	0.345	0.343

[a] Initial millimoles of $H_2PO_4^-$, M_1 = 4.936 throughout.

Plots of each of the sets of $\Delta pK'$ values as a function of ionic strength, shown in Figure 2, exhibit the expected linear dependence. Extrapolation to zero ionic strength gives $\Delta pK = 0.341 \pm 0.005$ at 25° for all three sets.

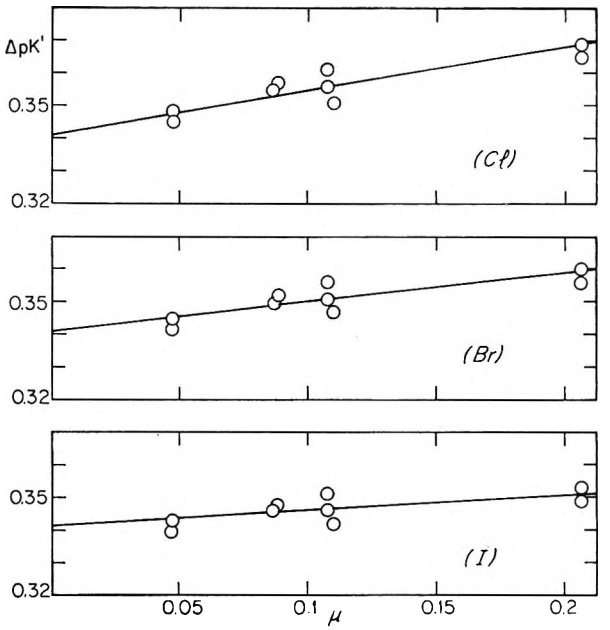

Figure 2. Evaluation of ΔpK at 25° by extrapolation of $\Delta pK'$ values computed with log f_r data for chloride, bromide, and iodide systems, respectively.

Similar data and computed parameters for the experiments at other temperatures are presented in Table V. Unfortunately, the arrangements used for temperature control did not reproduce temperatures exactly for experiments conducted several weeks apart. As a result the temperatures of individual experiments at each level sometimes differed several tenths of a degree from the mean for the group even though good constancy was maintained for each experiment.

Corrections of the $\Delta pK'$ to the mean temperature at each level were made by plotting the data at each ionic strength as a function of temperature and estimating corrections per degree to be applied on the basis of smooth curves drawn through the points. The factors ranged from 0.006 unit/deg at 34° to 0.0075 unit/deg at 4°. Values of $\Delta pK'$ corrected to the mean rounded temperatures are given in the last column of Table V. The maximum correction was 0.013 unit; only three values had corrections greater than 0.005 unit.

Plots of the corrected $\Delta pK'$ as a function of ionic strength are shown in Figure 3. The straight lines for extrapolation of the data have all been drawn with the same slope as that observed for the 25° data with the chloride system, for this constraint appeared to provide over-all the best consistent representation of the data.

The extrapolated values of ΔpK are listed in the

Table V: Computation of pK_c and $\Delta pK'$ at Temperatures other than 25°

Temp, °C	Ionic strength, μ	Initial mmoles of $H_2PO_4^-$, M_1	Initial mmoles of HPO_4^{2-}, M_2	Initial mmoles of HOCl, M_a	Equil fraction for OCl^-, F_b	Equil phosphate ratio	pK_c	Log f_r	$\Delta pK'$	$\Delta pK'$ (cor)
					a. 4°					
4.4	0.207	4.934	5.310	0.867	0.1401	1.026	0.799	0.288	0.511	0.514
4.0	0.201	4.934	5.053	0.871	0.1365	0.976	0.791	0.286	0.505	0.505
4.0	0.198	4.934	4.970	0.864	0.1328	0.962	0.798	0.284	0.514	0.514
3.9	0.107	4.934	5.531	2.093	0.1505	0.994	0.749	0.229	0.520	0.519
4.3	0.107	4.934	5.590	2.572	0.1509	0.977	0.740	0.229	0.511	0.513
3.8	0.046	4.928	6.164	3.070	0.1802	1.023	0.665	0.166	0.499	0.498
5.8	0.045	4.977	5.980	2.588	0.1843	1.005	0.648	0.165	0.483	0.496
					b. 10°					
11.5	0.212	5.238	5.352	0.605	0.1547	0.986	0.732	0.291	0.441	0.452
10.3	0.213	5.054	5.436	0.901	0.1564	0.020	0.748	0.291	0.457	0.459
11.5	0.210	5.052	5.345	0.899	0.1560	1.002	0.734	0.290	0.444	0.455
10.2	0.108	4.992	5.598	1.795	0.1737	0.997	0.676	0.230	0.446	0.448
10.2	0.111	5.038	5.621	1.793	0.1733	0.993	0.677	0.233	0.444	0.446
9.4	0.045	5.066	6.007	2.603	0.1955	0.986	0.608	0.165	0.443	0.438
					c. 16°					
16.5	0.215	5.172	5.408	0.775	0.1646	0.997	0.704	0.293	0.411	0.414
16.3	0.207	4.985	5.245	0.770	0.1648	1.001	0.705	0.289	0.416	0.418
16.6	0.108	5.053	5.555	1.919	0.1846	0.962	0.628	0.231	0.397	0.401
15.3	0.108	4.993	5.601	1.522	0.1886	1.006	0.636	0.231	0.405	0.401
15.6	0.056	6.049	7.598	3.041	0.2137	1.037	0.582	0.182	0.400	0.397
15.5	0.047	5.027	6.357	3.030	0.2107	1.009	0.577	0.169	0.408	0.404
					d. 34°					
34.2	0.206	4.928	5.224	0.587	0.2013	1.012	0.604	0.295	0.309	0.310
34.5	0.210	4.928	5.319	0.585	0.2042	1.030	0.604	0.297	0.307	0.310
34.0	0.107	4.928	5.567	1.455	0.2247	0.997	0.537	0.236	0.301	0.301
33.9	0.109	5.043	5.673	1.509	0.2265	0.990	0.529	0.238	0.291	0.290
34.4	0.112	5.121	5.859	1.507	0.2261	1.010	0.539	0.240	0.299	0.301
33.5	0.047	4.928	6.374	2.918	0.2539	0.994	0.465	0.173	0.292	0.289
34.2	0.051	5.032	7.068	3.722	0.2589	1.018	0.465	0.179	0.286	0.287
33.2	0.050	5.021	6.914	3.721	0.2542	1.000	0.468	0.178	0.290	0.285

second column of Table VI; from them the values of pK_a in the fifth column are obtained by addition of the pK_2 values for H_3PO_4 given in the fourth column.

Data of Bates and Acree[8], Ender, Teltschik, and Schäfer,[11] and Grzybowski[12] for pK_2 of H_3PO_4 are in good agreement for the temperature range of these measurements, the maximum spread being 0.004 pK unit. The equations derived from these data, however, yield a figure for $\Delta H°_{298}$ about 200 cal/mole greater than the value $\Delta H°_{298}$ = 800 cal/mole determined calorimetrically by Pitzer[13] and by Dumbaugh.[14] This discrepancy introduces some ambiguity into evaluation of pK_a for HOCl as a function of temperature.

Table VI: Evaluation of pK_a for Hypochlorous Acid

Temp, °C	ΔpK (obsd)	ΔpK (eq 11)	pK_2 (H_3PO_4)	pK_a (exptl)	pK_a (eq 12)	pK_a (eq 13)
4.0	0.490	0.480	7.286	7.776	7.756	7.768
10.0	0.432	0.437	7.254	7.686	7.685	7.690
16.0	0.391	0.397	7.228	7 619	7.621	7.622
25.0	0.341	0.339	7.199	7.540	7.540	7.537
34.0	0.282	0.284	7.184	7.466	7.474	7.469

The data for ΔpK can be expressed as a function of temperature by the simple equation

$$\Delta pK = \frac{555}{T} - 1.5228 \qquad (11)$$

(11) F. Ender, W. Teltschik, and K. Schäfer, *Z. Elektrochem.*, **61**, 775 (1957).

(12) A. K. Grzybowski, *J. Phys. Chem.*, **62**, 555 (1958).

(13) K. S. Pitzer, *J. Am. Chem. Soc.*, **59**, 2365 (1937).

(14) W. H. Dumbaugh, Jr., Thesis, Penn State University, 1959; University Microfilms 59-5104.

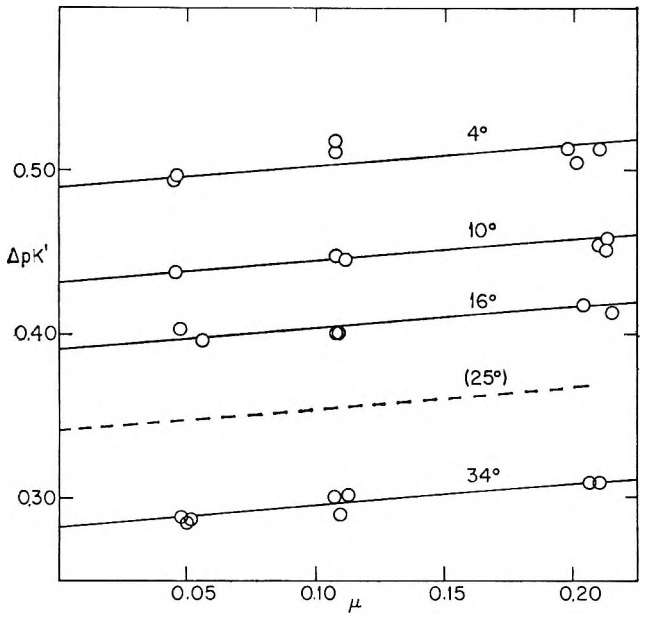

Figure 3. Evaluation of ΔpK by extrapolation of $\Delta pK'$ at temperatures of 4, 10, 16, and 34°.

Values of ΔpK computed from this equation, given in the third column of Table VI, show a maximum deviation from the measured quantities equal to 0.010 at 4°, the temperature for which the data are least reliable. The calculated $\Delta H°$ from this equation, 2540 cal, is in reasonable agreement with the combined thermochemical value for the second ionization of H_3PO_4 with that for the ionization of HOCl determined to be $\Delta H°_{291} = 3688$ cal/mole by Neumann and Müller.[15] The closeness of the accord, however, is dependent on the procedure used to adjust the two sets of calorimetric data to the same temperature.

If the equation representing the pK_a as a function of temperature is constrained to yield Neumann and Müller's value for $\Delta H°_{291}$, then a fair fit is obtained with the equation

$$pK_a = \frac{2500.00}{T} - 6.8018 + 0.01998T \qquad (12)$$

Values for pK_a computed from this equation, shown in the sixth column of Table VI, fit the experimental data closely at 10, 16, and 25° but give deviations of −0.020 at 4° and +0.008 at 34°. Change of the final term of eq 12 to 0.01970, a shift that corresponds to the maximum probable error in the thermochemical data, with adjustment of the constant term to 6.7195, reduces the deviation at 4° to −0.015 and that at 34° to +0.005 without significant effect on the concordance with the three central values.

An over-all best fit of the pK_a data is obtained with the equation

$$pK_a = \frac{3000.00}{T} - 10.0686 + 0.0253T \qquad (13)$$

Values of pK_a computed with this equation, given in the last column of Table VI, show maximum deviation from the experimental values equal to −0.008, at 4°. The $\Delta H°_{291}$ value is now about 3900 cal/mole, however, 200 cal greater than the thermochemical value, nearly the same as the discrepancy in the values for the second ionization of H_3PO_4 upon which these data are based.

Table VII presents values for pK_a of HOCl computed from eq 13 for 5° temperature intervals from 0 to 35°. These values are believed to be accurate within 0.01 unit, except possibly at 0°. Good agreement with the values of Caramazza, within the limits of precision of his work, is shown.

Table VII: pK_a for Hypochlorous Acid at Even Temperature Intervals

Temp, °C	pK_a (eq 11)	pK_a (Caramazza)	pK_a (others)
0	7.825	7.82	7.72 (S and K)
5	7.754		7.63 (K and H)
10	7.690	7.72	
15	7.633	7.65	7.58 (B and D)
20	7.582		7.55 (A and M)
25	7.537	7.53	7.53 (H)
30	7.497		
35	7.463	7.50	

Acknowledgments. The assistance of Frances T. Jewell, who conducted substantially all of the described experiments, is much appreciated. The work was performed under Research Grant RG-2378 from the National Institutes of Health, U. S. Public Health Service.

(15) B. Neumann and G. Müller, *Z. Anorg. Chem.*, **182**, 235 (1929); **185**, 428 (1930).

Stochastic Approach to Nonequilibrium Thermodynamics of First-Order Chemical Reactions

by Kenji Ishida

Laboratory of Radiochemistry, Japan Atomic Energy Research Institute, Tokai-mura, Naka-gun, Ibaraki-ken, Japan *(Received April 22, 1966)*

Since chemical reaction is in general a random process, the probability for a reaction state in the reaction system, in which the probability distribution for reaction states is determined by the stochastic theory of reaction process, is connected with the entropy change due to chemical reaction. It is then possible to formulate stochastically the nonequilibrium thermodynamics of chemical reaction. It is also shown that the relation between entropy and fluctuation is obtainable from such stochastic considerations.

Introduction

Throughout this paper, attention is confined to homogeneous gas reactions of first order in a closed system maintained at uniform temperature T. It is assumed that the reactions proceed sufficiently slowly so as not to disturb seriously the equilibrium energy distribution of each component to any appreciable extent.[1] Such a reaction system will be said to be in thermal equilibrium.[2] This assumption usually has been made also in the study of nonequilibrium thermodynamics of chemical reactions,[3] in which the notion of entropy production plays a central role. It is an interesting problem, however, to investigate how to include the condition of thermal equilibrium in the formula for entropy change due to chemical reactions.

To obtain the answer to this question, we apply the theory of stochastic process to chemical kinetics. Then the chemical reaction in thermal equilibrium can be treated as a temporally homogeneous Markov process.[2,4-8] It is possible, in some simple cases, to find the probability distribution for reaction states. In addition, if it is physically justified that entropy is closely related to the probability of a reaction state, the nonequilibrium thermodynamics of chemical reaction may be stochastically constructed without starting from the thermodynamic Gibbs relation.

Preliminary Approach

According to the theory of irreversible thermodynamics,[9,10] the entropy production d_iS resulting from a chemical reaction in closed system is given by

$$d_iS = Ad\xi/T \geq 0 \tag{1}$$

where A is the chemical affinity for the reaction and ξ is the degree of advancement. The last equality of (1) holds for the equilibrium state. Of course, as explained in the previous section, thermal equilibrium is tacitly assumed in eq 1.

The integral of (1) may be written in the form

$$S = \frac{1}{T}\int_{\text{equilibrium state}}^{\text{arbitrary reaction state}} Ad\xi + S_e \tag{2}$$

where S_e denotes the entropy for the equilibrium state. We shall for the sake of brevity consider the nonequilibrium thermodynamics of the reaction $A \rightleftarrows B$. In this case A and $d\xi$ are given by eq 3 and 4, respectively.

(1) R. H. Fowler, "Statistical Mechanics," Cambridge University Press, Cambridge, 1936, p 700.

(2) K. Ishida, *Bull. Chem. Soc. Japan*, **33**, 1030 (1960).

(3) I. Prigogine, "Introduction to Thermodynamics of Irreversible Processes," 2nd ed, Interscience Publishers, Inc., New York, N. Y., 1961, p 93.

(4) G. F. Bartholomay, *Bull. Math. Biophys.*, **20**, 175 (1958).

(5) A. T. Bharucha-Reid, "Elements of the Theory of Markov Processes and Their Applications," McGraw-Hill Book Co., Inc., New York, N. Y., 1960, Chapter 8.

(6) D. A. McQuarrie, *J. Chem. Phys.*, **38**, 433 (1963).

(7) D. A. McQuarrie, C. J. Jachimowski, and M. E. Russell, *ibid.*, **40**, 2914 (1964).

(8) K. Ishida, *ibid.*, **41**, 2472 (1964).

(9) See ref 3, p 23.

(10) S. R. de Groot, "Thermodynamics of Irreversible Processes," North-Holland Publishing Co., Amsterdam, 1952, Chapter 9.

$$A = RT \ln \frac{n_{B,e}/n_{A,e}}{n_B/n_A} \tag{3}$$

and

$$d\xi = -dn_A = dn_B \tag{4}$$

where n_γ (γ = A, B) is the number of moles per unit volume. Substituting (3) and (4) into (2) and carrying out the integration, we obtain

$$\begin{aligned} S &= -R\sum_\gamma n_\gamma \ln \frac{n_\gamma}{n_{\gamma,e}} + S_e \\ &= -nR\sum_\gamma f_\gamma \ln \left[\frac{f_\gamma}{f_{\gamma,e}\exp(s_e/R)}\right] \end{aligned} \tag{5}$$

where $n = \sum_\gamma n_\gamma$ is the total number of moles per unit volume, f_γ is the mole fraction, and $s_e = S_e/n$. If it is physically and stochastically justified that f_γ can be replaced by the probability $p_\gamma(t)$ for a γ molecule to be found in the reaction system at time t, then the entropy is closely related to the probability of a reaction state.

Stochastic Entropy Production

To visualize the last statement, first of all, it is necessary to find the probability distribution for reaction states. According to the stochastic theory of chemical reactions in thermal equilibrium, the probability distribution $P(N_A, N_B; t)$ for the reaction $A \rightleftarrows B$ satisfies

$$\begin{aligned} \frac{d}{dt}P(N_A, N_B; t) = \\ -(k_1N_A + k_1'N_B)P(N_A, N_B; t) + \\ k_1(N_A + 1)P(N_A + 1, N_B - 1; t) + \\ k_1'(N_B + 1)P(N_A - 1, N_B + 1; t) \end{aligned} \tag{6}$$

where $P(N_A, N_B; t)$ denotes the probability of finding the numbers N_A and N_B of A and B molecules in the reaction system during the time interval from 0 to t, k_1 and k_1' are the transition probabilities for the forward and reverse reactions, respectively. Solving this system of differential-difference equations under the initial condition

$$P(N_A^0, N_B^0; 0) = \frac{N!}{N_A^0!N_B^0!}p_A^{0N_A^0}p_B^{0N_B^0} \tag{7}$$

we obtain the binomial distribution[11]

$$P(N_A, N_B; t) = \frac{N!}{N_A!N_B!}\{p_A(t)\}^{N_A}\{p_B(t)\}^{N_B} \tag{8}$$

where N is the total number of molecules, $p_A(t)$ and $p_B(t)$ are given by, respectively

$$p_A(t) = \frac{k_1'}{k_1 + k_1'} + \frac{p_A^0k_1 - p_B^0k_1'}{k_1 + k_1'}\exp[-(k_1 + k_1')t] \tag{9}$$

and

$$p_B(t) = \frac{k_1}{k_1 + k_1'} - \frac{p_A^0k_1 - p_B^0k_1'}{k_1 + k_1'}\exp[-(k_1 + k_1')t] \tag{10}$$

In eq 8

$$\pi_R(t) = \{p_A(t)\}^{N_A}\{p_B(t)\}^{N_B} \tag{11}$$

represents the probability for a reaction state at time t.

We are now in a position to introduce a mathematical expression for the condition that the reaction proceeds in thermal equilibrium. This condition implies that for the relaxation time τ, which may be short compared with observed time but sufficiently long on the microscopic time scale,[12] one has

$$\lim_{\tau\to\infty} p_\gamma(\tau) = q_\gamma \tag{12}$$

where q_γ (γ = A, B) denotes the probability of a γ molecule in thermal equilibrium and is independent of the initial condition. Therefore, the probability $\pi_{T,E}(t)$ for such a thermal equilibrium state in the course of reaction is given by

$$\pi_{T,E}(t) = q_A^{N_A}q_B^{N_B} \tag{13}$$

Let us define by the following relation the stochastic entropy S due to the chemical reaction in thermal equilibrium

$$S = -k\left\langle \ln \frac{\pi_R(t)}{\pi_{T,E}(t)\exp(S_e/k)} \right\rangle \tag{14}$$

where k is Boltzmann's constant and the symbol $\langle\ \rangle$ stands for the mean with respect to the probability distribution for reaction states. Substituting (11) and (13) into (14), we have

$$S = -k\sum_\gamma \langle N_\gamma\rangle \ln \frac{p_\gamma(t)}{q_\gamma\exp(s_e/k)} \tag{15}$$

$$= -kN\sum_\gamma p_\gamma(t) \ln \frac{p_\gamma(t)}{q_\gamma \exp(s_e/k)} \tag{16}$$

where $\langle N_\gamma\rangle = Np_\gamma(t)$ and $s_e = S_e/N$. The stochastic entropy (16) is in form identical with the deterministic entropy (5) and analogous to the so-called Gibbs

(11) See the footnote for (19) and (20).

(12) In other words, this means that the thermal equilibrium may be instantaneously established owing to the rapid energy exchange between molecules.

entropy postulate in nonequilibrium statistical mechanics.[13] It follows with the help of (13) that S approaches the value of entropy for the equilibrium state as t tends to infinity

$$\lim_{t\to\infty} S = S_e \tag{17}$$

The differential of (15), *i.e.*, the stochastic entropy production, is given by

$$\begin{aligned} dS &= -k\sum_\gamma d\langle N_\gamma\rangle \ln (p_\gamma(t)/q_\gamma) \\ &= -k\sum_\gamma d\langle N_\gamma\rangle \ln (\langle N_\gamma\rangle/\langle N_\gamma\rangle_e) \end{aligned} \tag{13}$$

where $\sum_\gamma \langle N_\gamma\rangle d \ln p_\gamma(t) = 0$, $\langle N_\gamma\rangle = Np_\gamma(t)$, and $\langle N_\gamma\rangle_e = Nq_\gamma$ have been used. We now require the following differential equations with respect to the means $\langle N_A\rangle$ and $\langle N_B\rangle$

$$\frac{d\langle N_A\rangle}{dt} = -k_1\langle N_A\rangle + k_1'\langle N_B\rangle \tag{19}$$

and

$$\frac{d\langle N_B\rangle}{dt} = k_1\langle N_A\rangle - k_1'\langle N_B\rangle \tag{20}$$

which can be easily derived by the method of moment-generating function (mgf).[14] Since, on the other hand, the degree of advancement ξ is defined by the relation

$$d\langle N_\gamma\rangle = \nu_\gamma\, d\xi \tag{21}$$

where $\nu_A = -1$ and $\nu_B = -1$, eq 18 becomes

$$dS = -\frac{1}{T}\{kT \ln (\langle N_A\rangle/\langle N_A\rangle_e) - kT \ln (\langle N_B\rangle/\langle N_B\rangle_e)\}\, d\xi \tag{22}$$

This can be also written as the function of time t

$$dS = kT(p_A{}^0k_1 - p_B{}^0k_1')\exp[-(k_1 + k_1')t] \times \ln\left\{\frac{1 + \frac{p_A{}^0k_1 - p_B{}^0k_1'}{k_1'}\exp[-(k_1 + k_1')t]}{1 - \frac{p_A{}^0k_1 - p_B{}^0k_1'}{k_1}\exp[-(k_1 + k_1')t]}\right\} dt \tag{23}$$

Since in the theory of the Markov process time is no longer reversible,[15] it follows that $dt > 0$. Thus from (23) we have $dS \geq 0$, which holds for all the values of $t \geq 0$. On the right-hand side of (22)

$$kT \ln (\langle N_A\rangle/\langle N_A\rangle_e) - kT \ln (\langle N_B\rangle/\langle N_B\rangle_e)$$

corresponds to the chemical affinity $A = \mu_A - \mu_B$, because the chemical potential for a mixture of ideal gases may be written in the form $\mu_\gamma = \mu_{\gamma,e} + kT \ln (\langle N_\gamma\rangle/\langle N_\gamma\rangle_e)$. In consequence, we have

$$dS = A\, d\xi/T \geq 0 \tag{24}$$

which is on the average in agreement with the deterministic entropy production d_iS. We need to emphasize at this stage that in the present treatment all the variables are the means with respect to the probability distribution for reaction states, and that the stochastic entropy (16) enables us to formulate the nonequilibrium thermodynamics of chemical reaction without using the notion of chemical affinity.

Example

In order to illustrate the validity of the stochastic entropy production, we consider the reaction system of n components $A_1, A_2, \ldots, A_n$, between which all possible reactions of the type $A_i \rightleftarrows A_j$ occur. We then have $^1/_2n(n-1)$ of these possible reactions of which only $n-1$ are independent. The multidimensional Markov process for such a reaction system may be written in the form[16]

$$\begin{aligned} \frac{d}{dt}P(N_1, N_2, \ldots, N_i, \ldots, N_n; t) = \\ -\sum_i\sum_j{}'k_{ij}\{N_iP(N_1, N_2, \ldots, N_i, \ldots, N_n; t) + \\ (N_i + 1)P(N_1, N_2, \ldots, N_i + 1, \ldots, \\ N_j - 1, \ldots, N_n; t)\} \end{aligned} \tag{25}$$

where N_i is the number of A_i molecules at time t, k_{ij} is the transition probability of $A_i \to A_j$, and Σ' denotes the sum of all j's except $j = i$. As an initial condition, we assume $P(N, 0, \ldots, 0; 0) = 1$, where N is the total number of molecules. The solution of (25) is then given by the multinomial distribution (shown in eq 26)

(13) S. R. de Groot and P. Mazur, "Non-Equilibrium Thermodynamics," North-Holland Publishing Co., Inc., Amsterdam, 1962, Chapter 7, p 126.

(14) The mgf for $P(N_A, N_B; t)$ is defined by

$$M(\theta_1, \theta_2; t) = \sum_{N_A,N_B} e^{\theta_1 N_A}e^{\theta_2 N_B}P(N_A, N_B; t) \tag{a}$$

$$= 1 + \langle N_A\rangle\theta_1 + \langle N_B\rangle\theta_2 + {}^1/_2\langle N_A{}^2\rangle\theta_1{}^2 + \langle N_AN_B\rangle\theta_1\theta_2 + {}^1/_2\langle N_B{}^2\rangle\theta_2{}^2 + \ldots \tag{b}$$

where θ_1 and θ_2 are any real numbers and the summation is over all possible values of N_A and N_B. The differential-difference equation (6) is transformed into the partial differential equation, with the use of (a)

$$\frac{\partial M}{\partial t} = -k_1(1 - e^{-\theta_1+\theta_2})\frac{\partial M}{\partial \theta_1} - k_1'(1 - e^{\theta_1-\theta_2})\frac{\partial M}{\partial \theta_2} \tag{c}$$

From the solution of this equation we can get the probability distribution (8). If (b) and the expansions of $e^{-\theta_1+\theta_2}$ and $e^{\theta_1-\theta_2}$ in these Taylor series are substituted into (c), eq 19 and 20 are obtained as the coefficients of θ_1 and θ_2, respectively.

(15) E. Parzen, "Stochastic Processes," Holden-Day, Inc., San Francisco, Calif., 1962, p 187.

(16) I. M. Krieger and P. J. Gans, *J. Chem. Phys.*, **32**, 247 (1960).

$$P(N_1, N_2, \ldots, N_n; t) = \frac{N!}{\prod_i N_i!} \prod_i \{p_i(t)\}^{N_i} \quad (26)$$

where the probabilities $p_i(t)$ of finding an A_i molecule in the reaction system at time t satisfy $\sum_i p_i(t) = 1$. The probability $\pi_R(t)$ for a reaction state is

$$\pi_R(t) = \prod_i \{p_i(t)\}^{N_i} \quad (27)$$

Since, however, $p_i(t)$ is of the form

$$p_i(t) = q_i + \sum_{l=1}^{n-1} a_{il} \exp(-\lambda_l t) \quad (28)$$

where $\sum_i q_i = 1$, $\sum_i a_{il} = 0$, and $\lambda_l > 0$ for all l's, the probability $\pi_{T,E}(t)$ for a state in thermal equilibrium is given by

$$\pi_{T,E}(t) = \prod_i q_i^{N_i} \quad (29)$$

Thus, applying the formula (14) to the present case, we get, as the entropy production $\mathcal{P}_s = dS/dt$ per unit time

$$\mathcal{P}_s = -kN \sum_i \frac{dp_i(t)}{dt} \ln (p_i(t)/q_i) \quad (30)$$

$$= -k \sum_i \frac{d\langle N_i \rangle}{dt} \ln (\langle N_i \rangle / \langle N_i \rangle_e) \quad (31)$$

where $\langle N_i \rangle = N p_i(t)$ and $\langle N_i \rangle_e = N q_i$. From (25), on the other hand, we can derive the differential equations with respect to $\langle N_i \rangle$

$$\frac{d\langle N_i \rangle}{dt} = -\sum_j {}' k_{ij} \langle N_i \rangle + \sum_j {}' k_{ji} \langle N_j \rangle \qquad (i = 1, 2, \ldots, n) \quad (32)$$

Introducing the rates of reaction $d\langle N_i \rangle/dt = -v_i$ ($i = 1, 2, \ldots, n$), we may write (31) as

$$\mathcal{P}_s = \frac{1}{T} \sum_{i=1}^{n-1} v_i \left(kT \ln \frac{\langle N_i \rangle}{\langle N_i \rangle_e} - kT \ln \frac{\langle N_n \rangle}{\langle N_n \rangle_e} \right) \geq 0 \quad (33)$$

where use has been made of $-\sum_{i=1}^{n-1} v_i = v_n$. To prove the final equality and inequality of (33), we use the following observation. We first consider the behavior of (28). It is then shown that if $p_i(t) \geq q_i$, then

$$\sum_{l=1}^{n-1} a_{il} \exp(-\lambda_l t) \geq 0 \quad (34)$$

$$\frac{dp_i(t)}{dt} = -\sum_{l=1}^{n-1} a_{il} \lambda_l \exp(-\lambda_l t) \leq 0 \quad (35)$$

while if $p_i(t) < q_i$, then

$$\sum_{l=1}^{n-1} a_{il} \exp(-\lambda_l t) < 0 \quad (36)$$

$$\frac{dp_i(t)}{dt} = -\sum_{l=1}^{n-1} a_{il} \lambda_l \exp(-\lambda_l t) > 0 \quad (37)$$

Now, with the help of (28), we may write (30) in the form

$$\mathcal{P}_s = kN \sum_{i=1}^{n-1} \sum_{l=1}^{n-1} a_{il} \lambda_l \exp(-\lambda_l t) \times \ln \left\{ \frac{1 + \frac{1}{q_i} \sum_{l=1}^{n-1} a_{il} \exp(-\lambda_l t)}{1 - \frac{1}{q_n} \sum_{i=1}^{n-1} \sum_{l=1}^{n-1} a_{il} \exp(-\lambda_l t)} \right\} \quad (38)$$

where $\sum_{l=1}^{n-1} a_{nl} \exp(-\lambda_l t) = -\sum_{i=1}^{n-1} \sum_{l=1}^{n-1} a_{il} \exp(-\lambda_l t)$ has been used. It therefore follows from (34)–(37) that $\mathcal{P}_s \geq 0$, that is, the entropy production is always nonnegative.

Entropy and Fluctuation

In the present section, we shall investigate whether the relation between entropy and fluctuation[17] may be obtained on the basis of the definition of stochastic entropy established in the previous sections. The rate equations 19, 20, and 32, which have been stochastically derived, are consistent in the mean with the corresponding deterministic rate equations. Since, however, chemical reaction is a random process, the chance fluctuation must be inherent in chemical reaction. It may be expected, therefore, that under certain circumstances the entropy change due to chemical reaction is related to such fluctuations.

For this purpose, we rewrite the stochastic entropy (15) in the form

$$\Delta S/k = -\sum_\gamma \langle N_\gamma \rangle \ln (\langle N_\gamma \rangle / \langle N_\gamma \rangle_e) \quad (39)$$

where $\Delta S = S - S_e$ denotes the deviation of entropy from its equilibrium value. We return again to the reaction $A \rightleftharpoons B$, for which $\Delta S/k$ is written with the use of $\langle N_\gamma \rangle - \langle N_\gamma \rangle_e = \nu_\gamma (\xi - \xi_e)$ as

$$\Delta S/k = -\left\{ [\langle N_A \rangle_e - (\xi - \xi_e)] \ln \left(1 - \frac{\xi - \xi_e}{\langle N_A \rangle_e} \right) + [\langle N_B \rangle_e + (\xi - \xi_e)] \ln \left(1 + \frac{\xi - \xi_e}{\langle N_B \rangle_e} \right) \right\} \quad (40)$$

(17) This is used in the sense of $\langle (X - \langle X \rangle)^m \rangle$ or $\langle (X - \langle X \rangle)^m (Y - \langle Y \rangle)^n \rangle$, where X and Y are random variables and m and n positive integers. Refer also to T. L. Hill, "Statistical Mechanics," McGraw-Hill Book Co., Inc., New York, N. Y., 1956, Chapter 4.

For small deviations from equilibrium this becomes[18]

$$\Delta S/k = -{}^1/_2\frac{\alpha^2}{\langle N_A\rangle_e\langle N_B\rangle_e/N} < 0 \qquad (41)$$

where $\alpha = \xi - \xi_e$. The denominator $\langle N_A\rangle_e\langle N_B\rangle_e/N$ on the right-hand side of (41) is connected with the variance in the following way. Since the variance $\sigma_e^2 = \langle N_A^2\rangle_e - \langle N_A\rangle_e^2$ is given by $\sigma_e^2 = Nq_Aq_B = \langle N_A\rangle_e\langle N_B\rangle_e/N$ from the binomial distribution for equilibrium state, eq 41 is brought in the form

$$\Delta S/k = -{}^1/_2(1/\sigma_e^2)\alpha^2 \qquad (42)$$

This is in agreement with the deterministic formula[19]

$$\Delta_i S/k = -{}^1/_t\left[-\frac{1}{kT}\left(\frac{\partial A}{\partial \xi}\right)_e\right]\alpha^2 \qquad (43)$$

with the chemical affinity A [*cf.* (51)]. Equation 42 is also expressed in terms of time t as

$$\Delta S/k = -{}^1/_2(\alpha^0/\sigma_e)^2\exp[-2(k_1 + k_1')t] \qquad (44)$$

where $\alpha^0 = \xi^0 - \xi_e^0$ for the initial state has been introduced in the course of derivation. Equations 42 and 44, which tell us how entropy has a relation to fluctuation, result only from the stochastic considerations on the process of chemical reaction.

For more understanding of this problem, we consider the consecutive reaction A $\rightleftarrows$ B $\rightleftarrows$ C, for which the probability distribution is given by a trinomial distribution. For this case, we have analogous to (41)

$$\Delta S/k = -{}^1/_2\left\{\left(\frac{1}{\langle N_A\rangle_e} + \frac{1}{\langle N_B\rangle_e}\right)(\xi_1 - \xi_{1,e})^2 - 2\frac{1}{\langle N_B\rangle_e}(\xi_1 - \xi_{1,e})(\xi_2 - \xi_{2,e}) + \left(\frac{1}{\langle N_B\rangle_e} + \frac{1}{\langle N_C\rangle_e}\right)(\xi_2 - \xi_{2,e})^2\right\} \qquad (45)$$

where the degrees of advancement, ξ_1 and ξ_2, have been introduced by the relations $\langle N_A\rangle - \langle N_A\rangle_e = -(\xi_1 - \xi_{1,e})$, $\langle N_C\rangle - \langle N_C\rangle_e = \xi_2 - \xi_{2,e}$ and $\langle N_B\rangle = \langle N_B\rangle_e - (\xi_{1,e} - \xi_{2,e}) + (\xi_1 - \xi_2)$. From the trinomial distribution for equilibrium state, we can obtain the following formulas for fluctuations

$$\frac{1}{(1 - \rho_e^2)\sigma_{1,e}^2} = \frac{1}{\langle N_A\rangle_e} + \frac{1}{\langle N_B\rangle_e} \qquad (46)$$

$$\frac{-\rho_e}{(1 - \rho_e^2)\sigma_{1,e}\sigma_{2,e}} = \frac{1}{\langle N_B\rangle_e} \qquad (47)$$

and

$$\frac{1}{(1 - \rho_e^2)\sigma_{2,e}^2} = \frac{1}{\langle N_B\rangle_e} + \frac{1}{\langle N_C\rangle_e} \qquad (48)$$

where $\sigma_{1,e}^2 = \langle N_A^2\rangle_e - \langle N_A\rangle_e^2 = Nq_A(1 - q_A)$ and $\sigma_{2,e}^2 = \langle N_C^2\rangle_e - \langle N_C\rangle_e^2 = Nq_C(1 - q_C)$ are the variances and $\rho_e = (\langle N_AN_C\rangle_e - \langle N_A\rangle_e\langle N_C\rangle_e)/\sigma_{1,e}\sigma_{2,e} = -\sqrt{q_Aq_C/(1 - q_A)(1 - q_C)}$ is the correlation coefficient ($|\rho_e| \leq 1$).

On the other hand, differentiating the following chemical affinities with respect to ξ_1 and ξ_2

$$A_1 = kT\ln(\langle N_A\rangle/\langle N_A\rangle_e) - kT\ln(\langle N_B\rangle/\langle N_B\rangle_e) \qquad (49)$$

and

$$A_2 = kT\ln(\langle N_B\rangle/\langle N_B\rangle_e) - kT\ln(\langle N_C\rangle/\langle N_C\rangle_e) \qquad (50)$$

where the right-hand sides are obtained in the course of an entropy production such as (22), we find the relations

$$-\frac{1}{kT}\left(\frac{\partial A_1}{\partial \xi_1}\right)_e = \frac{1}{\langle N_A\rangle_e} + \frac{1}{\langle N_B\rangle_e} \qquad (51)$$

$$\frac{1}{kT}\left(\frac{\partial A_1}{\partial \xi_2}\right)_e = \frac{1}{kT}\left(\frac{\partial A_2}{\partial \xi_1}\right)_e = \frac{1}{\langle N_B\rangle_e} \qquad (52)$$

and

$$-\frac{1}{kT}\left(\frac{\partial A_2}{\partial \xi_2}\right)_e = \frac{1}{\langle N_B\rangle_e} + \frac{1}{\langle N_C\rangle_e} \qquad (53)$$

These three relations may also be derived in conventional nonequilibrium thermodynamics, but it is possible from the stochastic point of view that the thermodynamic quantities $(\partial A_1/\partial \xi_1)_e$, $(\partial A_1/\partial \xi_2)_e$, $(\partial A_2/\partial \xi_1)_e$, and $(\partial A_2/\partial \xi_2)_e$ are connected with the fluctuations through relations 46, 47, and 48.

Substituting (46)–(48) into (45), we obtain the expression in terms of the fluctuations $\sigma_{i,e}$ and ρ_e as

$$\Delta S/k = -\frac{1}{2(1 - \rho_e^2)}\left(\frac{\alpha_1^2}{\sigma_{1,e}^2} + 2\rho_e\frac{\alpha_1\alpha_2}{\sigma_{1,e}\sigma_{2,e}} + \frac{\alpha_2^2}{\sigma_{2,e}^2}\right) \qquad (54)$$

where $\alpha_i = \xi_i - \xi_{ie}$. This may reduce to

$$\Delta S = -{}^1/_2\sum_{i,j} g_{ij}\alpha_i\alpha_j \qquad (55)$$

which is in form completely identical with the general formula obtained on the basis of the Gibbs entropy postulate in nonequilibrium statistical mechanics,[20]

(18) Developing (40) in the Taylor series with respect to $\xi - \xi_e$, we obtain

$$\Delta S/k = -{}^1/_2(1/\sigma_e^2)(\xi - \xi_e)^2 \times \left\{1 - {}^1/_3\frac{\langle(N_A - \langle N_A\rangle)^3\rangle_e}{(\sigma_e^2)^2}(\xi - \xi_e) + \ldots\right\}$$

Since $\langle(N_A - \langle N_A\rangle)^3\rangle_e/(\sigma_e^2)^2 = \frac{1}{N}\left(\frac{1}{q_A} - \frac{1}{q_B}\right)$, the absolute value of the second term in the bracket { } is negligibly small compared with 1 for sufficiently large N.

(19) Reference 3, p 47.

(20) Reference 13, p 127.

since we have begun with (16). We should note, however, that in the case of the stochastic nonequilibrium thermodynamics of chemical reaction, the coefficients g_{ij} are explicitly expressed in terms of fluctuations with respect to the numbers of molecules in equilibrium state.

Wettability of Polyethylene Single Crystal Aggregates

by Harold Schonhorn and Frank W. Ryan

Bell Telephone Laboratories, Incorporated, Murray Hill, New Jersey *(Received May 4, 1966)*

The importance of describing fully the detailed physical properties (*e.g.*, density, degree of crystallinity, and molecular weight distribution) of materials to be classified with respect to their critical surface tension of wetting (γ_c) is stressed. This is illustrated by determining the γ_c for a well-characterized preparation of polyethylene single crystal aggregates. The γ_c of the crystalline polyethylene is shown to be 53.6 dynes/cm compared to the generally accepted value of 31 dynes/cm. An analysis based on Fowkes' approach to wettability data is consistent with our results.

Investigations in surface chemistry as applied to the wettability of polymers[1] have failed generally to specify with any precision the detailed physical properties (*e.g.* density, degree of crystallinity, and molecular weight distribution) of the materials to be classified with respect to their critical surface tension of wetting (γ_c). In this communication we shall endeavor to demonstrate the importance of describing fully the preparation of samples employed in wettability studies. We shall demonstrate that, for example, a variation in the surface density (ρ_S) of a polymer will change the critical surface tension of wetting.

Recently, Roe,[2] and Lee, Muir, and Lyman[3] have called attention to the concept of the density of the surface layer of polymers as being important in determining their ultimate wettability. To obtain agreement between the accepted critical surface tensions of wetting (γ_c) at 20° and empirical calculations based on the parachor concept, the above authors[2,3] had to employ the amorphous densities of the polymers. However, there is no *a priori* reason for choosing the amorphous density since polymers may assume a range of densities depending upon their molecular weight and degree of crystallinity, while retaining their chemical constitution. Polyethylene, for example, the subject of this investigation, has an amorphous bulk density (ρ_B) of 0.855 g/cm^3,[4] and a crystalline bulk density of 1.000 g/cm^3,[5] at 20°. Therefore, in principle, polyethylene should assume a spectrum of surface densities and γ_c values depending upon the ratio of amorphous to crystalline polymer present in the surface layer of the specimen.

Invariably, the polymer specimens which are employed in wettability experiments are of the melt-crystallized variety. That is, they are molded in the melt against a smooth surface, then cooled. Polymer molecules which cannot be accommodated into the crystal lattice during crystallization are rejected to the

(1) E. Wolfram, *Kolloid-Z.*, **182**, 75 (1962); K. L. Wolf, *Z. Physik. Chem.* (Leipzig), **225**, 1 (1964); V. R. Gray, *Forest Prod. J.*, **12**, 452 (1962); A. V. Neumann and P. J. Sell, *Z. Physik. Chem.* (Frankfurt), **41**, 183, 191 (1964).

(2) R. J. Roe, *J. Phys. Chem.*, **69**, 2809 (1965).

(3) I. J. Lee, W. M. Muir, and D. J. Lyman, *ibid.*, **69**, 3220 (1965).

(4) G. Allen, G. Gee, and G. J. Wilson, *Polymer*, **1**, 456 (1960).

(5) P. H. Geil, "Polymer Single Crystals," Interscience Publishers, Inc., New York, N. Y., 1963.

surface region and reside there in an amorphous or liquid-like state.[6] Apparently, polymers which have been melt crystallized have surface regions which have densities corresponding to the amorphous solid. Therefore, we decided to observe the effect of density on the wettability of polyethylene by using single crystal aggregates to determine γ_c. In this case, we would expect that the surface density would more closely approximate the bulk density, that is, $\rho_S \cong \rho_B$. Since the wettability of a polymer is governed solely by the nature of the outermost functional group,[7] orientation effects are probably unimportant with respect to the critical surface tension of wetting. However, orientation effects are important when solid–liquid interfacial tensions are considered.[5] For example, single-crystal aggregates of polyethylene have both a lateral and fold surface structure associated with them. The fold surface interfacial tension that exists at the crystal–melt interface has been estimated to be about 70 ergs/cm^2,[5] while the lateral surface interfacial tension is about 10 ergs/cm^2.[5]

Since Roe[2] has indicated that the critical surface tension of wetting is proportional to the fourth power of the amorphous density for polyethylene ($\gamma_c \propto \rho^4$), we should expect to obtain greater values of γ_c for polyethylene single-crystal aggregates where the surface density more closely approximates the bulk density of the polymer. If a surface density of 1.00 g/cm^3 for polyethylene were achieved, then we should expect a value of $\gamma_c > 60$ dynes/cm. If this were the case, it would show that an important parameter in wettability studies is the number of functional groups per square centimeter of polymer surface that interact with the wetting liquid. In effect, both the surface density of these functional groups and their chemical nature would govern the wettability with respect to a given liquid.

Experimental Section

1. Preparation of Polyethylene Single Crystals. Aggregates of crystals of linear polyethylene, having one branch per 1000 carbon atoms, $\bar{M}_w$ = 66,000 as determined from both light scattering and gel permeation chromatography (gpc) and $\bar{M}_n$ = 6000 as determined from gel permeation chromatography (Marlex 6000 series, Type 50, Phillips Petroleum Co., Bartlesville, Okla.) grown from 0.04% solution in xylene (Fisher, Certified ACS grade) have been studied. While gpc may not ordinarily be an absolute technique, it is here because of calibration with known fractions of linear polyethylene. Crystals were prepared by dissolving a portion of polyethylene in boiling xylene then pouring this solution into a larger volume (10×) of xylene thermostated at 85° to give a final concentration of 0.04%. The solution was allowed to crystallize overnight at 85° and then was filtered at 85°. Essentially none of the starting material remained in solution after filtration. Therefore, the molecular weight distribution of the single crystal aggregates was similar to the original material. When the solution was allowed to crystallize at 85° for 1 hr and then filtered at 85°, only 50% of the starting material was recovered. In this case, the molecular weight distribution was still broad, but the intrinsic viscosity of this preparation was greater than the original polymer. However, the wettability results obtained with both preparations were essentially identical. Crystals formed under both these conditions at 85° were essentially monolayer truncated lozenges while those formed at 75° and below are ridged true lozenges or dendrites.[8] Films formed by filtering crystals from suspension were dried at 40° in a vacuum oven for a minimum of 16 hr. The amount of solvent retained in a specimen was obtained by mass spectrophotometric analysis of gases evolved on melting samples at 150°.[9] In these thin films of single crystals, no xylene was noted after drying in the vacuum oven. The mats of single crystals prepared in the above manner were slowly formed into thin disks at pressures of 20,000 psi and a temperature of 20° in a die having a specularly smooth finish. Pressure was maintained for a period of several minutes. As a precaution, the die was cleaned scrupulously and air dried. This produced a glossy almost clear specimen suitable for wettability studies. X-Ray diffraction and infrared transmission analysis revealed no apparent changes in crystallinity before and after pressing the polymer mat into disks. The densities of the filtered mat and the molded polyethylene single crystals were both 0.972 g/cm^3, as measured with a density gradient column.

2. Contact Angle Measurements. For the contact angle measurements, the polyethylene film composed of single-crystal aggregates was mounted on a standard microscope slide, employing double-backed adhesive tape.

The advancing contact angles were measured directly by employing a telescopic device equipped with an ocular protractor which was built by the Gaertner Scientific Corp., Chicago, Ill. Three separate drops of the wetting liquid were placed on the polymer surface with opposite edges of the drops being measured. The surface tensions of the wetting liquids were measured prior to

(6) H. D. Keith and F. J. Padden, *J. Appl. Phys.*, **35**, 1270, 1286 (1964).

(7) W. A. Zisman, Advances in Chemistry Series, No. 43, American Chemical Society, Washington, D. C., 1964, p 1.

(8) D. C. Bassett and A. Keller, *Phil. Mag.*, **7**, 81 (1962).

(9) R. Salovey and D. C. Bassett, *J. Appl. Phys.*, **35**, 3216 (1964).

the wetting experiments. Excellent agreement with literature values for the γ_{LV} of the test liquids were obtained. The drops were equilibrated for a minimum of 10 min prior to reading the contact angle. The reproducibility of the readings was about ±2°. Subsequently, the pressed crystal aggregate was washed alternately in hexane and detergent, dried, and the wettability redetermined for both cleaning procedures. No significant changes in the contact angles were observed.

Analysis of Wettability Theory

It has been suggested that[10]

$$(\gamma_{SV}^{c} - \gamma_{SL}^{c}) \cong (\gamma_{SV}^{ac} - \gamma_{SL}^{ac}) \cong (\gamma_{SV}^{a} - \gamma_{SL}^{a}) \quad (1)$$

when

$$\rho_S^{c} \cong \rho_S^{ac} \cong \rho_S^{a} \quad (2)$$

where the superscripts a, ac, and c refer to amorphous, partially crystalline, and crystalline, respectively. In addition, it has been suggested that[10]

$$\gamma_{SV}^{a} = \gamma_{LV} = \gamma_c \quad (3)$$

where γ_{SV}^{a} is the surface free energy of the amorphous solid. If there is a difference in the density of the crystalline and amorphous states, then eq 1 may no longer be valid. Therefore, we suggest that

$$(\gamma_{SV}^{c} - \gamma_{SL}^{c}) \geq (\gamma_{SV}^{ac} - \gamma_{SL}^{ac}) \geq (\gamma_{SV}^{a} - \gamma_{SL}^{a}) \quad (4)$$

is probably true for the more general case when

$$\rho_S^{c} \geq \rho_S^{ac} \geq \rho_S^{a} \quad (5)$$

However, there may possibly be exceptions as in the case of poly-4 methylpentene-1, where it has been reported that $\rho_S^{a} > \rho_S^{c}$.[11]

We shall attempt to obtain a more useful form of eq 4 by employing the Fowkes expression[12]

$$(\gamma_{SV} - \gamma_{SL}) = 2(\gamma_{SV}^{d}\gamma_{LV}^{d})^{1/2} - \gamma_{LV} \quad (6)$$

where the superscript d refers to the dispersion component of the surface free energy of the solid. Previously, we suggested that[10]

$$(\gamma_{SV}^{a,ac,c} - \gamma_{SL}^{a,ac,c}) = 2(\gamma_{SV}^{ad}\gamma_{LV}^{d})^{1/2} - \gamma_{LV} \quad (7)$$

When $\rho^{ac,c} > \rho_S^{a}$, we have

$$\gamma_{SV}^{(ac,c)d} = (\gamma^*_{LV})_{ac,c}^{d} \neq \gamma_{LV}^{d} \quad (8)$$

where $(\gamma^*_{LV})^{d}$ is the dispersion component of the surface tension for a liquid having a density equivalent to ρ_S^{c} or ρ_S^{ac}.

Since Roe[2] and Lee, Muir, and Lyman[3] have shown that eq 9 occurs in the following relation

$$\gamma_{LV} = \left(\frac{P}{M}\rho_S^{a}\right)^4 \quad (9)$$

it is plausible to state that

$$(\gamma^*_{LV})_{ac,c} = \left(\frac{P}{M}\rho_S^{ac,c}\right)^4 \quad (10)$$

Combining eq 9 and 10 yields

$$(\gamma^*_{LV})_{ac,c} = \gamma_{LV}\left(\frac{\rho_S^{ac,c}}{\rho_S^{a}}\right)^4 \quad (11)$$

Substituting eq 11 into the geometric mean term of eq 7 we obtain

$$(\gamma_{SV}^{a,ac,c} - \gamma_{SL}^{a,ac,c}) = 2\left(\frac{\rho_S^{ac,c}}{\rho_S^{a}}\right)^2 [(\gamma_{LV}^{d})_p\gamma_{LV}^{d}]^{1/2} - \gamma_{LV} \quad (12)$$

where the subscript p refers to the polymer. Equation 12 is equivalent to eq 6 when $\rho_S^{ac,c} = \rho_S^{a}$.

To estimate the contact angle of a wetting liquid on the crystalline or partially crystalline polymer surface, eq 12 is employed with the Young equation. The general form of the Young equation for polymers becomes

$$(\gamma_{SV}^{a,ac,c} - \gamma_{SL}^{a,ac,c}) = \gamma_{LV}(\cos\theta)_{a,ac,c} \quad (13)$$

Combining eq 12 and 13 yields

$$(\cos\theta)_{a,ac,c} = \frac{2\left(\frac{\rho_S^{a,ac,c}}{\rho_S^{a}}\right)^2 [(\gamma_{LV}^{d})_p\gamma_{LV}^{d}]^{1/2}}{\gamma_{LV}} - 1 \quad (14)$$

Table I: The Calculated Contact Angles at 20° of Polar Liquids on Polyethylene Single Crystals Employing Eq 14

T, °C	ρ_S^{c}, g/cm³	ρ_S^{a}, g/cm³	$(\gamma_{LV}^{d})_p$,[a] dynes/cm	γ_{LV}, dynes/cm	γ_{LV}^{d}, dynes/cm	θ_{calcd}, deg	θ_{exptl}, deg
Water–Polyethylene Single Crystals							
20	0.972	0.855	36.2	72.8	21.8	90.3	93
Glycerol–Polyethylene Single Crystals							
				63.4	37.0	60.6	67
Formamide–Polyethylene Single Crystals							
				58.2	39.5	≤7.1	55

[a] Reference 15.

(10) H. Schonhorn, *J. Phys. Chem.*, **69**, 1084 (1965).

(11) J. H. Griffith and B. G. Ranby, *J. Polymer Sci.*, **44**, 360 (1960).

(12) F. M. Fowkes, *J. Phys. Chem.*, **66**, 1863 (1962); **67**, 2538 (1963); Advances in Chemistry Series, No. 43, American Chemical Society, Washington, D. C., 1964, p 99.

Table II: Wettability of Polyethylene at 20°

Liquid	γ_{LV}, dynes/cm	γ_{LV}^d, dynes/cm	$\sqrt{\gamma_{LV}^d}/\gamma_{LV}$, l./(dynes/cm)$^{1/2}$	Single crystal: θ, deg	Single crystal: Cos θ	Melt crystallized: θ,[a] deg	Melt crystallized: Cos θ[a]
Water	72.8	21.8	0.0641	93	−0.052	94	−0.070
Glycerol	63.4	37.0	0.0959	67	0.391	79	0.191
Formamide	58.2	39.5	0.1080	55	0.574	77	0.225
Methylene iodide	50.8	48.5	0.1404	40	0.760	52	0.616
α-Bromonaphthalene	44.6	44.6	0.1497	Spreads	1.000	35	0.818

[a] Reference 7.

The calculated values for the contact angles of several liquids on the polyethylene single crystal aggregates at 20° are shown in Table I.

Results

The wettability data for the pressure-molded aggregates of the polyethylene single crystals are presented in Table II. There is a significant difference in the advancing contact angles between the usual melt-crystallized polymer and the compressed single crystal aggregates for all the liquids employed except water. If we mold the single crystal aggregates of polyethylene above their melting point and cool rapidly or slowly, we again have the situation of a low γ_c, indicative of an amorphous surface layer.

A Zisman[7] type plot of the data in Table II for cos θ *vs.* γ_{LV} is shown in Figure 1. A narrow rectilinear band is obtained with an extrapolated range for γ_c of 44.6–47.2 dynes/cm. A Fowkes-type plot is shown in Figure 2. In this representation, cos θ is plotted as a function of $(\gamma_{LV}^d)^{1/2}/\gamma_{LV}$. Table II itemizes the accepted values of γ_{LV}^d for the wetting liquids. Apparently, the γ_{LV}^d for methylene iodide used in plotting Figure 2 is too high. The normal behavior of the Zisman plot strongly suggests that this is the case. The value proposed by Fowkes[13] for γ_{LV}^d of methylene iodide is 48.5 ± 9 dynes/cm. A value for γ_{LV}^d of about 40 dynes/cm would give better agreement with the linear representation in Figure 2. When cos θ = 1, then $\gamma_{LV}/(\gamma_{LV}^d)^{1/2} = (\gamma_{SV}^d)^{1/2}$. The value of γ_{SV}^d obtained from Figure 2 is 53.6 dynes/cm. It should be noted in this connection that the Fowkes-type plot yields a higher value for γ_{SV}^d or γ_c than the plot of Zisman. For melt-crystallized polyethylene, γ_c = 31 dynes/cm,[7] while employing the same contact angle data in a Fowkes-type representation $\gamma_{SV}^d \cong 35$ dynes/cm.[13]

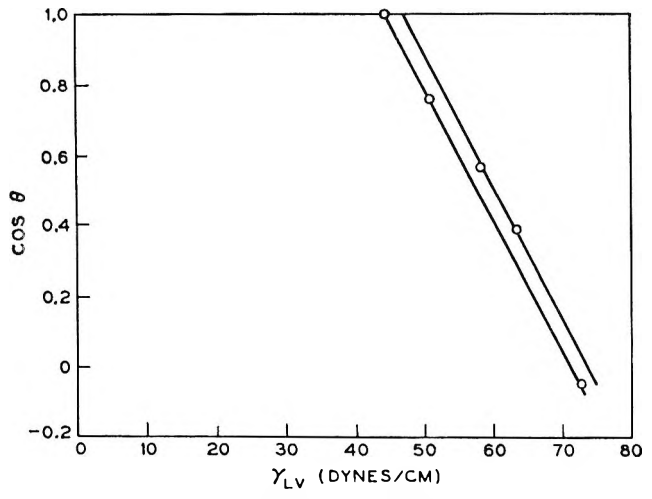

Figure 1. The critical surface tension of wetting for polyethylene single crystals is determined in a Zisman-type plot. A narrow rectilinear band results in an extrapolated range for γ_c between 44.6 and 47.2 dynes/cm.

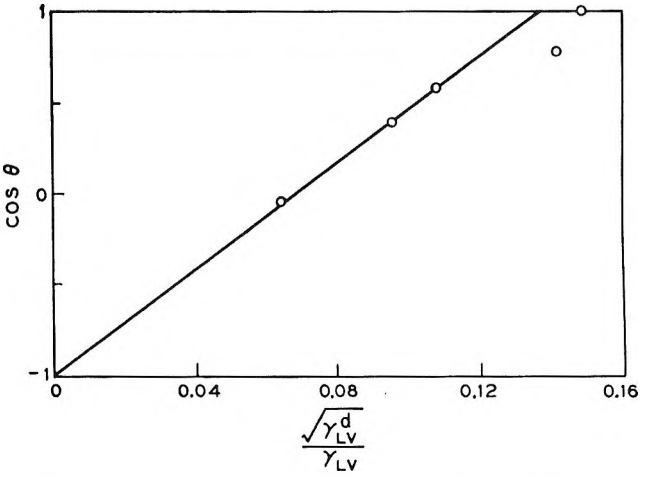

Figure 2. The wettability of polyethylene single crystals is shown in a Fowkes-type representation. The extrapolated value of 53.6 dynes/cm is similar to the values obtained in Figure 1.

Discussion

One implication of the present work is that wettability is not dependent solely upon the constitution of

(13) F. M. Fowkes, ASTM Special Technical Publication No. 360, 1964, p 20.

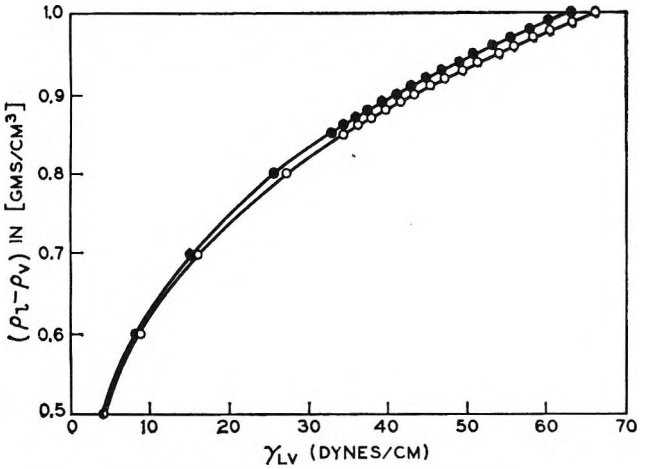

Figure 3. The density of the homologous series of *n*-hydrocarbons is plotted against their respective surface tensions as calculated employing the parachor concept. Two curves corresponding to parachor values of 39.0 and 40.0 are represented.

the surface. As evidenced from this investigation, polyethylene may assume a γ_c greater than that obtained for many polar polymers if the surface is crystalline. This investigation indicates the necessity to characterize fully any polymer studied with respect to preparation, degree of crystallinity, and history of the sample.

The liquid-like behavior in the surface region of melt-crystallized polymers is shown in Table III. The γ_c for several polymers are compared to the extrapolated values of their melt surface tensions. This suggests that eq 3 is appropriate for melt-crystallized nonpolar polymers. Apparently, this is why the parachor concept has been useful in analyzing wettability data.

Figure 3 illustrates the effect of density on the surface tension for a homologous series of *n*-hydrocarbons. The density is plotted against the calculated surface tensions for two parachor values. Parachors of 39.0 and 40.0 were chosen to be representative of the *n*-hydrocarbon series.[14] The density of the vapor at 20° is insignificant with respect to ρ_L. The density of 0.855

Table III: A Comparison of the Extrapolated Values for the Surface Tension of Several Polymers and Their Critical Surface Tension of Wetting

Polymer	γ_{LV}^{20}, dynes/cm	γ_c^{20}, dynes/cm
Polyethylene	36.2[a]	31[b]
Polypropylene	28.0[c]	29[b]
Poly(chlorotrifluoro-ethylene)	30.8[d]	31[b]
Poly(dimethylsiloxane)	20.6[e]	22[b]
	21.6[f]	
Polystyrene	32.4[g]	33[b]

[a] Reference 15. [b] Reference 7. [c] H. Schonhorn and L. H. Sharpe, *J. Polymer Sci.*, **B3**, 235 (1965). [d] H. Schonhorn, F. W. Ryan, and L. H. Sharpe, *J. Polymer Sci.*, **A2**, 538 (1966). [e] Reference 2. [f] H. Tarkow, *J. Polymer Sci.*, **27**, 35 (1958). T = 30°. [g] J. E. Marian, ASTM Special Technical Publication No. 340, 1963, p 122.

g/cm^3 for amorphous polyethylene yields a calculated surface tension of 35.4 dynes/cm for P = 40.0 and 33.6 dynes/cm for P = 39.0. Apparently, P = 40.0 is more appropriate for amorphous polyethylene since γ_{LV}^{20} is 36.2 dynes/cm.[15] It is obvious from Figure 3 that for a hypothetical *n*-hydrocarbon liquid having a density of 1.000 g/cm^3, the projected density for an ideal single crystal of polyethylene at 20°.

$$\gamma^*_{LV} = 66.1 \text{ dynes/cm} = \gamma_c$$

If the surface of the polymer consisted of both amorphous and crystalline regions, then we should expect a spectrum of γ_c values ranging from 35.4 dynes/cm for the completely amorphous surface layer to 66.1 dynes/cm for the completely crystalline surface layer. Consequently, it appears that

$$35.4 \text{ dynes/cm} \leqslant \gamma_c \leqslant 66.1 \text{ dynes/cm}$$

is appropriate for polyethylene.

(14) O. R. Quayle, *Chem. Rev.*, **53**, 439 (1953).

(15) H. Schonhorn and L. H. Sharpe. *J. Polymer Sci.*, **A3**, 569 (1965).

Effect of Self-Association on the Spectrophotometric Determination of Association Constants. A Computational Analysis

by Donald W. Tanner[1] and Thomas C. Bruice[2]

Department of Chemistry, University of California, Santa Barbara, California *(Received May 6, 1966)*

Association constants, calculated *via* the Benesi–Hildebrand method, contain inherent errors if either reactant self-associates to an observable extent. Moreover, the errors are not usually detectable from nonlinearity of the graphical plots. Synthetic data were generated and corresponding errors calculated *via* a computer for various combinations of extinction coefficients, association, and self-association constants. Experimental precautions and alternative methods of calculation of association constants are given.

Spectrophotometry is widely used to measure association constants where either reactant or product species appreciably absorbs radiation. The approaches of Benesi and Hildebrand,[3] Scott,[4] Rose and Drago,[5] and recently of Conrow, *et al.*,[6] Johnson and Bowen,[7] and De Tar and Silverstein,[8] are important graphical or mathematical methods for computing the association constant and molar extinction coefficients from optical density data. Conrow, *et al.*,[6] have stressed the importance of error analyses in reporting association constants and especially note the large errors induced in computer-calculated K and ϵ values caused by experimental errors and synthetic input error data. Also noteworthy was the evidence that the linearity of Benesi–Hildebrand plots (B–H plots) is an insufficient criterion for the existence of only 1:1 charge-transfer complexes. With many combinations of synthetic input parameters, K_1, K_2,[9] and ϵ_i, calculated deviations from linearity were not appreciably greater than expected from induced experimental errors except at relatively high complex concentrations.[7]

The purpose of the present work is to show that large errors may be induced in calculated association constants when reactants self-associate, as in the equilibria

$$aA + bB \overset{K}{\rightleftharpoons} C \quad (1)$$

$$nB \overset{K_n}{\rightleftharpoons} B_n \quad (2)$$

$$mA \overset{K'_m}{\rightleftharpoons} A_m \quad (3)$$

It will be assumed herein that the self-associated polymer is unreactive toward the second reactant.

The B–H plots of spectrophotometric data of these equilibria are similarly nearly linear within experimental error (except at high values of K_n). Examples are to be found in the equilibria between phenols and the various borate complexes and between amines and formaldehyde polymers in aqueous solutions.[10]

For simplicity, since $[B]_0 \gg [A]_0$ in the B–H treatment, this study can be divided into three cases, differing in mathematical treatment.

Case I.	B	self-associates
	A, C	absorb
Case II.	A	self-associates
	A, C	absorb
Case III.	A or B	self-associates
	A, B	absorb

(1) N.I.H. Predoctoral Fellow (1963–1966). Part of the work to be submitted by D. W. T. in partial fulfillment for the Ph.D. degree, Cornell University.

(2) To whom reprint requests should be addressed.

(3) H. A. Benesi and J. H. Hildebrand, *J. Am. Chem. Soc.*, **71**, 2703 (1949).

(4) R. L. Scott, *Rec. Trav. Chim.*, **75**, 787 (1956).

(5) N. J. Rose and R. S. Drago, *J. Am. Chem. Soc.*, **81**, 6138, 6141 (1959).

(6) K. Conrow, G. D. Johnson, and R. E. Bowen, *ibid.*, **86**, 1025 (1964).

(7) G. D. Johnson and R. E. Bowen, *ibid.*, **87**, 1655 (1965).

(8) D. F. De Tar and R. Silverstein, *ibid.*, **88**, 1013 (1966).

Case III will not be treated in detail here since it may be considered as an extension of the first two cases.

For case I, the following relationships pertain

$$K_n = \frac{[B_n]}{[B]^n} \tag{4}$$

$$[B]_0 = [B] + nK_n[B]^n \tag{5}$$

$$OD_i = \epsilon_A([A]_0 - a[C]) + \epsilon_C[C] \tag{6}$$

where OD_i is the optical density of the system (A,B,C) at equilibrium at initial concentrations $[A]_0$ and $[B]_0$. Defining an *apparent* equilibrium constant, K', as

$$K' = \frac{[C]}{([A]_0 - a[C])^a[B]_0^b} \tag{7}$$

and eliminating [C] from (6) and (7) gives, for the special case where $a = b = 1$, the rearranged B–H equation as

$$\frac{[A]_0(\epsilon_A - \epsilon_C)}{OD_i - \epsilon_A[A]_0} = \frac{1}{K'}\frac{1}{[B]_0} + 1 \tag{8}$$

Plotting the left-hand side *vs.* $1/[B]_0$ furnishes the value of $(-)K'$ as x intercept. Substituting (5) into (7) yields

$$K' = K\frac{1}{(1 + nK_n[B]^{n-1})^b} \tag{9}$$

Since [B] in (9) depends upon $[B]_0$, then K' will likewise depend upon $[B]_0$. Thus, the slope of (8) is not constant with varying $[B]_0$; consequently, the resulting B–H plot should be nonlinear and the calculated x intercept should vary depending upon the range of $[B]_0$ chosen experimentally.

For case II, the equilibrium constant may be expressed as

$$K = \frac{[C]}{([A]_0 - n[A_n] - a[C])^a[B]_0^b} \tag{10}$$

The optical density will be given by the Beer–Lambert law as

$$OD_i = \epsilon_A([A]_0 - n[A_n] - a[C]) + \epsilon_{An}[A_n] + \epsilon_C[C] \tag{11}$$

Derivation of an exact B–H equation in this case is precluded since there are now two concentration variables $[A_n]$ and [C], only one of which may be eliminated from (10) and (11). No prediction can therefore be made regarding linearity of B–H plots of experimental data of case II.

Experimental Section

To establish an upper limit for K_n above which curvature of the B–H plot would be experimentally observable and/or where the error in calculated K is less than 10%, synthetic data were generated and plotted *via* an IBM 1620 II computer for the simplest mathematical case, *i.e.*, $n = 2$ in (2) and (3). For case I, three values of K, eight values of K_2, three values of ϵ_A, and nine values of ϵ_C were used as parameters with $[A]_0 = 1.3 \times 10^{-4}$ *M*. For case II, three values of K, eight values of K_2, three values of ϵ_A, six values of ϵ_{A_2}, and seven values of ϵ_C were used with $[A]_0 = 2.0 \times 10^{-4}$ *M*. The optical density values so calculated fell with the practical limits of 0–1.5 OD units.

Utilizing nearly all combinations of given parameters, optical density data were computed over a range in $[B]_0$ from 0.01 to 0.10 *M*. The data were treated *via* eq 8 and fitted by the method of least-squares. Ordinate

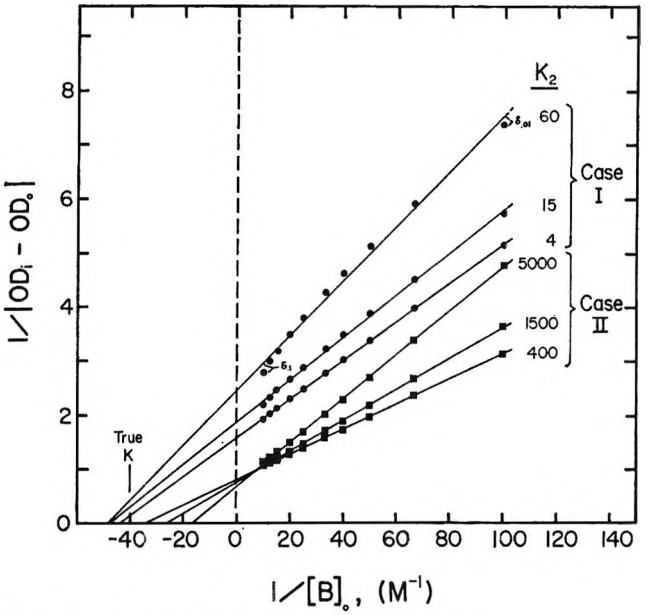

Figure 1. Benesi–Hildebrand plots of synthetic spectrophotometric input data. The circles (●) represent case I computations with ϵ_A 6000 and ϵ_C 500. The square symbols (■) represent case II data with ϵ_A 10, ϵ_{A_2} 100, and ϵ_C 6000. The parameter K_2 is the self-association constant and $K = 40$ in each plot. Curvature of case I plots is concave downward whereas for case II plots it is slightly concave upward. δ represents the deviation of the reciprocal of ΔOD from the least-squares line. δ corresponds to an error in ΔOD of 0.021 at $[B]_0 = 0.10$ *M* but only 0.003 OD unit at $[B]_0 = 0.01$ *M*.

(9) K_1 and K_2 are association constants for AB and AB_2 (or AB and A_2B).

(10) D. W. Tanner and T. C. Bruice, unpublished data; P. S. Skell and D. W. Tanner, unpublished data.

Table I: Synthetic Data and the Various Computed Errors in the Benesi–Hildebrand Treatment of Equilibria When Reactants Dimerize

	ϵ_A	ϵ_{A_2}	ϵ_C	K	K_2	K_2/K	$\Delta OD_{0.1}$[a]	$\Delta OD_{0.01}$[a]	Mole fraction of dimer[b]	PERK	PERXI	PSXI[c]
						Case I[d]						
1	6000		0	40	25	0.625	0.460	0.177	0.472	21.8	4.0	5.1
2	6000		0	40	8	0.20	0.533	0.203	0.301	16.1	1.7	4.5
3	500		8000	80	16	0.20	0.754	0.380	0.404	4.3	2.8	2.7
4	500		8000	80	8	0.10	0.791	0.402	0.301	5.3	1.6	2.6
5	500		8000	80	4	0.05	0.819	0.416	0.207	4.5	0.8	2.5
6	500		8000	40	16	0.40	0.613	0.236	0.404	20.2	3.0	3.8
7	500		8000	40	8	0.20	0.666	0.253	0.301	16.1	1.7	3.6
8	500		8000	40	4	0.10	0.706	0.265	0.207	11.3	0.8	3.4
9	500		8000	20	16	0.80	0.448	0.134	0.404	51.9	3.5	7.2
10	500		8000	20	8	0.40	0.505	0.145	0.301	37.7	2.1	6.9
11	500		8000	20	4	0.20	0.554	0.153	0.207	24.9	1.0	6.9
						Case II[e]						
1	6000	6000	1000	20	800	40	0.540	0.113	0.113	−32.9	0.8	13.6
2	6000	6000	10	20	800	40	0.670	0.141	0.113	−31.6	0.8	10.8
3	6000	10	10	20	800	40	0.569	0.113	0.113	−38.9	0.8	14.6
4	10	100	6000	40	800	20	0.945	0.299	0.113	−22.3	1.1	3.2
5	10	100	6000	40	400	10	0.951	0.318	0.067	−13.0	0.7	3.0
6	10	100	6000	40	200	5	0.955	0.329	0.036	−7.2	0.4	2.8
7	10	100	6000	20	800	40	0.771	0.168	0.11	−26.4	0.8	8.6
8	10	100	6000	20	400	20	0.784	0.181	0.067	−15.9	0.5	7.3
9	10	100	6000	20	200	10	0.792	0.189	0.036	−8.9	0.3	6.6

[a] Absolute value of $OD_i - OD_{[B]_0}$ computed at $[B]_0 = 0.10\ M$ (or 0.01 M). [b] Defined as $[X_2]/([X] + [X_2])$. Case I, computed at $[B]_0 = 0.10\ M$. Case II, computed at $[B]_0 = 0$. [c] Standard deviation of x intercept with $\sigma_{OD} = \pm 0.002$ OD unit. [d] $[B]_0 \gg [A]_0$, B dimerizes. [e] $[B]_0 \gg [A]_0$, A dimerizes.

values [$1/\Delta OD$, *i.e.*, $1/|OD_i - OD_{[B]=0}|$] over the entire range and the ratio [C]/[A] at the extremes of concentration of $[B]_0$ (*i.e.*, 0.01 and 0.10 M) were also computed. The ratio of [C]/[A] was found to be in the range of 6–0.2 for optimum experimental accuracy.[11] The criterion of Person was satisfied for each value of K chosen.[12]

Two types of error due to self-association were computed in each instance: (1) PERK–the per cent deviation of the calculated K (*i.e.*, the extrapolated x intercept of the B–H plot) from the input K, and (2) PERXI—the per cent variation of the calculated K due only to nonlinearity of the points of the B–H plot. The error PERXI is derived from a standard least-squares error analysis and would have the value of 0.0, were there no self-association, since the synthetic points would then be colinear.

For each set of a few selected values of the input parameters, all calculated OD values were assigned the reasonable standard deviation of 0.002. From this value the standard deviation of the x intercept yields PSXI, the per cent variation of the calculated K due to experimental errors in OD measurement (see Table I). Calculations with other values of σ_{OD} (0.001, 0.003, 0.005, or 0.010) yielded proportional values of PSXI (not shown in Table I).

Discussion

Inspection of Table I reveals that the error PERK due to self-association is the largest error one would encounter under the given conditions. PERK errors are independent of input ϵ values for case I and nearly so for case II. PSXI generally falls within 2–10% inversely proportional to the ΔOD value. The nonlinearity errors PERXI are surprisingly small, but should be seen graphically for data of case I at higher K_2 values (see Figure 1, $K_2 = 60$). Plots of case II data, however, show striking linearity. Thus, PERK errors as large as 80% may be incurred before curvature would be detected graphically. The two cases differ further in that (1) fractions of dimer A_2 higher than 0.05 cause PERK errors greater than 10%, whereas in case I, 0.30

(11) T. C. French and T. C. Bruice, *Biochemistry*, **3**, 1589 (1964); **4**, 77 (1965).

(12) W. B. Person, *J. Am. Chem. Soc.*, **87**, 167 (1965).

of B_2 may give PERK errors no higher than 10%, (2) at any constant K_2/K ratio, the PERK errors increase in case I as the absolute value of K_2 decreases, but decrease in case II as K_2 decreases, and (3) PERK errors in case I are always positive and in case II always negative. Interestingly, as $[B]_0$ is raised indefinitely, the extrapolated K' value approaches zero for any K for case I.

Sillén[13] has pointed out the various criteria for regression least-squares analysis. Two of these criteria are not met by any regression analysis of B–H plots (*i.e.*, an error in ΔOD shows a more pronounced deviation in the upper part of the plot as seen in Figure 1).

In measuring association constants, care should be taken to avoid the inherent, large errors induced by the B–H treatment, if (2) or (3) be present. For case I, if either ϵ_C (or ϵ_A) is negligibly small or if at any wavelength the ratio of ϵ_C/ϵ_A is known, K' should be computed by eq 7 at various values of $[B]_0$. Extrapolation of the so calculated K' values to zero $[B]_0$ provides the true association constant K. If the ϵ values are similar and ϵ_C is unknown, K_2 might be obtained by studying B solutions separately by previously described methods.[6,8,14]

If self-association is otherwise suspected, each reactant must be separately studied in very dilute solutions in order to detect deviations from the Beer–Lambert law and variations in shape of the ultraviolet (or visible) spectra over the experimental range of concentrations. If $\epsilon_{A_n(B_n)} = n\epsilon_{A(B)}$ at all wavelengths, separate spectral determination of K_n is impossible (this situation would pertain if the molecules self-associated leaving their exposed chromophonic groups completely unperturbed).

In case II, appreciable errors (10%) in K are caused by the presence of very small fractions of polymer, amounts which might escape spectrophotometric detection even though A_2 absorbs comparably to A. In such cases of self-association, the B–H treatment should not be used.

Obviously, these inherent errors would be encountered using modifications of the original Benesi–Hildebrand equation. Specifically, PERK errors of similar magnitude were found by treating synthetic data of the present study by the Scott equation.[4] In addition, where the dimer complexes further with the second reactant, computed PERK errors from the B–H treatment diminished in magnitude.

Although the numerical treatment presented herein applies only to the case of a bimolecular reaction occurring in the presence of a dimer, presumably similar PERK errors would be encountered if higher polymeric species (and combinations thereof) were involved.

Acknowledgment. This work was supported by a grant from the National Institutes of Health.

(13) L. G. Sillén, *Acta Chem. Scand.*, **16**, 159 (1962).

(14) F. J. C. Rossotti and H. Rossotti, "The Determination of Stability Constants," McGraw-Hill Book Co., Inc., New York, N. Y., 1961.

The Ionization Constant of Deuterium Oxide from 5 to 50°

by A. K. Covington,[1] R. A. Robinson, and Roger G. Bates

National Bureau of Standards, Washington, D. C. *(Received May 9, 1966)*

Electromotive force measurements of a cell without liquid junction have been used to determine the ionization constant of deuterium oxide from 5 to 50°. The value found for pK at 25° is 14.955 (molality scale), 14.869 (molarity scale), and 16.653 (mole fraction scale). Enthalpy, entropy, and heat capacity changes for the dissociation process have been evaluated.

Introduction

In preceding papers, a number of thermodynamic measurements using deuterium oxide as solvent have been described as part of a program directed toward establishing a pD scale in pure deuterium oxide. The standard potential of cell I

$$D_2, DCl \text{ in } D_2O, AgCl; Ag \qquad (I)$$

was determined,[2] permitting the second dissociation constant of deuteriophosphoric acid and pD values of KD_2PO_4–Na_2DPO_4 buffer solutions to be measured,[3] as well as the dissociation constants of acetic acid in deuterium oxide,[4] and of deuterioacetic acid both in ordinary water[5] and in deuterium oxide.[6]

The ionization constant of deuterium oxide

$$K_m = m_{D^+} m_{OD^-} \gamma_{D^+} \gamma_{OD^-} / a_{D_2O} \qquad (1)$$

was first determined by Abel, Bratu, and Redlich,[7] who employed cell II

$$D_2, NaOD, NaCl \text{ in } D_2O, AgCl; Ag \qquad (II)$$

Their microtechnique was tested by measurements on ordinary water, and pK was derived from measurements at 21° in solutions of 0.92–0.95 mole fraction of deuterium. Using some measurements effectively on cell I above to obtain the standard potential of cell II, the often quoted value of $K = 1.6 \times 10^{-15}$ at 25° was calculated on the assumption that $K(H_2O)/K(D_2O)$ is independent of temperature in the range from 21 to 25°.

Almost simultaneously, Wynne-Jones[8] had used cell III with liquid junction

$$D_2, KCl + DCl, \text{saturated } KCl, KCl + NaOD, D_2 \qquad (III)$$

to obtain pK at 15, 25, and 35°, employing better quality deuterium oxide. The apparent agreement at 25° with the value of Abel, Bratu, and Redlich[7] was based on a misunderstanding of the concentration scale used by them (moles per 55.51 moles of water, irrespective of whether it is H_2O or D_2O), a scale that is now often termed aquamolality.

The value reported by Kingerley and La Mer[9] is not an independent one but utilizes the difference in emf of cell II in light and heavy water as given by Abel, Bratu, and Redlich.[7]

More recent studies have been made using glass electrodes, but these too are discordant. Glasoe and Long[10] calibrated glass electrodes with ordinary aqueous buffer solutions and determined the difference between the operational pH and the pD in heavy water as solvent. They used the usual pH cell with the saturated KCl–calomel electrode prepared in ordinary water to determine pK values of some acids in deuterium

(1) On leave from the University of Newcastle upon Tyne, England.

(2) R. Gary, R. G. Bates, and R. A. Robinson, *J. Phys. Chem.*, **68**, 1186 (1964).

(3) R. Gary, R. G. Bates, and R. A. Robinson, *ibid.*, **68**, 3806 (1964).

(4) R. Gary, R. G. Bates, and R. A. Robinson, *ibid.*, **69**, 2750 (1965).

(5) M. Paabo, R. G. Bates, and R. A. Robinson, *ibid.*, **70**, 540 (1966).

(6) M. Paabo, R. G. Bates, and R. A. Robinson, *ibid.*, **70**, 2073 (1966).

(7) E. Abel, E. Bratu, and O. Redlich, *Z. Physik. Chem.*, **A173**, 353 (1935).

(8) W. F. K. Wynne-Jones, *Trans. Faraday Soc.*, **32**, 1397 (1936).

(9) R. W. Kingerley and V. K. La Mer, *J. Am. Chem. Soc.*, **63**, 2356 (1941).

(10) P. K. Glasoe and F. A. Long, *J. Phys. Chem.*, **64**, 188 (1960).

oxide. This work was then extended to the determination of the ionic product of H_2O–D_2O mixtures.[11]

Gold and Lowe[12] made measurements in a cell with a glass electrode but without liquid junction. Solutions of hydrochloric acid in H_2O–D_2O mixtures over the whole range of composition were titrated with barium hydroxide solution. Barium was the cation chosen in both studies[11,12] to minimize the alkaline error of the glass electrode.

In view of the considerable uncertainty in the value of such an important constant, a redetermination of the emf of cell II has been made over a temperature range. Cell II, with hydrogen gas and ordinary water, was used by Harned and his co-workers[13] in studies at constant hydroxide molality and variable chloride molality, but Roberts[14] had earlier used the same cell at a constant chloride–hydroxide ratio. The technique for preparing solutions is simpler when a constant ratio is maintained, and there is less danger of systematic error arising from a change in the low (0.01) hydroxide molality by absorption of carbon dioxide; hence the method of Roberts was preferred.

Experimental Section

Commercial deuterium gas, with an indicated hydrogen content of not more than 0.5 atom % by mass spectrometric analysis, was passed through a catalytic purifier to remove traces of oxygen, then through 5% potassium hydroxide in deuterium oxide and over potassium hydroxide pellets to remove traces of carbon dioxide (soda lime was used in the first run).

The heavy water had a density of 1.10417 g ml^{-1}, indicating an isotopic purity of 99.7 mole %.[15] Its specific conductance was 1.4×10^{-6} ohm^{-1} cm^{-1} at 25°.

Sodium hydroxide (NaOD) solution was prepared by an adaptation of the method of Marsh and Stokes[16] using the apparatus shown in Figure 1. The 1000-ml capacity separatory funnel contained 500 ml of triply distilled mercury and 400 ml of 30% (w/w) sodium hydroxide solution in deuterium oxide. Using a platinum anode (2 cm^2 in area), electrolysis was carried out for 3 hr at 4 amp. Stirring of the mercury was necessary to prevent solidification of the amalgam at the mercury–solution interface. At the conclusion of the electrolysis the amalgam was run into the flask containing 600 ml of deuterium oxide through which CO_2-free, dry nitrogen had been bubbled for some hours. The reaction between sodium amalgam and light or heavy water is very slow at room temperature. However, maintaining the flask for 8 hr on a hot plate at a temperature of 80–90° afforded sufficient reaction to give a solution about 0.5 *m* in NaOD. This was diluted under CO_2-free conditions with a solution of sodium chloride in deuterium oxide to yield a stock solution. Cell solutions were prepared from this by weight dilution. Vacuum corrections were made to all weighings.

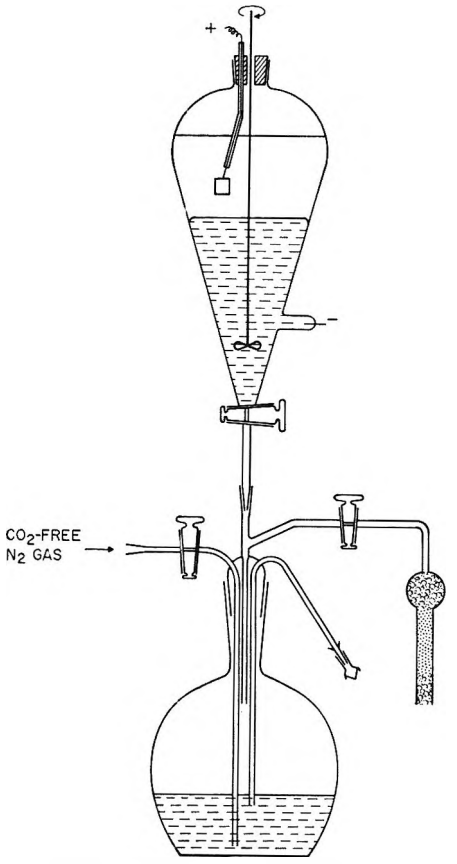

Figure 1. Apparatus for preparing a CO_2-free solution of NaOD in deuterium oxide.

Three runs were made at different chloride–hydroxide molality ratios. Hydroxide was determined by potentiometric weight titration against National Bureau of Standards potassium hydrogen phthalate sample 84 g. Chloride was estimated by coulometric titration[17] in the first run; in the last two runs the chloride

(11) P. Salomaa, L. L. Schaleger, and F. A. Long, *J. Am. Chem. Soc.*, 86, 1 (1964).

(12) V. Gold and B. M. Lowe, *Proc. Chem. Soc.*, 140 (1963).

(13) H. S. Harned and B. B. Owen, "Physical Chemistry of Electrolytic Solutions," 3rd ed, Reinhold Publishing Corp., New York, N. Y., Chapter 15, p 634.

(14) E. J. Roberts, *J. Am. Chem. Soc.*, 52, 3877 (1930).

(15) I. Kirshenbaum, "Physical Properties and Analysis of Heavy Water," H. C. Urey and G. M. Murphy, Ed., McGraw-Hill Book Co., Inc., New York, N. Y., 1951, p 17.

(16) K. N. Marsh and R. H. Stokes, *Australian J. Chem.*, 17, 740 (1964).

(17) Analysis by George Marinenko, Microchemical Analysis Section, National Bureau of Standards, Washington, D. C.

Table I: Electromotive Force (volts) of the Cell $D_2(g)$ at 1 atm, NaOD(m_1), NaCl(m_2), AgCl; Ag

I	5°	10°	15°	20°	25°	30°	35°	40°	45°	50°
					Run 1[a]					
0.015852[b]	1.09253	1.09332	1.09413	1.09505	1.09601	1.09690	1.09789	1.09887	1.09987	1.10081
0.019296[b]	1.09267	1.09339	1.09421	1.09511	1.09608	1.09684	1.09776	1.09868	1.09966	1.10042
0.029812	1.09274	1.09351	1.09437	1.09529	1.09618	1.09704	1.09800	1.09895	1.09995	1.10081
0.040675	1.09279	1.09358	1.09442	1.09534	1.09630	1.09719	1.09822	1.09925	1.10030	1.10130
0.045649	1.09281	1.09360	1.09443	1.09535	1.09630	1.09725	1.09823	1.09925	1.10033	1.10135
0.079372	1.09285	1.09364	1.09449	1.09542	1.09641	1.09737	1.09840	1.09945	1.10054	1.10161
					Run 2[c]					
0.017356[b]	1.09607	1.09701	1.09790	1.09885	1.09981	1.10060	1.10174	1.10285	1.10306	1.10479
0.035482	1.09628	1.09714	1.09805	1.09901	1.10003	1.10089	1.10206	1.10322	1.10427	1.10528
0.061815	1.09623	1.09714	1.09806	1.09902	1.10005	1.10097	1.10214	1.10334	1.10443	1.10548
0.083034	1.09631	1.09719	1.09809	1.09909	1.10014	1.10107	1.10226	1.10346	1.10456	1.10568
0.099905	1.09624	1.09710	1.09804	1.09902	1.10016	1.10102	1.10219	1.10341	1.10450	1.10558
0.15384	1.09619	1.09706	1.09800	1.09899	1.10016	1.10101	1.10220	1.10341	1.10451	1.10558
					Run 3[d]					
0.075411	1.10906	1.11013	1.11124	1.11243	1.11365	1.11487	1.11617	1.11749	1.11884	1.12018
0.075696	1.10909	1.11016	1.11127	1.11246	1.11368	1.11487	1.11618	1.11750	1.11886	1.12018
0.099380	1.10903	1.11008	1.11122	1.11244	1.11347	1.11491	1.11624	1.11758	1.11898	1.12034
0.13925	1.10895	1.11003	1.11115	1.11236	1.11359	1.11483	1.11615	1.11750	1.11890	1.12028
0.14322	1.10898	1.11006	1.11119	1.11240	1.11367	1.11491	1.11624	1.11760	1.11899	1.12039
0.19365	1.10890	1.10998	1.11111	1.11232	1.11359	1.11484	1.11617	1.11752	1.11891	1.12029

[a] $m_2/m_1 = 1.04617$. [b] Not used in calculating values of pK_m. [c] $m_2/m_1 = 0.89877$. [d] $m_2/m_1 = 0.53285$.

molality was calculated from the weight of sodium chloride in the solution added to the solution of NaOD. The sodium chloride was once recrystallized and low in bromide (0.003 mole % of the total salt).

The cells and the preparation of the electrodes have been described previously.[2,18] The electrodes were stored in deuterium oxide for 24 hr before placing them in the cells, which were flushed with deuterium gas before filling. The cell compartment with the electrodes in position was rinsed twice with solution; the rinsings were then forced under deuterium gas pressure into the presaturator section of the cell. The cell compartment was then filled, both electrodes being completely immersed in the solution.

The emf was measured over a temperature range in the order 25, 20, 15, 10, 5° (first day), 25, 30, 35, 40, 45, 50, 25° (second day), the deuterium gas being turned off overnight. In the second and third runs, an additional measurement at 25° was made at the end of the first day. The overnight values never differed by more than 0.06 mv except for the most dilute solutions in the second run, where it was suspected that the removal of carbon dioxide from the deuterium gas was not sufficiently adequate or that carbon dioxide had leaked into the cell. The third check at 25° yielded measurements lower on the average by 0.1 mv for the dilute solutions, but good agreement was found in the more concentrated solutions. In the third run, as an additional precaution, the thermostat was blanketed with nitrogen gas at atmospheric pressure throughout the whole series of measurements.

Results

The emf results, corrected to 1 atm partial pressure of deuterium gas, are shown in Table I. Values of pK_m' were calculated from the equation

$$pK_m' = pK_m - \log \gamma_{Cl^-}/\gamma_{OD^-} - \log a_{D_2O}$$
$$= (E - E^\circ)/k + \log m_{Cl^-}/m_{OD^-} \quad (2)$$

where k is written for $(RT \ln 10)/F$. Values of E° have been tabulated.[2] The values of pK_m' vary little with ionic strength (I) even with changes in m_{Cl^-}/m_{OD^-} ratio; this is to be expected since both the activity coefficient term $\gamma_{Cl^-}/\gamma_{OD^-}$ and a_{D_2O} are close to unity. The data for the two lowest concentrations in the first run and for the lowest one in the second run fall below the almost horizontal straight line at all temperatures. This is attributed to a slight contamination of the solutions with carbon dioxide, the effect of which is greatest at low concentrations. The largest

(18) R. G. Bates, "Determination of pH," John Wiley and Sons, Inc., New York, N. Y., 1964.

Table II: Self-Dissociation Constant of Deuterium Oxide from 5 to 50°

Temp, °C	D_2O			H_2O			$\frac{K_m(H_2O)}{K_m(D_2O)}$	$\frac{K_c(H_2O)}{K_c(D_2O)}$	$\frac{K_N(H_2O)}{K_N(D_2O)}$
	pK_m	pK_c	pK_N	pK_m	pK_c	pK_N			
5	15.740	15.653	17.438	14.734	14.734	16.478	10.14	8.30	9.12
10	15.526	15.439	17.224	14.535	14.535	16.279	9.79	8.02	8.81
15	15.326	15.239	17.024	14.346	14.347	16.090	9.55	7.80	8.59
20	15.136	15.049	16.384	14.167	14.169	15.911	9.31	7.59	8.38
25	14.955	14.869	16.653	13.997	14.000	15.741	9.08	7.40	8.17
30	14.784	14.699	16.482	13.833	13.837	15.577	8.93	7.28	8.04
35	14.622	14.538	16.320	13.680	13.685	15.424	8.75	7.13	7.87
40	14.468	14.385	16.166	13.535	13.542	15.279	8.57	6.97	7.71
45	14.322	14.241	16.020	13.396	13.405	15.140	8.43	6.85	7.59
50	14.182	14.103	15.880	13.262	13.272	15.006	8.32	6.78	7.48

difference (0.012 in pK_m) was found at 50°. Discarding these three points, pK_m at each temperature was derived by fitting the remaining 15 points by the method of least squares to an equation linear in I. These pK_m values on the molality scale are collected in Table II. The standard deviation was 0.001 at all temperatures. Table II also gives values of pK on the molarity (pK_c) and mole fraction (pK_N) scales and corresponding quantities for the self-dissociation of ordinary water.[19] The relation between the scales is

$$pK_c = pK_m - 2 \log d_0 \quad (3)$$

and

$$pK_N = pK_m + \log (1000/W) \quad (4)$$

where d_0 is the density and W the molecular weight of the solvent. Density data for deuterium oxide were taken from the paper of Chang and Tung.[20] Table II also gives values of the ratio $K(H_2O)/K(D_2O)$ on each concentration scale.

If all 18 solutions were considered, the value of pK_m derived would have been 0.002 to 0.004 lower, the higher difference being found at higher temperatures.

The values of pK_m from 5 to 50° were fitted, also by the method of least squares, to the equation[19]

$$pK_m = A_1/T - A_2 + A_3T \quad (5)$$

with 0°C = 273.15°K, giving A_1 = 4913.14 deg, A_2 = 7.5117, and A_3 = 0.0200854 deg^{-1}. The difference between the experimental value and that calculated by eq 5 did not exceed 0.001 in pK_m at any temperature.

From the constants of eq 5, values of $\Delta H°$, $\Delta S°$, and $\Delta C_p°$ for the self-dissociation of deuterium oxide were calculated; they are listed and compared with the values for ordinary water in Table III. The parameters of eq 5 for ordinary water[19] were originally computed on the basis of 0°C = 273.1°K; they have been recalculated with 0°C = 273.15°K to give A_1 = 4475.18 deg, A_2 = 6.1085, and A_3 = 0.0170890 deg^{-1}.

Table III: Thermodynamic Quantities[a] for the Self-Dissociation of Deuterium Oxide[b]

	Temp, °C	D_2O	H_2O
$\Delta G°$[b]	5	20,031	18,752
	25	20,403	19,095
	50	20,971	19,610
$\Delta H°$[b]	5	15,371	14,427
	25	14,311	13,526
	50	12,884	12,312
$\Delta S°$[b]	5	−16.76	−15.55
	25	−20.43	−18.68
	50	−25.03	−22.59
$\Delta C_p°$[b]	25	−54.8	−46.6
t_{max}, °C		221	239
$-\log K_{max}$		12.356	11.382

[a] The thermodynamic quantities listed refer to the molality scale of concentration. [b] $\Delta G°$ and $\Delta H°$ in cal mole^{-1}; $\Delta S°$ and $\Delta C_p°$ in cal deg^{-1} mole^{-1}; 1 cal = 4.1840 joules.

Discussion

The results appear to be higher by about 0.15 in pK than those previously reported.[7,8,11] There has, however, been some confusion over the concentration scales used by different workers. This and other factors make a reassessment of previous work desirable. The work of Abel, Bratu, and Redlich[7] depends essentially on two measurements at 21° on a combination of cells I and II

Ag; AgCl, DCl(m'), D_2 ----

D_2, NaOD(m'), NaCl(m'), AgCl; Ag (IV)

(19) H. S. Harned and R. A. Robinson, *Trans. Faraday Soc.*, **36**, 973 (1940).

(20) T. L. Chang and L. H. Tung, *Chinese J. Phys.*, **7**, 230 (1949).

where $m' = 0.1$ mole/55.51 mole of solvent. The two measurements gave 0.7402 and 0.7415 (absolute) v. In these two separate experiments the deuterium chloride was dissolved in deuterium oxide of mole fraction 0.946 and 0.970, respectively. The molalities were therefore 0.09056 and 0.09035 (moles/kg of solvent).

The emf of cell IV is given by

$$E/k = pK_m + 2 \log m_{DCl}\gamma_{DCl} + \log m_{OD^-}/m_{Cl^-} + \log \gamma_{OD^-}/\gamma_{Cl^-} - \log a_{D_2O} \quad (6)$$

The ratio of hydroxide to chloride ion concentration is unity whatever concentration scale is employed, and the present work indicates that $\gamma_{OD^-}/\gamma_{Cl^-}$ is almost unity. Moreover, $a_{D_2O} \rightarrow 1$ as $m \rightarrow 0$. In the absence of experimental measurements we set $\gamma_{DCl} = \gamma_{HCl}$ (= 0.8050) recognizing, however, that the value of γ_{DCl} is probably slightly lower than this.[2] Thus $pK_m = 14.958$ and 14.982 from eq 6. However, these measurements were made with alkali solutions which had a mole fraction of deuterium of 0.924 and 0.948, respectively. Assuming that pK_m varies linearly with the mole fraction of deuterium in H_2O–D_2O mixtures, then extrapolation gives 15.031 and 15.032 at 21°, compared with 15.099 from eq 5. The error resulting from the assumption of linearity is unlikely to increase pK_m by more than 0.02. A lower but reasonable value of γ_{DCl} would raise the value by only 0.01.

Wynne-Jones' extrapolated results[8] depend rather heavily on one point at low ionic strength (0.04) which is not collinear with the two points at higher ionic strengths ($I = 0.085$ and 0.10). However, the pK_c results ($I = 0$) given in Table II for 15, 25, and 35° are not inconsistent with these two higher ionic strength points. It does not seem unreasonable that the low concentration point may have been affected by contamination by carbon dioxide.

There remain the results obtained with the glass electrode. Those of Salomaa, Schaleger, and Long[11] for various H_2O–D_2O mixtures are based on measurements of the pH of barium hydroxide solutions. pK_c was calculated from the equation

$$pK_c = pH + \Delta pH - \log [\text{hydroxide}] - \log y_{\pm} \quad (7)$$

Here ΔpH is an empirical correction term and $y_{\pm}$ was estimated using a Debye–Hückel formula. The experimental values were found to fit the empirical equation

$$pK_c = 14.00 + 0.663n + 0.146n^2 \quad (8)$$

where n is the mole fraction of D_2O. This equation gives 14.81 for the pK_c of pure deuterium oxide. The results of Gold and Lowe, of which only a preliminary announcement has been made,[12] give, for pure deuterium oxide, $pK_c = 14.86 \pm 0.015$, yielding $pK_m = 14.95$, in agreement with the present value at 25°.

A discrepancy of 190 cal mole^{-1} exists between the calorimetrically determined ΔH° value[21,22] for ordinary water dissociation and that derived from the cell measurements of Harned and his co-workers.[13] It will be of interest to see if calorimetric measurements now in progress[23] reveal that a similar discrepancy exists for heavy water.

It may be noted that the parameters of eq 5 permit calculation of the maximum value of pK_m and the temperature at which it will occur. These quantities are given in Table III where they are compared with similar quantities for ordinary water.

Acknowledgment. A. K. C. wishes to express his gratitude to the University of Newcastle upon Tyne, England, for study leave.

(21) J. D. Hale, R. M. Izatt, and J. J. Christensen, *J. Phys. Chem.*, **67**, 2605 (1963).

(22) C. E. Vanderzee and J. A. Swanson, *ibid.*, **67**, 2608 (1963).

(23) L. G. Hepler, private communication.

Detection of Metal Ion Hydrolysis by Coagulation. VII. Neptunium(IV)[1,2]

by J. O. Wear and E. Matijević

Southern Research Support Center, Veterans Administration, Little Rock, Arkansas, and Department of Chemistry and Institute of Colloid and Surface Science, Clarkson College of Technology, Potsdam, New York *(Received May 9, 1966)*

The coagulation and reversal of charge of silver chloride, silver bromide, and silver iodide sols *in statu nascendi* by neptunium(IV) perchlorate have been investigated as a function of pH. The entire log $[Np(ClO_4)_4]$–pH domain for all three sols is given delineating the regions of uncoagulated sol, coagulated sols, and sols reestabilized due to charge reversal. The results have been discussed in terms of the hydrolyzed neptunium(IV) species.

Introduction

Apparently only one study of the hydrolysis of neptunium(IV) ion has been made.[3] Since hydrolytic species are frequently proposed in mechanisms for reactions involving Np(IV),[4–6] further study of the hydrolysis seemed desirable.

In this work the coagulation method has been employed which is essentially based upon the determination of the critical coagulation concentration (ccc) of an electrolyte for a known sol as a function of pH. In fortuitous cases, the change in ccc can give the actual *ionic charge* of the coagulating species. If negative lyophobic sols are coagulated, metal ions act as counterions, and if these ions undergo hydrolytic change due to variation in pH, the charge of the hydrolyzed species can be established. The method was described in detail earlier,[7] and the results of the hydrolysis studies on various ions have been given in the previous communications of this series. The advantages of the method are: (a) the charge of the complex species is determined directly, (b) the concentrations of counterions are generally extremely low and therefore activity effects and complexing with ions other than OH^- are as a rule negligible, and (c) the addition of large amounts of neutral electrolytes (such as alkali perchlorates) is not required.

Furthermore, it has been established that hydrolyzed species adsorb on various surfaces more strongly than nonhydrolyzed ions of the same metal.[8,9] When hydrolyzed ions adsorb in sufficient quantity, a reversal of charge of the sol particles may take place leading to the stabilization of colloid systems. Thus this effect is dependent on the concentration of the hydrolyzed species and could be utilized as a method for their detection. The charge reversal of silver halide sols by neptunium (IV) hydrolyzed species was also determined in this work. This information may be useful in the separation of neptunium from solutions by adsorption.

It is then obvious that coagulation and reversal of charge effects will depend on two parameters: the concentration of the neptunium(IV) salt and pH. The entire domain [Np(IV)]–pH has been obtained for silver iodide, silver bromide, and silver chloride sols; regions of uncoagulated sols, coagulated sols, and sols reestabilized by charge reversal have been delineated.

Experimental Section

Materials. The neptunium(IV) perchlorate stock solution was prepared and analyzed as described

(1) Part VI: E. Matijević, *J. Colloid Sci.*, **20**, 322 (1965).

(2) This investigation was supported in part by Public Health Service Research Grant WP-00815-01 from the Division of Water Supply and Pollution Control and in part by the U. S. Atomic Energy Commission. Most of the laboratory work was performed at Sandia Laboratory, Albuquerque, N. M.

(3) J. C. Sullivan and J. C. Hindman, *J. Phys. Chem.*, **63**, 1332 (1959).

(4) J. C. Hindman, J. C. Sullivan, and D. Cohen, *J. Am. Chem. Soc.*, **76**, 3278 (1954).

(5) J. R. Huizenga and L. B. Magnusson, *ibid.*, **73**, 3202 (1951).

(6) J. O. Wear, N. K. Shastri, and E. S. Amis, U. S. Atomic Energy Commission Report SC-RR-65-219.

(7) E. Matijević, M. B. Abramson, K. F. Schulz, and M. Kerker, *J. Phys. Chem.*, **64**, 1157 (1960).

(8) E. Matijević, M. B. Abramson, R. H. Ottewill, K. F. Schulz, and M. Kerker, *ibid.*, **65**, 1724 (1961).

(9) E. Matijević, G. E. Janauer, and M. Kerker, *J. Colloid Sci.*, **19**, 333 (1964).

previously.[6] Dilute Np(IV) solutions were prepared from this stock solution by the addition of doubly distilled water. The second distillation of water was carried out in an all-Pyrex still over permanganate. The water was boiled and cooled with argon bubbling through it. All other chemicals were of the highest purity grade and were used without further purification. All solutions were prepared oxygen free and kept under argon.

Methods. The critical coagulation concentration (ccc) and the critical stabilization concentration (csc) were determined from turbidity measurements using silver halide sols *in statu nascendi*. The procedure was a modification of the method described in detail earlier.[10,11]

Turbidity measurements were carried out in a Brice–Phoenix Model 2000DM light-scattering photometer at 45° using the incident beam of 546-mμ wavelength. The cell compartment was kept oxygen free by a steady flow of nitrogen. Measurements were made with a 24 × 24 mm semioctagonal cell which was placed in a thermostated cell jacket. The temperature was maintained at 25.0 ± 0.1° and monitored with a thermocouple.[12]

Samples of 18 ml volume were prepared by mixing all of the reagents [neptunium(IV) salt, potassium halide, and the acid or base] except $AgNO_3$ in the cell and thermostating this solution mixture in the instrument. Silver nitrate solution (2 ml) was then pipetted (~10 sec flow time) into the cell while stirring with a magnetic stirrer to bring the total volume to 20 ml; 30 sec after adding $AgNO_3$ the magnetic stirrer was turned off and the recorder of the light-scattering photometer was started. This method of mixing was found to give better results than the previously described technique.[7,10,11] At higher pH values the mixture was checked for precipitation of neptunium(IV) hydroxide and when necessary neptunium(IV) perchlorate was added with $AgNO_3$. The rest of the procedure remained unchanged. All concentrations were calculated for the final volume obtained after mixing all the components.

The pH measurements were carried out with a Beckman Model GS pH meter using glass electrodes. The meter was always calibrated using appropriate buffer solutions within 1 pH unit of the pH of the sample to be measured.

Results

In Figure 1 are shown three examples of curves for the coagulation of a silver iodide sol *in statu nascendi* by neptunium(IV) perchlorate. From the "time–turbidity" plots on the recorder, turbidities have been

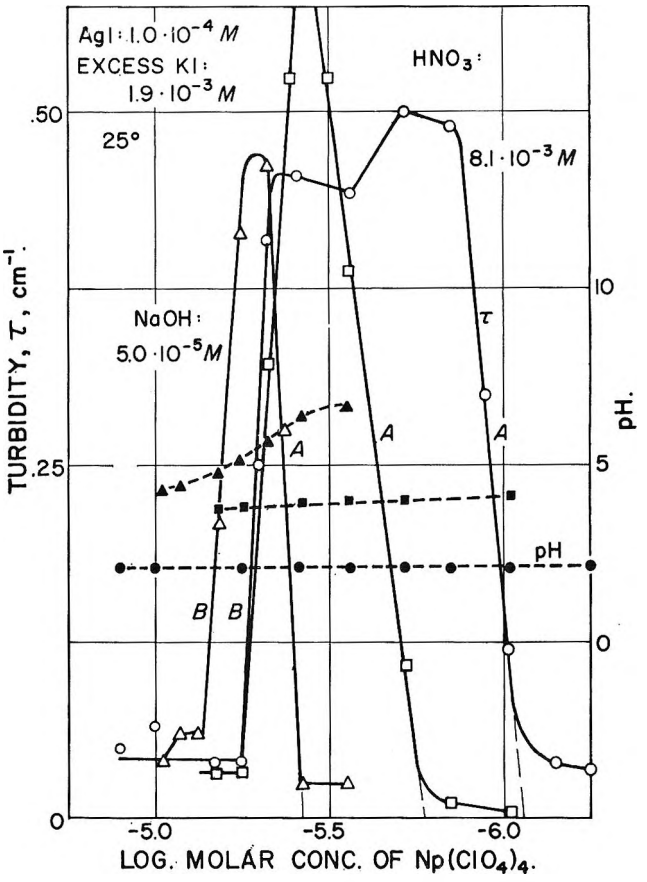

Figure 1. Coagulation curves of neptunium(IV) perchlorate for silver iodide sol *in statu nascendi*, 10 min after mixing the reacting components. Concentrations: $AgNO_3$: 1×10^{-4} *M*, excess KI 1.9×10^{-3} *M*; $Np(ClO_4)_4$ varied. –O–, HNO_3 8.1×10^{-3} *M*; –□–, HNO_3 8.1×10^{-5} *M*; –△–, NaOH 5×10^{-5} *M*. Full lines and open points represent turbidity measurements. A denotes the coagulation limit and B the stabilization limit. Dashed curves and blackened points give the corresponding pH values.

taken 10 min after mixing the reacting components (τ_{10}) and plotted against the concentration of added neptunium(IV) perchlorate; 10 min has been found to be a critical time for the coagulation of silver iodide sols.[11] In all cases the concentrations of $AgNO_3$ = 1.0×10^{-4} *M* and of KI = 2.0×10^{-3} *M*. Two curves represent measurements in the presence of 8.1×10^{-3} and 8.1×10^{-5} *M* HNO_3, respectively, while the third curve is for a system to which 5.0×10^{-5} *M* NaOH was added. All three curves show two low turbidity ranges and a turbidity maximum. At a very low Np(IV) salt concentration no coagulation takes place. Above turbidity limit A, neptunium

(10) E. Matijević and M. Kerker, *J. Phys. Chem.*, 62, 1271 (1958).
(11) B. Težak, E. Matijević, and K. Schulz, *ibid.*, 55, 1557 (1951).
(12) J. O. Wear, *J. Chem. Soc.*, 5596 (1965).

cationic species coagulate the negatively charged silver iodide sol, causing a sharp increase in turbidity. Above a certain concentration of neptunium(IV) perchlorate (limit B) another stability range appears due to the reversal of charge of silver iodide particles. By extrapolating the limits A and B to turbidity zero, one obtains the values of ccc and csc, respectively. The corresponding pH values can be read from the pH–concentration plots which are also included in Figure 1 (dashed lines). The curves given in Figure 1 clearly show that pH has a pronounced effect upon the coagulation and reversal of the charge process.

Figure 2 gives the complete domains as a "log molar concentration of neptunium perchlorate *vs.* pH" plot for the three silver halide sols investigated. Below the solid lines (ccc values) the sols remain uncoagulated, and above the dashed lines connecting blackened symbols (csc values) the sols are reestabilized due to the charge reversal. In between the two lines coagulation takes place. The most significant effect to observe is the increase in the coagulation concentration of neptunium(IV) perchlorate as the pH values become higher.

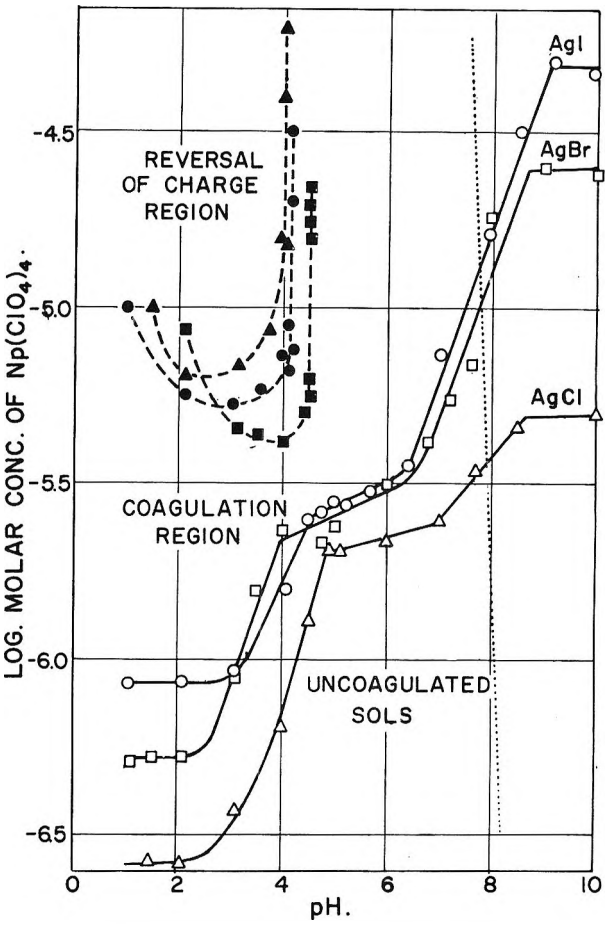

Figure 2. The entire log $[Np(ClO_4)_4]$–pH domain for AgCl, AgBr, and AgI sols *in statu nascendi*. The open symbols give the critical coagulation concentrations (ccc) and the blackened symbols the critical stabilization concentrations (csc). Between the two the sols are coagulated. Below the ccc the sols remain uncoagulated and above the csc they are stabilized due to reversal of charge. The dotted line represents the precipitation limit of neptunium hydroxide.

Discussion

Spectrophotometric data obtained by Sullivan and Hindman[3] indicate as the first hydrolysis step of neptunium(IV) ion the formation of $NpOH^{3+}$ species

$$Np^{4+}(aq) + H_2O \rightleftharpoons NpOH^{3+}(aq) + H_3O^+ \quad (1)$$

for which the hydrolysis constant, K_H, was found to be $5.0 \pm 0.3 \times 10^{-3}$. There was also evidence for the existence of polymerized neptunium hydrolyzed species at higher pH values, but no attempt was made to define their composition.

The coagulation experiments show that for all three silver halide sols the ccc is nearly constant up to pH ~2 and then increases to a plateau over the pH range 4–7. Above pH ~7 the ccc increases again to reach a maximum value over the pH range 8.5–10.

The coagulation values at pH <2 are 9×10^{-7} *M* for AgI, 5×10^{-7} *M* for AgBr, and 2.5×10^{-7} *M* for AgCl sols. These values are characteristic for counterions of charge +4 and are in excellent agreement with the ccc as obtained for the nonhydrolyzed $Th(aq)^{4+}$ ion (1×10^{-6} *M*, 6×10^{-7} *M*, and 3×10^{-7} *M* for AgI, AgBr, and AgCl sol, respectively).[7] One can therefore conclude that at pH <2 and the concentration of neptunium(IV) perchlorate used in these experiments the predominant species is the nonhydrolyzed $Np(aq)^{4+}$ ion.

According to the Schulze–Hardy rule, an increase in the ccc would indicate a lowering of the counterion charge. The plateau observed over the pH range 4–7 would normally be thought to indicate a new predominant species of lower charge. Using the hydrolysis constant given by Sullivan and Hindman,[3] the composition of the solutions was calculated for a number of combinations along the coagulation curve for the silver iodide sol, and the results are given in Table I.

The hydrolytic constant used was obtained at ionic strength 2.0. The systems used in this work contain less electrolyte. However, the effect of ionic strength upon the hydrolysis constant is usually sufficiently small so that the qualitative conclusions made from the data in Table I will still be valid.

It appears that the first plateau does coincide with

Table I: Calculated Concentrations of $NpOH^{3+}$ Species in Solution along the Coagulation Curve for Silver Iodide (Figure 1) Using $K_H = 5 \times 10^{-3}$ *M*

$[Np(IV)]_{tot}$, *M*	pH	$[NpOH^{3+}]$, *M*	%
9.0×10^{-7}	1.0	4.3×10^{-8}	4.8
9.0×10^{-7}	2.0	3.0×10^{-7}	33.0
1.60×10^{-6}	4.0	1.57×10^{-6}	98.3
2.80×10^{-6}	5.0	2.79×10^{-6}	99.6
3.20×10^{-6}	6.0	3.199×10^{-9}	99.98

the almost complete hydrolysis of neptunium(IV) ion although the ccc is much too low for counterions of +3 charge.[13] It is most likely that over this pH range the predominant species is $NpOH^{3+}$, accompanied by a minute amount of a higher charged species. Highly charged ions were found among hydrolysis products of other tetravalent ions, such as thorium.[14] It was shown that counterions of high charges (*e.g.*, +6) coagulate at extremely low concentrations ($\sim 10^{-8}$ *M*).[13]

The further increase in ccc over the pH range > 7 would indicate the formation of species of a still lower charge. For example, $Np(OH)_2^{2+}$ was postulated in an attempt to explain some kinetic processes involving the oxidation of Np(IV) ions, but no evidence was given for their existence. As will be shown below, it is more likely that the increase in the ccc at pH >7 is due to the formation of the uncharged, *soluble* $Np(OH)_4$ species and to precipitation of $Np(OH)_4$.

The upper stability region indicates that the Np^{4+} ion does not reverse the charge. It was impossible to delineate the boundary at the very low pH because further addition of acid would alone cause coagulation. As the pH value becomes higher, hydrolyzed neptunium species, if present in sufficient concentrations, cause sol stabilization due to charge reversal. However, above approximately pH 4 another coagulation–stabilization boundary is observed. If the charged hydrolyzed species were only present, the stability range of sols of reversed charge would be extended over the entire pH region above a certain concentration of the added neptunium salts such as is the case with aluminum[9] or ferric salts.[15] The disappearance of the stability range is an indication that the concentration of the charged hydrolyzed species has become too low to reverse the charge but is still high enough to coagulate the sols. One possible explanation of this effect is to assume the formation of a soluble molecular $Np(OH)_4$ species, the concentration of which will increase as the pH becomes higher. Such neutral species were found, for example, in aqueous solutions of ferric[9,16] and hafnium[17] salts. Recently, it was demonstrated that hafnium adsorbs strongly on silver halide sols over the entire pH range. While at lower pH values reversal of charge takes place, at higher pH values the sols remain negative.[18] The latter region coincides with the conditions at which almost all of the hafnium is in the form of soluble $Hf(OH)_4$.[17] This is why an analogous explanation is offered for the tetravalent neptunium ion.

At still higher pH, the concentration of counterions in solution falls below the ccc and the sols remain uncoagulated. This would then explain the coagulation curve above the first plateau. The big difference between the three silver halide systems over the pH range of the second plateau supports the given hypothesis.

The solubility of $Np(OH)_4$ in water was found to be 0.00011 g/l.[19] Assuming only the first hydrolysis step (eq 1), the solubility product constant can be given as

$$K_{sp} = \frac{[Np]_{tot}[OH^-]^4}{1 + K_H/[H^+]} \qquad (2)$$

The pH of a saturated solution of neptunium hydroxide, as calculated from the solubility data and K_H, is equal to 8. Using this value we obtain for $K_{sp} = 7.2 \times 10^{-37}$, which in turn yields the precipitation limit of neptunium hydroxide plotted as a dotted line in Figure 2. It appears that a better part of the coagulation region is still unsaturated with regard to solid $Np(OH)_4$. However, at the highest pH values the increase in ccc may at least in part be due to the precipitation of neptunium hydroxide. The big difference in the concentration of neptunium perchlorate at which the plateau is observed for the three silver halides as well as the order of the sols further indicates that this is not due to the coagulation by a lower charged complex counterion but to a more complicated process.

Apparently no adsorption phenomena of neptunium ions on solid–liquid interfaces have been reported. However, it was found that adsorption of plutonium

(13) E. Matijević, D. Broadhurst, and M. Kerker, *J. Phys. Chem.*, **63**, 1552 (1959).

(14) K. A. Kraus and R. W. Holmberg, *ibid.*, **58**, 325 (1959).

(15) E. Matijević and G. E. Janauer, *J. Colloid Sci.*, **21**, 197 (1966).

(16) A. B. Lamb and A. G. Jacques, *J. Am. Chem. Soc.*, **60**, 1215 (1938).

(17) V. M. Peshkova and Ang P'êng, *Russ. J. Inorg. Chem.*, **7**, 1091 (1962).

(18) E. Matijević, S. Kratohvil, and L. J. Stryker, *Discussions Faraday Soc.*, in press.

(19) T. J. LaChapelle, L. B. Magnusson, and J. C. Hindman, National Nuclear Energy Series, Division IV, 14B; Transuranium Elements, Part II, 1949, p 1097.

ions is strongly dependent on pH.[20] It is interesting that the adsorption on glass increases strongly up to pH 3.0 and then sharply declines above this pH value.[21] This is consistent with our observation of reversal of charge by neptunium. The comparison is justified because plutonium(IV) seems to undergo the same hydrolysis process as neptunium; at least as the first step, several investigators proposed $PuOH^{3+}$ species[22-24] with a hydrolysis constant of ~ 0.02. It would then seem that the adsorption in Pu(IV) on solid–liquid interfaces also takes place in the form of charged hydrolyzed species and the decline in adsorption above a certain pH is due to the removal of such species either in the form of soluble or precipitated $Pu(OH)_4$. However, since the solubility of $Pu(OH)_4$ is considerably smaller[25] than that of $Np(OH)_4$, and since plutonium has a higher tendency to form radio colloids than neptunium,[26] the latter explanation involving the formation of colloidal hydroxide is more likely.

(20) M. Haïssinsky and Y. Paiss, *J. Chim. Phys.*, **56**, 915 (1959); M. Haïssinsky and Y. Laflamme, *ibid.*, **55**, 510 (1958).

(21) V. I. Grebenshchikova and Yu. P. Davydov, *Radiokhimiya*, **3**, 165 (1960).

(22) S. W. Rabideau and R. J. Kline, *J. Phys. Chem.*, **64**, 680 (1960).

(23) K. A. Kraus and F. Nelson, *J. Am. Chem. Soc.*, **72**, 3901 (1950).

(24) J. C. Hindman, ref 19, Part I, p 370.

(25) M. Kasha, ref 19, Part I, p 295.

(26) E. L. King, ref 19, Part I, p 434.

Coagulation of Lyophobic Colloids in Mixed Solvents. II. The Effect of High Dielectric Constant[1,2]

by E. Matijević, M. E. Ronayne,[3] and J. P. Kratohvil

Department of Chemistry and Institute of Colloid and Surface Science, Clarkson College of Technology, Potsdam, New York *(Received May 31, 1966)*

The critical coagulation concentrations (ccc) of K^+, Li^+, Ba^{2+}, and La^{3+} have been determined for silver bromide sols *in statu nascendi* at various excess concentrations of Br^- in mixtures of N-methylpropionamide–water (dielectric constant at 25°, $\epsilon = 140$) and of N,N-dimethylformamide–water ($\epsilon = 66$). These new results are compared with previously obtained critical coagulation concentrations (ccc) in various solvent mixtures having dielectric constants of 30–126. Below $\epsilon \sim 120$ the log ccc decreases linearly with $1/\epsilon$. Above $\epsilon \sim 120$ there is an abrupt increase in the sol stability. The effect of ϵ upon the ccc is greater the higher the charge of the counterion. For example, for monovalent cations the ccc increases by two orders of magnitude, while for La^{3+} the ccc increases by approximately five orders of magnitude when ϵ is changed from 30 to 140.

Introduction

The stability of lyophobic sols toward electrolytes is most strongly affected by the charge of the counterion and by the dielectric properties of the medium. While the charge effects have been the subject of many studies, the influence of the medium has been investigated mainly in solvent mixtures of low dielectric constants (ϵ). Only very few studies of electrolytic coagulation in media of dielectric constant higher than that of water have been reported. It was found earlier that the stability of silver halide sols in aqueous glycine solutions[4,5] and of As_2S_3 in N-methylacetamide[6] is considerably higher than in corresponding aqueous solutions containing the same coagulating electrolytes. The use of single solvents or solvent mixtures of high dielectric constant in coagulation studies offers certain advantages over media of low ϵ. The coagulating electrolytes are more completely ionized and the probability of ion-pair formation is greatly reduced.

In this work the effect of N-methylpropinionamide–water mixture of dielectric constant $\epsilon = 140$ upon the coagulation of silver bromide sols *in statu nascendi* by lithium, barium, and lanthanum salts is presented. Also, data obtained with N,N-dimethylformamide–water mixtures of low dielectric constants for the same sol and various electrolytes are given. The latter systems were studied because of similar chemical composition of the two organic solvents used and great difference in their dielectric properties.

These new results are then compared with coagulation values of counterions of charge +1, +2, and +3 previously reported for the same sol in a variety of organic solvent–water mixtures.

Experimental Section

Eastman White Label N,N-dimethylformamide (DMF) was used without further purification. All measurements were carried out in a DMF–water mixture containing 20 mole % DMF (50.4 wt %). All salt solutions were prepared using aqueous 20 mole % DMF solution as the solvent and all dilutions were made with the same solvent mixture, the dielectric constant of which is $\epsilon = 66$.[7] The original intention

(1) Part I: J. P. Kratohvil, M. Orhanović, and E. Matijević, *J. Phys. Chem.*, **64**, 1216 (1960).

(2) Supported by a grant from the Army Research Office, No. DA-ARO-D-31-124-G656.

(3) National Science Foundation Undergraduate Research Participant.

(4) J. Kratohvil and B. Težak, *Arhiv Kem.*, **27**, 73 (1955).

(5) B. Jirgensons, *Kolloid-Z.*, **51**, 290 (1930).

(6) L. R. Dawson and D. G. Oei, *J. Colloid Sci.*, **20**, 282 (1965).

(7) R. D. Lanier, *J. Phys. Chem.*, **69**, 2697 (1965).

was to perform coagulation experiments in solutions of higher mole concentration of DMF (the same as for N-methylpropionamide). However, it was found that, in media with high concentrations of DMF, silver ions are reduced to metallic silver and the solubility of 1–1-valent salts was too small to prepare solutions above critical coagulation concentration.

The N-methylpropionamide (NMP) employed was also Eastman White Label. Several shipments of this were used. While no difficulty was encountered with the first sample, two subsequently obtained samples produced precipitates when silver nitrate or barium nitrate was dissolved in 85.43 mole % solutions of NMP. It was established that the precipitates were colloidal metal hydrous oxides formed because of higher alkalinity of the NMP samples. Addition of nitric acid to make the solution 5×10^{-3} M in H^+ eliminated the precipitation. All measurements were made in solutions containing 85.43 mole % NMP (96.59 wt. %). This concentration was chosen to give the dielectric constant of 140 at 25°.[8,9] Because in this concentration range small changes in water content result in considerable variation in the dielectric constant, all solutions were prepared by weighing. While solutions of $AgNO_3$, KBr, and $La(NO_3)_3$ of desired concentrations were prepared without difficulty, $Ba(NO_3)_2$ and $LiNO_3$ dissolved only after prolonged heating in a water bath with constant agitation. In preparing the solutions, the water content of the salts

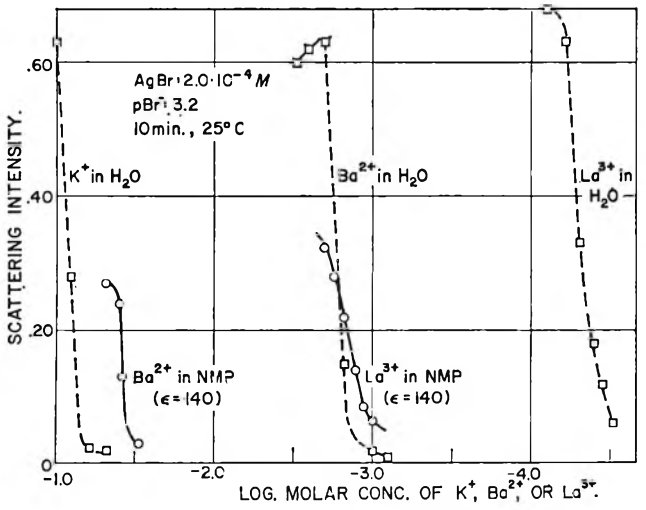

Figure 1. Coagulation curves for a silver bromide sol *in statu nascendi* in the presence of $Ba(NO_3)_2$ and $La(NO_3)_3$ in a mixture of N-methylpropionamide (NMP)–water (NMP 85.43 mole %, ϵ = 140) (solid lines) and in the presence of KNO_3, $Ba(NO_3)_2$, $La(NO_3)_3$ in water (dashed lines). Scattering intensities measured at 546 mμ, 10 min after mixing the reacting components. Concentrations: AgBr 2×10^{-4} M; excess Br^-, 6×10^{-4} M.

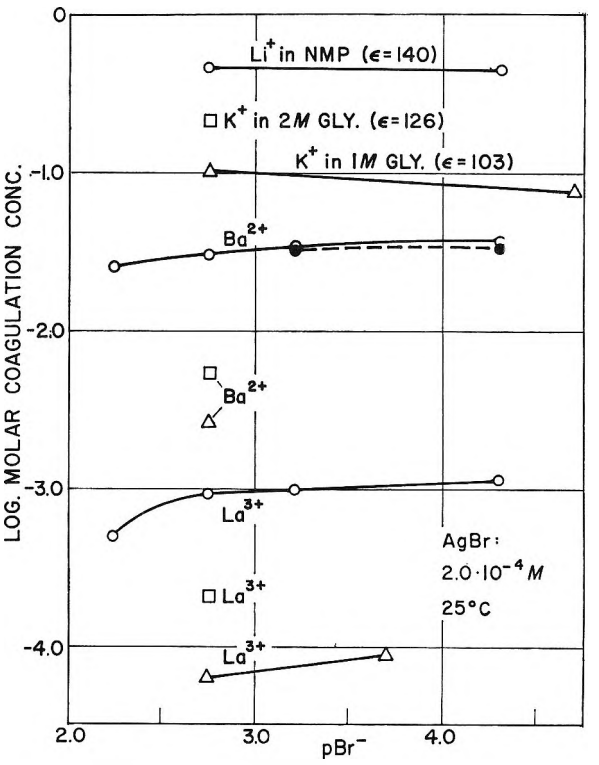

Figure 2. Plot of the critical coagulation concentration (ccc) of a silver bromide sol *in statu nascendi* against excess concentration of the stabilizing ion (pBr^-) for Li^+, Ba^{2+}, and La^{3+} in 85.43 mole % N-methylpropionamide (NMP)–water mixture (ϵ = 140) (open circles, in presence of 5×10^{-3} M HNO_3; full circles, no acid added). Squares and triangles give the ccc values for K^+, Ba^{2+}, and La^{3+} in 2 and 1 M glycine, respectively.[4]

and the small amounts of nitric acid used to acidify NMP were always taken into consideration.

All salts used were of the highest purity grade. The water was doubly distilled, the second distillation being carried out in an all-Pyrex still.

The coagulation process was studied using a silver bromide sol *in statu nascendi*. In all cases the concentration of the sol was 2×10^{-4} M while the concentration of excess KBr was varied. The turbidity changes were followed with time in presence of various amounts of coagulating electrolyte using an Aminco light-scattering photometer. The method of measurement and the procedure for the determination of the critical coagulation concentration (ccc) have been described in detail previously.[10,11]

(8) R. K. Wolford and R. G. Bates, *J. Phys. Chem.*, 66, 1496 (1962).

(9) T. B. Hoover, unpublished data. The authors gratefully acknowledge the receipt of unpublished values for the dielectric constant and for the density of NMP–water mixtures as measured by Dr. T. B. Hoover and Dr. R. G. Bates, National Bureau of Standards.

(10) E. Matijević and M. Kerker, *J. Phys. Chem.*, 62, 1271 (1958).

Results

The effect of N-methylpropionamide (NMP) upon coagulation of a silver bromide sol *in statu nascendi* by barium and lanthanum ions is shown in Figure 1. Full lines give coagulation curves obtained in NMP–water mixture of dielectric constant 140. The dashed lines represent the corresponding coagulation curves in water only. The critical coagulation concentration (ccc) is obtained by extrapolation of the coagulation limit (the steep part of the coagulation curve) to zero scattering intensity. The great stabilizing effect of NMP is expressed in the shift of the coagulation limits to considerably higher concentrations of the electrolyte. This shift is such that the trivalent lanthanum ion in 85.43 mole % NMP coagulates at about the same concentration as barium ion in water. A similar effect is observed with the divalent barium ion.

In Figure 2 the ccc of Li^+, Ba^{2+}, and La^{3+} ions in 85.43 mole % NMP is plotted as a function of excess bromide ion (pBr^-) for the same silver bromide sol *in statu nascendi*. In the case of barium nitrate two points were obtained in absence of nitric acid. It was found that addition of nitric acid had negligible effect upon the ccc. In the same diagram are plotted the ccc values obtained earlier in presence of 2 *M* (ϵ = 126) and 1 *M* (ϵ = 103) glycine.[4] Excess stabilizing ion (Br^-) has little effect upon the coagulation behavior of various ions. Furthermore, the ccc increases in all cases with increasing value of the dielectric constant of the medium.

Figure 3 gives the ccc for K^+, Ba^{2+}, and La^{3+} in a 20 mole % solution of N,N-dimethylformamide (DMF) (ϵ = 66) as a function of excess stabilizing Br^- ion (circles). Also included are corresponding data for water as the medium (squares). The full squares represent new measurements, while open squares are taken from previous work.[4,12] The reproducibility is quite good. As expected, the ccc's for Ba^{2+} and La^{3+} are lower in DMF–water mixtures than in water alone. However, the potassium ion coagulates the AgBr sol at higher concentration in 20 mole % DMF than in water. A similar effect has been observed before, in particular, for univalent coagulating ions in various solvent mixtures, the dielectric constants of which are not much lower than that of water.[4,13]

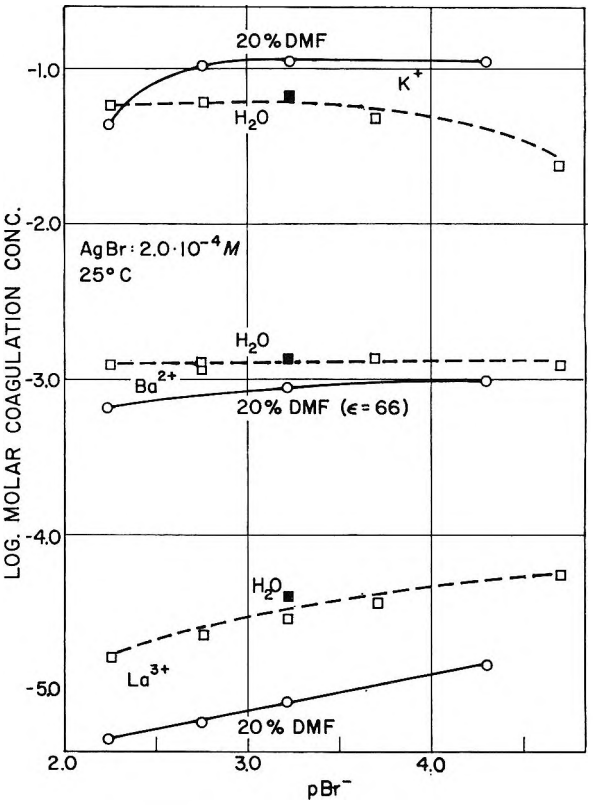

Figure 3. Plot of the critical coagulation concentration (ccc) of a silver bromide sol *in statu nascendi* against excess concentration of the stabilizing ion (pBr^-) for K^+, Ba^{2+}, and La^{3+} in 20 mole % N,N-dimethylformamide–water mixture (ϵ = 66) (solid lines) and in water alone (dashed line). Full squares represent data obtained in this work; empty squares are taken from previous work.[4,12]

Discussion

According to the stability theory of Derjaguin–Landau–Verwey–Overbeek (D–L–V–O)[14,15] in its original form, the coagulation concentration should be proportional to ϵ^3. However, experimental results on various sols strongly deviate from this requirement.[4,13] In order to reconcile the experimental data obtained on silver iodide sols in water–acetone solutions and Na^+, Ba^{2+}, and La^{3+} as coagulating ions with the D–L–V–O theory, Mackor[13] made a number of assumptions and modified the power law. However, there is no way to prove that the approximations made and the changes in constants introduced in that work are actually justified.

Adding a second solvent to a hydrosol in order to change the dielectric constant of the medium introduces a number of new parameters which have to be considered in any attempt to interpret the coagulation results. Some of these are (a) the change in the solu-

(11) B. Težak, E. Matijević, and K. Schulz, *J. Phys. Chem.*, **55**, 1557 (1951).

(12) E. Matijević, K. F. Schulz, and B. Težak, *Croat. Chem. Acta*, **28**, 81 (1956).

(13) E. L. Mackor, *Rec. Trav. Chim.*, **70**, 841 (1951).

(14) B. Derjaguin and L. Landau, *Acta Physicochim. U.R.S.S.*, **14**, 633 (1941).

(15) E. J. Verwey and J. Th. G. Overbeek, "Theory of the Stability of Lyophobic Colloids," Elsevier Publishing Co., New York, N. Y., 1948.

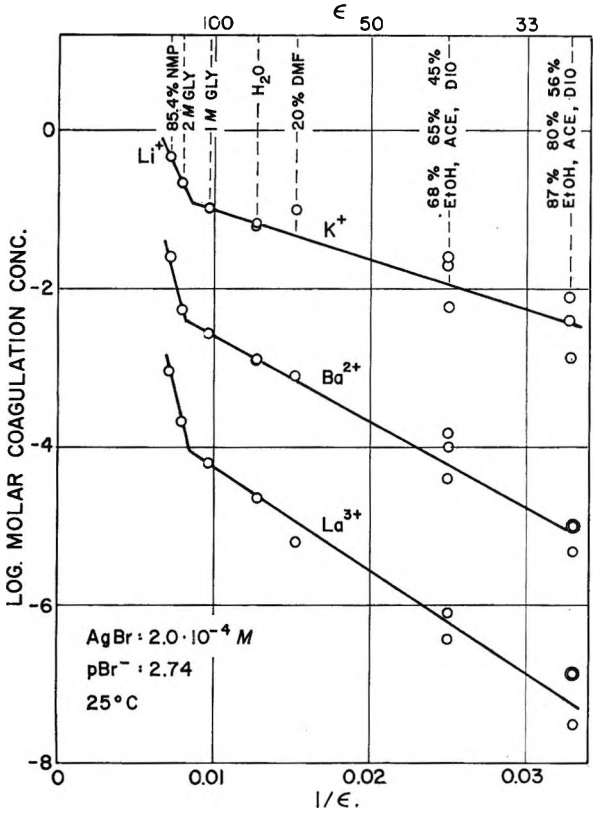

Figure 4. Plot of the critical coagulation concentration (ccc) for a negative silver bromide sol *in statu nascendi vs.* $1/\epsilon$ for K^+, Ba^{2+}, and La^{3+} for various solvent mixtures as indicated at top of the figure. Concentrations: AgBr, 2.0×10^{-4} *M*; excess concentration of Br^-, 6×10^{-4} *M* (GLY = glycine, DIO = dioxane, ACE = acetone, EtOH = ethanol).

bility of the dispersed material, (b) the adsorption of the second solvent on the colloid particles, (c) the effect of the second solvent upon the ionization of the coagulating electrolyte, (d) complexing between the electrolyte and solvent species, (e) change in the adsorption of the stabilizing ion and the counterion on the colloid particles. Most of these effects will influence the composition and the properties of the double layer, such as the zero point of charge, the χ potential across the interface, the integral capacity of the inner region, etc. Also the local dielectric constants will be different for various mixed solvents although the bulk dielectric constant may be the same. If chemical changes take place in addition (complexing!), the picture becomes even more involved.

Except for a certain amount of data on solubilities and the zero point of charge in mixed solvents, information on the remaining parameters is as a rule not available.

In the present work we employed one solvent having a high dielectric constant and a chemically similar solvent of low dielectric constant. It would appear from the measurements on AgI in DMF[16] that the solubility of silver bromide is only little influenced by these solvents. While it is expected that, owing to the very high dielectric constant of the solvent, the electrolytes are fully ionized in NMP, there is experimental evidence that ionization is not affected by DMF. For example, it has been shown that KI is completely dissociated in DMF.[17]

Since no other information necessary to compare the experimental results with the D–L–V–O theory is available, it would seem that the only way to do this is to make assumptions which are necessarily arbitrary and therefore of little value.

It was shown earlier[1,4,18] that in many cases a linear relationship is obtained when log ccc is plotted against $1/\epsilon$. We have used our present results and some previously obtained data on the same sol in various solvent mixtures for making a plot given in Figure 4. So far, this is the most complete set of data for a given sol, representing the coagulation values for three counterions of different charges in solvent mixtures with dielectric constants ranging from 30 to 140. It is apparent that an approximately linear relationship is obtained over the ϵ range from 30 to $\sim$120. At low dielectric constants, data are given for various solvent mixtures having the same ϵ value and the scatter indicates the specific solvent effects.[1,4] Above $\epsilon \sim 120$ an abrupt increase in sol stability is observed. This does not seem to be due to a specific solvent effect of NMP because values obtained with two different concentrations of glycine are located on both sides of the breaking point for all three counterions. The higher stability of the sols above $\epsilon \sim 120$ could be due to increased adsorption of the high dielectric solvent as a result of which the double layer is expanded. The $1/\epsilon$ dependence of log ccc would result if only the electrostatic attraction between the stabilizing ion and the counterion were responsible for the sol stability. This is obviously an oversimplification. It is, however, useful in that one can approximately predict the stability of a lyophobic colloid in a mixed solvent from the $1/\epsilon$–log ccc linear relationship once its coagulation value in water, or any other solvent, has been determined.

Figure 4 shows how strongly the stability of sols can be influenced by varying the dielectric constant of the solvent media. This result is indeed remarkable. In the case of La^{3+} the critical coagulation concentration

(16) H. Chateau and M. C. Moncet, *J. Chim. Phys.*, 60, 1060 (1963).
(17) D. P. Ames and P. G. Sears, *J. Phys. Chem.*, 59, 16 (1955).
(18) B. Težak, E. Matijević, K. F. Schulz, J. Kratohvil, M. Mirnik, and V. B. Vouk, *Discussions Faraday Soc.*, 18, 63 (1954).

changes by nearly five orders of magnitude when ϵ varies from 30 to 140. This is about 1000 times as great an effect as that predicted by the simple ϵ^3 relationship. Effects of such an order can be observed otherwise only when ions of various charges are used in the electrolytic coagulation (Schulze–Hardy rule).

Thermodynamic Quantities in the Exchange of Lithium with Cesium Ion on Cross-Linked Phosphonic Acid Cation Exchangers[1]

by K. E. Becker, S. Lindenbaum, and G. E. Boyd

Oak Ridge National Laboratory, Oak Ridge, Tennessee 37831 *(Received May 12, 1966)*

Calorimetric measurements showed that heat was absorbed in the preferential uptake of lithium ion from dilute alkaline aqueous solutions in exchange reactions with cesium ion in cross-linked nuclear and methylene phosphonic acid type cation exchangers. Standard free energies, $\Delta G°$, heats, $\Delta H°$, and entropies, $\Delta S°$, of exchange were -0.33 and -0.72 kcal mole^{-1}, 0.89 and 1.20 kcal mole^{-1}, and 4.1 and 6.4 eu, respectively. As with cross-linked polymethacrylic acid ion exchangers, the increase in $\Delta S°$ was attributed principally to the decrease in Li^+ ion hydration in the exchange reaction. Site binding of Li^+ was postulated as the cause for the preferential uptake of this ion by phosphonic acid type cation exchangers.

The order of the preferred uptake of the alkali metal ions from their dilute aqueous solutions by strong-acid cation exchangers, $Cs^+ > Rb^+ > K^+ > Na^+ > Li^+$, has been shown to be reversed in weak-acid exchangers of the polymethacrylate[2-4] and polyphosphonate[2,5] types. The selective absorption of the lighter alkali metal cations by carboxylic acid exchangers was found,[4] moreover, to be accompanied by the absorption of heat and an increase in entropy, whereas with strong-acid exchangers (*i.e.*, cross-linked polystyrenesulfonic acid) the preferential uptake of the heavier cation occurred with the evolution of heat and a decrease in entropy.[6] These observations have been interpreted as indicating that ion–water interactions are of primary importance in determining the alkali metal cation selectivity sequence with polystyrenesulfonate exchangers; with polymethacrylates, ion-pair formation between Li^+ (and possibly Na^+) ion and the carboxylate exchange group has been assumed. The specific interaction between Li^+ and COO^- may obey the "localized hydrolysis" mechanism proposed by Robinson and Harned[7] and result from the fact that the density of electric charge on a carboxylate group is greater than on a sulfonate group. Accordingly, it was of interest to examine the thermodynamics of the lithium–cesium ion exchange with a cation exchanger in which the electric charge density was even greater. The phosphonate exchange group resembles

(1) Research sponsored by the U. S. Atomic Energy Commission under contract with the Union Carbide Corp.

(2) J. I. Bregman, *Ann. N. Y. Acad. Sci.*, 57 [3], 126 (1953).

(3) H. P. Gregor, M. J. Hamilton, R. J. Oza, and F. Bernstein, *J. Phys. Chem.*, 60, 263 (1956).

(4) S. Lindenbaum and G. E. Boyd. *ibid.*, 69, 2374 (1965).

(5) J. Kennedy, J. Marriott, and V. J. Wheeler, *J. Inorg. Nucl. Chem.*, 22, 269 (1961).

(6) G. E. Boyd, F. Vaslow, and S. Lindenbaum, *J. Phys. Chem.*, 68, 590 (1964).

(7) R. A. Robinson and H. S. Harned, *Chem. Rev.*, 28, 419 (1941).

the sulfonate group in that three oxygens are combined in it but differs in that, when fully ionized, it carries two rather than one negative charge.

Experimental Section

Materials. Two types of phosphonic acid exchangers were used: a polystyrene–divinylbenzene cross-linked (5.5% DVB) preparation, $-CH-C_6H_4-PO(OH)_2$, in which the phosphonate groups were attached to a benzene nucleus, and a polystyrene–divinylbenzene cross-linked (5.5% DVB) methylene phosphonic acid exchanger, $-CH-C_6H_4CH_2-PO(OH)_2$, in which the phosphonate was separated from the benzene ring by a methylene group.[8] The ion-exchange capacities of these preparations were determined by shaking their acid forms which had been pretreated to remove impurities and unreacted monomers with a measured excess of standard NaOH solution for periods up to 7 days and back-titrating an aliquot of the supernatant solution with standard HCl. Values of 5.50 and 5.75 mequiv/g of dry hydrogen form resin were obtained for the nuclear and methylene phosphonic acid exchangers, respectively. Our experience, and that of others,[2,5] has indicated that these exchangers are stable in the presence of alkaline aqueous solutions and that their exchange capacity remains constant during experiment. The homo-ionic lithium and cesium salt forms employed as starting materials in the calorimeter reactions were prepared by treating the acid forms with an excess of aqueous LiOH or CsOH solution, respectively. The preparation of these solutions has been described.[4]

Calorimetric Measurements. A description of the calorimeter and its associated measuring circuits has been presented in other publications from this laboratory.[4,9] The procedure and methods of analysis[10] were identical with those described for the exchange of Li^+ with Cs^+ ion on polymethacrylate ion exchangers.[4] The reaction temperature was 25.00°, and the exchange reaction was conducted with aqueous LiOH + CsOH solutions at an ionic strength of 0.1 *M*. The heat of opening of the calorimeter pipet, which initially contained the exchanger, was determined as 0.010 ± 0.005 cal. This correction was applied to the observed heat effect expressed in terms of 1 cal = 4.184 joules. The performance of the calorimeter was checked by measurements of the heat of solution of KCl(c) in water and of tris(hydroxymethyl)aminomethane (THAM) in 0.100 *N* HCl. A heat of solution to infinite dilution for KCl of 4134 ± 12 cal $mole^{-1}$ was found, which may be compared with a recently proposed "best value"[11] of 4115 ± 10 cal $mole^{-1}$. An average value of −7118 ± 18 cal $mole^{-1}$ was measured for the heat of solution of THAM at a final concentration of *ca.* 5 g $l.^{-1}$. This may be compared with the value of −7107 cal $mole^{-1}$ recently reported by Gunn.[12]

Results and Discussion

Selectivity Coefficients. Selectivity coefficients computed from the measured equilibrium concentrations of Li^+ and Cs^+ ions in the aqueous solution and in the exchanger phases after the calorimetric experiments are plotted in Figure 1 as a function of the equivalent fraction of lithium ion, x_{Li^+}, in the exchanger. With both phosphonic acid exchangers log $D_{Cs^+}^{Li^+}$ was a linear function of x_{Li^+}. Both exchangers showed a strong preference for Li^+ over most of the range in x_{Li^+}; however, there was a selectivity inversion at large (0.8–0.9) lithium equivalent fractions where cesium was the preferred cation. A similar reversal was observed with polymethacrylate exchangers[4] at slightly lower values of x_{Li^+}.

Heats of Exchange. The measured heats of partial exchange are shown in Figure 2 by a chord for each experiment. The curves for the differential heat of exchange, $\Delta\bar{H} = (\partial H/\partial x_{Li^+})$, are the best least-squares fit through the midpoints of the chords. With the nuclear phosphonic acid preparation, $\Delta\bar{H}$ was linear with respect to x_{Li^+}, whereas the data for the methylene phosphonic acid exchanger were better fitted by a quadratic equation. The preferred uptake of lithium ion was accompanied by the absorption of heat over most of the composition range. The absorption of small amounts of Li^+, however, gave an evolution of heat with both exchangers. From the magnitudes of $\Delta\bar{H}$ at $x_{Li^+} = 0.0$ and $x_{Li^+} = 1.0$, it may be predicted that at temperatures above 48° lithium ion will be selectively absorbed over the entire composition range.

Standard-State Thermodynamic Values. Standard enthalpies, $\Delta H°$, free energies, $\Delta G°$, and entropies, $\Delta S°$, of exchange were calculated for the hypothetical reaction

$$CsR(a = 1, \text{equil with } 0.1\ N\ CsOH) + LiOH(aq, a = 1) \rightleftharpoons LiR(a = 1, \text{equil with } 0.1\ N\ LiOH) + CsOH(aq, a = 1) + nH_2O(a_w = 1)$$

(8) The authors are indebted to Dr. I. M. Abrams, Diamond Alkali Co., Western Division, Redwood City, Calif., for providing these materials. The nuclear phosphonic acid exchanger is commercially available as Duolite ES-63.

(9) S. Lindenbaum, *J. Phys. Chem.*, **70**, 814 (1966).

(10) The authors thank M. Ferguson of the ORNL Analytical Chemistry Division for the flame spectrophotometric determinations of lithium and cesium.

(11) V. B. Parker, "Thermal Properties of Aqueous Uni-univalent Electrolytes," National Standard Reference Data Series, National Bureau of Standards, Washington, D. C., 1965, NSRDS-NBS 2.

(12) S. R. Gunn, *J. Phys. Chem.*, **69**, 2902 (1965).

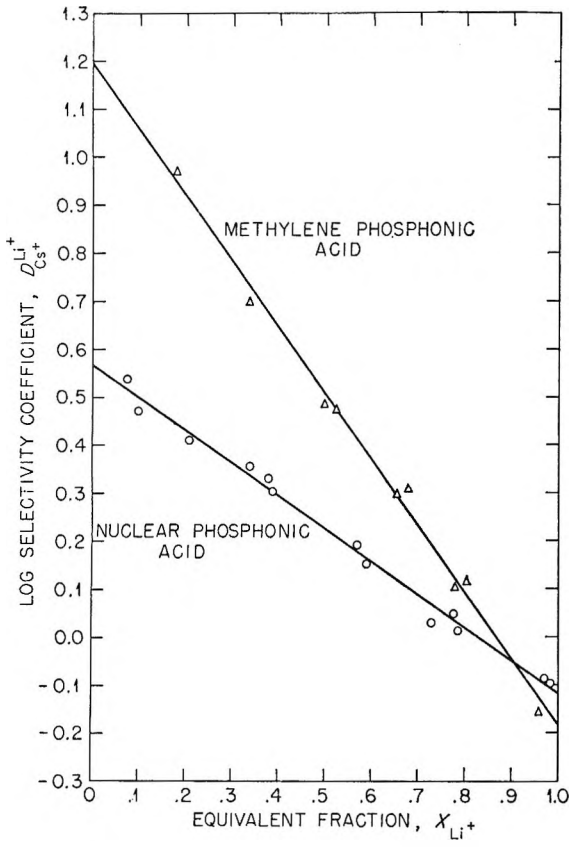

Figure 1. Selectivity coefficients for the exchange of Li^+ with Cs^+ in nominal 5.5% DVB cross-linked phosphonic acid ion exchangers.

where n is the number of moles of water lost (or gained) by the exchanger.

The desired standard enthalpy changes, $\Delta H°$, were derived from the integral heats of exchange, ΔH, corrected by the difference, $\Delta\phi_L = -50$ cal mole^{-1}, in the relative apparent molal heat contents between the 0.1 N LiOH and 0.1 N CsOH solutions. Integral exchange heats, defined by

$$\Delta H = \int_0^1 (\partial \Delta H/\partial x_{Li^+}) dx_{Li^+}$$

were evaluated by integrating the empirical least-squares equations fitted to the data of Figure 2. Corrections to the differential heat of exchange, $(\partial \Delta H/\partial x_{Li^+})$, for changes in the ionic strength from its initial value of 0.1 N because of the loss or gain of water by the exchanger during the ion-exchange reaction and for thermal effects caused by the mixing of aqueous electrolytes were always sufficiently small to be neglected.[13]

Standard free energy changes were found by graphical integration of the corrected selectivity coefficients, D_0, according to the equation

$$-\Delta G° = 2.3RT \int_0^1 \log D_0 \, dx_{Li^+}$$

The required D_0 values were obtained by correcting the observed selectivity coefficients (Figure 1) by the activity coefficient ratio, $\gamma_\pm^2(CsOH)/\gamma_\pm^2(LiOH)$, which was evaluated for aqueous 0.1 m mixtures following the method outlined by Robinson and Stokes.[14] This correction did not exceed 5%.

Standard-state thermodynamic quantities for the exchange of lithium with cesium ion on a nuclear and on a methylene phosphonic acid are summarized in Table I, where it may be observed that the entropy increase accompanying the uptake of Li^+ ion was sufficiently large to overcome the increased enthalpy required and thus give a free-energy decrease for the

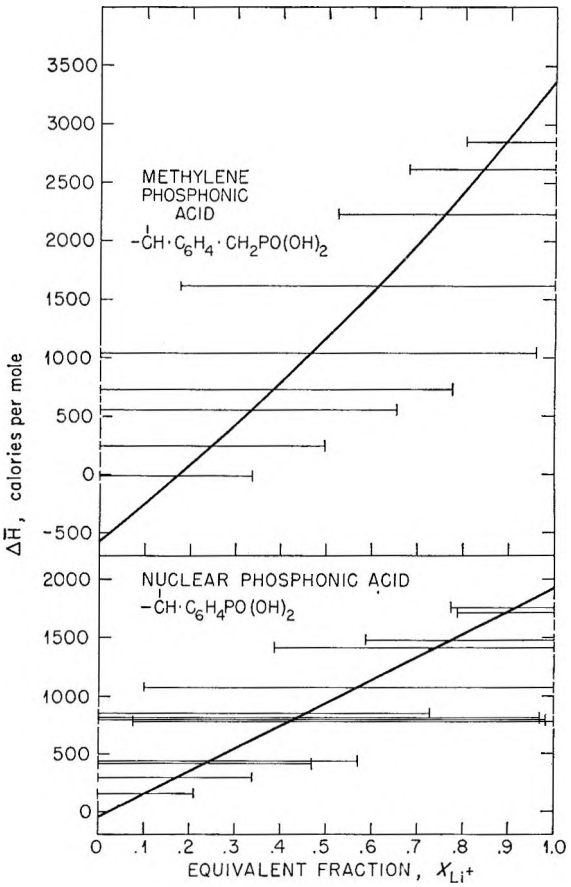

Figure 2. Differential heat of exchange of Li^+ with Cs^+ ion in nominal 5.5% DVB cross-linked phosphonic acid exchangers.

(13) Changes in the heat contents of the ion exchanger caused by changes in its swelling are included in the standard heat of exchange, $\Delta H°$, as defined.

(14) R. A. Robinson and R. H. Stokes, "Electrolyte Solutions," Butterworth & Co., Ltd., London, 1955, p 440.

Table I: Standard Free Energies, Heats, and Entropies of Exchange at 298.2°K of Lithium with Cesium Ion on Nuclear and on Methylene Phosphonic Acid Type Cation Exchangers

Exchanger	$-\Delta G°$, kcal mole^{-1}	$-\Delta H°$, kcal mole^{-1}	$\Delta S°$, eu
Nuclear phosphonic	0.33	−0.89	4.1
Methylene phosphonic	0.72	−1.20	6.4

reaction. Interestingly, the magnitude of the increase in enthalpy and entropy depended on the acid strength of the phosphonate group: the weaker the acid, the greater the selectivity for Li^+ over Cs^+ ion.[15] This result suggests that the observed increases in $\Delta H°$ and $\Delta S°$ cannot be attributed entirely to a decrease in the hydration of Li^+ ion when it is absorbed by weak-acid type cation exchangers.

As with cross-linked polymethacrylic acid exchangers,[4] it appears necessary to assume that there is a specific association between lithium ion and the phosphonate group of the exchanger (*i.e.*, "site-binding"). It is postulated that this interaction involves a water molecule as an intermediary between Li^+ and PO_3^{2-} as in the "localized hydrolysis" hypothesis previously employed by Robinson and Harned[7] to account for the reversal in the activity coefficient sequence of the alkali metal salts in aqueous solution from that for the halides when the anion is a proton acceptor. The second acid dissociation constants for phosphonic acids are quite small, indicating that the ion, $-PO_3H^-$, is a much weaker acid than acetic acid. An activity coefficient reversal between the sodium and potassium mono- and disalts of phosphoric acid has been reported,[16] and this may be understood on the basis of the "localized hydrolysis" mechanism for ion association. The binding of Li^+ ion in the association complex would be expected to increase as the proton accepting strength of the $-PO_3^{2-}$ group increases. Thus, the stronger binding of Li^+ by the methylene phosphonic acid compared with the nuclear phosphonic acid exchanger can be anticipated.

Dilatometric measurements[17] with doubly charged polyvinylphosphonates in aqueous solution have revealed that a relatively large volume increase accompanies the replacement of tetramethylammonium by lithium or by sodium ions. This result is consistent with the entropy increase (Table I) found by us if it is assumed that a partial dehydration of the Li^+ ions accompanies their interaction with the structurally bound PO_3^{2-} groups.

(15) *p*-Methylbenzenephosphonic acid shows $pK_1 = 1.98$ and $pK_2 = 7.2$ according to H. H. Jaffé, L. D. Freedman, and G. O. Doak, *J. Am. Chem. Soc.*, **75**, 2209 (1953), whereas for propanephosphonic acid $pK_1 = 2.4$ and $pK_2 = 8.2$, respectively. Corresponding values for phosphoric acid are $pK_1 = 2.1$ and $pK_2 = 7.1$, respectively.

(16) G. Scatchard and P. C. Breckenridge, *J. Phys. Chem.*, **58**, 596 (1954).

(17) U. P. Strauss and Y. P. Leung, *J. Am. Chem. Soc.*, **87**, 1476 (1965).

A Thermally Induced Transition in the Intensity of the Infrared Absorption of Water at 2100 Cm^{-1}

by C. Salama and D. A. I. Goring

Physical Chemistry Division, Pulp and Paper Research Institute of Canada, and the Department of Chemistry, McGill University, Montreal, Quebec, Canada *(Received May 13, 1966)*

The temperature dependence of the intensity of the infrared absorption peak of water in the vicinity of 2100 cm^{-1} has been shown to possess a well-defined inflection at 32°. This result is compared with several previous reports in the literature of discontinuities in the properties of water in the temperature range between 30 and 40°. The frequency of the peak decreased with increase in temperature but no definite inflection was observed

In a recent investigation[1] of the thermal expansion of cellulose and other wood polymers, a second-order transition in volume *vs.* temperature was detected at about 25°. When the dilatometric measurements were repeated with water-soaked materials, the transition was still apparent but was negative in the sense that the expansion coefficient decreased instead of increasing at temperatures above the transition. These results were interpreted as being due to the perturbation of the structure of the layer of water adjacent to the carbohydrate molecule.[2,3] Apparently the perturbed layer showed discontinuities in certain of its properties with an increase in temperature. It was therefore of interest to enquire whether the properties of water itself were discontinuous at or near the second-order transition temperature of the water-soaked carbohydrates.

There are several descriptions in the literature of transitions in the properties of water between 30 and 40°. Magat[4] has listed some examples in an earlier paper. Feates and Ives[5] have cited two sets of data which provide strong evidence for a structural "melting" of water in this temperature range. The accurate measurements of the heat capacity of water at constant pressure by Ginnings and Furukawa[6] show a shallow but definite minimum between 30 and 40°. Bridgman[7] showed that the minimum in the pressure dependence of the viscosity of water was eliminated at about 30°. The temperature at which the initial pressure coefficient of viscosity is zero has been recently determined more accurately to be 33.5°.[8] Drost-Hansen[9] has demonstrated a distinct thermal anomaly at about 30° in the interfacial behavior of water.

A change in the structure of water at 30° should be readily detectible by Raman or infrared spectroscopy. It is well known that both the frequency and intensity of the bands associated with the librational movement of the water molecule are markedly affected by changes in temperature.[4,10,11] The question is whether or not there is any evidence for a discontinuity or inflection point in the temperature dependence of the spectrum which would indicate a transition or phase change in the water.

In order to examine this question, the band at 2100 cm^{-1} in the infrared spectrum of water has been recorded at 5° intervals between 5 and 75°. Three tracings of this peak are shown in Figure 1. As

(1) M. V. Ramiah and D. A. I. Goring, *J. Polymer Sci.*, **C11**, 27 (1965).

(2) G. Némethy and H. A. Scheraga, *J. Chem. Phys.*, **36**, 3382 (1962).

(3) A. Ben-Naim, *J. Phys. Chem.*, **69**, 3245 (1965).

(4) M. Magat, *Trans. Faraday Soc.*, **33**, 114 (1937).

(5) F. S. Feates and D. J. G. Ives, *J. Chem. Soc.*, 2798 (1956).

(6) D. C. Ginnings and G. T. Furukawa, *J. Am. Chem. Soc.*, **75**, 522 (1953).

(7) P. W. Bridgman, "The Physics of High Pressures," Bell, London, 1952, p 346.

(8) K. E. Bett and J. B. Cappi, *Nature*, **207**, 620 (1965).

(9) W. Drost-Hansen, *Ind. Eng. Chem.*, **57**, No. 4, 18 (1965).

(10) P. A. Giguère and K. B. Harvey, *Can. J. Chem.*, **34**, 798 (1956).

(11) G. E. Walrafen, *J. Chem. Phys.*, **40**, 3249 (1964).

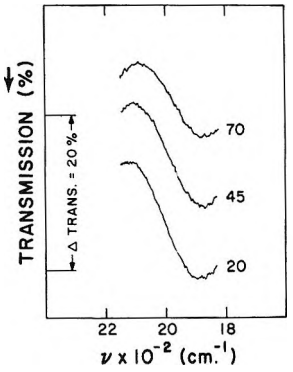

Figure 1. Spectrophotometer tracings of the infrared absorption of water between 1850 and 2150 cm^{-1} at temperatures of 20, 45, and 70°. Cam change was required at 2150 cm^{-1} and in some cases the high frequency side of the peak was not completed.

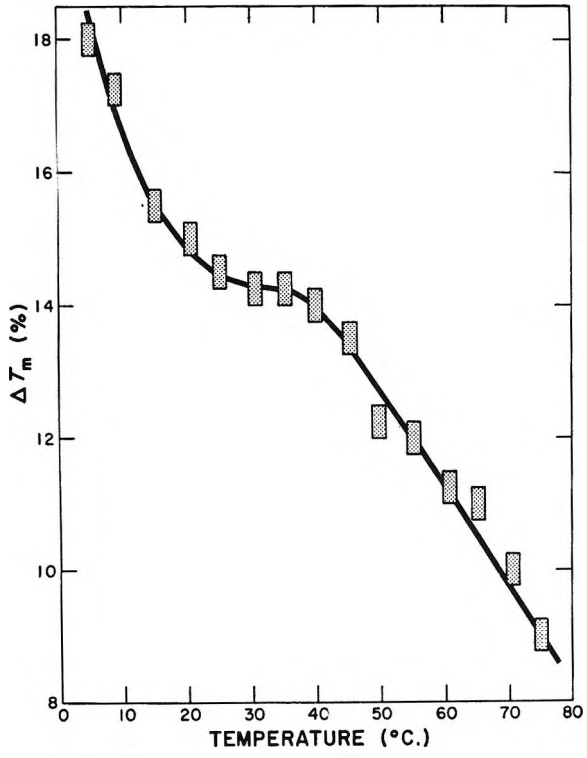

Figure 2. ΔT_m *vs.* temperature. The size of the rectangles approximately represents the possible error in the coordinates.

expected, the frequency and the intensity decrease with an increase in the temperature.

The temperature dependence of ΔT_m, the difference in transmission between the maximum at 2100 cm^{-1} and the minimum at 1900 cm^{-1}, is shown in Figure 2. The rectangles indicate, on the abscissa, the estimated uncertainty in the temperature of the cell, and on the ordinate, the maximum spread in ΔT_m between two sets of readings taken on the same instrument at an

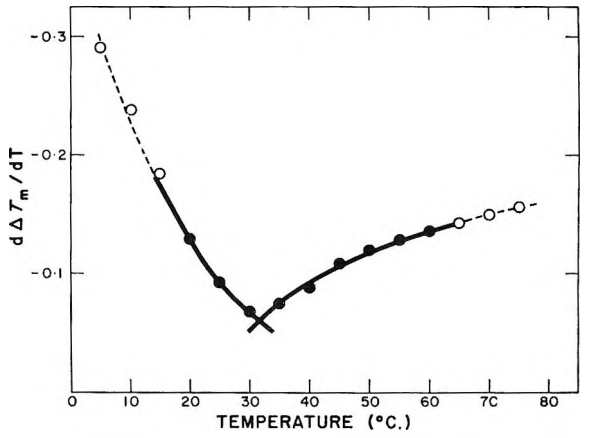

Figure 3. $d\Delta T_m/dT$ *vs.* T derived from the data in Figure 2. The filled circles are midpoint slopes on quadratics through seven points of the curve. The three terminal points (empty circles) at each end of the curve are slopes taken from the quadratic through the terminal seven points.

interval of 4 months. There is no doubt that a marked inflection in the curve occurs between 30 and 40°. In order to locate the inflection point more precisely, the first derivatives were calculated on a computer using a numeric technique of "moving quadratics." A quadratic curve is fitted by the method of least squares to the first seven points of the data, and from this the derivative is calculated at the center (*i.e.*, the fourth) point. A second mid-point derivative is obtained by fitting the next seven points taken by dropping the first point and adding the eighth point to the section. In this way, moving along by adding and dropping terminal points to successive seven-point sections, a series of mid-point derivatives are determined until the last datum point has been reached. The three initial derivatives are calculated from the first quadratic fitted, and similarly the last three are calculated from the last quadratic fitted. (These points are shown as empty circles in Figure 3 which are joined by dotted lines.) The graph of $d\Delta T_m/dT$ *vs.* T (temperature) in Figure 3 shows that the inflection point is at 32°. Some of the infrared traces were analyzed by the base-line method to give the optical density at the maximum of the 2100 cm^{-1} peak. The transition was still found. However, in presenting the data we prefer the simple and unambiguous result of the difference between the maximum and the minimum shown in Figure 1.

The variation with temperature of the frequency of the maximum near 2100 cm^{-1} is shown in Figure 4. The rectangles have the same significance as those in Figure 2. Here, evidence for a transition cannot be claimed, but close examination of the points reveals an indication of an inflection between 30 and 40°.

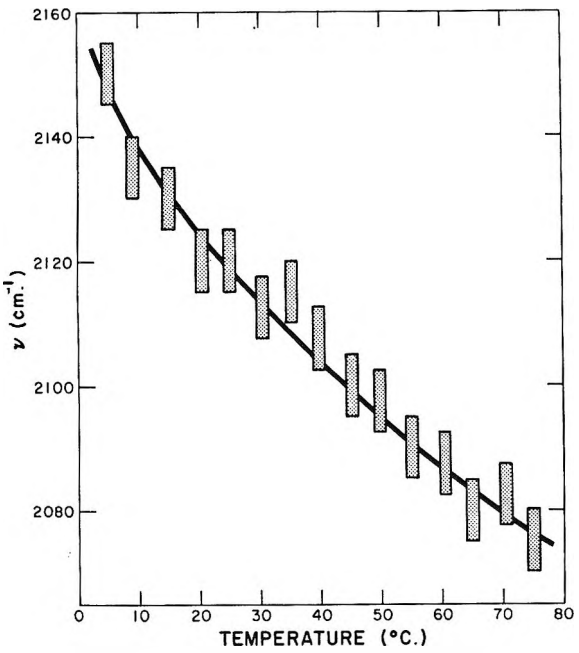

Figure 4. Variation of frequency with temperature for the 2100 cm^{-1} band of water. The size of the rectangles approximately represents the possible error in the coordinates.

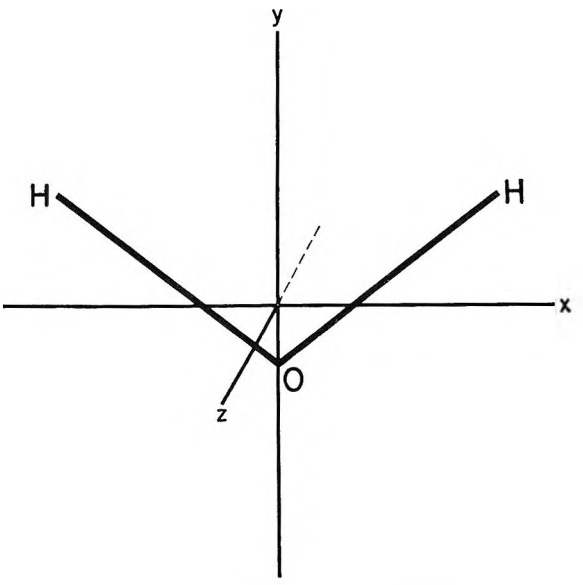

Figure 5. The three atoms of the water molecule are located in the xy plane.

More precise measurement of the frequency is required to confirm or disprove this point. The temperature dependence of the wave number, ν, agrees reasonably well with the three points reported by Fox and Martin[12] some time ago and also with the more recent data of Draegert, *et al.*[13]

The infrared absorption of water in the vicinity of 2100 cm^{-1} is a combination band made up of the symmetrical bending fundamental ν_2 at 1646 cm^{-1} and the librational modes at 500–700 cm^{-1}.[10,11] In the temperature range studied, the position of the maximum in the absorption of the ν_2 band was constant at 1646 $\pm$ 1 cm^{-1} between 11 and 71°. The value of ΔT_m of this band increased from 65.8 to 67.8% between 11 and 71° and showed a slight maximum at 30°. The constancy of the frequency and the slight increase in intensity with temperature parallel the earlier results of Fox and Martin.[12]

The constancy of the 1646 cm^{-1} band suggests that the temperature dependence of the combination band at 2100 cm^{-1} resides in the sensitivity of the librational modes to changes in the thermal energy available to the molecules.[10] This subject was discussed in classical terms by Magat[4] nearly 30 years ago. Magat computed the activation energy for rotation of a water molecule around the axes shown in Figure 5. For rotation around the x and z axes, activation energies of 17.6 and 22.5 kcal/mole were required. Magat noted that these figures were high because cooperative effects of neighboring molecules were not taken into account. Nevertheless, he concluded that rotation of an individual water molecule about the x or z axes is negligibly small at room temperature. The infrared and Raman absorptions between 500 and 700 cm^{-1} correspond to librations about x or z axes. Rotation about the y axis was found to correspond to an activation energy of only 3.6 kcal/mole. Magat suggested that the rapid decrease at 40° in the intensity of the Raman bands at 500 and 700 cm^{-1} was due to the onset of rotation about the y axis.

It should be noted that inflection points in the temperature dependence of both the frequency and intensity of certain bands in the near-infrared spectrum of water have been reported recently. Baistrocchi and Costa[14] characterized the absorption at 0.76 and 0.94 μ between 20 and 90°. They reported one characteristic temperature between 30 and 40° and a second at 70° but did not give the detailed data from which their curves were derived. In an investigation on the association of water, Luck[15] discovered a sharp break in the temperature dependence of the 1.15-μ band between 30 and 40°.

In conclusion, it can be claimed that the present result supports the original observation of Magat.[4] The transition observed is also in accord with several

(12) J. J. Fox and A. E. Martin, *Proc. Roy. Soc.* (London), **A174**, 234 (1940).

(13) D. A. Draegert, N. W. B. Stone, B. Curnutte, and D. Williams, *J. Opt. Soc. Am.*, **56**, 64 (1966).

(14) R. Baistrocchi and M. Costa, *Ann. Idrol.*, **1**, 111 (1963).

(15) A. P. Luck, *Ber. Bunsenges. Physik. Chem.*, **69**, 626 (1965).

other instances in the literature of discontinuities in the properties of water in the temperature range between 30 and 40°.

Experimental Section

Spectra were recorded on a Unicam SP100G vacuum grating spectrophotometer set for maximum resolution. The resolution at 1000 cm^{-1} was 0.3 cm^{-1}.

Calcium fluoride windows were used in a cell with lead spacers which was 0.012 mm thick as determined by the fringe method. Thermostatically controlled water was passed through a jacket which surrounded the cell. The temperature of the sample between the cell windows was determined by means of a copper–constantan thermocouple inserted into the body of the cell to a distance of $^1/_{16}$ in. from the water film between the two windows. The temperature as read by the thermocouple varied ±0.5°.

The water sample used was distilled and then boiled to eliminate dissolved gases.

Measurements were made at intervals of 5°. However, temperatures were not chosen in regular increasing or decreasing order but were selected randomly in order to avoid contributing any minor systematic trend with time to the results of the series of experiments.

Two series of measurements were made. In the first series, spectra were taken at 9, 20, 30, 35, 40, 45, 50, 60, and 70°. The second series was taken about 4 months later and consisted of 15 spectra taken at intervals of 5° between 5 and 75°. In the second series several scans were made at each temperature in order to ensure reproducibility. The results in Figures 2 and 4 are average values for the two sets of measurements. The average mean deviation in ΔT_m was ±0.15% and the maximum mean deviation was ±0.25%. The height of the rectangles in Figure 2 corresponds to the maximum mean deviation. The average mean deviation in ν was ±2.5 cm^{-1}, and the maximum mean deviation was ±5 cm^{-1}. The maximum deviation is given by the height of the rectangles in Figure 4.

A further possible source of error was pointed out by one of the referees. It concerns the increase in the blackbody radiation of the cell on being heated from 5 to 75°. The Nernst filament in the spectrophotometer was maintained at 1700–1800°. Calculations of comparative intensity were made from the classical blackbody equation. Equal divergence at the filament and at the cell was assumed. It was found that at a frequency of 2100 cm^{-1} the radiation generated by the 70° rise in temperature of the cell was approximately 0.05% of the radiation from the Nernst filament. Since the precision of the transmission measurement was ±0.25%, the effect of a 0.05% increase spread over 70° may be assumed to be negligible.

Acknowledgments. The authors wish to thank Mr. E. Koller for suggesting the computer analysis by the method of moving quadratics and Miss R. Sova for making the blackbody calculations. One author (C. S.) is now with Canadian National Technical Research Centre, Montreal.

General Computer Techniques for Evaluating the Time–Concentration Relationships Predicted by Reaction Mechanisms, Including Complex Enzyme Mechanisms[1,2]

by DeLos F. DeTar and Carleton E. DeTar

Department of Chemistry and the Institute of Molecular Biophysics, Florida State University, Tallahassee, Florida *(Received May 17, 1966)*

General techniques are described for computation of reactant and product concentrations as a function of time for a proposed reaction mechanism of almost any complexity. The mechanisms may include equilibria and steady-state systems.

Introduction

The study of reaction mechanisms from the standpoint of kinetics has proved very fruitful, but full use of the technique has been limited since mathematical expressions describing a given mechanism often become intractable with even quite simple mechanisms. Methods of chemical analysis have reached the point that experimental sophistication has outstripped the capabilities of traditional theoretical approaches.[3] A number of workers have therefore turned to computer techniques for the study of complex systems.[4-9] In most cases these have concerned solutions of the specific problems at hand.

A computer program provides tables of numerical values of concentrations at given times. Even when analytical solutions are available, as for example in eq 7 and 12 of ref 3d, these may be so complex as to be useful primarily for preparing similar tabular output. The analytical solutions provide the necessary reference points, but the contrast between the complexity of these hard won expressions and the simplicity of the corresponding iterative computer programs is striking. The introduction of powerful and sophisticated computer techniques into the study of reaction mechanisms provides a wholly new dimension and may be expected to yield a wealth of new developments.

Method of Computation

General. The basic computation involves numerical integration of systems of differential equations. The equation for the decrement D of a given reaction step is eq 1. The simplest form of integration in eq 1 consists of computing reaction decrements for each reaction in turn using the reactant concentrations present at the beginning of the interval. The concentration of a given compound is decremented by D for each equa-

$$D = kx_1x_1 \ldots x_n\Delta t \quad (1)$$

(1) This work was supported by the Division of Biology and Medicine, U. S. Atomic Energy Commission, under Contract No. AT-(40-1)-2690.

(2) We wish to express appreciation to Dr. E. P. Miles and to other members of the Computing Center at Florida State University for generous help and to the computing Center for making available the many hours of computer time needed for developing the programs.

(3) Among the many excellent references to traditional treatments are the following: (a) A. A. Frost and R. G. Pearson, "Kinetics and Mechanism," 2nd ed, John Wiley and Sons, Inc., New York, N. Y., 1961; (b) S. Benson, "The Mathematical Foundation of Chemical Kinetics," McGraw-Hill Book Co., Inc., New York, N. Y., 1960. The mathematical complexities of several relatively simple systems have been elegantly treated, for example, by (c) R. A. Alberty, *J. Am. Chem. Soc.*, **80**, 1777 (1958); (d) W. G. Miller and R. A. Alberty, *ibid.*, **80**, 5146 (1958).

(4) (a) B. Chance, D. Garfinkel, J. Higgins, and B. Hess, *J. Biol. Chem.*, **235**, 2426 (1960), and earlier papers; (b) D. Garfinkel and B. Hess, *ibid.*, **239**, 971 (1964); (c) B. Chance, *ibid.*, **235**, 2440 (1960).

(5) C. Perrin and F. H. Westheimer, *J. Am. Chem. Soc.*, **85**, 2773 (1963).

(6) K. Wiberg, "Computer Programming for Chemists," W. A. Benjamin, Inc., New York, N. Y., 1965, p 168.

(7) C. F. Walter and M. F. Morales, *J. Biol. Chem.*, **239**, 1277 (1964).

(8) (a) C. J. Collins, J. B. Cristee, and V. F. Raaen, *J. Am. Chem. Soc.*, **83**, 4267 (1961); (b) C. J. Collins, *Advan. Phys. Org. Chem.*, **2**, 44 (1964).

(9) See also the RMCH series and RMCHSS, simple programs of moderate generality: D. F. DeTar, *J. Chem. Educ.*, in press.

tion in which it appears as a reactant and incremented by D for each equation in which it is a product. Stoichiometry is preserved by applying the incrementing or decrementing to each appearance of a given reactant or product. Hence for the second-order reaction A + A → B (with rate constant k,) the amount of B produced is D, and the amount of A which disappears is $2D$. The effect is to interpret the rate constant as equal to k with respect to B and $2k$ with respect to A.

Certain of the more sophisticated forms of integration are more efficient.[10] A modification of the trapezoidal method (eq 2) appears to be the best compromise. The more elaborate Runge–Kutta method is slower.[9]

$$\Delta_t = 1.5D_i - 0.5D_{i-1} \tag{2}$$

Steady-State Intermediates. Obviously, the simple incrementing and decrementing approach is not applicable to a reaction involving steady-state intermediates, for a definition of a steady-state intermediate appropriate to an interative calculation is a species whose concentration is less than, perhaps very much less than, the reaction flux, *i.e.*, the decrement D for that reaction. Therefore, the concentration of a steady-state intermediate is never incremented or decremented but is determined instead by direct calculation.

The problem of calculating concentrations of a set of steady-state intermediates admits of no simple general solution. Iterative procedures must therefore be used, and two independent approaches have been devised.

In the first, the regular method, the concentration of a given steady-state intermediate, S_n, is given by eq 3; the i summation includes all those reactions in which S_n is a product, and the j summation includes all those reactions in which S_n is a reactant and A_j's are the re-

$$S_n = (\sum_i^{p} k_i A_i B_i)/(\sum_j^{r} k_j A_j) \tag{3}$$

spective coreactants. A and B are the concentrations of A and B, respectively. Inclusion of further terms is obvious if there are more than two reactants or products. A_i, B_i, and A_j may also be steady-state intermediates (including S_n). If the set of equations for a given steady-state intermediate does not contain any steady-state intermediates among the A_i, etc., then the concentrations are obtained without iteration.

In the more general case the solutions are only approximate. One possible iterative procedure is to keep substituting the values of S_n found in the previous iteration. However, this primitive approach is not very effective.

The first step toward a workable method is to replace eq 3 by the equivalent equations (4 and 5). (D values are defined in eq 1.) In eq 4 the summation over p includes only reactions in which S_n is a product and

$$R_n = \sum^{p} D_i / \sum^{r} D_j \tag{4}$$

$$S_n(\text{new}) = R_n S_n(\text{old}) \tag{5}$$

that over r only reactions in which S_n is a reactant. If S_n has its correct value, then $R_n = 1$, while $R_n > 1$ means that the estimate of S_n is too small. Equation 4 permits incorporation of a damping factor (DF) to reduce the tendency toward over compensation and hence oscillation.

$$S_n(\text{new}) = [(\text{DF})^* R_n + 1 - \text{DF}]S_n(\text{old}) \quad (\text{for } R_n > 1) \tag{6a}$$

$$S_n(\text{new}) = S_n(\text{old})/[\text{DF}/R_n + 1 - \text{DF}] \quad (\text{for } R_n < 1) \tag{6b}$$

This method of calculation has worked very well with several different mechanisms. The first round of iterations may run to 20–30 to bring all S_n to within 0.2%, *i.e.*, until $R = 1.000 \pm 0.002$ for each R. Once the "reaction" is underway, however, from three to five iterations usually suffice to touch up the concentrations of steady-state intermediates.

In some mechanisms it is necessary to keep the total concentrations of certain families of steady-state intermediates constant. This corresponds physically to a closed system such as an enzyme system in which one family of steady-state intermediates is represented by all the species containing this enzyme. In this case the concentration of each species is normalized by a factor equal to the ratio of the apparent total enzyme concentration to the desired total concentration.

In the second method, the perturbation method of obtaining steady-state concentrations, the D_n is written in generalized form as eq 7; S_{n1} is the first steady-state intermediate in reaction n, S_{n2} is the second, X_{n1} is the first other type of reactant (X = concentration of X), etc. Usually there will be only one or two reactants,

$$D_n = k_n S_{n1} S_{n2} \ldots X_{n1} X_{n2} \ldots \Delta t \tag{7}$$

but it is necessary to formulate general expressions. It is now assumed that for each steady-state intermediate in each equation there is available a preliminary estimate S' which is reasonably good, and that it is desired to find the correction term δS which gives the correct value S, through eq 8. Substitution of (8)

(10) (a) E. Whittaker and G. Robinson, "The Calculus of Observations," 4th ed, Blackie & Son Ltd., London, 1944, p 132; (b) H. Margenau and G. M. Murphy, "The Mathematic of Physics and Chemistry," D. Van Nostrand Co., Inc., New York, N. Y., 1943, p 450.

into (7) gives (9) where g_n is the number of steady-

$$S_{n1} \longleftarrow S_{n1}' + \delta S_{n1} \tag{8}$$

$$D_n = D_n'\left\{1 + \sum_{k=1}^{g_n} \frac{\delta S_{nk}}{S_{nk}'}\right\} \tag{9}$$

state intermediates in reaction n. All terms involving products of two or more δS have been discarded as representing high-order corrections. If the method converges, any error so introduced is corrected by iteration.

The general steady-state relationship (*cf.* eq 4 with $R_n = 1$) is eq 10. All summations are taken over only those D terms in which radical S_n is a product (summation over p) or a reactant (summation over r). Substi-

$$\sum^{p} D_i - \sum^{r} D_j = 0 \tag{10}$$

tution of eq 9 into eq 10 gives eq 11. It may be noted that eq 11 is linear in the δS terms and that with one

$$\sum^{p}\left\{\sum_{k=1}^{g_n} \frac{\delta S_{nk}}{S_{nk}'}\right\} D_n' - \sum^{r}\left\{\sum_{k=1}^{g_n} \frac{\delta S_{nk}}{S_{nk}'}\right\} D_n' = \sum^{r} D_n' - \sum^{p} D_n' \tag{11}$$

equation for each intermediate it is possible to solve for these corrections.

To treat the case of closed systems, the first equation for each family which comprises a closed system is arbitrarily replaced by the constraining equation 12 in which the total concentration is specified as the sum of the concentration of the component species V_{ik}. The perturbation form of eq 12 is eq 13.

$$T_k = \sum_{i=1}^{n_k} V_{ik} \tag{12}$$

$$\sum_{i=1}^{n_k} \delta V_{ik} = T_k - \sum_{i=1}^{n_k} V_{ik}' \tag{13}$$

Which version, the regular or the perturbation, is better must be ascertained by trial. In some mechanisms one is clearly superior; occasionally both must be used in a cyclic order. The direct method is effective for many very complex sets of steady-state intermediates but does not converge well if both numerator and denominator contain a functionally related dominant term. Such an example is a polymerization mechanism with respect to the dominant polymerization step: $RM\cdot + M \rightarrow RM\cdot$. The perturbation method requires solution of an $N \times N$ determinant where N is the number of steady-state species. This rapidly loses efficiency as N becomes large.

Acid–Base Equilibria.[11,12] The equilibria referred to in this section are those that determine the concentration of hydrogen ion or other lyonium ion or conversely of hydroxide or other lyate ion.

For n acid–base systems with m_i species in the ith system, with q_{ij} representing the charge and c_{ij} the concentration of the jth species of the ith system, and c_{it} the family total for the ith system, then eq 14 is the conservation of mass expression and eq 15 defines a term Q which may be called the charge excess. If a buffer system is established by mixing certain volumes of

$$c_{it} = \sum_{j=1}^{m_i} c_{ij} \tag{14}$$

$$Q = \sum_{i=1}^{n} \sum_{j=1}^{m_i} c_{ij} q_{ij} - c_{H^+} + c_{OH^-} \tag{15}$$

0.1 M phosphoric acid and 0.1 M sodium hydroxide, then Q is equal to the concentration of sodium ion, for example. Acidity constants for each dissociation step are denoted K_{ij} for dissociation of a proton from the jth species to produce the $j + 1$ species of the ith system (eq 16). The concentration of the jth species of the ith system is given in terms of the initial species by eq 17, with the proviso that the product function is unity for $j = 1$. Finally, the concentration of the

$$c_{ij+1} c_{H^+} = c_{ij} K_{ij} \tag{16}$$

$$c_{ij} = \frac{c_{it}}{c_{H^+}^{\,j-1}} \prod_{k=1}^{j-1} K_{ik} \tag{17}$$

jth species of the ith system is given in terms of c_{it}, the total concentration of the system, by combining eq 17 and 14 to give eq 18.

$$c_{ij} = c_{it}\left\{\frac{1}{c_{H^+}^{\,j-1}} \prod_{k=1}^{j-1} K_{ik}\right\}\left\{\sum_{j=1}^{m_i} \frac{1}{c_{H^+}^{\,j-1}} \prod_{k=1}^{j-1} K_{ik}\right\}^{-1} \tag{18}$$

The computation proceeds as follows. A preliminary very rough estimate for c_{H^+} is supplied. The individual species concentrations are computed through eq 18, and an estimate of Q $(= Q')$ is evaluated by eq 15. If Q' is smaller than Q, then the c_{H^+} estimate was too small. By means of an iterative procedure involving logarithmic steps, successive values of c_{H^+} are tested until the change is less than some predetermined amount, *e.g.*, c_{H^+} accurate to 0.01%.

Equilibrium Reactions. These concern potentially complex systems such as those involving carboxylic acid monomers and dimers and their salts in nondissociating solvents. The general equations are given

(11) *Cf.* L. G. Sillén, "Treatise on Analytical Chemistry," I. M. Kolthoff and P. J. Elving, Ed., The Interscience Encyclopedia Inc., New York, N. Y., 1959, p 277.

(12) (a) A. R. Emery, *J. Chem. Educ.*, **42**, 131 (1965); (b) A. J. Bard and D. M. King, *ibid.*, **42**, 127 (1965); (c) S. L. Cooke, Jr., *ibid.*, **42**, 620 (1965).

in eq 19, in which the R_{ij}'s are reactants and the P_{ij}'s are products of the ith reaction with equilibrium constant K_i, and the equilibrium expression eq 20. Each of the R_{ij} and P_{ij} may be assigned to a specific family

$$R_{i1} + R_{i2} + \ldots + R_{im_i} \underset{}{\overset{k_i}{\rightleftharpoons}} P_{i1} + P_{i2} + \ldots + P_{in_i} \quad (19)$$

$$K_i \prod_{j=1}^{m_i} R_{ij} = \prod_{j=1}^{n_i} P_{ij} \quad (20)$$

such as the acetate family, the triethylamine family, etc. If the family total is represented as t_m, then the conservation of mass equation (21) holds, assuming k_m species in family m.

$$t_m = \sum_{1}^{k_m} S_{km} \quad (21)$$

Each S_{km} corresponds to one or more of the R_{ij} or P_{ij} and, *vice versa*, the connections being uniquely determined by the equilibrium equations. Hence eq 20 and 21 uniquely define the equilibrium concentrations. The general solution cannot be achieved in closed form and is therefore carried out by a perturbation technique. Setting $S = S' + \delta S$, $R = R' + \delta R$, $P = P' + \delta P$, and substituting into eq 20 and dropping terms with more than one δ gives eq 22. (It is also assumed in obtaining eq 22 that the $\Sigma(\delta R/R)$ is small compared with unity so that ln $[1 + (\Sigma\delta R/R)]$ can be taken as $\Sigma(\delta R/R)$.) Similarly, substitution into eq 21 gives eq 23. These linear equations in the

$$\sum_{j=1}^{m_i} \frac{\delta R_{ij}}{R_{ij}'} - \sum_{j=1}^{n_i} \frac{\delta P_{ij}}{P'} = \ln \left[\prod_{j=1}^{n_i} P_{ij}' \Big/ K_i \prod_{j=1}^{m_i} R_{ij}' \right] \quad (22)$$

δ terms can be solved providing the initial estimates are reasonably good and provided further that the total number of unique species is equal to the number of equilibrium reactions plus the number of families.

$$\sum_{k=1}^{k_m} \delta S_{km} = t_m - \sum_{k=1}^{k_m} S_{km}' \quad (23)$$

The family stoichiometries can contain both negative and positive terms. The equilibrium computation thus overlaps the acid–base computations described above.

Preliminary estimates may be found by a semiempirical method. For each appearance of a given species as an equilibrium reactant in reaction i the quantity $(K_i)^{-1/2}$ is added to a distribution factor for that species, and for each appearance as a product the quantity $(K_i)^{1/2}$ is added. If the factor for species k of family m is denoted by f_{km}, then the preliminary estimates are those given by eq 24.

$$S_{km}' = t_m f_{km} \Big/ \sum_{m=1}^{k_m} f_{km} \quad (24)$$

The literature on application of computer techniques to equilibrium calculations is moderately extensive. There are two general problems, one the converse of the other. One problem is to find the best values of a series of equilibrium constants given a set of equations and concentration data. This problem has been treated by several workers.[13,14] The converse problem treated here is to find the concentrations of a series of reactants and products given the equilibrium conditions. The equilibrium conditions may be expressed in terms of equations and equilibrium constants or in terms of free energies of formation.[15-17]

Selected Results

The iterative procedures have been checked with reference to exact calculations of several relatively simple reactions.[18] For a first-order reaction defined by eq 25, the concentration of x was determined as a

$$x = x_0 e^{-kt} \quad (25)$$

function of time using uniform Δt values ranging from very coarse steps of $^1/_2$ of a half-time, through progressively finer steps of $^1/_{10}$, $^1/_{50}$, and $^1/_{200}$ half-times. For a reaction period of 8 half-lives, these correspond to 16, 80, 400, and 1600 iterations. For the latter, the calculated values of x agreed with theoretical to within better than one part in 10,000 *relative* at all points from 7 to 99.6% of reaction. The error with 400 iterations was about three parts in 10,000, with 80 iterations it was about one part in 300 relative, and for 16 iterations it was about 4% relative.

A slightly more complex reaction is one in which a reactant A disappears by parallel first- plus second-order steps (eq 26). The theoretical kinetic expression for the concentration of A at any time is given in eq 27. For a series of runs using values of k_1 and k_2 such

$$\begin{aligned} A &\xrightarrow{k_1} B \\ A + A &\xrightarrow{k_2} C \end{aligned} \quad (26)$$

that the mechanism ranged from pure first order through a variety of mixed orders (5, 10, 50, 75%,

(13) L. G. Sillén, *Acta Chem. Scand.*, **16**, 159 (1962); N. Ingri and L. G. Sillén, *ibid.*, **16**, 173 (1962).

(14) J. A. Chopoorian, G. R. Choppin, H. C. Griffith, and R. Chandler, *J. Inorg. Nucl. Chem.*, **21**, 21 (1961).

(15) H. B. Levine, *J. Chem. Phys.*, **36**, 3049 (1962).

(16) G. Anderegg, *Helv. Chim. Acta*, **45**, 901 (1962).

(17) J. Marek and R. Holub, *Collection Czech. Chem. Commun.*, **29**, 1085 (1964).

(18) We wish to acknowledge the valuable help of Victor M. Day in carrying out many of these computations.

initial second order) up to pure second order, the values

$$A = A_0k_1e^{-k_1t}/(k_1 + k_2A_0e^{-k_1t}) \qquad (27)$$

calculated showed comparable concordance with theory. For example, with 2000 iterations of a reaction initially 75% second order, observed and calculated values agreed to better than one part in 10,000 relative from 3 to 90% of reaction. Such high accuracy is seldom required, but the capability is available upon demand.

The described computational methods have been tested on several complex problems for which exact solutions are available only under special conditions, or perhaps not at all.

One type of moderately complex mechanism is a polymerization with induced decomposition of peroxide and with a retarder or inhibitor.[19] A still more complex set of equations is required by chain transfer.[20] Various such mechanisms have been investigated, ranging in complexity from 8 to 35 equations, and from 1 to 8 different steady-state intermediates. In all cases computation proceeded without difficulty, although in some cases the steady-state options had to be chosen correctly. In limiting cases, the concentrations of steady-state intermediates agreed closely with those predicted by simple theory.

The deamination of 1,2,2-triphenylethylamine was studied by Collins, *et al.*[8] Products included four forms of carbinol: rearranged, racemized, unrearranged, and unracemized in all combinations. Using the rate constant ratios given in Table 5 of ref 8b, the predicted proportions of the four products agreed exactly with the published values for the two examples examined (first and last). The product distribution, of course, remains constant throughout this particular reaction.

Perhaps the most complex reaction schemes for which detailed parameters are available are the multienzyme systems described in a pioneering series of papers by Chance and his co-workers.[4] One study by Garfinkel and Hess concerned a computer model to describe the glycolytic pathway in the metabolism of Ascites cells. The published model mechanism consists of 89 equations, with 24 normal reactants and products, and 13 different enzyme systems consisting of a total of 41 enzyme intermediates.[4b]

This problem offers a challenge to any computer program. In setting up the data, there arose certain questions of interpretation in spite of the wealth of detail in the paper. We elected to treat the problem as one involving steady states since this is inherently more difficult than is the treatment as a set of sequential reactions. Any serious study of such a system would, of course, require a judicious selection of several combinations of steady-state and nonsteady-state runs. We were concerned primarily with the computational aspects of this problem and not greatly with biochemical, biological, or fundamental kinetic aspects.

Our method of computation can hold total enzyme family concentrations constant, and these were taken as the sums of the concentrations listed as initial. A few modifications were made in the published values:[4b] k for eq 5 should apparently be 3×10^3 rather than 3×10^{-3}, DHA was apparently inadvertantly omitted as a product in eq 87, and eq 15–21 were rewritten so as to be in accord with the principle of microscopic reversibility, *i.e.*, forward and reverse versions of each reaction must have the same catalyzing species.

```
ASSUMED REACTION SCHEME
       EQUILIBRIUM SYSTEMS *
      .AMINE, RNH2, RCOO-RNH3+, (RCOOH)2 RNH2 *
      .ACID, RCOOH, (RCOOH)2, (RCOOH)2, RCOO-RNH3+, (RCOOH)2 RNH2,
      .(RCOOH)2 RNH2
       STEADY STATE INTERMEDIATES * ACISUREA * ACISUR.ACID*(RCO)2O
       REACTANTS AND PRODUCTS * DIIMIDE, UREA, ACUREA, RCONHR
       EQUILIBRIUM REACTIONS
 1      RCOOH    * RCOOH      = (RCOOH)2
 2      RNH2     * RCOOH      = RCOO-RNH3+
 3      RCOOH    * RCOOH    * RNH2      * (RCOOH)2 RNH2
       NORMAL REACTIONS
 4      RCOOH    * DIIMIDE    = ACISUREA
 5      RCOOH    * ACISUREA   = (RCO)2O  * UREA
 6      ACISUREA              = ACUREA
 7      (RCOOH)2 * DIIMIDE    = ACISUR.ACID
 8      ACISUR.ACID           = (RCO)2O  * UREA
 9      ACISUR.ACID           = ACUREA   * RCOOH
10      (RCO)2O  * RNH2       = RCONHR   * RCOOH
11      ACISUREA * RNH2       = RCONHR   * UREA
12      ACISUREA              = RNH2 + ACUREA
       END OF MECHANISM * INDEX *
```

Figure 1. Amide formation by reaction with carbodiimides including acid–base equilibria and direct acylation by acylisourea. The date, set identification, and page number have been omitted to save space. The printout shown is largely a reproduction of the data cards except for the format of the header, the Assumed Reaction Scheme, and the sequential numbering of the equations. Equation 3 illustrates the presence of three reactants, and eq 12 shows catalysis by RNH_2.

```
      INITIAL TRIALS

PROBLEM CARDS
       TABLE* ACID, AMINE, DIIMIDE, (RCO)2O, ACUREA, UREA, RCONHR, RNH2
       TABLE * RCOO-RNH3+, (RCOOH)2 RNH2, (RCOOH)2, ACISUREA, RCOOH,
      .ACISUR.ACID, RCT, 5, RCT, 7
       TABLE * RCT, 9, RCT,10, RCT,11, RCT,12, RCT, 6, RCT, 8, RCT, 4
       YIELDS BASED ON * DIIMIDE, ACID, AMINE
       INITIAL CONCENTRATIONS * M/L, RNH2 = .1, RCOOH = .2, DIIMIDE = .1
       PARAMETERS * DT=100, SEC. * ITERATE, 10, 1
       DT =   1.00E 02 SEC.    T =    0.        NP =   10 NINTER =    1
       DISP RG = 0. AB = 0. EQ = 0. SS = 0. NREPAB =   6 NREPEQ =  20 NREPS1 = 15
       NREPS2 = 15 OPT = 1 NCYCLE = 1 EVEN INCREMENT = 0.          (REACTION  01
       TOLEQU =   2.0E-03 TOLSTS =   2.0E-03 NEGCHK = 1 DAMPSS = 0.70
       REACTION CONSTANTS * 1,          5,          10000.
      .    .01,       600,        10,         1,          6000,       10.
      .    1E3,       1 E 3,      100
```

Figure 2. Amide formation by reaction with carbodiimides including acid–base equilibria and direct acylation by acylisourea. This is largely a reproduction of problem set data cards except for the two lines of header, and the four lines beginning with DT, DISP, NREPS2, and TOLEQU. The date, set identification, and page numbers have been omitted.

(19) C. Walling, "Free Radical Reaction," John Wiley and Sons, Inc., New York, N. Y., 1957.

(20) R. A. Gregg and F. R. Mayo, *J. Am. Chem. Soc.*, **70**, 2373 (1948); F. R. Mayo, *ibid.*, **70**, 3689 (1948).

INITIAL TRIALS

TABLE 1

CONCENTRATIONS IN M/L

TIME SEC.	ACID	AMINE	DIIMIDE	(RCO)2O	ACUREA	UREA	RCONHR	RNH2
INITIAL	0.	0.	1.0000E-01	1.0000E-10	0.	0.	0.	1.0000E-01
0.	2.0000E-01	1.0000E-01	1.0000E-01	6.0214E-06	0.	0.	0.	1.2780E-02
1.0000E 02	1.9071E-01	9.1469E-02	9.0717E-02	8.0698E-06	7.4835E-C4	8.5341E-03	8.5310E-03	1.0184E-02
2.0000E 02	1.8087E-01	8.2385E-02	8.0878E-02	1.1542E-05	1.4967E-C3	1.7625E-02	1.7614E-02	7.7258E-03
3.0000E 02	1.7041E-01	7.2678E-02	7.0427E-02	1.7769E-05	2.2309E-C3	2.7341E-02	2.7322E-02	5.5179E-03
4.0000E 02	1.5915E-01	6.2144E-02	5.9183E-02	2.9565E-05	2.9303E-C3	3.7885E-02	3.7856E-02	3.6566E-03
5.0000E 02	1.4705E-01	5.0672E-02	4.7077E-02	5.2082E-05	3.5631E-C3	4.9358E-02	4.9328E-02	2.2285E-03
6.0000E 02	1.3442E-01	3.8600E-02	3.4466E-02	9.1254E-05	4.0900E-C3	6.1442E-02	6.1400E-02	1.2592E-03
7.0000E 02	1.2258E-01	2.7146E-02	2.2627E-02	1.4439E-04	4.4764E-C3	7.2896E-02	7.2854E-02	6.7998E-04
8.0000E 02	1.1337E-01	1.8161E-02	1.3411E-02	1.8702E-04	4.7163E-C3	8.1873E-02	8.1839E-02	3.7588E-04
9.0000E 02	1.0763E-01	1.2526E-02	7.6539E-03	1.9320E-04	4.8459E-C3	8.7500E-02	8.7474E-02	2.3175E-04
1.0000E 03	1.0435E-01	9.3242E-03	4.3811E-03	1.6762E-04	4.9165E-C3	9.0702E-02	9.0676E-02	1.6233E-04

YIELDS BASED ON

DIIMIDE	109.13	9.75	4.58	0.18	5.14	94.86	94.83	0.17
ACID	109.10	9.75	4.58	0.18	5.14	94.83	94.80	0.17
AMINE	115.08	10.28	4.83	0.18	5.42	100.03	100.00	0.18

Figure 3. Amide formation by reaction with carbodiimides including acid–base equilibria and direct acylation by acylisourea. Yield calculations are based on reactant used. The figures for the yield of amine based on amine of acid based on acid and of diimide on diimide are to be disregarded. Only the first of three tables is shown. ACID is total acid concentration; AMINE is total amine concentration. RCOOH, free acid, appeared in Table 2; RNH_2 is free amine.

After initial adjustment, and during the early portions of the computation, the steady-state adjustment required only about ten passes through the "regular" steady-state subroutine to reach limiting values at each iteration. Δt was taken as 0.05 sec since 0.5-sec intervals caused certain concentrations to become negative very early. The program ran smoothly for the 100 iterations required to give 5 sec of real time, then the 0.01 M glucose was added, and computation was continued until it ceased at 22 sec when 2GA[4b] became negative (360 more iterations). The total run time was as follows: 1 min to read, compile, and write the mechanism; 35 sec to read, compile, and write the rate constants, concentrations, table specifications, and other parameters; the 460 iterations required 27 min, of which about 1.5 min was required to write the tables.

The previous authors emphasized problems involving oscillations, a plaguing form of computational instability they encountered in several parts of the program. We encountered no such instability but have occasionally observed oscillations with other mechanisms. However, in all of our cases this has resulted from concentration terms inadvertently becoming negative. A whole series of such mysteries cleared up in rapid order when we made the check for negative concentrations automatic unless specifically disabled.

The computation has been tested with a variety of other enzyme mechanisms including the fumarase system of Alberty,[21] which involves three levels of protonation for each enzyme species, and a general multienzyme system, which includes two substrates, two products, eight forms of the enzyme, and a multiplicity of closed paths.

Description of the Program

REMECH consists of about 7000 source program cards containing about 2500 comment and dimension cards. It is written primarily in FORTRAN-II for the IBM 709, but there are several FAP subroutines. Within the limits of our resources we will supply a tape copy of the program and of sample data and also an instruction manual to anyone who will send a tape. Separate copies of the manual and decks of cards cannot be furnished. Eventually the program will be converted to FORTRAN IV and MAP and to the CDC-6400 languages.[22]

An example of the output is given in Figures 1–3. For the most part the output shown in Figures 1 and 2 is simply a listing of the input cards. Input is in free format with the asterisk, the comma, and the equals sign used as field delimiters. The program automatically establishes all computing arrays.

The mechanism shown is taken from current research on the mechanisms of carbodiimide reactions.[23] It is chosen primarily to show a variety of features of REMECH including equilibrium reactions, steady-state intermediates, and catalysis. Only one table is illustrated although three were printed by the computer.

It is worth observing that no computer program can be a substitute for research judgment, nor can it be used profitably by a mere technician. Neither does it replace traditional approaches to a problem involving kinetics. A computer program is a tool and, used properly, can be a powerful aid in the study of reaction mechanisms and for providing insights not otherwise attainable.

(21) D. A. Brant, L. B. Barnett, and R. A. Alberty, *J. Am. Chem. Soc.*, **85**, 2204 (1963).

(22) REMECH if now available in all three versions. Run times on the CDC 6400 with the "RUN 1.1" computer are about 1/15 of those on the 709.

(23) D. F. DeTar and R. Silverstein, *J. Am. Chem. Soc.*, **88**, 1013 (1966).

Photoconductivity of Electron Acceptors. I. Nitro Derivatives of Fluoren-$\Delta^{9\alpha}$-malononitrile

by Tapan K. Mukherjee

Energetics Branch, Air Force Cambridge Research Laboratories, Bedford, Massachusetts
(Received June 3, 1966)

The phenomenon of photoconduction in four dinitro isomers of fluoren-$\Delta^{9\alpha}$-malononitrile, 2,4,7-trinitrofluoren-Δ-$^{9\alpha}$-malononitrile, and 2,4,5,7-tetranitro fluoren-$\Delta^{9\alpha}$-malononitrile has been investigated. The bulk and surface photoelectrical characteristics of the 2,7-dinitro isomer have been studied in some detail. The large photocurrent in this compound is associated with the excitation energy corresponding to 515 mμ. A strong fluorescence emission peak at 520 mμ is observed.

Introduction

The photoconductivity of molecular solids possessing polynuclear aromatic structures, *viz.*, anthracene,[1] perylene,[2] and heterocyclic amines,[3] has been studied extensively. These materials are typical electron donors. On the basis of the fact that the photoconductive dyes,[4] like malachite green, rhodamine B, pinacyanol etc., form donor–acceptor complexes[5] and anion radical salts[6] with electron acceptors, they can also be classified as donors. Recently some studies on the photoconduction in several donor–acceptor complexes have been published.[7,8] In contrast, very little information is available about the light-induced conductivity of electron acceptor molecules. In connection with the work on sensitization of electrostatic imaging processes, Hoegl[9] lists a number of electron acceptors as photoconductive materials. The photoconductivity observed in the partially nitrated polyacenaphthylene[10] probably arises from the donor–acceptor interaction. Reucroft and co-workers thoroughly investigated the nature[11] and origin[12] of the bulk photoconductivity of *p*-chloranil, along with several other halogenated benzoquinones.

As a part of a program on organic p–n junctions, the photoelectric characteristics of several electron acceptors have been examined in this laboratory. In this paper we wish to report the preparation and photoconductive properties of a number of nitro derivatives of fluoren-$\Delta^{9\alpha}$-malononitrile.

Experimental Section

Materials. Malononitrile was condensed with 2,4-dinitrofluorenone (Ia),[13] 2,5-dinitrofluorenone (Ib),[14] 2,6-dinitrofluorenone (Ic),[15] 2,7-dinitrofluorenone (Id),[14] 2,4,7-trinitrofluorenone (Ie), and 2,4,5,7-tetranitrofluorenone (If), respectively, by a previously published procedure[16] to give the corresponding dicyanomethylene

(1) J. Kommandeur, *J. Phys. Chem. Solids*, **22**, 339 (1961).

(2) B. J. Mulder, *Rec. Trav. Chim.*, 713 (1965).

(3) H. Inoue, K. Noda, and E. Imoto, *Bull. Chem. Soc. Japan*, **37**, 332 (1964).

(4) H. Meier, *Angew. Chem.*, **77**, 633 (1965).

(5) J. E. LuValle, A. Leifer, M. Koral, and M. Collins, *J. Phys. Chem.*, **67**, 2635 (1963).

(6) T. K. Mukherjee, to be published.

(7) H. Akamatu and H. Kuroda, *J. Chem. Phys.*, **39**, 3364 (1963).

(8) M. C. Tobin and D. P. Spitzer, *ibid.*, **42**, 3652 (1965).

(9) H. Hoegl, *J. Phys. Chem.*, **69**, 755 (1965).

(10) A. Inami, K. Morimoto, and Y. Hayashi, *Bull. Chem. Soc. Japan*, **37**, 842 (1964).

(11) P. J. Reucroft, O. N. Rudyi, R. E. Solomon, and M. M. Labes, *J. Phys. Chem.*, **69**, 779 (1965).

(12) P. J. Reucroft, O. N. Rudyi, R. E. Solomon, and M. M. Labes, *J. Chem. Phys.*, **43**, 767 (1965).

(13) F. Ullmann and J. Broido, *Ber.*, **39**, 360 (1906). We are thankful to Professor Allan K. Colter for a sample of this compound.

(14) C. Courtot, *Ann. Chim.*, **14**, 5 (1930).

(15) This compound as obtained from Aldrich Chemical Co. was found to be quite impure. It was purified by repeated chromatography over a silica gel column using chloroform as the eluent, followed by crystallization from acetonitrile, mp 235–236°.

(16) T. K. Mukherjee and L. A. Lavasseur, *J. Org. Chem.*, **30**, 644 (1965).

Table I: Melting Points, Elemental Analyses, and Fluorescence Emission of Nitro Derivatives of Fluoren-$\Delta^{9\alpha}$-malononitrile

Compound	Mp, °C	Calcd C	Calcd H	Calcd N	Found C	Found H	Found N	Fluorescence
2,4-Dinitro (IIa)	259–162	60.38	1.90	17.60	60.61	2.06	17.45	Yellow (+++)
2,5-Dinitro (IIb)	250–252	60.38	1.90	17.60	60.35	2.08	17.57	Orange (++)
2,6-Dinitro (IIc)	225–226	60.38	1.90	17.60	60.42	1.98	17.48	Yellow-orange (+)
2,7-Dinitro (IId)	298–299	60.38	1.90	17.60	60.47	2.04	17.80	Yellow-green (++++)
2,4,7-Trinitro (IIe)	266–268[a]	52.89	1.38	19.25	52.49	1.56	19.33	Yellow (+)
2,4,5,7-Tetranitro (IIf)	>400[b]	47.07	0.98	20.58	47.25	1.05	20.57	Yellow-green (++)

[a] See ref 16. [b] T. K. Mukherjee and A. Golubovic, Abstracts, 149th National Meeting of the American Chemical Society, Detroit, Mich., April 1965, p 53P.

derivatives (IIa–IIf) shown below.

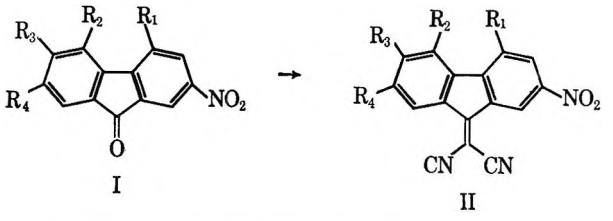

I II

(a) $R_1 = NO_2$, $R_2 = R_3 = R_4 = H$
(b) $R_2 = NO_2$, $R_1 = R_3 = R_4 = H$
(c) $R_3 = NO_2$, $R_1 = R_2 = R_4 = H$
(d) $R_4 = NO_2$, $R_1 = R_2 = R_3 = H$
(e) $R_1 = R_4 = NO_2$, $R_2 = R_3 = H$
(f) $R_1 = R_2 = R_4 = NO_2$, $R_3 = H$

Table I records their melting points and elemental analyses. The last column shows a comparison of fluorescence emission of the solids, as observed visually under ultraviolet excitation. Purification of these compounds by zone-refining technique was not successful due to partial carbonization of the melt. The compounds (I and II) were extensively purified by a combination of column chromatography, crystallization, and vacuum sublimation. The purity was checked by melting points, thin layer chromatography, and molecular extinction coefficients. It is important to note that the compounds IIa–IIe are fairly strong electron acceptors and react readily with alkali. Consequently, all operations were performed in acid-washed glassware.

Photoconductivity Measurements. The surface conductivity experiments were performed on a "comb"-type gold grid deposited on glass plate. The interelectrode spacing was 0.25 mm. Thin layers of the substances were deposited either by solvent evaporation or by vacuum sublimation techniques. The latter method was extensively used in the case of the 2,7-dinitro compound (IId). The surface cell was held by electrical leads in an evacuable glass chamber fitted with an optically flat quartz window. The cell was attached to a thermocouple, and heat was supplied by preheated nitrogen. The assembly was essentially of the same design described by Meier.[17]

For bulk conductivity measurement, the substances were solution-evaporated on the conductive sides of NESSA quartz plates. The other electrode consisted of a spring-activated aluminum disk. For the evaluation of the bulk photoconductivity efficiency (I_p/I_d), the "sandwich" cell was placed at a distance of 7 cm from a 200-w incandescent lamp (100 μw/cm^2, intensity of incident radiation), and the system was protected from stray light.

For spectral dependence of photoconduction, a 900-w xenon light source in conjunction with a Bausch and Lomb grating monochromator was used. The output from the monochromator was focused on the cell with two quartz lenses; the spectral distribution was determined by a bismuth–silver thermopile. The photocurrent was corrected to an incident illumination intensity corresponding to 38 μv developed by the light source at 470 mμ. The regions between 313 and 366 mμ were scanned by using a G.E. 100-w mercury arc.

For photoconduction activation energy, the 1-mm exit slit of the monochromator was used, while for spectral dependence studies, the exit slit was placed at the 0.25 mm position. Light intensity was varied by the use of Kodak neutral density filters, followed by calibration with a thermopile.

The field applied to the specimen was taken from a Keithley Model 241 regulated high voltage power supply, and the current measurement was carried out with the aid of a Keithley Model 610A micromicroammeter and an x–y recorder (EAI Variplotter Model 1110).

Results and Discussion

Room temperature bulk resistivities of the four

(17) H. Meier, *Z. Physik. Chem.*, **208**, 340 (1958).

Table II: Volume Resistivities of Nitro Derivatives of Fluoren-$\Delta^{9\alpha}$-malononitrile

Compound	Thickness mm	Dark, ohm-cm	Light, ohm-cm	Efficiency = I_p/I_d
2,4-Dinitro (IIa)	0.14	8×10^{15}	9×10^{11}	8,800
2,5-Dinitro (IIb)	0.20	2×10^{14}	5×10^{10}	4,000
2,6-Dinitro (IIc)	0.24	9.0×10^{14}	1.0×10^{11}	6,000
2,7-Dinitro (IId)	0.18	2.0×10^{15}	1×10^{11}	20,000
2,4,7-Trinitro (IIe)	0.29	1.0×10^{13}	7.0×10^{10}	142
2,4,5,7-Tetranitro (IIf)	0.23	2.0×10^{13}	8.0×10^{10}	250

dinitro isomers (IIa–IId), the trinitro (IIe), and the tetranitro (IIf) derivatives measured in the dark and under steady-state polychromatic illumination are listed in Table II. The photoconduction efficiencies are shown in the last column.

In view of the polycrystalline nature of the materials and the variable thicknesses of the cells, the photoconductive efficiencies are relative to each other. The fact that on illumination the bulk conductivities of these compounds increase by 2–4 orders of magnitude qualifies them as good photoconductive materials. In contrast, the photocurrents in the starting ketones (Ia–Ie) were higher than the corresponding dark currents by 0–1 order of magnitude. *Thus, replacement of the carbonyl group by the dicyanomethylene function results in the enhancement of photoconductivity in this series of compounds.* 2,7-Dinitrofluoren-$\Delta^{9\alpha}$-malononitrile (IId), the best photoconductor in this series, was selected for further investigation.

2,7-Dinitrofluoren-$\Delta^{9\alpha}$-malononitrile: Absorption Spectra and Spectral Dependence of Photoconductivity. The structure of 2,7-dinitrofluoren-$\Delta^{9\alpha}$-malononitrile (IId) was established by (a) analogy,[16] (b) elemental analyses of itself and that of the 1:1 molecular complex with pyrene, and (c) infrared and ultraviolet spectra. The electronic absorption spectrum, taken in mineral oil, shows peaks at 343, 360, and 410 mμ (shoulder) (Figure 1). A solution in acetonitrile showed peaks at 360 mμ (log ε 4.30), 342 mμ (log ε 4.40), 312 mμ (log ε 4.74), and 300 mμ (log ε 4.62). In the fluorescence spectrum the mirror image relationships of the absorption peaks are nearly retained, except that the long wavelength emission is considerably shifted to 520 ± 5 mμ (Figure

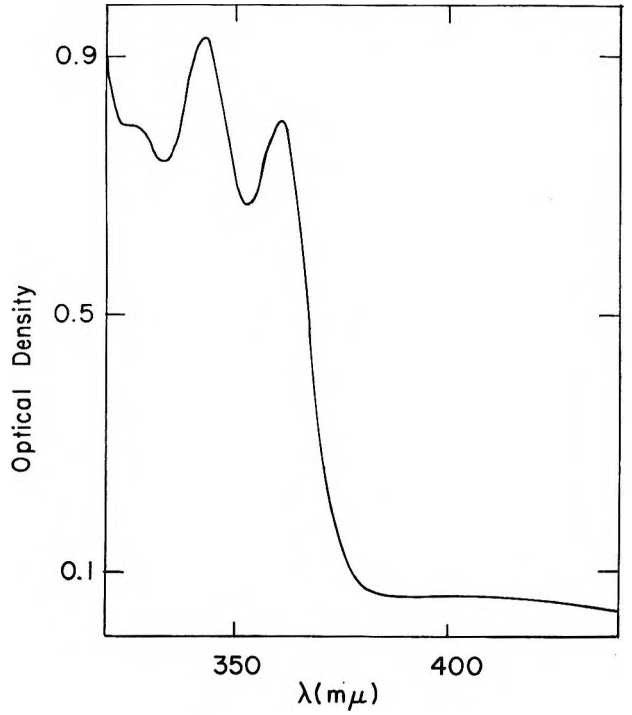

Figure 1. Absorption spectrum of 2,7-dinitrofluoren-$\Delta^{9\alpha}$-malononitrile in Nujol.

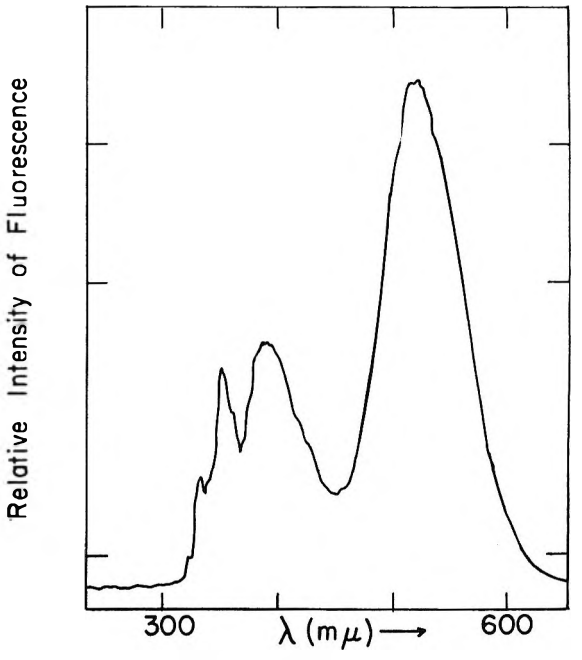

Figure 2. Fluorescence spectrum of 2,7-dinitrofluoren-$\Delta^{9\alpha}$-malononitrile in dioxane. Excitation at 350 mμ.

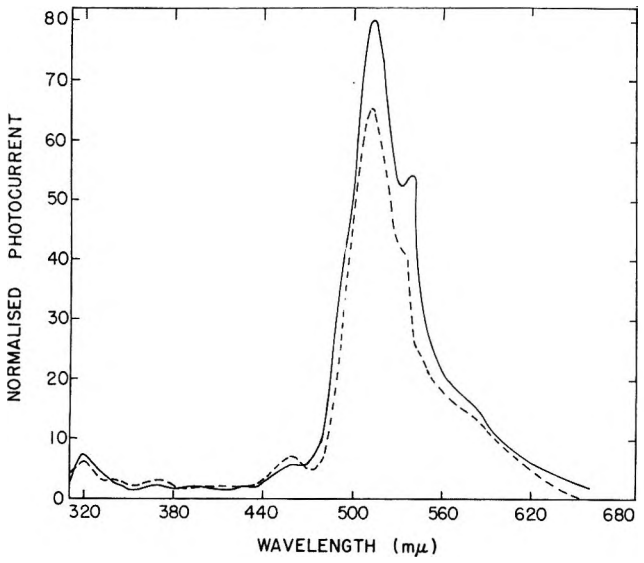

Figure 3. Spectral response of bulk photoconductivity of 2,7-dinitrofluoren-$\Delta^{9\alpha}$-malononitrile: full curve, photocurrent at 400 v (amp × 10^{10}); broken curve, photocurrent at 10 v (amp × 10^{12}); thickness of the layer, 0.07 mm.

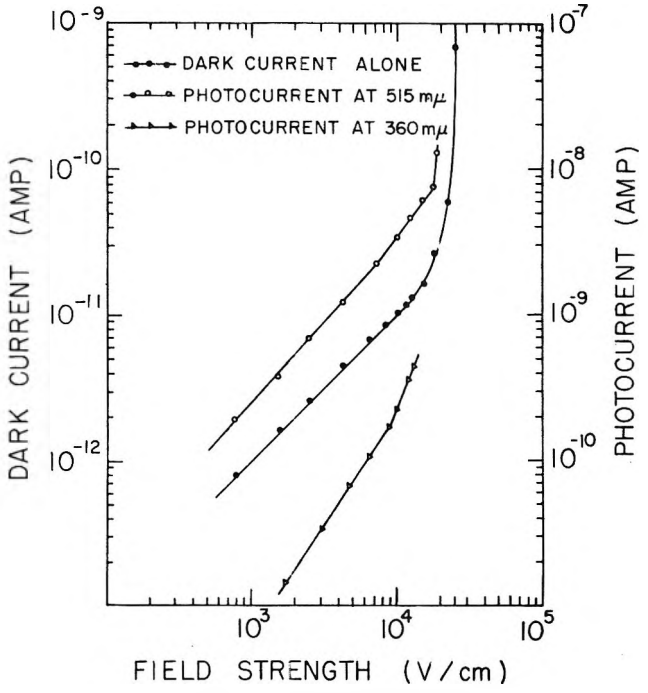

Figure 4. The surface current as a function of applied field strength of 2,7-dinitrofluoren-$\Delta^{9\alpha}$-malononitrile photocell.

2). The emission spectrum of a thin layer of the compound was complicated by scattering, although the strongest peak at 520 mμ was clearly observed. The phosphorescence emission from compound IId could not be detected in single crystals, glycerine, or EPA (ether–pentane–alcohol) glass.

The photocurrent action spectrum of IId was characterized by a strong response at the 515-mμ region. Comparatively, only a small response was noticed in the expected region, 360 mμ, of maximum absorption. The possibility of photoconduction at 515 mμ due to second-order excitation from the grating was avoided by the use of an ultraviolet cutout filter. Burshtein[18] and Avdeenko and co-workers[19] have shown that the anticorrelation of the photoconductivity and absorption spectra is more pronounced at weak fields and is due to weak charge separation masking the spectral dependence of the quantum yield of carrier generation. Conversely, at higher fields the carriers are effectively ionized. By a careful study of the effect of the external field on the photoconductivity at different wavelengths, Reucroft and co-workers[12] were able to prove that pure *p*-chloranil showed normal dependence of the photocurrent on the wavelength of the exciting light. The bulk photoconductivity action spectra (positive electrode illuminated) for solution-evaporated layers of IId were obtained at several field strengths. In Figure 3 the spectra at 10 and 400 v are shown. The maxima of photocurrents at intermediate fields showed regular variation of intensity without any shift of the peak at 515 mμ. Similar behavior was also observed in vacuum-deposited surface cells.[20]

Dependence on the Potential. The dark and light (at 360 and 515 mμ) current–voltage characteristics of the sublimed surface cells show an ohmic dependence up to an approximate field strength of 8 × 10^3 v/cm[2] (Figure 4). Above this, the dark current varies as the square of the field strength until the region of very high current is reached. This is the typical behavior of space–charge-limited currents. In the case of the photocurrent at 515 mμ, the region of square law dependence is very short, and the current rises steeply, indicating that traps are rapidly filled.[21]

Intensity Dependence. The intensity dependence of the photocurrent is shown in Figure 5. A good linear plot is obtained for light intensities at each of the spectral regions at 360 and 515 mμ. The photocurrent–intensity follows an $I_p = kI^z$ relationship,

(18) A. I. Burshtein, *Soviet Phys.-Solid State*, 5, 922 (1963).

(19) A. Avdeenko, Y. V. Naboikin, and S. P. Asina, *ibid.*, 6, 2779 (1965).

(20) In several experiments on sublimed surface cells, the maximum of the photocurrent varied between 520 and 525 mμ. By illumination from the back side of the cell [G. Tollin, D. R. Kearns, and M. Calvin, *J. Chem. Phys.*, 32, 1013 (1960)] this discrepancy was eliminated. It is important to sublime a very thin layer of the substance; otherwise a high dark current, giving erratic electrometer reading, will result.

(21) S. Matumoto, *Bull. Chem. Soc. Japan*, 38, 997 (1965).

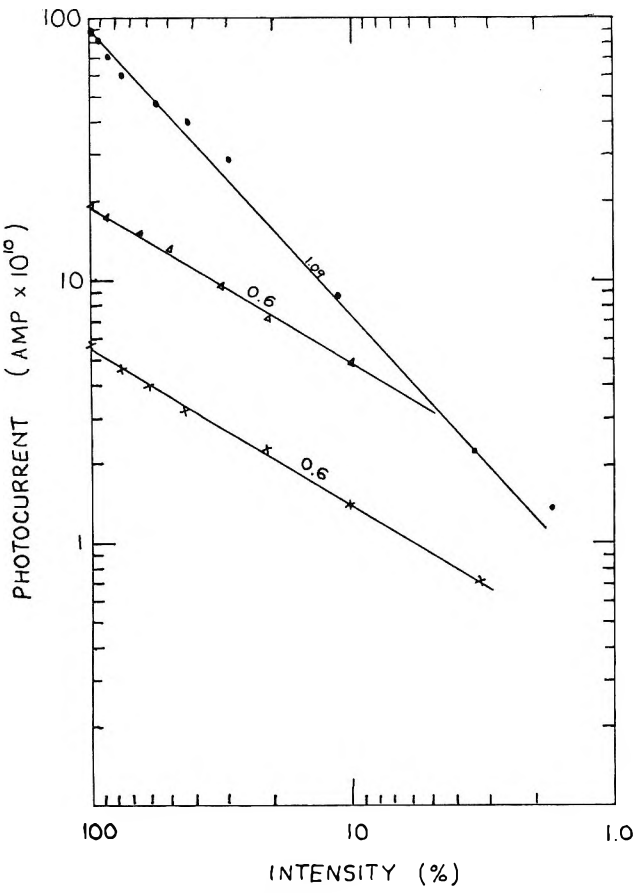

Figure 5. Surface photocurrent *vs.* light intensity of 2,7-dinitrofluoren-$\Delta^{9\alpha}$-malononitrile photocell: ×—×—×, 360 mμ; Δ—Δ—Δ, 515 mμ; ·—·—·, white light.

where I_p is photocurrent and I is intensity. A value of $x = 0.60$ was obtained at 360 and 515 mμ. By following the argument developed by Almelch and Harrison,[22] one can infer that the charge carriers are produced at these wavelengths by a single excitation mechanism. The current–intensity plot for intense polychromatic light shows a slope of 1.09.

Rise and Decay. Since the rate of rise of photocurrent in 2,7-dinitro compound (IId) is very fast, it has not been possible to measure the "rise characteristic." The rate of decay of conductance in darkness from steady state in light (at 515 mμ) followed second-order kinetics with a rate constant 0.15×10^{10} ohm/sec. Approximately 98% of the conductivity is lost within 5 sec of cessation of illumination.

Effect of Oxygen. Both the dark and the photoconductivity of the material IId decreased when oxygen was adsorbed by the surface, indicating that electrons[23] may be the majority carriers.

Dependence on Temperature. The temperature dependence of the dark and photo- (at 515 mμ) conductivity were measured on the surface cells. The activation energies (ΔE) were calculated from the relationship $i = i_0 \exp(-\Delta E/KT)$, where i is the current, i_0 is a constant, K is the Boltzmann constant, and T is the absolute temperature. The slopes obtained at an ascending temperature were identical with those at the descending temperature. These experiments provided the values of dark activation energy (ΔE_d) as 1.14 ev, and photoactivation energy (ΔE_p) as 0.5 ev, respectively.

Conclusion

The outstanding feature in this work is represented by the high photoconductivity of 2,7-dinitrofluoren-$\Delta^{9\alpha}$-malononitrile (IId), especially at the spectral region of weak absorption. This behavior is persistent even at higher fields. Although numerous experiments on different batches of highly purified samples confirm the findings, the possibility of the presence of traces of sensitizing impurities cannot be completely eliminated. This caution is necessary in photoconductivity studies of most organic materials due to the fact that available analytical tools are not sensitive enough to detect and characterize impurities below a certain concentration level. In the absence of any phosphorescence in IId, the participation of the triplet state in the conduction phenomenon cannot be considered. Alternatively, it can be speculated that the excited singlet state (A*) on reaction with the ground state (A) generate the "excimer" (AA*), which decays by emitting at longer wavelength. Further studies are required to examine the nature of this excited level and its possible impact on the photoconduction process.

Acknowledgment. The author wishes to express his thanks to Dr. A. Golubovic for his help in the instrumentation. Thanks are also due to Mr. D. Bogan and Mr. R. Andersson for technical assistance.

(22) N. Almelch and S. E. Harrison, *J. Phys. Chem. Solids*, **26**, 1571 (1965).

(23) H. Meier, *Z. Wiss. Phot.*, **53**, 1 (1958).

Medium Effects on the Rate of Hydrogen Evolution

by Mark Salomon

School of Chemistry, Rutgers, The State University, New Brunswick, New Jersey *(Received June 3, 1966)*

The hydrogen evolution reaction at mercury cathodes in water and mixtures of water and methanol is examined theoretically. Using a simple electrostatic model for the activated complex, the ratio, R, of the exchange currents in H_2O to that in H_2O–CH_3OH mixed solvents can be predicted in satisfactory agreement with experiment.

Introduction

Although the hydrogen evolution reaction (h.e.r.) in aqueous solutions has been studied in great detail over the last 60 years or so,[1-4] relatively little attention has been paid to the h.e.r. in nonaqueous solutions. Several papers have been published[5-10] on the h.e.r. at mercury cathodes in alcoholic solutions and Bockris and Parsons[7] have reported detailed experiments in H_2O–CH_3OH mixtures. These authors found that the exchange current density, i_0, decreases as the mole fraction of methanol (MeOH) is increased, but at high MeOH mole fractions i_0 begins to increase, and finally in pure MeOH the exchange current density is greater than in pure water. A detailed discussion of the variation of rate in mixed solvents has not been offered to date. In the present paper a quantitative explanation is offered for the effect of the dielectric constant on the rate of hydrogen evolution. The activated complex is treated as a charged species,[11] and simple electrostatic theory is used to calculate the ratio of exchange current densities, R, in various solvents.

Method

There can be no doubt that the discharge of protons is the slow step at the mercury cathode.[11,12] In this paper the rate-determining step is assumed to proceed with the formation of a fully charged activated complex[11] according to

$$Hg + H_3O^+ \rightleftharpoons X^{\ddagger} \longrightarrow HgH^+ + H_2O \quad (1)$$

Electron transfer then occurs as the fast step producing the neutral HgH species. According to eq 1 the rate at the reversible potential, ϕ_r, is given by

$$i_0 = F(kT/h)(a_{H^+})(1 - \theta) \times [\exp -(1 - \beta)\psi_1 F/RT] \times [\exp -\Delta G^{\ddagger}/RT][\exp -\beta\phi_r F/RT] \quad (2)$$

where a_{H^+} is the bulk activity, θ is the coverage by adsorbed hydrogen which is negligible at mercury cathodes,[2] ψ_1 is the potential at the outer Helmholtz plane, and β is the symmetry factor which has been defined as the ratio of the gradients of the potential energy distance relations of the initial and final states.[1] Experimentally β is quite close to $^1/_2$ in aqueous and methanolic pure and mixed solutions.[5-10] $\Delta G^{\ddagger}$ is the free energy of activation. Since a practically identical relation can be written for the exchange current density in a solvent of varying dielectric constant, we can define a ratio, R, of exchange current densities as

$$R = i_0/i_{0,s} = a_{H^+}/a_{H^+,s}[\exp(1 - \beta)][(\psi_{1,s} - \psi_1)F/RT] \times [\exp(\Delta G^{\ddagger}_s - \Delta G^{\ddagger})/RT][\exp \beta(\phi_{r,s} - \phi_r)F/RT] \quad (3)$$

In eq 3 the subscript s refers to the solvent of varying

(1) J. O'M. Bockris, *Mod. Aspects Electrochem.*, 1, 180 (1954).

(2) A. N. Frumkin, *Advan. Electrochem. Electrochem. Eng.*, 1, 65 (1961); *ibid.*, 3, 1 (1963).

(3) P. Delahay, "Double Layer and Electrode Kinetics," John Wiley and Sons, Inc., New York, N. Y., 1965.

(4) B. E. Conway, "Theory and Principles of Electrode Processes," Ronald Press, New York, N. Y., 1965.

(5) S. Levenia and S. Sarinsky, *Acta Physicochim.*, 6, 491 (1937).

(6) V. M. Novoselski, *Russ. J. Phys. Chem.*, 11, 369 (1938).

(7) J. O'M. Bockris and R. Parsons, *Trans. Faraday Soc.*, 45, 916 (1949).

(8) J. O'M. Bockris, R. Parsons, and H. Rosenberg, *ibid.*, 47, 766 (1951).

(9) S. Minc and J. Sobkowski, *Bull. Acad. Polon. Sci.*, 8, 29 (1959).

(10) B. E. Conway and M. Salomon, *J. Chem. Phys.*, 41, 3169 (1964).

(11) M. Salomon and B. E. Conway, *Discussions Faraday Soc.*, 39, 223 (1965).

(12) J. O'M. Bockris and S. Srinivasan, *J. Electrochem. Soc.*, 111, 844 (1964).

composition. Considering mixtures of H_2O–MeOH, the term in $\phi_{r,s} - \phi_r$ refers to the cell

$$Pt|H_2|H_2O,\ a_{H^+}||H_2O(X_1),\ MeOH(X_2),\ a_{H^+}|H_2|Pt \quad (4)$$

where X_1 and X_2 are the mole fractions of H_2O and MeOH, respectively. According to eq 4 we have

$$\phi_{rs} - \phi_r = \phi_{rs}^\circ - \phi_r^\circ + 0.0591 \log a_{H^+,s}/a_{H^+} \quad (5)$$

where $\phi_{rs}^\circ - \phi_r^\circ$ is the difference in standard reversible potentials for the hydrogen electrode in pure water against one in a solvent s of varying composition. Since the mean activity coefficients for HCl in methanol and ethanol solutions are known,[13,14] the main problem involves the evaluation of $\Delta\phi_r^\circ$ $(= \phi_{rs}^\circ - \phi_r^\circ)$ (assuming that the mean activity values can be used to calculate the activity ratio in eq 5). $\Delta\phi_r^\circ$ values for the pure solvents can be calculated from the equilibrium constant of the reaction

$$ROH + H_3O^+ \rightleftharpoons ROH_2^+ + H_2O;\quad K \quad (6)$$

since

$$\Delta\phi_r^\circ = (RT/F) \ln K \quad (7)$$

From conductivity,[15] indicator,[16] and emf[17] studies, the equilibrium constant is approximately 0.01 for MeOH and 0.004 for EtOH. As discussed by Ives[18] these are approximate values and a more accurate method is required.

In this paper the data of Feakins and Watson are used.[19] These authors have evaluated the free energy of transfer of individual ions from water to $H_2O(X_1)$–$MeOH(X_2)$ mixtures. From emf data they measure the total free energy of transfer of an acid halide, ΔG_t°, and to obtain the free energy of transfer for the H^+ species, $\Delta G_t^\circ(H^+)$, they write

$$\Delta G_t^\circ = \Delta G_t^\circ(H^+) + ar_a^{-1} \quad (8a)$$

where a is a constant and r_a is the Pauling[20] radius of the anion; or taking the data from amalgam cells, an equation similar to the above can be used; *i.e.*

$$\Delta G_t^\circ = \Delta G_t^\circ(Cl^-) - ar_c^{-1} \quad (8b)$$

where c represents the cation employed in the amalgam electrode.[19] Taking these data, the values of $\Delta\phi_r^\circ$ can then be calculated as a function of X_2 (the MeOH mole fraction) as shown in Figure 1. The $\Delta\phi_r^\circ$ value for transfer to pure MeOH ($X_2 = 1$) is 0.108 v and is significantly different from the value of 0.118 v calculated from eq 7 taking $K = 0.01$.

To evaluate the ψ potentials the data of Parsons and Devanathan[21] were used. The difference $\psi_{1,s} - \psi_1$ as a function of X_2 was obtained by assuming a linear free energy relation as is often found in solvents of

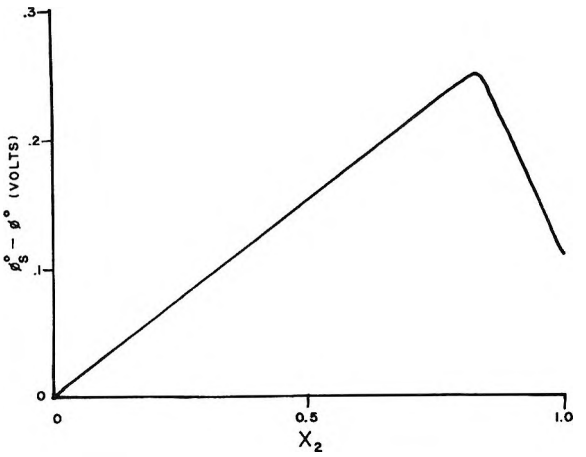

Figure 1. Potential for the cell in eq 4 as a function of the mole fraction of methanol, X_2.

varying composition.[22,23] Any error possibly involved in this assumption would be small anyway due to the small differences in the ψ potentials as seen in Table I. Grahame has also reported detailed experiments in HCl–MeOH solutions,[24] but since he used a salt bridge to an aqueous calomel electrode as his reference electrode, there exists the uncertainty in the magnitude of the MeOH–H_2O liquid junction potential and therefore his data were not used in this paper.

The remaining quantity $\Delta G^\ddagger$ (the Gibbs free energy of activation) corresponding to the process

$$C_nH_{2n+1}OH_2^+ + Hg \longrightarrow HgH^+ + C_nH_{2n+1}OH \quad (9)$$

can be evaluated in several ways. In eq 9 $C_nH_{2n+1}OH_2^+$ is H_3O^+, $CH_3OH_2^+$, $C_2H_5OH_2^+$, etc., for n = 0, 1, 2,..., respectively. In this equation the process involves the reaction between a proton and a charged

(13) H. S. Harned and B. B. Owen, "Physical Chemistry of Electrolytic Solutions," Reinhold Publishing Corp., New York, N. Y., 1950.

(14) R. G. Bates and R. A. Robinson, "Chemical Physics of Ionic Solutions," B. E. Conway and R. G. Barradas, Ed., John Wiley and Sons, Inc., New York, N. Y., 1966.

(15) H. Strehlow, *Z. Physik. Chem.* (Frankfurt), **24**, 240 (1960).

(16) L. S. Guss and I. M. Kolthoff, *J. Am. Chem. Soc.*, **62**, 1494 (1940).

(17) J. Koskikallio, *Suomen Kemistilehti*, **B38**, 30 (1957).

(18) F. Franks and D. J. G. Ives, *Quart. Rev.* (London), **20**, 1 (1966).

(19) D. Feakins and P. Watson, *J. Chem. Soc.*, 4734 (1963).

(20) L. Pauling, "Nature of the Chemical Bond," 3rd ed, Oxford University Press, London.

(21) R. Parsons and M. A. V. Devanathan, *Trans. Faraday Soc.*, **49**, 673 (1953).

(22) K. J. Laidler, "Reaction Kinetics," Vol. II, Pergamon Press Ltd., London, 1963.

(23) K. J. Laidler, *Suomen Kemistilehti*, **A33**, 44 (1960).

(24) D. C. Grahame, *Z. Elektrochem.*, **59**, 740 (1955).

Table I: Numerical Data Used for the Evaluation of Eq 3

X_2	ψ_1, v	$\phi_{rs}^\circ - \phi_r^\circ$, v	$\gamma_\pm(H^+)$	$\Delta G^{\pm}_s - \Delta G^{\pm}$, kcal mole^{-1}
0.0	0.092	0.000	0.797	0.00
0.1	0.090	0.032	0.773	0.14
0.3	0.086	0.097	0.720	0.44
0.5	0.083	0.154	0.652	0.81
0.7	0.079	0.212	0.572	1.24
0.8	0.077	0.240	0.527	1.46
0.9	0.075	0.208	0.482	1.71
1.0	0.073	0.108	0.431	1.98

mercury surface and according to Laidler,[25,26] for ions in solution the following energies would contribute to the $\Delta G^{\pm}$ values: (1) ion–ion type forces; (2) ion–dipole forces; (3) ion–induced dipole forces; (4) ion–quadrupole forces; (5) ion–induced quadrupole forces; (6) dipole–dipole forces; (7) dispersion forces; (8) charge-transfer forces; and since in the present case we are dealing with a metallic surface, one should also include (9) mirror image forces. For the reaction between two ions, the contributions 1–8 are not fully known, *e.g.*, with regard to 4 and 5 about which little is known and are therefore usually neglected.[25,26] For the reaction given by eq 1 and 9 even less is known, and an evaluation of the contributions 1–9 is prohibitive at the present and another method must be sought for the evaluation of $\Delta G^{\pm}$. The method used is discussed below.

A simplified model permits one to split $\Delta G^{\pm}$ into an electrostatic term $\Delta G^{\pm}_{es}$ and a nonelectrostatic term $\Delta G^{\pm}_{nes}$ according to

$$\Delta G^{\pm} = \Delta G^{\pm}_{nes} + \Delta G^{\pm}_{es} \qquad (10)$$

where $\Delta G^{\pm}_{nes}$ is assumed to be independent of solvent composition and $\Delta G^{\pm}_{es}$ is given by the Born equation[27]

$$\Delta G^{\pm}_{es} = \frac{Ne^2}{2\epsilon}\frac{1}{(r)} = \frac{1.66\ 10^{-6}}{\epsilon}\frac{1}{(r)}\ \text{kcal mole}^{-1} \qquad (11)$$

where r is a radius which can be associated either with the distance between two ions as in the "double sphere model"[22,23] or with the radii of all initial and activated complex species as in the single sphere model.[22,23] In the calculations presented here r was chosen to be 1.6 A so that $\Delta G^{\pm}_{es} = 103/\epsilon$ kcal mole^{-1}, where ϵ is the bulk dielectric constant of the solvent. It has long been considered that use of the Born equation with the macroscopic dielectric constant is unrealistic for the solvent close to an ion.[14,19,22,23,28,29] The use of the macroscopic dielectric constant often leads to small values of r in eq 11 and has therefore detracted from the fact that the Born equation does indeed successfully predict $\Delta G^{\pm}_{es}$ in many cases even though the required r values are small. The work of Feakins and Watson[19] described above in reference to eq 8 utilizes quite successfully a modified Born-type equation in the term ar_a^{-1} where r_a is the Pauling (nonsolvated) radius of the ion involved. Also recently Amis[30] has fitted the potentials of galvanic cells in a medium of varying composition and has used the Born equation. Despite the low values of r found by Amis, he has given a successful discussion of the energetics of the processes involved. One could always take into account the fact that the microscopic dielectric constant varies according to the distance from the ion in terms of continuous or discontinuous models,[23,25,26,28,29,31,32] but the fact remains that this does not appear to be necessary in the present case and in several other cases cited above.[19,30,33] One could conclude that the small values of r required by eq 11 result from the fact that

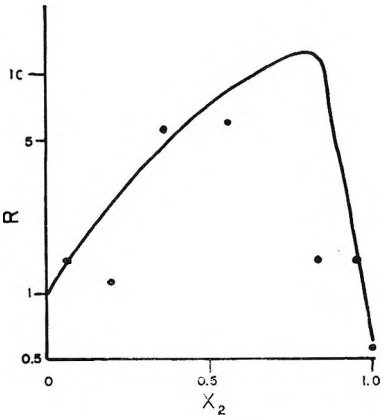

Figure 2. Ratio of exchange currents (normalized) as a function of the mole fraction of methanol, X_2. The solid line is that calculated from eq 3 for $\beta = 1/2$ at 25° and the points are experimental from ref 7.

(25) K. J. Laidler, Symposium of Solvation Phenomena, The Chemical Institute of Canada, Symposium Reprint No. 1, July 1963.

(26) J. S. Muirhead-Gould and K. J. Laidler, "Chemical Physics of Ionic Solutions," B. E. Conway and R. G. Barradas, Ed., John Wiley and Sons, Inc., New York, N. Y., 1966.

(27) M. Born, *Z. Physik*, **1**, 45 (1920).

(28) B. E. Conway, A. C. Smith, and J. Desnoyers, *Phil. Trans. Roy. Soc. London*, **A256**, 389 (1964).

(29) L. G. Hepler, *Australian J. Chem.*, **17**, 587 (1964).

(30) E. S. Amis, *J. Electroanal. Chem.*, **8**, 413 (1964).

(31) K. J. Laidler, *Can. J. Chem.*, **34**, 1107 (1956).

(32) K. J. Laidler and C. Pegis, *Proc. Roy. Soc.* (London), **A241**, 80 (1957).

(33) L. M. Mukherjee, *J. Phys. Chem.*, **58**, 1042 (1954); **60**, 974 (1956).

one is actually correcting the macroscopic value of ϵ in eq 11 which should be lower due to dielectric saturation. It should also be mentioned that although the r values have been referred to as being small, they are by no means unreasonably small. The value of 1.6 A for r used here is in fact consistent with the model used elsewhere[11] and is quite a reasonable value.

Finally in reference to this last discussion, it is indeed very reasonable to conclude that this simple treatment is indeed useful and can predict *trends* in the kinetics of the reactions in mixed solvents semiquantitatively in some cases, qualitatively in others, and in many reactions the use of a continuous solvent model medium of constant ϵ fails badly. In the present case, as in others, agreement with experiment is surprisingly good.

In Table I the relevant quantities used to evaluate eq 3 are listed. The results of this calculation are shown in Figure 2, where the ratio R is plotted against the mole fraction of methanol, X_2. The points shown are the experimental values of Bockris and Parsons,[7] and agreement is quite satisfactory.

Conclusion

The rate of hydrogen evolution at mercury cathodes in solvents of varying H_2O–MeOH composition has been theoretically treated in terms of a simple electrostatic model of the activated complex. The results confirm the mechanism of the h.e.r. at mercury cathodes in terms of a slow discharge theory as does more recent work involving isotopes[10-13] and reaction order.[1-4] This treatment can be extended to other systems such as H_2O–EtOH, H_2O–dioxane, etc., providing some relevant experimental data are available. Such data must include $\Delta G_t^\circ(H^+)$ and ψ_1 potentials. For the case of H_2O–EtOH mixed solvents, $\Delta G_t^\circ(H^+)$ values are known approximately for the case of transfer from pure water to pure EtOH. This quantity is calculable from eq 7 or from theoretical models involving free energies of solvation for individual ions ΔG_s°, which is particularly covered in the Russian literature.[34,35] Since these values are approximate, they cannot be used in a calculation of the type performed here since an error of ± 2 kcal mole^{-1} in ΔG_s° gives rise to an error of ± 0.1 v in ϕ_r° values. Ethanol–water mixtures are of interest and calculations of $\Delta G_t^\circ(H^+)$ as a function of the ethanol mole fraction could be calculated by the method of Feakins and Watson.[19] That such measurements are experimentally feasible in H_2O–EtOH mixtures is shown from the work of Mukherjee.[33]

Acknowledgments. I would like to thank the Chemistry Department and the Research Council of Rutgers, The State University, for financial support.

(34) N. A. Izmailov, *Dokl. Akad. Nauk SSSR*, **149**, 884 (1963).
(35) N. E. Khomutov, *Russ. J. Phys. Chem.*, **39**, 336 (1965).

Determination of Excited State pK_a Values Using Photopotentiometry

by Donald D. Rosebrook[1] and Warren W. Brandt

Chemistry Department, Kansas State University, Manhattan, Kansas *(Received June 6, 1966)*

Photopotentiometry is herein defined as the measurement of the potential developed between one illuminated electrode and one dark electrode in a solution. This potential, which is primarily a function of the various species in solution, was used to produce data leading to excited state pK_a values. The values found were −2.89 and 12.3 for the 2-naphthylamine cation and anion, respectively; 13.5 for the 1-naphthylamine anion; and 4.37 and 9.5 for the 3-pyridinol anion and cation, respectively. The presence of ethanol in the aqueous systems acted to shift the position of the excited-state pK_a values and to enhance the potentials. The first effect is attributed to differences in solvating power while the cause of the second effect is not clear.

I. Introduction

Forster was the pioneer in the study of pK_a values of the excited state. His studies consisted of the examination of hydroxypyrene derivatives[2a] and naphthalene derivatives.[2b] Weller[3-5] has given extensive consideration to the determination of the physical constants of protolytic reactions of the excited states of the mononaphthols. Derkacheva[6] and Hercules and Rogers[7] have reported pK_a values for excited naphthalene diols; however, there is little agreement in their results. The pK_a* values determined by these workers vary by as much as 1.8 units, and neither worker has found values which are consistently high or low. All of the above studies produced the same result: bases become weaker in the excited state by 5–10 pK units and acids become stronger in the excited state by 5–10 pK units.

Kokubun[8] reported the excited state pK_a for acridone and found indications that the heterocyclic nitrogen became more basic in the excited state, as well as indications that in this type of molecule the hydroxy group became a stronger acid in the excited state. Weller[9] noted that the heterocyclic nitrogen in acridine also becomes a stronger base in the excited state.

Bartok, *et al.*,[10] measured the dissociation constants of some excited phenols. They also measured pK_a* for phenol in glycerol and found that the value of pK_a* − pK_a was significantly larger in the nonaqueous solvent than in water.

Up to this time excited singlet-state pK_a values have been measured by fluorescence. This paper presents a new technique which we have called photopotentiometry. The technique has been applied to the determination of excited singlet-state pK_a values.

Levin and White[11-13] first showed that a positive correlation existed between the photopotential and the wavelength of the incident light such that a plot of photopotential *vs.* wavelength bore a very strong resemblance to the absorption spectrum. They were unsuccessful in an attempt to correlate fluorescence and what they called "photovoltaic" behavior Surash[14] later showed that in deoxygenated solutions the primary reaction was a photoreduction and that

(1) To whom correspondence should be addressed at Midwest Research Institute, Kansas City, Mo.

(2) (a) T. Forster, *Z. Elektrochem.*, **54**, 42 (1950); (b) *ibid.*, **54**, 531 (1950).

(3) A. Weller, *ibid.*, **56**, 662 (1952).

(4) A. Weller, *Z. Physik. Chem.* (Frankfurt), **3**, 238 (1955).

(5) A. Weller, *ibid.*, **17**, 224 (1958).

(6) L. D. Derkacheva, *Opt. Spectry.*, **9**, 209 (1960).

(7) D. M. Hercules and L. B. Rogers, *Spectrochim. Acta*, 393 (1959).

(8) H. Kokubun, *Z. Elektrochem.*, **62**, 599 (1958).

(9) A. Weller, *ibid.*, **61**, 956 (1957).

(10) W. Bartok, P. J. Luechesi, and N. S. Snider, *J. Am. Chem. Soc.*, **84**, 1842 (1962).

(11) I. Levin and C. E. White, *J. Chem. Phys.*, **18**, 417 (1950).

(12) I. Levin and C. E. White, *ibid.*, **19**, 1079 (1951).

(13) I. Levin and C. E. White, *ibid.*, **21**, 1654 (1953).

(14) J. J. Surash, Ph.D. Dissertation, Lehigh University, Bethlehem, Pa., 1960.

this produced negative potentials. Pitts, *et al.*,[15] have since utilized negative photopotentials to show the occurrence of photoreduction. Tsepalov and Shlyapintokh[16] have employed photopotential measurements to study qualitatively the kinetics of the low-temperature photoreduction of eosin, erythrosin, and rose bengal.

II. Theory

The absorption of energy sufficient to cause an electronic transition perturbs the ground-state electronic configuration of the molecule. The electronic distribution then changes to conform to the new total energy. This change usually results in an alteration of the acid–base properties of a molecule. Many methods have been utilized to study the new molecular properties of the excited molecule. Foremost among the methods employed has been fluorescence because of the relative ease of obtaining meaningful data. For this reason nearly all of the pertinent data on excited singlet-state acid–base characteristics has resulted from the interpretation of fluorescent measurements. However, we propose to show that a second technique is now available which provides data pertaining to the acid–base characteristics of excited molecules.

The validity of the interpretation of these data will be shown by an analogy to the situation in fluorescence. Consider a simple series of reactions involving a base and its conjugate acid BH^+ and their respective excited states.

$$B + h\nu_1 \longrightarrow B^* \quad (1)$$

$$BH^- + h\nu_2 \longrightarrow BH^{+*} \quad (2)$$

$$B^* \longrightarrow B + h\nu_3 \quad (3)$$

$$\longrightarrow P_1 \quad (4)$$

$$BH^{+*} \longrightarrow BH^+ + h\nu_4 \quad (5)$$

$$\longrightarrow P_2 \quad (6)$$

$$\longrightarrow B^* + H^+ \quad (7)$$

Because the total concentration of species in the excited state is very small, it is correct to refer to the point at which the concentration of B* equals the concentration of BH^{+*} as pK_a^*. The normal procedure is to measure the intensity of the fluorescence of either species at different pH values and to designate pK_a^* to be the pH value at which half-intensity occurs. The analogy is this: one of the alternative means of deactivation of the excited state is by a chemical reaction as shown in eq 4 and 6. In the case of reaction 4, the product P_1 is produced as an alternative to or coincidentally with fluorescence $h\nu_3$, which is indicative of the species B*. In the simplest situation the reaction leading to P_1 is

$$B \xrightarrow{h\nu_1} P_1$$

Thus we may postulate the Nernstian expression

$$-\frac{RT}{nF} \ln \frac{[P_1]}{[B]} = E_A - E_A^\circ = A$$

The potentials E_A and E_A° found in the Nernst equation depend on the concentration and the identity of the various materials in solution. We shall show later that neither E_n° or the identity of P_1 is important in this application of photopotentiometry. So long as the concentrations of B and P_1 remain constant the value of potential A will remain constant regardless of the pH. When the pH is such that B is consumed to form BH^+, three alternatives present themselves: (1) B is excited to B* from whence P_1 is formed. B, disappearing by reaction, is supplemented from the equilibrium involving BH^+. In this case, the ratio of P_1/B is the same, but the reaction takes longer due to the competing equilibrium with BH^+. (2) P_1 is formed in the following sequence of reactions: (2) followed by (7) followed by (4). The result here is the same as above because there will always be a finite concentration of B produced through reaction 3. (3) P_2 is formed by reaction 6; this necessitates the introduction of a second Nernstian expression

$$\frac{-RT}{nF} \ln \frac{[P_2]}{[BH^+]} = E_C - E_C^\circ = C$$

The general considerations for the magnitude of potential C are similar to the arguments for potential A. The over-all effect is to change the absolute value of the potential until the point where consideration of A is no longer significant. Graphically this looks as shown in Figure 1.

Under these circumstances the nature of the reactions and of the reaction products is not important as long as B* always forms product P_1 and BH^{+*} always forms product P_2. In general, any time the extent of a photoprocess is being measured at two conditions the nature of the reaction is unimportant, as is the nature of the product, so long as the identity of the product is the same under both sets of conditions. The analogy in this case is to a concentration cell.

To apply this technique to the determination of pK_a^*,

(15) J. N. Pitts, Jr., H. W. Johnson, Jr., and T. Kuwana, *J. Phys. Chem.*, 66, 2456 (1962).

(16) V. F. Tsepalov and J. Ya. Shlyapintokh, *Izv. Akad. Nauk SSSR, Otd. Khim. Nauk*, 637 (1959).

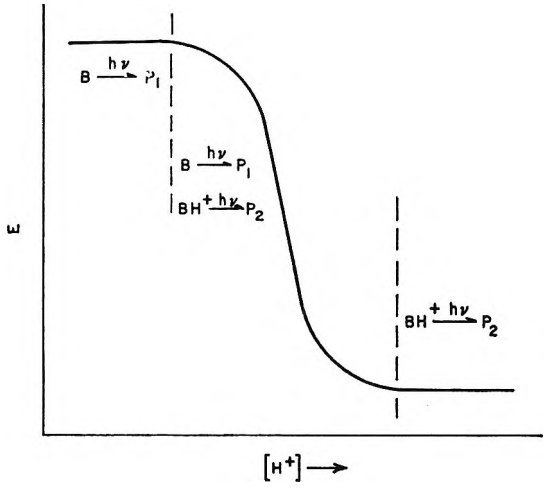

Figure 1.

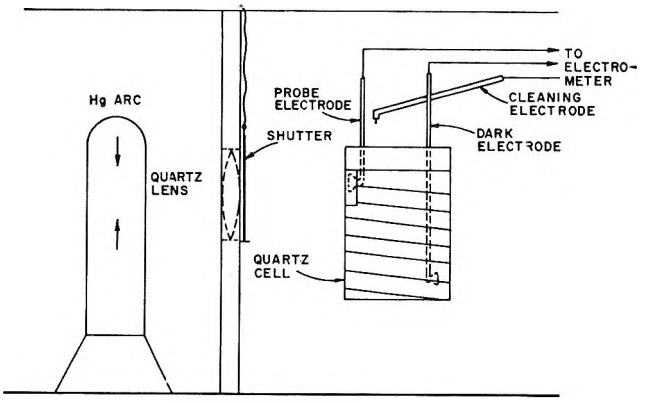

Figure 2. Core of the photopotentiometric apparatus.

one has only to record the photopotential as a function of pH. So long as one product, P_1, is being produced and the ratio P_1/B is constant, the photopotential will remain constant. When the excited-state equilibria shift and a different product, P_2 (or no product at all), is produced, the photopotential will change. The pH at the midpoint of the change between the two constant values of the photopotential may be assumed to be numerically equal to the pK_a^*.

III. Experimental Section

Photopotential is measured between one illuminated and one dark electrode in a solution and is defined as the actual electrometer reading of the illuminated electrode at any time *vs.* ground. For experimental purposes the term photodeflection is defined as the photopotential *vs.* ground at photoequilibrium minus the potential *vs.* ground at dark equilibrium.

The apparatus used to obtain photopotentials is shown in Figure 2. The sample was placed in the quartz cell which was wrapped in black electrical tape except for a window of 1 cm^2 area. The solutions were deaerated 10 min with nitrogen from which oxygen had been removed by bubbling the gas through two successive solutions of 0.08 *M* chromous sulfate. The gas was also passed through sulfuric acid and over Drierite to remove water, then over Ascarite to remove carbon dioxide. The pH of the solutions was measured after deaeration. The pH was also checked after irradiation to ensure that the potential change was not due to a pH change.

The electrodes were made from platinum wire, and during the deaeration period they were cleaned in another cell by anodizing and cathodizing for 5 min in 1 *M* $HClO_4$. A Micro Tek HCP-500 power supply provided 3 ma at 3 v for this purpose. In order to clean both electrodes simultaneously a third electrode was provided as well as provisions for connecting the indicating electrode and the reference electrode together. The "cleaning" electrode was on a swivel and was removed from the solution and grounded when not in use. After several days of use the electrodes were soaked in 72% $HClO_4$ for 1 hr. The electrodes were then rinsed with deionized water and dried with absorbant tissue. This treatment was found to be sufficient to give reproducible dark potentials.

The cell with the deaerated sample was placed in the cell holder such that the indicating electrode was against the side of the cell at the window. The reference electrode was in a dark portion of the cell. The electrodes were allowed to equilibrate in the dark until the potential change was less than 0.3 mv/min for at least 10 min. (The dark potential was not always zero because of the difficulty in maintaining two electrodes exactly alike. This necessitated the determination of a dark potential and the introduction of the relative term photodeflection.) After determination of the dark equilibrium potential the shutter was opened and the unfiltered radiation of the mercury arc was allowed to strike the solution around the indicating electrode. The change of the potential of the indicating electrode was measured with a Keithley 610A electrometer and recorded as a function of time. The reference electrode was connected to an earth ground and to the ground terminal of the electrometer. When the deflection dropped below 0.3 mv/min, the shutter was closed and pH was again recorded.

pH measurements were made with a Beckman Expanded Scale pH meter. When a normal glass electrode was used, the potassium error was calculated according to the equation of Jordan.[17] In some of the work a Beckman 0–14 glass electrode was utilized.

(17) D. O. Jordan, *Trans. Faraday Soc.*, 34, 1305 (1938).

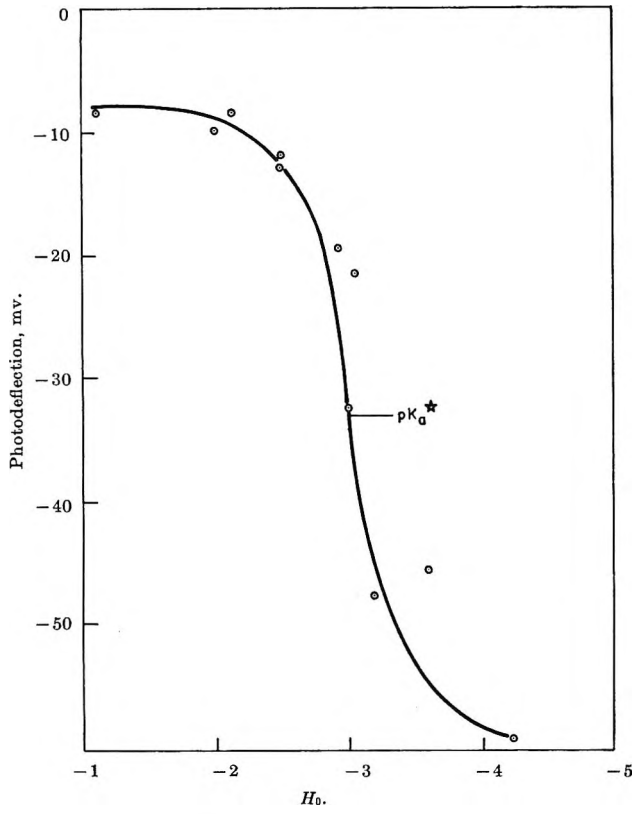

Figure 3. 2-Naphthylamine in acid solution.

In concentrated H_2SO_4 the hydrogen ion activity was interpolated from the concentration data of Paul and Long.[18] When necessary a correction for ethanol was applied according to the recommendations of Gutsbezahl and Grunwald.[19] The solutions were not buffered because the use of buffers in many cases introduced spurious potentials that resulted in unintelligible data.

The magnitude of the photopotential was found to be directly related to the purity of the solute in question. Therefore all solids were purified by four successive vacuum sublimations. Ethanol was treated according to the instructions of Lappin and Clark[20] to remove carbonyl impurities and distilled; the fraction boiling at 77° (uncorrected) was collected and chromatographed through a segmented column of absorption alumina and charcoal.

"Blank" experiments were performed and the measured photodeflections varied from +0.5 mv for absolute ethanol to −8 mv for some aqueous acids. These potentials in all cases were negligible, relative to the potentials measured in the corresponding samples.

The effect of the intensity of the Hg arc was examined qualitatively by defocusing the radiation. The only effect noted was a decrease in the rate of attaining photoequilibrium. The position of photoequilibrium was not affected.

IV. Results and Discussion

2-Naphthylamine. Forster[2b] has measured pK_a* for the excited-state reaction

$$BNH_3^{+*} \rightleftharpoons BNH_2^* + H^+ \qquad (8)$$

and obtained a value of approximately −2. This determination was completed in aqueous H_2SO_4 and Hammett acidity values, H_0, were used to denote hydrogen ion activities. Figure 3 shows the same equilibrium determined photopotentiometrically. In this case, a pK_a* of approximately −2.9 was found.

When the cationic species are irradiated, only a small fraction of the ions are excited, owing to the low absorptivity of the solution at the wavelengths of the mercury arc. This low absorptivity is reflected in the small photodeflections depicted in Figure 3. Since the photodeflection is small in the region from pH 2 to $H_0 = -2$, where the species BNH_2^* was produced according to reaction 8, and then it increases to a maximum at $H_0 = -4$, where the equilibrium favors BNH_3^{+*}, the indication is that the reduction of the species BNH_3^{+*} is more efficient than the reduction BNH_2^* because the solutions absorb the same amount of energy in both cases.

In alkaline solution another break in the photodeflection *vs.* pH curve occurs as is shown in Figure 4. This break was assigned to the pK_a* for formation of the amide ion in the excited state according to the following reaction

$$BNH_2^* \rightleftharpoons BNH^{-*} - H^+ \qquad (9)$$

The value of this pK_a* was found to be 12.3.

Forster[2b] observed the same phenomenon by following the change in the wavelength of fluorescence and assigned the value 12.2 to this pK_a*. Forster also states that the parallel ground-state reaction is only observed in a strong alkaline solvent such as liquid ammonia.

In alkaline solution the production of the species BNH^{-*} *via* reaction 9 occurs at the expense of BNH_2^* thus effectively reducing the observed photodeflection.

When the solvent system was changed from water to 42.2 wt % ethanol in water, the break in the photodeflection *vs.* pH curve appeared at 8.95. The shift of pK_a* for 2-naphthylamine from 12.3 in water to 8.95 in aqueous ethanol is in general agreement with the work of Bartok, *et al.*,[10] who found that pK_a* for phenol

(18) M. A. Paul and F. A. Long, *Chem. Rev.*, 5, 71 (1957).

(19) B. Gutsbezahl and E. Grunwald, *J. Am. Chem. Soc.*, 75, 565 (1953).

(20) G. R. Lappin and L. C. Clark, *Anal. Chem.*, 23, 541 (1951).

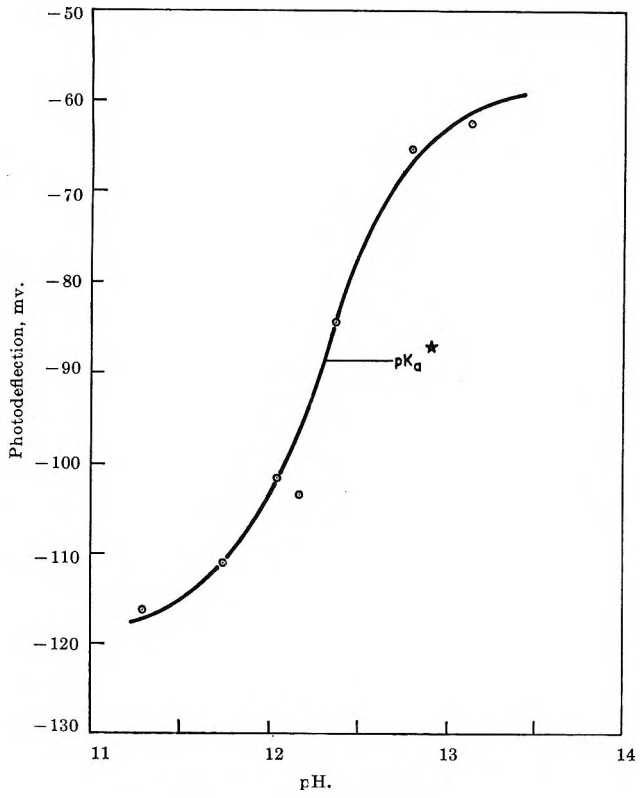

Figure 4. 2-Naphthylamine in alkaline solution.

goes from 5.7 in water to 3.2 in glycerol.

This shift in pK_a^* is attributed to the difference in the solvating power of the various solvents. The effect of solvating power is such that a polar solvent such as water exerts a stronger pull on the nonbonding electrons of the amine (or hydroxy group) than does the ethanol or glycerol. This solvation pull reduces the interaction of the nonbonding electrons with the π cloud of the aromatic ring according to the polarity of the solvent. The most polar solvent induces the greatest part of the electron density due to the n electrons to remain on the atom where those electrons originate. A higher concentration of electron density on an acidic or basic group in an aromatic molecule causes that group to be less acidic or more basic. This argument is true in the ground state and generally holds for the excited state except that the dielectric relaxation time of the solvent cage may cause some anomalous shifts in pK_a^* values.

1-Naphthylamine. No pK_a^* could be determined for 1-naphthylamine in acid solution. The magnitude of the photodeflection remained at −5 mv from pH 2 to $H_0 = -7.4$. pK_a^* for this compound for reaction 8 has not been determined by fluorescence either because of fluorescence quenching which occurs at the ground-state pK_a.

Forster[2b] also found this type of situation with 2-naphthol. He postulated that the rearrangement time of 2-naphthol was severely limited by the short lifetime of the excited state of this molecule. (By rearrangement time is meant the time required for protonation or deprotonation in the excited state.) The limited rearrangement time resulted in the appearance of the neutral molecule fluorescence at a pH corresponding to a point just less than the ground-state dissociation constant and far above the excited-state pK_a where fluorescence of the anion should have been observed. The analogy in this case is that the protonated naphthylamine should have exhibited the fluorescence of the neutral molecule and should have undergone the photoreduction of the neutral molecule at pH values below the pK_a and above the pK_a^*. Since it did not do this, the protonated species must not have had time to rearrange during the excited-state lifetime.

In alkaline solution a pK_a^* was again observed for reaction 9. The potential change over the break in the curve of photodeflection *vs.* pH was 40 mv and quenching of the fluorescence was visually observed. Weller[4] concluded that pK_a^* for 1-naphthylamine in alkaline solution fell somewhere between 13 and 14. This study showed the $pK_a^* = 13.5 \pm 0.15$. The high uncertainty in this study is due to the difficulty in calculating the potassium error at this pH.

The Effect of Ethanol. In aqueous solution the photodeflection from 2-naphthylamine was relatively low (−120 mv) while in 8.7 wt % ethanol at a similar pH the photodeflection was substantially increased (−290 mv). Increasing the ethanol content to 42.2 wt % ethanol produced no further increase in photodeflection.

The addition of ethanol was observed to accelerate decomposition even in semidarkness. Ethanol-containing solutions could not be stored longer than 24 hr, whereas aqueous solutions were stable for several days. The decomposition of a solution upon standing would be evidenced first by low photodeflections, and within a short time colored decomposition products could be observed visually.

For 1-naphthylamine, aqueous solutions gave a −50-mv photodeflection; addition of 1 wt % ethanol increased the photodeflection to −210 mv, and 4 wt % ethanol caused a further increase to −240 mv.

The effect of ethanol on photoreductions in aqueous solutions was extensively studied by Imamura and Kaizumi,[21] who found that in deaerated aqueous solu-

(21) M. Imamura and M. Kaizumi, *Bull. Chem. Soc. Japan*, **29**, 989 (1956).

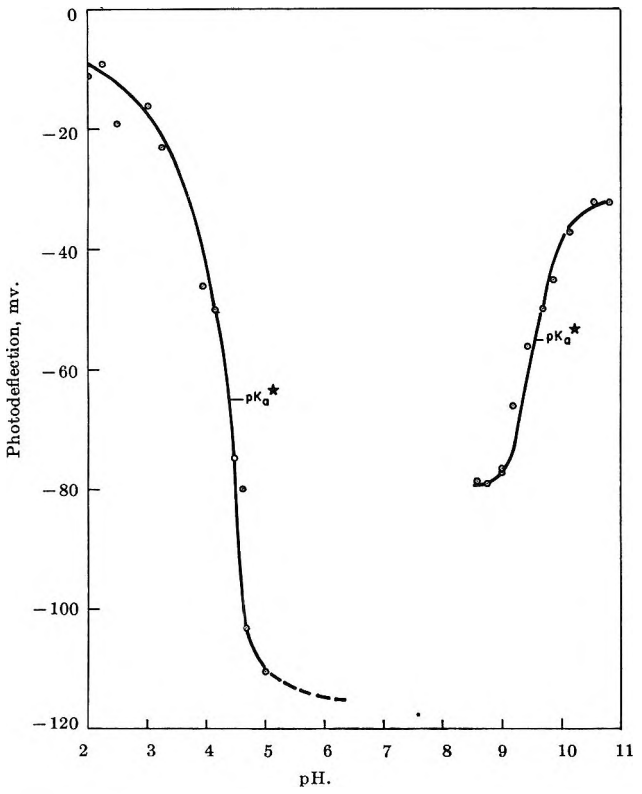

Figure 5. Determination of pK_a^* values for 3-pyridinol.

tions of eosin a small amount of ethanol caused a large increase in the extent of photoreactions. These workers also found that further increase in the ethanol concentration continued to increase the extent of reaction and that a maximum effect was attained at some concentration of ethanol after which no further change was observed. Their study showed that different reduction products were formed in the presence of alcohols.

3-Pyridinol. Several inflections appeared in the curve of photodeflection *vs.* pH for 3-pyridinol. Two of these were assigned to the excited-state pK_a values and are shown in Figure 5. The inflection at pH 4.37 was assigned to a pK_a^* for the dissociation of the proton of the hydroxyl group in the excited state because of the general similarity to phenol. The $pK_a^* - pK_a$ for phenol was −4.3 according to Bartok, *et al.*[10] 3-Pyridinol, which is isoelectronic with phenol, yielded $pK_a^* - pK_a = -4.25$ in this study. This observed shift of the pK_a to stronger acids for a hydroxy group is in accord with the shifts found in the literature for this type of group.

The inflection in alkaline solution at 9.5 was assigned to the pK_a^* for the protonation of the ring nitrogen. The $pK_a^* - pK_a$ would be 4.5 and is comparable with literature results for similar compounds. Mataga, *et al.*,[22] have obtained the value $pK_a^* - pK_a = 2$ for quinoline, 5.5 for acridine, and 3 for protonation of the ring nitrogen in 2,8-diaminoacridine. Kokubun[8] has found that acridone becomes a stronger base in the excited state with $pK_a^* - pK_a = 1.86$. Weller[23] found a ΔpK_a of approximately 5 for acridine by using NH_4^+ as the protonating agent.

Aromatic bases normally become weaker bases in the excited state with the exception of heterocyclic nitrogen bases as indicated above.

Normally, excitation of the unshared or n electron into the aromatic π cloud is regarded as the lowest energy transition. Such a transition would certainly cause a decrease in the basic strength. But in a very polar solvent the nitrogen is usually associated with a proton either through a strong hydrogen bond with a solvent molecule or by abstraction of a proton from a stronger acid in the system.

Association with a proton or hydrogen atom is generally sterically facilitated in heterocyclic molecules and this shifts the transition to a higher energy so that it is no longer the lowest energy transition. This argument also applies to aromatic carbonyl groups which become weaker acids in the excited state as opposed to the strengthened acidity found in excited hydroxy compounds.

The heterocyclic nitrogen atom becomes more basic in the excited state because the π–p interaction is between orthagonal orbitals. This means that electron–electron repulsions become a dominant factor. Strong electron–electron repulsions will affect the orbital angular momentum of the p orbital. Thus the p orbitals extend out further from the nitrogen to facilitate bonding between the nitrogen and a protonating agent.

V. Summary

The present study has outlined a new technique which provides a method of determining excited-state pK_a values. It has been shown that results from photopotentiometry are compatible with results from fluoresence measurements.

(22) N. Mataga, Y. Kaifu, and M. Kaizumi, *Bull. Chem. Soc. Japan*, 29, 373 (1956).

(23) A. Weller, *Z. Elektrochem.*, 61, 956 (1957).

Kinetic Studies of Permanganate Oxidation Reactions. I. Reaction with Iodide Ion

by Louis J. Kirschenbaum and John R. Sutter

Department of Chemistry, Howard University, Washington, D. C. *(Received June 10, 1966)*

The reaction of $8H^+ + MnO_4^- + 5I^- \rightarrow {}^5/_2I_2 + Mn^{2+} + 4H_2O$ has been studied in acidic media using phosphate buffers. At 35° and at ionic strength $I = 0.9\ M$ over the pH range 3 to 6 the reaction follows the rate expression

$$-d(MnO_4^-)/dt = (MnO_4^-)(I^-)\{k_2 + k_3 a_{H^+}\}$$

In the pH 5 region, $k_2 = 51.2$ l./mole sec and $k_3 = 1.70 \times 10^7$ l.^{2}/mole^2 sec. The activation parameters for the second-order path at $\Delta H^{\ddagger} = 1.30$ kcal and $\Delta S^{\ddagger} = -45.8$ eu, while those for the third-order path are 3.77 kcal and −14.4 eu, respectively. Mechanisms for the two paths involving the formation of a $(MnO_4I)^{2-}$ complex prior to the rate-determining step are consistent with the data.

Introduction

The reaction between the permanganate ion and iodide ion affords an opportunity to study kinetically the five-equivalent reduction of permanganate. It should be noted that the formation of either iodine or HOI as a product of a step in which manganate would be produced as a reduction product of permanganate would constitute a barrier to the progress of the reaction. The I^-–I_2 couple has a potential[1] approximately equal to that of the MnO_4^-–MnO_4^{2-} couple, and the I^-–HOI reaction is thermodynamically forbidden. In spite of these factors, the reaction is extremely rapid. The formation of Mn(V) and HOI in a two-equivalent reduction is thermodynamically favorable.

Experimental Section

Reagent grade chemicals were used in all cases. Initially, they were recrystallized several times from water before kinetic use; results showed no difference in the experimental rate constant before and after recrystallization, and further runs were made without purification. Water was freshly distilled from a Barnstead still. Potassium iodide solutions were made up by weight while the potassium permanganate solutions were standardized spectrophotometrically at 520 mμ where $\epsilon = 2184\ M^{-1}$ cm^{-1}. The stock solution of permanganate used in the Beer's law experiments was standardized against standard arsenious trioxide by titration.

Verification that the reaction proceeded quantitatively to manganous ion and iodide (I_3^-), exclusively, under the conditions of the experiment ($K_{I_3^-} = 720$) was accomplished in two ways. First, the amount of I_3^- produced in the reaction was observed spectrophotometrically at the end of the reaction,[2] and secondly, experiments were performed in such a way that the amount of I_3^- produced could be titrated with standard thiosulfate. In both experiments the amount of I_3^- formed in the reaction agreed very well with the amount calculated from permanganate present initially.

The rate of the reaction was determined by following the disappearance of permanganate at 520 mμ spectrophotometrically, using a specially adapted Beckman DU. In all reactions the iodide ion concentration was maintained constant by having it in large (from 40- to 100-fold) excess. Thus the kinetic disappearance of permanganate was pseudo-first order throughout the course of the reaction, as determined from the plots of

(1) W. M. Latimer, "Oxidation Potentials," 2nd ed, Prentice-Hall, Inc., New York, N. Y., 1952. All thermodynamic estimates taken from this source.

(2) A. D. Awtrey and R. E. Connick, *J. Am. Chem. Soc.*, **73**, 1842 (1951).

log $(A_\infty - A)$, the difference in the absorbance at infinite time and at time t.

The order of the reaction with respect to permanganate and iodide was determined by this technique to be first order in each. The results are summarized in Table I. In certain runs the reaction was followed through five half-lives to ensure a noncomplicated reaction scheme independent of products.

The phosphate buffers were made up by weight to the approximate desired pH, using K_2HPO_4 and KH_2PO_4. These solutions were used to make up the stock solutions of the reactants. In this way the solutions were made up to the same ionic strength and pH prior to mixing. The ionic strength was calculated in the usual fashion and was held constant in all reactions at $I = 0.933$ by keeping the total concentration of salts fixed. The buffers thus functioned to hold both pH and ionic strength constant. In the low pH range, the buffers were made from KH_2PO_4 to which small amounts of H_3PO_4 were added to adjust the pH.

Table I: Rate Dependence on MnO_4^- and I^- [a]

Run	$[MnO_4^-]$, moles/l. $\times 10^5$	$[I^-]$, moles/l. $\times 10^2$	k, sec^{-1}	$k_2' = k/I^-$, l. $mole^{-1}$ sec^{-1}
1a	8.22	3.49	1.98	56.7
1b	8.22	3.49	2.08	59.6
2a	8.50	2.57	1.52	59.1
2b	8.50	2.57	1.50	58.4
3a	3.40	1.29	0.737	57.1
3b	3.40	1.29	0.740	57.4
4a	3.28	1.74	1.01	58.0
4b	3.28	1.74	1.08	62.1
5a	1.86	0.872	0.518	59.4
5b	1.86	0.872	0.535	61.4
5c	1.86	0.872	0.556	63.8
6a	1.92	0.643	0.410	63.8
7a	15.3	6.97	4.06	58.2
7b	15.3	6.97	4.28	61.4
8a	2.88	0.697	0.400	57.4
8b	2.88	0.697	0.399	57.2
9a	2.88	6.97	4.10	58.8
				59.3 ± 1.8

[a] $t = 34.92°$; $I = 0.933\ M$; λ 5200 A; 2-cm cell; $\epsilon_{MnO_4^-} = 2184\ M^{-1}\ cm^{-1}$; pH 6.13.

The pH of the reactant solutions was measured before and after individual runs, using a Metrohm E-300 pH meter which was standardized at the temperature of the reaction mixtures against standard buffers of known temperature dependence.

In order to follow the kinetics of this rapid reaction, a rapid mixing device was utilized. The permanganate solution was diluted to the desired initial concentration and ionic strength with phosphate buffer of the proper pH. A calibrated volume (3 ml) was pipetted into a special water-jacketed quartz cell of 2-cm path length.[3] The solution in this was thermostated by flowing water, and the temperature was regulated to $\pm 0.05°$ or better. Five-tenths of a milliliter (calibrated) of the iodide solution, made up to the same ionic strength and pH as the permanganate solution was taken up with a 2-ml hypodermic syringe equipped with an 18-gauge needle. The iodide ion concentration was adjusted so that the iodide concentration after mixing the two solutions would be in the proper excess necessary for the isolation technique. The syringe was housed in a thermostated brass cylinder which also served to hold it in a vertical position on top of the DU cell compartment, with the needle dipping into the permanganate solution. The syringe plunger was fitted with a tight compression spring[4] which, when released, rapidly mixed the two solutions by forcing one into the other. In a separate series of experiments, the mixing time was determined using hydrochloric acid and sodium hydroxide solutions of equivalent composition, and observing the disappearance of the phenolphthalein color. The mixing time for complete color disappearance was approximately 30 msec. The change in absorbance during the kinetic runs was followed by taking the signal from the anode of an IP28 photomultiplier and leading it into a Type D Tektronix differential amplifier and Model 532 oscilloscope. The triggering of the oscilloscope was made to coincide with the mixing of the solution by coupling the release arm of the spring on the rapid mixing device to a microswitch and the external trigger input of the oscilloscope. The resultant change in absorbance was photographed with a Tektronix C-12 Polaroid oscilloscope camera. The film was read under a microscope equipped with a movable Vernier stage. The data so obtained were plotted in order to determine the rate law.

Results and Discussion

Dependence on hydrogen ion activity was determined in the pH range 6.2 to 3.2 (Table II). A plot of the observed second-order rate constant, k_2' *vs.* a_{H^+} is linear in the high pH region (pH 5–6) showing a two-part rate law of the form

$$\text{rate} = (MnO_4^-)(I^-)\{k_2 - k_3 a_{H^+}\}$$

where the term in braces is k_2', the observed second-

(3) Constructed by Optical Cell Co., Brentwood, Md.

(4) Design by R. G. Thompson and G. Gordon, University of Maryland, private communication. The reader may refer to R. Thompson and G. Gordon, *J. Sci. Instr.*, 41, 480 (1964).

order rate constant. Values of the slope and intercept are consistent with a value of $k_2' = 51.2 + 1.70 \times 10^7 a_{H^+}$. It is to be noted that this equation gives values for k_3 in the pH 3 region that are higher than those observed experimentally. However, a plot of log $(k_2' - k_2)$ *vs.* pH is linear over the entire pH 3 to pH 6 range, with a slope of -0.94, indicating that the two-part rate law is probably maintained throughout, but that the "long" extrapolation is responsible for the lack of agreement in the numbers. Examination of the last three entries of Table II lends support that the two-part rate law is being obeyed throughout the entire pH range studied. Here, although the pH spread is admittedly not large, the values of $k_2'/a_{H^+} = k_3$ result in a rate constant of $9.66 \pm 0.2 \times 10^6$ (l./mole)^2 sec^{-1}, showing a simple first-order dependence on a_{H^+}, in agreement with the expected behavior of the two-part rate law on going to low pH. It is apparent that the errors in the rate constants determined in the pH 5–6 region, although reasonable, will not allow a proper extrapolation to the pH 3 region without including values from the intermediate pH 4 region, which are inaccessible in a system using phosphate buffers.

The dependence of rate on temperature was determined at both a pH of 3.3 and of 5.49 (Tables III and IV). A plot of log (k_2'/T) *vs.* $1/T$ at the low pH gives a straight line and a calculated $\Delta H^{\pm}$ and $\Delta S^{\pm}$ of 3.77 kcal and -14.42 eu, respectively. In these calculations k_2'/a_{H^+} was taken equal to k_3, and no correction was made for the small contribution to k_3 from the rate constant k_2 of the nonprotonated path in this low pH region.

A plot of log (k_2'/T) *vs.* $1/T$ at the high pH value yields a curved line which is expected, due to the sizable contribution from k_3. These k_2 values were corrected by subtracting $k_3 a_{H^+}$ from the k_2', giving a value of k_2 at each temperature. These data plot linearly to give $\Delta H^{\pm}$ and $\Delta S^{\pm}$ of 1.3 kcal and -45.85 eu, respectively. The treatment of the data in this fashion is justified even though a given set of parameters k_2 and k_3 will not span the entire pH range because of the argument presented above. Once the form of the rate law has been shown to be obeyed over this range, the subtraction of the experimental product $k_3 a_{H^+}$ from k_2', even though they are of comparable magnitude at high pH, will yield values of k_2 without appreciable loss of precision.

Since the $\Delta H^{\pm}$ is quite low for both the protonated and nonprotonated paths, the formation of an intermediate complex is indicated.[5] This seems more likely than the formation of OI^- through the rupture or partial rupture of an Mn–O bond in a single step, and even more likely than the formation of either I or I^+ species in solution. The energy necessary to form such species in solution is in excess of 1 ev.[6] In the hydrogen ion independent step of the two-part rate law, the mechanism

Table II: Dependence of Rate on pH

pH	k_2', l./mole sec[a]	$[KH_2PO_4]$, *M*	$[K_2HPO_4]$, *M*	$[I^-] \times 10^3$, *M*
6.13	59.3	0.133[b]	0.533[b]	*c*
5.86	79.1	0.626	0.102	8.66
5.46	104.8	0.780	0.0587	8.66
5.16	177.0	0.833	0.033	8.72
3.40	3.77×10^3	0.930	*d*	4.33
3.34	4.38×10^3	0.930	...	4.33
3.18	6.58×10^3	0.930	...	4.33

[a] All rate constants are the average of two to four runs. [b] These are approximate values that were adjusted to correspond to $I = 0.933$. [c] See Table I. [d] Small amount of H_3PO_4 added to adjust pH. All runs at $t = 34.92°$, $I = 0.933$.

Table III: Temperature Dependence at Low pH[a]

t, °C	pH	$k_2' \times 10^{-4}$, l./mole sec	$k_3 = (k_2'/a_{H^+}) \times 10^{-6}$, (l./mole)^2 sec^{-1}
6.40	3.46	1.61	4.63
15.16	3.44	2.14	5.89
18.95	3.38	2.62	6.28
25.20	3.33	3.56	7.59
34.92	3.34	4.38	9.59

[a] $[I^-] = 4.33 \times 10^{-3}$ *M*; $[MnO_4^-] = 2.47 \times 10^{-5}$ *M*; $I = 0.933$.

Table IV: Temperature Dependence at High pH

t, °C	pH	k_2'	$k_3 \times 10^{-6}$[a]	Correction to k_2' ($k_3 \times a_{H^+}$)	k_2
6.40	5.52	68.1	4.63	13.9	54.2
15.16	5.48	77.6	5.89	19.5	58.1
19.40	5.49	82.5	6.54	21.2	61.3
23.90	5.49	88.3	7.35	23.8	64.5
34.92	5.46	105.3	9.59	33.3	72.0
45.00	5.40	130.1	12.10	48.2	81.9

[a] From Table III by extrapolation or interpolation.

(5) J. P. Hunt, "Metal Ions in Aqueous Solution," W. A. Benjamin, Inc., New York, N. Y., 1963, p 114.

(6) Z. Simon, *Can. J. Chem.*, **38**, 2373 (1960).

$$MnO_4^- + I^- \overset{K}{\rightleftharpoons} (O_3MnOI)^{2-} \quad \text{(rapid, } K\text{)} \quad \text{(I)}$$

$$(O_3MnOI)^{2-} + HOH \xrightarrow{k} HOI + HMnO_4^{2-}$$

(rate determining) (II)

is consistent with the observed kinetics. The observed $\Delta H^{\ddagger}_{obsd}$ being the sum of the ΔH° for the complex formation step and the $\Delta H^{\ddagger}_{II}$ of the rate-determining step. The HOI formed would be rapidly reduced

$$HOI + H_3O^+ + 2I^- \longrightarrow I_3^- + 2H_2O$$

(rapid and complex)

with $HMnO_4^{2-}$ present to further the reaction. The formation of this hypomanganate species and transfer of oxygen is in keeping with arguments put forth by Carrington and Symons[7] and by Stewart and van der Linden[8] in the permanganate–cyanide reaction. The $(MnO_4I)^{2-}$ complex is to be considered a derivative of hypomanganate with the character of the kinetic intermediates $(OI^-) + (MnO_4)^{3-}$ being fairly well established prior to the rate-determining step.

The hydrogen ion dependent path parallels the above mechanism

$$MnO_4^- + I^- \rightleftharpoons (O_3MnOI)^{2-} \quad \text{(rapid, } K\text{)}$$

$$(O_3MnOI)^{2-} + H_3O^+ \xrightarrow{k} HOI + H_2MnO_4^-$$

(rate determining) (III)

In this case, the change from second to third order with decrease in pH is seen in terms of a competition between H_2O and H_3O^+ as an electrophile.

Under the conditions of our experiments in the low pH range, permanganate is present almost exclusively in the nonprotonated form, *e.g.* and although the formation of the $HMnO_4$ species may be important to the kinetics, it would be kinetically indistinguishable from the above mechanism.

$$H^+ + MnO_4^- = HMnO_4 \qquad (k = 5.6 \times 10^{-3})^9$$

Five runs were made at 34.92° and pH 6.18 with various permanganate–iodide concentrations, and in addition, at ionic strength $I = 0.0933$. The observed second-order rate constant, k_2', at this ionic strength was 18.6 ± 0.7 l./mole sec. No attempt was made to correlate the increase in rate with increasing ionic strength in terms of the Brønsted–Bjerrum equation.

The increase in $\Delta S^{\ddagger}$ in comparing the nonprotonated and protonated paths (with activation entropies of −45.8 and −14.4 eu, respectively) reflects the release of water molecules by the proton during the formation of the transition state. Assuming three water molecules released per proton, a value of −10 eu per water molecule is obtained for this entropy.

Acknowledgment. The authors acknowledge partial support of this work through a grant from the donors of the Petroleum Research Fund, administered by the American Chemical Society. L. J. K. acknowledges support under a National Science Foundation Undergraduate Summer Research Program grant.

(7) A. Carrington and M. C. R. Symons, *Chem. Rev.*, **63**, 443 (1963).

(8) R. Stewart and R. van der Linden, *Can. J. Chem.*, **38**, 2237 (1960).

(9) N. Bailey, A. Carrington, T. A. K. Lott, and M. C. R. Symons, *J. Chem. Soc.*, 290 (1960).

Mercury Porosimetry: Filling of Toroidal Void Volume Following Breakthrough between Packed Spheres

by Raymond P. Mayer and Robert A. Stowe

Research and Development Laboratory, The Dow Chemical Company, Ludington, Michigan
(Received June 13, 1966)

The treatment covering penetration of fluids into the void space of a collection of uniform solid spheres has been extended to the filling of the toroidal void space following initial breakthrough. The pressure–volume relationships are derived by consideration of the energy balance involved. Data are presented for a range of pressures from breakthrough to infinity and for fluid–solid systems exhibiting contact angles between 100 and 180°. Various concepts regarding the experimental phenomena of penetration, filling, retraction, and withdrawal are discussed in terms of the theoretical treatment.

I. Introduction

The use of the mercury porosimeter is common in the characterization of porous solids. The usual interpretation of the pressure data is in terms of cylindrical capillaries, as first proposed by Washburn.[1] The limitations of this model have been pointed out by de Boer.[2] Kruyer[3] and, more recently, Frevel and Kressley,[4] recognizing the failure of many experimental solids to meet the criteria of the Washburn model, treated various aspects of the problem of the penetration and retraction of mercury into a solid composed of a collection of nonporous uniform spheres.

The mathematical relationships describing the penetration of fluids into the void spaces of such spheres have been developed by the present authors.[5] The pressure required for initial penetration or "breakthrough" pressure was defined in terms of the porosity of the spherical model and the contact angle of the fluid. These relationships allow the determination of particle radius from standard mercury penetration and porosity data.

It is the purpose of the present paper to extend this treatment to cover the filling of the toroidal void space with mercury under increasing hydraulic pressure following initial breakthrough.

II. Derivation of Pressure Relationship

The pressure required to force mercury, or other nonwetting fluid, into the constricted regions between solid particles is a function of the geometry of the system. The function may be derived by a consideration of the surface free energies involved.

At equilibrium, the pressure on the mercury is constant. The work associated with infinitesimal changes in the surfaces is equal to the net change in surface energies. This work is given by

$$P\mathrm{d}V = \gamma_{\mathrm{L,V}}\mathrm{d}S_{\mathrm{L,V}} + \gamma_{\mathrm{L,S}}\mathrm{d}S_{\mathrm{L,S}} + \gamma_{\mathrm{S,V}}\mathrm{d}S_{\mathrm{S,V}} \quad (1)$$

where P, V, γ, and S are terms referring to pressure differential, volume, surface free energy, and surface area, respectively, and the subscripts L, S, and V refer to liquid, solid, and vapor, respectively. Under conditions of intrusion

$$\mathrm{d}S_{\mathrm{L,S}} = -\mathrm{d}S_{\mathrm{S,V}} \quad (2)$$

In addition

$$\gamma_{\mathrm{S,V}} - \gamma_{\mathrm{L,S}} = \gamma_{\mathrm{L,V}} \cos\theta \quad (3)$$

where θ is the contact angle between the liquid and solid. Substitution of eq 2 and 3 in eq 1 followed by rearrangement, gives

(1) E. W. Washburn, *Proc. Natl. Acad. Sci. U. S.*, **7**, 115 (1921).
(2) J. H. de Boer, *Advan. Catalysis*, **9**, 139 (1959).
(3) S. Kruyer, *Trans. Faraday Soc.*, **54**, 1758 (1958).
(4) L. K. Frevel and L. J. Kressley, *Anal. Chem.*, **35**, 1492 (1963).
(5) R. P. Mayer and R. A. Stowe, *J. Collcid Sci.*, **20**, 893 (1965).

$$P = \frac{\gamma_{L,V}(dS_{L,V} + dS_{S,V} \cos \theta)}{dV} \quad (4)$$

The above equation gives directly

$$P = \frac{-2\gamma_{L,V} \cos \theta}{r}$$

when applied to an opening having a circular cross section. In such a case, the advancing L,V surface does not change and $dS_{L,V} = 0$. Also the quantity $dS_{S,V}/dV$ reduces to $-2/r$.

Similarly, for a parallel-sided fissure of length b and width $2r$, with $b \gg r$, eq 4 simplifies to

$$P = \frac{-\gamma_{L,V} \cos \theta}{r}$$

The general relationship shown by eq 4 is the starting point for the more specific expression given for breakthrough pressure as eq 9 in the previous paper.[5] For a portion of an L,V surface, not in contact with a solid, the right side of eq 4 reduces to $\gamma_{L,V}dS_{L,V}/dV$. Using the principal radii of curvature for expressing the surface and volume terms gives rise to the familiar Young and Laplace equation.[6]

III. Application of Spherical Model

The model of packed nonporous uniform spheres was discussed in the previous paper. Two types of packing were outlined, differing mainly in the maximum porosity which they can attain. However, after initial breakthrough, the geometry of the isolated void rings around the points where the spheres make contact is the same for either case. Figure 1 represents a system of isolated void spaces during filling. The void volumes represented by an area such as m in the cross-sectional view are bounded by the S, V surfaces of the spheres and the L, V surfaces of the advancing mercury. A given toroidal void ring is provided by rotation of this area around the line A_1A_2.

An enlarged view showing construction details is given in Figure 2. The centers of the spheres, A_1 and A_2, are placed on the X axis with the Y axis intersecting at D, the point of contact between the spheres. The intersection of the liquid–solid, the liquid–vapor, and the solid–vapor interfaces occurs at point C. The extension of the spherical radius, r, through C intersects the Y axis at point G, and defines the basic parameter, angle ϕ. The curvature of the L, V surface shown by arc CH is a function of the contact angle θ. A general contact angle is shown as angle NCM, where NC is perpendicular to A_2G. Line CJ is constructed perpendicular to CM and defines the radius of curvature, g, of the arc CH. The angle, κ, by simple geometry, is

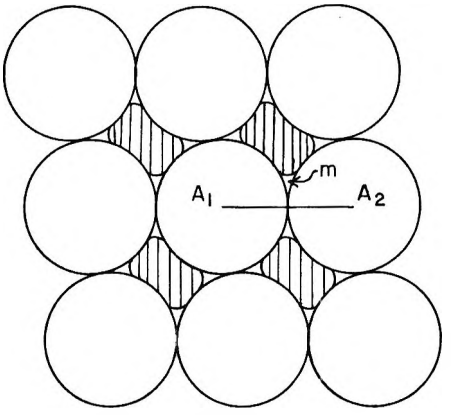

Figure 1. Cross section of spheres during filling.

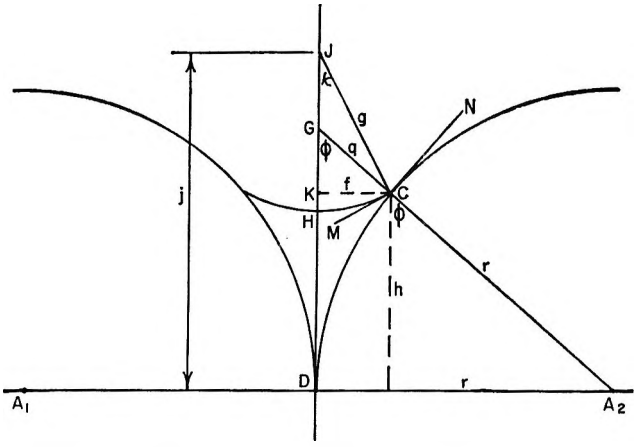

Figure 2. Construction for toroidal void space.

found to be $(\phi - \pi + \theta)$ radians. Distances f and h are the x and y coordinates of point C. For convenience, the distances CJ, CG, and DJ are represented by g, q, and j, respectively.

Differentiation of eq 4, with respect to the parameter ϕ, and rearranging gives

$$\frac{P}{\gamma_{L,V}} = \frac{\dfrac{dS_{L,V}}{d\phi} + \dfrac{dS_{S,V} \cos \theta}{d\phi}}{\dfrac{dV}{d\phi}} \quad (5)$$

For a single toroid, the surface, $S_{L,V}$, is given analytically as twice the surface of revolution of the arc CH. Likewise, the surface, $S_{S,V}$, is twice the surface generated by revolution of arc CD.

The volume term in eq 4 and 5 refers to the volume of mercury. A change in volume of the toroidal void space results in an equal but opposite change in the

(6) A. W. Adamson, "Physical Chemistry of Surfaces," Interscience Publishers, Inc., New York, N. Y., 1960, pp 1–6.

volume of the mercury. The volume of the toroid, itself, is given analytically by the difference in volume generated by revolution of arc CH and arc CD.

The general expression for arc CD is

$$(x - r)^2 + y^2 = r^2 \tag{6}$$

Similarly, arc CH is given by

$$x^2 + (y - j)^2 = g^2 \tag{7}$$

By calculus, the S, V surface is given by the general expression

$$S_{S,V} = 2 \cdot 2\pi \int_0^f (2rx - x^2)^{1/2}[1 + (r - x)^2(2rx - x^2)^{-1}]^{1/2} dx = 4\pi rf \tag{8}$$

Similarly, the L, V surface is given by

$$S_{L,V} = 2 \cdot 2\pi \int_0^f [j - (g^2 - x^2)^{1/2}] \times [1 + x^2(g^2 - x^2)^{-1}]^{1/2} dx = 4\pi g(j\varkappa - f) \tag{9}$$

The toroidal volume, V_t, is given by

$$V_t = 2\pi \int_0^f [j^2 - 2j(g^2 - x^2)^{1/2} + g^2 - x^2] dx - 2\pi \int_0^f (2rx - x^2) dx = 2\pi[fj^2 - f^2 j \operatorname{ctn} \varkappa - g^2 j\varkappa + fg^2 - rf^2] \tag{10}$$

Differentiation of eq 8, 9, and 10 with respect to ϕ provides the terms required for substitution in eq 5. Thus

$$\frac{dS_{S,V}}{d\phi} = 4\pi r \frac{df}{d\phi} \tag{11}$$

$$\frac{dS_{L,V}}{d\phi} = 4\pi\left[gj + \varkappa\left(g\frac{dj}{d\phi} + j\frac{dg}{d\phi}\right) - g\frac{df}{d\phi} - f\frac{dg}{d\phi}\right] \tag{12}$$

and as noted before for the change in volume of the mercury

$$\frac{dV}{d\phi} = \frac{-dV_t}{d\phi} = -2\pi\left[j^2\frac{df}{d\phi} + 2fj\frac{dj}{d\phi} + f^2 j \csc^2 \varkappa - \operatorname{ctn} \varkappa\left(2fj\frac{df}{d\phi} + f^2\frac{dj}{d\phi}\right) - g^2 j - \varkappa\left(2gj\frac{dg}{d\phi} + g^2\frac{dj}{d\phi}\right) + g^2\frac{df}{d\phi} + 2fg\frac{dg}{d\phi} - 2rf\frac{df}{d\phi}\right] \tag{13}$$

In the above equations, we note that

$$f = r(1 - \sin \phi)$$

$$g = f/\sin \varkappa$$

$$j = r \cos \phi + g \cos \varkappa$$

and

$$\frac{df}{d\phi} = -r \cos \phi$$

$$\frac{dg}{d\phi} = \frac{\sin \varkappa \dfrac{df}{d\phi} - f \cos \varkappa}{\sin^2 \varkappa}$$

$$\frac{dj}{d\phi} = -r \sin \phi - g \sin \varkappa + \cos \varkappa \frac{dg}{d\phi}$$

The various terms in eq 5 now having been defined, values for $P/\gamma_{L,V}$ are readily computed for various values of the parameters ϕ and θ. The equations are in a form readily adapted to computer evaluation. Therefore, no attempt was made to provide further substitution or simplification.

IV. Residual Void Volume

In the preceding section, the volume associated with a single toroidal void was given by eq 10. Within the system of packed spheres, partially filled with mercury, each point of contact between spheres gives rise to such a toroidal void space. The number of such contacts depends upon the packing model chosen.

Two models for packing have been discussed in the previous paper. In one of these, the spheres are arranged in simple cubic array and vary uniformly in three dimensions as the packing changes to hexagonal close-packed. The alternate model starts with cubic stacking of hexagonally close-packed layers and by nesting of such layers reaches the same hexagonal close-packed array.

The first model will have six points of contact between a given sphere and its neighbors throughout the range of packing. By contrast, the second model has eight points of contact throughout its range of packing. However, when the hexagonal close-packed state is reached, the number of contacts increases to 12 for both models.

The toroidal void space associated with each point of contact is shared by the two spheres. Hence, the volume of residual void space associated with each sphere or unit cell is $nV_t/2$, where n is the number of contacts per sphere. Because of the various values which n may assume, it is convenient to compute V_t directly from eq 10 and then apply separately the appropriate factor for the points of contact associated with the packing model.

Accordingly, values were computed for the reduced hydraulic pressure difference, $P/\gamma_{L,V}$, and the toroidal void space, V_t, over a range of ϕ from 45 to 90° and for θ

Table I: Selected Values of Reduced Pressure *vs.* Toroidal Void Space

ϕ, deg	θ = 180°		θ = 170°		θ = 160°		θ = 150°		θ = 140°		θ = 130°		θ = 120°		θ = 110°		θ = 100°	
	$P/\gamma_{L,V}$	V_t	$P/\gamma_{L,V}$	V_t	$P/\gamma_{L,V}$	V_t	$P/\gamma_{L,V}$	V_t	$P/\gamma_{L,V}$	V_t	$P/\gamma_{L,V}$	V_t	$P/\gamma_{L,V}$	V_t	$P/\gamma_{L,V}$	V_t	$P/\gamma_{L,V}$	V_t
90	∞	0.0000	∞	0.0000	∞	0.0000	∞	0.0000	∞	0.0000	∞	0.0000	∞	0.0000	∞	0.0000	∞	0.0000
89	6519.07	0.0000	6398.90	0.0000	6082.02	0.0000	5578.44	0.0000	4903.71	0.0000	4078.50	0.0000	3128.01	0.0000	2081.23	0.0000	970.00	0.0000
88	1617.51	0.0000	1582.39	0.0000	1498.04	0.0000	1367.21	0.0000	1194.01	0.0000	983.80	0.0000	743.01	0.0000	479.02	0.0000	199.87	0.0000
87	713.13	0.0000	695.28	0.0000	655.53	0.0000	595.22	0.0000	516.26	0.0000	421.13	0.0000	312.75	0.0000	194.45	0.0000	69.84	0.0000
86	397.72	0.0000	386.43	0.0000	362.81	0.0000	327.68	0.0000	282.17	0.0000	227.72	0.0000	166.02	0.0000	98.95	0.0000	28.58	0.0000
85	252.25	0.0001	244.23	0.0001	228.30	0.0001	205.06	0.0001	175.24	0.0001	139.81	0.0001	99.86	0.0001	56.63	0.0001	11.43	0.0001
84	173.50	0.0002	167.38	0.0002	155.77	0.0002	139.11	0.0002	117.93	0.0002	92.93	0.0002	64.88	0.0002	34.65	0.0002	3.16	0.0002
83	126.19	0.0003	121.29	0.0003	112.36	0.0003	99.73	0.0003	83.84	0.0003	65.19	0.0003	44.36	0.0003	22.00	0.0003	−1.19	0.0003
82	95.59	0.0005	91.53	0.0005	84.39	0.0005	74.44	0.0005	62.01	0.0005	47.52	0.0006	31.41	0.0006	14.19	0.0006		
81	74.68	0.0008	71.24	0.0008	65.36	0.0008	57.27	0.0008	47.25	0.0009	35.64	0.0009	22.79	0.0009	9.11	0.0009		
80	59.78	0.0011	56.80	0.0012	51.85	0.0012	45.12	0.0013	36.85	0.0013	27.31	0.0013	16.81	0.0014	5.67	0.0014		
79	48.79	0.0016	46.18	0.0017	41.92	0.0018	36.22	0.0018	29.25	0.0019	21.27	0.0020	12.52	0.0020	3.27	0.0021		
78	40.47	0.0022	38.14	0.0024	34.43	0.0025	29.52	0.0026	23.56	0.0027	16.77	0.0028	9.35	0.0028	1.55	0.0029		
77	34.01	0.0030	31.92	0.0032	28.65	0.0034	24.36	0.0035	19.20	0.0036	13.34	0.0038	6.97	0.0039				
76	28.91	0.0039	27.01	0.0042	24.10	0.0045	20.31	0.0047	15.79	0.0049	10.68	0.0050	5.15	0.0052				
75	24.80	0.0051	23.07	0.0055	20.45	0.0058	17.08	0.0061	13.08	0.0063	8.58	0.0066	3.73	0.0068				
74	21.46	0.0064	19.86	0.0069	17.49	0.0074	14.47	0.0078	10.89	0.0081	6.90	0.0085	2.61	0.0088				
73	18.69	0.0080	17.22	0.0087	15.06	0.0093	12.32	0.0098	9.11	0.0103	5.54	0.0107						
72	16.39	0.0098	15.01	0.0107	13.04	0.0115	10.55	0.0122	7.64	0.0128	4.43	0.0134						
71	14.44	0.0120	13.16	0.0131	11.34	0.0141	9.06	0.0149	6.42	0.0157	3.51	0.0165						
70	12.79	0.0144	11.59	0.0158	9.90	0.0170	7.81	0.0181	5.39	0.0192	2.74	0.0201						
69	11.37	0.0171	10.24	0.0189	8.67	0.0204	6.74	0.0218	4.53	0.0231								
68	10.14	0.0202	9.08	0.0224	7.62	0.0243	5.83	0.0260	3.79	0.0276								
67	9.08	0.0236	8.08	0.0263	6.71	0.0286	5.04	0.0307										
66	8.15	0.0274	7.20	0.0306	5.91	0.0335	4.36	0.0360										
65	7.33	0.0316	6.43	0.0355	5.22	0.0389	3.77	0.0420										
64	6.60	0.0363	5.75	0.0409	4.61	0.0449												
63	5.96	0.0413	5.15	0.0468	4.07	0.0516												
62	5.39	0.0469	4.61	0.0532														
61	4.88	0.0529	4.14	0.0603														
60	4.42	0.0595																

in 10° increments from 100 to 180°. Selected values of $P/\gamma_{L,V}$ and the corresponding toroidal volume are listed in Table I. These relationships are illustrated in Figure 3, in which V_t is expressed in units of r^3, and $P/\gamma_{L,V}$ is a log scale with units of r^{-1}. It is seen that the toroidal void space becomes zero at $P/\gamma_{L,V} = \infty$. Also, for a fluid having a lower contact angle with the solid, less pressure is required to reduce the void space to a given value.

It should be pointed out that the general relationship depicted in Figure 3 fails to hold at the lower end of the pressure scale. Thus, as discussed in the previous paper, a characteristic breakthrough pressure, depending upon the packing and the contact angle, is required to penetrate the porous solid initially. The void space will be partially filled at this pressure. The relationship between V_t and $P/\gamma_{L,V}$ shown in Figure 3 holds only at pressures greater than P^*, the reduced breakthrough pressure.

The various features of the lower pressure end of the scale can be more clearly seen in Figure 4. In this figure, the values of breakthrough pressure[5] for selected values of the packing angle, σ, and contact angle, θ, are added to the V_t *vs.* $P/\gamma_{L,V}$ relationship.

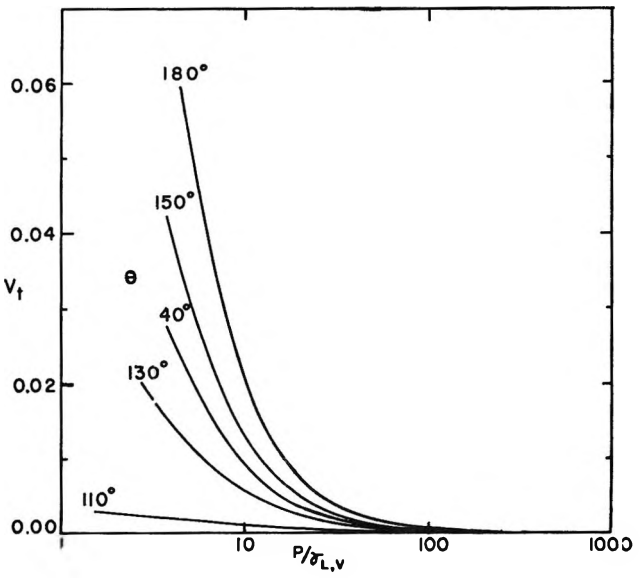

Figure 3. Toroidal void space *vs.* pressure.

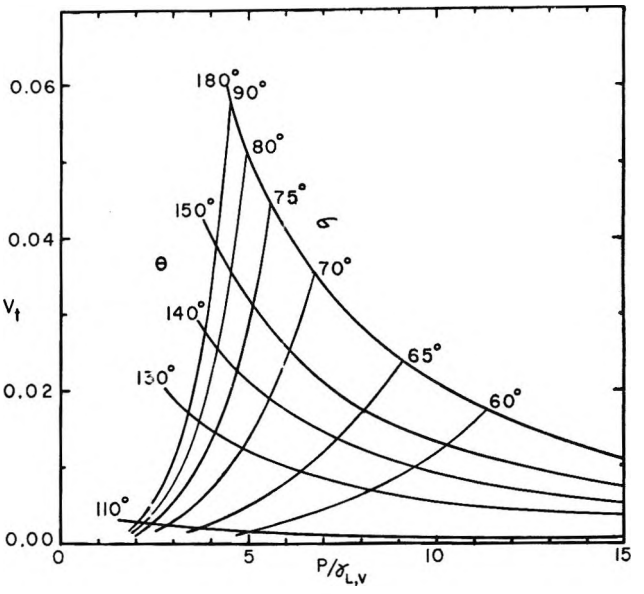

Figure 4. Pressure–volume relationship combined with breakthrough pressure.

V. Discussion

After a porous solid has been subjected to a pressure equal to the breakthrough pressure, the original void volume will partially fill with mercury. Filling ceases when the residual void volume of each toroid reaches the value shown in Figure 4 for the appropriate value of the breakthrough pressure and contact angle. Further increases in pressure cause a further filling with mercury. The resulting decrease in residual void volume follows the relationship shown in Figure 4. Conveniently, this residual void volume may be related to the volume, V, of the mercury per unit cell. This relationship is given by

$$V = \epsilon V_a - \frac{nV_t}{2} \qquad (14)$$

where ϵ is the porosity and V_a is the apparent volume of the unit cell. V_a is given by

$$V_a = \frac{4\pi r^3}{3}\left(\frac{1}{1-\epsilon}\right) \qquad (15)$$

The pressure–volume relationship for mercury penetration of a porous solid comprised of uniform spheres can now be completely described using the preceding data in conjunction with the breakthrough data. This relationship is illustrated in Figure 5 for a solid with which mercury exhibits a contact angle of 140°. Using the model for packing of uniform spheres represented by porosity, ϵ, in the previous paper, four configurations at different packing angles, σ, are illustrated. At the breakthrough pressure, filling occurs along an isobar of pressure. Increased pressure causes further intrusion of mercury. The volume fraction of mercury in the solid approaches the value for the porosity, ϵ, as the pressure becomes infinitely large.

The volume filled, expressed as a fraction of the volume of the original voids is given by $(V/V_a)(1/\epsilon)$, where V and V_a are given by eq 14 and 15. Selected values of the volume fraction filled after the isobaric

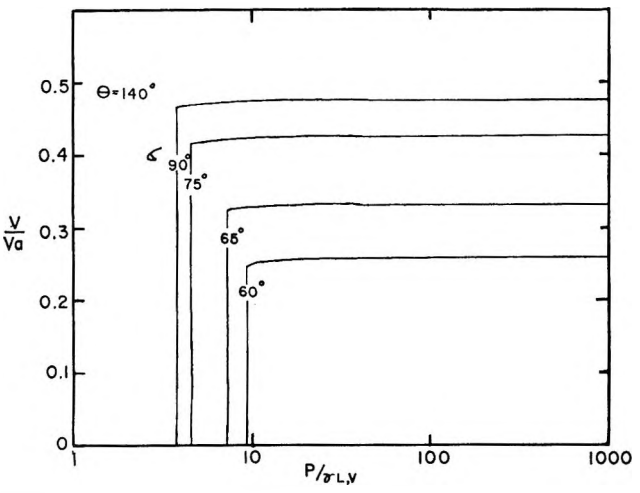

Figure 5. Penetration curves for packed spheres.

filling at the breakthrough pressure are given in Table II. The four packing configurations shown in Figure 5 are presented at the two additional contact angles of 180 and 100°. Note that at $\theta = 100°$, filling after breakthrough is essentially complete at all values of σ. Also, the extent of filling for $\theta = 140°$ and $\theta = 180°$ is reduced at $\sigma = 60°$, due to the additional void space around the increased number of points of contact between spheres.

Table II: Volume Fraction Filled Following Breakthrough

σ, deg	θ, deg 100	140	180
90	1.000	0.978	0.954
75	1.000	0.978	0.957
65	1.000	0.980	0.966
60	1.000	0.959	0.932

It is interesting to compare the above extent of filling with the values suggested by Frevel and Kressley. This is conveniently done only at $\sigma = 60°$, where the two models are identical and $\epsilon = \epsilon' = 0.2595$. In Figure 3 of their paper, the curve for $s/r = 2/\sqrt{3}$ corresponds to $\sigma = 60°$. The value of V/V_a after breakthrough is 0.1964. This value, as a fraction of the porosity, is 0.7569. The comparable value from Table II is 0.932. The value of 0.7569 arises from the assumption that mercury passes through the access opening in the shape of the inscribed circle. This assumption leads to a larger value for the void space remaining and thus, to a lower fraction filled following penetration.

Kruyer,[3] in his discussion of the penetration and retraction of mercury into collections of uniform spheres, limited his theoretical calculations to the retraction branch. His treatment is developed using a construction angle which is the complement of the ϕ angle used here. The volumes associated with the toroidal voids for various configurations are identical with the similar calculations presented above. However, for finding the pressure differential corresponding to these volumes, he makes use of a hyperboloid surface which approximates but is in good agreement with the more correct nodoid surface proposed by Radushkevich[7] and Fisher.[8] Thus, for retraction of mercury from a completely filled solid model, Kruyer's pressure–volume relationship for the early part of the retraction branch is the same as presented here for the later part of the penetration branch except for slight differences in pressure at corresponding volumes. The agreement in these pressures can be seen in Table III which tabulates several values of ϕ, $V_t/2\pi r^3$, and reduced pressures, $P/\gamma_{L,V}$. The reduced pressures listed for Kruyer were calculated from his tabulated values of ρ/R, and thus can be compared directly with the values obtained from this work.

Table III: Comparison with Kruyer at $\theta = 140°$

ϕ, deg	$V_t/2\pi r^3$ × 10³	Reduced pressure, $P/\gamma_{L,V}$ Kruyer	This work
60	14.26	0.528	0.524
65	7.14	2.139	2.133
70	3.05	5.405	5.394
75	1.01	13.098	13.077
80	0.21	36.900	36.846

Kruyer considers retraction from the isolated void rings to occur as pressure is decreased until suddenly the retreating mercury sets free the whole pore space. This discontinuity was considered to occur at the configuration where the isolated L, V surfaces of the retreating mercury interfere with one another. Kruyer's model for the solid lacks the uniformity of packing of the model used here. Therefore, such interference was assumed to occur first in the narrowest access opening possible. These openings are the triangular accesses in hexagonally close-packed spheres and for $\theta = 180°$, the configuration for interference of surfaces corresponds to the inscribed circle.

It appears that with a combination of treatments, one

(7) L. V. Radushkevich, *Izv. Akad. Nauk. SSSR, Otd. Khim. Nauk*, 885 (1952).

(8) R. A. Fisher, *J. Agr. Sci.*, 16, 492 (1926).

could completely describe on theoretical grounds the initial breakthrough, the penetration and retraction branches, and the sudden withdrawal of mercury from a solid model of uniform spheres. Since withdrawal is predicted to occur at pressures lower than those predicted for initial breakthrough into the packing, it would seem that this combination of treatments might adequately account for the observed phenomenon of hysteresis.

This argument may be examined briefly by using Kruyer's experimental data presented for glass spheres of 0.42–0.35-mm diameter. Estimating a breakthrough pressure from the midpoint of his penetration curve of 8 cm pressure, and taking values of $\theta = 140°$, 474 ergs/cm^2 for surface tension, and a porosity of $\epsilon' = 0.363$, a particle diameter of 0.40 mm is calculated by employing the method of the previous paper.[5]

However, Kruyer's experimental value of 5 cm pressure from the midpoint of his withdrawal curve does not agree well with his predicted value of 1.07 cm pressure (calculated from $\rho/R = 3.79$). Several attempts were made to apply Kruyer's concept of interfering surfaces to the geometry of the solid models discussed here. The agreement between the predicted and experimental points for sudden withdrawal was not improved, however.

Other workers have proposed the concept of advancing and receding contact angles to explain hysteresis effects. It is interesting to apply these concepts to the models comprising uniform spheres. Focusing attention first on the higher pressure portions of the penetration and retraction branches, it is noted that the two branches no longer coincide if different contact angles are used. However, they would not differ greatly, especially at the higher pressures. Now, the pressure at which sudden withdrawal will occur might be assumed to be the same as the breakthrough pressure, calculated for the same conditions of packing and contact angle. Thus, retraction at a lower contact angle would provide for a lower withdrawal pressure and account for hysteresis. On this basis, a receding contact angle of about 115° for θ *vs.* an advancing angle of 140° would be required to account for the observed pressures of 5 and 8 cm in the above experiment. At this point, the basis for judging the validity of these various speculations is not evident, and it appears that withdrawal and hysteresis are neither simple nor completely understood.

A further point that may be seen in Figure 5 is the dissimilarity between the shape of the theoretical penetration curves and the usual S-shaped curves found experimentally. Such a smooth S curve can be produced from the present spherical model by assuming a distribution of packing configurations on either side of the principal configuration. Likewise, irregular shapes, as well as a distribution of spherical sizes, would contribute to producing the experimental deviation from the theoretical curves of Figure 5. Thus, the models chosen here do not perfectly represent the real solids, and this emphasizes again that in characterizing experimental solids, various types of supplemental information may be needed.

On the Knudsen Limiting Law of Thermal Transpiration

by George A. Miller and Ralph L. Buice, Jr.

School of Chemistry, Georgia Institute of Technology, Atlanta, Georgia *(Received June 14, 1966)*

Transmission probabilities for gaseous free molecular flow under a temperature gradient have been calculated for various capillaries with a scattering law in which the faster moving molecule has a higher probability of being specularly reflected. This model can explain recent experimental observations of deviations from the Knudsen limiting law. Also the model indicates that the limiting law may be obtained approximately from isothermal free molecular flow data at the two temperatures of interest.

In working at low pressures one must take into account often the thermal molecular pressure difference (TPD) which arises from thermal transpiration along temperature gradients in the apparatus. Thus in measuring the vapor pressure of a substance at low temperatures one must apply a correction to the reading of the manometer, which is normally at room temperature. There are two theoretical treatments of TPD which start from first principles, the Weber equation[1] and the Dusty Gas model.[2] The latter, especially interesting in its bearing on rotational relaxation, is concerned with porous media. If extended to include capillaries, it is in essential agreement with the former. The Weber equation has, in its crudest form, no adjustable constants, since it is derived by joining Maxwell's kinetic theory solution in the slip flow region to the Knudsen limiting law in differential form. It is, however, an approximate equation, and a consideration of data and certain details of the theory led Weber to adjust the constants and form somewhat.

One of us[3] has made a study of numerous TPD data in light of the Weber equation. It appears that the prediction of TPD is rather uncertain in the middle or transition region of pressure and that it is best to work at either higher pressures, where the effect is small, or at pressures sufficiently low that the Knudsen limiting law is approached to within a few per cent. However, whereas certain sets of data studied approached the limiting law within about 3% while following the Weber equation closely, other data deviated widely from the equation at the same low pressures and left doubt as to the applicability of the Knudsen limiting law. More recently, careful experiments carried to very low pressures by Hobson and co-workers[4,5] have shown a clear deviation from the law for the light gases helium and neon. In this paper we present a theoretical model to explain these results, and we examine the consequences of our calculations in broader terms.

The limiting law is directly traceable to the problem of free molecular flow. Clausing[6] first recognized free molecular flow as a probability problem in which the collision density of gas molecules at the solid surface is the important function. Referring to Figure 1, the rate of flow of molecules from reservoir 2 to reservoir 1 is equal to the rate at which they enter the capillary times the probability that they will leave through the exit. The latter quantity is commonly called the transmission probability (Q) and is a function of the dimensions of the capillary and the scattering law for the gas molecules at the capillary wall. In the free molecular flow region, then, TPD involves a steady state between two independent, opposing flows, and the limiting law is, in more general form

$$\frac{P_2}{P_1} = \left(\frac{T_2}{T_1}\right)^{1/2} \frac{Q_{12}}{Q_{21}} \tag{1}$$

The subscripts to the Q's refer to the direction of flow.

(1) S. Weber, *Commun. Phys. Lab. Univ. Leiden*, No. 246b (1937).

(2) E. A. Mason, R. B. Evans, III, and G. M. Watson, *J. Chem. Phys.*, **38**, 1808 (1963).

(3) G. A. Miller, *J. Phys. Chem.*, **67**, 1359 (1963).

(4) J. P. Hobson, T. Edmonds, and R. Verreault, *Can. J. Phys.*, **41**, 983 (1963).

(5) T. Edmonds and J. P. Hobson, *J. Vacuum Sci. Tech.*, **2**, 182 (1965).

(6) P. Clausing, *Ann. Phys.*, **12**, 961 (1932).

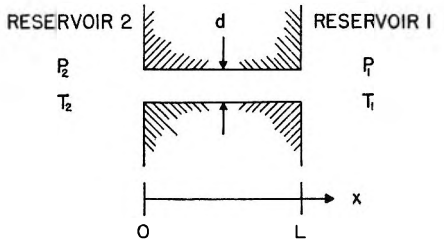

Figure 1. Diagram for the discussion of thermal transpiration through a capillary.

It should be noted that eq 1 contains the assumption that the number of molecules entering the capillary per unit time and area of opening from either reservoir is given by the usual kinetic theory expression, $P/(2\pi mkT)^{1/2}$. Since we are dealing with a nonequilibrium situation in which at least a very small deviation from a Maxwell distribution must take place, this cannot be exact. We have put this difficult question aside in order to be able to study the more obvious aspects of TPD.

Accepting therefore a Maxwellian distribution of velocities in either reservoir, we can say that the Knudsen limiting law is based on the assumption that $Q_{12} = Q_{21}$, which will be true for certain simple reflection laws: (1) totally specular reflection, (2) totally diffuse reflection, *i.e.*, the cosine law, or (3) a fixed degree of specular reflection, in which the impinging molecule has a fixed probability of being specularly reflected regardless of its previous history. In order to explain the experimentally demonstrated deviations from the Knudsen limiting law cited above it is necessary to show that

$$Q_{12} < Q_{21}, \text{ where } T_2 > T_1 \qquad (2)$$

which requires that the scattering law varies in some way with temperature. Unfortunately not enough is known about the details of the scattering of molecules at ordinary surfaces. Molecular beam experiments[7-9] indicate that at this stage Maxwell's picture of a mixture of diffuse and specular reflection is still useful. On the other hand, flow experiments have brought out the importance of preferential back scattering, which is rather the opposite of specular reflection. The model we present below is therefore a compromise between simplicity and experimental fact as we know it.

The Model. It is reasonably clear from the work of DeMarcus[10] that a scattering law capable of explaining the inequality (2) will not be amenable to an analytical solution for Q. We have accordingly set up the problem as a Monte Carlo or random number calculation. Since the problem of the scattering law is far from settled, we thought it to be as important to gain some insight into the details of free molecular flow as to arrive at numerical values of Q. Therefore we have split the calculation into two parts, endeavoring to solve as much of the problem as is possible analytically and performing the remainder by the Monte Carlo technique. Some accuracy is actually sacrificed by this procedure. For an example of a purely random number approach to free molecular flow, we refer to the calculations of Davis[11] on variously shaped ducts in which he assumed the diffuse law of scattering.

Our model consists of the following points: (1) Gas molecules are either diffusely reflected with complete accommodation with the wall or specularly reflected with no accommodation. (2) The probability that a molecule of translational energy, ϵ, be reflected specularly is given by

$$P(\epsilon) = 1 - e^{-\epsilon/\epsilon_0}$$

where ϵ_0 is a sort of critical energy for specular reflection. (3) The distribution of energies of molecules impinging on the capillary wall directly from the reservoir, as well as of the molecules which have just undergone accommodation and diffuse reflection, is assumed to be of the simplified form

$$F(\epsilon) = \frac{1}{T}e^{-\epsilon/T}$$

where ϵ is the translational energy measured in units of k, the Boltzmann constant. This equation is easier to handle in the already time consuming Monte Carlo calculations and gives the correct qualitative behavior as long as the fraction of molecules for which $\epsilon > \epsilon_0$ is not large and as long as ϵ_0 is looked upon as an adjustable parameter not to be predicted with any accuracy from first principles. The correct expression, however, would be that of an effusing gas

$$\frac{1}{T^2}\epsilon e^{-\epsilon/T}$$

Now imagine a gas flowing from a reservoir at temperature T_2 into a capillary of the dimensions shown in Figure 1. The gas is sufficiently rarefied that there are no collisions in the gas phase. Following DeMarcus[10] we define the following probability functions,

(7) F. C. Hurlbut, *J. Appl. Phys.*, **28**, 844 (1957).

(8) S. Datz, G. E. Moore, and E. H. Taylor, *Proc. Intern. Symp. Rarefied Gas Dyn., 3rd (1962)*, **1**, 347 (1963).

(9) J. N. Smith, Jr., *J. Chem. Phys.*, **40**, 2520 (1964).

(10) W. C. DeMarcus, *Proc. Intern. Symp. Rarefied Gas Dyn., 2nd, Berkeley, 1960*, 161 (1961).

(11) D. H. Davis, *J. Appl. Phys.*, **31**, 1169 (1960).

normalized to one molecule entering per second: $s(x)$ is the diffuse collision density per unit length of capillary; $s_1(x)$, the density of first diffuse collisions by entering molecules per unit length; $S_1(x)$, $\int_x^\infty s_1(t)dt$, the density of first diffuse collisions anywhere beyond x; $\Gamma(y, x)$, the probability that a molecule which has diffusely collided at y will suffer its next diffuse collision at x; and $f(x, L)$, the probability that a molecule which has diffusely collided at x will eventually leave through the exit rather than the entrance. Clausing's equations then take the form

$$s(x) = s_1(x) + \int_0^L s(y)\Gamma(y, x)dy$$

$$Q = S_1(L) + \int_0^L s_1(x)f(x, L)dx \qquad (3)$$

An analytical form can be derived for the entrance formula, $s_1(x)$; values of the exit formula $f(x, L)$ are obtained by the Monte Carlo technique. We have chosen the parameters $T_2 = 300°K$ and $T_1 = 100°K$ to approximate conveniently room temperature and the boiling point of liquid nitrogen, $L/d = 1$, 10, and 50, and finally $\epsilon_0 = 900$ for all lengths and 2100 for length 10. The degree of specular reflection as defined below is abnormally high with these values of ϵ_0, but the computer time required is shortened and the over-all effect of ϵ_0 more firmly established.

The Entrance Formula. For that part of the problem which is to be solved analytically we are able to follow closely the procedure developed by DeMarcus[10] for the case of a constant probability of specular reflection, [$P(\epsilon)$ = constant]. Therefore we omit much of the detail of the derivation.

Consider a beam of molecules at temperature T striking the wall of the capillary. The fraction which undergoes n successive specular reflections is, by our model

$$\int_0^\infty P(\epsilon)^n F(\epsilon)d\epsilon = r_1r_2r_3 \cdots r_n$$

$$r_n = nT/(nT + \epsilon_0)$$

We define $r_1 = 1/(1 + \epsilon_0/T)$ as the degree of specular reflection for the sake of discussion. Due to the nature of our model, the function $\Gamma(y, x)$ is symmetrical about y in spite of the temperature gradient along the capillary, *i.e.*

$$\Gamma(y, y + a) = \Gamma(y, y - a)$$

Following DeMarcus[10] it can be shown that

$$\Gamma(y, x) = K(|x - y|)(1 - r_1) + (1/2)K\left(\left|\frac{x - y}{2}\right|\right)r_1(1 - r_2) + (1/3)K\left(\left|\frac{x - y}{3}\right|\right)r_1r_2(1 - r_3) + \ldots$$

where

$$K(y, x) = \lim_{\epsilon_0 \to \infty} \Gamma(y, x)$$

and r_n is characterized by the temperature of the wall at y.

Now consider the equilibrium situation: In Figure 1, set $P_1 = P_2$ and $T_1 = T_2$. Using the well-known properties of an equilibrium gas and Clausing's integral equation for the collision density, we arrive at the formula

$$s_1(x) = (1 - r_1)[(1 - r_1)n_1(x) + r_1(1 - r_2)n_1(x/2) + r_1r_2(1 - r_3)n_1(x/3) + \ldots]$$

where

$$n_1(x) = \lim_{\epsilon_0 \to \infty} s_1(x) = \frac{2}{d}\left[(x^2 + d^2)^{1/2} + \frac{x^2}{(x^2 + d^2)^{1/2}} - 2x\right]$$

and now r_n is characterized by the temperature of the reservoir at the entrance. This formula holds equally well if there is a temperature gradient along the capillary, again due to the nature of our model. Similarly, we can derive the formula

$$S_1(x) = (1 - r_1)[(1 - r_1)N_1(x) + 2r_1(1 - r_2)N_1(x/2) + 3r_1r_2(1 - r_3)N_1(x/3) + \ldots]$$

where

$$N_1(x) = \lim_{\epsilon_0 \to \infty} S_1(x) = \frac{4}{d^2}[2x^2 - 2x(x^2 + d^2)^{1/2} + d^2]$$

The Exit Formula. The calculation outlined below was performed on a Burroughs 5500 digital computer. Random numbers, R, where generated with a power residue formula (sometimes called the multiplicative congruential method), $R_{n+1} = CR_n$ (modulo 8^{13}), where $C = 541755813883$ and $R_0 = 1$ in the decimal number system, and the computer was used at double its normal capacity of 13 octal digits through a special routine. The R_n are considered to be integers in the generating formula and an additional division by 8^{13} is required to normalize them to the unit interval. This particular sequence has a period of 2^{37}.

Figure 2 shows the coordinate system of a molecule leaving the surface of the capillary. The distance

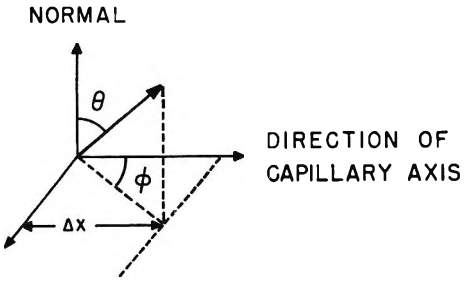

Figure 2. Coordinates of a molecule leaving the capillary wall.

traveled down the tube between successive wall collisions is

$$\Delta x = \frac{\sin\theta\cos\theta\cos\varphi}{1 - \sin^2\theta\cos^2\varphi}$$

It should be noted that in our program the angles θ and φ were always chosen successively in that order. Since the random number generator does not really produce random numbers, one of the severest tests to which it can be put is that successive values of R appear to be random for the purposes of the problem being solved. Statistical tests have shown that the power residue method scores well in general on this point. Nevertheless, the coupling between θ and φ could very well have produced a small bias in favor of one direction down the capillary. Therefore we introduced the following artifice to ensure that "random" values of Δx were symmetrically distributed about $\Delta x = 0$. The angle φ was limited to the range $[0, \pi/2]$ and a new random number was chosen to decide whether Δx was to be positive or negative. The temperature gradient along the capillary was taken to be constant.

The various random variables were related to the uniformly distributed random numbers, R, by integrating the corresponding distribution function. Let r be a random variable which follows a distribution function, $P(r)$, over the range $0 < r < a$. Then each value of r is obtained by the relation

$$R_n = \int_0^{r_n} P(t)\mathrm{d}t$$

where the R_n are adjusted to fall in a range determined by $0 < r < a$. The exit function was evaluated by starting a molecule at a chosen position at the wall with a diffuse bounce. The positions chosen tended to be clumped near either end, where the exit function is of greatest importance in determining the transmission probability. A brief outline of the generation of a molecular history is given here. The adjusted intervals of the random numbers are given in brackets; the natural interval of the random numbers as generated by the power residue formula is always [0, 1].

Let x be the starting position. Choose four random numbers: $R_1 = [0, 1] = \sin\theta$, $R_2 = [0, \pi/2] = \varphi$, $R_3 = [0, 1]$, and $R_4 = [0, 1] = e^{-\epsilon/T}$, where $T = 300 - (200/L)x$. Calculate $|\Delta x|$ by eq 4; if $R_3 < 1/2$, then $\Delta x = -|\Delta x|$, otherwise $\Delta x = |\Delta x|$. Calculate ϵ from R_4 and choose $R_5, R_6, \ldots R_n = [0, 1]$ until $R_n < e^{-\epsilon/\epsilon_0}$. The new starting position or next diffuse reflection is $x + (n - 4)\Delta x$. The calculation ends when a diffuse reflection occurs at a position greater then L or less than zero.

Results

The results of the Monte Carlo runs are summarized in Table I. Values of $f(x, L)$ are given by the ratio of the number of molecules exiting to the number of trials or histories generated. Transmission probabilities were calculated for both directions, the integral in eq 3 being evaluated graphically. For the reverse direction, cold to hot, the definitions of exit and entrance were interchanged. Transmission probabilities were also calculated for the case of no temperature gradient using the variational solution of DeMarcus[10]

$$Q = 8\left(\frac{ABL - AC - B^2}{4AL^2 - C}\right)$$

$$A = 1 + S_1(L)$$

$$B = \int_0^L S_1(x)\mathrm{d}x$$

Table I: Monte Carlo Results for the Exit Function; Entrance at 300°K, Exit at 100°K

	Starting position	No. exiting		Starting position	No. exiting
$L/d = 1$	0	126	$L/d = 10$	0	49
$\epsilon_0 = 900$	0.2	168	$\epsilon_0 = 2100$	1	147
500 trials	0.4	214	1000 trials	5	512
per position	0.6	290		9	859
	0.8	354		10	963
	1.0	385			
$L/d = 10$	0	65	$L/d = 50$	0	12
$\epsilon_0 = 900$	1	177	$\epsilon_0 = 900$	0.4	27
1000 trials	5	547	1000 trials	1	47
	9	866		4	96
	10	953		10	206
				25	468
				40	780
				46	892
				49	969
				50	991

$$C = \int_0^L xS_1(x)\mathrm{d}x$$

For our model the above integrals become

$$B = (1 - r_1)[(1 - r_1)I(x) + 4r_1(1 - r_1)I(x/2) + 9r_1r_2(1 - r_3)I(x/3) + \ldots]$$

$$I(x/n) = \int_0^{L/n} N_1(x)\mathrm{d}x$$

$$C = (1 - r_1)[(1 - r_1)J(x) + 8r_1(1 - r_2)J(x/2) + 27r_1r_2(1 - r_3)J(x/3) + \ldots]$$

$$J(x/n) = \int_0^{L/n} xN_1(x)\mathrm{d}x$$

For the special case of no specular reflection, *i.e.*, $\epsilon_0 \rightarrow \infty$, the calculations have been performed elsewhere;[12] Q is then independent of temperature.

Figure 3 shows the exit function for the three capillaries with the entrance ($x = 0$) at the hot end. The curve for $\epsilon_0 = 2100$ and $L/d = 10$ is omitted. For the case of no temperature gradient or of only diffuse reflection the exit function would obey the relations

$$f(L/2, L) = {}^1/_2$$

$$f(x, L) + f(L - x, L) = 1$$

As can be seen, perhaps better from the data in Table I than from the graph, the presence of a temperature gradient results in a detectable deviation from these relations. The effect is of minor importance however.

A summary of transmission probabilities is given in Table II. The variational solutions are listed as "exact," whereas in fact they are known only to be much more accurate than our Monte Carlo calculations. The standard deviation of the Monte Carlo values of $f(x, L)$ for N trials is given by

$$\sigma = \left(\frac{f(x, L)(1 - f(x, L))}{N}\right)^{1/2}$$

All of the uncertainty in the calculation of Q came from evaluating the integral in eq 3. The trapazoidal rule was used to weight the various data points in determining the standard deviation. For example, for $L = 10$, the standard deviation of Q was given by

$$\sigma = [(1/4)\sigma_0^2 + (25/4)\sigma_1^2 + 16\sigma_5^2 + (25/4)\sigma_9^2 + (1/4)\sigma_{10}^2]^{1/2}$$

where σ_0 is the standard deviation of $s_1(0)f(0, L)$, etc.

In examining the results two points stand out. First, as the degree of specular reflection increases, the values of the forward and reverse transmission probabilities diverge more and more and the deviation from the Knudsen limiting law increases as anticipated (Figure 4). Second, the existence of a temperature gradient along the tube has only a secondary influence on the transmission probability, the important variable being the reservoir temperature (Figure 5). Apparently the decisive event is the initial specular reflection of an entering molecule which places its first diffuse reflection farther down the tube, where the exit function has a larger value. Mathematically stated, the functions $s_1(x)$ and $S_1(x)$, which are dependent on the reservoir temperature, essentially determine the temperature

Table II: Transmission Probabilities for Free Molecular Flow

Capillary length to diam ratio, L/d	Entrance temp, °K	Exit temp, °K	Specular parameter, ϵ_0	Transmission probability, Q	Std deviation, σ
1	...	...	∞	0.514	Exact
1	300	300	900	0.695	Exact
1	300	100	900	0.719	0.007
1	100	100	900	0.558	Exact
1	100	300	900	0.539	0.008
10	...	...	∞	0.109	Exact
10	300	300	2100	0.142	Exact
10	300	100	2100	0.140	0.010
10	100	100	2100	0.118	Exact
10	100	300	2100	0.113	0.009
10	300	300	900	0.232	Exact
10	300	100	900	0.245	0.011
10	100	100	900	0.133	Exact
10	100	300	900	0.123	0.009
50	...	...	∞	0.0253	Exact
50	300	300	900	0.0691	Exact
50	300	100	900	0.0653	0.0044
50	100	100	900	0.0322	Exact
50	100	300	900	0.0300	0.0040

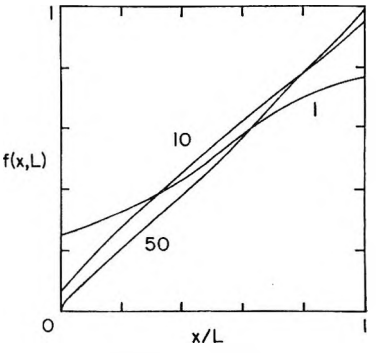

Figure 3. The exit function for various capillary length to diameter ratios with the critical energy of specular reflection equal to 900.

(12) L. M. Lund and A. S. Berman, *J. Appl. Phys.*, **37**, 2489 (1966).

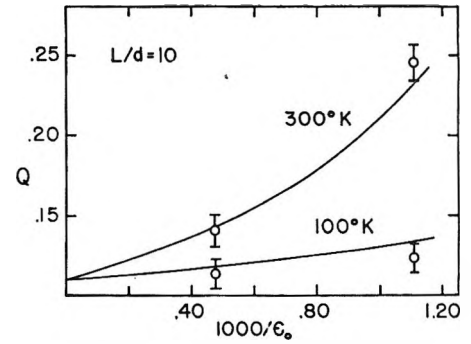

Figure 4. Capillary transmission probabilities for the entrance at 300°K (upper curve) and 100°K (lower curve) as a function of the critical energy of specular reflection. Solid curves are for no temperature gradient. Circles are Monte Carlo values for a capillary with a uniform temperature gradient between 300 and 100°K.

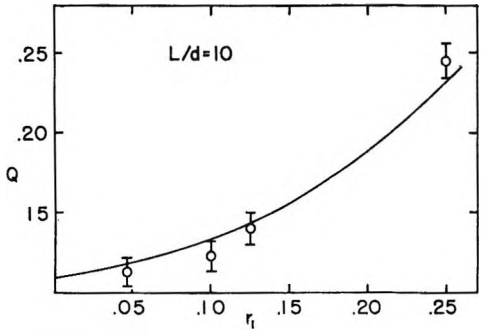

Figure 5. Unified plot of capillary transmission probabilities as a function of the degree of specular reflection at the entrance temperature. Solid curve is for no temperature gradient. Circles are Monte Carlo values.

dependence of Q, whereby $Q_{12} < Q_{21}$, and the exit function plays only a minor role in this respect. Within the limits of our model this leads to the important conclusion that free molecular flow experiments performed under differing, uniform temperature conditions should reveal the same order effects observed by Hobson and co-workers in connection with the limiting law.

Before discussing capillary flow data, however, it is necessary to deal with the problem of back scattering. Transmission probabilities may be decreased by artifically roughening the capillary wall.[13] Due to a sort of "roof top" effect,[14] molecules impinging at low angles are preferentially scattered backward. The effect appears to be important on normal surfaces as well. We have assumed that back scattering causes a small and equal diminishing of the transmission probabilities in either direction. The effect of temperature on Q is to be attributed as before to the temperature sensitive degree of specular reflection. Our calculated values of Q are too large by whatever amount must be subtracted for back scattering, but the ratios of the forward and backward values of Q should be independent of the effect in the first order.

Lund and Berman[15,16] have made precise measurements of the gaseous flow in metal and ionic crystal capillaries at low pressures. Although their data cover a temperature range of only 0 to 50°, transmission probabilities could be correlated in terms of the Lennard-Jones gas interaction parameter over a much wider range of effective or reduced temperature. Taking arbitrary pairs of reduced temperatures which correspond to $T_2 = 300°K$ and $T_1 = 100°K$, we find that the ratio of transmission probabilities is always close to unity

$$Q_{21}/Q_{12} \cong Q_{22}/Q_{11} = 1.02 \text{ to } 1.03$$

The correlation included the light gases hydrogen and neon, but the behavior of helium was anomalous and no conclusion can be drawn about this gas. Eschbach, Jaeckel, and Müller[17] have measured transmission probabilities of helium through a glass capillary over a very wide temperature range, −200 to +600°. Within the ±5% uncertainty of their results they observed no temperature dependence of Q.

The evidence from flow experiments, then, is that the ratio Q_{21}/Q_{12} should be within a few per cent of unity between room temperature and liquid nitrogen temperature and that the Knudsen limiting law should be obeyed within the same limits. Nevertheless the extensive TPD measurements of Hobson and co-workers[4,5] have clearly established larger deviations from the Knudsen limiting law (Table III). Also the deviations decrease with increasing capillary length, whereas our calculations show the opposite trend. It would be interesting to know if these apparent contradictions lie in the assumptions of our model, including possible entrance effects caused by a non-Maxwellian distribution in the reservoirs. The answer might well come from further molecular beam work, but such studies are difficult to carry out, particularly at angles involving back scattering. We suggest that simple flow experiments would be quite informative.

For example, it would be very helpful to have precise data on free molecular flow through glass capillaries (1) under isothermal conditions, but over a wide temperature range, and (2) under positive and negative

(13) D. H. Davis, L. L. Levenson, and N. Milleron, *J. Appl. Phys.*, **35**, 529 (1964).

(14) W. C. DeMarcus, U. S. AEC Report K-1435, 1959.

(15) A. S. Berman and L. M. Lund, *Proc. Intern. Conf. Peaceful Uses At. Energy, 2nd, Geneva, Sept 1958*, **4**, 359 (1959).

(16) L. M. Lund and A. S. Berman, *J. Appl. Phys.*, **37**, 2496 (1966).

(17) H. L. Eschbach, R. Jaeckel, and D. Müller, *Trans. Natl. Vacuum Symp.*, **8**, 1110 (1961).

Table III: Neon Transmission Probability Ratios for Pyrex Tubing[a]

L/d[b]	Q_{21}/Q_{12}
5.8	1.23
8.0	1.23
11	1.15
24	1.14
210	1.05

[a] Based on thermal transpiration data from ref 4 and 5; T_2 = 295°K, T_1 = 77.4°K. [b] The distance over which the temperature gradient takes place is much smaller.

temperature gradients. Deviation from the Knudsen limiting law should be established by TPD measurements on the same capillaries. The effect of grinding or etching the capillary wall might throw further light on the role of back scattering and also might prove to be a practical method of attaining Knudsen limiting law behavior. One attractive feature of flow measurements is that only relative pressures are needed since the logarithmic decay of pressure is determined. The manometer may be operated at the reservoir temperature without the need for calibration, provided the response is known to be linear. In the measurement of TPD, on the other hand, there are two reservoirs at two different temperatures, which presents a basically different problem in pressure measurement.

Acknowledgment. This research was supported in part by National Aeronautics and Space Administration Grant NsG-657.

The Effect of Impurities on the Activity of Oxygen Chemisorbed on Silver[1]

by Y. L. Sandler, S. Z. Beer, and D. D. Durigon

Westinghouse Research Laboratories, Pittsburgh, Pennsylvania 15235 *(Received June 17, 1966)*

A previous study of the isotopic exchange reaction $O^{16}_2 + O^{18}_2 \rightarrow 2O^{16}O^{18}$ and the desorption of oxygen from pure silver showed that evacuation and oxygen pretreatment at high temperatures of a well-cleaned silver powder reversibly increases and reduces the desorption rate of oxygen below 200° without a change in activation energy (32.5 kcal/mole). This is due to reversible changes in the topography of the surface. It is now shown that pretreatment of silver with hydrogen reduces the activation energy of oxygen desorption. The presence of residual hydrogen appears to be the reason for many discrepancies found in the literature. Isotopic dilution experiments reveal that residual hydrogen is firmly held at centers containing strongly bound oxygen. A silver powder containing MgO or alloyed with gold, even when pretreated with hydrogen, gives the same activation energy of desorption as hydrogen-free pure silver. Exchange experiments on Ag–MgO also show that no firmly bound oxygen or hydrogen exists in or on these materials. The activity changes produced by the additives, as are those produced by high-temperature oxygen pretreatment, are due to changes in the topography of the silver surface and not to changes in the work function or to lattice expansion as previously suggested in the literature.

Introduction

In a previous communication[2] (paper I) it was shown that at temperatures above 160° at least two modes of chemisorption of oxygen exist on pure silver. Pretreatment with oxygen at 500° changes the relative amounts of the two types of chemisorption. The rate of desorption is thus changed but not the activation energy. It was concluded that the observed phenomena must be caused by a change in surface topography. The experiments described in paper I were carried out on silver particles of high analytical purity which had been carefully freed of carbonaceous impurities and of trapped hydrogen. It became apparent in the course of this work that hydrogen is very hard to remove even at temperatures as high as 500° and that it has a profound influence on the properties of the adsorbed oxygen.

This paper discusses the effect of the residual hydrogen on the oxygen adsorption. The desorption of oxygen and the homonuclear exchange reaction $O^{16}_2 + O^{18}_2 \rightarrow 2O^{16}O^{18}$ were studied. As shown in paper I, the rate of the two reactions is the same, but additional information can be obtained by studying the isotopic exchange.

Also investigated were the effects of other types of impurities: gold (alloyed) and magnesium oxide. These impurities are frequently used to modify the catalytic properties of silver catalysts.[3,4] A study of the effect of MgO was also of interest in view of its effect on the properties of silver as an oxygen electrode.[5,6] As in paper I, all experiments were carried out under conditions at which silver oxide is not formed as a separate phase.

Experimental Section

The reaction system was the same as previously described.[2,7] It consisted of 2–4 g of metal powder in a quartz vessel of 18–30-cc volume which could be isolated from the gas-handling systems, diffusion pumps, and liquid nitrogen traps by means of a metal valve.

(1) Work sponsored in part by the U. S. Army Electronics Command and the Office of Naval Research.

(2) Y. L. Sandler and D. D. Durigon, *J. Phys. Chem.*, **69**, 4201 (1965).

(3) *Cf.* L. Ya. Margolis, *Advan. Catalysis*, **14**, 479 (1963).

(4) K. E. Hayes, *Can. J. Chem.*, **37**, 583 (1959).

(5) S. Z. Beer and Y. L. Sandler, *J. Electrochem. Soc.*, **112**, 1153 (1965).

(6) Y. L. Sandler and E. A. Pantier, Extended Abstract, Theoretical Division, Cleveland Meeting of The Electrochemical Society, May 1966, p 57.

(7) Y. L. Sandler and D. D. Durigon, *Trans. Faraday Soc.*, **62**, 215 (1966).

Two thermistor gauges attached to either side of the metal valve served to measure gas pressures. Surface areas were determined by the BET method with krypton. For pure silver these varied from 600 cm^2/g after initial oxygen pretreatment to 230 cm^2/g after continued hydrogen and oxygen pretreatment. A small mass spectrometer was coupled to the system to monitor gaseous impurities desorbing from the metals and to analyze the oxygen isotopes. Only the isotopic dilution experiments with silver at 500° were carried out on a larger system. This system, which consisted of 20 g of silver in a vessel of 135 cc, was degassed on the vacuum system and transferred to an analytical mass spectrometer of higher accuracy.

The silver powder was supplied by Handy and Harman, gold by American Smelting and Refining Co. Though both were of 99.999% guaranteed purity, the carbon content[7] was considerably higher than the given impurity limit.

Silver–gold alloys were produced by repeated levitation melting of compressed powder mixtures. They were then formed by swaging to provide wires approximately 1 mm in diameter. To assure homogeneity of the wires and to lower the carbon content, the wires were kept for 2 days at 750° in a flow of purified oxygen. The alloy powders were then prepared by spark erosion under triple-distilled water. Figure 1 shows the automatic spark erosion milling machine (Servomet, Metals Research Ltd., Cambridge) adapted for the purpose. The alloy wire to be sparked, extended by a gold wire welded to it, is connected to the anode of the Servomet output and is fed down the vertical capillary of the vessel by means of the servo-controlled arm. The feed of the vertical wire toward the cathode is controlled by the machine in such a way that a fixed voltage of 140–180 v is maintained across the gap. One gram of powder was produced in about 2 hr. To oxidize any carbonaceous impurity present, pure oxygen was bubbled through the water. The colloidal particles coagulated rapidly, and the water could be decanted.

A silver–1.7 mole % magnesium powder was produced by precipitating a mixture of the carbonates from an aqueous solution of the nitrates with ammonium carbonate, followed by thermal decomposition *in vacuo*.

All powders were degassed at a temperature that was gradually raised to 520° with frequent contact with low-pressure oxygen until the desorbed impurities were reduced to a negligible level.

Desorption rates were determined after first allowing oxygen at a certain pressure to equilibrate with the powder. The gas phase was then rapidly removed by pumping, the valve was closed, and the pressure rise was recorded. The technique is accurate and simple;

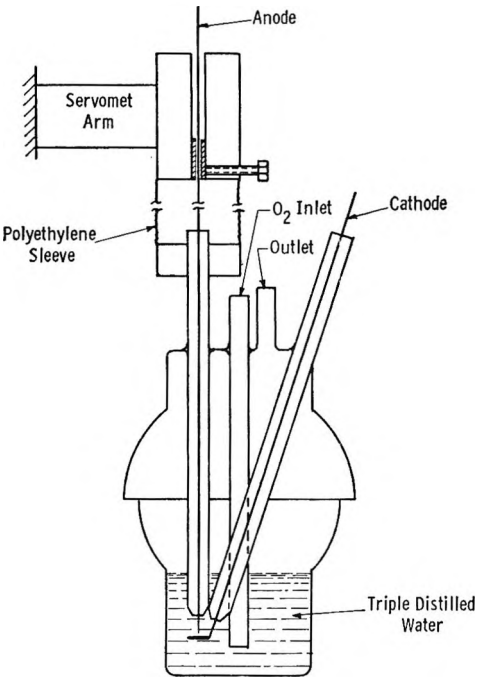

Figure 1. Setup for producing powders from wires by sparking.

however, if the measured rate is to be equal to the desorption rate at equilibrium with the oxygen (before its removal), it must first be shown that no weakly chemisorbed gas is removed during the pumping period. This was done in paper I.

Results

The Effect of Residual Hydrogen in Silver on the Desorption Rate of Oxygen. The previous experiments[2] showed that the activation energy of the homonuclear oxygen-exchange reaction is high, about 32 kcal/mole of O_2, if the silver contains no hydrogen. The rate-determining step in the exchange reaction is the desorption of oxygen. The desorption rate was then measured directly by the rate of pressure increase in the reaction vessel after rapid removal of the gas phase.

In Figure 2, the two broken lines represent the previously measured[2] desorption rates, in molecules/cm^2 sec, as a function of the inverse absolute temperature. The lower curve was obtained when the sample contained a high concentration of strongly bound oxygen and was obtained by cooling the sample in 5 torr of oxygen from 500°. The upper curve was obtained after cooling from 500° *in vacuo* before contact of oxygen at a lower temperature. As shown by the sequence of the measurements, the change in the state of the surface is completely reversible. The independence of the activation energy of desorption of the relative amount of

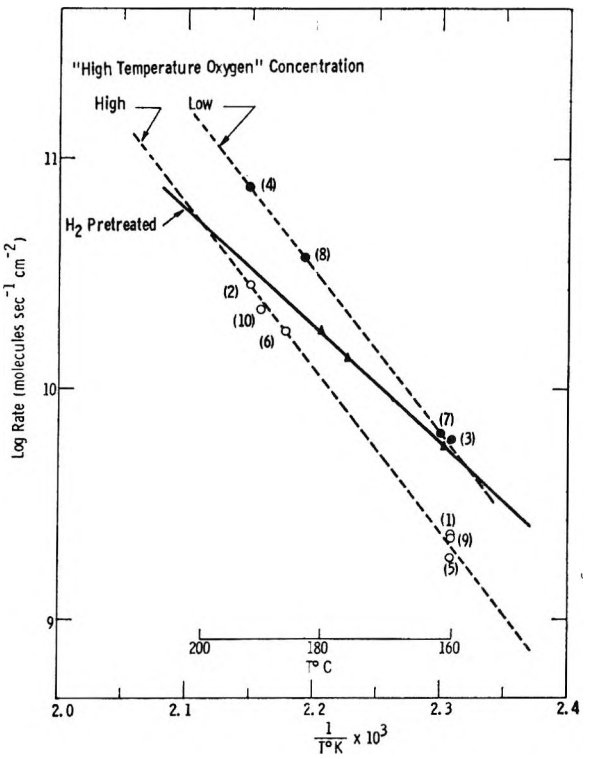

Figure 2. Effect of gas pretreatment at 500° on the oxygen desorption between 160 and 190°: oxygen pretreatment, broken lines; hydrogen pretreatment, solid line.

the two modes of adsorption was interpreted as showing that the surface sites for the weaker chemisorption are unchanged. The oxygen pretreatment causes a change in the distribution of crystallographic planes (faceting).

At the end of the experiment just described, it was ascertained that the silver had contained no appreciable amount of hydrogen. A small dose of deuterium was equilibrated with the powder at 500°. The small amount of HD evolved showed that the total amount of light hydrogen in the silver was less than the equivalent of 10^{-3} monolayer.

The effect of sorbed hydrogen on the desorption rate of oxygen was then tested. The silver was brought into contact with 20 torr of hydrogen for about 0.5 hr at 500° and was then pumped overnight at the same temperature. Oxygen was then adsorbed at 160° and pumped, in the same manner as described[2] for the oxygen pretreated samples. Figure 2 shows that the activation energy of desorption of the oxygen was now lower, being 24 kcal/mole between 160 and 180°. A similar result will be described below. As will be shown, residual hydrogen is firmly bound to silver (in the presence of residual oxygen) and it modifies the adsorption properties of the surface for oxygen.

Residual Oxygen and Hydrogen in Pure Silver. Oxygen cannot be completely removed from silver by prolonged pumping at 500° (paper I). In part, the residual oxygen resides at the surface and rapidly exchanges with chemisorbing oxygen at temperatures as low as 160° (the lowest temperature at which desorption was fast enough to make measurement of the isotopic exchange possible). The current experiments show that contact of hydrogen produces changes in the surface which affect the reversibility of the oxygen adsorption.

In the following, isotopic dilution experiments are summarized. These were carried out at 500°, a temperature high enough to make the diffusion of both hydrogen and oxygen through a silver particle fast so that the oxygen in the gas phase rapidly equilibrates with the oxygen in the silver. The amounts of residual oxygen and hydrogen in the silver were determined after different hydrogen and oxygen pretreatments. It will be seen that hydrogen is as strongly retained as is oxygen.

In the oxygen dilution experiments a mixture of argon and O^{18} (containing 6% O^{16}) was admitted to a pure silver sample after certain pretreatments with oxygen (O^{16}) and hydrogen and pumping at 500°. The amounts of the different isotopes (in cc atm) in the gas phase at any given time were determined by measuring the composition of small samples and the total amount of argon present; the latter was measured by expansion into a large standard volume and by a pressure reading on a capacitance micromanometer.

For analyzing the hydrogen content of the samples a known pressure (usually 2 torr) of 98.4% deuterium was admitted at 500°. No inert gas was used in this case and the results are somewhat less accurate. The amount admitted was calculated (1) from the approximate pressure of the admitted gas and the volume of the reaction vessel and (2) by expansion of the gas at the end of an experiment into the standard volume and reading the pressure. In all cases, the two methods agreed to better than 30%.

Table I summarizes some of the experiments. The pretreatment before starting the dilution experiment is stated in each case, then the type and amount of gas added, the time of equilibration of the gas with the metal before measurement, the isotopic ratio found, and the total residual gas, for 20 g of silver. In the first example, the sample was first contacted several times with O^{16} and pumped, to remove O^{18} from previous experiments and to remove carbonaceous impurities. After repeated contact with hydrogen and pumping, the oxygen exchange with O^{18} was carried out. From the samples taken between 5 and 160 min it may be seen that, as expected, equilibrium is rapidly attained. The residual O^{16} found in the sample

Table I: Isotopic Dilution Experiments with Pure Silver at 500°

Ag sample 9 run no.	Pretreatment at 500°	Gas added at $t = 0$, cc	Time t, min	$(O^{16}/O^{18})_{eq}$ or $(H/D)_{eq}$	Residual gas (20 g of Ag), cc
1	Repeated contact with $O^{16}{}_2$ and pumping; pumped 1 hr. Contacted two times with 5 torr of H_2 for 15 min; pumped 5 hr at 500°	O^{18}, 0.106	5 20 160	2.2 2.4 2.5	$O^{16}{}_2$, 0.27 (=17 ppm (wt))
	Pumped 2 hr	D, 0.13	30	0.93	H_2, 0.12
2	Admitted 10 torr of $O^{16}{}_2$ and pumped; four times in 3 hr. Then admitted 30 torr of H_2 and pumped; seven times in 5 hr; pumped 17 hr	D, 0.32	30 60	2.45 3.26	H_2, 0.10
	Pumped 2 hr	O^{18}, 0.041	30		$O^{16}{}_2$, 0.21
3	Admitted 30 torr of H_2 and pumped; seven times in 26 hr (in H_2 overnight). Then pumped 45 min	O^{18}, 0.038	30		$O^{16}{}_2$, 0.062

amounted to 0.27 cc atm. This corresponds to 17 ppm (weight) of the bulk (or about 1.5 monolayers; the surface area was 230 cm^2/g). The isotopic hydrogen dilution experiment carried out immediately after pumping the sample for 2 hr showed that the residual hydrogen concentration was of the same order as the residual oxygen concentration, about half its amount.

In the next experiment, run no. 2, the procedure was reversed; the hydrogen was exchanged first and then the oxygen. A more thorough hydrogen pretreatment was given here, as indicated in the column headed "Pretreatment at 500°." Nevertheless, the result was almost the same: the residual oxygen concentration was only slightly lower than in the first run and the amount of hydrogen was again about half of the oxygen concentration.

Other dilution experiments with hydrogen, not carried out in conjunction with oxygen dilution, also showed that at least the order of magnitude of the retained hydrogen is the same as found for oxygen. This leaves little doubt that the strong retention of the hydrogen in the silver is caused by the presence of firmly bound oxygen in the solid. The result is analogous to a previous conclusion[7] that firmly bound hydrogen, formed on the silver surface at high temperatures, is caused by strongly chemisorbed oxygen. In run no. 3, the silver was pretreated with hydrogen for 26 hr; this included contact with hydrogen overnight. A liquid nitrogen trap was used to keep the H_2O pressure low. In this way the residual oxygen concentration could be reduced to 0.003 cc/g of Ag, or 4 ppm, corresponding in the present case to one-third of a monolayer. The best way to remove residual hydrogen appears to be continued contact with more hydrogen. It removes the residual oxygen which causes retention of the hydrogen.

Example 2, as well as other exchange experiments at 500° with hydrogen, showed a slow increase with time of the amount of exchanged hydrogen after the initial fast exchange. The silica walls of the reaction vessel may have been responsible for the slow exchange. Another vessel without silver powder, treated in similar fashion with oxygen and hydrogen, showed no noticeable exchange after 16 hr. However, it is possible that water formed during the initial phase of hydrogen pretreatment of the silver may have produced exchangeable OH in the silica walls.

The Homonuclear Oxygen Exchange on Silver with and without Additives. The rate of the reaction $O^{16}{}_2 + O^{18}{}_2 \rightarrow 2O^{16}O^{18}$ was measured with pure silver, silver–gold alloys, and a silver–magnesium oxide (coprecipitated). The powders received a degassing pretreatment at temperatures up to 520° for several days with frequent oxygen and hydrogen contact at decreasing pressures. All samples were pumped at 450–500° overnight, immediately before measurements were made.

The results are presented in Figure 3 where the logarithm of the rate of exchange (in molecules cm^{-1} sec^{-1}) is plotted against the inverse absolute temperature. The curve marked "Ag(O)" was oxygen-pretreated only and was taken with the same sample as used for the desorption experiments before contact

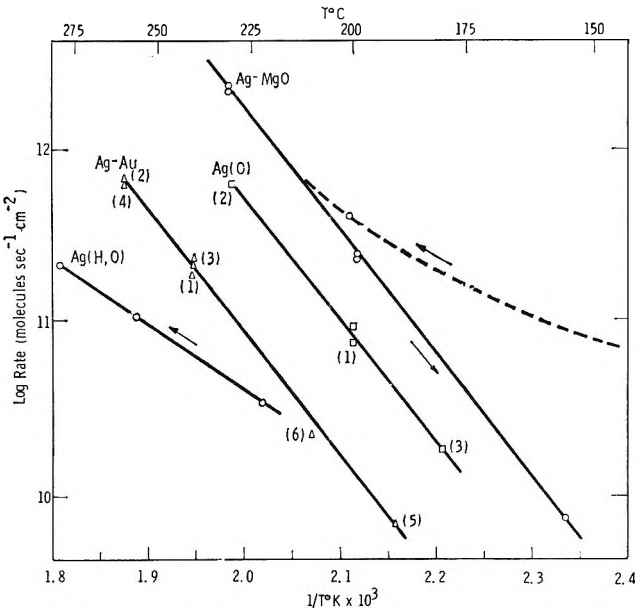

Figure 3. Isotopic oxygen exchange rate for oxygen-pretreated silver, Ag(O), for hydrogen- and oxygen-pretreated pure silver, Ag(H,O), alloy Ag–Au, and Ag–MgO.

with hydrogen. Rates and activation energy are the same as obtained in the desorption experiment (Figure 1, upper solid line).

All the other samples used in the experiments of Figure 3 were pretreated with both hydrogen and oxygen. "Ag(H,O)" was a 1.8-g sample produced by spark erosion for comparison with the similarly prepared silver–gold alloy. It was cleaned with oxygen up to 420° and treated with 10 doses of hydrogen for 2 hr at 500°. On pumping, a slow desorption of hydrogen was first observed, then mainly of water vapor. After 3 hr, no measurable desorption was obtained at 400°. After this, the parahydrogen conversion at −195° was measured[7] and the sample was found to have a strongly paramagnetic surface. After pumping off the parahydrogen at low temperatures, the sample was pumped for 16 hr at room temperature. The homonuclear oxygen exchange was then measured as a function of temperature. The activation energy was roughly 17 kcal/mole. Since the rate at a given temperature strongly decreased with time, the sample was further treated with oxygen. After alternate oxygen contact and pumping for 24 hr at 500°, the run was made. The result of this run is presented in Figure 3, marked "Ag(H,O)," and in Table II. The activation energy was still 17 kcal/mole, as compared to 32.5 kcal/mole obtained with the samples which were pretreated with oxygen only.

The behavior of silver containing impurity additions was different. A silver–75 at. % gold alloy was pretreated with hydrogen and oxygen, similar to the silver sample "Ag(H,O)." However, it gave the same slope as the silver sample "Ag(O)" containing no hydrogen. The surface area was 1200 cm²/g. The points were taken in random sequence, as indicated by the numbers in Figure 3. When it is considered that only one-fourth of all atoms are silver, the absolute rate appears to be the same as for oxygen-treated pure silver (Ag(O)). However, this conclusion is not reliable. The thermal pretreatment may have decreased somewhat the silver content of the surface.

Table II: Reaction of 3 Torr of $O^{16}_2 + O^{18}_2$ on Ag, Pretreated with O^{16}_2 after H_2

Sample	Time, min	Temp, °C	Mole % of O^{16}_2	Mole % of $O^{16}O^{18}$	Mole % of O^{18}_2	O^{16}/O^{18}
New O_2 mixture	0	24	48.2	6.2	45.6	1.05
1	1065		47.1	8.5	44.4	1.05
2	0	222	46.9	9.9	43.2	1.08
3	345		47.7	11.5	40.8	1.15
4	0	256	48.5	14.6	36.9	1.26
5	53		51.2	21.6	27.2	1.63
New O_2 mixture	0	280	48.4	6.4	45.2	1.07
1	60		47.3	21.2	31.5	1.38
2	985		45.0	43.9	11.1	2.07

This was clearly seen in an experiment with a second silver–gold alloy that contained 80 at. % silver. It was heated in oxygen and hydrogen to a higher temperature, 520° (instead of about 480° for the first alloy), and was found to be inactive up to 500°. A gold film visibly covered the inside of the reaction vessel and must have covered the alloy surface. The rate per silver surface atom for the silver–gold alloy in Figure 3 may be higher than for pure silver.

The silver–magnesium oxide (7 mole %) sample was also pretreated with hydrogen and oxygen up to 500° and pumped for 24 hr. It had a surface area of 1200 cm²/g. Again there was no effect of the hydrogen pretreatment. The curve is shown in Figure 3 and marked "Ag–MgO." After pumping at 500°, a relatively high activity was found at low temperatures. The activity here is due to the presence of defect magnesium oxide. It is measurable down to −130° and is due to the existence of a very weak

chemisorption on this and other defect oxides.[8,9] The activity is suppressed by contact with oxygen at 300°. On lowering the temperature from 300 to 160°, the slope is the same as obtained with oxygen-treated pure silver or the silver–gold alloy. The higher specific activity is significant. It is connected with the fact that the silver contained no firmly bound oxygen, which would reduce the activity as seen in the desorption experiments (Figure 2).

The absence of firmly bound oxygen is proved by the experiment shown in Table III. The table shows data of an exchange experiment made with an O^{16}_2 + O^{18}_2 mixture at various temperatures on the same material after prior contact with O^{16}_2 at 500°. The ratio of O^{16}/O^{18} can be seen to be constant up to the highest temperature, 300°. With pure silver, all experiments of this type showed an increase in the ratio. This is due to exchange with residual, firmly bound oxygen in and on the surface of the silver which cannot be removed by pumping at 500° before the start of an experiment (compare Table II and paper I). The impure silver evidently contains no firmly bound oxygen and therefore no firmly bound hydrogen. (The latter, as shown earlier, requires the presence of firmly bound oxygen.)

Table III: Reaction of 11 Torr of O^{16}_2 + O^{18}_2 on Ag–MgO, Pretreated with O^{16}_2 after H_2

Sample	Time, min	Temp, °C	Mole % of O^{16}_2	Mole % of $O^{16}O^{18}$	Mole % of O^{18}_2	O^{16}/O^{18}
New O_2 mixture	0	24	46.1	5.6	48.3	0.95
1	1061	24	42.4	13.8	43.8	0.97
2	0	100	41.4	15.5	43.1	0.97
3	4320	100	32.4	32.0	35.6	0.94
4	0	200	32.0	33.2	34.8	0.95
5	90	200	29.3	41.9	28.8	1.01
New O_2 mixture	0	300	45.1	6.6	48.3	0.94
1	16	300	24.9	49.0	26.1	0.97

Conclusions

Hydrogen is very strongly retained in pure silver, just as is oxygen. No such strong retention of hydrogen would be expected in a pure s metal. Actually, the true (endothermal) equilibrium solubility[10] of hydrogen in silver at 500° and 10 torr is about 100 times lower than the residual amounts of hydrogen found in our experiments (Table I). The fact that the amount of residual hydrogen is of the same order as the residual oxygen shows that the very strong binding of the hydrogen is caused by the presence of the oxygen.

The presence of hydrogen at the surface changes the binding energy of the more weakly chemisorbed oxygen, as seen from the change in the activation energy of desorption. The good reproducibility of the present results with hydrogen-free silver stands in sharp contrast to the often-noticed[11] lack of reproducibility of previous data. The latter were usually taken with catalysts that were pretreated with hydrogen and evacuated at relatively low temperatures. Presumably, the low value found by Margolis[12] and co-workers for the activation energy of the homonuclear oxygen exchange (~12 kcal/mole) is due to the presence of hydrogen in the silver.

The current results, in which the total residual oxygen and hydrogen were determined in the same experiment, are too few to say whether the value 2 found for the oxygen to hydrogen ratio is significant. The corresponding complex at the surface was found[7] to be paramagnetic and might consist of two chemisorbed oxygen atoms with a proton trapped between them.

It was found that alloy formation with gold and incorporation of MgO does not change the activation energy for the oxygen desorption (or the exchange reaction, the rate of which is the same). There is no apparent effect of a possible change in work function[3] or change in the dimensions of the lattice by the presence of the additive. No strong oxygen chemisorption was found and, consequently, no residual hydrogen. The added impurities eliminate the sites for the stronger chemisorption and stabilize those planes which cause the weaker O_2 adsorption; there is no direct effect on the binding energy of the oxygen.

The presence of hydrogen may also cause topographic changes,[13] but here the bond strength of the oxygen is also affected as seen from the change in the activation energy of desorption.

It is difficult at the present stage to state definite correlations of the effects of oxygen pretreatments or

(8) G. K. Boreskov, *Advan. Catalysis*, **15**, 327 (1964).

(9) Y. L. Sandler and D. D. Durigon, to be published.

(10) E. H. Steacie and F. M. G. Johnson, *Proc. Roy. Soc.* (London), **A117**, 662 (1928).

(11) M. I. Temkin and N. V. Kulkova, *Dokl. Akad. Nauk SSSR*, **105**, 1021 (1955).

(12) L. Ya. Margolis, *Izv. Akad. Nauk SSSR, Otd. Khim. Nauk*, 225 (1959).

(13) B. E. Sunquist, *Acta Met.*, **12**, 67 (1964).

impurity additions with topographic changes described in the literature. With face-centered-cubic structures the {111} and {100} facets are stabilized by treatment with oxygen, and the rounded edges between the facets become sharper as the oxygen pressure increases.[13,14] The changes in shape with pressures are reversible, as are the observed desorption characteristics with oxygen pretreatment. Similarly, the presence of impurities is known[13] to affect the morphology of the surface.

A marked effect of thermal pretreatment and impurity content on the oxygen reduction at a silver electrode in an alkaline electrolyte was recently found[6] which is due to similar causes. Work on a more definite identification of the exposed crystal planes is now in progress.

Acknowledgment. The authors are indebted to W. M. Hickam and his group for carrying out the isotopic dilution experiments.

(14) R. Y. Meelheim, *et al.*, *Actes Congr. Intern. Catalyse, 2e, Paris, 1960*, 2, 2005 (1961).

Solvent Effects on ^{13}C–H Coupling Parameters and Chemical Shifts of Some Halomethanes

by V. S. Watts and J. H. Goldstein

Department of Chemistry, Emory University, Atlanta, Georgia 30322 *(Received June 17, 1966)*

Medium effects on the chemical shift and ^{13}C–H coupling of bromoform have been determined in a series of 30 solvents representing a variety of functional groups. Similar observations have been carried out for 13 substituted methanes as the neat liquids and as solutions in cyclohexane, carbon tetrachloride, and dimethylformamide. The observed behavior can in general be correlated with the structure of the solvents and solutes studied. The results are adequately explained in terms of specific molecular interactions, in particular, hydrogen bonding. The advantages of using ^{13}C–H couplings as a criterion for molecular interactions are pointed out.

Introduction

The effect of solvent media on nmr coupling parameters has been the subject of considerable recent interest. Variability with solvent and/or concentration has been established for the cases of geminal H—H,[1-5] directly bonded ^{13}C—H[6,7] geminal P—H (PCH),[8] and vicinal H—F couplings through C—C and C=C bonds.[9] At the present time it is not entirely clear whether these changes are primarily produced by specific interactions[6] or whether they arise from more general effects such as the reaction fields induced by solutes in the dielectric solvent medium.[10,11]

In an effort to clarify this problem further we have carried out solvent-effect studies of two types: (1) the effect of an extended series of both saturated and

(1) V. S. Watts, G. S. Reddy, and J. H. Goldstein, *J. Mol. Spectry.*, 11, 325 (1963).

(2) B. L. Shapiro, R. M. Kopchik, and S. J. Ebersole, *ibid.*, 11, 326 (1963).

(3) B. L. Shapiro, R. M. Kopchik, and S. J. Ebersole, *J. Chem. Phys.*, 39, 3154 (1963).

(4) P. Bates, S. Cawley, and S. S. Danyluk, *ibid.*, 40, 2415 (1964).

(5) V. S. Watts and J. H. Goldstein, *ibid.*, 42, 228 (1965).

(6) D. F. Evans, *J. Chem. Soc.*, 5575 (1963).

unsaturated organic solvents on the ^{13}C–H coupling of a single solute, $CHBr_3$, and (2) the effect of certain selected saturated organic solvents on the ^{13}C–H coupling in a number of halogen- and cyano-substituted methanes. A study similar to (1) above was carried out by Evans on $CHCl_3$ but with a less extensive series of solvents.[6]

In the first phase of the investigation correlations were sought between observed changes in J(CH) and various properties of the solvent such as the dielectric constant, dipole moment, structural features, etc. For the 30 solvents employed there is no indication of a significant correlation with the dielectric constant or dipole moment, but the magnitudes of the effects observed do tend to group together according to the solvent type (alcohol, amine, etc.). These results suggest specific interactions as the predominant or, perhaps, sole factor involved.

The second phase of this work was designed to reveal the influence of the substituents on the sensitivity of J(CH) to the medium. Previously, infrared studies have indicated that a single electronegative substituent does not render an α proton appreciably hydrogen bonding.[12] Our results, however, show that even a single iodine is sufficient to produce noticeable proton-donor activity.

Experimental Section

The solutes and solvents used were commercially available products. Where their nmr spectra indicated the presence of impurities these were removed by distillation using a spinning-band column. Each of the solutes was observed as the neat liquid and at 20–25 mole % in cyclohexane (CH), carbon tetrachloride (CCl_4), and dimethylformamide (DMF). Bromoform was also observed at 20–25 mole % in each of the solvents listed in Table I. Samples of the liquid solutes were prepared by weighing the solute and solvent into an nmr tube and adding a few drops of TMS to serve as the internal reference. Samples of the gaseous solutes were prepared by using a vacuum system to condense the solute into a weighed amount of solvent and TMS in an nmr tube and then reweighing.

All spectra were taken on a Varian Associates Model A-60 spectrometer and were calibrated by the usual side-band technique using an audio oscillator continuously monitored by a frequency counter. Normal proton frequencies were obtained as the average of three forward and three reverse sweeps. For the ^{13}C–H satellite spectra at least four forward and four reverse sweeps were used. The average deviation for each peak was approximately 0.04 cps.

In some cases both the upfield and downfield ^{13}C–H satellite patterns could not be observed owing to the solvent protons. In such cases the value of J was obtained from that half which could be observed plus or minus approximately 0.4 cps to correct for the asymmetry of the proton peak with respect to the two ^{13}C–H patterns.

Table I: Solvent Effects on Nmr Parameters of $CHBr_3$[a]

Solvent	Mole % $CHBr_3$	ω	J_{CH}
Cyclohexane	25.19	406.10	204.31
Carbon tetrachloride	23.28	409.72	204.60
Bromoform	...	410.55	205.40
Chloroform	21.70	410.64	205.25
Methyl alcohol	22.18	428.82	208.12
Ethyl alcohol	22.67	433.18	208.36
Isopropyl alcohol	22.39	433.18	208.39
t-Butyl alcohol	23.63	432.31	208.34
Diethyl ether	23.61	434.44	208.89
Diisopropyl ether	25.17	433.58	208.91
Isobutyraldehyde	23.15	419.52	206.83
n-Heptaldehyde	23.16	425.68	207.68
Acetyl chloride	24.43	416.55	206.79
Acetone	22.13	443.39	209.89
4-Heptanone	23.33	444.13	209.65
Cyclohexanone	23.57	442.99	209.98
n-Hexylamine	22.71	471.32	210.92
Cyclohexylamine	23.16	474.43	211.19
t-Butylamine	22.60	478.68	211.38
Diisopropylamine	23.40	464.78	210.00
Triethylamine	24.06	458.38	209.19
Tri-*n*-propylamine	22.76	432.52	207.33
Tributylamine	25.39	431.77	207.15
Dimethylformamide	22.12	458.97	211.60
Benzene	23.25	362.73	206.17
Thiophene	22.71	373.88	205.81
Bromobenzene	23.12	392.48	205.66
Chlorobenzene	22.48	386.66	205.38
Benzonitrile	22.55	419.00	208.04

[a] Parameters are given in cps; ω is referenced to internal TMS.

Results

The chemical shifts (ω) and ^{13}C–H coupling parameters (J) of $CHBr_3$ were determined in 24 aliphatic and 6 aromatic solvents and are listed in Table I. As shown in Figure 1 there is a fair correlation between the sol-

(7) V. S. Watts, J. Loemker, and J. H. Goldstein, *J. Mol. Spectry.*, **17**, 348 (1965).

(8) M. Gordon and C. E. Griffin, *J. Chem. Phys.*, **41**, 2570 (1964).

(9) S. Ng, J. Tang, and C. H. Sederholm, *ibid.*, **42**, 79 (1965).

(10) A. D. Buckingham, T. Schaefer, and W. G. Schneider, *ibid.*, **32**, 1227 (1960).

(11) A. D. Buckingham, *Can. J. Chem.*, **38**, 300 (1960).

(12) A. Allerhand and P. von R. Schleyer, *J. Am. Chem. Soc.*, **85**, 1715 (1963).

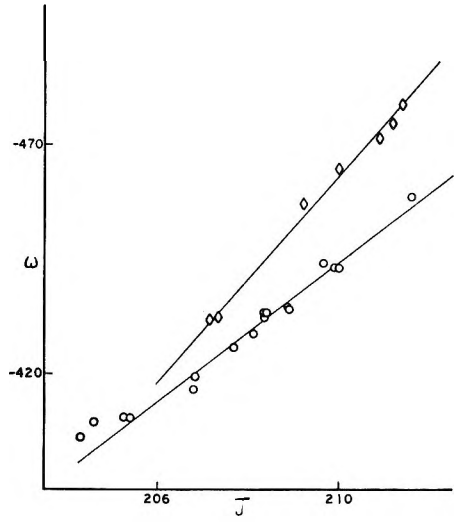

Figure 1. Plot of ω *vs.* $J(^{13}C\text{–}H)$ for bromoform in nonaromatic solvents.

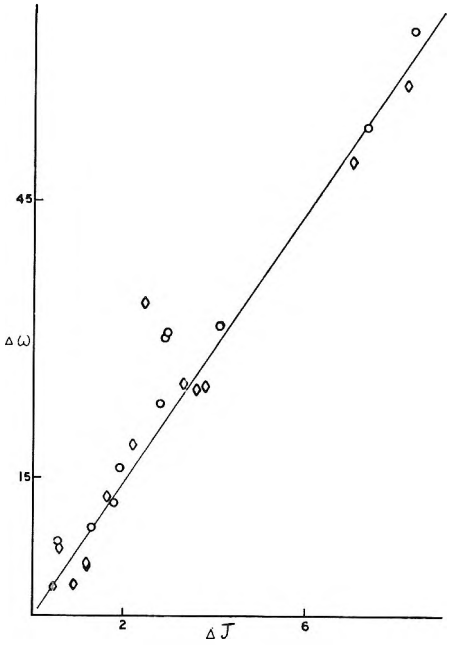

Figure 2. Plot of differential solvent effects on ω and J for the substituted methanes: circles, values of $\Delta\omega$ and ΔJ (see text); diamonds, values of $\omega_{DMF} - \omega_{CCl_4}$ and $J_{DMF} - J_{CCl_4}$.

vent effects on J and ω for the aliphatic solvents. It is possible to group the magnitudes of the solvent effect on J and ω according to the type of solvent molecule. However, because of the limited number of solvents of each type, such a classification must be regarded as tentative. When considered in terms of the functional groups in the aliphatic solvent molecules, the increases in $|J|$ and $|\omega|$, relative to the corresponding values in CH, occur in the following order. J: halogen $<$ CHO $=$ $NR_2 <$ OH $<$ OR $<$ C=O $=$ NHR $<$ NH_2; ω: halogen $<$ CHO $<$ OH $=$ $NR_2 <$ OR $<$ C=O $<$ NHR $<$ NH_2.

The aromatic solvents produced an upfield displacement in the chemical shifts and a slight increase in J with respect to the cyclohexane values. In these solvents there appears to be no correlation between the effects on J and ω.

In the second phase of this study eight halomethanes, acetonitrile, chloroacetonitrile, and methylchloroform were observed as neat liquids and as solutions with mole ratios of 1:4–1:5 in cyclohexane (CH), carbon tetrachloride (CCl_4), and dimethylformamide (DMF). The values of ω and J so obtained are listed in Table II, from which it can be seen that in each case $\omega_{DMF} < \omega_{CH}$ and $J_{DMF} > J_{CH}$. The observed changes in ω and J on going from CH to CCl_4 are relatively small. The considerably larger differences between the values in DMF and those in CH represent the effect experienced on replacing an inert medium, CH, by the highly polar, proton-acceptor solvent, DMF. Figure 2 shows that there is a reasonably good linear correlation between $\Delta\omega = |\omega_{DMF} - \omega_{CH}|$ and $\Delta J = J_{DMF} - J_{CH}$.

There is also a fair correlation between ΔJ and J (although this is not shown graphically here), the points tending to cluster somewhat according to the number of substituents present. The value of ΔJ increases with the degree of substitution, increasing roughly twofold for each substitution of hydrogen by a particular halogen.

Insofar as the values for the halomethanes in Table II permit generalization, there appears to be a relationship between the solvent effects on J and both the structural type of the solute and the nature of its substituent. In terms of ΔJ (the difference between J in DMF and CH) the solvent effect decreases in the order $CHX_3 > CH_2X_2$ or $CH_2XY > CH_3X$, and the effect of the substituents follows the order Cl $>$ Br $>$ I. The differences $J_{neat} - J_{CH}$ are rather small (0.8–1.6 cps) for all the halomethanes, but in addition are clearly largest for the group of dihalomethanes.

For acetonitrile the solvent effects on J are very small (as is also true in the case of methylchloroform). When Cl is replaced by CN in both CH_3Cl and CH_2Cl_2 the parallelism of the solvent effects on ω and J no longer holds. The result of this substitution is to increase the effect on ω but decrease it for J.

Discussion

The effect of the aliphatic solvents of Table I on the chemical shift and C–H coupling of bromoform (a proton donor) tends to increase with the proton-accept-

Table II: Solvent Effects on the Nmr Parameters of Some Halogenated Methanes[a]

Solute	Solvent	Mole % compd	ω	$J^{13}C-H$	Av dev[b]
$CHCl_3$	DMF	24.36	−492.32	216.46	0.04
		100.00	−434.17	208.91	0.03
	CCl_4	21.46	−434.77	208.26	0.07
	CH	22.53	−429.17	208.11	0.05
$CHBr_3$	DMF	22.12	−458.97	211.60	0.05
		100.00	−410.55	205.40	0.04
	CCl_4	23.28	−409.72	204.60	0.06
	CH	25.19	−406.10	204.31	0.04
CH_2Cl_2	DMF	22.35	−341.99	180.55	0.05
		100.00	−319.56	178.11	0.06
	CCl_4	21.48	−317.22	176.75	0.04
	CH	24.02	−310.74	176.48	0.05
CH_2BrCl	DMF	23.66	−333.96	181.33	0.02
		100.00	−312.78	178.96	0.04
	CCl_4	22.83	−309.60	177.70	0.07
	CH	24.04	−303.17	177.38	0.05
CH_2Br_2	DMF	21.17	−321.16	181.63	0.07
		100.00	−300.06	179.22	0.05
	CCl_4	22.92	−295.99	177.98	0.05
	CH	23.61	−290.90	177.74	0.05
CH_2BrI	DMF	22.26	−292.68	177.54	0.06
		100.00	−276.90	176.20	0.02
	CCl_4	21.71	−274.12	175.28	0.03
	CH	23.67	−269.79	174.73	0.06
CH_2I_2	DMF	21.25	−246.98	173.80	0.05
		100.00	−235.00	172.92	0.03
	CCl_4	22.46	−234.10	172.15	0.03
	CH	24.28	−231.02	171.93	0.03
CH_2ClCN	DMF	23.42	−280.81	162.16	0.03
		100.00	−251.18	161.22	0.03
	CCl_4	23.06	−246.87	159.69	0.04
	CH[c]	...	...	...	...
CH_3Cl	DMF	21.68	−184.28	150.40	0.05
		100.00	−179.09	149.64	0.03
	CCl_4	25.18	−179.06	149.18	0.03
	CH	19.22	−172.05	148.58	0.04
CH_3Br	DMF	23.20	−163.46	152.14	0.04
		100.00	−158.58	151.44	0.03
	CCl_4	27.74	−157.73	150.98	0.05
	CH	26.07	−151.08	150.54	0.05
CH_3I	DMF	22.38	−132.79	151.59	0.03
		100.00	−130.97	151.09	0.06
	CCl_4	21.72	−129.49	150.65	0.05
	CH	23.42	−123.18	150.31	0.05
CH_3CN	DMF	22.66	−125.89	135.99	0.05
		100.00	−117.70	136.15	0.04
	CCl_4	22.18	−118.17	135.66	0.05
	CH[c]	...	...	...	...
CH_3CCl_3	DMF	24.16	−167.08	133.77	0.04
			−163.71	133.46	0.04
	CCl_4	24.50	−164.03	133.31	0.04
	CH	22.37	−159.05	133.25	0.04

[a] Parameters are given in cps; ω is referenced to internal TMS. [b] Average deviation of the calibrated values of ω. [c] Not observed because of limited solubility.

ing ability of the solvent. The values of $\Delta\omega$ and ΔJ (Table II) provide a measure of the hydrogen-bonding effect of DMF relative to the inert medium CH. These quantities on the whole tend to increase with the expected proton-donating ability of the solutes. On the other hand, in the highly polar CH_3CN J is only slightly affected by the transition from CCl_4 to DMF, although the shift is affected appreciably.

These observations can be more plausibly accounted for in terms of the specific interactions between the solvent and solute, in particular hydrogen bonding, than by any more general mechanism. In comparing the situation in any solvent with that in the neat solute, consideration must also be given to association in the latter state.

In the hydrogen-bonded complex the electron-rich proton acceptor repels the charge from the vicinity of the bonded proton toward the carbon atom.[6] This increases the s character of the carbon orbital bonded to the proton with a corresponding increase in the value of J. The parallelism between the solvent effects on J and ω (see Figure 1) is qualitatively in accord with such a mechanism.

The points in Figure 1 fall on two distinct curves. The values for all of the amines studied fall on the upper curve while those for all the solvents containing oxygen are on the lower curve. It is impossible to decide whether the values for those solvents containing only halogen substituents fall on one of these two curves or define a third, owing to the small magnitudes of their effects. This separation into groups must arise in the differences in the relative importance of the factors responsible for the observed solvent effects. The probable source of these differences is the anisotropy contribution of the acceptor atom in the hydrogen-bonded complex, which has been discussed in this connection elsewhere.[13,14] The correlation between ΔJ and $\Delta\omega$ is linear for both solvent groups but has a greater slope for the amines. This appears reasonable since as the strength of the hydrogen bond increases, the proton would be expected to approach more closely to the seat of anisotropy.

There is no apparent correlation between the solvent effects and the basicities of the amines used.[15] However, these amines do not differ greatly in their pK_a values ($\sim$10.5–11.0). In this situation steric effects might be expected to be important in hydrogen bonding to the bulky bromoform molecule. That such is the case is supported by the relative order of solvent effects: primary > secondary > tertiary amines. Finally it is interesting to note that DMF falls on the curve for oxygen compounds indicating that it bonds through its oxygen atom.

On the basis of the above mechanism of interaction it is to be expected that the solvent effect in a strong acceptor such as DMF would increase with the proton-donor ability of the solute. The observed effect, as measured by ΔJ, does indeed increase in the order $CH_3X < CH_2X_2 < CHX_3$ in the approximate ratio 1:2:4. (A somewhat different order is found for the less polar solvents, CH and CCl_4, namely $CH_2X_2 > CHX_3 \cong CH_3X$. The differences in J observed for all these structures are not very large.) These results may reasonably be attributed to the breakup of self-associated complexes of the solute on dilution with CH or CCl_4. McClellan and Nicksic have recently reported studies of the chemical shifts of a series of halomethanes and haloethanes as pure liquids and as solutions in DMSO, CH, and CCl_4.[16] From the results they concluded that all these compounds are weakly associated to about the same extent. In these loose complexes it is possible that statistical factors can become important. Thus there are six ways to form hydrogen-bonded dimers in CH_3X or CHX_3 and eight in the case of CH_2X_2, which might explain the observed order of the solvent effect in CH or CCl_4 for these structures.

In general the solvent effect observed here for $CH_{3-m}X_m$ follows the order Cl > Br > I. For the haloforms Creswell and Allred have found the enthalpies of hydrogen-bond association to fall in the same order: $CHCl_3 > CHBr_3 > CHI_3$.[17] Infrared methods have also been used to investigate the hydrogen bonding of these compounds to bases using dilute solutions in CCl_4. In this way Allerhand and Schleyer found the order of changes in the C–H stretching frequencies to be $CHBr_3 > CHI_3 > CHCl_3$.[12] They also found that the replacement of Cl by CCl_3 and CN as well as by Br and I resulted in the enhancement of the spectral shifts produced by a common base. The use of very dilute solutions to study ^{13}C–H couplings would likewise be desirable, but it is not practical at the natural abundance of this isotope with the usually available techniques.

Both $\Delta\omega$ and ΔJ correlate reasonably well with the Taft inductive parameters of the halogens,[18] as is shown for ΔJ in Figure 3. The correlation for ΔJ

(13) B. B. Howard, C. F. Jumper, and M. T. Emerson, *J. Mol. Spectry.*, **10**, 117 (1963).

(14) D. P. Eyman and R. S. Drago, *J. Am. Chem. Soc.*, **88**, 1617 (1966).

(15) H. K. Hall, Jr., *ibid.*, **79**, 5441 (1957).

(16) A. L. McClellan and S. W. Nicksic, *J. Phys. Chem.*, **69**, 446 (1965).

(17) C. J. Creswell and A. L. Allred, *J. Am. Chem. Soc.*, **85**, 1723 (1963).

(18) R. W. Taft, Jr., and I. C. Lewis, *Tetrahedron*, **5**, 210 (1959).

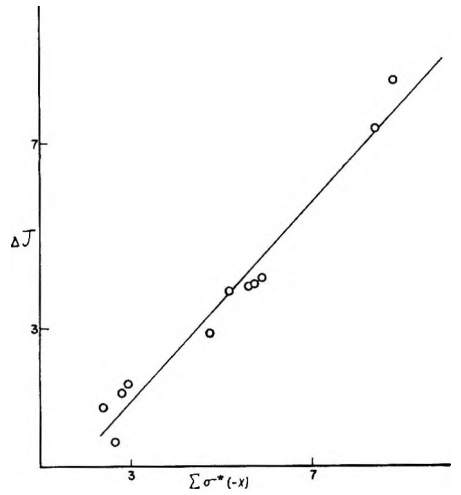

Figure 3. Plot of ΔJ *vs.* the sum of the Taft substituent parameters for the substituted methanes.

(but not for $\Delta\omega$) is poorer for the CN substituent, and it has been pointed out above that the solvent effect on J for acetonitrile is small.

The effect of aromatic solvents on J is interesting. In benzene $J(CHBr_3)$ is ~2 cps larger than in CH and ~0.8 cps greater than the value for the pure compound. This difference, though small, is significant and suggests the existence of a characteristic aromatic effect. Such an effect could arise, for example, from the complexing of the proton with the π charge of the aromatic ring as has been postulated elsewhere.[15] The values of J and ω in each substituted aromatic solvent are intermediate between those in benzene and those in aliphatic solvents with the same substituent. This suggests a competition between the complexes of the bromoform proton with the aromatic π cloud[19] and with the aromatic substituent. Rapid equilibration between the two types of complexes must obviously be assumed to account for the observation of only one spectrum.

We should like finally to discuss some of the more general aspects of the method employed here to study solute–solvent interactions. In similar investigations nmr spectroscopists have usually relied upon changes in chemical shifts as an index of such interactions. In those instances where investigators noted the importance of anisotropy effects it has been found necessary to attempt an estimation of these contributions on the basis of an assumed model and suitable theoretical calculations.[13,14]

In this study we have perferred instead to place primary reliance on the ^{13}C–H coupling parameter of the solutes while at the same time comparing its behavior with that of the chemical shifts. The use of this parameter (J) is advantageous because of its insensitivity to anisotropy effects which are a major source of difficulty in the use of chemical shifts. Since the factors influencing ΔJ and $\Delta\omega$ are likely to be different, their simultaneous use offers obvious advantages.

Acknowledgments. This work was supported in part by grants from the National Science Foundation and the National Institutes of Health. We are indebted to Lee H. Altmayer and K. M. Pryse, both National Science Foundation Undergraduate Research Participants, for their assistance in various phases of this study.

(19) W. G Schneider, *J. Phys. Chem.*, 66, 2653 (1962).

Reaction of Oxygen Atoms with Tetrafluoroethylene in the Presence of Molecular Oxygen[1]

by Julian Heicklen and Vester Knight

Aerospace Corporation, El Segundo, California *(Received June 20, 1966)*

Oxygen atoms were produced in the presence of C_2F_4 and O_2 from the mercury-photosensitized decomposition of N_2O. Besides N_2, the products were CF_2O, C_2F_4O (tetrafluoroethylene oxide), and cyclo-C_3F_6. CF_3CFO was not found. The mechanism involves a short chain which produces CF_2O: $CF_2O_2 + C_2F_4 \rightarrow 2CF_2O + CF_2$ $\xrightarrow{O_2}$ CF_2O_2. The chain carrier CF_2O_2 is removed by either $2CF_2O_2 \rightarrow 2CF_2O + O_2$ or $CF_2O_2 + C_2F_4 \rightarrow CF_2O + C_2F_4O$. At room temperature, O_2 suppresses cyclo-C_3F_6 formation, but at 125° its presence enhances cyclo-C_3F_6 production. The detailed mechanism is given by reactions a through p in the text. A number of rate constant ratios were determined, and they are included. The mechanism and rate constant ratios are compared to those for C_3F_6 and found to be similar.

I. Introduction

Earlier communications[2,3] from our laboratory have discussed the reactions of $O(^3P)$ (prepared from the Hg-sensitized photolysis of N_2O) with C_2F_4. The reaction scheme between room temperature and 150° seems reasonably well established. The detailed mechanism and pertinent rate constant ratios,[3] as well as the absolute rate constant parameters for the $O + C_2F_4$ reaction,[2b] are known. Briefly, the results are: first, the only products are CF_2O and cyclo-C_3F_6; tetrafluoroethylene oxide C_2F_4O as well as CF_3CFO is definitely absent for all conditions studied; second, $\Phi(CF_2O) = 1.0$ for all conditions; and third, Φ(cyclo-C_3F_6) can vary from zero to 1.0 and is dependent on the temperature, the C_2F_4 pressure, and the absorbed intensity.

A few preliminary runs at room temperature in the presence of molecular oxygen have been reported,[2a] and $\Phi(CF_2O)$ was roughly doubled by the addition of oxygen. In the present work, we have extended this investigation.

II. Experimental Section

Matheson Co. N_2O and O_2 were used. The N_2O was degassed at −196° before use, but the O_2 was used without further purification. C_2F_4 was prepared by the debromination of the vicinal dibromide $C_2F_4Br_2$ (E. I. du Pont de Nemours, Freon 114-B-2). Liquid Freon was added dropwise to a warm (50°) slurry of zinc dust and methanol containing some $ZnCl_2$. The rate of addition was adjusted to keep the solvent gently refluxing, and the effluent C_2F_4 was subsequently purified by passing it through water, then Drierite, and finally through a trap at −126° to separate any heavy ends. Before use, the C_2F_4 was degassed at −196°.

The general analytical procedure has been described previously.[2] At room temperature, mixtures of reactants were prepared in a cylindrical Pyrex cell, 10 cm long and 5 cm in diameter, with sodium chloride windows. Irradiation was from two Hanovia low-pressure spiral mercury lamps, one at each window. After irradiation an infrared spectrum of the cell contents was taken on a Perkin-Elmer Model 21 infrared spectrometer. At 125°, a T-shaped cell was used. Both the stem and cross were 10 cm long and 5 cm in diameter. Irradiation was through a Corning 9-54 filter (to remove radiation below 2200 A) and a quartz window on the stem of the cell. The cross of

(1) This work was supported by the U. S. Air Force under Contract No. AF 04(695)-669.

(2) (a) D. Saunders and J. Heicklen, *J. Am. Chem. Soc.*, **87**, 2088 (1965); (b) D. Saunders and J. Heicklen, *J. Phys. Chem.*, **70**, 1950 (1966).

(3) N. Cohen and J. Heicklen, *ibid.*, **70**, 3082 (1966).

the T had NaCl windows and was situated in the sample beam of a Beckman IR-4 infrared spectrometer. During any irradiation, only one product band was followed, and it was followed continuously.

The absorbed intensity I_a was measured from the CF_2O production for runs with oxygen absent, where $\Phi(CF_2O) = 1.0$.

III. Results

The products of the Hg-photosensitized decomposition of N_2O in the presence of both C_2F_4 and O_2 are N_2, which was not monitored, and CF_2O, cyclo-C_3F_6, and C_2F_4O, which were easily identified and analyzed by infrared spectroscopy. CF_3CFO was never found, though we looked for it specifically and would have detected it easily if it were present. At room temperature, a small amount of polymer was also formed, but it did not interfere. However, at 125° the polymer formation was appreciable, and it was necessary to clean the cell occasionally during the series of runs.

The infrared bands used for analysis were at 5.12, 6.22, and 11.65 μ, respectively, for CF_2O, C_2F_4O, and cyclo-C_3F_6. The absolute absorption coefficients are known for CF_2O from previous work.[2b] The absorption coefficients for cyclo-C_3F_6 were found by performing photolyses in the absence of O_2 and using as absolute quantum yields those predicted from earlier results.[3,4] The value for the absorption coefficient (to base 10) is 530 l./mole cm at both 23 and 125°. For C_2F_4O, we used a value (to base 10) of 123 l./mole cm for the extinction coefficient at 6.22 μ based on the infrared spectrum reported by Caglioti, Lenzi, and Mele.[5]

Spot checks showed that at room temperature the products grew linearly with time. However, at 125° this was definitely not the case. The rates of growth of CF_2O and cyclo-C_3F_6 were markedly enhanced as the reaction proceeded. On the other hand, the rate of growth of C_2F_4O was retarded. These effects were most pronounced at the lowest intensities where longer times were needed to obtain measurable amounts of products. Under these conditions, it was extremely difficult to determine accurately initial rates of growth, and the initial quantum yields we report for cyclo-C_3F_6 and C_2F_4O easily may be in error by 50% at the lowest intensities at 125°. Because more CF_2O is formed, its analysis is much more reliable.

After the irradiation was discontinued at 125°, both the CF_2O and cyclo-C_3F_6 continued to grow, whereas the C_2F_4O decayed until it eventually vanished. When the C_2F_4O was consumed, the CF_2O stopped growing, but the cyclo-C_3F_6 continued to grow indefinitely. (We sometimes monitored it for about 1 hr after the CF_2O had stabilized.) Lenzi and Mele[6] found that C_2F_4O rapidly decomposes at 125° to CF_2O and CF_2 (which could show up as either CF_2O or cyclo-C_3F_6 in our system). Thus some of these results are not unexpected.

For some experiments, we measured the increase in CF_2O and found it to be roughly about two or three times the C_2F_4O consumed. Consequently, some of the CF_2O growth, but not all of it, can be explained as due to C_2F_4O decomposition. On the other hand, the continual growth of cyclo-C_3F_6, even after the C_2F_4O is exhausted, is a complete mystery.

The results at 23° are reported in Table I, and the initial quantum yields at 125° are reported in Table II. At room temperature and at low C_2F_4 pressures and high values of I_a, $\Phi(CF_2O)$ rises slightly as O_2 increases from 5.0 mm. Eventually a plateau is reached, and then further increases in O_2 markedly reduce $\Phi(CF_2O)$. As (C_2F_4) increases or I_a falls, the plateau area becomes more important; eventually $\Phi(CF_2O)$ is essentially independent of (O_2) and approaches a value of 3.0. For the latter region, Φ(cyclo-C_3F_6) is independent of I_a but rises with the ratio $(C_2F_4)/(O_2)$. $\Phi(C_2F_4O)$ is independent of (O_2) but is enlarged as either (C_2F_4) is enhanced or I_a is diminished. Its absolute value varies between zero and unity.

At 125° under our experimental conditions, all initial quantum yields are essentially independent of (O_2) though they are all larger than in the absence of O_2. All of the yields increase with increasing (C_2F_4) or declining I_a. $\Phi(CF_2O)$ varies from about 3 to 10; Φ(cyclo-C_3F_6), from about 0.1 to about 2.0; and $\Phi(C_2F_4O)$, from about 0.6 to about 4.

IV. Discussion

In the absence of O_2, the reaction mechanism is[3]

$$Hg + h\nu \longrightarrow Hg^* \quad (a)$$

$$Hg^* + N_2O \longrightarrow Hg + N_2 + O(^3P) \quad (b)$$

$$O + C_2F_4 \longrightarrow CF_2O + CF_2 \quad (c)$$

$$O + C_2F_4 \longrightarrow C_2F_4O^* \quad (d)$$

$$2CF_2 \longrightarrow C_2F_4 \quad (e)$$

$$CF_2 + C_2F_4 \longrightarrow \text{cyclo-}C_3F_6 \quad (f)$$

$$C_2F_4O^* + C_2F_4 \longrightarrow CF_2O + \text{cyclo-}C_3F_6 \quad (g)$$

where the asterisk denotes an excited state. For the time being, the multiplicity of the CF_2 species will not be specified, though we believe it to be triplet.

(4) N. Cohen and J. Heicklen, *J. Chem. Phys.*, **43**, 871 (1965).
(5) V. Caglioti, M. Lenzi, and A. Mele, *Nature*, **201**, 610 (1964).
(6) M. Lenzi and A. Mele, *J. Chem. Phys.*, **43**, 1974 (1965).

Table I: Results at 23° for N_2O–C_2F_4 Mixtures [$(N_2O) \sim 500$ mm, $\lambda = 2537$ A]

(C_2F_4), mm	(O_2), mm	Exposure time, min	$\Phi(CF_2O)$	Φ(cyclo-C_3F_6)	$\Phi(C_2F_4O)$
	$I_a = 64 \times 10^{13}$ quanta/cc sec				
6.0	6.0	5.0	0.83	0.009	0
4.6	8.0	2.0	1.10	0	0
5.2	15	2.0	1.07	0	0
5.0	16	2.0	1.07	0	0
5.0	54	2.0	0.58	0	0
5.1	56	3.0	0.49	0	0
5.3	106	5.0	0.31	0	0
5.0	150	6.0	0.22	0	0
5.2	152	13.0	0.113	0	0
18.5	4.5	3.0	1.27	0.025	0.08
16	5.0	2.0	1.31	0.019	0.09
17	18	2.0	1.04	0	0
17	62	2.0	0.88	0	0
15	147	3.0	0.35	0	0
64	5.0	1.0	2.39	0.103	0.24
59	7.0	1.5	1.59	0.065	0.24
55	15	1.5	2.06	~0.03	0.29
47	58	1.5	1.64	0.008	0.20
50	103	1.5	1.08	0.008	0.20
167	6.0	1.0	1.81	0.128	0.58
160	17	2.0	1.77	0.09	0.47
159	55	1.5	1.02	~0	~0.25
	$I_a = 22 \times 10^{13}$ quanta/cc sec				
5.0	6.0	8.0	0.83	0	0
7.0	14	6.0	1.08	...	0
5.0	55	10.0	0.48	0	0
6.0	147	25.0	0.22	0	0
15	5.0	5.0	1.62	0.016	0
16	22	5.0	1.55	0.008	0
15	52	6.0	1.00	0	0
16	147	10.0	0.38	0	0
55	6.0	5.0	1.60	0.048	0.24
53	16	5.0	1.80	0.045	0.30
52	67	4.0	1.55	0.016	0.21
50	173	5.0	0.82	0.01	...
139	6.5	3.0	1.93	0.121	0.55
146	17	6.0	1.82	0.093	0.52
139	49	5.0	1.07	0.016	0.37
	$I_a = 4.0 \times 10^{13}$ quanta/cc sec				
6.4	5.6	31.0	0.93	0	0
6.4	12.6	20.0	1.00	0	0
6.2	63	30.0	0.54	0	0
6.8	168	90.0	0.22	0	0
17.5	5.0	15.0	2.00	0.06	0
16	19	15.0	1.75	0	0
16	51	20.0	1.37	0	...
16	154	30.0	0.56	0	0
48	5.5	15.0	2.46	0.105	0.66
56	17	17.0	1.77	0.052	0.50
51	61	15.0	2.25	0	0.56
49	140	15.0	1.75	0.01	0.41
146	5	10.0	2.12	0.144	0.63
162	17	20.0	2.74	0.097	0.91
163	51	15.0	2.75	0.118	0.92
	$I_a = 0.98 \times 10^{13}$ quanta/cc sec				
7.7	5.3	60.0	1.58	0	0
16	16	30.0	1.84	0	0
14	141	60.0	1.25	0	0
51	57	50.0	2.50	0.03	0.83
50	155	45.0	2.34	0.03	0.74
141	15	60.0	3.4	0.22	1.35
192	49	45.0	2.56	0.15	1.11
	$I_a = 0.24 \times 10^{13}$ quanta/cc sec				
14	19	90.0	2.7	0.03	0
51	60	150.0	2.3	0.03	0.92
137	49	155.0	2.8	0.17	1.08

Actually, $C_2F_4O^*$ also can decompose in a first-order step, but this is only important for C_2F_4 pressures less than 1 mm and need not be considered here. The ratio of $k_d/(k_c + k_d)$ is 0.15 at 23° and ~0.10 at 125°.

It is also necessary to consider the reaction

$$Hg^* + O_2 \longrightarrow Hg + O_2^*$$

O_2 is about as efficient as N_2O in quenching Hg*. Thus for $(O_2) = 150$ mm, about 25% of the Hg* reacts with O_2. We will ignore this reaction in the subsequent analysis, though we realize that to do so introduces some error. Fortunately, the O_2^* reacts rapidly with C_2F_4 to give results very similar[7] to that of the O + C_2F_4 reaction in the presence of O_2. Thus the importance of this complicating competition is masked. For smaller O_2 pressures the removal of Hg* by O_2 is not sufficiently important to influence the results.

At 23°. At room temperature, in the presence of molecular oxygen, Φ(cyclo-C_3F_6) falls as $(C_2F_4)/(O_2)$ is diminished, even in the regions where the other product yields are independent of the O_2 pressure, and even at low intensities and high C_2F_4 pressures where reaction f should be important. In fact, with 50 mm of C_2F_4, 60 mm of O_2, and $I_a = 0.24 \times 10^{13}$ quanta/cc

(7) J. Heicklen, V. Knight, and S. A. Greene, *J. Chem. Phys.*, **42**, 221 (1965).

Table II: Initial Results at 125° for N_2O–C_2F_4 Mixtures [$(N_2O) \sim 500$ mm, $\lambda = 2537$ A]

(C_2F_4), mm	(O_2), mm	$\Phi(CF_2O)$	Φ(cyclo-C_3F_6)	$\Phi(C_2F_4O)$	Φ(cyclo-C_3F_6)/ Φ_0(cyclo-C_3F_6)	$[\Phi(C_2F_4O) - 1]/\Phi$(cyclo-C_3F_6)	η^a	k_m/k_n^b
			$I_a = 11.2 \times 10^{13}$ quanta/cc sec					
16	18	3.3	0.12	0.64	0.87	...	...	...
55	15	3.5	0.29	1.17	1.32	...	...	...
52	56	3.8	0.32	1.10	1.48	...	...	...
53	151	3.4	0.26	1.00	1.18	...	...	...
147	50	5.1	~0.75	1.67	~1.8	0.9	2.5	0.7
			$I_a = 1.65 \times 10^{13}$ quanta/cc sec					
16	16	5.0	0.22	0.92	1.44	...	...	...
52	14	6.4	0.68	1.84	2.1	1.2	2.2	1.0
50	56	6.6	0.64	1.51	2.0	0.8	3.0	1.3
51	147	10.4	0.76	1.60	2.4	0.8	2.7	2.4
150	49	9.8	1.6	3.1	2.8	1.3	1.5	0.9
			$I_a = 0.31 \times 10^{13}$ quanta/cc sec					
16	18	6.5	0.44	1.0	2.2	...	...	...
51	16	6.8	1.15	1.8	2.4	0.7	2.2	1.1
52	53	7.4	1.35	2.4	2.8	1.0	1.7	0.8
52	151	8.4	1.4	1.5	3.4	0.3	3.1	2.0
149	52	9.2	1.8	2.6	3.0	0.9	1.6	1.1
			$I_a = 0.061 \times 10^{13}$ quanta/cc sec					
16	17	9.1	0.88	~2.0	0.7	1.1	2.0	1.5
53	17	9.0	1.45	2.9	1.9	1.3	1.5	0.9
54	55	11.2	1.2	2.9	1.3	1.6	1.5	1.3
54	153	6.2	...	2.6	...	...	1.6	0.5
149	51	9.2	2.0	4.2	2.0	1.6	1.3	0.5

[a] From eq 9. [b] From eq 10.

sec, Φ(cyclo-C_3F_6) is 0.04, whereas in the absence of O_2 it would be 0.11 from reaction f alone (ignoring any contribution from g). With $C_2F_4 = 150$ mm and the same (O_2) and I_a, Φ(cyclo-C_3F_6) is 0.17, which can be accounted for completely by reaction g plus the CF_2 produced from

$$Hg^* + C_2F_4 \longrightarrow Hg + 2CF_2^1 \qquad (h)$$

where the superscript 1 denotes the singlet state. The latter reaction gives about 20% as many CF_2 radicals as reaction c when $C_2F_4 = 150$ mm,[2a] and these singlet radicals are not scavenged by O_2.[7] Φ(cyclo-C_3F_6) predicted from reaction f alone would be 0.28. *Consequently, it seems clear that either the CF_2 radical produced in reaction c or its precursor must be removed by O_2. There appears to be no way of escaping this conclusion.*

Alternatively, we can examine the chain-terminating step. C_2F_4O can be formed only in a chain-terminating step. If there are no branched chains at 23°, then when $\Phi(C_2F_4O) = 1.0$, every reaction of an oxygen atom with C_2F_4 must lead ultimately to C_2F_4O. Again the conclusion is reached that either the CF_2 radicals from reaction c or their precursors are scavenged by O_2.

Now we consider the precursor to C_2F_4O formation. In the absence of O_2, this molecule is not formed;[2] thus the $O + C_2F_4$ reaction is too energetic to yield a stable C_2F_4O molecule. Another intermediate must be formed when O_2 is present which can donate an oxygen atom to C_2F_4 in a less exothermic reaction. The indicated intermediate is the CF_2O_2 radical, and it is most easily formed in the reaction

$$CF_2^3 + O_2 \longrightarrow CF_2O_2 \qquad (i)$$

where the superscript 3 denotes a triplet state.

The molecular oxygen can also react with O atoms and the $C_2F_4O^*$ intermediate

$$O + O_2 + N_2O \longrightarrow O_3 + N_2O \qquad (j)$$

$$C_2F_4O^* + O_2 \longrightarrow CF_2O + CF_2O_2 \qquad (l)$$

Reaction j is well known, and reaction l must occur to account for the diminution in Φ(cyclo-C_3F_6) in the pres-

ence of O_2. (In the absence of O_2, most of the cyclo-C_3F_6 comes from reaction g.)

The intermediate CF_2O_2 can react with C_2F_4

$$CF_2O_2 + C_2F_4 \longrightarrow CF_2^3 + 2CF_2O \qquad (m)$$

$$CF_2O_2 + C_2F_4 \longrightarrow CF_2O + C_2F_4O \qquad (n)$$

where reaction m is the chain-propagating step and reaction n is a chain-terminating step. Since $\Phi(C_2F_4O)$ is often less than unity and there is an intensity effect, another chain-terminating step must be

$$2CF_2O_2 \longrightarrow 2CF_2O + O_2 \qquad (o)$$

There is an alternative mechanism that can explain the results. Instead of reactions c and m producing CF_2^3 radicals, they might form some other intermediate that is scavenged by O_2 but does not react with C_2F_4. However, it would seem odd that such an intermediate could exist in lieu of the fact that $C_2F_4O^*$ reacts with both C_2F_4 and O_2.

On the other hand, the complication introduced by reaction i concerns the fact that CF_2 radicals produced in three other systems are not scavenged by O_2.[7-9] Presumably, those radicals were singlets. Spin conservation would require the CF_2 produced in this system to be triplets, and we have reported this to be the case.[2a,10] Our results here seem to confirm this hypothesis. However, if this is so, then $k_f/k_e^{1/2}$ appears to be the same for both singlet and triplet CF_2 radicals,[3] a result that would be too fortuitous to be true. Presumably, the initially formed triplet CF_2 radicals pass over to the singlet state in the absence of O_2 before reaction.

Except at low I_a and high (C_2F_4), the cyclo-C_3F_6 comes essentially from reaction g. Thus, the mechanism predicts that

$$\frac{\Phi(\text{cyclo-}C_3F_6)}{\Phi_0(\text{cyclo-}C_3F_6)(1+\alpha)^{-1} - \Phi(\text{cyclo-}C_3F_6)} = \frac{k_g}{k_1}\frac{(C_2F_4)}{(O_2)} \qquad (1)$$

where $\Phi_0(\text{cyclo-}C_3F_6)$ is the quantum yield of cyclo-C_3F_6 in the absence of O_2, and

$$\alpha = \frac{k_j(O_2)(N_2O)}{(k_c + k_d)(C_2F_4)} \qquad (2)$$

Under the conditions of interest, α can be neglected, and $\log\{\Phi(\text{cyclo-}C_3F_6)/[\Phi_0(\text{cyclo-}C_3F_6) - \Phi(\text{cyclo-}C_3F_6)]\}$ is plotted *vs.* $\log\{(C_2F_4)/(O_2)\}$ in Figure 1. The few data points of Saunders and Heicklen[2a] are included. (It should be pointed out that Saunders and Heicklen misinterpreted their results concerning this competition.) There is considerable scatter in the data; yet it is easy to draw a straight line of unit slope through them. The value of k_g/k_1 is about 0.10.

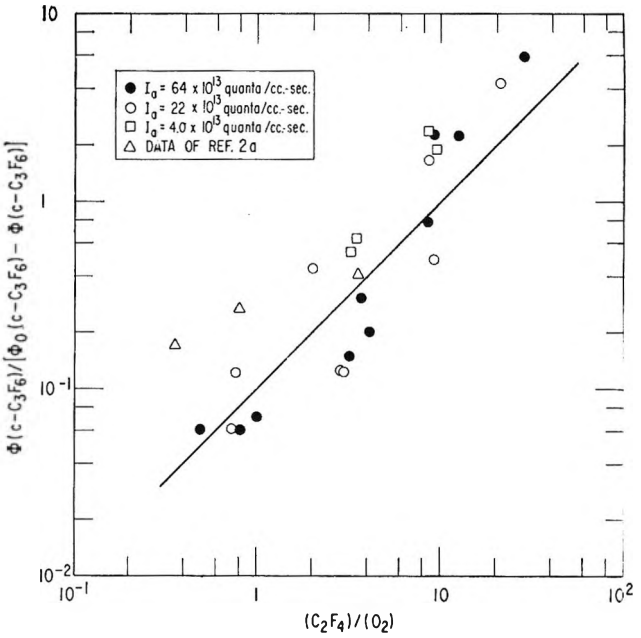

Figure 1. Log–log plot of $\Phi(\text{cyclo-}C_3F_6)/[\Phi_0(\text{cyclo-}C_3F_6) - \Phi(\text{cyclo-}C_3F_6)]$ *vs.* $(C_2F_4)/(O_2)$ at 23°.

When reaction n is small compared to reaction o [*i.e.*, when $\Phi(C_2F_4O)$ is small], a condition that prevails at high I_a and low C_2F_4, then the mechanism requires that

$$[\Phi(CF_2O)]^{-1} = \frac{1}{2} + \frac{k_j(N_2O)(O_2)}{2(k_c + k_d)(C_2F_4)} \qquad (3)$$

as long as all the CF_2^3 radicals and $C_2F_4O^*$ are scavenged by O_2. Since (N_2O) is constant, $[\Phi(CF_2O)]^{-1}$ can be plotted against $(O_2)/(C_2F_4)$, and a straight line should result. This is done in Figure 2 for the runs where $\Phi(C_2F_4O)$ is small. The data fit a straight-line plot which we have forced to pass through an intercept of 0.5. It can be seen that the high-intensity points at low $(O_2)/(C_2F_4)$ lie about a factor of 2 high, a result that could be caused by the removal of CF_2 by reaction e rather than reaction i. Roughly, $k_j/k_c^{1/2}$ can be estimated to be about 0.13 (mm min)$^{-1/2}$ if this explanation is correct. From the slope, a value of 95 l./mole is obtained for $k_j/(k_c + k_d)$. Now k_j is about 5.5 × 10^9 l.^{2}/mole^2 sec with N_2O as a third body,[11] and $k_c + k_d$ is 0.6 × 10^9 l./mole sec at room temperature.[2a] Consequently, the observed ratio is 10 times too large.

(8) F. W. Dalby, *J. Chem. Phys.*, **41**, 2297 (1964).

(9) J. P. Simons and A. J. Yarwood, *Nature*, **192**, 943 (1961).

(10) J. Heicklen, N. Cohen, and D. Saunders, *J. Phys. Chem.*, **69**, 1774 (1965).

(11) F. Kaufman, private communication.

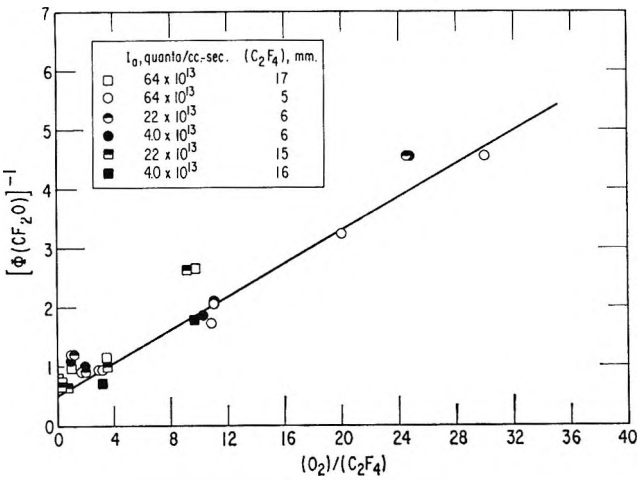

Figure 2. Plot of $[\Phi(CF_2O)]^{-1}$ *vs.* $(O_2)/(C_2F_4)$ for low values of $(C_2F_4)I_a^{1/2}$ at 23°.

From the limited data of ref 2a, a more favorable comparison can be made. In a comparable study of the reactions of O atoms with C_3F_6 in the presence of O_2,[12] the value for k_j was found to be too high by a factor of 2. Furthermore, an odd feature of both systems is that product formation is suppressed by reaction j in spite of the fact that O_3 reacts rapidly with perfluoroolefins.[13] The O_3 must either react with the Hg or absorb the radiation, or both, in a manner to suppress product formation, and the amount of suppression may be characteristic of the system. In other systems we have found HgO when O_3 is produced. Thus, the value of $k_j/(k_c + k_d)$ obtained in this study is not reliable. Nevertheless, it is useful in the subsequent analysis to correct for reaction j. However, because of the uncertainty we shall limit our analysis of the data to the region where $(O_2)/(C_2F_4)$ is less than about 3, so as to minimize any complications resulting from reaction j.

Finally, the room-temperature mechanism predicts

$$\Phi(CF_2O)\{1 + \alpha\} = 1 + \gamma \qquad [R(o) > R(n)] \quad (4)$$

$$\Phi(CF_2O)\{1 + \alpha\} = 2 + \frac{2\gamma k_m}{k_n} \qquad [R(o) < R(n)] \quad (5)$$

and

$$\Phi(C_2F_4O)\{1 + \alpha\}^{1/2} = \frac{k_n\gamma^{1/2}}{(2k_o)^{1/2}}\frac{(C_2F_4)}{I_a^{1/2}} \qquad [R(o) > R(n)] \quad (6)$$

$$\Phi(C_2F_4O)\{1 + \alpha\}^{1/2} = \frac{\gamma}{\{1 + \alpha\}^{1/2}} \qquad [R(o) < R(n)] \quad (7)$$

where γ is the fraction of the CF_2 plus $C_2F_4O^*$ produced from reactions c and d which react with O_2, and $R(x)$ is the rate of reaction x. Except at very high I_a and low (O_2) where reaction e can be important, γ varies from 0.85 to 1.00. We set it equal to unity as our experimental error would outweigh any minor trends in γ. The factor $1 + \alpha$ can be estimated from the results of Figure 2. Consequently, the left-hand sides of eq 4 through 7 can be computed under all conditions, and they are plotted *vs.* $(C_2F_4)/I_a^{1/2}$ in Figure 3. For low values of $(C_2F_4)/I_a^{1/2}$, $R(o)$ is greater than $R(n)$ and $\Phi(CF_2O)\{1 + \alpha\}$ is slightly less than 2.0, as indicated by eq 4, and $\Phi(C_2F_4O)\{1 + \alpha\}^{1/2}$ rises linearly with $(C_2F_4)/I_a^{1/2}$ (unit slope on the log–log plot). The value of $k_n/k_o^{1/2}$ is found to be 5.6×10^{-3} (mm min)$^{-1/2}$. For high values of $(C_2F_4)/I_a^{1/2}$, $R(o)$ is less than $R(n)$ and $\Phi(CF_2O)\{1 + \alpha\}$ rises to a value of about 3.0, yielding a value of 0.5 for k_m/k_n. Under these conditions, $\{1 + \alpha\}$ is essentially unity and $\Phi(C_2F_4O)\{1 + \alpha\}^{1/2}$ becomes 1.0, as predicted by eq 7. An alternate but less accurate method of computing k_n/k_o is from the break point of the $\Phi(CF_2O)\{1 + \alpha\}$ curve. When $\Phi(CF_2O)$ is about halfway between its limiting values, $R(o) \sim R(n)$ and $k_n/k_o^{1/2}$ can be estimated to be about 5×10^{-3} (mm min)$^{-1/2}$, in good agreement with that found from eq 6.

At 125°. At the elevated temperature, both k_g/k_i and $k_i/k_e^{1/2}$ are probably similar to their room-temperature values. On the other hand, $k_j/(k_c + k_d)$ is smaller, both because $k_c + k_d$ has a small positive activation energy[2b] and because k_j has a negative activation energy.[14] Therefore, we could design our experiments with $(O_2)/(C_2F_4)$ ratios to minimize the importance of reactions e, f, g, and j. Thus, these reactions can be ignored under our conditions at 125°. The simplified mechanism explains the trends in the data. As expected, the quantum yields are independent of (O_2) and rise with increasing (C_2F_4) and falling I_a.

However, there are two marked differences from the room temperature data. In the first place, the addition of O_2 does not inhibit cyclo-C_3F_6 production but actually promotes it; in many cases Φ(cyclo-C_3F_6) is measurably greater than unity. In the second place, both Φ(cyclo-C_3F_6) and $\Phi(C_2F_4O)$ often exceed 1.0. Since these molecules must be formed in chain-terminating steps, a branched-chain mechanism must be operative. An examination of the data in Table II shows that both Φ(cyclo-C_3F_6) and $\Phi(C_2F_4O)$ rise with $(C_2F_4)/I_a^{1/2}$. Consequently, chain branching is more important when termination occurs by reaction n rather

(12) D. Saunders and J. Heicklen, *J. Am. Chem. Soc.*, **87**, 4062 (1965).

(13) J. Heicklen, *J. Phys. Chem.*, **70**, 477 (1966).

(14) W. M. Jones and N. Davidson, *J. Chem. Phys.*, **84**, 2868 (1962).

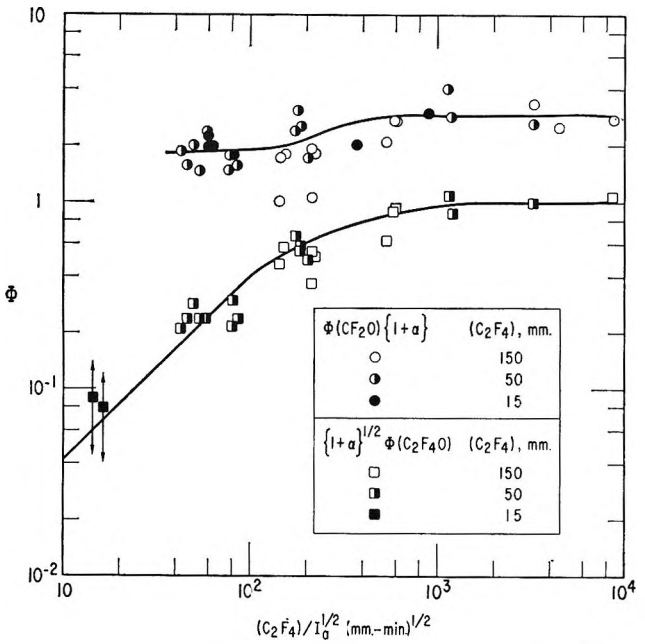

Figure 3. Log–log plots of $\{1 + \alpha\}\Phi(CF_2O)$ and $\{1 + \alpha\}^{1/2} \times \Phi(C_2F_4O)$ *vs.* $(C_2F_4)/I_a^{1/2}$ for $(C_2F_4)/(O_2) \geq 0.3$ at 23°.

than by reaction o. Thus, the chain-branching step can be associated with reactions m and n.

C_2F_4 is thermally stable up to temperatures of about 600°. In the presence of O_2, however, CF_2O and cyclo-C_3F_6 are formed, even at 200° in both static and flow experiments. The process accelerates with time and a branched-step mechanism undoubtedly is involved.[15] At 200°, there are only two thermodynamically possible chain-initiating steps, and these are

$$2C_2F_4 \longrightarrow CF_2^1 + \text{cyclo-}C_3F_6$$

$$C_2F_4 + O_2 \longrightarrow CF_2^1 + CF_2O_2 \qquad \text{(p)}$$

The first reaction can be discarded for two reasons. First, such a reaction would occur in the absence of (O_2) and some cyclo-C_3F_6 should be observed, even in spite of the fact that it readily decomposes back to C_2F_4 at this temperature. A more severe objection results from a consideration of the type of CF_2 formed. Surely such a reaction would produce the less energetic, spin-allowed, singlet CF_2 which at 125° does not oxidize. Thus, there would be no way for $\Phi(C_2F_4O)$ to rise above unity.

On the other hand, reaction p adequately explains our observed results. Again, for energetic reasons, the CF_2 must be singlet and does not enter the oxidation scheme. It ultimately results in either C_2F_4 or cyclo-C_3F_6. However, the CF_2O_2 is the additional radical that enters the oxidation mechanism.

The remaining problem is why reaction p occurs during but not prior to illumination at 125° and how it is related to reactions m and n. The answer can be related to the energetics of the reaction scheme. Reactions m and n are the most exothermic of all the reactions, the heats of reaction being about 200 kcal/mole. Clearly, the product molecules will be extremely energetic when first formed. Because the bonds formed are carbonyl bonds, the energy can be expected to reside mainly in the CF_2O product. These energetic molecules will transfer energy to C_2F_4 or O_2 or both by collision, and thus initiate reaction p.

If reaction p is the chain-branching step, then at large (C_2F_4) and small I_a, all the CF_2 radicals from p and only those from p and h will appear as cyclo-C_3F_6. Also, reaction o will be unimportant. The mechanism would then require that

$$\frac{\Phi(C_2F_4O) - 1}{\Phi(\text{cyclo-}C_3F_6)} = 1.0 \qquad (8)$$

and

$$\frac{\Phi(C_2F_4O)}{\Phi(C_2F_4O) - 1} = \eta \qquad (9)$$

where η is the ratio of rates of reaction n to p, *i.e.*, the number of times reaction n must take place for reaction p to be induced. Unfortunately, at high C_2F_4 and low I_a, our data are the most unreliable. However, the left-hand sides of eq 8 and 9 are listed in Table II for the appropriate runs. Considering the uncertainty in the data, we see that eq 8 is well obeyed. Also, η is reasonably constant and averages to 2.0.

Furthermore, at high C_2F_4 and low I_a where reaction o is unimportant, the mechanism predicts that

$$\frac{k_m}{k_n} = \frac{\Phi(CF_2O) - 1}{2\Phi(C_2F_4O)} - \frac{1}{2} \qquad (10)$$

The right-hand side of (10) is listed in Table II for the appropriate runs, and k_m/k_n is about 1.1, or approximately twice as large as at 23°. The enhancement is in the expected direction, as the less exothermic reaction should be more favored by raising the temperature. It should be recognized that if η had been less than unity, an unstable situation would have resulted, and the oxidation would have become self-sustaining.

An evaluation of $k_n/k_o^{1/2}$ can be made by considering the situation at low (C_2F_4) and high I_a, *i.e.*, when $R(o) > R(n)$. The expressions for $\Phi(CF_2O)$ and $\Phi(C_2F_4O)$ are given by eq 4 and 6, respectively. Unfortunately, our results are never entirely in this region, as can be seen from an examination of Table II. $\Phi(CF_2O)$ never

(15) Unpublished results of the Aerospace Corp. Laboratories.

Table III: Summary of Rate Constant Data

Ratio	T, °C	Value	Units	Source	Comments
k_e/k_1	23	0.10	None	Eq 1, Figure 1	...
$k_j/(k_c + k_d)$	23	95	l./mole	Eq 3, Figure 2	Ten times too large; see Discussion
$k_i/k_e^{1/2}$	23	~0.13 ~2.3	$(\text{mm min})^{-1/2}$ $(\text{l./mole sec})^{1/2}$	Figure 2	Competition not well established. Result very approximate and only valid if (e) actually competes with (i)
$k_n/k_o^{1/2}$	23	5.6×10^{-3} 0.098	$(\text{mm min})^{-1/2}$ $(\text{l./mole sec})^{1/2}$	Eq 6, Figure 3	...
	23	$\sim 5 \times 10^{-3}$ ~0.09	$(\text{mm min})^{-1/2}$ $(\text{l./mole sec})^{1/2}$	Figure 3	Based on break point in $\Phi(CF_2O)$—approximate value
	125	$\sim 1 \times 10^{-2}$ ~0.2	$(\text{mm min})^{-1/2}$ $(\text{l./mole sec})^{1/2}$	Table II	Based on break point in $\Phi(CF_2O)$—approximate value
k_m/k_n	23	0.5	None	Eq 5, Figure 3	...
	125	1.1	None	Eq 5, Table II	...
η	125	2.0	None	Eq 9, Table II	...

drops to 2 and $\Phi(C_2F_4O)$ is not proportional to $(C_2F_4)/I_a^{1/2}$. For example, at our highest intensities, a factor of 9 change in (C_2F_4) gives less than a factor of 3 change in $\Phi(C_2F_4O)$. Thus a good computation for $k_n/k_o^{1/2}$ cannot be performed. However, an approximate value can be found by realizing that when $\Phi(CF_2O)$ is halfway between its limits of 2 and 9, then $R(o) \approx R(n)$. Thus $k_n/k_o^{1/2}$ can be estimated crudely to be about 1×10^{-2} $(\text{mm min})^{-1/2}$.

V. Summary

The products of the reaction of oxygen atoms with C_2F_4 in the presence of O_2 are CF_2O, C_2F_4O, and cyclo-C_3F_6; CF_3CFO is not produced. The mechanism involves a simple but small chain at room temperature, and a larger, branched chain at 125°. The mechanism is given by reactions c–f, which occur in the absence of O_2, and reactions i–p which occur in the presence of O_2. An important result is that the reaction of $O(^3P)$ with C_2F_4 is so exothermic that the intermediate C_2F_4O molecule is so energetic that it cannot be stabilized and thus is not found in the absence of O_2. However, the triplet CF_2 radical produced can add to O_2, if it is present; the resulting CF_2O_2 radical can donate an oxygen atom to C_2F_4 in a less exothermic reaction than direct addition of oxygen atoms. Thus, the C_2F_4O intermediate is more easily stabilized and appears as a product.

A number of rate constant ratios were estimated, and they are tabulated in Table III. Both $k_n/k_o^{1/2}$ and k_m/k_n rise very slightly from 23 to 125°. Thus both k_n and k_m have small, but measurable, activation energies (~2 kcal/mole), that of k_m being slightly larger, as might be expected, since reaction m is less exothermic than reaction n. It should be noted that if both k_n and k_o have normal frequency factors (*i.e.*, about 10^{10} l./mole sec), then the activation energy difference $E_n - {}^1/_2E_o$ should be about 7 kcal/mole, somewhat larger than found. However, our high-temperature value for $k_n/k_o^{1/2}$ is sufficiently inaccurate to accommodate this discrepancy.

It is interesting to compare the results with those of the C_3F_6 system where the oxidation is principally of the CF_3CF radical.[12] In that system, the reaction of oxygen atoms with C_3F_6 also led to two sets of products. About 85% of the time (at 23°), CF_2O and CF_3CF were produced in an analogous fashion to reaction c. About 15% of the time, CF_3CFO was produced, perhaps in a reaction sequence similar to reactions d and g (though this has not been ascertained). If so, then in the presence of O_2, a reaction analogous to reaction l could occur also. In the C_3F_6 system, reactions analogous to m, i, and o were shown to be important. At 23°, the only temperature for which data exist for the C_3F_6 system, reaction p is unimportant in both the C_2F_4 and C_3F_6 systems. Thus the only reported difference between the systems is that reaction n produces C_2F_4O in the C_2F_4 system, but no analogous reaction produces perfluoropropylene oxide in the C_3F_6

system. Recent work in our laboratory has now established the formation of the epoxide in the O–C_3F_6–O_2 system. The rate constant ratio $k_m/k_o^{1/2}$ is 0.05 (l./mole sec)$^{1/2}$ for the C_2F_4 system compared to 0.068 (l./mole sec)$^{1/2}$ for the analogous ratio in the C_3F_6 system.

Acknowledgment. The authors wish to thank Mr. Dennis Saunders for preparation of the C_2F_4 and Drs. Caglioti, Lenzi, and Mele for access to their original infrared spectrum of C_2F_4O. They also wish to thank Mrs. Barbara Peer and Miss Jeanne Kiley for assistance with the manuscript.

A Reexamination of the Mercury-Photosensitized Oxidation of Tetrafluoroethylene

by Julian Heicklen and Vester Knight

Aerospace Corporation, El Segundo, California *(Received June 20, 1966)*

The mercury-photosensitized oxidation of C_2F_4 was studied at 29 and 127°. The absorbed intensity was varied by a factor of 1000, and the O_2 and C_2F_4 pressures by a factor of 30. The products of the reaction were cyclo-C_3F_6, CF_2O, and C_2F_4O (tetrafluoroethylene oxide). Important intermediates in the oxidation are an electronically excited C_2F_4 molecule and the CF_2O_2 radical. In addition, both singlet and triplet CF_2 radicals are involved. A detailed reaction mechanism is presented, and several rate constant ratios are obtained. Where comparisons with literature values could be made, agreement is good. The important oxidation step that generates the CF_2O_2 radicals is $E_0^* + O_2 \rightarrow CF_2O_2 + CF_2^1$, where E_0^* is a vibrationally equilibrated electronically excited C_2F_4 molecule, and CF_2^1 is the singlet CF_2 radical.

I. Introduction

The mercury-sensitized photolysis of C_2F_4 has been studied previously, both in the absence of O_2[1-3] and in the presence of O_2.[2] In the absence of O_2, the mechanism has been reasonably well established to be

$$Hg + h\nu \longrightarrow Hg^* \quad (a)$$

$$Hg^* + E \longrightarrow Hg + E_n^* \text{ (112.7 kcal/mole)} \quad (b)$$

$$E_n^* \longrightarrow 2CF_2^1 \quad (c)$$

$$E_n^* + E \longrightarrow E_0^* + E \quad (d)$$

$$E_0^* + E \longrightarrow 2E \quad (e)$$

$$CF_2^1 + C_2F_4 \longrightarrow \text{cyclo-}C_3F_6 \quad (f)$$

$$2CF_2^1 \longrightarrow C_2F_4 \quad (g)$$

where E is C_2F_4, the asterisk represents an electronically excited molecule (surely a triplet), the subscript n represents vibrational excitation, and the subscript 0 represents vibrationally unexcited molecules. The CF_2 radicals formed are in the singlet state, which is shown by the superscript 1. That the singlet CF_2 is formed was indicated in the oxidation studies where the results excluded the possibility of CF_2 radicals reacting with O_2. However, with oxygen present, oxidation products were formed from the oxidation of the electronically excited C_2F_4. In the absence of O_2,

(1) B. Atkinson, *J. Chem. Soc.*, 2684 (1952).

(2) J. Heicklen, V. Knight, and S. A. Greene, *J. Chem. Phys.*, **42**, 221 (1965).

(3) N. Cohen and J. Heicklen, *ibid.*, **43**, 871 (1965).

Table I: Results of Photolyses at 29°

(C_2F_4), mm	(O_2), mm	$\Phi(CF_2O)$	$\Phi(C_2F_4O)$	Φ(cyclo-C_3F_6)	α	β	γ	ψ
			I_a = 17.9 μ/sec (Aerospace C_2F_4)					
9.5	0.0	...	...	0.0022	...	...	...	...
16	0.0	...	...	0.0028	...	...	...	...
17	16	...	0.003	...	0.077	0.77	0.58	0.54
29	0.0	...	...	0.0069	...	...	...	...
53	0.0	...	...	0.0077	...	...	...	...
54	16	0.30	0.050	...	0.21	0.92	0.54	0.42
147	16	0.30	...	0.026	0.42	0.97	0.55	0.32
169	17	...	0.110	...	0.46	0.97	0.56	0.32
152	51	0.40	...	...	0.43	0.97	0.70	0.56
164	151	...	0.088	...	0.45	0.97	0.83	0.76
325	16	...	...	0.038	0.62	0.99	0.67	0.255
440	15	0.65	0.074	0.096	0.69	0.99	0.80	0.191
			I_a = 7.8 μ/sec (Peninsular C_2F_4)					
15	0.0	...	...	0.0056	...	...	...	...
16	16	0.76, 0.63	0.047	0.0035 0.0028	0.074	0.76	0.58	0.54
49	0.0	...	...	0.0120	...	...	...	...
53	16	0.48	...	0.0097 0.0187	0.21	0.92	0.54	0.42
64	16	0.48	...	...	0.24	0.93	0.52	0.40
50	64	...	0.076	0.0116	0.20	0.92	0.77	0.73
149	0.0	...	...	0.033	...	...	...	...
153	16	0.32, 0.42	0.107	...	0.43	0.97	0.56	0.31
156	52	0.44, 0.44	...	0.037	0.44	0.97	0.70	0.56
180	50	...	0.158	...	0.47	0.97	0.70	0.54
115	175	...	0.22	...	0.36	0.96	0.84	0.81
140	166	0.69	~0.23	0.032	0.41	0.97	0.84	0.80
445	0.0	...	...	0.073	...	...	...	...
455	4.5	0.146	...	...	0.70	0.99	0.71	0.079
410	15	...	...	0.093	0.67	0.99	0.70	0.22
465	16	0.21, 0.22	0.092	0.079	0.70	0.99	0.72	0.217
465	52	0.40	0.160	0.091	0.70	0.99	0.76	0.45
395	152	...	...	0.081	0.66	0.99	0.76	0.62
465	150	0.73	0.25, 0.26	0.099	0.70	0.99	0.84	0.67
			I_a = 4.0 μ/sec (Aerospace C_2F_4)					
19	16	...	~0.016	...	0.087	0.79	0.58	0.53
65	16	0.67	0.040	...	0.245	0.93	0.53	0.40
138	16	0.86, 1.05	0.20	...	0.41	0.97	0.54	0.32
168	50	0.88	0.143	...	0.46	0.97	0.70	0.55
147	130	...	...	0.031	0.42	0.97	0.86	0.79
149	158	...	0.078	...	0.43	0.97	0.84	0.78
150	185	0.40	...	...	0.43	0.97	0.85	0.80
300	17	...	...	0.174	0.60	0.99	0.66	0.27
375	17	...	0.26	...	0.65	0.99	0.68	0.245
			I_a = 2.1 μ/sec (Peninsular C_2F_4)					
17	0.0	...	...	0.0086	...	...	...	...
16	16	0.55	0.076	...	0.074	0.76	0.58	0.54
47	0.0	...	...	0.0246	...	...	...	...
50	65	0.55	0.114	...	0.20	0.92	0.77	0.70
149	0.0	...	...	0.046	...	...	...	...
164	17	0.41	0.092	...	0.45	0.97	0.56	0.33
170	52	0.57	0.174	...	0.46	0.97	0.70	0.55
148	159	0.72	0.197	...	0.43	0.97	0.84	0.78
504	0.0	...	...	0.128	...	...	...	...

(C_2F_4), mm	(O_2), mm	$\Phi(CF_2O)$	$\Phi(C_2F_4O)$	Φ(cyclo-C_3F_6)	α	β	γ	ψ
475	16	0.21	...	...	0.72	0.99	0.72	0.214
490	18	0.33	0.093	...	0.71	0.99	0.73	0.23
482	51	0.47	0.162	...	0.71	0.99	0.78	0.44
502	50	0.53	0.21	...	0.72	0.99	0.78	0.44
480	148	0.79	0.26	...	0.71	0.99	0.84	0.66
491	150	0.78	0.32	...	0.71	0.99	0.81	0.64
			I_a = 0.91 μ/sec (Aerospace C_2F_4)					
17	18	0.82	...	...	0.073	0.77	0.60	0.56
58	18	0.89	0.032	0.041	0.225	0.92	0.55	0.44
150	17	1.30	0.28	0.119	0.43	0.97	0.56	0.33
136	51	...	0.32	0.061	0.40	0.97	0.70	0.58
163	51	1.43	...	...	0.45	0.97	0.70	0.58
151	163	1.71	0.48	0.107	0.43	0.97	0.84	0.78
430	17	...	...	0.38	0.68	0.99	0.72	0.236
			I_a = 0.142 μ/sec (Peninsular C_2F_4)					
150	0.0	...	...	0.23, 0.23	...	...	...	..
158	15	0.61, 0.64	0.27	0.26	0.44	0.97	0.55	0.30
150	164	1.51	0.57	0.20	0.43	0.97	0.84	0.78
510	0.0	...	...	0.55	...	...	...	...
432	16	0.75	0.35	...	0.68	0.99	0.72	0.226
467	15	0.51	...	0.55	0.70	0.99	0.72	0.21
485	150	2.6	0.73	0.55	0.71	0.99	0.84	0.67
			I_a = 0.041 μ/sec (Peninsular C_2F_4)					
477	0.0	...	...	0.66	...	...	...	...
468	150	2.7	0.61	0.56	0.70	0.99	0.84	0.67
			I_a = 0.018 ± 0.008 μ/sec (Peninsular C_2F_4)					
505	0.0	...	...	0.42	...	...	...	...
511	150	2.6	...	0.35	0.72	0.99	0.84	0.56

the fate of E_0* was not ascertained, though ultimately it must return to ground-state C_2F_4. The deactivation could either be by collision or by a first-order process. We anticipate the results of this study and write the deactivation step e as a collision-induced transition.

In the previous oxidation study, the products were found to be cyclo-C_3F_6, CF_2O, and an unidentified product with infrared absorption bands at 6.22 and 8.85 μ. This product has since been shown to be tetrafluoroethylene oxide (C_2F_4O).[4] The analyses were performed by gas chromatography after the oxidation products had been converted to CO_2. Thus, products were reported as cyclo-C_3F_6 and CO_2. In the study reported in the present paper, analyses were made continuously during a run for each of the products by *in situ* infrared analysis. In the previous study, the C_2F_4 pressure was varied from 0.6 to 60 mm, the intensity by a factor of 5, and the temperature not at all. In the present study, the C_2F_4 pressure was varied from 15 to 500 mm, and the intensity by a factor of 10^3. Furthermore, runs were made at both 29 and 127°.

II. Experimental Section

Matheson Co. N_2O and O_2 were used. The O_2 was not further purified, but the N_2O was degassed at −196° before use. Two samples of C_2F_4 were used. One was obtained from Peninsular ChemResearch, Inc., and was purified by collecting only that fraction volatile at −126° and condensable at −196°. The other sample was prepared in our laboratory by the debromination of vicinal dibromide $C_2F_4Br_2$ (E. I. du Pont de Nemours, Freon 114-B-2). The liquid Freon was added dropwise to a warm (50°) slurry of zinc dust and methanol containing some $ZnCl_2$. The rate of addition was adjusted to keep the solvent gently refluxing, and the effluent C_2F_4 was subsequently purified by passing it through water, through Drierite, and then through silica gel. Finally, it was degassed at −196°. Analyses of both samples of C_2F_4 were performed using a Beckman GC-2A programmed-temperature gas

(4) V. Caglioti, M. Lenzi, and A. Mele, *Nature*, **201**, 610 (1964).

Table II: Results of Photolyses at 127°[a]

(C_2F_4), mm	(O_2), mm	$\Phi(CF_2O)$	$\Phi(C_2F_4O)$	Φ(cyclo-C_3F_6)	α	β	γ	ψ
				$I_a = 18.2\ \mu$/sec				
15	0.0	...	...	0.029	...	...	...	...
18	15	0.70	0.073	0.025	0.083	0.78	0.57	0.52
51	0.0	...	...	0.044	...	...	...	...
50	15	1.12	0.129	...	0.20	0.91	0.52	0.41
65	16	...	...	0.063	0.245	0.93	0.52	0.42
153	0.0	...	...	0.079	...	...	...	...
140	16	...	0.24	0.095	0.41	0.97	0.54	0.32
156	15	0.97	...	...	0.44	0.97	0.55	0.30
140	55	...	0.28	...	0.41	0.97	0.71	0.59
162	50	1.40	...	0.096	0.45	0.97	0.70	0.55
150	154	1.65	0.38	...	0.43	0.97	0.84	0.77
148	170	...	...	0.102	0.42	0.97	0.84	0.80
503	0.0	...	...	0.135	...	...	...	...
503	17	...	0.24	0.21	0.72	0.99	0.76	0.224
551	15	0.81	...	...	0.73	0.99	0.76	0.193
400	150	1.68	...	...	0.67	0.99	0.84	0.69
465	150	...	0.46	0.154	0.70	0.99	0.84	0.67
				$I_a = 3.4\ \mu$/sec				
17	0.0	...	...	0.056	...	...	...	...
16	18	1.02	0.111	0.040	0.074	0.76	0.60	0.56
51	0.0	...	...	0.104	...	...	...	...
55	15	1.46	0.30	0.121	0.216	0.92	0.54	0.42
150	0.0	...	...	0.191	...	...	...	...
155	16	1.20	0.34	0.22	0.44	0.97	0.56	0.31
152	52	1.95	0.53	0.20	0.43	0.97	0.70	0.57
150	148	2.42	0.64	...	0.43	0.97	0.82	0.76
150	170	...	...	0.20	0.43	0.97	0.84	0.79
485	0.0	...	...	0.38	...	...	...	...
489	17	0.75	0.28	0.40	0.71	0.99	0.74	0.22
487	150	2.15	0.75	0.35	0.71	0.99	0.84	0.66

[a] Peninsular C_2F_4 used in all runs.

chromatograph utilizing a silica gel column. Both samples showed less than 0.1% of any impurity.

The vacuum manifold, T-shaped cell, and the optical arrangement have been described previously.[5-8] The infrared analyses were performed *in situ* in a Perkin-Elmer Model 13 Universal spectrometer. Both the stem and the cross of the T-shaped cell were 10 cm long and 5 cm in diameter. Irradiation was from a Hanovia low-pressure, spiral mercury lamp. The radiation passed through a Corning 9-54 filter (to remove radiation below 2200 A), through 0–10 Corning 9–30 filters (to reduce the intensity), and through a quartz window on the stem of the cell. The cross of the T had NaCl windows and was situated in the sample beam of the infrared spectrometer. During any irradiation, only one product band was followed, and it was followed continuously.

The infrared bands and extinction coefficients used for analysis were the same used previously.[8] Absolute intensities were measured continually by following CF_2O production in separate experiments of the mercury-sensitized photolysis of 500 mm of N_2O in the presence of 30 mm of C_2F_4. Under these conditions, $\Phi(CF_2O)$ is equal to 1.00.[5,7]

III. Results

As in the previous studies,[1-3] the products were found to be cyclo-C_3F_6 in the absence of O_2, and cyclo-C_3F_6, CF_2O, and C_2F_4O (tetrafluoroethylene oxide) in the presence of O_2. In the absence of O_2, the cyclo-C_3F_6 grew linearly with exposure time. However, in the presence of O_2, the rates of growth of the products

(5) D. Saunders and J. Heicklen, *J. Am. Chem. Soc.*, 87, 2988 (1965).

(6) D. Marsh and J. Heicklen, *J. Phys. Chem.*, 69, 4410 (1965).

(7) D. Saunders and J. Heicklen, Report No. TDR-669(6250-40)-3, Vol. I, Aerospace Corp., Jan 1966; *J. Phys. Chem.*, 70, 1950 (1966).

(8) J. Heicklen and V. Knight, *ibid.*, 70, 3893 (1966).

(C_2F_4), mm	(O_2), mm	$\Phi(CF_2O)$	$\Phi(C_2F_4O)$	Φ(cyclo-C_3F_6)	α	β	γ	ψ
				$I_a = 0.64$ μ/sec				
15	0.0	...	...	0.131	...	...	...	...
16	17	0.99	0.099	0.102	0.074	0.76	0.59	0.56
51	0.0	...	...	0.23	...	...	...	...
45	15	1.83	...	...	0.184	0.90	0.52	0.42
60	17	...	0.39	0.28	0.23	0.92	0.54	0.42
150	0.0	...	...	0.37	...	...	...	...
141	15	1.24	...	...	0.41	0.97	0.54	0.30
158	18	...	0.41	0.46	0.44	0.97	0.56	0.33
154	51	2.22	...	...	0.43	0.97	0.70	0.56
166	51	...	0.52	0.46	0.45	0.97	0.70	0.56
151	162	2.70	0.71	0.40	0.43	0.97	0.84	0.79
460	0.0	...	...	0.63	...	...	...	...
480	16	1.21	0.47	0.68	0.71	0.99	0.74	0.22
482	151	2.22	0.99	0.67	0.71	0.99	0.84	0.68
				$I_a = 0.24$ μ/sec				
15	0.0	...	...	0.160	...	...	...	...
16	16	...	0.21	0.102	0.074	0.76	0.58	0.53
15	18	0.81	...	...	0.070	0.75	0.60	0.56
53	0.0	...	...	0.31	...	...	...	...
57	17	0.93, 0.95	0.20	0.26	0.222	0.92	0.54	0.42
151	0.0	...	...	0.35	...	...	...	...
150	16	0.91	0.34	...	0.43	0.97	0.56	0.32
174	16	...	...	0.35	0.47	0.97	0.58	0.31
160	51	...	0.42	0.38	0.44	0.97	0.54	0.44
199	51	1.26	...	...	0.50	0.97	0.71	0.54
150	158	1.78	0.54	0.29	0.43	0.97	0.84	0.78
465	0.0	...	...	0.44	...	...	...	...
480	16	1.14	0.54	0.46	0.71	0.99	0.74	0.215
498	150	2.6	0.90	0.57	0.71	0.99	0.84	0.67

were not constant. At room temperature, there was a mild inhibition of all product formation as irradiation continued. This effect became more pronounced as the $(O_2)/(C_2F_4)$ ratio increased. At 127°, there was a mild acceleration of CF_2O and cyclo-C_3F_6 formation and a mild inhibition of C_2F_4O formation. However, the effect was not nearly as large as found in another system.[8] After irradiation at 127°, the C_2F_4O slowly disappeared.

The initial quantum yields of product formation are given in Tables I and II. Double entries indicate the results of duplicate runs. The variation of the yields is a complex function of temperature, intensity, and reactant pressures. Nevertheless, the over-all trends can be summarized as follows.

First, Φ(cyclo-C_3F_6) is nearly unaffected by the presence of O_2, but it does rise by enhancing the C_2F_4 pressure or diminishing the intensity. For comparable conditions, Φ(cyclo-C_3F_6) is larger at the higher temperature, but the upper limit is about 0.6 at both temperatures.

Second, $\Phi(CF_2O)$ is always greater than $\Phi(C_2F_4O)$, and neither is markedly affected by a change in temperature.

Third, $\Phi(CF_2O)$ rises from about 0.2 to 2.7 and $\Phi(C_2F_4O)$ rises from about 0.003 to 1.0 as either the C_2F_4 pressure is increased or the absorbed intensity is decreased.

Fourth, for constant (C_2F_4) and I_a, both $\Phi(CF_2O)$ and $\Phi(C_2F_4O)$ rise measurably as the O_2 pressure is raised.

IV. Discussion

In the absence of O_2, the mechanism is given by reactions a through g. A steady-state analysis leads to the following predictions. For large $(C_2F_4)[1 + (k_d/k_c)(C_2F_4)]^{1/2}/I_a^{1/2}$ where $R(f) > R(g)$ we have

$$\Phi(\text{cyclo-}C_3F_6)\left[1 + \frac{k_d}{k_c}(C_2F_4)\right] = 2.0 \qquad (1)$$

For small $(C_2F_4)[1 + (k_d/k_c)(C_2F_4)]^{1/2}/I_a^{1/2}$ where $R(f) < R(g)$

$$\Phi(\text{cyclo-}C_3F_6)\left[1 + \frac{k_d}{k_c}(C_2F_4)\right] = \frac{k_f}{k_g^{1/2}}(C_2F_4)\frac{[1 + (k_d/k_c)(C_2F_4)]^{1/2}}{I_a^{1/2}} \qquad (2)$$

where $R(X)$ is the rate of reaction X, $\Phi(X)$ is the quantum yield of production of X, and I_a is the absorbed intensity. The rate constant ratio k_d/k_c can be estimated from eq 1 and the fact that the upper limiting value of $\Phi(\text{cyclo-}C_3F_6)$ is 0.6 with 500 mm of C_2F_4 at both temperatures. Thus, k_d/k_c is found to be 5×10^{-3} mm^{-1}, which is in good agreement with an earlier estimate of 4×10^{-3} mm^{-1} at 175°.[3] Using the value of 5×10^{-3} mm^{-1} for k_d/k_c permits us to calculate the quantities on both sides of eq 2 from the data in Tables I and II. For the runs in the absence of O_2, the appropriate quantities are plotted in Figure 1. For low values of the coordinates, the log–log plots are linear with slope unity at both temperatures. However, the intercept is higher at the elevated temperature. For large values of the abscissa, the ordinate levels off at 2.0. Thus, the predictions of eq 1 and 2 are fulfilled.

Comparable studies have been made previously,[3,9] and those results are indicated in Figure 1 by solid lines. Saunders' experiments were performed in an X-shaped cell at 24°, and the results agree exactly with ours. On the other hand, Cohen and Heicklen's experiments were performed in a cylindrical cell, and the results lie above ours at both temperatures. The apparent discrepancy is easily explained because the abscissa is an intensity-dependent function. In our calculations, we have assumed a uniform intensity throughout the cell, when in fact the ultraviolet radiation was absorbed nonuniformly in the stem of the T-shaped cell. Therefore, the effective absorbed intensity in Saunders' and in our experiments was greater than the average intensity, and the points lie below those of Cohen and Heicklen. A further corroboration of this point is achieved from a careful examination of the data points. The points at the higher pressures (where diffusion is slower and the effective absorbed intensity is larger) lie slightly below the straight-line extension of those at lower pressures. The more accurate value of $k_f/k_g^{1/2}$ is that obtained from Cohen and Heicklen's data where the radical concentration is more nearly uniform; even those values may be slightly low.

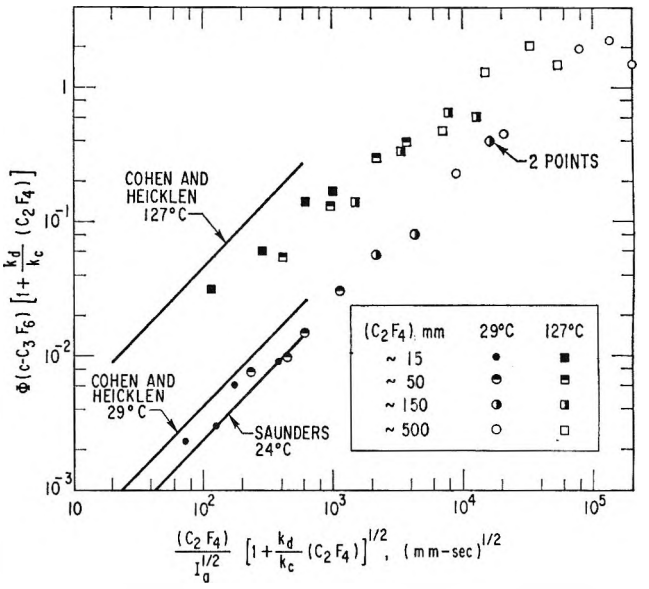

Figure 1. Log–log plots of $\Phi(\text{cyclo-}C_3F_6)[1 + (k_d/k_c)(C_2F_4)]$ in the absence of O_2 *vs.* $(C_2F_4) \times [1 + (k_d/k_c)(C_2F_4)]^{1/2}/I_a^{1/2}$ at 29 and 127°.

In the presence of O_2, additional reactions occur. In the first place, the excited mercury atom can transfer its energy to O_2

$$Hg^* + O_2 \longrightarrow Hg + O_2^* \qquad (h)$$

A summary of all the evidence indicates that O_2^* is the $c^1\Sigma_u^-$ electronic state of O_2.[10] The excited molecule must contain sufficient energy to react with an unexcited O_2 and produce O_3 and oxygen atoms some of the time. Furthermore, the spin conservation rules predict that a singlet level be formed. The $c^1\Sigma_u^-$ state is the only state that meets both requirements. Additional supporting evidence has been obtained in this laboratory,[11,12] where it has been shown that O_2^* transfers its energy to C_3F_6 to form an electronically excited molecule (presumably a triplet). The spin rules and energetic considerations favor the $c^1\Sigma_u^-$ state for O_2^*. The present study with C_2F_4 further supports this hypothesis.

The electronically excited oxygen can transfer its energy to C_2F_4

$$O_2^* + E \longrightarrow O_2 + E_m^* \ (\leq 104 \text{ kcal/mole}) \qquad (i)$$

where the subscript m refers to less vibrational energy than the subscript n. Two other reactions of O_2^* are possible

(9) D. Saunders, unpublished work of this laboratory, 1964.
(10) D. Volman, *Advan. Photochem.*, 1, 43 (1963).
(11) J. Heicklen and V. Knight, *J. Phys. Chem.*, 69, 3641 (1965).
(12) J. Heicklen and T. Johnston, to be published.

$$O_2^* + O_2 \longrightarrow \text{products}$$

$$O_2^* + E \longrightarrow CF_2O,\ C_2F_4O$$

In these studies we kept the $(O_2)/(C_2F_4)$ ratio below unity. Under these conditions, the results of ref 2 indicate that the first reaction is negligible compared to reaction i. The second reaction cannot be important, for if it were, the rates of formation of the oxidation products would not fall off with diminishing C_2F_4 pressure. The results of ref 2 clearly establish the falloff.

The initially formed vibronically excited molecule behaves like E_n^*

$$E_m^* \longrightarrow 2CF_2^1 \qquad (j)$$

$$E_m^* + E \longrightarrow E_0^* + E \qquad (l)$$

For both reactions d and l, C_2 has been excluded as a deactivating gas for simplicity. Such a simplification is justified because $(O_2)/(C_2F_4)$ was kept below unity, and O_2 is surely a much less efficient deactivator than C_2F_4.

The vibrationally inactive molecule E_0^* can react with oxygen

$$E_0^* + O_2 \longrightarrow CF_2O_2 + CF_2^1 \qquad (m)$$

Reaction m must produce singlet CF_2 radicals in order to keep the cyclo-C_3F_6 yield from falling in the presence of O_2. Triplet CF_2 radicals would be scavenged by O_2,[13] and are thus ruled out. The alternate reaction

$$E_0^* + O_2 \longrightarrow CF_2O,\ C_2F_4O$$

may play some role, but it cannot be important. If it were, Φ(cyclo-C_3F_6) should fall markedly when O_2 is added, contrary to fact.

The CF_2O_2 radicals have been shown to react *via*[8]

$$CF_2O_2 + C_2F_4 \longrightarrow 2CF_2 + CF_2^3 \xrightarrow{O_2} CF_2O_2 \qquad (n)$$

$$CF_2O_2 + C_2F_4 \longrightarrow CF_2O + C_2F_4O \qquad (o)$$

$$2CF_2O_2 \longrightarrow 2CF_2O + O_2 \qquad (p)$$

Under our conditions here, where (O_2) is greater than 15 mm, the triplet CF_2 radicals are always scavenged by O_2.[8] Two other reactions that need to be considered in this system are

$$CF_2^1 + CF_2O_2 \longrightarrow 2CF_2O \qquad (q)$$

$$CF_2^1 + CF_2O_2 \longrightarrow C_2F_4 + O_2 \qquad (r)$$

The oxidation mechanism predicts that

$$\theta = \frac{k_j}{k_1}(E)^{-1} \qquad (3)$$

where θ is defined as

$$\theta \equiv \left\{\left[\Phi(CF_2O) - \frac{2k_n}{k_o}\Phi(C_2F_4O)\right]\left[1 + \frac{k_h}{k_b}\frac{(O_2)}{(E)}\right] \times \left[1 + \frac{k_e(E)}{k_m(O_2)}\right] - \alpha\right\}^{-1} \frac{k_h}{k_b}\frac{(O_2)}{(E)} - 1 \qquad (4)$$

The quantity α is the fraction of E_n^* which is deactivated to E_f^* and is

$$\alpha \equiv \frac{k_d(E)/k_c}{1 + k_d(E)/k_c} \qquad (5)$$

It can be calculated from the known value of k_d/k_c of 5×10^{-3} mm^{-1}, and the values are listed in Tables I and II. The ratio k_h/k_b can be obtained from data already in the literature. The ratio of the rate constants for Hg* quenching by O_2 and N_2O has been found to be 1.00 by Yarwood, Strausz, and Gunning,[14] although Calvert and Pitts[15] report a value of 1.26. The relative rate constants for Hg* quenching by C_2F_4 and N_2O have been reported to be 0.31,[5] 0.35,[16] 0.36,[17] and 0.43.[18] We use 1.00 and 0.35, respectively, for the two ratios and obtain a value of k_h/k_b of 2.8. The value for k_e/k_m is more elusive. However, by fitting our data, we estimate an approximate value of 0.08.

For the data obtained in this study, it is necessary to subtract two similar numbers to obtain θ. Thus, the errors are very large. However, in the work of ref 2 at low C_2F_4 pressures, more accurate values can be obtained for θ. Furthermore, in that work a number of simplifications exist: α is negligibly small; $k_h(O_2)/k_b(E) >> 1.0$; $k_e(E)/k_m(O_2) << 1.0$; and $\Phi(C_2F_4O) << \Phi(CF_2O)$. The analytical scheme used in that work quantitatively converted the oxidation products to CO_2. Since $\Phi(C_2F_4O) << \Phi(CF_2O)$, the CO_2 production can be equated with CF_2O production, and eq 3 reduces to

$$[\Phi(CO_2)]^{-1} - 1 = \frac{k_j}{k_1}(E)^{-1} \qquad (6)$$

In the Heicklen, Knight, and Greene study,[2] quantum

(13) J. Heicklen, N. Cohen, and D. Saunders, *J. Phys. Chem.*, **69**, 1774 (1965).

(14) A. J. Yarwood, O. P. Strausz, and H. E. Gunning, *J. Chem. Phys.*, **41**, 1705 (1964).

(15) J. G. Calvert and J. N. Pitts, Jr., "Photochemistry," John Wiley and Sons, Inc., New York, N. Y., 1966, p 74.

(16) B. de B. Darwent, M. K. Phibbs, and F. G. Hurtubise, *J. Chem. Phys.*, **22**, 859 (1954).

(17) M. G. Bellas, Y. Rousseau, O. P. Strausz, and H. E. Gunning, *ibid.*, **41**, 768 (1964), as quoted in ref 14.

(18) A. R. Trobridge and K. R. Jennings, *Proc. Chem. Soc.*, 335 (1964).

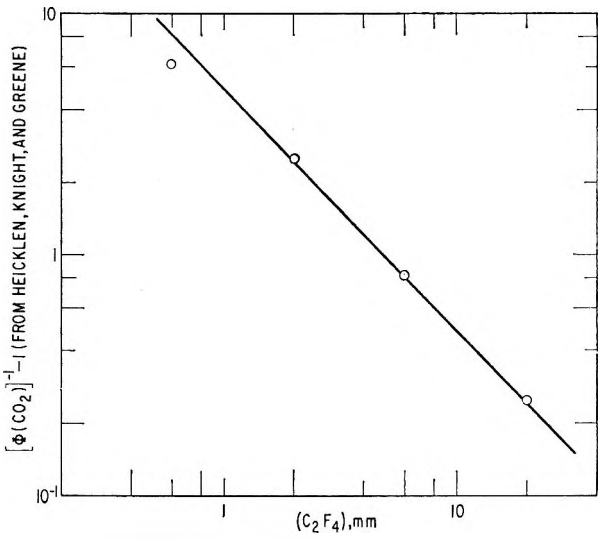

Figure 2. Log–log plot of $[\Phi(CO_2)]^{-1} - 1$ *vs.* (C_2F_4) at 23°.

yields were not reported because the absorbed intensity was not known. With 60 mm of C_2F_4 and excess O_2, $\Phi(CF_2O)$ should be near unity. Thus if we assume $\Phi(CO_2)$ is 1.2 (to allow for some C_2F_4O formation), then the absorbed intensity and the quantum yield can be calculated. To check this assumption, this value of I_a and the rates of cyclo-C_3F_6 formation were used to calculate $k_f/k_g^{1/2}$. The value thus obtained corresponds exactly to that from this study.

Figure 2 is a plot of $[\Phi(CO_2)]^{-1} - 1$ *vs.* the C_2F_4 pressure based on the data of ref 2. The log–log plot is linear with a slope of -1.0 and yields a value of 5.0 mm of k_j/k_1. The rate constants for energy removal k_d and k_1 probably correspond to the collision frequency and therefore are similar. Thus, k_c/k_j is about 40, a result to be expected since E_n^* has about 10 kcal/mole more energy than E_m^*.

From the rate constant information we now have, we can compute three more important quantities

$$\beta \equiv \frac{k_1(E)/k_j}{1 + k_1(E)/k_j} \tag{7}$$

$$\gamma \equiv \frac{\alpha + \beta k_h(O_2)/k_b(E)}{1 + k_h(O_2)/k_b(E)} \tag{8}$$

$$\psi \equiv \frac{\gamma}{1 + k_e(E)/k_m(O_2)} \tag{9}$$

where β is the fraction of E_m^* deactivated to E_0^*, γ is the quantum yield of E_0^* production, and ψ is the quantum yield of CF_2O_2 production. Values for these three quantities are listed in Tables I and II.

The quantum yield of production of CF_2^1 is $2(1 - \gamma) + \psi$, which is always larger than ψ, the quantum yield of CF_2O_2 production. Therefore, when CF_2 radicals are removed primarily by radical–radical reactions, reaction g must play some role, no matter how fast reactions q and r are. For the pertinent conditions in our experiments, CF_2^1 is always produced at least 50% faster than CF_2O_2, and in some cases, three times as fast. Thus, it is safe to make the simplification that CF_2^1 removal by reactions q and r is unimportant compared to removal by reaction g without introducing much error. A steady-state treatment leads to the following results: at high $(C_2F_4)/I_a^{1/2}(1 - \gamma + \psi/2)^{1/2}$ where $R(f) > R(g) + R(q) + R(r)$

$$\frac{\Phi(\text{cyclo-}C_3F_6)}{1 - \gamma + \psi/2} = 2.0 \tag{10}$$

At low $(C_2F_4)/I_a^{1/2}[1 - \gamma + \psi/2]^{1/2}$ where $R(g) > R(f)$

$$\frac{\Phi(\text{cyclo-}C_3F_6)}{1 - \gamma + \psi/2} = \frac{k_f}{k_g^{1/2}} \frac{(C_2F_4)}{I_a^{1/2}(1 - \gamma + \psi/2)^{1/2}} \qquad [R(g) > R(q) + R(r)] \tag{11}$$

The appropriate quantities from eq 10 and 11 are plotted in Figure 3. Equations 10 and 11 are analogous to eq 1 and 2, respectively. For low values of the abscissa, the log–log plots should be linear with unit slope and an intercept of $k_f/k_g^{1/2}$, whereas at high values of the abscissa, the ordinate should approach 2.0. It is clear that Figure 3 follows the expected behavior. The lines that best fit the data points from Figure 1 in the absence of O_2 are shown in Figure 3. The remarkable agreement is gratifying.

Let us now consider the oxidation products. At high C_2F_4 pressures and low radical concentrations, CF_2O_2 is removed principally by reaction o, whereas for the reverse conditions, removal is primarily by reactions p, q, and r. Then the steady-state analysis leads to: at high $(C_2F_4)/(I_a\psi)^{1/2}$ or $(C_2F_4)/I_a^{1/2}(1 - \gamma + \psi/2)^{1/2}$, where $R(o) > R(p) + R(q) + R(r)$

$$\frac{\Phi(CF_2O)}{\psi} = 1 + \frac{2k_n}{k_o} \tag{12}$$

$$\frac{\Phi(C_2F_4O)}{\psi} = 1.0 \tag{13}$$

At low $(C_2F_4)/(I_a\psi)^{1/2}$, where $R(p) > R(o)$

$$\frac{\Phi(CF_2O)}{\psi} = 1.0 \qquad [R(p) > R(q) + R(r)] \tag{14}$$

$$\frac{\Phi(C_2F_4O)}{\psi} = \frac{k_o}{(2k_p)^{1/2}} \frac{(C_2F_4)}{(I_a\psi)^{1/2}} \qquad [R(p) > R(q) + R(r)] \tag{15}$$

At low $(C_2F_4)/I_a^{1/2}(1 - \gamma + \psi/2)^{1/2}$, where $R(q) + R(r) > R(o)$, we have relationships 16 and 17

$$\frac{\Phi(CF_2O)}{\psi} = \frac{2k_q}{k_q + k_r} \qquad [R(q) + R(r) > R(p)] \quad (16)$$

$$\frac{\Phi(C_2F_4O)}{\psi} = \frac{k_o k_g^{1/2}}{(k_q + k_r)} \frac{(C_2F_4)}{I_a^{1/2}(1 - \gamma + \psi/2)^{1/2}} \qquad [R(q) + R(r) > R(p)] \quad (17)$$

Equations 14 through 17 are all based on the already justified simplification that $R(g) > R(p)$. For eq 14 and 15, reactions q and r have been neglected in the steady-state assumption, whereas in eq 16 and 17, reaction p has been neglected in the steady-state assumption. It was necessary to do this to make the expressions tractable. As shall be seen, neither assumption is justified, and reactions p, q, and r play competing roles.

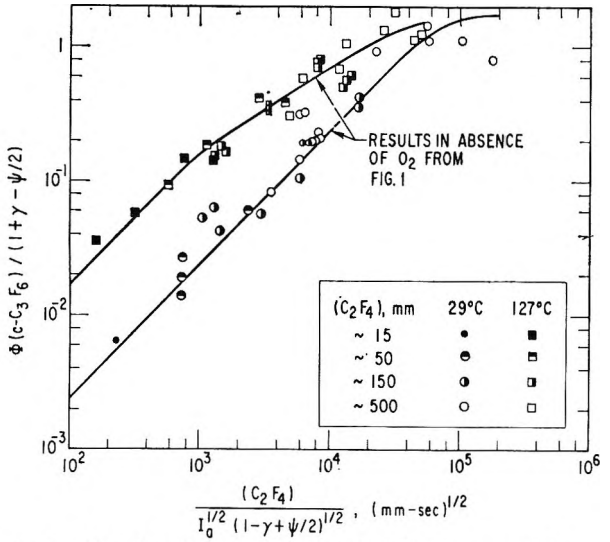

Figure 3. Log–log plots of Φ(cyclc-C_3F_6)/(1 + γ − ψ/2) in the presence of O_2 *vs.* $(C_2F_4)/I_a^{1/2} \times (1 - \gamma + \psi/2)^{1/2}$ at 29 and 127°.

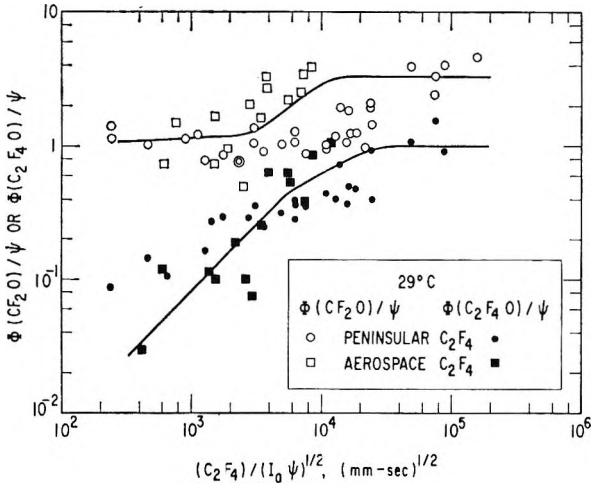

Figure 4. Log–log plots of $\Phi(CF_2O)/\psi$ and $\Phi(C_2F_4O)/\psi$ *vs.* $(C_2F_4)/(I_a\psi)^{1/2}$ at 29°.

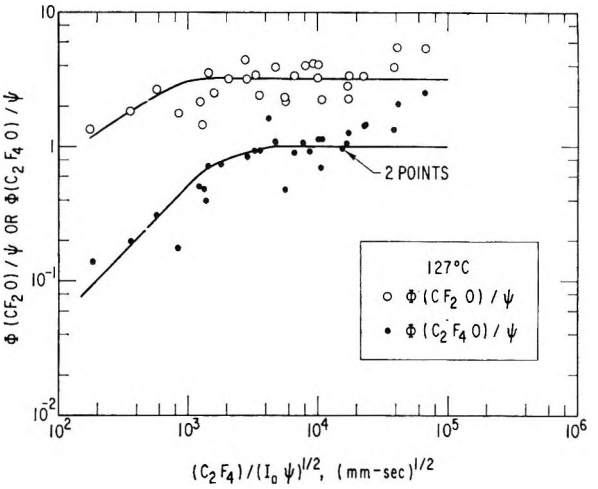

Figure 5. Log–log plots of $\Phi(CF_2O)/\psi$ and $\Phi(C_2F_4O)/\psi$ *vs.* $(C_2F_4)/(I_a\psi)^{1/2}$ at 127°.

Figures 4 and 5 present plots of $\Phi(CF_2O)/\psi$ and $\Phi(C_2F_4O)/\psi$ *vs.* $(C_2F_4)/(I_a\psi)^{1/2}$. The data are badly scattered, but the trends predicted by eq 12 through 15 are evident The large scatter can be attributed to three causes. First, the experimental determination of C_2F_4O for $\Phi(C_2F_4O)$ less than 0.1 is extremely difficult because of the low intensity of the 6.22-μ band of C_2F_4O and the inhibition of C_2F_4O as products accumulate. An experimental error of a factor of 2 is not unlikely. Second, the points which deviate most from the curves are those corresponding to low values of ψ, where the correction factors are of most importance. This is particularly true at high $(C_2F_4)/(I_a\psi)^{1/2}$. Finally, some of the scatter can be attributed to the fact that reactions q and r were neglected in the analysis. Nevertheless, estimates of appropriate rate constant ratios can be made.

From the figures and eq 12, k_n/k_o is found to be about 1.1 at both temperatures. In a study of the reaction of oxygen atoms with C_2F_4 in the presence of O_2,[8] k_n/k_o was found to be 1.1 at 125° and 0.55 at 23°. In that study, the room temperature value was computed by subtracting two similar numbers, so that the uncertainty was large. In view of the scatter in this study, the agreement between the two studies is quite satisfactory.

From Figures 4 and 5 and eq 15, a lower limit to $k_o/k_p^{1/2}$ can be found. The intercept of the portion of the C_2F_4O curve with unit slope gives a lower limit of $k_o/(2k_p)^{1/2}$. That this is a lower limit is due to the neglect of reactions q and r. Thus $k_o/k_p^{1/2} \geq 1.1 \times 10^{-4}$ (mm sec)$^{-1/2}$ at 29° and $\geq 7.0 \times 10^{-4}$

Table III: Rate Constant Data

Ratio	Value	Units	Source	Comments
k_d/k_c	5×10^{-3}	mm^{-1}	Eq 1	From upper limit of Φ(cyclo-C_3F_6)
	100	M^{-1}	Eq 1	From upper limit of Φ(cyclo-C_3F_6)
	100	M^{-1}	Ref 3	...
k_b/k_b	2.8	None	Ref 5, 14–18	See Discussion
k_e/k_m	~0.08	None	...	Best fit of data
k_j/k_l	5.0	mm	Eq 6, Figure 2	From data of ref 2
	2.2×10^{-4}	M	Eq 6, Figure 2	From data of ref 2
k_n/k_o	1.1	None	Eq 12, Figures 4, 5	...
	1.1[a]	None	Ref 8	...
	0.55[b]	None	Ref 8	...
$k_o/k_p^{1/2}$	$\geq 1.1 \times 10^{-4}$[c]	$(mm\ sec)^{-1/2}$	Eq 15, Figure 4	...
	≥ 0.015[c]	$(M\ sec)^{-1/2}$	Eq 15, Figure 4	...
	≥ 0.098[b]	$(M\ sec)^{-1/2}$	Ref 8	...
	$\geq 7.0 \times 10^{-4}$[d]	$(mm\ sec)^{-1/2}$	Eq 15, Figure 5	...
	≥ 0.11[d]	$(M\ sec)^{-1/2}$	Eq 15, Figure 5	...
	~0.2[a]	$(M\ sec)^{-1/2}$	Ref 8	...
k_q/k_r	~1	None	Eq 16, Figures 4, 5	...
$k_o k_g^{1/2}/(k_q + k_r)$	$\geq 0.8 \times 10^{-4}$[c]	$(mm\ sec)^{-1/2}$	Eq 17, Figure 6	...
	≥ 0.011[c]	$(M\ sec)^{-1/2}$	Eq 17, Figure 6	...
	$\geq 6.0 \times 10^{-4}$[d]	$(mm\ sec)^{-1/2}$	Eq 17, Figure 6	...
	≥ 0.095[d]	$(M\ sec)^{-1/2}$	Eq 17, Figure 6	

[a] At 125°. [b] At 23°. [c] At 29°. [d] At 127°.

$(mm\ sec)^{-1/2}$ at 127°. The values found for this ratio in ref 8 were 7.2×10^{-4} and about 13×10^{-3} $(mm\ sec)^{-1/2}$ at 23 and 125°, respectively. Thus the lower limits found here lie close to but below those found previously. The obvious conclusion is that reactions c and r play an important role in the mechanism.

If we ignore reaction p, then the importance of (q) and (r) can be estimated from eq 16 and 17 and Figure 6. If (p) is negligible, then k_q should be similar to k_r to satisfy (16) and the fact that $\Phi(CF_2O)/\psi$ approaches a lower limit of unity. However, since (p) is not negligible, this conclusion is quite crude.

Figure 6 is log–log plot based on eq 17. The scatter in the data is similar to that in Figures 4 and 5 for similar reasons [reaction p neglected rather (q) and (r)]. From the intercepts of the portion of the curves with unit slope, a lower limit to $k_o k_g^{1/2}/(k_q + k_r)$ can be estimated. Again, only a lower limit is obtained because reaction p was neglected. Thus $k_o k_g^{1/2}/(k_q + k_r) \geq 0.8 \times 10^{-4}$ $(mm\ sec)^{-1/2}$ at 29° and $\geq 6.0 \times 10^{-4}$ $(mm\ sec)^{-1/2}$ at 127°.

Finally, we wish to comment on the absence in this system of the branched-chain mechanism or the marked acceleration that was observed at 125° in our study of the reaction of oxygen atoms with C_2F_4 in the presence of O_2. It seems to us that this discrepancy reflects a temperature difference in the two systems, even though both high temperatures are reported to be the same. The two studies were done in different vacuum systems with different reaction cells. The thermocouple was placed at the intersection of the stem

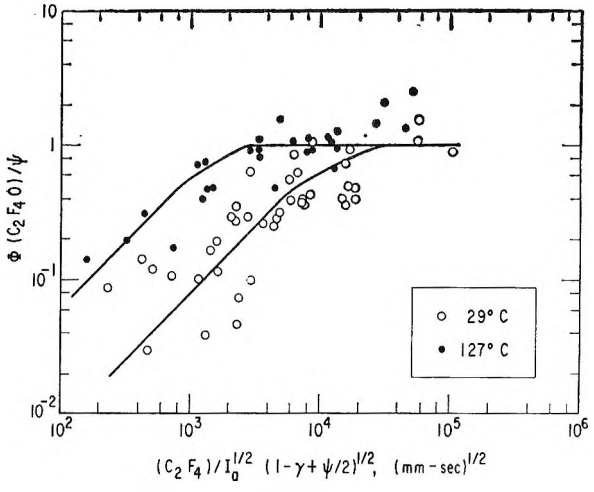

Figure 6. Log–log plots of $\Phi(C_2F_4O)/\psi$ *vs.* $(C_2F_4)/I_a^{1/2}(1 - \gamma + \psi/2)^{1/2}$ at 29 and 127°.

and the cross. However, most of the reaction occurs near the stem window, and perhaps the temperature there was several degrees higher in our previous study or several degrees lower in this study, or both. The branched-chain step should be markedly temperature dependent, and a temperature difference of several degrees could have a profound effect. The supposition that the effective temperature was less than 127° in this study is supported by an examination of the cyclo-C_3F_6 data. As explained earlier, our results in Figure 1 should lie below those of Cohen and Heicklen[3] because of the differences in cell shape in the respective systems. However, at room temperature, our results are only 30% below Cohen and Heicklen's, whereas at 127° they are almost a factor of 2.5 lower. This excessive lowering would be expected if in fact the effective temperature in this study were less than 127°. Fortunately, all other rate constants are nearly temperature independent. Thus, even if the high temperatures are somewhat in error, the effect on those rate constants would be negligible.

V. Summary

A reasonable and consistent mechanism is given by reactions a through r. A number of rate constant ratios could be ascertained, and they are tabulated in Table III along with literature values where available. The ratios obtained all seem reasonable and compare favorably with previous estimates.

Acknowledgment. The authors wish to thank Mr. Dennis Saunders for preparation of the Aerospace C_2F_4 and Mrs. Barbara Peer for assistance with the manuscript. This research was supported by the U. S. Air Force under Contract No. AF 04(695)-669.

The Surface Tension and Density of Binary Hydrocarbon Mixtures: Benzene–*n*-Hexane and Benzene–*n*-Dodecane

by Raymond L. Schmidt, James C. Randall, and H. Lawrence Clever

Department of Chemistry, Emory University, Atlanta, Georgia 30322 *(Received June 21, 1966)*

The surface tension and density of benzene–*n*-hexane and benzene–*n*-dodecane mixtures were determined over the full composition range at temperatures of 25, 30, 35, and 40°. The Guggenheim ideal and regular solution equations, the Hildebrand and Scott ideal equation for molecules of different size, and the Eckert and Prausnitz cell model equation have been tested with the benzene–*n*-hexane system. The cell model equation is best for this system. The Hildebrand and Scott equation has been further tested by fitting it to the experimental surface tension of six binary hydrocarbon systems by varying one surface area per molecule and comparing the fit area with a calculated surface area per molecule assuming spherical molecules. The density data have been used to calculate the excess volume of mixing, which is more temperature dependent for the benzene–*n*-hexane system than for the benzene–*n*-dodecane system.

Gibbs enrichment of a binary mixture surface by the component of lower surface tension is well known. The normal result is a lowering of the mixture surface tension which results in a negative deviation from a linear function of bulk mole fraction.

Many attempts to explain the surface tension of a binary nonelectrolyte mixture have been made. Semiempirical ideal and regular solution equations were developed by Schuchowitzky[1] and by Belton and Evans.[2] Guggenheim,[3] using a quasicrystalline model, has derived equations for ideal and regular solutions. Hildebrand and Scott[4] have extended the Guggenheim ideal equation to mixtures of molecules of different size. Bellemans and Stecki[5] point out that it is not necessary to specify layers in which the "surface" and bulk phases differ in composition, and they derive an equation identical with Guggenheim's regular solution equation through second-order terms. Englert-Chwoles and Prigogine[6] use a cell model with an averaged interaction potential to obtain an expression for a binary mixture surface tension. Eckert and Prausnitz[7] apply a grand partition function to a cell model of the liquid–vapor interface and obtain an expression for the surface tension that works well for simple cryogenic liquid mixtures.[8] Eberhart[9] has shown that the surface tension–composition isotherms of many binary systems can be fit by a function which is linear in surface composition.

This work was initiated to test the applicability of the available theories for surface tension to binary hydrocarbon mixtures.

Experimental Section

Materials. The hydrocarbons were Phillips Petroleum pure grade (99 mole %). They were shaken with concentrated H_2SO_4, water-washed until neutral, and dried over metallic sodium. The benzene was distilled through a 50-plate spinning band column, the *n*-hexane was distilled through a 20-plate packed col-

(1) A. Schuchowitzky, *Acta Physicochim. URSS*, **19**, 176 (1944).

(2) J. W. Belton and M. G. Evans, *Trans. Faraday Soc.*, **41**, 1 (1945).

(3) E. A. Guggenheim, "Mixtures," Oxford University Press, London, 1952, Chapter 9.

(4) J. H. Hildebrand and R. L. Scott, "Solubility of Nonelectrolytes," 3rd ed, Reinhold Publishing Corp., New York, N. Y., 1950, Chapter 21.

(5) A. Bellemans and J. Stecki, *Mol. Phys.*, **3**, 203 (1960).

(6) A. Englert-Chwoles and I. Prigogine. *Nuovo Cimento*, **9**, Suppl. 1, 347 (1958).

(7) C. A. Eckert and J. M. Prausnitz, *A.I.Ch.E. J.*, **10**, 677 (1964).

(8) F. B. Sprow and J. M. Prausnitz, *Trans. Faraday Soc.*, **62**, 1105 (1966).

(9) J. G. Eberhart, *J. Phys. Chem.*, **70**, 1183 (1966).

umn, and the *n*-dodecane was purified in 10-ml lots by passage through a preparative gas chromatograph with column temperature about 10° above the dodecane normal boiling point. The purified samples were stored over metallic sodium until used. Boiling points and refractive indices checked well with accepted values.[10]

Surface Tension. Surface tensions were measured by the maximum bubble-pressure technique on an apparatus built and described by Quayle.[11]

The bubbler was calibrated with highly purified samples of benzene and *n*-octane. The hydrocarbon mixtures were prepared by weight. The surface tension bubbler air was presaturated with vapor from the mixture being measured to prevent evaporation losses and cooling of the surface during the measurement.

The temperature was controlled to ±0.05° at 25, 30, 35, and 40° for the surface tension and density measurements. Temperatures were measured on a thermometer calibrated against an NBS certified thermometer.

Density. Mixture densities were determined in a Sprengel–Ostwald type 5-ml pycnometer previously calibrated with freshly boiled distilled water.

Discussion and Results

The surface tensions and densities are given in Table I and the surface tensions in Figure 1 as functions of temperature and composition. Figure 2 shows the benzene–*n*-hexane excess surface tension, calculated from $\sigma^E = \sigma - (X_1\sigma_1 + X_2\sigma_2)$, at 25°. σ is the solution surface tension, σ_1 and σ_2 the pure liquid surface tensions, and X_1 and X_2 the respective bulk mole fractions. The figure compares experimental with calculated excess surface tensions obtained from several theoretical equations. All of the theoretical approaches require a surface area per molecule and this has been calculated from the two-thirds power of the pure liquid molar volume assuming a spherical molecule. The areas are 28.03 and 36.28 A²/molecule for benzene and *n*-hexane, respectively.

Guggenheim's[3] symmetrical, single-parameter equation for the surface tension of an ideal mixture of compounds with molecules of similar size and shape and his regular solution equation can seldom be fit to surface tension data with physically meaningful size parameters and interaction energies.[12-14] Figure 2 shows the excess surface tension calculated from the Guggenheim ideal equation using the average surface area of 32.15 A²/molecule and from the regular equation assuming a close packed lattice, 32.15 A²/molecule, and an interaction energy of 141 × 10^{-16} ergs/molecular pair. The interaction energy was obtained from the benzene–*n*-hexane heat of mixing at 20°.[15] Both equations give the observed negative excess surface tension with the regular solution equation giving the better agreement with experiment. The Hildebrand and Scott[4] extension of Guggenheim's ideal solution equation to systems containing molecules of significantly different size is also tested in Figure 2. The equation for the mixture surface tension, σ, is

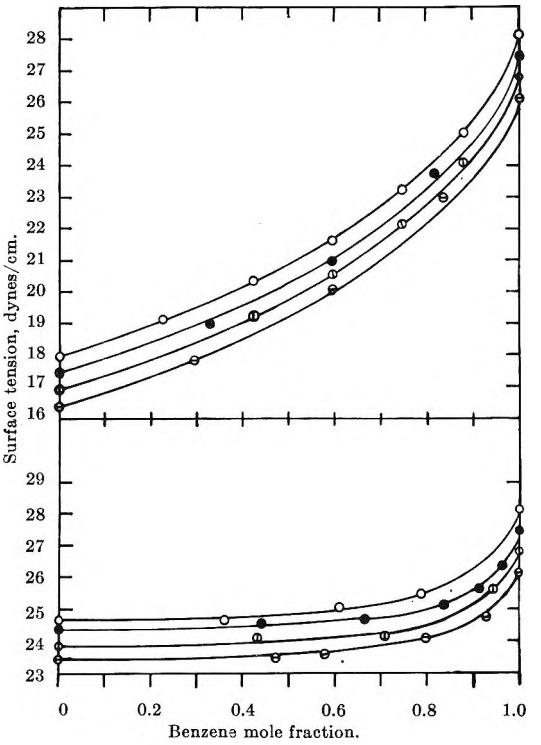

Figure 1. Surface tension *vs.* benzene mole fraction. Top, benzene–*n*-hexane: bottom, benzene–*n*-dodecane: O, 25°; ●, 30°; ⊙, 35°; and ⊖, 40°.

$$\sigma = Y_1\sigma_1 + Y_2\sigma_2 - \frac{(\sigma_1 - \sigma_2)^2}{2kT} \times (Y_1a_2 + Y_2a_1)Y_1Y_2 \quad (1)$$

where, in addition to terms defined above, Y_1 and Y_2 are surface area fractions given by $Y_i = X_ia_i/(X_1a_1 + X_2a_2)$, a_1 and a_2 are surface area per molecule, k is the

(10) F. D. Rossini, *et al.*, "Selected Values of Properties of Hydrocarbons," National Bureau of Standards Circular 461, U. S. Government Printing Office, Washington, D. C., 1947.

(11) O. R. Quayle, *Chem. Rev.*, 53, 439 (1953).

(12) H. L. Clever and W. E. Chase, *J. Chem. Eng. Data*, 8, 291 (1963).

(13) H. L. Clever and C. C. Snead, *J. Phys. Chem.*, 67, 918 (1963).

(14) H. B. Evans, Jr., and H. L. Clever, *ibid.*, 68, 3433 (1964).

(15) A. R. Mathieson and J. C. J. Thynne, *J. Chem. Soc.*, 3708 (1956).

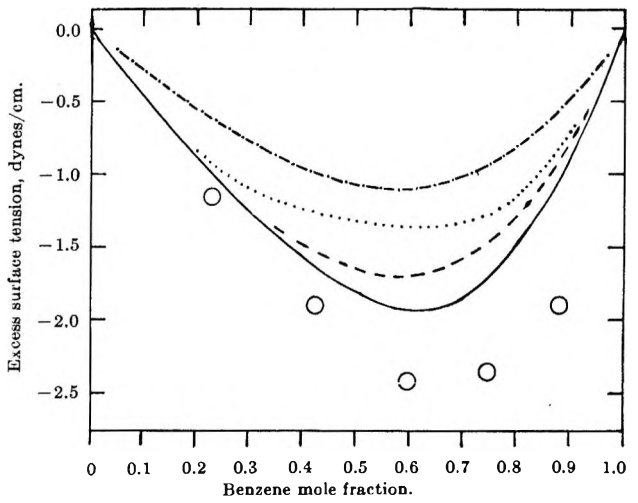

Figure 2. Benzene–*n*-hexane system, 25°. Excess surface tension *vs.* benzene mole fraction. O, experimental points; — · —, calculated from the Guggenheim ideal equation; . . . ., calculated from the Guggenheim regular equation; – – –, calculated from the Hildebrand and Scott equation; and ———, calculated from the Eckert and Prausnitz equation.

Boltzmann constant, and T is the absolute temperature. The agreement with experiment is fair.

Eckert and Prausnitz[7] have used the cell model of the liquid–vapor interface of a nonpolar liquid mixture to obtain an expression for the surface properties. The surface tension is expressed in terms of the surface composition, the pure component properties, and the activity coefficients of the bulk mixture by the equation

$$\sigma = Y_1'\sigma_1 + Y_2'\sigma_2 + Y_1'Y_2'\eta + \frac{kT}{X_1'a_1 + X_2'a_2} \times \left[X_1' \ln \frac{X_1'}{X_1\gamma_1} + X_2' \ln \frac{X_2'}{X_2\gamma_2}\right] \quad (2)$$

where in addition to the terms defined before

$$Y_i' = \frac{X_i'a_i}{X_1'a_1 + X_2'a_2}$$

X_1' and X_2' are surface mole fractions, γ_1 and γ_2 are the activity coefficients in the bulk phase, and η is the configurational energy density difference given by

$$\eta = C_1' + C_2' - 2\sqrt{C_1C_2}$$

C_i' is the surface configurational energy densities given by

$$C_i' = \frac{\Delta h_i^{vap} + (h_i^{id} - h_i^{sat}) - (RT - P_i^{sat}V_i)}{a_i} - \sigma_i + T\frac{d\sigma_i}{dT}$$

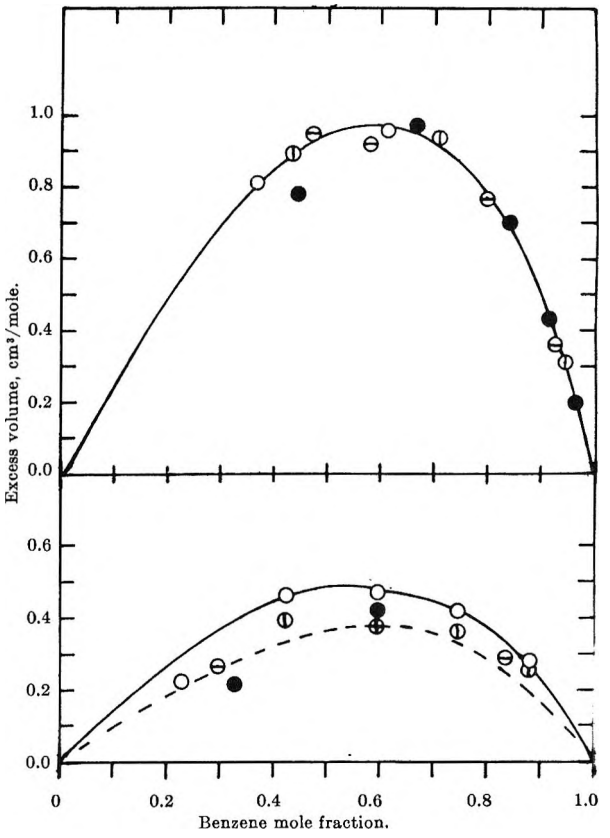

Figure 3. Excess volume *vs.* benzene mole fraction. Top, benzene–*n*-dodecane; bottom, benzene–*n*-hexane: O, 25°; ●, 30°; ⊙, 35°; and ⊖, 40°.

where Δh_i^{vap} is the enthalpy of vaporization of component i and superscripts id and sat refer to the ideal gas state and saturation condition, respectively.

The pure component data necessary to calculate the benzene–*n*-hexane surface tension from the Eckert and Prausnitz equation are given in Table II. The surface configurational energy density requires the enthalpy of vaporization[10,16] and the difference in the enthalpy of the ideal and real vapors at the saturation pressure. This difference was calculated from the second virial coefficients and from the temperature dependence of the second virial coefficients.[17] The surface tension and its temperature dependence were taken from the data in Table I. The bulk activity coefficients, at 20°, were taken from Christian, Neparko, and Aff-

(16) J. F. Connolly and G. A. Kandalic, *J. Chem. Eng. Data*, 7, 137 (1962).

(17) (a) G. N. Lewis and M. Randall, "Thermodynamics," revised by K. S. Pitzer and L. Brewer, McGraw-Hill Book Co., Inc., New York, N. Y., 1961, p 191; (b) H. G. David, S. D. Hamann, and R. B. Thomas, *Australian J. Chem.*, 12, 309 (1959); (c) G. A. Bottomley and C. G. Reeves, *J. Chem. Soc.*, 3794 (1958). The virial coefficients were fit with a third degree polynomial by the method of least squares.

Table I: Surface Tensions and Densities of Benzene–*n*-Hexane and Benzene–*n*-Dodecane Mixtures

	Benzene–*n*-hexane			Benzene–*n*-dodecane		
Temp, °C	Mole fraction benzene	*d*, g/ml	Surface tension, dynes/cm	Mole fraction benzene	*d*, g/ml	Surface tension, dynes/cm
25.0	0.0000	0.6548	17.94	0.0000	0.7452	24.69
	0.2274	0.6900	19.11	0.3604	0.7649	24.68
	0.4239	0.7248	20.36	0.6100	0.7887	25.03
	0.5955	0.7609	21.60	0.7869	0.8312	25.49
	0.7465	0.7974	23.22	1.0000	0.8737	28.15
	0.8803	0.8347	25.04			
	1.0000	0.8737	28.15			
30.0	0.0000	0.6503	17.43	0.0000	0.7417	24.31
	0.3293	0.7035	18.98	0.4404	0.7677	24.55
	0.5957	0.7563	20.97	0.6662	0.7916	24.68
	0.8154	0.8138	23.75	0.8384	0.8214	25.11
	1.0000	0.8683	27.48	0.9139	0.8402	25.66
				0.9620	0.8549	26.35
				1.0000	0.8683	27.48
35.0	0.0000	0.6459	16.90	0.0000	0.7383	23.85
	0.4239	0.7157	19.21	0.4330	0.7630	24.10
	0.5955	0.7517	20.56	0.7084	0.7934	24.16
	0.7465	0.7877	22.14	0.9432	0.8436	25.61
	0.8803	0.8244	24.10	1.0000	0.8629	26.81
	1.0000	0.8629	26.81			
40.0	0.0000	0.6413	16.38	0.0000	0.7349	23.42
	0.2959	0.6877	17.85	0 4732	0.7625	23.48
	0.5955	0.7467	20.05	0 5786	0.7731	23.58
	0.8375	0.8070	22.99	0 7987	0.8044	24.10
	1.0000	0.8575	26.14	0 9271	0.8341	24.75
				1 0000	0.8575	26.14

Table II: Parameters Used in the Calculation of the Benzene–*n*-Hexane Surface Tension at 25° from the Eckert and Prausnitz Equation

Property	Benzene	*n*-Hexane	Ref
Surface tension, dynes/cm	28.15	17.94	
Temp coeff of surface tension, dynes/cm-deg	−0.134	−0.104	
Surface area, A^2/molecule	28.03	36.28	
Saturation pressure, mm	95.133	151.25	10
Vol., cm^3/mole	89.41	131.61	
Enthalpy correction, $(h^{id} - h^{sat})$, cal/mole	14.61	53.18	16
Enthalpy of vaporization, cal/mole	8082.5	7540.0	10, 17

sprung[18] and used without temperature corrections to calculate the 25° surface tensions.

Of the equations tested, the Eckert and Prausnitz equation gives the best agreement with experiment (Figure 2). Considering that the equation was developed for simple cryogenic liquid mixtures, the agreement for the benzene–*n*-hexane system is satisfactory, showing a slightly skewed minimum at about the same mole fraction as the experimental data.

The Hildebrand and Scott equation has been further tested by fitting it to the experimental surface tension of the six binary hydrocarbon systems[12,14] listed in Table III. The test was made by comparing the fit area with a calculated area. The fit was accomplished by assuming component 2 to be preferentially adsorbed in the surface. The a_2/a_1 ratio was varied in eq 1 in a computer program until the best reproduction of the experimental data was obtained. The surface area per molecule of component 1 was calculated from the molar volume, and the surface area of component 2 was then determined from the best a_2/a_1 ratio.

The resulting size parameters, given in Table III, when substituted into eq 1 give an empirical equation which reproduces the experimental surface tension with an average deviation of less than 0.10 dyne/cm.

(18) S. D. Christian, E. Neparko, and H. E. Affsprung, *J. Phys. Chem.*, 64, 442 (1960).

Table III: Size Parameters: Hildebrand and Scott Equation, A^2 per Molecule[a]

Temp, °C	Ref component: Benzene	Second component: *n*-Hexane	Second component: *n*-Dodecane	Second component: 2,2,4-Trimethylpentane
25.0	28.03	46.54	221.5	
30.0	28.15	47.58	258.4	53.27
35.0	28.27	46.36	180.9	
40.0	28.39	46.27	227.1	
	Ref component: Cyclohexane	Second component: *n*-Hexane	Second component: 2,2,4-Trimethylpentane	
25.0	31.95	38.34		
30.0	32.08	38.49	51.32	
35.0	32.21	37.04		
	Ref component: *n*-Dodecane	Second component: 2,2,4-Trimethylpentane		
30.0	52.58	37.34		

[a] The surface area for the reference component was calculated from the molar volume assuming a spherical molecule. Surface areas for the second component gave the best fit of eq 1 to the experimental data. If spherical molecules were assumed for the second component, molar volumes would give a surface area of 36.28–36.79 A^2 for *n*-hexane, 42.50 A^2 for 2,2,4-trimethylpentane, and 52.42–52.91 A^2 for *n*-dodecane.

It is of interest to compare the best fit size parameters of component 2 in each mixture with the area calculated from the bulk molar volume assuming a spherical molecule. The best agreement is in the cyclohexane–*n*-hexane system, where fit and calculated areas differ by 6%. The best fit *n*-hexane area is 27% larger than calculated in the benzene–*n*-hexane system. The poor agreement between best fit and calculated surface area of *n*-dodecane in benzene mixtures is not surprising in view of the spherical molecule assumption. It would appear that the Hildebrand and Scott equation would be a good approximation to unknown surface tensions of mixtures of quasispherical molecules.

Excess volumes of mixing were calculated for these mixtures from the density data given in Table I. Gomez-Ibanez and Liu[19] have found that the excess volume of cyclohexane when mixed with *n*-dodecane and *n*-hexane is independent of temperature. Our data for benzene mixtures indicate that the excess volume of the benzene–*n*-dodecane system is independent of temperature, but that the benzene–*n*-hexane system is not. The data are not of sufficient accuracy to establish the magnitude of the temperature dependence for the benzene–*n*-hexane system, but the excess volume does decrease with increased temperature as expected. Gomez-Ibanez and Liu have also shown the magnitude of the excess volume to be related to *n*-paraffin chain length for cyclohexane–*n*-paraffin mixtures. Our results show that similar conclusions can be made for benzene–*n*-paraffin mixtures. The two systems reported here show positive deviation from ideal behavior with the *n*-dodecane deviation being about twice that for the *n*-hexane solutions. The extremum in the excess volume occurred at about the same mole fraction as the extremum in the excess surface tension. (See Figure 3.)

Acknowledgment. This work was initiated and supported in part by National Science Foundation Grant G 7357.

(19) J. Gomez-Ibanez and C. Liu, *J. Phys. Chem.*, 65, 2148 (1961).

The Osmotic Coefficients and Other Related Properties of Aqueous 12-Tungstosilicic Acid ($H_4W_{12}SiO_{40}$) at 25°[1]

by S. Y. Tyree, Jr., R. L. Angstadt, F. C. Hentz, Jr., R. L. Yoest, and George Scatchard

Department of Chemistry, University of North Carolina, Chapel Hill, North Carolina, and Department of Chemistry and Laboratory of Nuclear Science, Massachusetts Institute of Technology, Cambridge, Massachusetts
(Received June 21, 1966)

We have measured the osmotic coefficient, ϕ, of aqueous 12-tungstosilicic acid at 25° from 0.04 to 0.87 *m* by isopiestic (isotonic) comparison with KCl and with NaCl, and determined an analytic expression for it by which ln $\gamma_\pm$ and $\partial \ln \gamma_\pm / \partial \ln m$ may be computed. We have compared our results with earlier measurements of light scattering and ultracentrifuge equilibrium. We confirm the earlier findings that this acid is a typical highly ionized strong electrolyte.

12-Tungstosilicic acid ($H_4W_{12}SiO_{40}$), often called silicotungstic acid, is a very interesting substance. It is one of the few strong electrolytes known with one quadrivalent and four univalent ions, perhaps the only acid. However, the anion is large enough that the properties of its dilute solutions may be studied by light scattering or by equilibrium ultracentrifugation. The most concentrated solution for which we have measured the osmotic coefficient, though only 0.8725 *m*, contains 2.5 g of $H_4W_{12}SiO_{40}$ to 1.0 g of H_2O.

Kronman and Timasheff[2] have measured the light scattering of the sodium salt in dilute solution; Johnson, Kraus, and Scatchard[3] have measured both the light scattering and ultracentrifuge equilibrium of both the acid and the sodium salt; and Kerker, Kratohvil, Ottewill, and Matijević[4] have measured the light scattering of the acid up to higher concentrations.

The osmotic coefficients were measured by Angstadt from 0.05 to 0.8725 *m*. Since the measurements in dilute solution were not consistent with those of JKS by other methods, they were repeated by Hentz and in dilute solutions by Yoest.

Materials. The TSA studied at North Carolina was prepared by purifying J. T. Baker silicotungstic acid essentially by the method of Matijević and Kerker[5] but with additional steps. The acid was extracted six times from a very concentrated solution with HCl and ether. The ether was removed by pumping in a vacuum desiccator for 15 hr and the residue was left *in vacuo* over P_2O_5 for 2 days; then it was ground, dissolved in a small amount of distilled water, filtered through a medium-porosity glass filter, and evaporated to a small volume, with the temperature kept below the boiling point. The crystals which separated on cooling were removed by filtration and dried *in vacuo* over P_2O_5. The product was ground, recrystallized in the same way, dried for 4 days over Drierite, and ground to a fine powder.

The final material was very hygroscopic and was allowed to equilibrate with the atmosphere until it did not change in weight perceptibly in 1 or 2 hr. It then contained 4.5 to 5.5% water. For analysis it was dried to $H_4SiW_{12}O_{40}$ by heating to constant weight at 240–250°, and some samples were dried to $SiO_2 \cdot 12WO_3$ by igniting to constant weight at 700°.

The tungstosilicic acids studied at the Massachusetts

(1) Based on the Ph.D. Thesis of R. L. Angstadt, U.N.C., 1961, unpublished results of F. C. Hentz, Jr., University of North Carolina, 1961, and the Ph.D. Thesis of R. L. Yoest, Massachusetts Institute of Technology 1964.

(2) M. J. Kronman and S. N. Timasheff, *J. Phys. Chem.*, **63**, 629 (1959) (KT). Dr. Timasheff informs us that L. D. Cerankowski and S. N. Timasheff have taken up again the study of dilute solutions of TSA and find that with carefully purified material "the downturn at low concentration is not observed."

(3) J. S. Johnson, K. A. Kraus, and G. Scatchard, *ibid.*, **64**, 1697 (1960) (JKS).

(4) M. Kerker, J. R. Kratohvil, R. H. Ottewill, and E. Matijević, *ibid.*, **67**, 1097 (1963).

(5) M. Kerker and E. Matijević, *J. Am. Chem. Soc.*, **81**, 5560 (1959).

Institute of Technology were Baker and Adamson reagent grade and Fisher reagent grade silicotungstic acid used without further purification. They were taken from the same bottles as part of the material used for light scattering by JKS.

Procedures. The apparatus and procedure at North Carolina were the same as previously used there.[6] Triplicates of TSA were compared with triplicates of KCl to determine the isopiestic ratios. The quantities of solutes were determined by weighing the solids. To determine the moisture content of the TSA three other samples were exposed to the atmosphere at the same time and analyzed by drying to $H_4SiW_{12}O_{40}$ as above. Water was added to the cups, which were then placed in the isopot. This was evacuated to the vapor pressure of water stepwise, put into the bath, and rocked through angles of about 22° from the horizontal with constant stirring of the gas phase by a magnetic stirrer.

The apparatus and procedure used at the Massachusetts Institute of Technology were the same as previously used there[7] except that, because of the failure of the threads, the lead gasket was replaced by a rubber O ring which could be sealed by the weight of the cover and the atmospheric pressure. The quantity of solute in the cups was determined by using weighed amounts of stock solutions whose concentrations were determined by evaporating and drying to NaCl for the standard and to $SiO_2 \cdot 12WO_4$ for the TSA. Two cups were filled with each of the acids and two with NaCl. A few drops of water were put into the bottom of the bomb before each evacuation to help sweep out the air. Slow evacuation was attained by slowly doubling the volume of gas until the vapor pressure of water was reached, and then doubling it ten times more. The apparatus was then placed in the thermostat and rotated at an angle of 45°.

In both laboratories the concentration of the equilibrium solutions and the isopiestic ratio was obtained from the weight of the empty bottles, of the bottle plus solid or plus known stock solution, and of the bottle plus final solution.

Results

The osmotic coefficients of the TSA were computed from the isopiestic (isotonic) ratios and the equations of Lietzke and Stoughton[8] for the Robinson and Stokes osmotic coefficients of KCl and NaCl.[9,10]

The results are shown in Figure 1 as ϕ *vs.* $\sqrt{I}$ (= $\sqrt{10m}$), the circles and squares from the University of North Carolina, the triangles from the Massachusetts Institute of Technology. All the measurements are

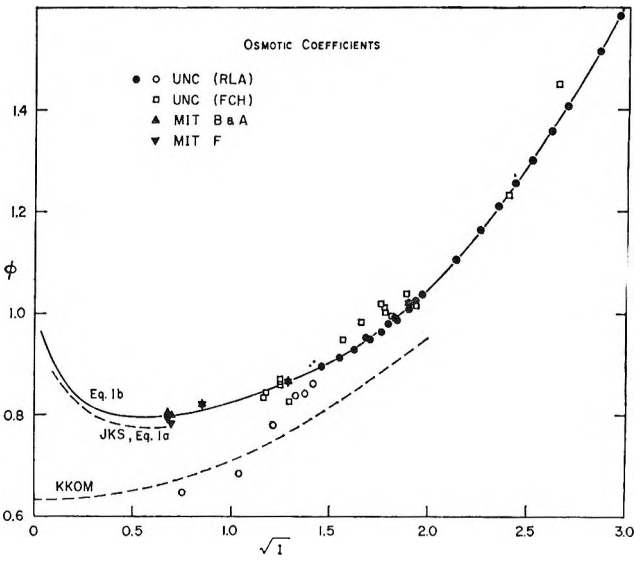

Figure 1. Osmotic coefficients.

exhibited except those few where disagreement between duplicates showed failure to attain equilibrium.

Discussion

We note first that the differences between the results for the two acids studied at the Massachusetts Institute of Technology are within the apparent experimental error. Those at $\sqrt{I} = 1.9$ agree excellently with the results from the University of North Carolina. At $\sqrt{I} = 1.3$ and at lower concentrations the agreement becomes progressively worse.

When expressed as a function of the molality of tungstosilicate ion the osmotic coefficient increases very rapidly, but when expressed as a function of the molality of hydrogen ion, which is probably a better comparison, the increase is about as rapid as that for HCl or that for $HClO_4$.

Several equations of the form

$$\phi = 1 - 4 \times 1.1710[1 + A\sqrt{I} - 1/(1 + A\sqrt{I}) - 2 \ln (1 + A\sqrt{I})]/A^3 I + BI + CI^2 + DI^3 \quad (1)$$

(6) C. S. Patterson, S. Y. Tyree, Jr., and K. Knox, *J. Am. Chem. Soc.* 77, 2195 (1955).

(7) G. Scatchard, W. J. Hamer, and S. E. Wood, *ibid.*, 60, 3061 (1938); G. Scatchard and R. G. Breckenridge, *J. Phys. Chem.*, 58, 596 (1954).

(8) M. H. Lietzke and R. W. Stoughton, *ibid.*, 66, 508 (1962).

(9) R. A. Robinson and R. W. Stokes, "Electrolyte Solutions," Academic Press Inc., New York, N. Y., 1955; R. A. Robinson and D. A. Sinclair, *J. Am. Chem. Soc.*, 56, 1830 (1934).

(10) Dr. R. M. Rush and Dr. J. S. Johnson of the Oak Ridge National Laboratory have very kindly made these computations for us and have computed several least-squares analytical expressions for them.

Table I: Parameters for Eq 1[10]

Eq	A	B	C	D	Std dev
1a	2.5	0[a]	0[a]	0[a]	
1b	2.690 ± 0.049	0.0061 ± 0.0044	0.0133 ± 0.0012	−0.000544 ± 0.000096	0.0062
1c	2.510 ± 0.047	0.0295 ± 0.0025	0.00627 ± 0.0003(	0[a]	0.0090
1d	2.570 ± 0.196	0.0125 ± 0.0125	0.0120 ± 0.0026	−0.00047 ± 0.00016	0.0044
1e	2.686 ± 0.084	−0.0005 ± 0.0075	0.0156 ± 0.0021	−0.00072 ± 0.00016	0.0108
1f	2.435 ± 0.065	0.031 ± 0.0039	0.00621 ± 0.0004[illegible]	0[a]	0.0137
1g	2.583 ± 0.121	0.0132 ± 0.0112	0.0126 ± 0.0031	−0.000549 ± 0.00024	0.0174
1h	2.388 ± 0.077	0.0372 ± 0.0048	0.00555 ± 0.00056	0[a]	0.0182

[a] Arbitrarily fixed. 1a from ultracentrifuge, JKS; 1b and 1c from black circles and triangles; 1d from black circles; 1e and 1f from black circles and triangles and three most concentrated open circles; 1g and 1h from black circles and triangles, three most concentrated open circles and open squares.

were determined by least squares to represent the measurements exhibited in Figure 1.[10] The values of the parameters are given in Table I. The full curve in Figure 1 represents eq 1b, determined from the triangles and full circles of Figure 1. None of the other equations differs from eq 1b by more than 0.01 at any concentration except for those with no cubic terms at the extreme concentrations. This is less than the diameters of the circles. We believe that eq 1b is the best representation of our measurements. The broken line labeled JKS, eq 1a in Figure 1, represents eq 1a, determined from ultracentrifuge measurements. The broken line labeled KKOM is determined from eq 6 and 7 of the paper of KKOM which lead to

$$-\partial \ln a_1/\partial c = \bar{V}_1 H c/\tau = \bar{V}_1(1.10 + 1.16c + 0.88c^2)10^{-3} \quad (2)$$

in which a_1 is the activity of water, $\bar{V}_1$ is its partial molal volume, c is the concentration of TSA is grams per milliliter, τ is the turbidity, and H is a parameter defined in that paper. Then

$$-\ln a_1 = \bar{V}_1 c(1.10 + 0.58c + 0.293c^2)10^{-3} = \bar{V}_1 \nu m \phi/1000 \quad (3)$$

in which νm is the stoichiometric number of moles of ions per kilogram of water. This equation will be discussed later.

The equations for $\ln \gamma_\pm$ and for $\partial \ln \gamma_\pm/\partial \ln I$ which correspond to eq 1 for the osmotic coefficient are

$$\ln \gamma_\pm = -\frac{4 \times 1.1710\sqrt{I}}{1 + A\sqrt{I}} + 2BI + {}^3/_2 CI^2 + {}^4/_3 DI^3 \quad (4)$$

$$\partial \ln \gamma_\pm/\partial \ln I = \frac{1}{I}\partial[I(\phi - 1)]/\partial \ln I = \frac{-4 \times 1.1710\sqrt{I}}{2(1 + A\sqrt{I})^2} + 2BI + 3CI^2 + 4DI^3 \quad (5)$$

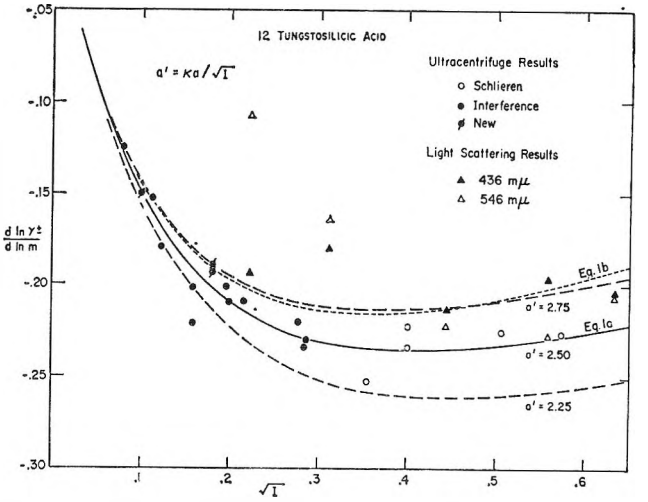

Figure 2. Ultracentrifuge equilibrium and light scattering (Johnson, Kraus, and Scatchard).

The first equality in eq 5 is determined by the Gibbs–Duhem relation. Equation 5 is used to relate ultracentrifuge equilibrium and light scattering to the osmotic coefficient.

Figure 2 is adapted from Figure 1 of the JKS paper by deleting the points for the sodium salt, by distinguishing more clearly between the measurements by the schlieren and by the interference method, by adding three results of the study by the interference method of TSA purified at the University of North Carolina, by adding the values of d ln $\gamma_\pm$/d ln I from the light-scattering measurements of JKS, and by adding a curve for $\partial \ln \gamma_\pm/\partial \ln I$ calculated from eq 5 with the parameters of eq 1b. This is of course beyond the range of the measurements from which the parameters were determined, except for unity at zero ionic strength.

Figure 3 is Figure 2 of KKOM with the addition of a curve from our measurements of the osmotic

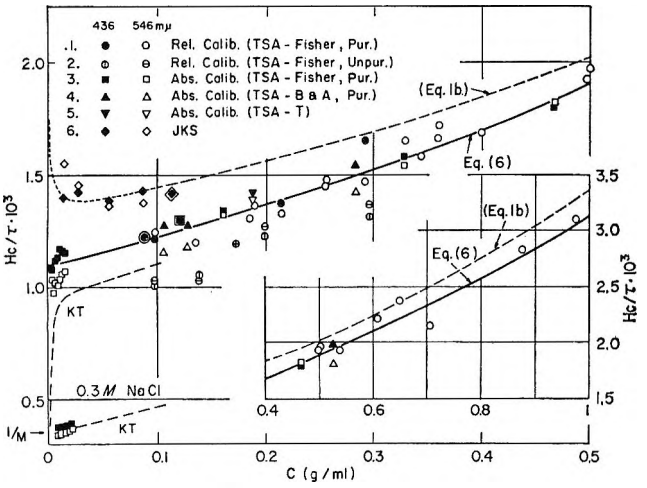

Figure 3. Light scattering (Kerker, Kratohvil, Ottewill, and Matijević).

coefficients (eq 1b) using the KKOM values for the index of refraction, n, and for dn/dc. In computing these curves we have recognized that KKOM have used an approximate form, applicable only to very dilute solutions, in which c and dn/dc replace w and dn/dw of the exact expression. Here w is grams of solute per gram of water. The net result is that their results should be multiplied by $(d \ln c/d \ln w)^2$ to be compared with those obtained by other methods, or that the results obtained by other methods should be multiplied by $(d \ln w/d \ln c)^2$ to be placed in this figure. The density measurements of KKOM up to $c = 1.0$ lead to the equations

$$c/w = 1 - 0.1512w + 0.0296w^2 \quad (6)$$

$$(d \ln w/d \ln c)^2 = (1 - 0.1512w + 0.0296w^2)^2/(1 - 0.3024w + 0.0888w^2)^2 \quad (7)$$

The line drawn by KKOM from their light-scattering measurements is lower than that from the osmotic coefficients by about 0.64, 0.21, 0.15, and 0.24 at c = 0.0, 0.1, 0.5, and 1.0, respectively, which correspond to 37, 14, 7, and 7%. Although the difference is certainly real, it is not greater than the scatter of their results, except for those at extreme dilution.

KKOM criticize the results of JKS because they indicate a negative slope in very dilute solutions. They say "...other workers have invariably obtained positive slopes for solutions of similar systems...." They apparently overlooked the very careful measurements of Timasheff, Dintzis, Kirkwood, and Coleman[11] on the light scattering of deionized bovine serum albumin and mercaptalbumin, which have been confirmed by Scatchard and Bregman.[12] The decrease in Hc/τ proportional to the square root of the concentration, in spite of the fact that the average charge is zero, is interpreted as an electrostatic effect arising from the nonzero average square of the charge.

We have added at the University of North Carolina another to the several titrations which indicate that TSA is a very highly ionized tetrabasic acid. The best evidence that it is a typical strong 4–1 electrolyte is from the ultracentrifuge measurements of JKS illustrated in Figure 2, and similar measurements on the sodium salt which were deleted from that figure. The measurements with the acid go to dilute enough solutions so that $-\partial \ln \gamma_{\pm}/\partial \ln m$ is little more than half the maximum value. Their measurements by ultracentrifuge equilibrium and by light scattering for the acid and for the sodium salt agree very well with each other and with the Debye–Hückel value for a strong 4–1 electrolyte. However, a much fairer test of the precision of the light-scattering measurements is the direct comparison of the turbidities given in Table II and Figure 1 of JKS.

We believe that the ultracentrifuge values of JKS for the osmotic coefficient are the best up to 0.04 m and that the isopiestic values cannot be far wrong in the more concentrated solutions. They fit together not too badly, but there is room for improvement. It may be that eq 1 is inadequate. The use of a more complete expression than that of Debye and Hückel for the electrostatic effect leads to a much more complicated expression than eq 1. It may be, however, that either the ultracentrifuge or the isopiestic measurements are in error near 0.04 m. As shown in Figure 2, the light-scattering measurements of JKS do not help to choose between them.

It is clear that the light-scattering measurements of KKOM do not determine the activity and osmotic coefficients. The curve labeled KKOM in Figure 1 fits little better than the assumption of ideal solutions, $\phi = 1$. In fact it does not fit so well over much of the range. Most of the discrepancy is caused by the error of the integration from $c = 0$ to $c = 1$ with values which are much too small. The results of this error persist to the highest concentrations, but they are partially compensated for by the error of the approximate equation they use. The best comparison between the two sets of measurements is shown in Figure 3 although this contains, in the curve calculated from ϕ, any errors from the KKOM measurements of n.

(11) S. N. Timasheff, H. M. Dintzis, J. G. Kirkwood, and B. D. Coleman, *Proc. Natl. Acad. Sci. U. S.*, **41**, 710 (1955); *J. Am. Chem. Soc.*, **79**, 782 (1957).

(12) G. Scatchard and J. Bregman, *ibid.*, **81**, 6095 (1959).

There are two reasons why light scattering should approach that of the un-ionized acid at infinite dilution. The first effect has been noted and calculated by Hermans[13] and is discussed by JKS. This effect rises from the fact that the ion concentrations begin to fluctuate independently as their concentrations become extremely small and that scattering by four hydrogen ions is very small compared to that by one tungstosilicate ion. This does not affect measurements by methods other than light scattering. In the group of measurements by KKOM very near the origin in Figure 3, the concentration varies from approximately $m = 5 \times 10^{-4}$ to $m = 5 \times 10^{-3}$. The Hermans effect varies from 1 to 0.1%, or about one-tenth of the variation of the measurements within that group.

The second effect, that the activity of the hydrogen ion is not equal to the equivalent concentration of acid in extremely dilute solutions because of the ionization of water, has been stressed recently by Erlander.[14] It applies to any method and to all acids (and bases) in water. It has been well recognized for at least half a century and taken into account when necessary. For example, the reference state of unit activity coefficient for an acid is customarily taken as an idealized un-ionized solvent which resembles water in every other respect. Since the concentration of hydrogen ion furnished by the water is equal to that of the hydroxyl ion, or 10^{-14} divided by the total hydrogen ion concentration at 25°, the fraction of H^+ furnished by the water is 0.01 when $(H^+) = 10^{-6}$ and is only 10^{-4} when $(H^+) = 10^{-5}$.[15,16]

Acknowledgment. The University of North Carolina part of this work was supported by the Office of Naval Research, and the Massachusetts Institute of Technology part by the AEC, under Contract AT(30-1)-905.

(13) J. J. Hermans, *Rec. Trav. Chim.*, **68**, 859 (1951).

(14) S. R. Erlander, *Iowa State J. Sci.*, **38**, 323 (1964); S. R. Erlander and F. R. Senti, *Makromol. Chem.*, **73**, 14 (1964).

(15) For the discussion of other confusions in Erlander's paper, see G. Scatchard, "Chemical Physics of Ionic Solutions," B. E. Conway and R. G. Baradas, Ed., John Wiley and Sons, Inc., New York, N. Y., 1966, Chapter 10.

(16) NOTE ADDED IN PROOF. Recently, J. P. Kratohvil, L. E. Oppenheimer, and M. Kerker, *J. Phys. Chem.*, **70**, 2834 (1966), have published an equation for the activity of water in TSA solutions from which we calculate osmotic coefficients about 7% higher than the curve labeled KKOM in Figure 1. It is thus about 2% lower than curve 1b in the more concentrated range, but falls far below in the dilute range because they still ignore the fact that TSA is a strong 1–4 electrolyte. They do not give the lower limit of concentration studied.

Determination of the Second Dissociation Constant of Sulfuric Acid by Donnan Membrane Equilibrium[1]

by Richard M. Wallace

Savannah River Laboratory, E. I. du Pont de Nemours and Co., Aiken, South Carolina *(Received June 21, 1966)*

A method was developed for determining the degree of dissociation of sulfuric acid by measuring the distribution of ^{22}Na tracer between solutions of sulfuric acid and perchloric acid separated by a cation-permselective membrane. The degree of dissociation and the stoichiometric activity for sulfuric acid were combined to obtain the second dissociation equilibrium constant. Equilibrium constants at 25, 35, and 50° were 0.0131, 0.0094, and 0.0062 mole kg^{-1}, respectively. An average ΔH was calculated to be -5.6 kcal/mole.

Donnan membrane equilibrium across permselective membranes is used for the determination of charges on ions in solution.[2] This paper describes the extension of this technique to measure dissociation constants of acids. The method was tested by determining the second dissociation constant of sulfuric acid because previous measurements of this constant by a variety of methods[3] are available for comparison. Also, knowledge of the free sulfate ion concentration in sulfuric acid solutions of varying concentration is necessary for further studies of complex formation between sulfate and metal ions in progress in this laboratory.

Basis of Method

The distribution of $^{22}Na^+$ tracer between a solution of perchloric acid on one side (p) of a cation-permselective membrane and a solution of sulfuric acid on the other side (s) is measured. From this distribution and knowledge of the concentrations of the solutions, the concentration of free hydrogen ion in the sulfuric acid solution can be calculated along with other quantities necessary for determining the degree of dissociation. The use of sodium tracer $^{22}Na^+$ permitted convenient and accurate measurement of the relative concentration of sodium ion in the two solutions at an absolute concentration too low to affect the concentrations of other ions in the solutions.

The following assumptions were made in developing equations for calculating the equilibrium constant for the bisulfate dissociation ($HSO_4^- \rightleftharpoons H^+ + SO_4^{2-}$): (1) perchloric acid is completely dissociated; (2) the first stage of the dissociation of sulfuric acid is complete; (3) sodium ion is not complexed by any of the anions present.

Conditions for Donnan membrane equilibrium across cation-permselective membranes require that

$$\frac{(H_s^+)}{(H_p^+)} = \frac{(Na_s^+)}{(Na_p^+)} \frac{\gamma_{Na_s}}{\gamma_{Na_p}} \frac{\gamma_{H_p}}{\gamma_{H_s}} \qquad (1)$$

where (H^+) and (Na^+) are the respective concentrations of hydrogen and sodium ions, while the subscripts s and p refer to the sulfuric acid and perchloric acid solutions, respectively. The symbol γ with the appropriate subscript is the activity coefficient of the designated ion.

The concentration of free hydrogen ion in the sulfuric acid solution can then be calculated from the equation

$$(H_s^+) = (H_p^+)\frac{(Na_s^+)}{(Na_p^+)}\beta \qquad (2)$$

where β is the collection of activity coefficients in eq 1, which is assumed to be unity when the ionic strength of the solutions on opposite sides of the

(1) The information contained in this article was developed during the course of work under Contract AT(07-2)-1 with the U. S. Atomic Energy Commission.

(2) R. M. Wallace, *J. Phys. Chem.*, 68, 2418 (1964).

(3) L. G. Sillén and A. E. Martell, "Stability Constants of Metal-Ion Complexes," The Chemical Society, London, 1964, p 232.

membranes are the same. This assumption will be discussed in detail later.

The total analytical sulfate concentration, S_t, and the total analytical acidity, H_t, can be represented in terms of the concentrations of free hydrogen ion (H_s^+), bisulfate ion (HSO_4^-), and sulfate ion (SO_4^{2-})

$$S_t = (SO_4^{2-}) + (HSO_4^-) \quad (3)$$

$$H_t = (H_s^+) + (HSO_4^-) \quad (4)$$

Since the sulfuric acid solution is essentially pure

$$H_t = 2S_t \quad (5)$$

Finally, if the degree of dissociation, α, of bisulfate is defined as

$$\alpha = \frac{(SO_4^{2-})}{S_t} \quad (6)$$

then a combination of eq 2–6 yields

$$1 + \alpha = \frac{(H_p^+)}{S_t}\frac{(Na_s^+)}{(Na_p^+)}\beta \quad (7)$$

from which α can be determined if β is known.

In solutions of moderate concentration (up to a few tenths molar), the activity of an ion can be represented quite well by the Debye–Hückel equation

$$\log \gamma_i = \frac{-AZ_i^2\sqrt{\mu}}{1 + \mathring{a}B\sqrt{\mu}} \quad (8)$$

Where A and B are known constants, Z_i is the charge on the ion, μ is the ionic strength, and $\mathring{a}$ is the ion-size parameter. $\mathring{a}$ need not be the same for two different cations in the same solution. Differences in $\mathring{a}$ between the hydrogen ion and sodium ion in the two solutions will cause β to differ significantly from unity, particularly in the more concentrated solutions.

Differences in $\mathring{a}$ are awkward to handle because of the form of eq 8. However, Robinson and Stokes[4] have shown that in dilute solutions, variations in $\mathring{a}$ produce approximately the same effect as an additional term, linear in μ. The activity coefficients can therefore be most simply represented by

$$\log \gamma_i = \frac{-AZ_i^2\sqrt{\mu}}{1 + \bar{\mathring{a}}B\sqrt{\mu}} + C_i\mu \quad (8')$$

where $\bar{\mathring{a}}$ is an average ion-size parameter, assumed to be constant for a given solution, which may however vary from one solution to another, while C_i will depend on the particular ion and the solution.

With the above assumption

$$\log \beta = (C_{Na_s} - C_{H_s})\mu_s - (C_{Na_p} - C_{H_p})\mu_p \quad (9)$$

If $\bar{\Delta}$ is the average of the two values of $C_{Na} - C_H$ in (9) and δ is the difference between the actual value and the average, then eq 9 can be written

$$\log \beta = \bar{\Delta}(\mu_s - \mu_p) + \delta(\mu_s + \mu_p) \quad (10)$$

The first term on the right of eq 10 becomes zero when $\mu_s = \mu_p$, while the second term represents an uncertainty in $\log \beta$ that cannot be evaluated exactly. A comparison of the activity coefficients of the sodium salts and acids of various univalent anions indicates that the absolute value of δ is probably no greater than 0.03. This value would cause an uncertainty of only 0.006 in $\log (1 + \alpha)$ at $\mu = 0.1$; and the uncertainty decreases with decreasing ionic strength, approaching zero at infinite dilution. For the present purposes δ can therefore be assumed to be zero. The validity of this assumption is derived from the internal consistency of the results and their agreement with other observations, as will be apparent later in this paper.

The best value of α should be obtained by equilibrating a solution of sulfuric acid with one of perchloric acid of the same ionic strength. Unfortunately, the ionic strength of sulfuric acid depends on α, and the correct concentration of perchloric acid to use is not known *a priori*. The problem may be solved, however, by equilibrating a given concentration of sulfuric acid with several different concentrations of perchloric acid that bracket the ionic strength of the sulfuric acid solution. The correct value of α can then be obtained by interpolation, as shown below.

From eq 7 and 10, assuming $\delta = 0$

$$\log \frac{(H_p^+)}{S_t}\frac{(Na_s^+)}{(Na_p^+)} = \log (1 + \alpha) - \bar{\Delta}\mu_s + \bar{\Delta}\mu_p \quad (11)$$

with distribution measurements at constant sulfuric acid concentration but variable perchloric acid concentrations. The value of the left side of eq 11 can be determined as a function of perchloric acid concentration. The graph of this relationship should be a straight line with a slope equal to the constant $\bar{\Delta}$. When the value of $\bar{\Delta}$ has been established, α can be determined from eq 12, which is derived from (11) by substituting the equivalent $S_t(1 + 2\alpha)$ for μ_s.

$$\log \frac{(H_p^+)}{S_t}\frac{(Na_s^+)}{(Na_p^+)} - \bar{\Delta}\mu_p = \log (1 + \alpha) - \bar{\Delta}S_t(1 + 2\alpha) \quad (12)$$

With a constant sulfuric acid concentration, the left side of eq 12 must remain constant (except for small variations caused by scatter in the data). Equation 12 can then be graphically solved for α.

(4) R. A. Robinson and R. H. Stokes, "Electrolytic Solutions," Butterworth and Co. Ltd., London, 1955, p 234.

Calculation of Equilibrium Constants

The usual procedure for determining equilibrium constants when the degrees of dissociation are known at various concentrations is to calculate the equilibrium quotient, Q, in terms of concentrations or molalities, and then by trial and error to determine a value of the ion-size parameter, $\mathring{a}$, that will yield a constant value for the equilibrium constant, K, in terms of activities. Since stoichiometric activity data for sulfuric acid are available,[4] equilibrium constants can be calculated in a more convenient manner and simultaneously tested for the consistency of the two types of measurements. The equation for this calculation is derived as follows.

The equilibrium constant, K, to be determined is defined by eq 13, where a is the activity of the designated ion.

$$K = \frac{a_{H^+}a_{SO_4^{2-}}}{a_{HSO_4^-}} \tag{13}$$

The stoichiometric activity of sulfuric acid, a_2, in (14) can be represented in terms either of (1) the activities of the hydrogen ions and sulfate ions or (2) the molality, m, of sulfuric acid, the degree of dissociation of bisulfate, α, and the activity coefficients, γ, of the individual ions.

$$a_2 = a_{H^+}{}^2 a_{SO_4^{2-}} = m^3(1 + \alpha)^2\alpha\gamma_{H^+}{}^2\gamma_{SO_4^{2-}} \tag{14}$$

The equilibrium constant can also be expressed in terms of the stoichiometric activity and the activities of the hydrogen and bisulfate ions or in terms of m, α, and the activity coefficients of these ions. Thus

$$K = \frac{a_2}{a_{H^+}a_{HSO_4^-}} = \frac{a_2}{m^2(1 + \alpha)(1 - \alpha)\gamma_{H^+}\gamma_{HSO_4^-}} \tag{15}$$

Equations 14 and 15 can each be solved for the product of activity coefficients to give

$$\gamma_{H^+}{}^2\gamma_{SO_4^{2-}} = \frac{a_2}{m^3(1 + \alpha)^2\alpha} \tag{16}$$

$$\gamma_{H^+}\gamma_{HSO_4^-} = \frac{a_2}{Km^2(1 + \alpha)(1 - \alpha)} \tag{17}$$

If eq 17 is divided by the cube root of eq 16 and a_2 is expressed in terms of the molality and the stoichiometric mean activity coefficient, $\gamma_\pm$, of sulfuric acid ($a_2 \equiv 4m^3\gamma_\pm{}^3$), then

$$\left(\frac{\gamma_{H^+}\gamma_{HSO_4^-}{}^3}{\gamma_{SO_4^{2-}}}\right)^{1/3} = \frac{4^{2/3}m\gamma_\pm{}^2}{K}\left(\frac{\alpha}{1 + \alpha}\right)^{1/3}\left(\frac{1}{1 - \alpha}\right) \tag{18}$$

If a single ion-size parameter $\mathring{a}$ in the Debye–Hückel equation (eq 8) exists that applies to all of the ions involved, then the left side of eq 18 will be unity, and K can be expressed in terms of experimentally determined quantities

$$K = 4^{2/3}m\gamma_\pm{}^2\left(\frac{\alpha}{1 + \alpha}\right)^{1/3}\left(\frac{1}{1 - \alpha}\right) \tag{19}$$

Experimental Section

Membrane equilibrations were run in an apparatus described previously[1] that consists of two Teflon (Du Pont trademark for its fluorocarbon plastic) blocks each containing a 20-ml cylindrical cavity and a filling passage. The equilibration cell was assembled by placing a circular membrane between the two blocks and bolting them together. Solutions were added to the cavities on each side of the membrane through the filling passages, which were subsequently sealed. The solutions were agitated during equilibration by rotating the cells at 60–120 rpm in a constant-temperature bath.

The membranes were AMFion C103 (Trademark of American Machine and Foundry Co.) cation-permeable membranes, converted from the sodium form to the hydrogen form.

About 15 ml of water containing a small amount of ^{22}Na tracer was introduced into the cell on each side of the membrane. The cells were rotated for about 1 hr to absorb the tracer on the membranes; then the water was removed and the cells were disassembled, carefully dried, and reassembled. Accurately analyzed solutions of sulfuric and perchloric acids were placed in each cell on opposite sides of the membrane and equilibrated in a constant-temperature bath, after which the solutions were removed for analysis.

The length of the equilibrations varied with the temperature: 6 hr at 25 ± 0.1°, 4 hr at 35 ± 0.1°, and 2 hr at 50 ± 0.1°. Preliminary kinetic studies indicated that equilibrium with respect to the distribution of sodium ions was virtually complete after 1 hr at 25°, but longer periods were desirable to assure that equilibrium was more nearly attained. Attempts to equilibrate for 20 hr or more resulted in a significant leakage of sulfate ion; *e.g.*, after 24 hr at 25° almost 1% of the sulfate was transferred into the perchloric acid solutions and even larger fractions were transferred at the higher temperatures. At the equilibration times used, however, less than 0.3% of the sulfate was transferred in the worst case. No direct analysis of the amount of perchlorate transferred into the sulfate solutions was made, but a material balance based on acid and sulfate analyses indicated that it was no greater than the sulfate transport.

The solutions were counted for the ^{22}Na γ activity after removal from the cells. Because of osmosis during the equilibrations, the solutions in which the acid concentrations were ≥ 0.05 M were reanalyzed for total acidity.

^{22}Na was counted in a well-type γ-scintillation counter with an RIDL solid-state scaler and timer. All solutions were counted for a sufficient time to obtain at least 10^5 counts, which limited statistical error to about 0.3%.

Perchloric and sulfuric acids were determined by titrating (to pH 7.0 on a pH meter) with carbonate-free sodium hydroxide using a 1-ml micrometer buret. Duplicate results always agreed within 0.4%.

Sulfate leakage across the membrane was determined independently by titration with $BaCl_2$. Titrations were performed in 80% ethanol–20% water mixture at an apparent pH between 2.5 and 4 with Thoron as an indicator. This titration was not nearly so precise as the acid–base titration. Consequently, the pure sulfuric acid was titrated with base.

Results and Discussion

Detailed results of equilibrium measurements at 25° are shown in Table I. The distribution of ^{22}Na was determined among three different concentrations of perchloric acid for each of six concentrations of sulfuric acid.

Table I: Dissociation of HSO_4^- at 25°

H_2SO_4 molarity (S_t)	$HClO_4$ molarity (H_p)	$(Na_s^+)/(Na_p^+)$	$\frac{(H_p^+)}{S_t}\frac{(Na_s^+)}{(Na_p^+)}$	α
0.001010	0.001013	1.894	1.899	
0.001010	0.001520	1.253	1.886	0.895
0.001010	0.002018	0.951	1.900	
0.005026	0.005056	1.688	1.698	
0.005026	0.007613	1.126	1.706	0.699
0.005026	0.01018	0.836	1.693	
0.01004	0.01018	1.573	1.596	
0.01004	0.01529	1.048	1.597	0.590
0.01004	0.02021	0.783	1.577	
0.02515	0.02522	1.433	1.437	
0.02515	0.03751	0.954	1.424	0.420
0.02515	0.05030	0.7091	1.418	
0.05050	0.05065	1.3414	1.345	
0.05101	0.07491	0.8998	1.321	0.314
0.05123	0.09985	0.6669	1.300	
0.1015	0.1008	1.2556	1.248	
0.1022	0.1502	0.8374	1.231	0.227
0.1033	0.1984	0.6268	1.204	

Fractional dissociations, α, for the three higher concentrations of sulfuric acid for which $(H_p)(Na_s)/S_t(Na_p)$ varied significantly with the concentration of perchloric acid were calculated by interpolation to the conditions at which the ionic strength was the same on both sides of the membrane using eq 12. This procedure was developed assuming constant sulfuric acid concentration for a set of measurements; however, this condition was difficult to maintain exactly at the higher concentrations because of differences in the amount of osmosis, and consequently the sulfuric acid concentration varied slightly. Hence, the average value of the sulfuric acid concentration was used in the calculations. Since α changes slowly with concentration in the more concentrated solutions, these small variations in the concentration did not contribute significantly to the error.

At concentrations below 0.025 M, where differences between the ionic strength on opposite sides of the membranes were small, the quantity $(H_p^+)(Na_s^+)/S_t(Na_p^+)$ was virtually independent of the perchloric acid concentration. α was calculated from eq 7 with $\beta = 1$ in these cases, and an average of the three measurements was taken.

Table II summarizes the dissociation values calculated from membrane equilibrium measurements at 25, 35, and 50°. The values of α which were measured as a function of molarity have been interpolated to the nearest round value of the molality for easy comparison with activity data.[5] The values of α at 35 and 50° were determined in the same manner except that distribution measurements were made at only two different perchloric acid concentrations for each sulfuric acid concentration. The values of the stoichiometric activity coefficients of sulfuric acid $\gamma_\pm$ are those of Harned and Hamer[5] determined potentiometrically with a hydrogen and a lead peroxide–lead sulfate electrode. Quadratic interpolation was used where necessary to obtain values not given explicitly in their tables. The values of K shown were calculated from the other data in the table using eq 19. Average values of K at each temperature together with their standard deviations are given at the bottom of each column.

The average value of ΔH between 25 and 50° for the reaction was determined to be -5.6 ± 0.5 kcal/mole from a least-squares fit of log K as a linear function of the reciprocal of the absolute temperature.

The constancy of K at 25° over a 100-fold variation in the concentration demonstrates consistency between the values of α determined by membrane equilibrium

(5) H. S. Harned and W. J. Hamer, *J. Am. Chem. Soc.*, **57**, 27 (1935).

Table II: Dissociation Data for HSO_4^- at Various Temperatures

H_2SO_4 molality	α	$\gamma_\pm$	K
	25°		
0.001	0.896	0.830	0.0130
0.005	0.700	0.639	0.0128
0.010	0.591	0.544	0.0131
0.025	0.421	0.423	0.0130
0.050	0.316	0.340	0.0133
0.100	0.229	0.265	0.0131
			Av 0.0131 ± 0.0002
	35°		
0.001	0.857	0.814	0.0090
0.005	0.635	0.608	0.0093
0.010	0.500	0.511	0.0091
0.025	0.361	0.392	0.0097
0.050	0.268	0.313	0.0100
0.100	0.182	0.240	0.0095
			Av 0.0094 ± 0.0004
	50°		
0.001	0.784	0.790	0.0055
0.005	0.534	0.566	0.0061
0.010	0.409	0.467	0.0062
0.025	0.270	0.352	0.0064
0.050	0.191	0.279	0.0066
0.100	0.139	0.214	0.0067
			Av 0.0062 ± 0.0004

measurements and the stoichiometric activity coefficients determined potentiometrically. K varied more at the higher temperatures, although the variations were still small. The larger variations at the higher temperatures may derive from the experimental technique in the present work. Although the equilibrations were run in a constant-temperature bath, the cells had to be removed for sampling. The cells were sampled as rapidly as possible, but some reequilibration may have occurred. The changes in K with molality at 50° which appear to be systematic rather than random may be a result of this reequilibration.

The ion-size parameters $\hat{a}$ (eq 8) were calculated as follows. The product of activity coefficients, $\gamma_{H^+}{}^2\gamma_{SO_4^{2-}}$, at each molality was first calculated with eq 16. These values were then substituted into the Debye–Hückel equation together with the appropriate value of the ionic strength $\mu = m(1 + 2\alpha)$ and values of A and B at the appropriate temperatures tabulated by Robinson and Stokes.[6] The equation was then solved for $\hat{a}$.

Values of $\hat{a}$ calculated for the five highest concentrations are shown in Table III. The most reliable values are those obtained at the highest concentrations, where deviations from the limiting law are the greatest. Virtually the same value of $\hat{a}$ was obtained at the highest concentration at all three temperatures, and very good agreement was obtained in all cases between the values at 25 and 35°. The most reliable values of $\hat{a}$ are ~6.0 A, which is a reasonable value for the ion-size parameter of acid solutions.

Table III: Calculated Values of the Ion-Size Parameter $\hat{a}$

H_2SO_4 molality	$\hat{a}$, A		
	25°	35°	50°
0.005	4.5	5.7	10.7
0.010	4.7	7.7	9.9
0.025	6.5	6.5	9.0
0.050	6.4	6.3	8.1
0.100	5.9	6.0	6.1

Membrane equilibrium measurements are consistent with activity data, and the ΔH of reaction, -5.6 ± 0.5 kcal mole^{-1}, obtained is in substantial agreement with the calorimetric values of Pitzer[7] (-5.2 ± 0.5 kcal mole^{-1}) and of Austin and Mair[8] (-5.74 ± 0.20 kcal mole^{-1}).

K values did not agree very well with results of other methods. Davies, Jones, and Monk[9] obtained a value of 0.0103 for K at 25° by potentiometric measurements on mixtures of hydrochloric acid and sulfuric acid using hydrogen and silver–silver chloride electrodes. Nair and Nancollas[10] obtained a value of 0.0110 by the same method. Young, Klotz, and Singleterry[11] obtained a value for K of 0.01015 by a spectrophotometric method, while Kerker[12] derived a value of 0.0102 from conductance and transport data. All these values are considerably lower than 0.0131 found in the present study. Similar discrepancies also occur at other temperatures.

The potentiometric method with mixtures of sulfuric and hydrochloric acids or mixtures of sodium sulfate, sodium bisulfate, and sodium chloride has

(6) See ref 4, p 491.

(7) K. S. Pitzer, *J. Am. Chem. Soc.*, **59**, 2365 (1937).

(8) J. M. Austin and A. D. Mair, *J. Phys. Chem.*, **66**, 519 (1962).

(9) C. W. Davies, H. W. Jones, and C. B. Monk, *Trans. Faraday Soc.*, **48**, 921 (1952).

(10) V. S. K. Nair and G. H. Nancollas, *J. Chem. Soc.*, 4144 (1958).

(11) I. M. Klotz and C. R. Singleterry, Thesis, University of Chicago, 1940.

(12) M. Kerker, *J. Am. Chem. Soc.*, **79**, 3664 (1957).

been criticized by Hamer[13] because the extrapolated value of the equilibrium constant depends upon the ion-size parameter chosen for the calculations. He showed that the choice of $\mathring{a} = 4$ A gave agreement between the two potentiometric methods and the spectrophotometric method but stated that the agreement might be fortuitous. The agreement between the values obtained by the potentiometric methods and these of the present study would, however, not be improved by using $\mathring{a} = 6$ A in the potentiometric calculation, since an increase in the ion-size parameter causes K to change in the wrong direction.

The discrepancy between the results of the present study and those obtained by conductivity measurements is probably not serious. Kerker's[12] values for α are only 3–5% lower than those of the present study in the region between 0.001 and 0.005 M. This difference decreases with increasing concentration until both methods give essentially the same value at 0.025 M. At still higher concentrations the conductance method gives higher values for α than the membrane method (0.266 for the conductance method *vs.* 0.229 for membrane method at 0.1 M).

The exact method of extrapolation used with the conductance data was not specified. It appears, however, that Q, the equilibrium quotient in terms of concentrations, was calculated, and a plot of log Q *vs.* some function of the concentration was extrapolated to zero concentration by drawing a line through the last few points. This procedure places greatest weight on the points that are most sensitive to slight errors in α; for example, at 0.00025 M where α was found to be 0.959 a 1% error in α would cause a 24% error in either Q or K. A recalculation of K from the values of α obtained from conductivity data using eq 19 gave values that varied between 0.0107 at 0.001 M and 0.0143 at 0.1 M; all values of K obtained at concentrations above 0.01 M were in excess of 0.0120. It therefore appears that the results from the conductance method agree reasonably well with those from the membrane method.

Although the values of α obtained by the membrane method are consistent with the activity data for sulfuric acid, the lower values of K obtained by other methods need explanation. This question can be answered by assigning any desired value of K in eq 19 and calculating values of α consistent with it and the stoichiometric activity coefficients of sulfuric acid. These values of α may then be substituted into eq 15 to determine $\gamma_{H^+}{}^2\gamma_{SO_4^{2-}}$, the product of activity coefficients of the free ions. This product can then be substituted into the Debye–Hückel equation, and the ion-size parameter, $\mathring{a}$, determined. This procedure was carried out for $K = 0.0110$ and resulted in values of $\mathring{a}$ that varied between 11 and 16 A (values of $\mathring{a}$ for completely dissociated acids fell between 5.6 and 8.2 A when calculated with eq 8 at $\mu = 0.1$ from data in ref 4, p 476). Since these values are unreasonably high, it appears that the lower values of K are not consistent with activity data.

The purpose of the present paper was to demonstrate the utility of the Donnan membrane equilibrium method in determining dissociation constants of acids and not to challenge previously determined values of the dissociation constant of bisulfate ion. The consistency of the values of α obtained by the membrane method with the activity data for sulfuric acid over a large range of concentrations, together with fair agreement with conductivity measurements at the higher concentrations, indicates that the equilibrium constants found in the present study may be more reliable than those reported previously.

(13) W. J. Hamer, "The Structure of Electrolytic Solutions," John Wiley and Sons, Inc., New York, N. Y., 1959, Chapter 15.

A Possible Method for Distinguishing between Triplet–Triplet Annihilation and Direct Singlet Formation in Electrogenerated Chemiluminescence[1]

by Stephen W. Feldberg

Brookhaven National Laboratory, Upton, New York *(Received June 24, 1966)*

Several workers have suggested that the observed singlet emission in electrogenerated chemiluminescence arises from a triplet–triplet annihilation mechanism rather than from direct singlet formation by the cation radical–anion radical reaction. The cation radical–anion radical reaction yields a triplet instead of an excited singlet; two triplets then annihilate producing the excited singlet. The quantitative aspects of parallel direct singlet and triplet–triplet mechanisms are calculated and compared to previously calculated relationships for the direct singlet formation. The difference between the two mechanisms becomes most apparent only when there is significant triplet quenching.

A recent publication[2] presented the relationship of the current, time, and light emission parameters for the electrogeneration of chemiluminescence at a single electrode using a double-step controlled-potential technique. The quantitative relationships were calculated for the following mechanism (to be referred to as mechanism a)

$$R + e^- \longrightarrow R^- \quad \text{first potential step} \tag{1}$$

$$\left.\begin{aligned} R &\longrightarrow R^+ + e^- \\ R^- &\longrightarrow R^+ + 2e^- \end{aligned}\right\} \text{second potential step} \quad (2), (3)$$

$$R^- + R^+ \xrightarrow{k_4} {}^1R^* + R \tag{4}$$

$${}^1R^* \xrightarrow{k_5} R + h\nu \quad \text{light emission} \tag{5}$$

$${}^1R^* + Z \xrightarrow{k_6} R \quad \text{quenching} \tag{6}$$

$${}^1R^* + R \xrightarrow{k_7} 2R \quad \text{self-quenching} \tag{7}$$

The calculations indicated that when the rate constant for reaction 4 was very high, one could write the following simple expression for the generation of light as a function of time

$$\log \omega_a = -1.45(t_r/t_f)^{1/2} + 0.71 \tag{8}$$

where t_f and t_r are the durations of the first and second potential steps and ω_a, the normalized rate of light generation, is defined in relationship 9

$$\omega_a = \frac{It_f^{1/2}}{\varphi C_R D^{1/2} A} = \frac{IF}{\pi^{1/2}\varphi i_f} \tag{9}$$

where I is the rate of singlet emission in moles of photons per second, C_R is the bulk concentration of R, D is the diffusion coefficient of all species, A is the electrode area, F is the faraday, and i_f is the current at time t_f. The quantum efficiency, φ, is defined as

$$\varphi = \frac{k_5}{k_5 + k_6 C_Z + k_7 C_R} \tag{10}$$

where C_Z is the concentration of quencher Z. If the output of a photomultiplier tube, P, is proportional to I, then a plot of log $Pt_f^{1/2}$ *vs.* $(t_r/t_f)^{1/2}$ should have a slope of -1.45. This relationship has been verified by Lansbury, Hercules, and Roe,[3] who investigated the chemiluminescence of rubrene in acetonitrile and dimethylformamide. Visco[4] has also obtained verification in studies of rubrene in benzonitrile. The plots he obtained, however, had slopes of -1.9, slightly more negative than the theoretical -1.45.

Virtually all workers have at one time or another

(1) Research supported by the U. S. Atomic Energy Commission.

(2) S. W. Feldberg, *J. Am. Chem. Soc.*, **88**, 390 (1966).

(3) R. C. Lansbury, D. M. Hercules, and D. K. Roe, presented at the Winter Meeting of the American Chemical Society, Phoenix, Ariz., Jan 1966, Abstract No. 28.

(4) R. E. Visco, Bell Telephone Laboratories, Murray Hill, N. J., private communication.

suggested the possibility that reaction 4 generates a triplet state (instead of a singlet) and that a triplet–triplet annihilation produces the excited singlet. This may be written as the following sequence of parallel reactions (to be referred to as mechanism b)

mechanism a (reactions 1–7) +

$$R^+ + R^- \xrightarrow{k_{11}} {}^3R^* + R \qquad (11)$$

$${}^3R^* + {}^3R^* \xrightarrow{k_{12}} {}^1R^* + R$$

triplet–triplet annihilation (12)

$${}^3R^* + Q \xrightarrow{k_{13}} R \qquad \text{triplet quenching} \qquad (13)$$

The objective of the calculations in this paper is to show that the slopes greater than -1.45 might be a manifestation of mechanism b and to show further what experimental conditions might be best suited for distinguishing mechanism a from b.

On the basis of eq 8 and 9, it is possible to obtain a modified equation describing the behavior of mechanism b by introducing the added parameters k_{11}, k_{12}, k_{13}, and C_Q, the concentration of quencher, Q. The term I/φ of eq 9 is really the rate of production of excited species and thus ω_a may also be defined as the normalized rate of production of excited species. The details of the derivation are presented in the Appendix. The normalized light emission for mechanism b, ω_b, is defined in the same way as ω_a in eq 9, and

$$\omega_b = \frac{\beta}{8}\left[1 - \left(1 + \frac{8\gamma\omega_a}{\beta}\right)^{1/2}\right] + (1 - {}^1/_2\gamma)\omega_a \qquad (14)$$

where β is defined as

$$\beta = \frac{C_Q{}^2 k_{13}{}^2 t_f}{k_{12} C_R} \qquad (15)$$

and γ is defined as the fraction of cation radical–anion radical reactions producing triplets

$$\gamma = \frac{k_{11}}{k_4 + k_{11}} \qquad (16)$$

The behavior of mechanism b as described by eq 14 is interesting. When $\gamma = 0$ (*i.e.*, 100% direct singlet production), one obtains the trivial result

$$\omega_a = \omega_b \qquad (17)$$

When $\gamma > 0$, the equation depends greatly upon the magnitude of the triplet quenching term, β. When $\beta = 0$, eq 14 reduces to

$$\omega_b = (1 - {}^1/_2\gamma)\omega_a \qquad (18)$$

If the light-measuring system is accurately calibrated and one can obtain an experimental value for ω which is close to the theoretical value predicted by eq 8 and 9 for $\varphi = 1$, then mechanism b can be ruled out. If, however, ω is found to be less than the theoretical value, this does not necessarily imply $\gamma > 0$ since the lower value may also be explained by $\varphi < 1$ as well as by $\gamma > 0$.

When the triplet-quenching term, β, becomes significant, however, the distinction between the two mechanisms becomes more apparent. For $\beta \gg 8\gamma\omega_a$, eq 14 reduces to (see Appendix, eq A9 and A10)

$$\omega_b = \frac{\gamma^2\omega_a{}^2}{\beta} + (1 - \gamma)\omega_a \qquad (19)$$

When $\gamma = 1$, eq 19 further simplifies and may be written in the form (substituting from eq 8)

$$\log \omega_b = -2.90(t_r/t_f)^{1/2} - \log \beta + 1.42 \qquad (20)$$

This expression may explain the slopes more negative than -1.45 observed by several workers[3,4] in their plots of $\log Pt_f{}^{1/2}$ *vs.* $(t_r/t_f)^{1/2}$. For those values of γ and β, which do not lead to simplified equations, eq 14 may have to be graphed for various values of these parameters and compared to plots of experimental data.

Discussion

Equations 20 and 8 indicate that the difference in slope (-2.90 instead of -1.45) could provide an unambiguous method of distinguishing between mechanisms a and b. The major experimental difficulty may be in finding a suitable triplet quencher. It must be sufficiently electroinactive so that it will not be oxidized or reduced at the electrode surface or react with the anion or cation radicals.

Chandross and Visco[5] have suggested that the radicals themselves may act as triplet quenchers. Calculations of this mode of quenching are much more complex since they involve the radical concentrations. In that region of the diffusion layer where triplet concentration is greatest (the region of maximum light output[2]), the radical concentration will be a minimum and the exact value of the concentrations will depend on the rate constant for the anion radical–cation radical reaction. The fact that several workers have obtained data plots close to the theoretical -1.45 slope[3,4] indicates that if the triplet–triplet annihilation mechanism obtains, triplet–radical quenching either does not occur or has only a small effect upon the behavior of the system.

Appendix

The rate of production of excited triplets and sin-

(5) E. A. Chandross and R. E. Visco, Bell Telephone Laboratories, Murray Hill, N. J., private communication.

glets by the counter-ion reaction may be defined as

$$L = I/\varphi \tag{A-1}$$

where I is defined following eq 9. Assume that the number of triplets formed is a constant fraction, γ, of L. Thus, if T = triplet concentration

$$dT/dt_r = \gamma L/\Delta - k_{12}T^2 - k_{13}C_Q T \tag{A-2}$$

where Δ is a reaction volume. Assume

$$\Delta = fA(Dt_f)^{1/2} \tag{A-3}$$

where f is a constant to be evaluated later. Since k_{12} is probably quite large, the right-hand side of (A-2) may be set equal to zero. The resulting quadratic equation is easily solved

$$T = \frac{-k_{13}C_Q + \left(k_{13}^2C_Q^2 + \dfrac{4\gamma Lk_{12}}{\Delta}\right)^{1/2}}{2k_{12}} \tag{A-4}$$

The rate of production of excited singlet by triplet–triplet annihilation and by direct singlet production is

$$\frac{dS}{dt} = \Delta k_{12}T^2/2 + (1 - \gamma)L \tag{A-5}$$

and the rate of singlet light emission is

$$I = \varphi\frac{dS}{dt} \tag{A-6}$$

Substituting from (A-1), (A-4), (A-5), and (A-6)

$$I = \varphi\left(\frac{\Delta k_{13}^2C_Q^2}{4k_{12}}\left[1 - \left(1 + \frac{4\gamma Lk_{12}}{\Delta k_{13}^2C_Q^2}\right)^{1/2}\right] + \gamma L/2 + (1 - \gamma)L\right) \tag{A-7}$$

Dividing both sides by the term $\varphi C_R A D^{1/2}/t_f^{1/2}$ gives

$$\omega_b = \frac{f\beta}{4}\left[1 - \left(1 + \frac{4\gamma\omega_a}{f\beta}\right)^{1/2}\right] + (1 - {}^1/_2\gamma)\omega \tag{A-8}$$

where β is defined in eq 15, and f by eq A-3. The approximation for the term $(1 + X)^{1/2}$ is (for $X \ll 1$)

$$(1 + X)^{1/2} = 1 + \frac{X}{2} - \frac{X^2}{8} \tag{A-9}$$

Thus for large values of β, eq A-8 reduces to

$$\omega_b = \omega_a(1 - \gamma) + \frac{\gamma^2\omega_a^2}{2f\beta} \tag{A-10}$$

or for $\gamma = 1$

$$\log \omega_b = -2.90(t_r/t_f)^{1/2} - \log f - \log \beta + 1.12 \tag{A-11}$$

When $\gamma = 1$, it is possible to obtain a solution to the problem directly by using the computer technique described previously[2,6,7] and thereby evaluate the constant f. The equation that may be written directly from the computer solution is

$$\log \omega_b = -2.90(t_r/t_f)^{1/2} - \log \beta + 1.40 \tag{A-12}$$

From eq A-11 and A-12, one can calculate

$$\log f = -0.28 \tag{A-13}$$

or

$$f = 0.525 \cong 0.5 \tag{A-14}$$

Substituting this value for f in eq A-8 leads directly to eq 14.

Acknowledgment. The author wishes to thank Professor R. A. Marcus of the University of Illinois, Urbana, Ill., who suggested that an investigation of quenching effects might permit distinguishing a triplet–triplet annihilation mechanism from a pure singlet mechanism (mechanisms a and b in this paper.) The author also wishes to thank Professor David Roe, Massachusetts Institute of Technology, Cambridge, Mass., Dr. Robert Visco, Bell Telephone Laboratories, Murray Hill, N. J., Dr. Donald Maricle, American Cyanamid, Stamford, Conn., and Dr. Jack Fajer, Brookhaven National Laboratory, for their helpful discussions and suggestions.

(6) S. W. Feldberg and C. Auerbach, *Anal. Chem.*, 36, 505 (1964).

(7) S. W. Feldberg, presented at the Meeting of the Electrochemical Society, San Francisco, Calif., May 1965, Abstract No. 156.

A Hydrodynamic Effect in the Rates of Diffusion-Controlled Reactions[1]

by Harold L. Friedman

Department of Chemistry, State University of New York, Stony Brook, New York *(Received June 24, 1966)*

There is a hydrodynamic interaction between the particles in a diffusion-controlled reaction. An estimate is made of its effect on the rate constant using Smoluchowski's method in the calculation. The hydrodynamic effect makes a reduction of about 15% in the computed rate constant for neutral species or ions in water.

1. Introduction

The theory of the rates of diffusion-controlled reactions, due first to Smoluchowski,[2] has been generalized by Debye[3] to include the effects of any forces between the reacting particles that may be derived from potentials. There is, however, another force acting between the particles that is not derivable from a potential: this is a hydrodynamic interaction resulting from the fact that each moving solute particle sets the solvent medium in motion. The resulting flux in the solvent medium then tends to move all of the other solute particles. The same interaction is responsible for the electrophoretic effect in the conductance of electrolyte solutions. It is an interaction which is certainly relevant for colloidal particles, the systems studied by Smoluchowski; on the other hand, its relevance for the diffusion-controlled reaction of ordinary small ions and solute molecules is precisely the same as that of the Smoluchowski–Debye theory, namely, somewhat uncertain because of the neglect of the molecular structure of the solvent.

Smoluchowski related the rate of combination of particles of radius l_1 and diffusion coefficient D_1 with those of radius l_2 and diffusion coefficient D_2 to the flow in the stationary state that results after a sink of radius $R = l_1 + l_2$ is inserted in an infinite solution of particles having diffusion coefficient $D_1 + D_2$.[4] The flow in this stationary state is quite easy to calculate.

Smoluchowski's method is readily shown to be exact when the motions of the particles are Brownian except when they collide and combine.[2b] The method is more difficult both to employ and to justify when not every collision between the Brownian particles leads to reaction[5,6] and when there are other forces, derivable from potentials, operating among the particles.[3,7] Very recently Smoluchowski's method had been shown to be incorrect when there are many-body effects due to interionic forces.[8] It is easy to see that Smoluchowski's method is at best uncertain when there are velocity-dependent forces such as we consider here, and, since these forces are required for physical consistency, it appears that Smoluchowski's method cannot be relied upon to give *exactly* the physically observable rate in any situation.

It would therefore be desirable to treat this problem in a more general statistical-mechanical framework, such as the correlation-function method,[9] but the problems involved in doing this have not yet been overcome. Therefore in this paper we use Smoluchowski's method to estimate the magnitude of the contribution of the hydrodynamic forces to the rate constant.

2. Calculation

If ζ_1 and ζ_2 are the friction coefficients of two particles of radii l_1 and l_2, then according to the Smoluchowski–Debye method one seeks the solution for the follow-

(1) The study was aided by a grant from the Office of Saline Water, U. S. Department of the Interior.

(2) (a) M. V. Smoluchowski, *Physik. Z.*, **17**, 557, 585 (1916); *Z. Physik. Chem.*, **92**, 129 (1917); (b) This calculation is described in a general framework by S. Chandrasekhar, *Rev. Mod Phys.*, **15**, 1 (1943).

(3) P. Debye, *Trans. Electrochemical Soc.*, **82**, 265 (1942).

(4) In general $l_1 + l_2$ need not be the collision diameter but may be a more general length: the radius of the so-called sphere of influence.

(5) F. C. Collins and G. Kimball, *J. Colloid Sci.*, **4**, 425 (1949).

(6) H. L. Frisch and F. C. Collins, *J. Chem. Phys.*, **20**, 1797 (1952).

(7) T. R. Waite, *Phys. Rev.*, **107**, 463 (1957); *J. Chem. Phys.*, **28**, 103 (1958).

(8) L. Bass and W. J. Greenhalgh, *Trans. Faraday Soc.*, **62**, 715 (1966).

(9) R. W. Zwanzig, *Ann. Rev. Phys. Chem.*, **16**, 67 (1965).

ing differential equation which describes the stationary state of diffusion into a sink centered at $r = 0$

$$I/4\pi r^2 = -kT[(1/\zeta_1) + (1/\zeta_2)]\mathrm{d}c/\mathrm{d}r + [(1/\zeta_1) + (1/\zeta_2)]Fc \quad (1)$$

where I is the number of particles per second flowing into the sink, $c = c(r)$ is the local concentration of the diffusing particles, and $F = F(r)$ is the outward force on the diffusing particles.

The force may be written as the sum of two terms

$$F = -\frac{\partial U}{\partial r} - H(r)v(r) \quad (2)$$

where $U = U_{12}(r)$ is the interaction potential considered by Debye[3] and the hydrodynamic force is the product of a positive scalar proportionality factor $H(r)$ and the average velocity $v(r)$ of the particles toward the origin. The justification for this form for the hydrodynamic force is given below.

In view of the fact that

$$v(r)c(r) = I/4\pi r^2 \quad (3)$$

we may write eq 1 in the form

$$\frac{\mathrm{d}c}{\mathrm{d}r} + \beta c\frac{\mathrm{d}U}{\mathrm{d}r} = -\frac{I}{4\pi D_{12}}f(r) \quad (4)$$

where

$$\beta \equiv 1/kT$$

$$D_{12} \equiv kT[(1/\zeta_1) + (1/\zeta_2)]$$

$$f(r) \equiv \{1 + [(1/\zeta_1) + (1/\zeta_2)]H(r)\}/r^2 \quad (5)$$

Equation 4 has the solution

$$c(r) = -\frac{I}{4\pi D_{12}}e^{-\beta U(r)}\int_R^r f(x)e^{\beta U(x)}\mathrm{d}x \quad (6)$$

where $R = l_1 + l_2$ and we have used the boundary condition $c(R) = 0$. We also have $c(\infty) = c_0$, the bulk concentration of the diffusing species, and we have $U(\infty) = 0$, so we can solve for the total flow into the sink

$$-I = 4\pi D_{12}c_0\Big/\int_R^\infty f(x)\exp(\beta U(x))\,\mathrm{d}x \quad (7)$$

Furthermore, from Smoluchowski's equivalence, as discussed above, we have, for the rate constant k_{12} of the bimolecular diffusion-controlled combination of species 1 and species 2

$$k_{12} = -I/2c_0 \quad (8)$$

If $H(r) = 0$ for all r, then k_{12} calculated from eq 5, 7, and 8 is the same as Debye's result,[3] but, if $H(r) \neq 0$, then k_{12} does not reduce to Smoluchowski's result, even if $U(r) = 0$.

To find the form of $H(r)$ it is appropriate to consider a solution with only two solute particles, say particle 1 at the origin and particle 2 at r. In such a system $c(r)$ still has a statistical meaning as a pair-distribution function. Now, as particle 2 diffuses with velocity $v_2(r)$, it generates a pattern of flow in the medium which may be expressed as the velocity $v_m(r')$ at each point r' in the medium. The well-known result may be expressed in the form

$$v_m(r') = \mathsf{A}\cdot v_2(r) \quad (9)$$

where $\mathsf{A} = \mathsf{A}(r,r')$ is a tensor evaluated by Stokes.[10,11] In the present case this expression takes a simple form; the flow at the origin, neglecting the presence of particle 1 for the moment, is

$$v_m(0) = \zeta_{12}v_2(r)/4\pi\eta r$$
$$\zeta_{12} \equiv [\zeta_1^{-1} + \zeta_2^{-1}]^{-1} \quad (10)$$

and is in a direction away from the incoming particle. (We neglect a shorter range component having r^{-3} distance dependence.) There being no restoring force on particle 1, it will, if initially located at the origin, tend to drift away with the velocity $v_m(0)$. Thus the net velocity of approach of the two particles has the magnitude

$$v_2(r) - v_m(0) = v_2(r)[1 - \zeta_{12}/4\pi\eta r] \quad (11)$$

The similarity to the electrophoretic effect in the Debye–Hückel–Onsager conductance theory is now obvious.

In order to restore the problem to one having spherical symmetry, *i.e.*, in order to account for this effect while keeping particle 1 at the origin, we may introduce a virtual force on particle 2 having the magnitude $v_m(0)\zeta_{12}$ and directed away from the origin. This leads to the same relative velocity as calculated in eq 11, and on comparison with eq 2 we see that we have

$$H(r) = \zeta_{12}^2/4\pi\eta r \quad (12)$$

In the case that $U(r)$ is the Coulomb potential, the integral in eq 7 is readily evaluated with this $H(r)$. The final result for k_{12} is

$$k_{12} = 2\pi RD_{12}\frac{x}{e^x - 1 + \frac{\zeta_{12}}{4\pi\eta R}\{e^x[1 - (1/x)] + (1/x)\}} \quad (13)$$

(10) H. Lamb, "Hydrodynamics," 6th ed, Dover Publications, New York, N. Y., 1956, p 597.

(11) H. L. Friedman, *Physica*, **30**, 537 (1964).

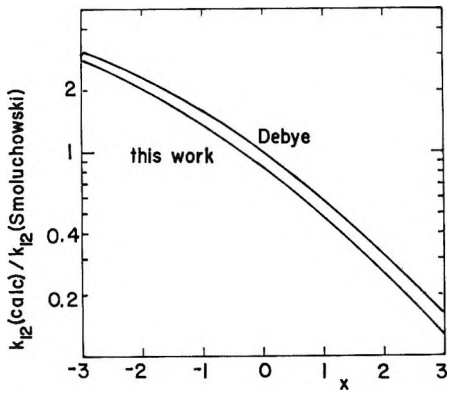

Figure 1. Effect of interactions on the rate constant for diffusion-controlled reactions. The abscissa is the coulomb potential in units of kT at the reaction distance (eq 14). For two sodium ions in water at room temperature $x = 1$ at a separation of 7.14 A. The upper curve is calculated for a Coulomb potential according to Debye's equation while the lower curve includes the hydrodynamic interaction dealt with in this paper. The results are expressed as the ratio of the calculated k_{12} to k_{12} (Smoluchowski) $= 2\pi D_{12}R$ to show the effect of all of the interactions.

where x is the Coulomb potential in units of kT at the reaction distance

$$x \equiv U(R)/kT = e_1e_2/\epsilon RkT \tag{14}$$

It is consistent with the other assumptions in this calculation to use Stokes' law to calculate the friction coefficients, in which case we have

$$\zeta_{12}/4\pi\eta R = \frac{3}{2}\frac{l_1l_2}{[l_1 + l_2]^2} \leq \frac{3}{8} \tag{15}$$

where the equality in the last member pertains to the case $l_1 = l_2$. This function falls off only slowly as l_1/l_2 is changed from unity. In Figure 1 we show a graph of eq 13 for the case $l_1 = l_2$.

It is apparent that the hydrodynamic interaction need be taken into account only in calculations of rather high accuracy. Its effect is to reduce the rate constant by about 15% over the whole range of charges covered in Figure 1. The hydrodynamic effect will be present equally in the reverse reaction; since it cannot contribute to the free energy of an association process, it must slow down the dissociation rate by the same amount as the association. In these respects the effect is equivalent to a decrease in diffusion coefficients of reacting or dissociating particles.

The possibility of finding experimental evidence for the hydrodynamic effect is made remote by the ease with which a 15% change can be introduced at various points in any comparison of calculated and observed rate constants for diffusion-controlled reactions. For one thing, the latter are difficult to determine with an uncertainty less than 15%. In the case of reaction between small molecules or ions, considerable uncertainty is introduced by neglect of the molecular structure of the solvent. In the case of reaction between colloidal particles the diameters are hard to determine independently as are the amount and distribution of electric charges, if any. Another source of uncertainty in the case of charged particles is the ionic strength correction discussed by Bass and Greenhalgh.[8] The hydrodynamic correction would only be important in a case in which these difficulties could be overcome and an exact comparison of an experimental rate constant and a calculation from a model were required.

The Radiation-Induced Addition of Methylsilane and Dimethylsilane to Ethylene. A Gas-Phase Ionic Reaction[1]

by F. W. Lampe, J. S. Snyderman, and W. H. Johnston

Johnston Laboratories, Inc., Baltimore, Maryland 21215 *(Received August 15, 1966)*

Methylsilane and dimethylsilane undergo radiation-induced addition to ethylene with the formation of telomeric products, 1:1 and 1:2 telomers being observed. At 50°, $G(1:1)$ values of 38 and 15 for methylsilane and dimethylsilane, respectively, are observed for a 3:1 reactant ratio of silane to ethylene. $G(1:1)$ values, in the case of methylsilane, of several hundred are observed at temperatures up to 250°. Nitric oxide inhibits these yields only slightly while NH_3 is a more efficient inhibitor. These facts plus an observed temperature dependence corresponding to about 1 kcal/mole strongly suggest that the chain reaction forming telomer is ionic.

The magnitude of the specific reaction rates of ion–molecule reactions, as measured in mass spectrometric studies, has long been suggestive of the importance of such reactions in gas-phase radiation chemistry.[2] A number of reports have appeared in the literature which show quite conclusively that ion–molecule reactions occur as elementary steps in complex radiation-induced chemical conversions[3] and as dominant chain propagation steps in isotopic exchange reactions.[4,5] We wish to report herewith some studies of the gas-phase radiation-induced reactions of methylsilanes with ethylene in which the dominant process appears to be an addition of the stoichiometry

$$(CH_3)_nSiH_{4-n} + C_2H_4 \longrightarrow (CH_3)_nSiH_{3-n}C_2H_5 \quad (1)$$

which occurs predominantly *via* an ionic chain reaction.

Experimental Section

Methylsilane and dimethylsilane were obtained from Peninsular ChemResearch Inc. These compounds were subjected to several freeze–pump–melt cycles on a standard high-vacuum line and then used directly in the experiments. An impurity of the order of about 1% was noted in each compound, but it was of such a nature that it did not interfere with the product analyses. Ethylene was Phillips research grade which was given one freeze–pump cycle. Nitric oxide, obtained from the Matheson Co., was given one freeze–pump cycle, and then the middle third from a vacuum distillation used.

Irradiations were conducted using γ-rays from an 8200 curie Co^{60} Irradiator (Model GR-9) manufactured by U. S. Nuclear Corp. The dose rate was determined using ethylene dosimetry ($G_{H_2} = 1.2$)[6] to be 7.5×10^{19} ev/g–hr. The irradiations were carried out in a stainless steel cell of 60-cm³ volume. Total pressures of reactants were maintained sufficiently low to ensure that none of the silane reactant was in the liquid state. Maximum conversion of the less abundant reactant was of the order of ~12%.

Products were analyzed quantitatively with a Varian Aerograph Model 202-1 gas chromatograph. The column used had a total length of 40 ft, consisting of 20 ft of 20% diethylene glycol succinate in series with 20 ft of 20% silicone GE SF-96, both on 45/60 firebrick.

(1) Report No. JLI-3655-2 on work supported by the AEC, Division of Isotopes Development, under Contract No. AT(30-1)-3655 and AT(30-1)-2901. Although the majority of this research was performed under Contract No. AT(30-1)-3655, the initial laboratory experiments were done under Contract No. AT(30-1)-2901.

(2) F. W. Lampe, J. L. Franklin, and F. H. Field, *Progr. Reaction Kinetics*, **1**, 67 (1961).

(3) For example, see (a) G. G. Meisels, W. H. Hamill, and R. R. Williams, *J. Phys. Chem.*, **61**, 1456 (1957); (b) J. H. Futrell, *J. Am. Chem. Soc.*, **81**, 5921 (1959); (c) F. W. Lampe, *ibid.*, **82**, 1551 (1960); (d) J. H. Futrell and T. O. Tiernan, *J. Chem. Phys.*, **38**, 150 (1963); (e) P. J. Ausloos and S. G. Lias, *ibid.*, **38**, 2207 (1963); (f) P. J. Ausloos and S. G. Lias, *ibid.*, **36**, 3163 (1962).

(4) (a) S. O. Thompson and O. A. Schaeffer, *J. Am. Chem. Soc.*, **80**, 553 (1958); (b) O. A. Schaeffer and S. O. Thompson, *Radiation Res.*, **10**, 671 (1959).

(5) T. H. Pratt and R. Wolfgang, *J. Am. Chem. Soc.*, **83**, 10 (1961).

(6) K. Yang and P. L. Gant, *J. Phys. Chem.*, **65**, 1861 (1961).

Table I:[a] Radiation Yields of Telomeric Products in the Radiolysis of CH_3SiH_3–C_2H_4 Mixtures

Run no.	Temp, °C	$P(CH_3SiH_3)$, atm	$P(C_2H_4)$, atm	P(NO) or $P(NH_3)$, atm	$G(1:1)$ $CH_3SiH_2C_2H_5$	$G(1:2)$ $CH_3SiH(C_2H_5)_2$
1	50	2.58	5.11	0	16	4.8
2	50	3.94	3.99	0	36	2.8
3	50	5.32	2.65	0	36	1.8
4	50	5.98	2.01	0	38	1.5
5	50	5.32	2.66	0.272	34	1.7
6	50	5.31	2.66	0.796	31	2.2
7	200	6.84	3.49	0	403	15.3
8	200	6.84	3.44	0.490	292	14.3
9	200	6.86	3.49	0.388 (NH_3)	239	9.8
10	70	7.08	3.54	0	74	2.4
11	100	7.08	3.54	0	158	5.5
12	150	6.99	3.45	0	220 ± 21[b]	8.4 ± 0.5[b]
13	200	7.10	3.51	0	192 ± 14[c]	7.5 ± 1.0[c]
14	250	7.08	3.54	0	215	11.3

[a] All experiments carried out with a dose of 3.00×10^{20} ev/g. [b] Average of two replicate runs. [c] Average of three replicate runs.

The column temperature employed was 108°; the helium carrier flow rate was 35 ml/min. Product identification was made by examination of chromatographically separated peaks with a Johnston Laboratories concidence mass spectrometer and by retention time checks.

Results

A. Methylsilane–Ethylene Reaction. The 100-ev yields of the 1:1 and 1:2 addition products of CH_3SiH_3 and C_2H_4 are shown in Table I. We have adopted arbitrarily the convention of basing G values on the total energy absorbed rather than on the energy absorbed by the silanes alone. This convention will take into account the probably important contribution of ionization of silanes by hydride transfer by ions from the ethylene. Irradiation of CH_3SiH_3 to a dose of 2.57×10^{21} ev/g in the absence of ethylene gave rise to about five chromatographically observable products that were condensable in liquid nitrogen; the largest (by a factor of at least 10) was identified mass spectrometrically as the dimer $C_2Si_2H_{10}$ with a G value for formation of 1.1. The dimer was definitely observed gas chromatographically in the runs with ethylene present, but its 100-ev yield was difficult to determine with any precision because of an overlap with the much larger peaks of the 1:1 and 1:2 telomeric products. However, it was *not* observed in any of the experiments in which NO was present.

Following runs 7–9, the reaction cell was cleaned before conducting runs 10–14. G values as high as those obtained in runs 7 and 8 were never obtained again, which indicates the sensitivity of the reaction to surface conditions. This is typical of chain reactions (which this obviously is) in which the surface conditions affect the termination rate and make precise reproducibility difficult. It does not affect the main conclusion of the paper. The day-to-day reproducibility, in the absence of adding foreign gases such as NO and NH_3, is indicated by runs 12 and 13, which are in actuality averages of replicate experiments. The purely thermal reaction at the highest temperature employed (250°) amounts to about 5% of the radiation-induced process.

B. Dimethylsilane–Ethylene Reaction. The 100-ev yields of the 1:1 and 1:2 telomeric products at 50° are shown in Table II. Runs 1–7 show the effect of varying the reactant ratio at a constant total pressure upon the G values. The variation of G under such conditions for both the 1:1 and 1:2 telomers is as expected with the maximum for the 1:1 occurring at about a 3:1 silane to ethylene ratio and the 1:2 maximum occurring at about a 1:3 ratio. Runs 8–10 show the effect of NO on the yield of the 1:1 telomer at a reactant ratio of 3:1 and should be compared with run 6. Dimer yields were not measured.

Discussion

The efficient, free-radical addition of silane and organo derivatives in which there is at least one Si–H bond has long been known to occur,[7] presumably *via* the chain-propagation steps 2 and 3. Higher addition prod-

$$R_1R_2R_3Si\cdot + CH_2{=}CHR \longrightarrow R_1R_2R_3SiCH_2\dot{C}HR \quad (2)$$

(7) C. Walling, "Free Radicals in Solution," John Wiley and Sons, Inc., New York, N. Y., 1957, pp 343, 344.

$$R_1R_2R_3SiCH_2\dot{C}HR + R_1R_2R_3SiH \longrightarrow R_1R_2R_3SiCH_2CH_2R + R_1R_2R_3Si\cdot \quad (3)$$

ucts occur when the radical product of (2) adds to another olefin molecule. Analogous free-radical reactions also occur for the cases in which SiH_2 groups are replaced by the isoelectronic groups PH and S.[8] Free radicals are certainly produced in the radiolysis and it is therefore not surprising that in both the methylsilane and dimethylsilane additions to ethylene, evidence of a chain reaction is observed (*cf.* Tables I and II). However, the effect of adding NO is rather surprising. As can be seen in Table I, with as much as 10% NO added to the reactants, the yield of 1:1 telomer is reduced by only about 15% at 50°, and a level of ~5% NO reduces the $G(1:1)$ at 200° from 403 to only 292. In the dimethylsilane–ethylene reactions, Table II, $G(1:1)$ is reduced only by about 50% when NO is added up to ~17%. In contrast, NO at a level of only 3% reduced $G(CH_3SC_2H_5)$ in a CH_3SH–C_2H_4 radiolysis from 7000 to essentially zero.[9] The nonreactivity of NO toward $\geq$Si· radicals can be ruled out on the basis of studies of the $Hg(^3P_1)$-photosensitized decomposition of alkylsilanes by Nay, Woodall, Strausz, and Gunning.[10] These authors found that addition of NO at levels less than 1% completely suppressed dimer formation *via* NO scavenging of $\geq$Si· radicals. From the magnitude of the unscavenged yields, particularly in the methylsilane case, we conclude that a nonradical chain process is occurring.

It has been proposed[11] that singlet radicals MeSiH: and Me_2Si: might be involved in reactions of substituted silanes. These singlet radicals would most likely react in our system by either insertion reaction with the silane to yield dimer or with ethylene to yield the corresponding vinyl silane, *viz.*

$$R_1R_2Si: + R_1R_2SiH_2 \longrightarrow R_1R_2SiHSiHMe_2 \quad (4)$$

$$R_1R_2Si: + C_2H_4 \longrightarrow R_1R_2SiCH{=}CH_2 \quad (5)$$

We have not detected the vinyl silane as a product although this does not preclude the occurrence of (4) and (5) as minor processes. The important point with regard to this paper is that the singlet radicals do not lead to telomer formation nor to a chain reaction. We must expect triplet radicals R_1R_2Si: to be scavenged by nitric oxide, and, therefore, we must look elsewhere for our explanation of the unscavenged (by NO) chain formation of telomer.

The only other major transient species present that will not contain an unpaired electron (rendering it unscavengeable by NO) is the siliconium ion $R_1R_2SiH^+$. This ion is one of the major ions in the mass spectra of $(CH_3)_2SiH_2$ and CH_3SiH_3 and will, in addition, be formed *via* hydride ion abstraction reactions of fragment ions of the two compounds. For example, in SiH_4 the predominent ion–molecule reaction[12] is

$$SiH_2^+ + SiH_4 \longrightarrow SiH_3^+ + SiH_3 \quad (6)$$

the analogs of which in $(CH_3)_2SiH_2$ and CH_3SiH_3 would result in the siliconium ion, $R_1R_2SiH^+$, being the most abundant ion present. We suggest that the residual chain reaction that is uneffected by NO proceeds *via* the gas-phase silane analog of the acid-catalyzed alkylation of a paraffin with an olefin, *viz.*

$$R_1R_2SiH^+ + C_2H_4 \longrightarrow \begin{matrix} & R_1 & \\ & \diagdown & \\ H & — & SiCH_2CH_2^+ \\ & \diagup & \\ & R_2 & \end{matrix} \quad (7)$$

$$\begin{matrix} & R_1 & \\ & \diagdown & \\ H & — & SiCH_2CH_2^+ + \\ & \diagup & \\ & R_2 & \end{matrix} \qquad R_1R_2SiH_2 \longrightarrow \begin{matrix} & R_1 & \\ & \diagdown & \\ H & — & SiC_2H_5 \\ & \diagup & \\ & R_2 & \end{matrix} + R_1R_2SiH^+ \quad (8)$$

$$\begin{matrix} & R_1 & \\ & \diagdown & \\ & Si^+ & — C_2H_5 \\ & \diagup & \\ & R_2 & \end{matrix} + R_1R_2SiH_2$$

Table II:[a] Radiation Yields of Telomeric Products in the Radiolysis of $(CH_3)_2SiH_2$–C_2H_4 Mixtures at 50°

Run no.	$P(Me_2SiH_2)$, atm	$P(C_2H_4)$, atm	$P(NO)$, atm	$G(1:1)$ $(CH_3)_2Si$-HC_2H_5	$G(1:2)$ $(CH_3)_2Si$-$(C_2H_5)_2$
1	0.782	3.13	0	3.3	1.6
2	1.01	3.05	0	4.0	1.5
3	1.32	2.64	0	6.5	1.6
4	1.97	1.97	0	10.6	0.7
5	2.60	1.32	0	10.0	...
6	2.95	0.99	0	15.3	0.2
7	3.21	0.64	0	12.0	...
8	2.97	0.99	0.12	7.6	...
9	2.90	0.97	0.36	9.0	...
10	2.97	0.99	0.80	5.8	...

[a] All experiments carried out with a dose of 3.00×10^{20} ev/g.

An Arrhenius plot of ln $G(1:1)$ *vs.* $1/T$ of the data in Table I for runs 10–14 yields a temperature coefficient of the order of 1 kcal/mole. This is what is expected if the principal mode of telomer formation proceeds by ion–molecule reactions.

The radiation yields of telomeric products in the CH_3SiH_3–C_2H_4 mixture are higher than those in the $(CH_3)_2SiH_2$–C_2H_4 mixture. One can rationalize the longer chains in the case of the $CH_3SiH_2^+$ ion because the expected greater stability of the $(CH_3)_2SiH^+$ ion should also lead to decreased reactivity and shorter chains with the dimethylsiliconium ion.

The effect of the added NH_3 is seen in Table I, run 9. We have not attempted to establish a level of NH_3 concentration at which $G(1:1)$ and $G(1:2)$ no longer decrease with further NH_3 addition, but it is clear that NH_3 is a more effective inhibitor than NO. Since NH_3 has been shown to be an excellent inhibitor of carbonium ion reactions[13] this effect is consistent with our suggestion that the telomerization is predominantly an ionic chain.

Acknowledgments. The authors wish to thank Dr. Gordon Fergusson and Dr. Larry Kevan for their many helpful suggestions and Marvin Vestal for his contribution to the mass spectrometer analyses and help in interpretation of the spectral data.

(8) C. Walling, ref 7, pp 313–322, 341–343.

(9) F. W. Lampe and W. H. Johnston, Proceedings of the 7th Japan Conference on Radioisotopes, Tokyo, 1966.

(10) M. A. Nay, G. N. C. Woodall, O. P. Strausz, and H. E. Gunning, *J. Am. Chem. Soc.*, **87**, 179 (1965).

(11) P. S. Skell and E. J. Goldstein, *ibid.*, **86**, 1442 (1964).

(12) G. G. Hess and F. W. Lampe, *J. Chem. Phys.*, **44**, 2257 (1966).

(13) M. A. Bonin, W. R. Busler, and F. Williams, *J. Am. Chem. Soc.*, **84**, 4355 (1962).

Vapor Pressure Measurements on Thorium Nitrides[1]

by S. Aronson and A. B. Auskern

Brookhaven National Laboratory, Upton, New York *(Received June 27, 1966)*

Three nitrides of thorium have been reported, ThN, Th_3N_4, and Th_2N_3. In the recent literature, the existence of Th_3N_4 has been questioned. Samples of thorium nitride were prepared by heating thorium metal in nitrogen at 500–900°. The composition of the nitride determined from the weight change corresponded to the formula Th_3N_4. The X-ray diffraction pattern of the nitride was different from that reported for ThN or Th_2N_3. Vapor pressure measurements over the two-phase system ThN–Th_3N_4 were made at temperatures of 1450–1800°. The nitrogen pressure ranged from 5 to 200 torr. The enthalpy and entropy changes calculated from the data for the reaction $6ThN(s) + N_2(g) = 2Th_3N_4(s)$ were −72.7 kcal/mole of N_2 and −32.7 eu/mole of N_2, respectively.

Three nitrides of thorium have been reported,[2–4] ThN, Th_3N_4, and Th_2N_3. In the recent literature, the existence of Th_3N_4 as a definite compound has been questioned[2–4] and reports of its occurrence have been attributed to incomplete formation of Th_2N_3.

In the present study, Th_3N_4 has been prepared and its existence has been established. Vapor pressures of nitrogen over the two-phase system ThN–Th_3N_4 were measured and thermodynamic information was obtained.

(1) This work was performed under the auspices of the AEC.

(2) P. Schwarzkopf and R. Kieffer, "Refractory Hard Metals," The Macmillan Co., New York, N. Y., 1953, p 254.

Experimental Section

Materials. Thorium metal powder was obtained from Electronic Space Products, Inc., Los Angeles, Calif. A chemical analysis was supplied with the sample and indicated the presence of the following impurities (in ppm): Ca (300), C (154), Ni (101), Fe (57), Cr (35), Mg (22), Ti (12), and O (1100). Nitrogen gas (prepurified grade, 99.997%) was obtained from the Matheson Co., East Rutherford, N. J., and was passed through a liquid nitrogen trap before using.

Th_3N_4 was prepared by treating thorium metal with nitrogen gas. Thorium powder was placed in a tungsten crucible and was heated in nitrogen at 200 torr to about 600°, at which temperature a rapid, exothermic reaction occurred. The pressure was then maintained at about 1 atm and the temperature was raised to 900°. Heating was continued for about 1 hr. The color of the resulting powder was maroon. The weight change which occurred upon nitriding corresponded to the formation of a compound of composition $ThN_{1.319\pm0.002}$ assuming no impurities were present in the thorium metal powder. If the oxygen found in the thorium metal (0.11 wt %) was combined with thorium in the form of ThO_2, and if the small amounts of metallic impurities in the thorium are ignored, then the calculated composition of the nitride is $ThN_{1.33}$ or Th_3N_4. The Th_3N_4 was stored and handled in an inert-atmosphere drybox to avoid air oxidation. In some operations the powder was exposed to air momentarily.

Apparatus. The heating arrangement used to make vapor pressure measurements on thorium nitrides is shown in Figure 1. Th_3N_4 powder (1.5–3 g) was pressed into a cylinder $^3/_8$ in. in diameter. A $^1/_{10}$-in. diameter hole was drilled halfway into the cylinder so that it could be supported on the end of a calibrated tungsten–5% rhenium *vs.* tungsten–26% rhenium thermocouple obtained from the Hoskins Manufacturing Co., Detroit, Mich. The temperature was controlled manually and was constant to better than ±5° at any setting. The use of a thermocouple was found to be more convenient than an optical pyrometer which was occasionally employed. The sample was contained in a tungsten-lined alumina crucible. The tungsten foil acted as a susceptor for the induction heating coil. Care was taken to avoid contact between the nitride and alumina during heating since thorium nitrides react with alumina at the temperatures employed.

The following procedure was followed in making vapor pressure measurements. The Th_3N_4 sample was first outgassed at 500° under a pressure of 10^{-5} torr. Nitrogen gas was then admitted to the system at a specified pressure. Pressure measurements were made

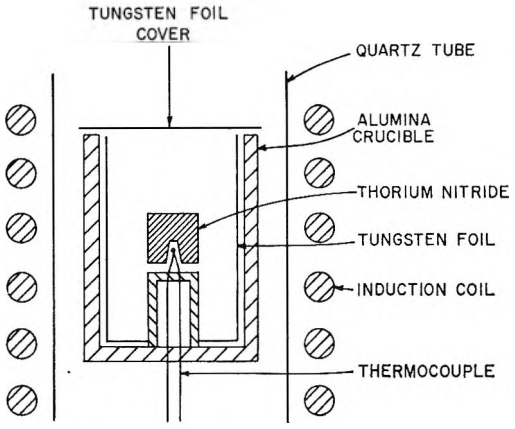

Figure 1. Apparatus for vapor pressure measurements on thorium nitrides.

with a cathetometer focused on a mercury manometer attached to the system. The sample was heated to temperatures of 1450–1800° and pressure readings were taken at various temperatures after waiting periods of 30 to 120 min. Although a large temperature difference existed between the sample and the manometer, pressure corrections for thermal transpiration effects were not required. The use of large-bore glass tubing in the region of the temperature gradient and the relatively high nitrogen pressures (>1 torr) ensured a uniform pressure throughout the system.

X-Ray Diffraction Measurements. X-Ray diffraction data on the powder samples were obtained with a Phillips Electronics diffractometer. Each sample was placed in a container consisting partly of a thin Mylar film through which the X-ray beam passed. The sample was protected from air and water vapor by flowing helium gas through the container. The lattice parameter of ThN was calculated using several values of θ in the back-reflection region. An extrapolation of the lattice parameter *vs.* $\sin^2\theta$ to $\theta = 90°$ was made.

Results and Discussion

X-Ray diffraction data were obtained on the as-prepared Th_3N_4, on the Th_3N_4 samples which were subjected to the vapor pressure measurements, and on ThN prepared by decomposing Th_3N_4 *in vacuo* at 1600–1700°. The diffraction data obtained on Th_3N_4 are shown in Table I. A comparison of the *d* spacings of Th_3N_4 with those of Th_2N_3[5,6] and those of ThN shows

(3) F. A. Rough and A. A. Bauer, "Constitutional Diagrams of Uranium and Thorium Alloys," Addison-Wesley Publishing Co., Reading, Mass., 1958, p 133.

(4) E. K. Storms, "A Critical Review of Refractories," AEC Report LA-2942, Aug 13, 1964.

(5) W. H. Zachariasen, "The Crystal Structure of Th_2N_3," AECD 2090, Jan 19, 1948.

(6) W. H. Zachariasen, *Acta Cryst.*, 2, 388 (1949).

that the diffraction pattern of Th_3N_4 is different from those of the other two nitrides. Th_2N_3 has a hexagonal unit cell of the La_2O_3 type with the lattice parameters a = 3.875 A and c = 6.175 A.[5,6] ThN is face-centered cubic with a lattice parameter of 5.159 A.[7] The diffraction peaks of Th_3N_4 could not be readily indexed. The crystal structure of the compound appears to be complex. The measured lattice parameter of ThN was 5.159 ± 0.002 A, which agrees with the other lattice parameter measurements on ThN.[7] In the X-ray patterns obtained on Th_3N_4 and ThN, a weak line occurred at 2θ values close to 27.5°. Since the strongest line in the ThO_2 pattern occurs at approximately this angle, the presence of a small amount of ThO_2 may be indicated.

The X-ray diffraction results and the consistent change in weight which occurs upon nitriding thorium establish the existence of Th_3N_4 as a stable phase.[8]

Table I: X-Ray Diffraction Data on Th_3N_4, Th_2N_3, and ThN

Th_3N_4		Th_2N_3[5,6]		ThN	
d, A	I	*d*, A	I	*d*, A	I
3.32	s	3.31	w		
3.25	w				
3.04	s	3.03	w		
3.01	vs			2.98	vs
		2.91	s		
2.86	s				
2.54	f			2.58	s
2.39	w				
		2.26	w		
2.12	f				
1.9	m	1.93	m	1.824	s
1.782	m				
		1.75	m		
1.690	w				
1.674	w	1.675	vw		
1.632	m	1.64	ms		
1.603	w	1.61	m−		
1.555	f			1.556	s
1.523	f	1.53	vw		
1.505	f				
		1.47	vw		
		1.40	vvw	1.489	m
1.310	f				
		1.298	m−	1.290	w
1.273	f				
1.276	f	1.265	vw		
1.245	w	1.24	s−		
1.235	w				
		1.205	m		
1.197	w				
1.188	f				
				1.181	m
1.167	f	1.17	w−		
		1.156	w		

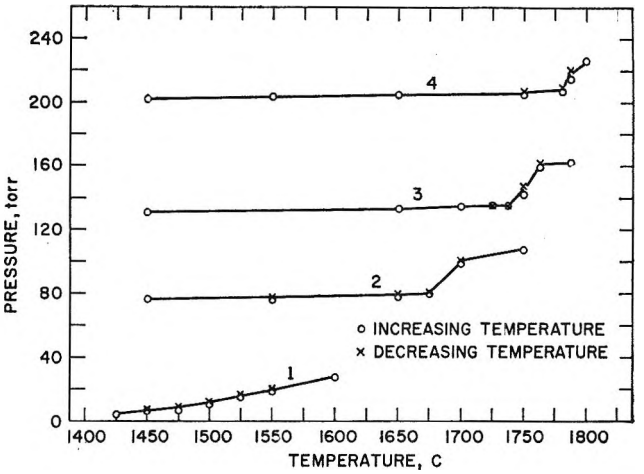

Figure 2. Pressures of nitrogen over thorium nitrides.

On the basis of the experimental conditions used to prepare Th_3N_4 in this study and upon examination of the vapor pressure data to be presented, it appears unlikely that Th_2N_3 can be formed from thorium metal and nitrogen at pressures below 1 atm. Chiotti prepared Th_2N_3 using ammonia gas.[9] It is possible, therefore, that ammonia or nitrogen at high pressures is required for the formation of Th_2N_3.

Vapor pressure data were obtained by heating samples of Th_3N_4 in various pressures of nitrogen. *In vacuo*, Th_3N_4 lost nitrogen at temperatures below 1300°. In the presence of nitrogen, the decomposition temperature increased with increasing nitrogen pressure. Some typical data are shown in Figure 2. The data are consistent with the assumption that two stoichiometric phases, ThN and Th_3N_4, exist. The data in Figure 2 are interpreted in the following manner.[10] In the case of curve 2, the Th_3N_4 sample did not lose nitrogen, upon increasing the temperature, until 1702°. The slow increase in pressure with temperature below 1702° is accounted for by the increase in the temperature of the cell in the fixed-volume system. The vapor pressure of the two-phase system, ThN–Th_3-

(7) W. M. Olson and R. N. R. Mulford, *J. Phys. Chem.*, 69, 1223 (1965).

(8) N. J. Bridger and R. M. Dell, unpublished data, give the formula $ThN_{1.30}$ for thorium nitride prepared by them. The reported composition is based on chemical analyses for nitrogen (Dumas method), thorium (ignition to ThO_2), and oxygen (vacuum fusion).

(9) P. Chiotti, *J. Am. Ceram. Soc.*, **35**, 123 (1952).

(10) Complete decomposition of Th_3N_4 to ThN (1.5–3-g samples) caused an increase in pressure in the system of 20 to 40 torr as the volume of the system was approximately 750 cc. The volume of the system was determined from pressure–volume experiments using calibrated volumes. The pressure in the system was also determined as a function of the temperature of the cell. Since the data were consistent with the assumption of a simple two-phase region between ThN and Th_3N_4, quantitative use of the temperature and pressure calibrations was not required.

N_4, at 1702° is taken as 101 ± 1 torr, which is the average pressure measured at ascending and descending temperatures. In general, as is observed in Figure 2, the pressures measured at descending temperatures were slightly higher than those measured at ascending temperatures. Decomposition of the nitride to ThN was complete at 1750°. The data represented by curves 3 and 4 can be described in a similar manner. The vapor pressures obtained from curves 3 and 4 are 145 ± 2 torr at 1751° and 218 ± 2 at 178°. In the case of curve 1, vapor pressure values for the two-phase region were obtained at temperatures of 1452, 1476, 1500, 1524, and 1550°.

The data obtained were not sufficiently accurate to determine whether narrow regions of nonstoichiometry occur in ThN and Th_3N_4. Examination of the pressure data showed no indication of nonstoichiometry in the vicinity of Th_3N_4. There was some irreversibility and sluggishness in obtaining pressure equilibrium in samples close in composition to ThN. The possibility, therefore, exists of some nonstoichiometry occurring between the composition ThN and about $ThN_{1.05}$. Since, however, Olson and Mulford[7] have reported, on the basis of X-ray lattice parameter measurements, that little or no nonstoichiometry occurs in ThN, it is likely that the sluggishness in attaining equilibrium is due to kinetic reasons.

A logarithmic plot of the vapor pressure *vs.* reciprocal absolute temperature was linear and is shown in Figure 3. The enthalpy and entropy changes for the reaction

$$6ThN(s) + N_2(g) = 2Th_3N_4(s)$$

calculated from the slope and intercept of the plot in Figure 3 are −72.7 ± 2 kcal/mole of N_2 and −32.7 ± 2 eu/mole of N_2, respectively. The limits of error which are presented are greater than the standard deviations and represent estimates of the accuracy of the values based on the reproducibility of the data and other experimental considerations.

The above data can be used to estimate the heat and entropy of formation of ThN. We first estimate a heat of reaction of −77.5 kcal/mole of N_2 and an entropy of reaction of −38.2 eu/mole of N_2 at 298°K by assuming a value for ΔC_p of 3 eu/mole N_2. The heat and entropy of formation of Th_3N_4 at 298°K have been given as −155.2 kcal/mole of N_2 and −44.8 eu/mole of N_2,[11] respectively. Combining the information on the formation of Th_3N_4 and the data on the reaction in eq 1, we obtain values for the heat and entropy of formation of ThN. The values for ThN are shown in Table II together with values obtained for group IV transition metal nitrides and uranium nitride. The mononitrides shown have face-centered-cubic structures. The thermodynamic properties of ThN are thus similar to those of ZrN, HfN, and TiN. This is quite reasonable since the metals are all quadrivalent and other refractory compounds of thorium, such as the monocarbide, have properties similar to

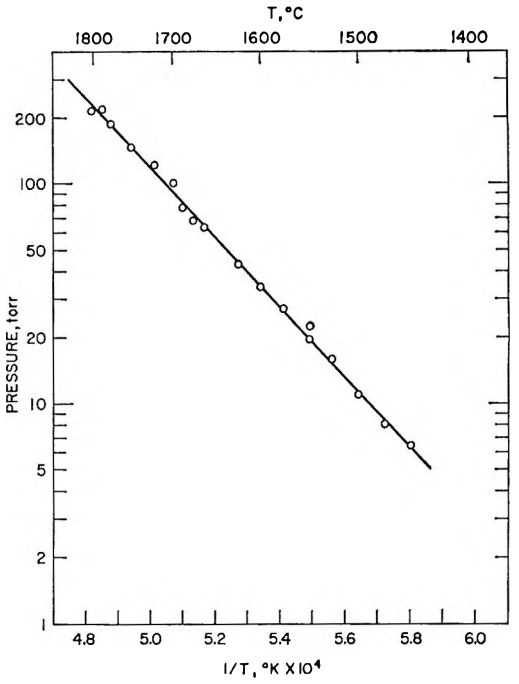

Figure 3. Vapor pressures of nitrogen over the two-phase system ThN–Th_3N_4.

Table II: Heats and Entropies of Formation of Selected Mononitrides

Compd	$-\Delta H°_{298}$, kcal/g-atom of N	$-\Delta S°_{298}$, kcal/g-atom of N	Ref
ThN	90.6	23.5	...
ZrN	87.6	22.9[a]	4
HfN	88.2	22.9	4
TiN	80.5	23.0	4
UN	70.4	21.9	12

[a] The values of $\Delta S°_{298}$ for ZrN, HfN, TiN, and UN were obtained by subtracting the standard entropies of the elements at 298°K[13] from those of the compounds.[4,12]

(11) L. Brewer, L. A. Bromley, P. W. Gilles, and N. L. Lofgren, "The Chemistry and Metallurgy of Miscellaneous Materials—Thermodynamics," L. L. Quill, Ed., McGraw-Hill Book Co., Inc., New York, N. Y., 1950, p 42.

(12) M. H. Rand and O. Kubaschewski, "The Thermochemical Properties of Uranium Compounds," Oliver and Boyd Ltd., Edinburgh, Scotalnd, 1963, p 41.

(13) D. R. Stull and G. C. Sinke, "Thermodynamic Properties of the Elements," American Chemical Society, Washington, D. C., 1956.

the corresponding refractory compounds of the group IV transition metals.[2,4]

Acknowledgments. The authors wish to thank Mrs. E. Cisney for obtaining the X-ray diffraction data. We thank J. G. Davis for his aid in performing the vapor pressure measurements.

The Surface Structure of Porous Silicas

by L. R. Snyder and J. W. Ward

Research Center, Union Oil Company of California, Brea, California *(Received June 27, 1966)*

A variety of experimental techniques (notably selective silanization and infrared spectroscopy) have been applied to a wide range of high surface area (139–824 m^2/g) silica samples in an effort to characterize the nature of their surfaces and to identify the types of surface groups which participate most effectively in adsorption on and reaction with the silica surface. A previously overlooked surface hydroxyl type (so-called "reactive hydroxyls") constitutes the strongest site for the adsorption of aromatic hydrocarbons such as fluoranthene. These hydroxyls also react most rapidly with trimethylchlorosilane and dimethyldichlorosilane. Reactive hydroxyls appear to consist of an adjacent pair of strongly hydrogen bonded surface hydroxyls. The proposal of DeBoer and Vleeskens that the silica surface can be annealed by thermal treatment now appears incorrect. The silica surface varies widely among various samples. Reactive hydroxyls predominate on fine pore silicas and are virtually absent from coarse pore samples.

The surface properties of silicas are important for both practical and theoretical reasons. The nature of the silica surface and its interactions with various adsorbates and reactants have been intensively studied (see review of Hockey[1] and subsequent work by Davydov, *et al.*[2]). On the basis of these studies, a fairly simple, reasonably consistent picture has emerged concerning the types of groups present on the silica surface and their respective roles in determining various surface phenomena. It is commonly accepted that the surface of a hydrated silica is covered with hydroxyl groups which are attached to silicon atoms, and that these surface hydroxyls may be classified into two distinct types: "free" hydroxyls which give rise to a narrow absorption band in the infrared near 3750 cm^{-1}, and hydrogen bonded ("bound") hydroxyl groups which are characterized by a broad absorption band in the infrared between 2800 and 3700 cm^{-1}. A major role has been accorded the free hydroxyls in adsorption on and reaction with the silica surface. Thus infrared absorption studies suggest that the selective adsorption of polar molecules and aromatic hydrocarbons on silica occurs primarily upon free hydroxyls.[3-6] The esterification of surface hydroxyls by extended reaction with trimethylchlorosilane (TMCS) and dimethyldichlorosilane (DMDCS) has also been shown to involve primarily free hydroxyls, with at most partial reaction of bound hydroxyls.[2] The greater importance of free hydroxyls in adsorption and reaction appears

(1) J. A. Hockey, *Chem. Ind.* (London), 57 (1965).

(2) V. Y. Davydov, A. V. Kiselev, and L. T. Zhuravlev, *Trans. Faraday Soc.*, **60**, 2254 (1964); *Russ. J. Phys. Chem.*, **38**, 1108 (1964).

(3) R. S. McDonald, *J. Am. Chem. Soc.*, **79**, 850 (1957).

(4) M. R. Basila, *J. Chem. Phys.*, **35**, 1151 (1961).

(5) G. A. Galkin, A. V. Kiselev, and V. I. Lygin, *Trans. Faraday Soc.*, **60**, 431 (1964).

(6) A. N. Sidorov and I. E. Neimark, *Russ. J. Phys. Chem.*, **38**, 1518 (1964).

superficially reasonable (see discussion of Kiselev, *et al.*[2,7]). Upon heating silicas above 200°, surface hydroxyls begin to condense to form siloxane bonds (Si–O–Si) or other oxide groups with loss of water. Siloxane groups appear unimportant in determining the specific adsorption properties of hydrated silicas; a fully dehydrated silica surface shows greatly reduced adsorption of both polar and unsaturated molecules.[7,8]

The variation of the silica surface among different samples has also received much attention. McDonald[9] has noted that the nature of the hydroxyl groups and the relative proportions of bound and free hydroxyls vary among different samples. Similarly, DeBoer and Vleeskens[10] and Hockey[1] have claimed that the surface of a fully hydrated silica can exhibit differences in hydroxyl concentration and in crystallinity or order. Kiselev and co-workers, on the other hand, have presented evidence that the surfaces of all but fine pore silicas are generally similar. For several maximally hydrated silicas and aerosils with surface areas between 39 and 750 m^2/g, it was observed[2] that the concentrations of surface hydroxyls are approximately constant for a given drying temperature between 200 and 1000°. Similarly, Kiselev, *et al.*,[7,8] found that relative adsorption and heats of adsorption on silica of various hydrocarbons (both saturated and unsaturated) and polar compounds are the same per unit area of surface for silicas of widely different origin and surface area. Only in the case of very fine pore silicas do differences in adsorption characteristics appear. These were attributed to increased adsorbent–adsorbate contacts which are possible in very fine pores.

In the present study, several different experimental techniques (infrared spectroscopy, selective silanization, liquid phase adsorption, chemical and physical analysis, and thermal treating) were applied to the characterization of eight widely different silica samples. The data obtained suggest a substantially revised view of the structure of the silica surface, the variability of the surface between different samples, the role of different surface groups in various adsorption and surface reaction phenomena, and the susceptibility of the silica surface to thermal treatment (*e.g.*, annealing).

Experimental Section

Materials. Eight different laboratory or commercial silica samples were investigated. These had the origin, geometrical characteristics, and aluminum contents listed in Table I.[11] The Davison silicas appeared to be hydrogels which had not been heated high enough to result in significant loss of structural water (see later discussion) and were used as received. The bulk density of the starting Cab-O-Sil was increased by mixing with water, drying at 110°, crushing, and sieving. The various gel preparations were not initially heated above 115° and were therefore assumed to be in a fully hydrated state. The particle sizes of all the samples of Table I fell in the 60–200 mesh range. Surface areas were determined by the BET method using nitrogen adsorption (16.2 A^2 assumed for N_2 molecular area).

Table I: History and Properties of the Silica Samples Studied in the Present Investigation

Sample no.	Sample description	Surface area, m^2/g	Pore diameter, A	% Al
I	Cab-O-Sil[a]	139	805	
II	Davison Code 62[b]	319	241	0.16
III	Ethyl silicate, pH 10[c]	380	243	0.01
IV	Ethyl silicate, pH <1[c]	496	120	0.01
V	Davison MS[b]	770	111	0.16
VI	Sodium silicate, MO[d]	792	70	
VII	Sodium silicate, blank[d]	824	64	
VIII	Davison Code 12[b]	748	41	0.11

[a] Cabot Corp. [b] W. R. Grace & Co., Davison Chemical Division. [c] Prepared by precipitation of hydrolyzed ethyl silicate from solution of indicated pH. [d] Prepared by precipitation of sodium silicate with HCl;[11] MO refers to the presence of methyl orange in the precipitation step.

The various silanes, TMCS, DMDCS, and hexamethyldisilazane (HMDS) were obtained from Applied Science Laboratories, Inc. (State College, Pa.) and were used as received.

Silica–Silane Reactions. Silane–silica reactions were carried out in a simple glass flow apparatus at 195 ± 5° using a nitrogen flow of 2 ml/sec as carrier gas and purge. The silica samples (3 to 6 g) contained in a detachable U-tube with glass wool plugs were first dried to constant weight in the apparatus (nitrogen flow) for removal of physically bound water. Incremental additions of the desired silane were made through a rubber septum by means of a syringe, with conditioning of the silica after each silane addition for 15 min (*i.e.*, to constant weight) to remove reaction products and unreacted silane. The weights of dry

(7) A. V. Kiselev, Y. S. Nikitin, R. S. Petrova, K. D. Shcherbakova, and Y. I. Yashin, *Anal. Chem.*, 36, 1526 (1964).

(8) A. V. Kiselev, "The Structure and Properties of Porous Materials," D. H. Everett and F. S. Stone, Ed., Butterworth and Co. Ltd., London, 1958, p 195.

(9) R. S. McDonald, *J. Phys. Chem.*, 62, 1168 (1958).

(10) J. H. DeBoer and J. M. Vleeskens, *Proc. Koninkl. Ned. Akad. Wetenschap., Ser. B*, 61, 2 (1958).

(11) F. H. Dickey, *J. Phys. Chem.*, 59, 695 (1955).

silica and of reacted silica after each silane addition were obtained to yield a plot of silica weight increase *vs.* silane addition.

Liquid Phase Adsorption Studies. The linear isotherm adsorption of the aromatic hydrocarbon fluoranthene ($C_{16}H_{10}$) by various silica samples (dried at 195° in a nitrogen stream to constant weight) from 5 vol % benzene–pentane was obtained in a standard procedure. A 160 × 10-mm column was packed with the silica to be tested, 10 ml of the latter solvent was passed through the column and rejected, 25 μl of 0.1% fluoranthene in benzene was charged to the column, and elution with solvent was continued at 3–5 cm³/min. Fractions (5 cc) were collected and measured for ultraviolet absorbance at 287 mμ. An equivalent retention volume $\underline{R}^0$ (equal to the distribution coefficient of fluoranthene in this system: K in cm³/g) was obtained in the usual way.[12]

Infrared Spectroscopic Measurements. The infrared spectra were determined with a Perkin-Elmer Model 221G double-beam spectrophotometer. The silicas, after various treatments, were compacted into 1-in. diameter plates of thickness 10 mg/cm² at 3000 psi. The transparency of the plates was such that the instrument conditions recommended by the manufacturer for normal operation could be used. The reference beam was attenuated by suitable screens. The silica samples were evacuated for 2 hr at each temperature investigated in a one-piece Pyrex–quartz cell. Hambleton, *et al.*,[13] noted that the properties of pressed disks differ from those of the original solid, and attributed this to the formation (by pressing) of surface regions inaccessible to adsorbing species, *i.e.*, simple blocking of original pores. Since adsorption experiments were not performed on our pressed disks, this potential complication was of no significance.

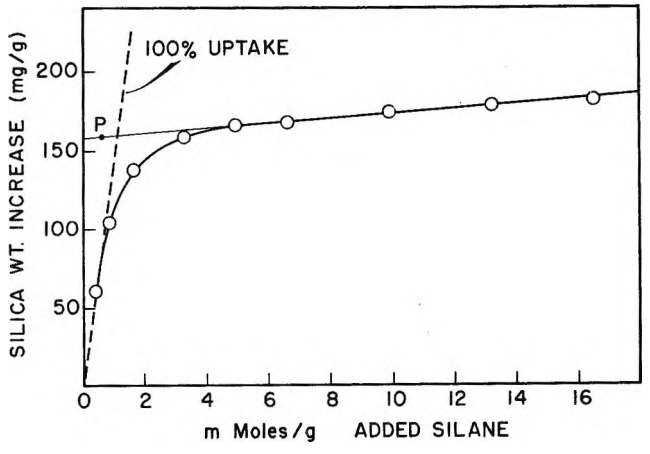

Figure 1. Reaction of silica sample VII with hexamethyldisilazane.

Water Determinations. The water contents of various silicas were desired after removal of physically adsorbed water. The samples of interest were first dried at 105–110° in air for 4 hr or more as recommended by DeBoer, *et al.*,[14] then in a stream of nitrogen at the same temperature to constant weight. An additional 5 to 10% of the total water in the sample after air drying was lost in the nitrogen drying. The water contents of the dried samples were then determined gravimetrically by dehydration of the samples at 1250° in a stream of dry air. Replicate determinations agreed within ±7%. Use of a Meker burner (recommended by DeBoer, *et al.*[14]) gave water contents which averaged 10% low, as is also shown by Zhuravlev, *et al.*[15]

Results

The esterification reactions of the silanes HMDS, TMCS, and DMDCS with the silica surface are assumed[2] to proceed as

$$\text{HMDS: } (CH_3)_3Si\text{–}NH\text{–}Si(CH_3)_3 + 2{\gtrdot}Si\text{–}OH \longrightarrow 2{\gtrdot}Si\text{–}O\text{–}Si(CH_3)_3 + NH_3 \quad (1)$$

$$\text{TMCS: } (CH_3)_3Si\text{–}Cl + {\gtrdot}Si\text{–}OH \longrightarrow {\gtrdot}Si\text{–}O\text{–}Si(CH_3)_3 + HCl \quad (1a)$$

$$\text{DMDCS: } (CH_3)_2SiCl_2 + {\gtrdot}Si\text{–}OH \longrightarrow {\gtrdot}Si\text{–}O\text{–}SiCl(CH_3)_2 + HCl \quad (1b)$$

In the case of DMDCS, the possibility of reaction with two adjacent surface hydroxyls (diesterification) also exists

$$(CH_3)_2SiCl_2 + 2{\gtrdot}Si\text{–}OH \longrightarrow \begin{matrix}{\gtrdot}Si\text{–}O\\ \diagdown\\ Si(CH_3)_2\\ \diagup\\ {\gtrdot}Si\text{–}O\end{matrix} + 2HCl \quad (2)$$

When physically adsorbed water is present on the silica surface, corresponding reactions of silane and water can be visualized. A difference of opinion exists[1,16] concerning the relative concentrations of molecular water on silicas heated above 115°. Under the conditions used in the present silanization studies, however, it seems unlikely that significant amounts of

(12) L. R. Snyder, *J. Chromatog.*, **6**, 22 (1961).

(13) F. H. Hambleton, J. A. Hockey, and J. A. G. Taylor, *Nature*, **208**, 138 (1965).

(14) J. H. DeBoer, J. H. Hermans, and J. M. Vleeskens, *Proc. Koninkl. Ned. Akad. Wetenschap., Ser. B*, **61**, 45 (1958).

(15) L. T. Zhuravlev, A. V. Kiselev, V. P. Naidina, and A. L. Polyakov, *Russ. J. Phys. Chem.*, **37**, 1216 (1963).

(16) J. J. Fripiat and J. Uytterhoeven, *J. Phys. Chem.*, **66**, 800 (1962).

water are present on the surface of the reacting silicas (compare ref 16). This is supported by TGA studies.[17] The unimportance of competing water–silane reactions was confirmed by noting that uptake of silane by silica was independent of temperature over the interval 110–250°.

The reaction of HMDS with the samples of Table I appears to give rapid, complete coverage of the silica surface. A typical reaction curve is shown in Figure 1, where sample weight increase is plotted *vs.* the amount of added silane. The dashed line through the origin ("100% reaction") is the calculated curve for complete reaction of added silane according to eq 1 (with loss of NH_3). After an initial, rapid reaction of silane and silica, a much slower, secondary reaction is apparent. Extrapolation of this secondary uptake of silane back to the point P gives the approximate weight increase ΔW (in milligrams) of the sample corresponding to completion of the initial fast reaction. The total concentration (milliequivalents per gram) of trimethylsilyl (TMS) groups introduced into the silica surface during the initial fast reaction (S_t) is $\Delta W/72W$); W is the weight (grams) of starting, dry silica. The determination of S_t was reproducible within ±4%. Values of S_t for the silicas of Table I are listed in Table II, along with derived values σ_t of the apparent molecular area of a TMS group for each sample. Additional σ_t values for some modified silicas are shown in Table III. The experimental σ_t values for these 13 samples (56 A^2 with a standard deviation of ±4 A^2) are reasonably constant and fall within the range of values indicated for complete coverage of the silica surface. (The standard deviations of BET surface area determinations (±7%) and S_t determinations (±4%) suggest an experimental uncertainty of σ_t of ±8% or ±5 A^2.) Thus close packing of TMS groups on any surface (van der Waals separation)[18] gives σ_t equal to 51 A^2; for a spacing of TMS groups as in normal physical adsorption,[19] σ_t equals 63 A^2.

The reaction of TMCS with the samples of Table I is similar to HMDS reaction in showing an initial fast reaction followed by slow secondary reaction. In the case of samples I, II, III, VII, and VIII, the rate of the initial fast reaction is sufficiently greater than that of the secondary slow reaction to permit an accurate determination of the amount of TMCS taken up by the silica during the initial fast reaction (S_r), similar to the determination of S_t (see Figure 2). For samples IV, V, and VI, the distinction between the rates of initial and secondary reaction was less pronounced and the determination of S_r more ambiguous. The determination of S_r in the latter cases was improved

Table II: Characterization of Samples of Table I by Means of Selective Silanization and Adsorption from Solution

	Silanization data[a]					—K, cm³/g[b]—	
Sample	S_t	S_r	S_r/S_t	σ_t	f_d	Orig. sample	TMCS product
I	0.50	0.01	0.02	47		3.2	1.4
II	0.87	0.03	0.03	61	0.07	3.2	1.5
III	1.16	0.03	0.03	54		5.4	3.6
IV	1.42	0.09	0.06	58	0.21	8.9	4.6
V	2.36	0.50	0.21	57	0.24	16.0	4.7
VI	2.24	0.72	0.32	59		17.1	4.3
VII	2.21	0.88	0.40	62	0.30	18.8	3.5
VIII	2.24	1.60	0.71	55	0.77	26.1	1.2

[a] For completion of initial fast reaction with silane; S_t, total uptake (mequiv/g) HMDS; S_r, total uptake (mequiv/g) TMCS; σ_t, experimental molecular area of TMS group (A^2) calculated from S_t and sample surface area; f_d, fraction diesterification in reaction with DMDCS. [b] Linear isotherm distribution coefficient for adsorption of fluoranthene from 5%v benzene–pentane.

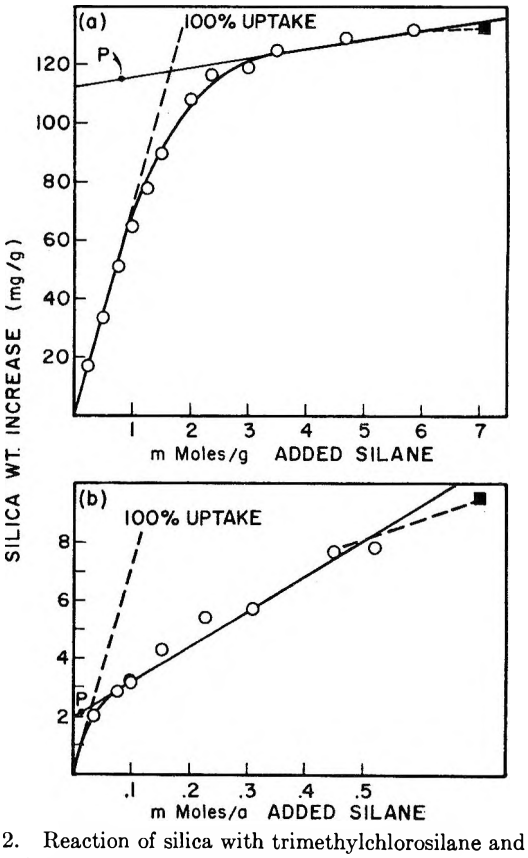

Figure 2. Reaction of silica with trimethylchlorosilane and dimethyldichlorosilane: (a) sample VIII; (b) sample II; O, TMCS; ■, DMDCS.

(17) K. R. Lange, *J. Colloid Sci.*, **20**, 231 (1965).

(18) L. Pauling, "The Nature of the Chemical Bond," Cornell University Press, Ithaca, N. Y., 1940, Chapter V.

(19) L. R. Snyder and E. R. Fett, *J. Chromatog.*, **18**, 461 (1965).

Table III: Properties of Rehydrated and Annealed Silicas

Sample	% H_2O	Surface area, m^2/g	S_r, mequiv/g	S_t, mequiv/g	σ_t	Apparent n_{OH} SA[a]	Apparent n_{OH} S_t[b]	Apparent n_{OH} Calcd[c]	S_r/S_t
				Rehydrated samples[d]					
II	2.42	217	0.02	0.69	52	7.4	6.8	6.9	0.03
V	5.80	714	0.50	2.15	55	5.5	5.2	5.4	0.23
VIII	5.93	668	1.60	1.95	57	6.0	6.1	5.5	0.82
				Annealed samples[e]					
II	0.90	129	0.04	0.39	55	4.7	4.5		0.10
V	3.32	520	0.46	1.48	58	4.2	4.4		0.31
VIII	2.97	436	...[f]	...[f]		4.6	...		...

[a] Determined from BET surface area. [b] Determined from surface area estimated from S_t. [c] Assumes n_{OH} (surface) = 4.8; bulk H_2O = 0.7%/g. [d] Contacted with liquid water at 95° for 16 hr, then dried (see procedure of DeBoer, *et al.*[13]). [e] Heated at 890° for 16 hr then rehydrated as in *d* (see procedure of DeBoer and Vleeskens[10]). [f] Silane reactions were quite slow, preventing the accurate measurement of S_t or S_r.

as described below. Values of S_r for the various silicas studied are listed in Table II; these values are repeatable within about ±0.02 mequiv/g. S_r is always less than S_t, from which it follows that TMCS is less reactive than HMDS, and a particularly reactive portion of the silica surface is involved in the addition of the initial S_r equivalents of TMCS to the sample. The ratio S_r/S_t, which represents the fraction of reactive surface for each silica, varies widely for the samples of Table II ($0.02 \leqslant S_r/S_t \leqslant 0.71$). The variation in the extent of initial reaction with TMCS of these samples is further illustrated in the reduced plots of Figure 3, where ΔW per unit of surface ($\Delta W/WS_t$) is plotted *vs.* added TMCS per unit of surface (mequiv TMCS/WS_t).

The reaction of DMDCS with the samples of Table II closely resembles reaction with TMCS. DMDCS uptake in the initial fast reaction averages only 80% of S_r, however. Addition of TMCS to DMDCS reacted sample gives an initial rapid uptake of TMCS until total silane uptake equals S_r (corrected for secondary reaction), followed by the normal secondary uptake of TMCS. As seen in Figure 2, addition of DMDCS to TMCS treated silicas gives a somewhat slower secondary uptake of silane. Thus DMDCS appears to react rapidly with the same part of the silica surface which is especially reactive toward TMCS, but at a slightly slower rate. This contrasts with the extended reaction of these two silanes with silica,[2] where DMCDS appears more reactive. The extent of diesterification in the initial uptake of 0.8 S_r equivalent of DMDCS was calculated for several of the samples of Table II from the chloride contents of the reacted samples (the initial silicas all had negligible chloride contents, as did TMCS-reacted samples). The fraction of

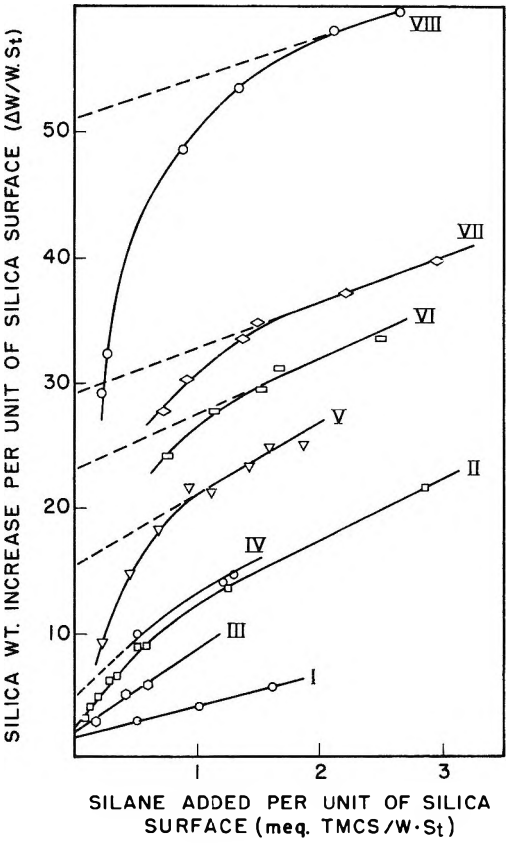

Figure 3. Reactions of different silica samples with trimethylchlorosilane.

diesterification f_d in the total reaction of DMDCS with the silicas of Table II is seen to vary widely ($0.07 \leqslant f_d \leqslant 0.77$) and to parallel values of S_r/S_t.

That portion of the silica surface which reacts rapidly with TMCS also preferentially adsorbs aromatic hy-

drocarbons from solution. This was shown by determining linear isotherm distribution coefficients K (cm^3/g) for the adsorption of fluoranthene from 5%v benzene–pentane onto the surfaces of the samples of Table II and their TMCS reaction products (*i.e.*, sample plus S_r mequiv/g of TMCS). These data are given in Table II. The K value for the original silica can be expressed as the sum of K values for reactive (K_r) and unreactive (K_u) surface (relative to rapid reaction with TMCS); K_u is then the value of K observed for the TMCS treated silica, and K_r is the K value for the original sample minus K_u. K_r is plotted *vs.* S_r and K_u *vs.* $(S_t - S_r)$ in Figure 4. K_r shows reasonably linear correlation with S_r, implying that TMCS reactive surface in the various samples is energetically similar with regard to fluoranthene adsorption. Thus for surfaces of identical energy or composition, K should be proportional to total surface area per gram of adsorbent, while S_r is proportional to the area per gram of reactive surface for a particular sample. Similarly, K_u correlates well with $(S_t - S_r)$, suggesting that TMCS unreactive surface for the various samples is approximately equivalent with regard to fluoranthene adsorption. From the relative slopes of the two plots of Figure 3, TMCS reactive surface appears about seven times more effective than unreactive surface in adsorbing fluoranthene from dilute solutions.

The much greater adsorption affinity of TMCS reactive surface permits a better determination of S_r in doubtful cases (*e.g.*, samples IV through VI) by plotting K *vs.* the amount of added TMCS for a series of partially reacted samples. This is illustrated in Figure 5a for sample V. A similar plot for the HMDS reaction of sample V is also shown (Figure 5b) for comparison. Extrapolation of the initially linear portion of the curve to the point P in Figure 5a gives the quantity S_r (equal to 0.5 in this case). This procedure was confirmed by the similar determination of S_r in samples II and VIII, whose S_r values were known unambiguously (from Figure 2); these samples gave S_r equal to 0.06 and 1.5, respectively, in reasonable agreement with previously determined values (0.03 and 1.60, respectively). The similar determination of S_t as in Figure 5b (extrapolation to $K = 0$) gave values of 0.8, 2.2, and 2.3 for samples II, V, and VIII, respectively, again in good agreement with previous values (0.87, 2.3, 2.24, respectively). With values of S_r available for samples I, II, III, V, VII, and VIII, the family of curves in Figure 3 could be used to more precisely define S_r from experimental silane uptake data.

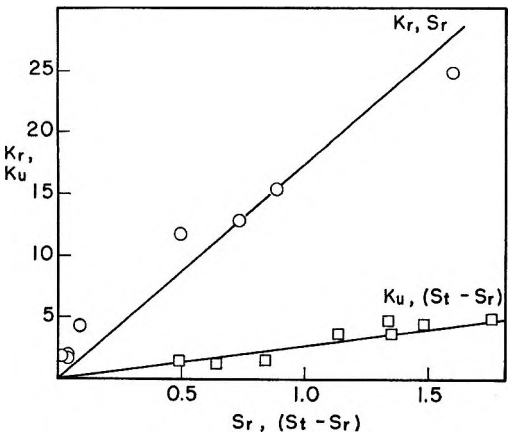

Figure 4. Preferential adsorption of fluoranthene on TMS reactive surface.

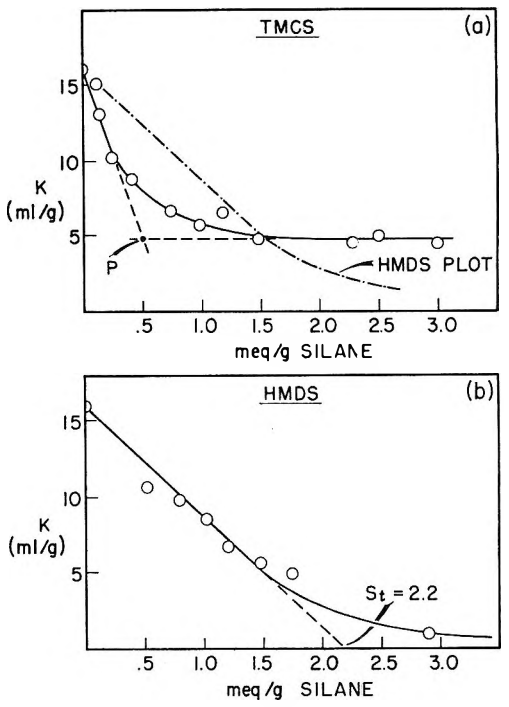

Figure 5. Silica adsorptivity *vs.* extent of silane reaction; sample V.

The infrared spectra as a function of temperature for several of the samples of Table II are shown in Figure 6. The spectra of samples III, IV, VI, and VII were also obtained but are not shown, since they are similar to the spectrum of sample V. An approximate measure of the relative concentrations of free and bound hydroxyls on the surfaces of these samples can be inferred from the area of the 3750-cm^{-1} band relative to that of the broad band between 3500 and 3700 cm^{-1}. It is clear from the spectra of Figure 6 that the relative concentration of free hydroxyls tends to decrease in the sequence sample I to VIII. This is contrary to expectation if it is assumed that TMCS reactive surface corresponds to surface covered by free hydroxyls (as

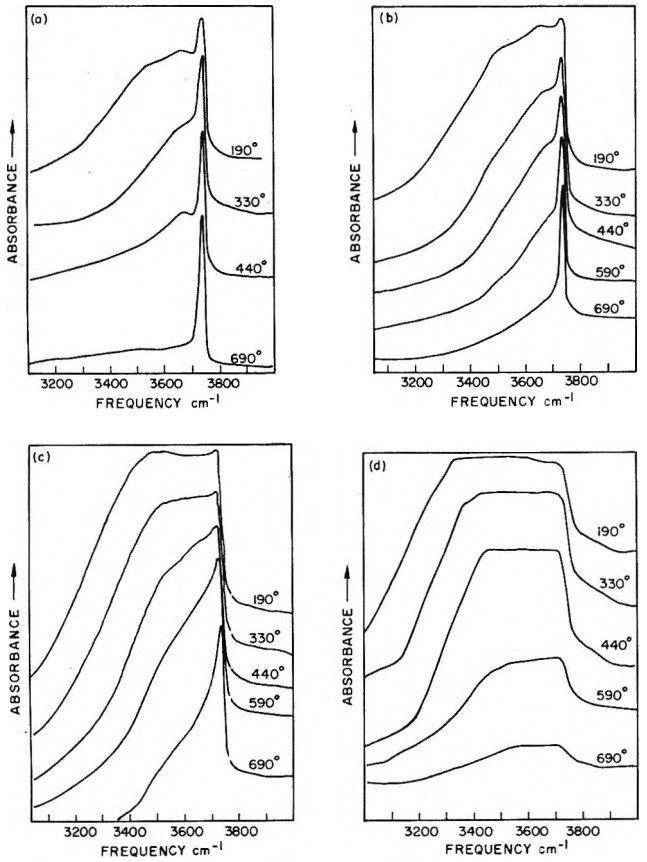

Figure 6. Infrared spectra of different silica samples *vs.* temperature: (a) sample I; (b) sample II; (c) sample V; (d) sample VIII.

would be indicated by earlier work). Rather, it appears that some third hydroxyl type ("reactive hydroxyls") is involved, differing from both free hydroxyls and "normal" bound hydroxyls, which reacts more rapidly with TMCS and DMDCS and is a stronger site for the adsorption of aromatic hydrocarbons. The nonequivalence of reactive and free hydroxyls was further demonstrated by examining the infrared spectrum of sample II after uptake of 0.09 mequiv/g of TMCS (*i.e.*, 3 times S_r). The intensity of the 3750-cm^{-1} band was reduced by only 15%, although reactive hydroxyls had been completely esterified. The extensive diesterification (77%) in the DMDCS reaction of sample VIII also rules out the equivalence of reactive and free hydroxyls, since it has been pointed out[2] that free hydroxyls must be separated by a minimum distance (to prevent hydrogen bonding) which is too large to permit bridging by a dimethylsilyl group.

Discussion

The data of the preceding section appear to establish the existence on the silica surface of a distinct class of reactive hydroxyl groups. The combined infrared, adsorptive, and reactive properties of these reactive hydroxyls differ markedly from those previously attributed either to free or to bound hydroxyls. Before inquiring into the detailed structure of these reactive hydroxyls, it is worth noting why previous workers have failed to recognize the presence or effects of reactive hydroxyls on the silica surface. First, the relative concentration (S_r/S_t) of reactive hydroxyls is generally small ($\leq 5\%$) on silicas with surface areas less than 500 m^2/g (to which previously reported infrared studies appear to have been exclusively confined). Second, the infrared absorption band for reactive hydroxyls (see below) is believed to be broader than that of free hydroxyls and to overlap the absorption of "normal" bound hydroxyls. Finally, previously adsorption[3-6] and silane reaction[2] studies have involved coverage or reaction of a substantial part of the silica surface. Under these conditions, the small number of reactive hydroxyls function as sites for initial adsorption or reaction, but the major number of surface hydroxyls finally involved in adsorption or reaction belong to the next most reactive set (*i.e.*, free hydroxyls). Changes in the silica infrared spectrum resulting from silanization or adsorption are then most readily attributed to the secondary involvement of free hydroxyls.

The Nature of Reactive Hydroxyls. The relative concentration of reactive hydroxyls (S_r/S_t) for the samples of Table II correlates closely with silica pore diameter (see Figure 7). Kiselev, *et al.*,[7] have emphasized the role of fine pores in altering the adsorption characteristics of the silica surface, and it might be argued that similar geometrical effects can explain the greater reactivity of reactive hydroxyls with TMCS. That is, reactive hydroxyls might be nothing more than otherwise normal hydroxyls which happen to be located in fine pores (diameter <20A), and their unique properties might be a simple consequence of the differing interactions peculiar to fine pores. Several facts suggest that this explanation is not correct. First, the presence of reactive hydroxyls in sample II seems to require the presence of at least some pores which are narrower than the widest pores of sample VIII; however, pore distribution studies show no overlap in the pore sizes of these two samples; all pores of sample VIII are narrower than 25 A, and all pores of sample II are wider than 25 A. Second, the narrow pore hypothesis must assume that reactive hydroxyls are similar in the various silicas studied, with these samples differing only in their content of fine pores (and of reactive hydroxyls). It is difficult to justify the correlation of Figure 4 otherwise. However, the varying values of f_d for the samples of Table II suggest that reactive

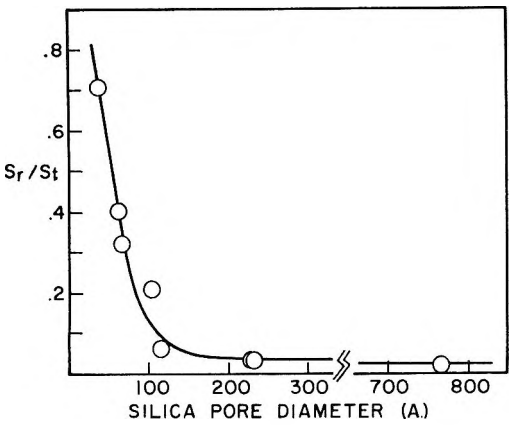

Figure 7. Correlation of reactive hydroxyl concentration with silica pore diameter.

hydroxyls are generally widely separated in samples with low concentrations (S_r/S_t) of reactive hydroxyls, and generally adjacent (to permit diesterification) in samples with high concentrations of reactive hydroxyls (the second chlorine of DMDCS cannot react either with "normal" bound or free hydroxyls for energetic and geometric reasons, respectively).[2] That is, a simple statistical distribution of reactive hydroxyls over the entire silica surface is indicated, rather than a concentration of these groups into narrow pores. Finally, various experimental studies[7,20] suggest that pore diameter has little effect *per se* on the *selective* adsorption of various unsaturated hydrocarbons on different silicas (relative to saturated hydrocarbons).

The possibility that reactive hydroxyls are the result of some surface impurity was also considered, in view of the experience of previous workers (*e.g.*, ref 1,9). Traces of aluminum seem most suspect in this respect, since aluminum could increase the acidity of surface hydroxyls and is generally the major metallic impurity in these samples.[21] As seen in Table I, however, there is no correlation between the aluminum contents and S_r values of these samples.

Previous workers, in using the classification of surface hydroxyls into "bound" and "free" types, have tended to assume that two distinct hydroxyl types are actually involved, and that their respective properties are sharply defined and markedly different (*cf.*, Davydov, *et al.*[2]). The major difference between these two hydroxyl types is one of *relative* separation of the hydroxyl group from the oxygen atom of an adjacent hydroxyl or siloxane group (d_{O-O}, the distance between oxygen atoms). Hydroxyls which are separated from adjacent oxygen atoms by more than 3.1 A appear incapable of hydrogen bonding[2,22] while the strongest hydrogen bonds must involve some optimum hydroxyl–oxygen distance d_O (value of d_{O-O}) which is considerably smaller than 3.1 A (2.4 to 2.8 A).[22] If a continuum of values of d_{O-O} is assumed for an amorphous silica surface, then a continuum of hydroxyl "types" necessarily follows, ranging gradually from free ($d_{O-O} >$ 3.1 A) to strongly bound ($d_{O-O} \approx d_O$) hydroxyls. This is in agreement with the infrared spectra of most silicas, which exhibit broad rather than sharp hydroxyl bands below 3750 cm^{-1}. It will next be argued that two surface hydroxyls so situated as to form a hydrogen bond of weak or intermediate strength (I) can explain all of the properties of "reactive" hydroxyls.

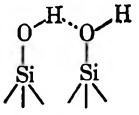

(I)

The adsorptive strength or surface energy of a small region of the silica surface (*i.e.*, strength of an adsorption site) toward an adsorbate such as benzene or fluoranthene is determined by two factors: the relative availability of hydroxyls in that region for hydrogen bonding to the adsorbate (*i.e.*, greater for free than for bound hydroxyls), and the relative number of hydroxyls in the region (*i.e.*, the more hydroxyls in the region, the greater the adsorption energy). As the distance d_{O-O} between a particular pair of surface hydroxyls on a crystalline silica surface decreases from the average value of 5.0 A (corresponding to n_{OH} equal 4.6; see Figure 10 of ref 9), the density of hydroxyls in that particular region is effectively increased, in the sense that a smaller area is required to encompass the two hydroxyls, and it is easier for a single adsorbate molecule to interact simultaneously with each group. As d_{O-O} decreases below 3.1 A, however, hydrogen bonding of the two hydroxyls begins to be significant. At some value of d_{O-O} below 3.1 A, an optimum situation for interaction of the two hydroxyls with a single adsorbate molecule should exist, such that further reduction in d_{O-O} increases hydrogen bonding between the groups more than is compensated for by increased concentration of hydroxyls in the adsorption region, and increasing d_{O-O} decreases the concentration of hydroxyls more than is compensated for by decreased hydrogen bonding. Hydroxyl pairs with values of d_{O-O} ranging a few tenths of an angstrom to either side of this optimum separation (for optimum adsorption)

(20) L. R. Snyder, *J. Phys. Chem.*, **67**, 2622 (1963).

(21) J. A. Hockey and B. A. Pethica, *Trans. Faraday Soc.*, **57**, 2247 (1961).

(22) G. C. Pimentel and A. L. McClellan, "The Hydrogen Bond," W. F. Freeman & Co., San Francisco, Calif., 1960.

can thus explain the adsorptive properties of "reactive" hydroxyls; such hydroxyl pairs can easily break the hydrogen bond between them, making both hydroxyls available for bonding with an adsorbate such as fluoranthene.

By analogy with substitution reactions on saturated carbon in solution, it seems unlikely that the reaction of TMCS with a surface hydroxyl involves a simple, direct attack on the Si–Cl bond by the surface hydroxyl, without intervention of some third species, *i.e.*, as written in eq 1a. Rather, a concerted mechanism seems probable, involving the reacting hydroxyl as entering group, and some other group to stabilize the leaving chloride group. Two adjacent hydroxyls, so situated as to permit weak hydrogen bonding, nicely fulfill this requirement. This is illustrated in the sequence below, visualized from a point directly overhead

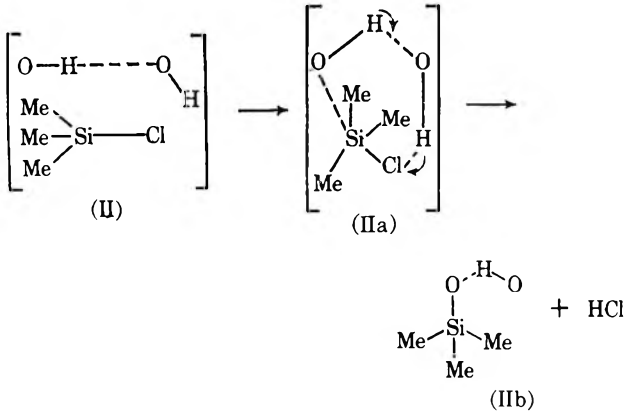

Finally, a pair of weakly bonded hydroxyls should show maximum absorption in the region 3600–3700 cm^{-1}, and this absorption is seen in Figure 6 to increase regularly (relative to free hydroxyl absorption) in the sequence sample I through VIII. Thus the expected reactive, adsorptive, and infrared properties of weakly bonded, adjacent hydroxyls satisfy all the experimental properties of "reactive" hydroxyls.

An alternative description of reactive hydroxyls seems possible in terms of the nonbonding proton in (I). Where two adjacent hydroxyls can hydrogen bond, the preferred position of the bonding proton is on the line of centers of the two oxygens,[22] which leaves one of the two protons in an unbonded state.[23] The acidity of this unbonded proton is expected to be greater than that of free hydroxyls, which in turn should increase both its ability to interact with adsorbing aromatic molecules such as fluoranthene and to react with molecules such as TMCS. The infrared absorption of this nonbonded hydroxyl group is at the same frequency or shifted to a lower frequency (<3750) than the free hydroxyl by virtue of weakening the O–H bond and increasing the reduced mass of the system.[23] A respectable match between the expected properties of the nonbonded hydroxyl in (I) and the experimental properties of reactive hydroxyls is thus apparent. The latter possibility differs from the former only in the strength of the hydrogen bond in (I): the most reactive hydroxyls will correspond to weakly bonded (I) in the first case, and to strongly hydrogen-bonded (I) in the second case. The infrared spectrum of sample VIII after TMCS treatment (Figure 8) shows selective removal of strongly bonded hydroxyls (compare Figure 6d), which suggests that reactive hydroxyls involve relatively strongly bonded hydroxyl pairs.

The Variation of Surface Type between Different Silicas. It is clear that substantial differences exist in the surfaces of the various silicas of Table I, and that these differences vary more or less smoothly from sample I to sample VIII. The concentrations of bound and reactive hydroxyls increase in this sequence, while the concentrations of free hydroxyls decrease in the same order. Similarly, pore diameter decreases in this sequence and the extent of DMDCS diesterification decreases. The differences in infrared absorption of

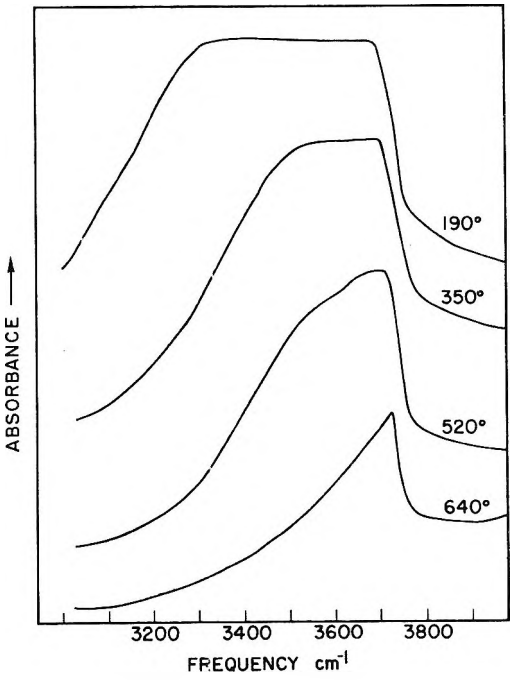

Figure 8. Infrared spectrum of silica sample VIII after reaction with TMCS.

(23) P. J. Krueger and H. D. Mettee, *J. Mol. Spectry.*, 18, 131 (1965); R. N. Jones and C. Sandorfy, "Chemical Applications of Spectroscopy," "Technique of Organic Chemistry," Vol. IX, A. Weissberger, Ed., Interscience Publishers, Inc., New York, N. Y., 1956, p 419–420.

the samples of Table I appear to resemble differences which can be created in the same silica by thermal treatment and rehydration. Thus, Hockey has observed[1] that the heating of a silica at 450° followed by rehydration gave a sample with reduced relative concentration of bound hydroxyls (by infrared analysis). We have confirmed this behavior for sample II of Table I, where heating at 700° followed by rehydration greatly reduced the absorption between 3500 and 3700 cm^{-1}, without affecting the absorption of the band at 3750 cm^{-1}. Hockey has related this behavior to the "annealing" of the silica surface as described by DeBoer and Vleeskens,[10] which is claimed to give a surface similar to that in various crystalline silicas (*e.g.*, β-tridymite). The concept that the samples of Table I exhibit decreased surface order or relative "crystallinity" in going from sample I to sample VIII is superficially attractive, since this proposal is capable of explaining most of the properties of these samples. However, the related hypothesis concerning the response of the silica surface to thermal treatment (*i.e.*, annealing) appears incorrect for reasons we will now discuss.

The concept that surface annealing of a silica can be effected by heating the sample above 400°, to give a more regular or near-crystalline surface, rests upon two pieces of evidence. DeBoer and Vleeskens' original study[10] showed that n_{OH} for a 500 m^2/g silica hydrogel could be reduced from a starting value of 6.2 to a limiting value of 4.6 ± 0.2 by various combinations of heating and intermediate hydration. Since the latter n_{OH} value corresponds fairly closely to the values expected for various crystalline silicas, it was logical to assume that annealing had re-ordered or "crystallized" the silica surface. Similarly, Hockey[1] has shown that annealing of a silica at 450° decreases the concentration of bound hydroxyls while maintaining the free hydroxyl concentration constant. Both observations have been shown by Hockey to be consistent with a simple picture of the silica surface and of the annealing process. An annealed silica is assumed to be approximately crystalline (at least in the region of the surface) while unannealed hydrogels can be regarded as partially hydrolyzed products of otherwise similar structure. The siloxane bond between first and second row silicon atoms (in crystalline silica) is assumed to be replaced by an additional hydroxyl group on each of these atoms (in an unannealed hydrogel). Annealing then consists of the simple dehydration of the latter hydroxyl pairs, with restoration of the crystal lattice. An annealed surface should consist exclusively of free hydroxyls, while bound groups exist in a hydrolyzed or unannealed silica. DeBoer and Vleeskens' treatment overlooks the possibility that bulk hydroxyls might exist in the original hydrogel, in addition to surface hydroxyls (*i.e.*, their values of n_{OH} include any bulk hydroxyls, if present). Similarly, Hockey's conclusions[21] from the infrared study of annealing rest on the assumption that bulk hydroxyls cannot be lost during heating of a silica at 450°, since the infrared absorption of bound surface hydroxyls and of bulk hydroxyls is quite similar.[2] Davydov, *et al.*,[2] have actually shown that substantial amounts of bulk hydroxyls are normally present in silica hydrogels. These authors have further shown that the true n_{OH} values of a wide range of silica hydrogels fall fairly close to a value of 4.8; *i.e.*, the initial hydrogels possess n_{OH} values close to that of the annealed sample of DeBoer and Vleeskens. This suggests that annealing as carried out by the latter workers has simply removed bulk water from the original hydrogel. This suspicion is supported by comparison of DeBoer and Vleeskens' annealing curves (n_{OH} *vs.* treatment, Figure 1 of ref 10) with the rate of removal of bulk hydroxyls from similar silicas as a function of temperature. For moderately high surface silicas (>180 m^2/g, *vs.* 500 m^2/g for DeBoer and Vleeskens sample), both Davydov, *et al.*,[2] and Fripiat and Uytterhoeven[15] have observed that bulk hydroxyls begin to leave the sample at a temperature of 500–600°, a major part of the bulk hydroxyls can be removed at temperatures between 700 and 800°, and virtually complete removal of bulk hydroxyls occurs at temperatures above 800 to 900°. Similarly, DeBoer and Vleeskens[10] found that heating their silica at 450° for an extended time (without intermediate hydration) gave little reduction in n_{OH} (6.2 to 5.8), heating at 650° gave substantial reduction (to 5.0), and heating at 890° gave complete "annealing" (n_{OH} equal to 4.6). Hockey's assumption that bulk hydroxyls cannot be lost from a silica at 450° rests exclusively upon observations on silica glasses.[21,24] This comparison seems basically unsound, since water is much more easily lost from the comparatively open structure of a hydrogel than from a solid sample of fused silica. Whereas bulk hydroxyls are not lost from silica glasses at 700° under vacuum,[24] silica hydrogels give up much of the bulk hydroxyls under these conditions (*cf.* above). Davydov, *et al.*,[2] have in fact observed extensive loss of bulk hydroxyls from one hydrogel (39 m^2/g surface area) at temperatures below 400°. The observations of both Hockey[1] and DeBoer and Vleeskens[10] can thus be explained on the basis of bulk

(24) A. J. Moulson and J. P. Roberts, *Trans. Faraday Soc.*, **57**, 1208 (1961).

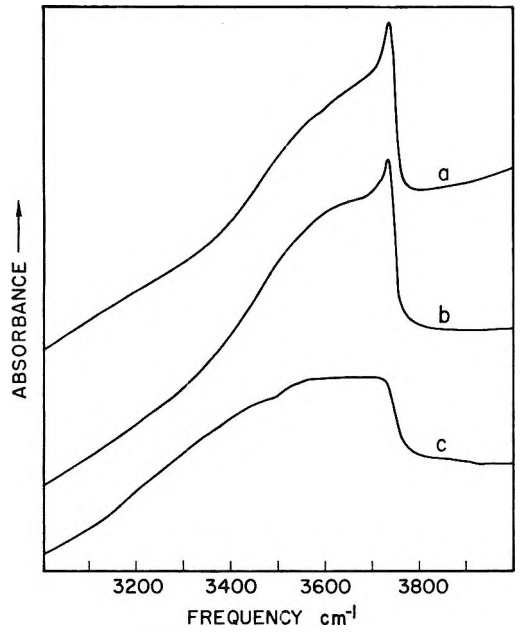

Figure 9. Infrared spectra of annealed and rehydrated silicas after heating to 330°; a, sample II; b, sample V; c, sample VIII.

hydroxyl removal, without any need to invoke surface annealing or alteration of surface structure.

The proposal of DeBoer and Vleeskens[10] and of Hockey[1] with regard to the nature of the "annealing" process was further studied, using samples II, V, and VIII. These samples were first rehydrated according to the procedure of DeBoer, *et al.*,[14] in order to ensure complete surface coverage by hydroxyls, then annealed (and again rehydrated) by the method of DeBoer and Vleeskens.[10] The water contents (and apparent n_{OH} values) and S_r and S_t values of both the rehydrated and annealed samples were obtained, along with the infrared spectra of the annealed samples. These data are summarized in Table III and Figure 9. The decrease in the absorbance of the free hydroxyl group is due to loss of surface area. Annealing and rehydration lowers n_{OH} for all three samples to an approximately constant value of 4.5. This is similar to the DeBoer and Vleeskens[10] average value (4.6) and verifies that the annealing of these samples was complete. The n_{OH} values of the unannealed samples are higher, as found by DeBoer and Vleeskens,[10] but show a correlation with the infrared spectra of these samples (Figure 6) which is the reverse of that predicted by Hockey. The data of Davydov, *et al.*,[2] suggest an average bulk hydroxyl content (as water) for silica hydrogels equal to 0.7%, and an average surface n_{OH} value equal to 4.8. This permits the estimation of *apparent* n_{OH} values (*i.e.*, as per DeBoer and Vleeskens[10]) for the rehydrated samples of Table III, and these calculated values are seen to be in good agreement with the experimental n_{OH} values. The similar calculation of the apparent n_{OH} value of the silica studied by DeBoer and Vleeskens[10] gives a value of 5.5, *vs.* 6.2 experimental. The annealing process is seen in Table III to have essentially no effect on the S_r values of samples II and V,[25] suggesting little change in silica surface type as a result of annealing. Similarly, the infrared spectra of annealed samples II, V, and VIII (Figure 9) differ little from the spectra of the unannealed samples (Figure 6). There is an apparent loss of bound hydroxyls from sample II, which can be attributed to the simple removal of bulk hydroxyls during annealing. Samples V and VIII, which according to Hockey's proposal should show the greatest change in surface hydroxyl type upon annealing, show essentially no change in infrared spectra. We conclude that the annealing of silicas as described by DeBoer, *et al.*, serves to remove bulk hydroxyls and to reduce surface area, but does not significantly alter the nature of the remaining surface hydroxyls. Reactive hydroxyls appear to survive the process of annealing and rehydration intact, while other hydroxyl types (and their associated surfaces) are partially destroyed. This is reasonable since reactive hydroxyls should be preferentially removed at low temperatures, while irreversible destruction of surface (and associated hydroxyls) by hydroxyl condensation occurs primarily at high temperatures.[26] Rehydration then serves to regenerate surface hydroxyl groups with the exception of those hydroxyl types which are involved in surface-to-surface condensation at high temperatures.

The Origin of Surface Differences. On the basis of the preceding discussion, it seems clear that the postulate of DeBoer and Vleeskens[10] and of Hockey[1] concerning the origin of surface differences among various silica samples must be modified. These differences cannot be reconciled in terms of varying concentrations of total surface hydroxyls (*cf.* annealed silicas of Table III). However, the corollary suggestion that differences in surface type reflect differing degrees of surface regularity or crystallinity appears reasonable. On this basis, it is proposed that large-pore diameter silicas such as samples I, II, and III are relatively crystalline, fine pore samples such as sample VIII are essentially amorphous, and silicas of intermediate pore size possess

(25) S_r and S_t values for annealed sample VIII could not be measured accurately, due to greatly reduced silane reaction rates. This was apparently a result of partial blocking of the fine pore network by sintering, with a resulting decrease in the rate of silane diffusion.

(26) J. H. DeBoer and Vleeskens, *Proc. Koninkl. Ned. Akad. Wetenschap., Ser. B*, **60**, 234 (1957).

an intermediate structure. Hockey[1] and others have noted that the surface of a crystalline silica will be covered exclusively by free hydroxyls, with a separation between adjacent hydroxyls of 5.0 A (as in the β-tridymite structure). With perturbation of an initially crystalline structure and randomization of the positions of surface hydroxyls, the average spacing between nearest hydroxyl neighbors must tend to decrease, and an increasing number of hydroxyls will be sufficiently close to permit hydrogen bonding. Reactive hydroxyls appear to comprise the closer, more tightly bound surface hydroxyls, and their concentration should increase regularly with decreasing silica crystallinity and decreasing concentration of free hydroxyls. The parallelism of surface crystallinity and average pore diameter probably reflects a dependence of each of these properties on some basic aspect of the original silica synthesis. Thus it seems likely that those factors which promote silica crystallinity during its synthesis will likewise favor large crystallite size and increased silica pore diameter.

Acknowledgment. The authors are grateful to W. P. Cummings of W. R. Grace and Company for making available pore size distribution data on samples II and VIII.

Partial Molar Volumes and Adiabatic Compressibilities of Tetraalkylammonium and Aminium Salts in Water. I. Compressibility Behavior

by B. E. Conway and R. E. Verrall[1]

Department of Chemistry, University of Ottawa, Ottawa, Canada *(Received July 6, 1966)*

Differential ultrasonic velocity measurements have been carried out on a series of aqueous solutions of symmetrical tetra-*n*-alkylammonium salts, corresponding salts of protonated methylamines, and the neutral methylamines themselves. The apparent molal adiabatic compressibilities $\phi_{K(s)}$ have been derived and the values $\phi^0_{K(s)}$ at infinite dilution estimated. The dependence of $\phi^0_{K(s)}$ upon the coordination of the N^+ center by H_2O molecules and by Me groups has been considered in relation to the variation of $\phi^0_{K(s)}$ with molecular weight in the homologous series of symmetrical R_4N^+ salts from R = Me to R = *n*-Bu. Effects due to electrostriction and structure promotion are considered as a function of alkyl substitution at the N center.

Introduction

In recent years, considerable interest[2-11] has arisen concerning the behavior of tetraalkylammonium salts in aqueous solution, particularly with regard to their anomalous thermodynamic behavior, hydration, and apparent structure-promoting influence in water. A review has also been given.[12] Elsewhere[9,12] we have examined the additivity of partial ionic volumes $\bar{V}$ of symmetrical homologous ions in this series, the concentration dependence[2,9] of $\bar{V}$ for various corresponding salts, and deduced the individual ionic contributions

(1) Work carried out in partial fulfillment of the requirements for the Ph.D. degree in the University of Ottawa, Ottawa, Canada.

(2) W. Y. Wen and S. Saito, *J. Phys. Chem.*, **68**, 2639 (1964).

(3) W. Y. Wen and S. Saito, *ibid.*, **69**, 3569 (1965).

(4) B. J. Levien, *Australian J. Chem.*, **18**, 1161 (1965).

with a very small thermodynamic uncertainty. Also attention has been directed[1c] to the role of nonelectrostatic relative size effects in the thermodynamics of solutions of these salts.

In the present two papers (see part II following), we report data on the compressibility and density behavior of a series of symmetrical R_4N^+ salts and of salts derived from corresponding primary, secondary, and tertiary aminium acids $R_nH_{4-n}N^+$ where n, an integer, is $1 \leq n \leq 3$. Measurements have also been made on the corresponding neutral amines $R_nH_{3-n}N$, so that the compressibility and volume changes on ionization[13] can be derived. The relation between ionic compressibilities, partial molal volumes, and electrostriction in relation to hydration has been dealt with theoretically in previously published papers.[14-17] The choice of the compounds studied in the present work was dictated by the desire to examine effects associated with changing coordination about the N^+ center in the aminium and tetraalkylammonium salt series.

In the compressibility measurements reported here in part I, the differential adiabatic method[18] was used as this gives satisfactory results down to concentrations of salt which are lower than can be studied by the static method or the direct interferometric method.[15] A slight disadvantage is that only the adiabatic compressibility β is obtained, but for aqueous solutions this quantity can be given meaningful interpretations (*cf.* ref 15, 16, 17, and also 19 where the isothermal compressibility α was calculated from β with the necessary partial molar heat capacity data) and is not too different (*ca.* 7–10%)[19] from α for alkali halide salts.

Experimental Section

(*1*) *Compressibility Determinations.* Compressibilities of the various salt and neutral amine solutions were determined from ultrasonic velocity measurements by the differential interferometric method of Carstensen[18] using barium titanate ultrasonic transducers operating at carrier frequencies (see below) of 5.2 and 8.4 MHz with pulsed signals of width 100–1000 μsec and having a repetition frequency of 2.5 to 500 kHz. Various improvements to the previously described apparatus[18] were made including a three-way screw adjustment for aligning the transducers and a transverse racking mechanism for the receiver transducer. The longitudinal traverse was constructed from a metric threaded shaft (pitch 1 mm) provided with a reading dial divided into 100 divisions per turn.

The two transducers dipped, respectively, into each half of a divided bath, in one side of which was the salt solution and in the other the pure solvent, water. A polyethylene membrane provided separation between the two sections of the bath.

The test vessel was mounted on four supports in an externally insulated stainless steel thermostat bath such that five sides of the test vessel were in constant contact with circulating thermostated water. This constant temperature water was thermostated in a well-lagged and covered bath situated next to the apparatus.

Around the stainless steel bath was situated a $^1/_4$-in. rigid rectangular aluminum frame supporting the sliding assembly which carried the two transducers at a predetermined fixed distance apart. This sliding frame was guided in its movement along the axis of the test vessel by means of two locating V blocks resting on a triangular rail.

A schematic diagram of the apparatus[18] and the associated electronic block units is given in Figure 1. A detailed description of the electronic apparatus used is given in a thesis;[20] the general design of most of the apparatus followed, in principle, that published previously[18] but took advantage of more recent advances in electronic circuitry.

The receiver transducer signal, after amplification by a broadband amplifier, was admitted to a tuned preamplifier, type PA-620 (Arenberg Ultrasonic Laboratory), F in Figure 1. The coils in F were slug-tuned and their inductance could easily be varied to peak the signal at any frequency in the range studied. An arrangement for the insertion of a second signal at a fixed impedance level for comparison purposes was

(5) L. G. Hepler, J. M. Stokes, and R. H. Stokes, *Trans. Faraday Soc.*, **61**, 20 (1965).

(6) S. Lindenbaum and G. E. Boyd, *J. Phys. Chem.*, **68**, 911 (1964).

(7) M. A. V. Devanathan and M. J. Fernando, *Trans. Faraday Soc.*, **58**, 784 (1962).

(8) H. S. Frank, *J. Phys. Chem.*, **67**, 1554 (1963).

(9) B. E. Conway, R. E. Verrall, and J. E. Desnoyers, *Trans. Faraday Soc.*, **62**, 2738 (1966).

(10) B. E. Conway and R. E. Verrall, *J. Phys. Chem.*, **70**, 1473 (1966); see also E. Glueckauf, *Trans. Faraday Soc.*, **51**, 1235 (1955).

(11) R. M. Diamond, *J. Phys. Chem.*, **67**, 2513 (1963).

(12) B. E. Conway, R. E. Verrall, and J. E. Desnoyers, *Z. Physik. Chem.* (Leipzig), Falkenhagen Anniversary Papers, **230**, 157 (1965); see also B. E. Conway, *Ann. Rev. Phys. Chem.*, **17**, 481 (1966).

(13) L. G. Hepler, *J. Phys. Chem.*, **69**, 965 (1965).

(14) J. E. Desnoyers, R. E. Verrall, and B. E. Conway, *J. Chem. Phys.*, **43**, 243 (1965); *cf.* E. Whalley, *ibid.*, **38**, 1400 (1963) and J. Padova, *ibid.*, **39**, 1552 (1963).

(15) A. G. Passynskii, *Acta Physiochim. U.R.S.S.*, **8**, 385 (1938).

(16) P. L. Khare, *Trans. Faraday Soc.*, **58**, 359 (1962).

(17) T. Isemura and S. Goto, *Bull. Chem. Soc. Japan*, **37**, 1690 (1964); *ibid.*, **37**, 1663, 1697 (1964).

(18) E. W. Carstensen, *J. Acoust. Soc. Am.*, **26**, 858 (1954).

(19) B. B. Owen and J. S. Simons, *J. Phys. Chem.*, **61**, 479 (1957); see also B. B. Owen and P. L. Kronick, *ibid.*, **65**, 84 (1961).

(20) R. E. Verrall, Ph.D. Thesis, University of Ottawa, Ottawa, Canada, 1966.

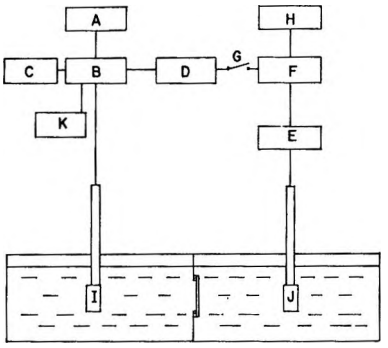

Figure 1. Block diagram of differential ultrasonic velocity apparatus: A, radiofrequency oscillator; B, pulse modulator; C, pulse generator; D, decade attenuator; E, broad-band amplifier; F, tuned amplifier and mixing circuit; G, phase comparison (on–off switch in mixing circuit); H, oscilloscope; I, source transducer; J, receiver transducer; K, frequency meter.

provided, and with proper phase adjustments, this stage can act as a cancelling device. An important feature of this apparatus is that it acts as an adjustable filter and provides a mixing circuit which enables a phase comparison to be made between the signal transmitted through the two-section bath and the directly transmitted signal from the radiofrequency source. This comparison is the basis of the velocity determination.

An essential part of the electrical system is the decade attenuator, which must be adjusted during measurement to achieve a good null in the phase comparison measurement. The attenuator network used was a Daven, three decade, direct reading unit that provided accurate performance in the radiofrequency range from 0 to 10 MHz. The three decades were ten step, 10, 1, and 0.1 db per step, respectively. The decade attenuator had a frequency characteristic of ±0.2 db at 0 to 10 MHz in each of the 0.1 and 1 db per step decades, and ±0.5 db in the 10 db per step decade.

The resulting pulsed wave form was viewed on a Tektronix 543A oscilloscope with a Tektronix Type L plug-in preamplifier in the vertical deflection system. The rise time of this unit was between 12 and 15 nsec.

(2) *Accuracy of Apparatus and Technique.* The technique described here has proven capable of giving precise velocity difference measurements equivalent to a sensitivity of the order of 2–3 parts in 10^5 in a measurement of the velocity itself.[15]

In order to measure the relative phase of the signal received at J (Figure 1), the output of the receiver transducer was added to the reference signal which came directly from the radiofrequency oscillator. A sharp minimum in the sum is observed on the oscilloscope when the signals are exactly out of phase and of equal amplitude (adjusted by means of the attenuator). The phase of the received signal depends, among other things, upon the number of acoustic wavelengths n which separate the source and receiver. If the physical separation of the transducers is a, and the path length in the reference solvent is y, then

$$n = \frac{y}{\lambda_w} + \frac{a - y}{\lambda_x} \tag{1}$$

where λ_w and λ_x are wavelengths of ultrasound in the reference solvent and test solution, respectively. If the transducer assembly is moved along the axis of the test vessel a distance Δy until the received signal undergoes a 360° phase change, then the acoustic path length is increased to

$$n + 1 = \frac{y + \Delta y}{\lambda_w} + \frac{a - y - \Delta y}{\lambda_x} \tag{2}$$

if $\lambda_x > \lambda_w$. Subtracting these equations and introducing velocities instead of wavelengths, the following expression is obtained[21]

$$u_x - u_w = u^2_w \frac{1}{f\Delta y - u_w} \tag{3}$$

where f is the frequency, and u_x and u_w are velocities in the reference solvent and test solution, respectively.

Equation 3 shows that the accuracy of the measurement of the difference of velocity is determined by the precision with which the frequency f (measured by K in Figure 1 to better than 0.03%) and the quantity Δy may be measured. The quantity $f\Delta y$ is much larger than u_w; hence, errors related to the measurement of Δy determine the limit of accuracy of the velocity difference technique.

In order to keep temperature effects in the velocity difference below one part in 10^4, the temperature difference between the reference solvent and the test solutions has to be 0.01°. The temperature coefficient of the difference in a velocity between, for example, water and an aqueous solution will, however, be smaller than the temperature coefficients of the absolute velocities themselves. Hence, the velocity difference technique is less sensitive to temperature fluctuations than are conventional direct methods.

The temperature of the divided bath was maintained constant to 25 ± 0.03° and measured on a previously calibrated thermometer having a 12-in. scale for a range

(21) The sign of Δu, *i.e.*, $u_x - u_w$, was determined for a given solute by employing the transducers in a direct[15] interferometric arrangement at suitable solute concentrations.

of 6°. The thermostating liquid (water) was pumped from an adjacent supply bath that was well lagged and heated by means of a partially immersed electric bulb. The apparatus, including the bath, was situated in a room, the temperature of which was maintained between 24–25°. Temperature differences between the two compartments of the bath were not greater than 0.01° and were generally not detectable.

Changes in concentration of the test solution through evaporation were minimized by covering both the divided bath and the outer bath. Only a narrow slot was provided in the test vessel cover to permit motion of the transducer assembly. Considering that the room temperature was very close to that of the bath, errors from changes of concentration due to evaporation were considered negligible.

The velocity difference measurements were obtained from Δy with an absolute precision of ± 0.04 m sec^{-1} or better, and the absolute accuracy of the measurement was determined with test runs on KCl solutions. For each concentration at least five consecutive measurements of Δy differing by not more than 0.5% were made. The values of the measured velocities for aqueous KCl agreed to within 0.1 m sec^{-1} of the data published by Owen and Kronick[19] in the concentration range 0.05–0.25 M.

In order to obtain the absolute velocity in the salt solution, the value of u for water was taken as 1497.07 m sec^{-1} at 25.0° from the data of Owen and Kronick.[19]

The adiabatic compressibility coefficients for the solutions indicated below were then calculated from the absolute velocities of sound u in cm sec^{-1} and corresponding measurements of density d using the relation

$$\beta = 10^6/u^2d \text{ bar}^{-1} \quad (4)$$

(3) *Systems Studied and Purification of Salts.* The following compounds were studied in double-distilled water as the solvent: (a) the series of tetra-*n*-alkylammonium iodides and bromides R_4NX with R = Me to R = *n*-butyl; (b) the series of alkylamine hydrochlorides from $CH_3NH_2 \cdot HCl$ to $(CH_3)_3NHCl$ including the quaternary salt $(CH_3)_4NCl$, and (c) the neutral amines CH_3NH_2, $(CH_3)_2NH$, and $(CH_3)_3N$.

(*i*) *Tetraalkylammonium Salts.* The procedure used for purification and analysis of the R_4NX salts has been described in detail elsewhere.[9,20] Usually two recrystallizations followed by suitable drying *in vacuo* at minimal temperatures were used.

(*ii*) *$CH_3NH_2 \cdot HCl$, $(CH_3)_2NH \cdot HCl$, and $(CH_3)_3N \cdot HCl$ Salts.* The salts used were Fisher high-purity reagent grade materials. They were recrystallized twice from methanol–diethyl ether mixtures of varying volume composition. Each salt, after purification, was dried at 50° *in vacuo* for 4–6 days prior to use. Purity was checked by melting point determinations and chloride analysis.

(*iii*) *Corresponding Neutral Amines.* Eastman reagent grade anhydrous dimethylamine and trimethylamine were obtained in sealed ampoules and used without any further purification. The methylamine employed was an Eastman reagent grade 30% aqueous solution and was used without further purification.

(4) *Actual Experimental Procedure.* The solutions were made up volumetrically in 1-l. volumetric flasks calibrated at 25°. The purified salts were weighed by difference and placed in the flasks, whereas the amine liquids were added to give approximate concentrations, the exact concentration being determined by titration with a standardized HCl solution. The neutral amine solutions were made up in 0.025 N aqueous KOH to suppress ionization. The reference solvent for the differential measurements in these cases was also 0.025 N KOH. The flasks containing the solutions were placed in a thermostat at 25 ± 0.05°, thermally equilibrated, and then made up to the mark.

Results

Values of the apparent molal adiabatic compressibilities $\phi_{K(s)}$ for the first four members of the homologous series of symmetrical tetraalkylammonium bromides in aqueous solution at 25° are shown in Table I, together with the values of the coefficient β at different concentrations and the apparent molar volume ϕ_V. Typical extrapolations of $\phi_{K(s)}$ with respect to $c^{1/2}$ are shown in Figures 2 and 3 for $(CH_3)_4NBr$, $(C_2H_5)_4NBr$, and $(n\text{-}C_4H_9)_4NBr$. Tables II, III, and IV contain corresponding data for the salt series CH_3NH_3Cl to $(CH_3)_4NCl$, $(CH_3)_4NI$ to $(n\text{-}C_4H_9)_4NI$, and the amines CH_3NH_2, $(CH_3)_2NH$, and $(CH_3)_3N$, respectively.

Extrapolations of $\phi_{K(s)}$ for the R_4NBr salts as $f(c^{1/2})$ down to $c^{1/2} = 0$ are shown in Figures 2 and 3. While these extrapolations leave something to be desired owing to the fact that the lower limit of c attainable was only 0.02–0.05 M, this is also the lower limit attained in other work with alkali halides;[19] the extrapolations are certainly no worse than previous ones that have been made[5,6] for other functions for these salts.

It was assumed that the concentration dependence of the apparent molal adiabatic compressibility $\phi_{K(s)}$ follows closely the simple form[22]

$$\phi_{K(s)} = \phi^0_{K(s)} + S_{K(s)}c^{1/2} \quad (5)$$

(22) H. S. Harned and B. B. Owen, "The Physical Chemistry of Electrolyte Solutions," 3rd ed, Reinhold Publishing Corp., New York, N. Y., 1964, p 376.

Table I: Values of the Apparent Molal Adiabatic Compressibility $\phi_{K(s)}$ for Four Tetraalkylammonium Bromide Aqueous Solutions at 25°

Salt	Concn, M	$\beta_{(s)} \times 10^6$ bar^{-1}	ϕ_V, cc mole^{-1}	$\phi_{K(s)} \times 10^4$ cc (mole bar)$^{-1}$
$(CH_3)_4NBr$	0.04158	44.521	114.52	−4.07
	0.04998	44.477	114.58	−3.55
	0.06187	44.413	114.59	−3.35
	0.07156	44.368	114.76	−2.17
	0.08926	44.271	114.74	−2.43
	0.10805	44.173	114.81	−2.12
	0.12715	44.071	114.86	−2.08
	0.15029	43.955	114.88	−1.55
	0.19960	43.703	115.05	−1.02
	0.28738	43.263	115.13	−0.26
$(C_2H_5)_4NBr$	0.02214	44.565	174.36	−5.98
	0.03052	44.496	174.11	−5.63
	0.04779	44.355	173.65	−5.15
	0.06187	44.241	173.74	−4.68
	0.07501	44.136	173.84	−4.20
	0.09981	43.938	173.97	−3.60
	0.14984	43.541	173.79	−2.98
	0.20123	43.143	173.64	−2.20
	0.30377	42.363	173.49	−0.97
$(n\text{-}C_3H_7)_4NBr$[a]	0.01567	44.567	239.42	−10.28
	0.02209	44.493	239.15	−9.76
	0.03075	44.393	239.31	−9.33
	0.03106	44.390	239.36	−9.12
	0.03332	44.362	239.28	−9.67
	0.03981	44.287	239.38	−9.42
	0.04106	44.275	239.30	−8.83
	0.04346	44.246	239.37	−9.08
	0.05855	44.075	239.23	−8.40
	0.06270	44.026	239.16	−8.61
$(n\text{-}C_4H_9)_4NBr$	0.01616	44.502	300.44	−19.64
	0.01758	44.480	300.58	−19.64
	0.01759	44.480	300.59	−19.51
	0.01806	44.472	300.95	−19.83
	0.02537	44.361	300.57	−19.19
	0.03068	44.281	300.65	−18.64
	0.03371	44.237	300.48	−19.03
	0.03500	44.217	300.32	−18.19
	0.04383	44.086	300.45	−17.27
	0.05659	43.900	300.40	−15.96
	0.07731	43.587	300.18	−16.22

[a] The $\bar{V}^0$ datum for this compound was incorrectly quoted in ref 10 owing to a transcription error.

Table II: Values of the Apparent Molal Adiabatic Compressibility $\phi_{K(s)}$ for Aqueous Solutions of CH_3NH_3Cl, $(CH_3)_2NH_2Cl$, $(CH_3)_3NHCl$, and $(CH_3)_4NCl$ at 25°

Salt	Concn, M	$\beta_{(s)} \times 10^6$ bar^{-1}	ϕ_V,[a] cc mole^{-1}	$\phi_{K(s)} \times 10^4$ cc (mole bar)$^{-1}$
CH_3NH_3Cl	0.04113	44.569	54.26	−19.99
	0.05037	44.532	54.28	−19.09
	0.06199	44.480	54.28	−19.35
	0.07026	44.444	54.30	−19.37
	0.14192	44.145	54.53	−18.25
	0.19630	43.910	54.67	−18.38
	0.30395	43.510	54.77	−16.32
	0.40769	43.107	54.93	−15.73
	0.45211	42.938	54.93	−15.52
	0.50749	42.751	55.03	−14.77
	0.59012	42.471	55.09	−13.97
$(CH_3)_2NH_2Cl$	0.02492	44.627	72.62	−17.27
	0.04425	44.535	72.66	−16.30
	0.06201	44.453	72.83	−15.47
	0.08180	44.362	73.00	−14.89
	0.09987	44.277	73.04	−14.78
	0.16114	43.996	73.16	−14.11
	0.21518	43.751	73.21	−13.71
	0.25043	43.611	73.23	−12.75
	0.31453	43.326	73.32	−12.50
$(CH_3)_3NHCl$	0.02545	44.610	90.90	−14.72
	0.03024	44.585	91.09	−14.13
	0.04066	44.531	90.88	−13.44
	0.04098	44.527	90.97	−13.95
	0.06158	44.425	90.94	−12.25
	0.07071	44.373	91.05	−12.72
	0.07813	44.340	91.09	−11.84
	0.09018	44.282	91.05	−11.26
	0.09369	44.261	91.12	−11.53
$(CH_3)_4NCl$	0.02187	44.616	107.59	−13.59
	0.02564	44.595	107.66	−12.67
	0.03384	44.548	107.41	−11.91
	0.04559	44.478	107.66	−11.71
	0.05203	44.442	107.61	−11.23
	0.05882	44.402	107.68	−11.14

[a] Values of ϕ_V are also recorded here and in Tables III and IV (see part II) for convenience of reference.

which is expected in the case of the apparent molal isothermal compressibility ϕ_K in dilute solutions. It may be shown[22] that the limiting slope S_K is given by

$$S_K = \left[\left(\frac{\partial S_{(V)}}{\partial P}\right)_H + \frac{\beta S_{(V)}}{2}\right] \quad (6)$$

where $S_{(V)}$ is the corresponding limiting slope for ϕ_V.

The values of the apparent molal adiabatic compressibilities at infinite dilution $\phi^0_{K(s)}$ and the slopes $S_{K(s)}$ for the three series of salts studied are shown in Table V. It was difficult to achieve the desired low concentration values of $\phi_{K(s)}$ for some of the salts on account of the restriction imposed by the length of the test vessel employed in the frequency range 8.3–8.45 MHz. At higher concentrations ($>\sim 0.15$ M), the slopes of plots of $\phi_{K(s)}$ as a function of $c^{1/2}$ decrease for most of the salts. In the case of $(CH_3)_4NI$, only a

Table III: Values of the Apparent Molal Adiabatic Compressibility $\phi_{K(s)}$ for Aqueous Solutions of $(CH_3)_4NI$, $(C_2H_5)_4NI$, $(n\text{-}C_3H_7)_4NI$, and $(n\text{-}C_4H_9)_4NI$ at 25°

Salt	Concn, M	$\beta_{(s)} \times 10^6$ bar^{-1}	ϕ_V, cc mole^{-1}	$\phi_{K(s)} \times 10^4$ cc (mole bar)$^{-1}$
$(CH_3)_4NI$	0.08993	44.319	126.24	+8.46
	0.09460	44.298	126.30	+8.64
	0.09997	44.274	126.37	+8.84
	0.10353	44.256	126.28	+8.70
	0.10967	44.228	126.34	+8.85
	0.11117	44.222	126.58	+9.05
	0.11888	44.189	126.51	+9.34
$(C_2H_5)_4NI$	0.03171	44.507	185.65	+6.14
	0.03286	44.498	185.74	+6.14
	0.04212	44.430	185.67	+6.89
	0.04851	44.383	185.68	+7.20
	0.04906	44.378	185.87	+7.15
	0.07458	44.199	185.48	+8.99
	0.09857	44.024	185.70	+9.33
$(n\text{-}C_3H_7)_4NI$	0.02643	44.460	250.94	+2.17
	0.04093	44.305	250.80	+3.25
	0.05071	44.201	251.14	+3.87
	0.06713	44.030	250.84	+4.80
	0.11407	43.550	250.76	+6.93
	0.14264	43.265	250.66	+8.02
$(n\text{-}C_4H_9)_4NI$	0.01564	44.520	312.25	−7.98
	0.01979	44.459	312.19	−7.85
	0.02035	44.450	312.30	−8.15
	0.03048	44.304	312.30	−6.89
	0.04959	44.031	312.16	−5.50

Table IV: Values of the Apparent Molal Adiabatic Compressibility $\phi_{K(s)}$ for Aqueous Solutions of CH_3NH_2, $(CH_3)_2NH$, and $(CH_3)_3N$ at 25° (in 0.025 N Aqueous KOH to Suppress Ionization; Same Solution Used in Reference Compartment)

Solute	Concn, M	$\beta_{(s)} \times 10^6$ bar^{-1}	ϕ_V, cc mole^{-1}	$\phi_{K(s)} \times 10^4$ cc (mole bar)$^{-1}$
CH_3NH_2	0.07120	44.672	40.73	+7.13
	0.07433	44.669	40.75	+7.20
	0.08092	44.664	40.78	+7.50
	0.09031	44.654	40.85	+7.55
	0.10053	44.644	41.06	+7.73
	0.10811	44.636	41.16	+7.78
	0.11882	44.622	41.14	+7.55
	0.14239	44.594	41.12	+7.38
$(CH_3)_2NH$	0.06468	44.638	58.78	+8.81
	0.07680	44.616	59.02	+8.83
	0.08372	44.607	58.32	+8.90
	0.09592	44.586	58.51	+8.98
	0.10630	44.566	59.06	+9.03
	0.12130	44.540	58.96	+8.99
	0.16497	44.457	59.01	+8.59
	0.19875	44.391	59.28	+8.42
$(CH_3)_3N$	0.03082	44.657	76.50	+3.73
	0.04499	44.614	78.15	+4.52
	0.04582	44.611	78.11	+4.40
	0.04615	44.611	78.22	+4.67
	0.04994	44.599	78.21	+4.56
	0.06312	44.563	78.19	+5.21
	0.09905	44.461	78.34	+5.78
	0.15623	44.272	78.65	+4.54

rather narrow concentration range could be studied owing to the limitation of the length of test vessel at low concentrations and the relative insolubility (*viz.*, *ca.* 0.12 M) of $(CH_3)_4NI$ at higher ones. $S_{k(s)}$ is positive as in the case of simple salts.[22]

Values of $\phi_{K(s)}$ for the aqueous mono-, di-, and trimethylamine solutions are shown in Figure 4 as a function of the molar concentration c. In each case, $\phi_{K(s)}$ passes through a slight maximum which arises in the concentration range 0.09–0.11 M for each of the three amines. This behavior cannot arise from hydrolysis at low concentrations since the measurements were carried out in 0.025 M aqueous KOH to eliminate this possibility.

The values of $\phi^0_{K(s)}$ for the three series of salts studied are shown in Figure 5 as a function of the number of carbon atoms in the salt.[9,12] It is seen that $\phi^0_{K(s)}$ increases linearly with the number of carbon atoms[23] in the methylamine hydrochloride series. However, in the $R_4N^+Br^-$ and $R_4N^+I^-$ series, $\phi^0_{K(s)}$ decreases nonlinearly with an increasing number of carbon atoms;

Table V: Values of $\phi_{K(s)}$ and $S_{K(s)}$ in Eq 5 (25°)

Salt	$\phi^0_{K(s)}$ (±0.25) × 10^4 cc (mole bar)$^{-1}$	$S_{K(s)}$ (±8%) × 10^5 cc l.$^{1/2}$ mole$^{-3/2}$ bar^{-1}
$(CH_3)_4NBr$	−7.1	+15.4
$(C_2H_5)_4NBr$	−8.2	+14.2
$(n\text{-}C_3H_7)_4NBr$	−11.8	+13.7
$(n\text{-}C_4H_9)_4NBr$	−23.3	+27.5
$(CH_3)_4NI$	+3.3	+17.2
$(C_2H_5)_4NI$	+1.6	+25.3
$(n\text{-}C_3H_7)_4NI$	−2.25	+27.2
$(n\text{-}C_4H_9)_4NI$	−11.9	+28.6
CH_3NH_3Cl	−22.0	+10.0
$(CH_3)_2NH_2Cl$	−20.2	+18.2
$(CH_3)_3NHCl$	−18.1	+21.5
$(CH_3)_4NCl$	−16.6	+23.4

(23) The datum for the NH_4^+ ion is considered in part II in relation to its partial molar volume. (See also ref 9.)

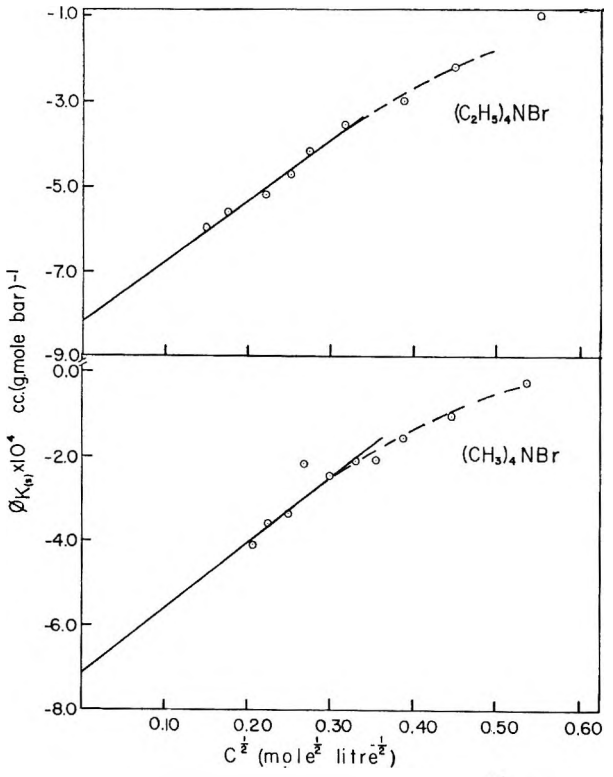

Figure 2. Extrapolations of $\phi_{K(s)}$ with respect to $c^{1/2}$ for aqueous tetramethyl- and tetraethylammonium bromides.

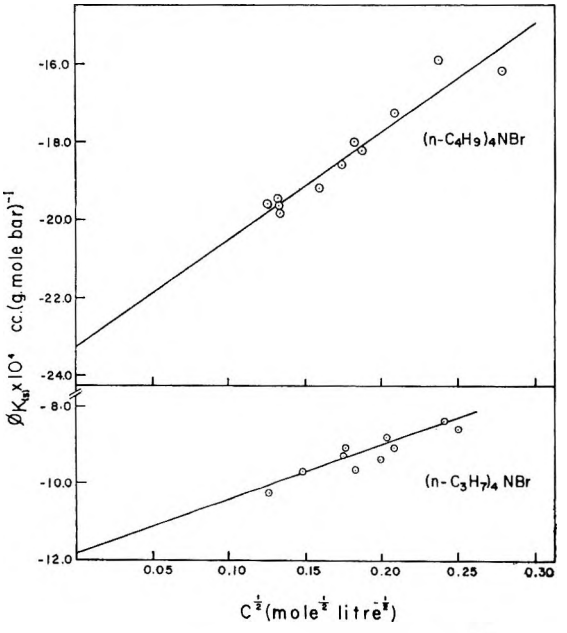

Figure 3. Extrapolations of $\phi_{K(s)}$ with respect to $c^{1/2}$ for aqueous tetra-*n*-propyl- and tetra-*n*-butylammonium bromides.

in regard to this fact, it is of interest to note that the corresponding $\bar{V}^0$ values for the R_4N^+ salts are remarkably linear in the number of carbon atoms in the salt.[9,12]

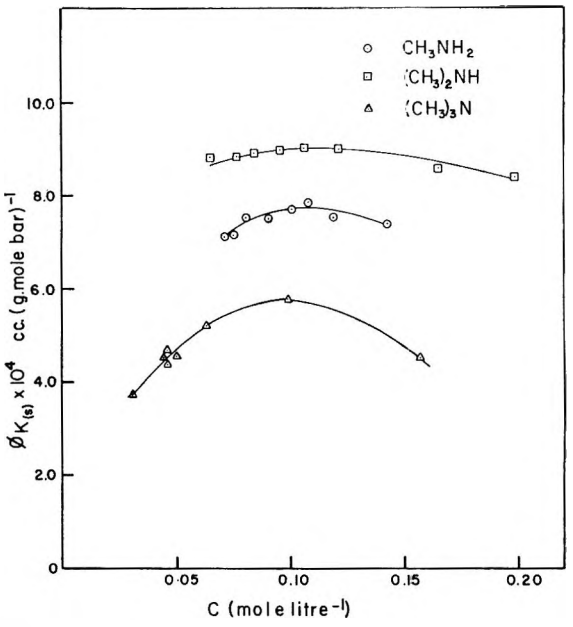

Figure 4. $\phi^0_{K(s)}$ as a function of $c^{1/2}$ for neutral primary, secondary, and tertiary methylamines in 0.025 *N* aqueous KOH.

Discussion

The experimental observations described above show some regularities, an interpretation of which may be offered in terms of two effects: (a) a structural one, due to the influence of the ions on the cluster equilibrium[11] in the water, and (b) an electrostatic one.[14,15]

The higher (less negative) apparent compressibility of the tetraalkylammonium halide solutions in comparison with that of corresponding inorganic salt solutions, *e.g.*, KCl, KBr indicates that the cation must cause this effect; for example, $\phi_{K(s)KCl} = -40 \times 10^{-4}$ whereas $\phi^0_{K(s)Me_4NCl} = -16.6 \times 10^{-4}$ cc (mole bar)$^{-1}$. It should be noted that this higher compressibility is not limited to the alkyl-substituted ammonium ions but that the NH_4^+ itself has a higher (*i.e.*, less negative) apparent compressibility[24] than that of other inorganic ions, *e.g.*, K^+. It appears that the ability of the NH_4^+ ion to form H bonds results in an influence on water structure which is less than that for the K^+ ion which has a similar radius. The same applies to H_3O^+.

Previous studies[2,3,6,9,11,25] on tetraalkylammonium salts seem to indicate a strong structural influence of the large cations upon water.

Interpretations of the present results may be made tentatively in terms of changes of the local compressibility of the solvent near the ions. The bulkiness of the large hydrophobic cations suggests that their in-

(24) V. B. Corey, *Phys. Rev.*, **64**, 350 (1943).

(25) H. S. Frank and W. Y. Wen, *Discussions Faraday Soc.*, **24**, 133 (1957).

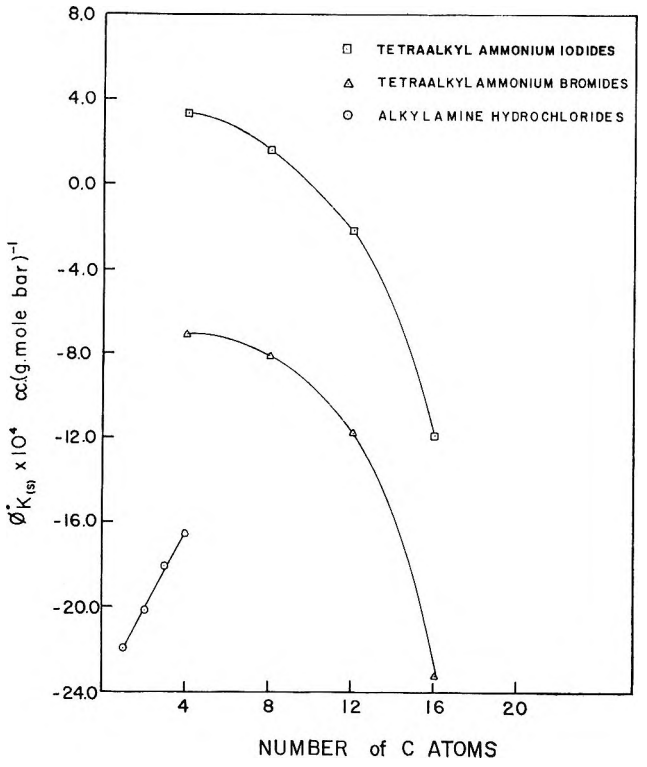

Figure 5. Values of $\phi^0_{K(s)}$ as a function of the number of carbon atoms in a series of tetraalkylammonium bromides and iodides, and in the methylamine hydrochloride series including Me_4NCl. (See also part II.)

trinsic molecular compressibilities might account for some of the apparent increase of compressibility in relation to that for small inorganic ions. However, in general, the intrinsic compressibility of ions themselves is expected to be much less than that of the solvent water since in the latter case, it is the free volume that is principally diminished with increasing pressure. The compressibility of the ion itself will presumably be similar to that for a substance, *e.g.*, a hydrocarbon, at very high pressures or to that for a close-packed metal. Previously it has been argued,[14] when the process of taking inorganic ions from the crystal lattice into the solution is considered, that the compression of the solute appears negligible in comparison with that of the solvent. The intrinsic compressibility of the tetraalkylammonium ions may, however, be somewhat greater than that of small monatomic ions since the former are, in effect, microscopic droplets of a different phase in the water, probably with some free space between the CH_2 groups in R particularly when R is large.

However, in the present case, if the intrinsic molecular compressibility of the cation made a significant contribution to the observed compression, the effect would be expected to be greatest for the largest cation, since it is reasonable to assume that any "free volume"[26] within the intrinsic volume of n-Bu_4N^+ is greater than that in Me_3NH^+ or Me_4N^+. If this were the case, then the plots of $\phi^0_{K(s)}$ as a function of the number of C atoms in Figure 5 for the R_4NX salts should show a trend in the opposite direction to that observed, *i.e.*, $\phi_{K(s)}$ should become less negative with increasing cation size for a given halide anion.

A different possibility arises if the R_4N^- ions are, in fact, relatively incompressible in comparison with water. Then with increasing size of R the apparent compressibility would tend to be more negative. However, since the volume of the ions increases almost in exact proportion to the number of carbon atoms,[9,12] it would be expected that the effect referred to above would lead to a linear decrease of $\phi_{K(s)}$ with molecular weight, which is not observed (Figure 5 and see part II). Therefore we must consider how the observed effects might arise from structure promotion or electrostriction in addition to the last possibility considered.

Qualitatively, it may be useful to distinguish, limitingly, three types[27] of local solvent water near the ions as shown in Figure 6; (1) is an ice-like configuration[25,28]; (2) is "free" water (*cf.* Némethy and Scheraga's[29] "unbonded" liquid state); and (3) is electrostricted water.[14]

Structure 1 in Figure 6 is regarded as being less compressible than bulk solvent water because of a stronger intermolecular framework of H bonds. This is supported by the fact that $\beta_{ice} << \beta_{water}$. Numerical values of β for ice I vary between 12×10^{-6} and 33×10^{-6} bar^{-1} [30,31] in the temperature range -15 to $0°$ and, in general, solids have a much lower value of β compared with that for water (*viz.*, 45×10^{-6} bar^{-1}). For example, Ag has a value of $\beta = 1 \times 10^{-6}$ bar^{-1}; it has been shown that compressed or electrostricted water can be expected to behave similarly.[14] Thus the unbonded water molecules (2) in Figure 6 may tend to possess the highest compressibility because they may be pushed closer together without H-bond rupture and the main effect will be to decrease the void space between the molecules; finally, the electrostricted water molecules (3) in Figure 6 will be expected[15] to

(26) However, any "free volume" that might be involved within the larger R_4N^+ ions will not have quite the same significance as that in a corresponding liquid hydrocarbon RH.

(27) For a review of recent structural theories of water in terms of various states, see ref 12 (B. E. Conway).

(28) J. D. Bernal and R. H. Fowler, *J. Chem. Phys.*, **1**, 515 (1933).

(29) G. Némethy and H. A. Scheraga, *ibid.*, **36**, 3382 (1962).

(30) T. W. Richards and C. L. Speyers, *J. Am. Chem. Soc.*, **36**, 491 (1914).

(31) P. W. Bridgman, *Proc. Am. Acad. Arts Sci.*, **47**, 473 (1912).

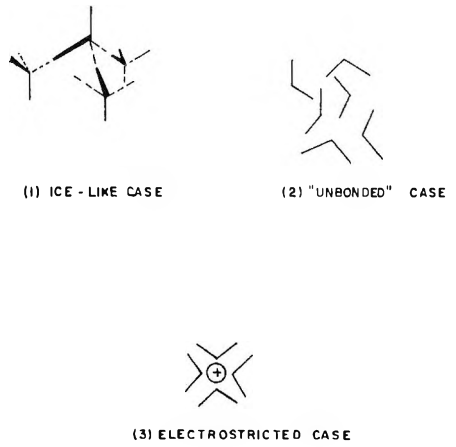

Figure 6. Schematic representation of three limiting types of water species considered.

have, of course, the least compressibility. Hence it seems reasonable to suppose that the relative order of increasing compressibility of the solvent species in Figure 6 would be (3) < (1) < (2).

For the three series of salts, $\phi^0_{K(s)}$ increases (becomes less negative) for a given cation with increase of the anion size in the order $I^- > Br^- > Cl^-$. This trend is consistent with a decreasing electrostrictive effect with increasing anion size (primary hydration effect).

Some estimate of the differences of individual $\phi^0_{K(s)}$ values deduced from the data for R_4NX salts with a common cation or anion are shown in Table VI. The difference in the values of $\Delta\phi^0_{K(s)}$ and $\Delta\bar{K}_2{}^0$ for Cl^-–Br^- [19] in Table VI is in part due to the fact that the adiabatic and isothermal compressibilities differ according to eq 4. However, in the case of NaCl or KCl,[19] neglect of the correction to the adiabatic quantities causes an error of only *ca.* 7.5% in $\bar{K}_2{}^0$.

Although a complete series of salts of alkyl-substituted ammonium cations ranging from $MeNH_3X$ to *n*-Bu_4NX having a common anion have not been studied, it may be assumed (using the thermodynamic differences for $\Delta\phi^0_{K(s)}(Br^-–Cl^-)$ from Table VI that the $\phi^0_{K(s)}$ values for such a series, *viz.*, the bromide series, tend to go through a discontinuous maximum (see part II, Figure 8). The maximum occurs at Me_4NBr, and in the series of cations NH_4^+, $MeNH_3^+$, etc., there is evidently an almost linear decrease in the amount of electrostricted water of type 3 (and possibly an increase in type 2). This would cause an apparent increase in $\phi^0_{K(s)}$. However, in comparison with the Me_4N^+ ion, Et_4N^+ appears to promote structure slightly, *i.e.*, it increases type 1 water at the expense of type 3, thus decreasing the compressibility. This structure promotion is evidently greatly increased by *n*-Pr_4N^+ and *n*-Bu_4N^+ with a consequent marked decrease in compressibility despite the lower electrostrictive field at the larger ions. Analogous explanations have been used[33] to explain the nonlinear decrease from Me_4N^+ to *n*-Bu_4N^+ of the ratio of the Walden product for D_2O to that for H_2O as a function of ion size.

Table VI: Differences of $\Delta\phi^0_{K(s)}$ at Infinite Dilution for Tetraalkylammonium Halides Having a Common Cation or Anion

Ions	$\Delta\phi^0_{K(s)} \times 10^4$ cc (mole bar)$^{-1}$	$\bar{K}_2{}^{0\,a} \times 10^4$ cc (mole bar)$^{-1}$
Cl^-–Br^-	−9.5	−8.6
Cl^-–I^-	−19.9	
Br^-–I^-	−10.4	
Me_4N^+–Et_4N^+ [d]	+2.4[b] (±0.3)[c]	
Et_4N^+–*n*-Pr_4N^+	+3.7[b] (±0.1)[c]	
n-Pr_4N^+–*n*-Bu_4N^+	+10.6[b] (±0.9)[c]	

[a] From ref 19 for sodium and potassium salts. [b] Average values from the bromide and iodide series. [c] Mean deviation. [d] A different value would follow from the recent data of Allam and Lee.[32] However, their measurements were not made to a sufficiently high dilution for extrapolation to be satisfactory and their data for NaCl, NaBr, and KCl are not in good agreement with those of Owen and Kronick for these salts (see Table 10 in ref 12).

The nonlinearity of the plots of $\phi^0_{K(s)}$ as a function of cation size precludes the possibility of using such a graph for estimating the $\phi^0_{i,K(s)}$ for individual anions *i* as was possible[9,12] in the case of the partial molal volumes.

No interpretation of the slopes $S_{K(s)}$ for the $R_4N^+X^-$ salts is attempted here on account of the complexity of the factors that determine $S_{K(s)}$ and also S_V to which it is related[9] (eq 6).

The values of $\phi_{K(s)}$ for the uncharged alkylamines CH_3NH_2, $(CH_3)_2NH$, and $(CH_3)_3N$ were also measured and show a nonlinear dependence on concentration (Figure 4); the $\phi_{K(s)}$ values are also positive, while for the corresponding protonated amine salts the values are negative. The order of $\phi_{K(s)}$ values is $(CH_3)_2NH > CH_3(NH_2) > (CH_3)_3N$.

Acknowledgments. Grateful acknowledgment is made to the National Research Council, Canada, for support of this work. R. E. V. acknowledges the award of Province of Ontario Graduate Scholarships

(32) D. S. Allam and N. H. Lee, *J. Chem. Soc.*, 6049 (1964); *ibid., Sect. A*, 5, 426 (1966).

(33) R. L. Kay and D. F. Evans, *J. Phys. Chem.*, **69**, 4216 (1965).

in 1964 and 1965. We are also indebted to Mr. A. Couture of the engineering staff of the Pure Chemistry Division of the National Research Council for fabrication of the ultrasonic velocity bath and racking mechanism, and to Dr. E. W. Carstensen for discussion on the design of the electrical circuit.

Partial Molar Volumes and Adiabatic Compressibilities of Tetraalkylammonium and Aminium Salts in Water. II. Volume and Volume Change Relationships

by R. E. Verrall[1] and B. E. Conway

Department of Chemistry, University of Ottawa, Ottawa, Canada *(Received July 6, 1966)*

Partial molal volumes of primary, secondary, and tertiary methylamine hydrohalides have been determined by a differential buoyancy method and compared with similar data for tetraalkylammonium salts in an aqueous medium. The volumes of acid ionization in reactions such as $R_nH_{4-n}N^+ \rightleftharpoons R_nNH_{3-n} + H^+$ have been determined, and values of the partial molar volume have been related to the apparent molal compressibilities and the partial specific compressibilities. The results are interpreted in terms of a change from electrostrictive effects to structure-promotion effects as the extent of coordination of the N^+ center by alkyl groups is increased.

Introduction

In previous papers[2,3] the partial molar volumes $\bar{V}$ of tetraalkylammonium ions have been considered in relation to the additivity[2a,3] of alkyl function contributions, the effects these ions have on the water structure,[2b,4,5] and to the concentration dependence of $\bar{V}$.[2a] In this paper we present data on $\bar{V}$ for primary, secondary, and tertiary alkylamine hydrohalides in relation to the $\bar{V}$ data for tetraalkylammonium salts published previously.[2] Measurements on the volumes of the neutral alkylamines together with the data for the corresponding hydrohalides lead to estimates of the volume change $\Delta\bar{V}$ for ionization. Relations between the $\bar{V}$ data and the $\phi_{K(s)}$ data presented in part I will be examined in terms of electrostriction and structure promotion effects. (See preceding paper.)

Experimental Section

(1) Partial Molar Volume Measurements. The determination of $\bar{V}$ values was made by evaluating the apparent molar volumes ϕ_V from density measurements. Densities were determined to six decimal places by the differential Archimedian balance method described by Wirth.[6] The details and accuracy of an improved procedure based on this method have been described and discussed previously[2a,3] in relation to determinations of $\bar{V}$ for a series of tetra-*n*-alkylammonium salts.

(2) Compounds Studied. Data for a series of tetra-

(1) Work carried out in partial fulfillment of the requirements for Ph.D. degree in the University of Ottawa, Ottawa, Canada.

(2) (a) B. E. Conway, R. E. Verrall, and J. E. Desnoyers, *Trans. Faraday Soc.*, 62, 2738 (1966); (b) W. Y. Wen and S. Saito, *J. Phys. Chem.*, 68, 2639 (1964).

(3) B. E. Conway, R. E. Verrall, and J. E. Desnoyers, *Z. Physik. Chem.* (Leipzig), Falkenhagen Anniversary Papers, 230, 157 (1965).

(4) R. M. Diamond, *J. Phys. Chem.*, 67, 2513 (1963).

(5) J. E. Desnoyers, G. E. Pelletier, and C. Jolicoeur, *Can. J. Chem.*, 43, 3222 (1965).

(6) H. E. Wirth, *J. Am. Chem. Soc.*, 59, 2549 (1937); see also F. Vaslow, *J. Phys. Chem.*, 70, 2286 (1966).

n-alkylammonium salts R_4NX are considered in relation to the behavior of a series of alkylamine hydrohalides. The preparation, purification, and analysis of the R_4NX salts have been described in detail elsewhere.[2a,7]

The purification of the primary, secondary, and tertiary methylamine hydrochlorides was described in part I. Other compounds were prepared and purified as follows.

(*a*) *Triethylamine Hydrogen Chloride.* Triethylamine hydrogen chloride was prepared by bubbling dried HCl gas into Eastman reagent grade triethylamine that had been purified by distillation under a nitrogen atmosphere at 55 mm. The impure salt was recrystallized twice from ethanol and dried *in vacuo* at 50° for 3 days prior to use.

(*b*) *Tri-n-propylamine Hydrogen Chloride.* Tri-*n*-propylamine hydrogen chloride was prepared by bubbling dried HCl gas into a 1:1 mixture of benzene and previously distilled Eastman reagent grade tri-*n*-propylamine under a nitrogen atmosphere. The reaction vessel was cooled to 0–5° to minimize the elimination of alkyl halide which can occur as a side reaction at higher temperatures. The resulting salt was washed with petroleum ether and then recrystallized from a chloroform–diethyl ether mixture. The recrystallized salt was washed with chilled diethyl ether and dried *in vacuo* without heating. The product, after grinding, was then placed in the vacuum oven at 50° for 4–6 days.

(*c*) *Alkylamine Hydrogen Iodide Salts.* The hydrogen iodide salts of *n*-propyl-, di-*n*-propyl-, and tri-*n*-propylamine were prepared in a way similar to that described above; HI gas, dried by passing through a tube of P_2O_5, was bubbled into a mixture of the amine and nitromethane. The amines had been previously purified by distillation under reduced pressure. The reaction system was essentially closed except for a P_2O_5 drying tube over a positive pressure safety outlet. The rate of bubbling was carefully controlled to prevent localized heating which produced a precipitate containing an appreciable amount of iodine which was undesirable. The reaction flask was cooled by a Dry Ice–acetone mixture to −15°.

The iodide salts were recrystallized from ethanol–diethyl ether mixtures at least three times, dried at 60° *in vacuo* for 4–6 days, and kept under subdued light.

(*3*) *Purity of the Compounds Used.* (*a*) *Tetra-n-alkylammonium Halides.* The careful recrystallization procedure (described previously[2a]) carried out on these reagent grade salts was considered sufficient to provide compounds of a sufficiently high degree of purity. Melting points or decomposition temperatures were determined in all cases and compared satisfactorily with literature data. In some cases, *e.g.*, $(n\text{-}C_3H_7)_4NBr$, a gravimetric determination of the halide was used to check purity.

(*b*) *Alkylamine Hydrogen Chloride Salts.* The melting points of the recrystallized alkylamine hydrochlorides were in good agreement with literature values[8] except in the case of the tri-*n*-propylamine salt. The reported melting point of 90° was in considerable disagreement with the experimental melting point of 137°. A standard gravimetric determination of chloride ion in tri-*n*-propylamine hydrogen chloride showed that the compound contained 99.95% of the theoretical amount of chloride ion expected for the compound $(n\text{-}C_3H_7)_3N \cdot HCl$. The literature melting point seems to be incorrect.

(*c*) *Alkylamine Hydrogen Iodide Salts.* The purity of all three compounds was determined volumetrically by a titration of the iodide[9] after treatment with a suitable oxidant.

Results

(*1*) *Alkylamine Hydrogen Halide Salts.* Plots of ϕ_V, the apparent molal volume, with respect to $c^{1/2}$

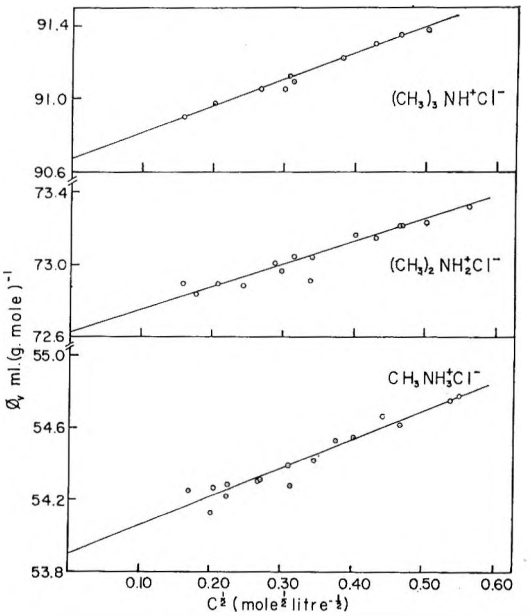

Figure 1. Apparent molal volumes ϕv as a function of $c^{1/2}$ for the three methylamine hydrogen chlorides (25°).

(7) R. E. Verrall, Ph. D. Thesis, University of Ottawa, Ottawa, Canada, 1966.

(8) "Dictionary of Organic Compounds," 4th ed, I. Heilbron and H. M. Bunbury, Ed., Eyre and Spottiswoode Ltd., London, 1965.

(9) I. M. Kolthoff and E. B. Sandell, "Textbook of Quantitative Inorganic Analysis," 3rd ed, The Macmillan Co., New York, N. Y., 1952, p 599.

Table I: Apparent Molal Volumes, Partial Molal Volumes, and Densities of Five Alkylammonium Chlorides at 25°

Salt	Concn, M	$\phi_2 \pm 0.06$,[a] ml mole^{-1}	$\bar{V}_2 \pm 0.1$, ml mole^{-1}	Density $\pm$ 3×10^{-6}, g ml^{-1}
CH_3NH_3Cl	0.02871	54.25	54.38	0.997433
	0.03985	54.13	54.29	0.997588
	0.04113	54.26	54.42	0.997600
	0.04961	54.22	54.40	0.997716
	0.05037	54.26	54.46	0.997723
	0.06199	54.28	54.52	0.997879
	0.07026	54.30	54.51	0.997988
	0.07271	54.31	54.52	0.998020
	0.09633	54.39	54.64	0.998328
	0.11969	54.42	54.69	0.998635
	0.14192	54.53	54.83	0.998915
	0.16167	54.54	54.85	0.999172
	0.19630	54.67	55.02	0.999602
	0.21805	54.62	54.99	0.999896
	0.28909	54.75	55.17	1.000785
	0.30395	54.77	55.20	1.000973
$(CH_3)_2NH_2Cl$	0.02489	72.89	72.99	0.997269
	0.03125	72.83	72.94	0.997327
	0.04323	72.89	73.02	0.997432
	0.05982	72.88	73.03	0.997580
	0.08180	73.00	73.17	0.997765
	0.08822	72.96	73.14	0.997825
	0.09987	73.04	73.23	0.997919
	0.11376	72.91	73.12	0.998056
	0.11575	73.04	73.25	0.998058
	0.16114	73.16	73.41	0.998435
	0.18412	73.15	73.41	0.998635
	0.21267	73.21	73.49	0.998890
	0.21518	73.21	73.49	0.998889
	0.25043	73.23	73.54	0.999185
	0.25143	73.23	73.53	0.999194
	0.31453	73.32	73.67	0.999704
$(CH_3)_3NHCl$	0.02545	90.90	91.02	0.997174
	0.04098	90.97	91.12	0.997248
	0.06158	90.94	91.13	0.997350

Salt	Concn, M	$\phi_2 \pm 0.06$,[a] ml mole^{-1}	$V_2 \pm 0.1$, ml mole^{-1}	Density $\pm$ 3×10^{-6}, g ml^{-1}
$(CH_3)_3NHCl$	0.07071	91.05	91.25	0.997387
	0.07813	91.09	91.32	0.997420
	0.09018	91.05	91.27	0.997481
	0.09369	91.12	91.35	0.997491
	0.14614	91.22	91.50	0.997724
	0.18379	91.30	91.62	0.997885
$(C_2H_5)_3NHCl$	0.01462	138.76	138.72	0.997038
	0.04288	138.69	138.63	0.997021
	0.05014	138.67	138.60	0.997018
	0.05579	138.57	138.49	0.997020
	0.06497	138.67	138.59	0.997009
	0.06603	138.64	138.56	0.997010
	0.06852	138.66	138.58	0.997007
	0.08426	138.63	138.54	0.997001
	0.10835	138.63	138.52	0.996986
	0.10904	138.67	138.57	0.996982
	0.13832	138.66	138.54	0.996965
	0.20805	138.54	138.43	0.996947
	0.29772	138.46	...	0.996929
	0.40967	138.31	...	0.996947
	0.53019	138.14	...	0.997003
$(n\text{-}C_3H_7)_3NHCl$	0.02083	186.77	186.65	0.996913
	0.02668	186.71	186.58	0.996877
	0.04702	186.76	186.57	0.996744
	0.06729	186.63	186.40	0.996621
	0.08194	186.75	186.49	0.996529
	0.08541	186.54	186.28	0.996524
	0.11845	186.48	186.16	0.996314
	0.12142	186.47	186.15	0.996298
	0.16959	186.35	186.00	0.996020
	0.20529	186.16	...	0.995843
	0.29128	185.80	...	0.995441
	0.33058	185.55	...	0.995309
	0.37189	185.41	...	0.995143

[a] See also Table II, part I.

for the alkylamine hydrogen chlorides are shown in Figures 1 and 2. Experimental data are given in Tables I and II. A similar plot for the alkylamine hydrogen iodides is shown in Figure 3. Partial molal volumes $\bar{V}$ were calculated from ϕ_V and $d\phi_V/dc$ in the usual way. Extrapolations[2a,10] of $\bar{V} - 2.792c^{1/2}$ with respect to c, down to zero c, are shown in Figures 4, 5, and 6 for the respective alkylamine hydrogen chlorides and iodides.[11] Numerical data for $\bar{V}^0$, the value of $\bar{V}$ at infinite dilution, and the resulting coefficient h of the remaining term in c[2a,10] for the alkylamine hydrogen halide salts are also given in Table III. Corresponding plots[10] of $\phi_V - 1.868c^{1/2}$ were also made for extrapolation purposes (see below) to obtain ϕ^0_V ($\equiv \bar{V}^0$ when $c \rightarrow 0$).

Previous studies on the partial molal volumes of CH_3NH_3Cl, $(CH_3)_2NH_2Cl$, and $(CH_3)_3NHCl$ were carried out pycnometrically by Hamann and Lim.[12] Their $\bar{V}^0$ values are only in fair agreement with the present data, the differences being 3% for the first member to 1% for the last. The differential float method employed here and in ref 2a allows accurate measurements to be made to a substantially higher dilution than in the pycnometric method.

(10) O. Redlich and D. M. Meyer, *Chem. Rev.*, 64, 221 (1964).

(11) The extent of hydrolysis of the methylammonium ions was calculated and found to be insignificant even at the lowest concentrations employed.

(12) S. D. Hamann and S. C. Lim, *Australian J. Chem.*, 7, 329 (1954).

Table II: Apparent Molal Volumes, Partial Molal Volumes, and Densities of Three Propylammonium Iodides at 25°

Salt	Concn, M	$\phi_2 \pm 0.06$, ml mole^{-1}	$\bar{V}_2 \pm 0.1$, ml mole^{-1}	Density $\pm$ 3×10^{-6}, g ml^{-1}
n-$C_3H_7NH_3I$	0.01923	105.95	106.04	0.998613
	0.02280	105.90	106.00	0.998905
	0.02812	106.00	106.11	0.999335
	0.04214	106.02	106.16	0.000475
	0.05692	106.17	106.23	1.001668
	0.05778	106.05	106.21	1.001745
	0.09755	106.13	106.34	1.004970
	0.17628	106.33	106.61	1.0111328
$(n$-$C_3H_7)_2NH_2I$	0.01868	157.23	157.31	0.998399
	0.02693	157.23	157.33	0.998996
	0.06048	157.33	157.47	1.001417
	0.09259	157.38	157.56	1.003733
	0.13474	157.48	157.69	1.006761
	0.16432	157.51	157.74	1.008890
$(n$-$C_3H_7)_3NHI$	0.01434	205.03	205.13	0.998005
	0.02209	205.06	205.18	0.998522
	0.03877	205.16	205.32	0.999631
	0.04330	205.20	205.37	0.999931
	0.05217	205.20	205.39	1.000522
	0.06343	205.23	205.43	1.001270

Table III: Values of $\bar{V}^0$ and h in the Equation $\bar{V} = \bar{V}^0 + 2.792\,c^{1/2} + hc$ for Alkylamine Hydrogen Halide Salts (25°)

Salt	$\bar{V}_2^0$ (± 0.2), ml mole^{-1}	h ($\pm 5\%$), ml mole^{-2}
$CH_3NH_3^+Cl^-$	53.81	−0.43 (9)
$(CH_3)_2NH_2^+Cl^-$	72.47	−1.33
$(CH_3)_3NH^+Cl^-$	90.59	−1.00
$(CH_3)_4N^+Cl^-$ (for comparison)	107.3	−4.60
$(C_2H_5)_3NH^+Cl^-$	138.6	−14.4
$(n$-$C_3H_7)_3NH^+Cl^-$	186.8	−22.4
n-$C_3H_7NH_3^+I^-$	105.7	−2.20
$(n$-$C_3H_7)_2NH_2^+I^-$	156.9	−1.60
$(n$-$C_3H_7)_3NH^+I^-$	204.8	−1.03
$(n$-$C_3H_7)_4N^+I^-$ (for comparison	250.7	−14.4

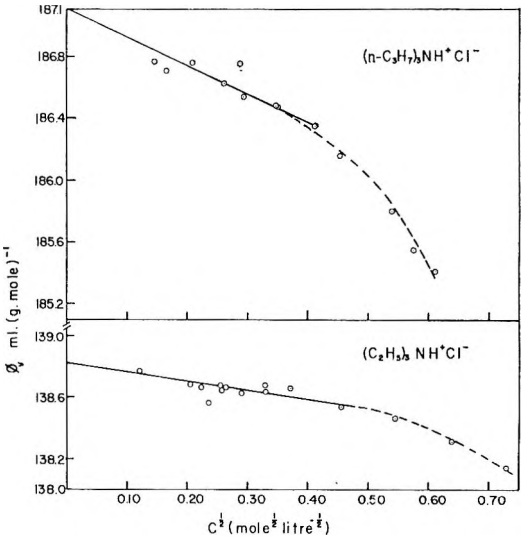

Figure 2. Apparent molal volumes ϕ_V as a function of $c^{1/2}$ for triethylamine and tri-n-propylamine hydrogen chlorides (25°).

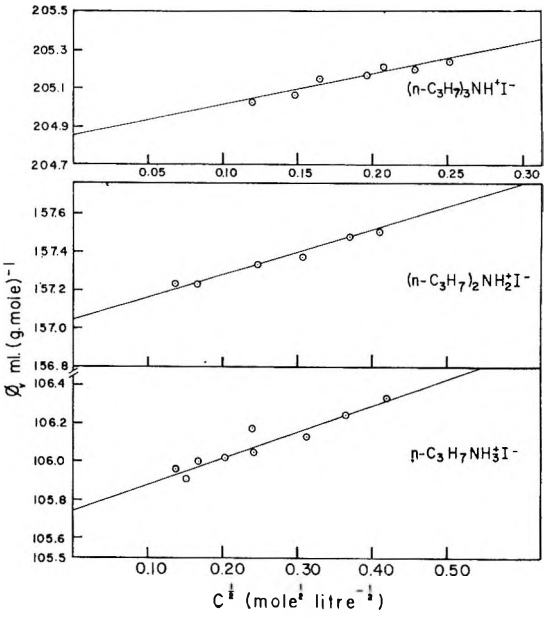

Figure 3. Apparent molal volumes ϕ_V as a function of $c^{1/2}$ for the three n-propylamine hydrogen iodides (25°).

2. Accuracy of Results. The experimental conditions employed in the determination of the apparent molal volumes enabled the density measurements to be obtained with a reproducibility of three in the sixth decimal place. A check on the absolute accuracy of the measurements was determined as described previously[2a] by means of test runs on KCl solutions; satisfactory agreement (to 0.06 ml mole^{-1}), *i.e.*, within 0.1% of the published data,[6] was obtained. A detailed discussion of the accuracy of the density measurements has been given previously[2a] with regard to the results for the $R_4N^+X^-$ salts.

3. Accuracy of Derived Results. Partial molal volumes $\bar{V}$ at finite concentrations were obtained from ϕ_V according to well-known principles. The precision for the partial molal volumes is ±0.1 ml mole^{-1} based on an estimated maximum error[13] in ϕ_V of 0.06 ml

(13) The error in ϕ_V becomes smaller however with increasing concentration.

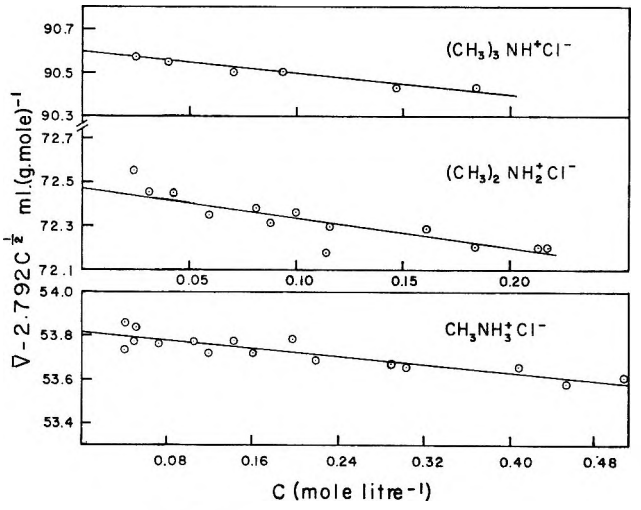

Figure 4. Plots of $\bar{V} - 2.792c^{1/2}$ for the three methylamine hydrogen chlorides (25°).

mole^{-1} and the least-squares uncertainty in the slope of ϕ_V as a linear function of $c^{1/2}$. Least-squares uncertainty in the intercepts $\bar{V}^0$ based on a linear plot of $\phi_V - 1.868c^{1/2}$ against c is ±0.2 ml mole^{-1}, and the uncertainty in the slopes is 5%.

Discussion

The present results can be examined usefully in regard to the following matters: (a) electrostriction as a function of coordination of the N^+ center by methyl groups; (b) changes of volume on ionization of the amines to give the protonated aminium salts; (c) the relation between the $\phi_{K(s)}$ values obtained in part I and the $\bar{V}$ data presented here; and (d) the additivity of partial molar volume contributions in solution.[2a,3]

(1) Volume Relationships in the Alkylamine Hydrohalide Series. The relationship between the partial molal volumes of consecutive members of an homologous series of alkylamine hydrogen halide salts having a common anion may be represented (as considered previously[2a,3] for R_4N^+ salts) by equations of a form equivalent to those for the homologous series of tetra-*n*-alkylammonium salts, *viz.*

$$\bar{V}^0_{Me_3NH^+} + \bar{V}^0_{X^-} = \bar{V}^0_{Me_2NH_2^+} + \bar{V}^0_{X^-} + b(\Delta\text{mol wt}) \quad (1)$$

where b is the volume increment[2a] per CH_3 minus H unit in the series primary, secondary, and tertiary aminium salts.

Values of the coefficient b, *i.e.*, the specific volume change per "CH_3" group added,[14] for the alkylamine hydrogen halide salts are shown in Table IV. The dependence of $\bar{V}^0$, the value of $\bar{V}$ for the solute salts at infinite dilution, on the number of carbon atoms in the salt is shown comparatively in Figure 7 for alkylamine hydrogen halide salts in relation to analogous data[2a] for the series of symmetrical tetraalkylammonium salts.

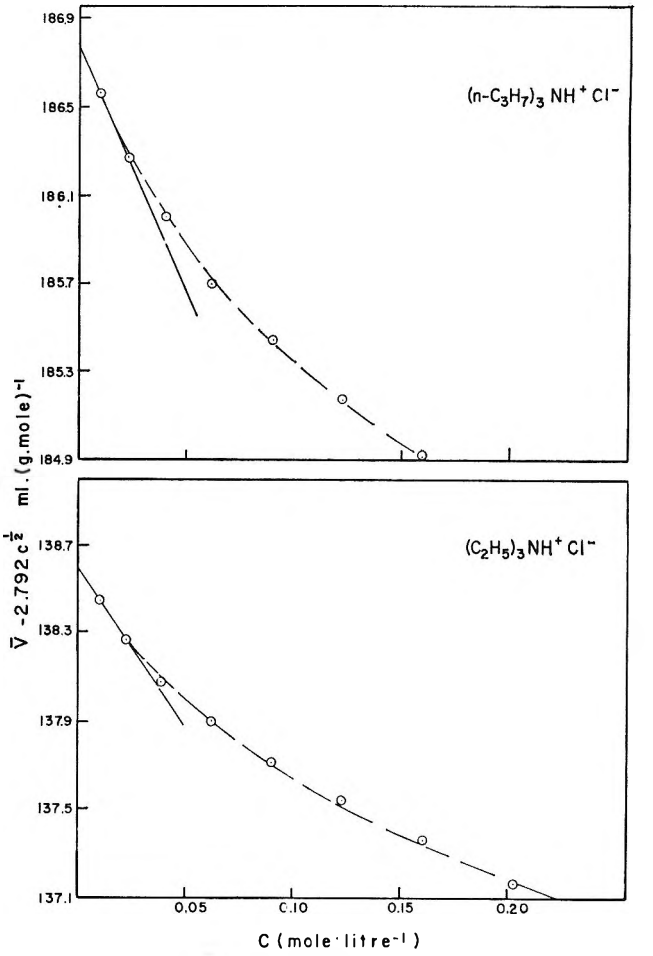

Figure 5. Plots of $\bar{V} - 2.792c^{1/2}$ for triethylamine and tri-*n*-propylamine hydrogen chlorides (25°).

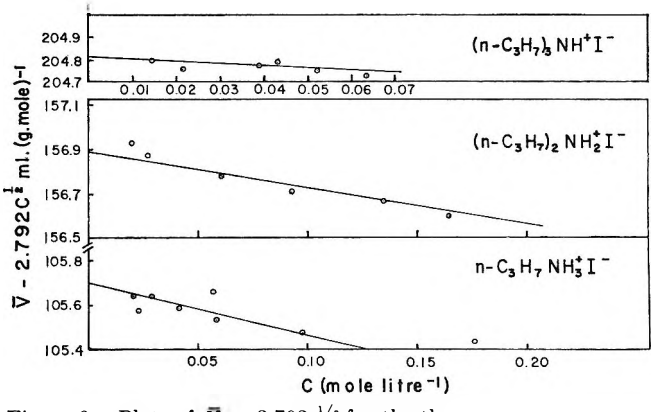

Figure 6. Plots of $\bar{V} - 2.792c^{1/2}$ for the three *n*-propylamine hydrogen iodides (25°).

(14) That is, including the loss of one H per CH_3 added.

In the series R_3NH^+, $R_2NH_2^+$, RNH_3^+ (and NH_4^+) (Figure 7 and Table IV), diminishing substitution at the N^+ center leads to a bigger local influence of the charge, and the b values are greater than those[2a] for the R_4N^+ series (see the change of slope in Figure 7 below Me_4N^+). This effect must be attributed to an increasing degree of hydration as the N^+ becomes more exposed in the direction of the above series. A similar trend of entropies of ionization is also observed.[15]

Table IV: Values of the Coefficient b in Eq 1 for Homologous Series of Alkylamine Hydrogen Halide Salts[a]

Salt	b
$CH_3NH_3^+Cl^-$	1.330
$(CH_3)_2NH_2^+Cl^-$	1.292
$(CH_3)_3NH^+Cl^-$	1.141
$(C_2H_5)_3NH^+Cl^-$	1.145
$(n\text{-}C_3H_7)_3NH^+Cl^-$	
$n\text{-}C_3H_7NH_3^+I^-$	1.217
$(n\text{-}C_3H_7)_2NH_2^+I^-$	1.139
$(n\text{-}C_3H_7)_3NH^+I^-$	

[a] Values for corresponding R_4N^+ salts are given in ref 2a.

The thermodynamic partial gram ionic volume difference $V^0_I - V^0_{Cl}$ may be verified in the case of the salts $(n\text{-}C_3H_7)_3NHI$ and $(n\text{-}C_3H_7)_3NHCl$ (Table III). The value of 18.0 ml (g-ion^{-1}) found is in reasonable agreement with the partial gram ionic volume difference obtained previously[2a] for the symmetrical tetraalkylammonium halide series.

(2) Concentration Dependence of $\bar{V}$ for the n-Alkylamine Hydrogen Halide Salts. The trend in the magnitude of the experimental h parameter[2a,10] (Table III) for the n-alkylamine hydrogen halide salts indicates that there is a general decrease in h as the size of the cation increases, but there is a reverse effect for a given cation with an increasing radius of the coanion. This behavior is similar to that found[2a] in the case of the R_4NX salts and offers evidence that the hydrophobic character of the cation is responsible, in part, for the negative slope of the concentration dependence of $\bar{V}$. Successive substitutions of a hydrogen atom by a methyl group in the series $MeNH_3Cl$ to Me_3NHCl do not appear to change the magnitude of h appreciably, although values of h for all three salts are greater than that for Me_4NCl, as would be expected (see Table III). Also h varies little in the iodide series n-$PrNH_3I$ to $(n\text{-}Pr)_3NHI$. However, as the size of the alkyl group is increased in the tri-n-alkylammonium chloride salts, there is a considerable decrease in h to more negative values.

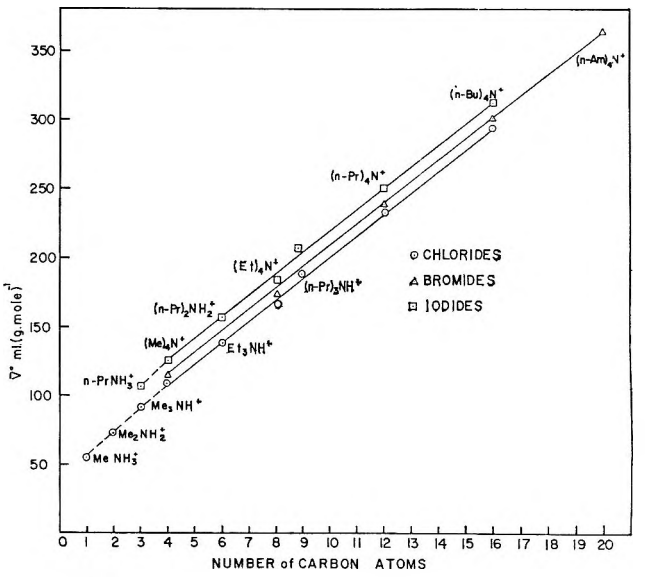

Figure 7. $\bar{V}_0$ for alkylamine hydrogen halides and tetraalkylammonium salts (the latter data from ref 2a) as a function of the number of carbon atoms in the salt.

These results generally indicate that the observed negative concentration dependence of $\bar{V}$ is larger (a) when the nitrogen atom in a salt of the type $R_nH_{4-n}N^+X^-$ is completely surrounded by four alkyl substituents ($n = 4$) and (b) when, for a given number of alkyl substituents in the cation, the size of the substituent alkyl group is increased;[5] in this case it must be borne in mind, however, that changes of the anion size lead to a reverse effect with regard to the variation of the experimental h values for a given cation.

Furthermore, it is seen that the charge-bearing nitrogen atom can evidently still exert an appreciable charge effect with regard to the values of h when the large ammonium-type cation is not completely substituted. The charge effect tends to give a positive concentration dependence of $\bar{V}$.

(3) Relation between $\bar{V}$ and $\phi_{K(s)}$. The relation between the $\phi^0_{K(s)}$ and $\bar{V}^0$ is shown in Figure 8. As in the case of the dependence of $\phi^0_{K(s)}$ on the number of carbon atoms (see Figure 7), there appears to be a linear relation between $\bar{V}^0$ and $\phi_{K(s)}$ in the case of the alkylamine hydrochloride salts only. Assuming this linear relationship and taking the value[16] of $\bar{V}^0$ for NH_4Cl as 35.98, a $\phi^0_{K(s)}$ value for NH_4Cl may be predicted to be -23.7×10^{-4}. Little work has been carried out on the apparent molal adiabatic compres-

(15) L. Hepler, *J. Phys. Chem.*, **69**, 965 (1965).

(16) H. S. Harned and B. B. Owen, "The Physical Chemistry of Electrolytic Solutions," 3rd ed, Reinhold Publishing Corp., New York, N. Y., 1958, p 361.

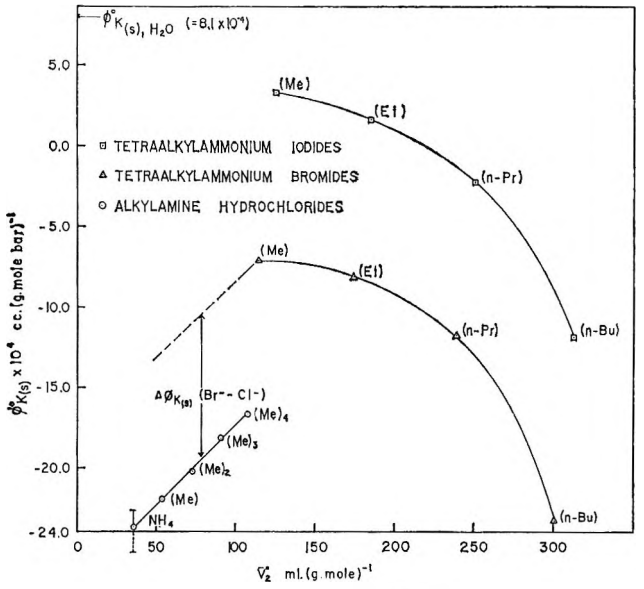

Figure 8. Relation between $\phi^0_{K(s)}$ and $\bar{V}_0$ for alkylamine hydrogen halides and related tetraalkylammonium salts.

sibility of NH_4Cl. However, Corey[17] gives one value of $\phi_{K(s)}$ for 25° and $c = 1.0827\ M$. Assuming $d\phi_{K(s)}/dc^{1/2}$ to be less than that obtained for CH_3NH_3Cl (see part I), and in fact using the one value of Corey and taking $S_{K(s)}$ as being in the range from 8×10^{-4} to 10×10^{-4}, values of $\phi^0_{K(s)}$ for NH_4Cl are obtained as -24.7×10^{-4} or -22.6×10^{-4}, respectively. These limits are shown by a vertical line in Figure 8 where the datum for NH_4Cl is shown for comparison with the data for the other substituted ammonium ions; it is evidently in the same linear relation with them.

In the ammonium ion series, the linear variation of $\phi^0_{K(s)}$ with increasing Me substitution (Figure 8) suggests a progressive diminution of the electrostriction effect as reflected by the compressibility.[18] Once the N^+ is completely coordinated by alkyl groups R, an increase of the size of R produces a continuously decreasing $\phi^0_{K(s)}$ with a discontinuity at the $(Me)_4N^+$ ion, as might be expected since the situation of the charge-bearing center in relation to its interaction with H_2O suffers qualitative change at the ion $(Me)_4N^+$. In Figure 8 this point is indicated more clearly by the dashed line which has been drawn to represent the change of $\phi^0_{K(s)}$ from NH_4^+ to Me_4N^+ that would occur in the bromide series by shifting the line for the chloride salts by the thermodynamic difference $\Delta\phi^0_{K(s)}$ ($Br^- - Cl^-$).

Since ϕ^0_K is defined as $-d\bar{V}^0/dP$, variations of ϕ^0_K in the series of salts studied can reflect effects due to the changing volume $\bar{V}^0$ of the salts in the series examined. It may therefore be suggested that the reduced function $\phi^0_K/\bar{V}^0$ may be a preferable quantity to relate to the number of carbon atoms in the cations. In the present work, however, we have only $\phi^0_{K(s)}$ data and therefore plot as a useful but approximate quantity $\phi^0_{K(s)}/\bar{V}^0$ ($=\beta$) as a function of the number of carbon atoms. The quantity β will thus be a partial specific compressibility and is plotted in Figure 9. In the series $NH_4^+ \rightarrow Me_4N^+$, β varies very markedly with N^+ coordination presumably due to the hydration effects discussed above; in the $R_4N^+I^-$ series (Figure 9),[19] however, β tends to diminish, but of course much less so than in the plot for $\phi^0_{K(s)}$ in Figure 8. This diminution we believe may reflect in terms of compressibility properties the progressive increase of a specific structure promotion effect now normalized to a unit volume quantity.

(4) *Solvation Effects in the Ionization Process.* (a) *Volume Relations.* The data obtained in the present work allow the volumes associated with acid ionization processes of the type

$$(R)_nH_{4-n}N^+ \longrightarrow (R)_nH_{3-n}N + H^+ \qquad (2)$$

to be estimated for the four protonated amines $CH_3NH_3^+$, $(CH_3)_2NH_2^+$, $(CH_3)_3NH^+$, and $(C_2H_5)_3NH^+$. The volume change associated with an ionization $BH^+ \rightarrow B + H^+$ may be expressed as

$$\Delta\bar{V}^0_{ioniz} = \bar{V}^0_B + \bar{V}^0_{H^+} - \bar{V}^0_{BH^+} \qquad (3)$$

or without any thermodynamic ambiguity as

$$\Delta\bar{V}^0_{ioniz} = \bar{V}^0_B + \bar{V}^0_{H^+Cl^-} - \bar{V}^0_{BH^+Cl^-} \qquad (3a)$$

In eq 3, $\bar{V}^0_B$ is the partial molal volume of the free alkylamine at infinite dilution obtained from the density data required in the compressibility studies of the alkylamines reported in part I. $\bar{V}^0_{BH^+}$ is the appropriate partial molal volume of the protonated alkylamine (Table I) calculated from the $\bar{V}^0$ value for the aminium hydrochloride salt and the value of the individual partial gram ionic volume for the chloride ion at infinite dilution deduced previously;[2a] $\bar{V}^0_{H^+}$ is -5.7 ± 0.4 ml (g-ion^{-1}) on this scale. Subtraction of $\bar{V}^0_{Cl^-}$ from $\bar{V}^0_{BH^+Cl^-}$ gives $\bar{V}^0_{BH^+}$. Alternatively, $\Delta\bar{V}^0_{ioniz}$ can be obtained directly from $\bar{V}^0_{BH^+Cl^-}$, $\bar{V}^0_B$, and $\bar{V}^0_{HCl}$ by eq 3a. The volumes for the respective species shown on the right-hand side of eq 2

(17) V. B. Corey, *Phys. Rev.*, 64, 350 (1943).

(18) A. G. Passynskii, *Acta Physicochim., U.R.S.S.*, 8, 385 (1938).

(19) In the R_4N^+ series of iodides and bromides, the data in Figure 9 indicate an apparent lack of constancy of the difference of the contributions to β from I^- and Br^-. This arises partly from the fact that the extrapolation for the $\phi^0_{K(s)}$ for $Me_4N^+I^-$ is based on only a limited range of concentrations due to the low solubility of this salt.

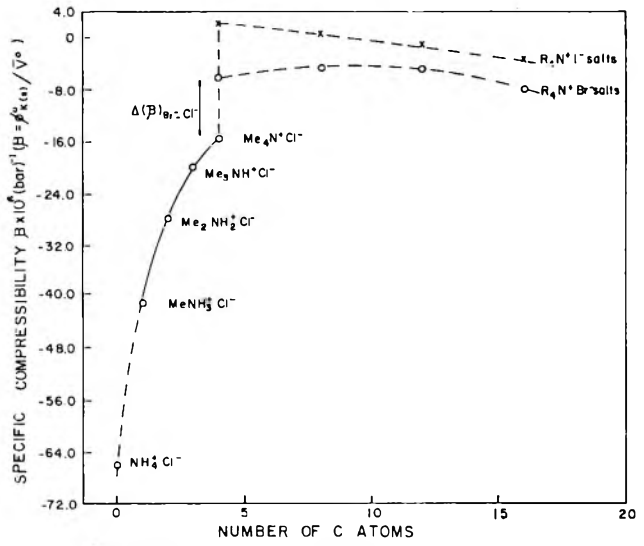

Figure 9. Plots of $\phi^0_{K(s)}$ as a function of the number of carbon atoms in the methylamine hydrochloride series and for four symmetrical homologous tetraalkylammonium salts.

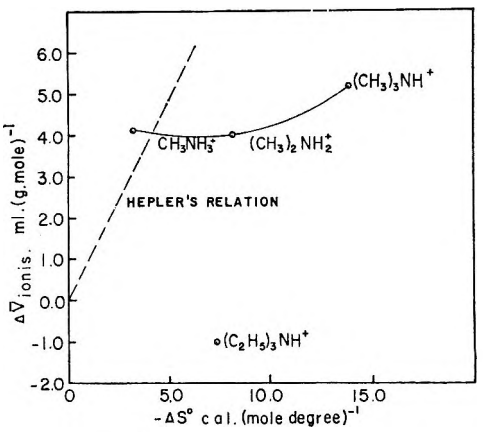

Figure 10. Plot of $\bar{V}_{ioniz}$ *vs.* $\Delta S°$, the entropy of ionization, for four alkylaminium ions in comparison with Hepler's relation[15] for a wide variety of other ionization processes.

and for $\Delta\bar{V}^0_{ioniz}$ are shown in Table V. The values of $\Delta\bar{V}^0_{ioniz}$ do not vary greatly with the different protonated bases.[15] Similarly, only slightly varying values of $\Delta\bar{V}^0_{ioniz}$ have been reported by Hamann and Lim[12] for the ionization of the series of bases NH_4OH to $(CH)_3NHOH$. Of course the values $\Delta\bar{V}^0_{ioniz}$ in the latter case are large and negative (-28 ml mole^{-1}) as would be expected from the net gain of charge which results when the above bases become ionized.

Table V: Volumes of Acid Ionization $\Delta\bar{V}^0_{ioniz}$ in Water for Processes of the Type $(R)_nH_{4-n}N^+ \rightleftharpoons R_nH_{3-n}N + H^+$, Where n Varies between 1 and 3 and R = Methyl or Ethyl

Base	$\bar{V}^0_B$, ml mole^{-1}	$\bar{V}^0_{BH^+Cl^-}$,[a] ml mole^{-1}	$\bar{V}^0_{BH^+}$, ml (g-ion^{-1})	$\Delta\bar{V}^0_{ioniz}$, ml mole^{-1}
CH_3NH_2	40.0	53.8	30.2	$+4.1 \pm 0.4$
$(CH_3)_2NH$	58.6	72.5	48.9	$+4.0 \pm 0.4$
$(CH_3)_3N$	77.9	90.6	67.0	$+5.2 \pm 0.4$
$(C_2H_5)_3N$	119.7	138.6	115.0	-1.0 ± 0.4

[a] From Table I.

It is difficult to draw any final conclusions from the results for $\Delta\bar{V}^0_{ioniz}$ for the methylamine series; the values are surprisingly independent of coordination of the N^+ center by Me groups and the consequent blocking of the hydration.[20]

The $\Delta\bar{V}^0_{ioniz}$ for the salts studied in this work are shown[15] in Figure 10 as a function of $\Delta S°$, the entropy of ionization.[21] It can be seen that whereas the $\Delta\bar{V}^0_{ioniz}$ increases by only about 1 ml mole^{-1} through the homologous series of methylammonium ions, $\Delta S°$ decreases by -10.6 eu, progressively. The slight change in $\Delta\bar{V}^0_{ioniz}$ as opposed to the appreciable change in $\Delta S°$ for ionization suggests that the entropy changes are perhaps more related to the interaction of the hydrophobic tails of the charged and uncharged molecules with the polar associated aqueous medium than to the normally predominant electrostrictive effects[3] arising from ion–dipole interaction.[22]

The role of such interactions is further indicated by the ΔC_p values, which are large and positive,[23] decreasing in the order $(CH_3)_3NH^+ > (CH_3)_2NH_2^+ > (CH_3)NH_3^+$. It is obvious that the normal electrostatic picture is inadequate to account for the ion–solvent interaction in these particular cases, especially in view of the tendency for $\Delta S°$ and ΔC_p to vary in opposite directions.[3,23] Structural effects seem to be of principal importance.[2b,24] In the present cases, the solvent molecules may see the asymmetric solute cation as an apparently bifunctional molecule; thus, on one hand, the hydrophobic "tails" (Me groups) on the ionic center may tend to increase solvent order through "freezing" of the normal water structure, *i.e.*, through an increase of type 1 water (part I); on the other hand, the N^+–H part of the molecule ion will tend to decrease the order or at best fit into the

(20) S. D. Hamann and A. G. Evans, *Trans. Faraday Soc.*, **47**, 34 (1951).

(21) R. P. Bell, "The Proton in Chemistry," Cornell University Press, Ithaca, N. Y., 1959, p 64.

(22) D. D. Eley and M. G. Evans, *Trans. Faraday Soc.*, **34**, 1093 (1938).

(23) D. H. Everett and W. F. K. Wynne-Jones, *Proc. Roy. Soc.* (London), **A177**, 499 (1941).

(24) H. S. Frank and M. W. Evans, *J. Chem. Phys.*, **13**, 507 (1945).

water structure without too much solvent structural disorganization. As a consequence of increased alkyl substitution, an incompatibility would tend to arise between the existence of two rather differing solvent-ordered regions in the solvent volume immediately adjacent to the cation (*cf.* the types of water referred to in part I). These observations indicate that it may be dangerous to make purely electrostatic interpretations of the hydration behavior of organic ions and hence of steric and substituent effects in the ionization properties of organic acids or bases.

(*b*) *Compressibility Relations.* From eq 2 it is evident that if $\phi^0_{K(s)}$ values are known for an $R_nH_{4-n}H^+X^-$ salt together with $\phi^0_{K(s)}$ for $R_nH_{3-n}N$ ($n \geq 3$) and the completely dissociated acid HX, the $\Delta\phi^0_{K(s)}$ for the ionization reaction can be calculated without any thermodynamic ambiguities (*cf.* eq 3a). Using the data for aqueous HCl for $\phi^0_{K(s)}$ [$= -8.3 \times 10^{-4}$ cc (mole bar)$^{-1}$], the $\Delta\phi^0_{K(s),ioniz}$ may be evaluated (as shown in Table VI) from an equation analogous to 3a but expressed in terms of the function $\phi^0_{K(s)}$. The resulting $\Delta\phi^0_{K(s),ioniz}$ values are all appreciable in magnitude and positive largely owing to the substantial negative values of $\phi^0_{K(s)}$ for the aminium salts which all have much more negative values of this function than that for aqueous H^+Cl^-. [Here it may be noted that the related quantity ϕ^0_K is defined as $-d\phi^0_V/dP$, *i.e.*, with the negative sign included in the defining equation (*cf.* that for β).] This is again a somewhat surprising result, reflecting presumably a stronger structure-promoting effect of the alkyl groups in the aminium cation in relation to that caused by the H_3O^+ ion. Addition of the third methyl group in the tertiary base evidently has the largest specific effect.

Table VI: $\Delta\phi^0_{K(s),ioniz}$ in cc (mole bar)$^{-1}$ for the Acid Ionization of Primary, Secondary, and Tertiary Methylaminium Chlorides at 25° (Compare Tables V for Corresponding $\Delta\bar{V}^0_{ioniz}$ Values)

Base B	$\phi^0_{K(s)}$ B $\times 10^4$	$\phi^0_{K(s)}$ BH^+Cl^- $\times 10^4$	$\Delta\phi^0_{K(s),ioniz}$ $\times 10^4$
CH_3NH_2	4 ± 1.5[a]	−22.0	17.7
$(CH_3)_2NH$	7.5 ± 1.5	−20.2	19.4
$(CH_3)_3N$	2.0 ± 1	−18.1	11.8

[a] Based on estimates of the extrapolated quantity $\phi^0_{K(s)}$ for the neutral bases from Figure 4, part I. These extrapolated quantities are rather less certain than those for the corresponding salts.

Acknowledgments. Grateful acknowledgment is made to the National Research Council, Canada, for support of this work. R. E. V. acknowledges the award of Province of Ontario Graduate Scholarships in 1964–1965.

Effects of Third Components on Critical Mixing in the Water–Triethylamine System

by Brian J. Hales, Gary L. Bertrand, and Loren G. Hepler

Carnegie Institute of Technology, Pittsburgh, Pennsylvania *(Received July 11, 1966)*

The phase diagram for the water–triethylamine liquid system has been redetermined for mole fractions of triethylamine ranging from 0.02 to 0.40, with results in general agreement with previous investigators. We have further determined the effects of small quantities of a variety of third components on the temperature of phase separation in this system. Timmermans' generalization that third components which are appreciably soluble in only water or triethylamine will lower the temperature of phase separation is supported by all of our relevant data. His other generalization that third components that are quite soluble in both water and triethylamine will raise the temperature of phase separation is supported by only some of our relevant data. We have found some alcohols (quite soluble in both water and triethylamine) that raise the temperature of phase separation for some water–triethylamine compositions, lower it for other compositions, and necessarily have no effect on the temperatures of phase separation at some intermediate composition.

Phase equilibrium investigations on two-component systems have been of considerable practical and theoretical importance for many years. Similar investigations on polycomponent systems have also been important and far from uncommon. Although the majority of the earlier investigations have been concerned with solid–liquid or liquid–gas equilibria, a variety of liquid–liquid systems have also been investigated. Measurements of the effects of salts on solubilities of nonelectrolytes as expressed by salting-out (or in) coefficients are most like our investigations of the effects of solutes (both electrolytes and nonelectrolytes) on mutual solubility in the water–triethylamine liquid–liquid system. There have been a few earlier investigations[1,2] of the effects of salts on the water–triethylamine system as well as thermodynamic description[3] of the effects of solutes on liquid–liquid miscibility.

The water–triethylamine system has long been known to have a lower critical solution temperature (LCST) at 18–19° at about 0.08 mole fraction of triethylamine. At lower temperatures the liquids are completely miscible, while at higher temperatures they separate into two liquid phases. This investigation has been concerned with systematic determinations of changes in the temperature of phase separation caused by the addition of small quantities of various solutes to water–triethylamine mixtures.

Experimental Section

Triethylamine was purified by vacuum distillation over KOH pellets not more than 48 hr before use. The material was stored in well-stoppered bottles. Since our experiments have been confined to the mixtures with mole fraction of triethylamine between 0.02 and 0.40, small quantities of water as an impurity in the triethylamine contribute negligible errors to the results. Other compounds that we used were purified by traditional methods. In all experiments the distilled water was freshly boiled to expel CO_2 and care was taken during the experiments to minimize absorption of CO_2 from the atmosphere.

For equilibrium determinations we used a 50-ml Pyrex beaker to the top of which was sealed a 15-cm tube of 25-mm diameter. Considerable care was taken

(1) J. Timmermans, *Z. Physik. Chem.*, **58**, 129 (1907).

(2) R. J. Kline and A. J. Ihde, *J. Colloid Sci.*, **13**, 163 (1958).

(3) I. Prigogine and R. Defay, "Chemical Thermodynamics," translated by D. H. Everett, John Wiley and Sons, Inc., New York, N. Y., 1954.

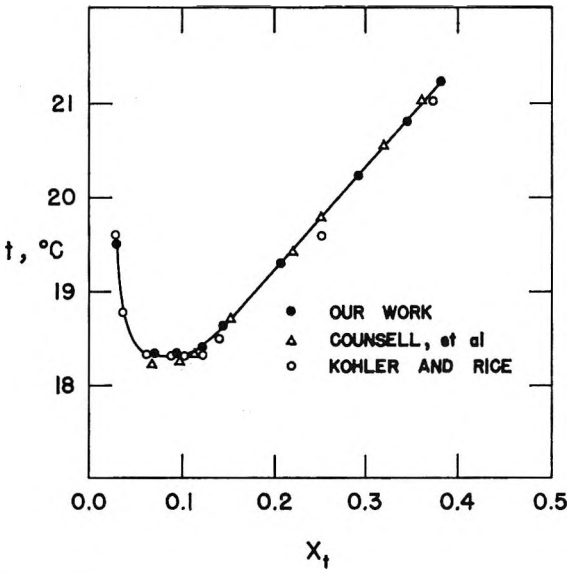

Figure 1. Phase diagram for the water–triethylamine system.

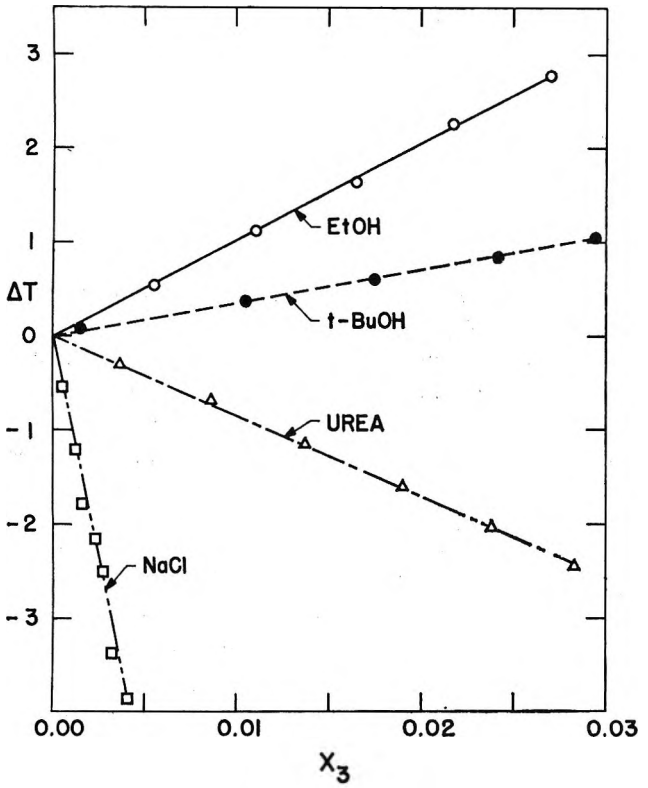

Figure 2. Effects of some third components on the temperature of phase separation in the water–triethylamine system.

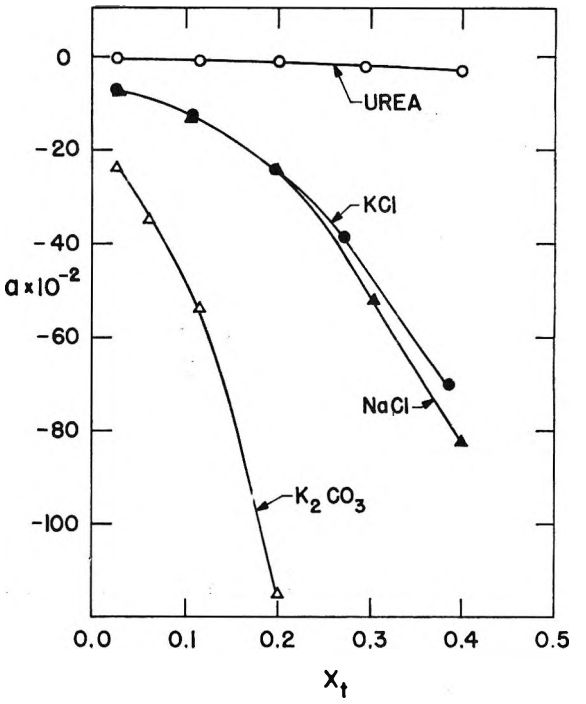

Figure 3. Initial effects of water-soluble third components on the temperature of phase separation in the water–triethylamine system.

to see that this equipment was clean for all experiments. This vessel was submerged in a 3-l. beaker containing water whose temperature could be changed slowly by heating or cooling. The water in the outer bath and the mixture of interest in the equilibrium vessel were both stirred magnetically. The stirrer bar in the equilibrium vessel was coated with Teflon. Temperatures could be read with an accuracy of about ±0.02° with a calibrated mercury-in-glass thermometer that registered temperatures from −1 to +51° over a length of 36 cm. The thermometer was introduced to the equilibrium vessel through a tightly fitting cork.

The experimental procedure began with preparation of a water–triethylamine mixture of the desired composition. The temperature of phase separation of this mixture was determined visually with the temperature both increasing and decreasing at rates of about 0.2–0.3°/min. The worst disagreement in these duplicate temperature determinations was 0.1°, which usually occurred in the extreme water-rich and triethylamine-rich regions. The usual difference in four determinations was less than 0.05°. After the determination of this equilibrium temperature for the two-component system, a measured small amount of third component was added and the phase separation temperature was redetermined on both heating and cooling. Increments of third components ranging from 0.003 to 1.5 g of solid or from 0.01 to 1.0 ml of liquid were added to known amounts (~65 ml) of water–triethylamine mixtures. This procedure was then repeated

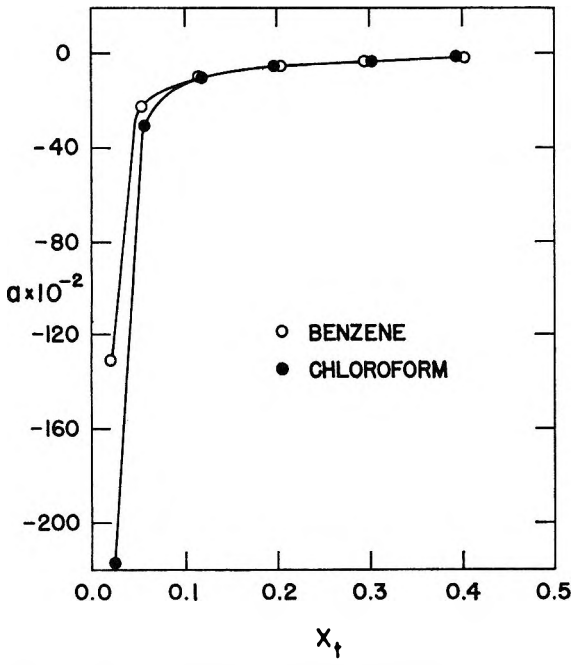

Figure 4. Initial effects of triethylamine-soluble third components on the temperature of phase separation in the water–triethylamine system.

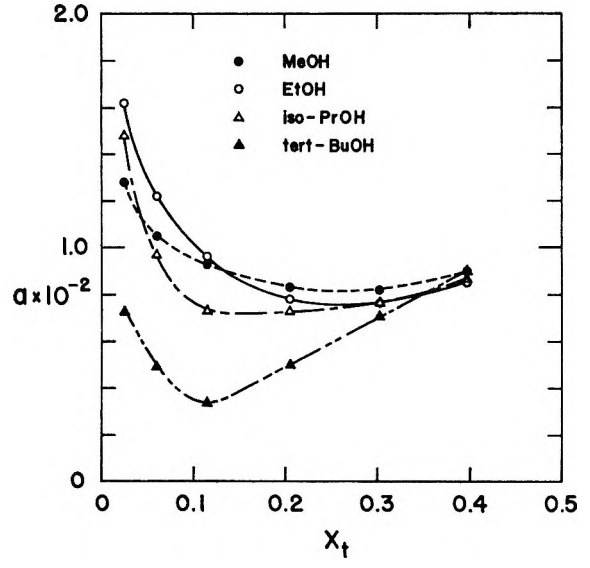

Figure 5. Initial effects of alcohols that raise the temperature of phase separation in the water–triethylamine system.

up to a maximum of 12 additions of the third component, although five or six additions were more usual.

Results

Our results for the water–triethylamine system are summarized in Figure 1 along with the results of two other recent investigations of this system.[4,5]

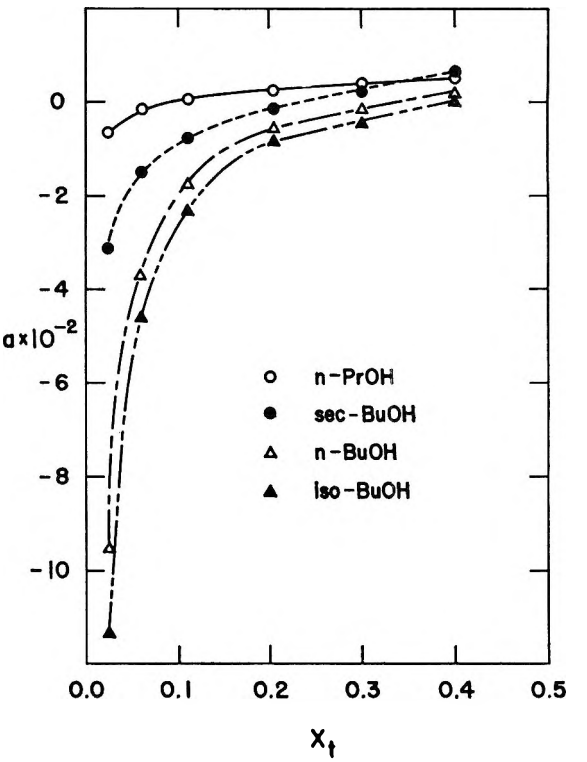

Figure 6. Initial effects of alcohols that lower the temperature of phase separation for water–triethylamine mixtures with small X_t, raise the temperature of phase separation for mixtures with larger X_t, and necessarily have no effect at some intermediate composition.

The curve is the so-called mutual solubility curve for the system—the area above the line represents the system existing in two liquid phases while the area below it represents the system as one liquid phase. In this figure and later in this paper we use X_t for mole fraction of triethylamine in the initial water–triethylamine system and X_3 for mole fraction of the third component.

Qualitative effects of third components on mutual solubilities of liquids have long been known. It has been pointed out[1] that a third component which is very soluble in both water and triethylamine will increase their mutual solubility when added to the system. This increase in miscibility corresponds to raising the mutual solubility curve in Figure 1. On the other hand, a third component which is very soluble in either water or triethylamine but very slightly soluble in the other liquid will decrease the mutual solubility and lower the curve shown in Figure 1.

Some of our results for various third components in

(4) F. Kohler and O. K. Rice, *J. Chem. Phys.*, **26**, 1614 (1957).

(5) J. F. Counsell, D. H. Everett, and R. J. Munn, *Pure Appl. Chem.*, **2**, 335 (1961).

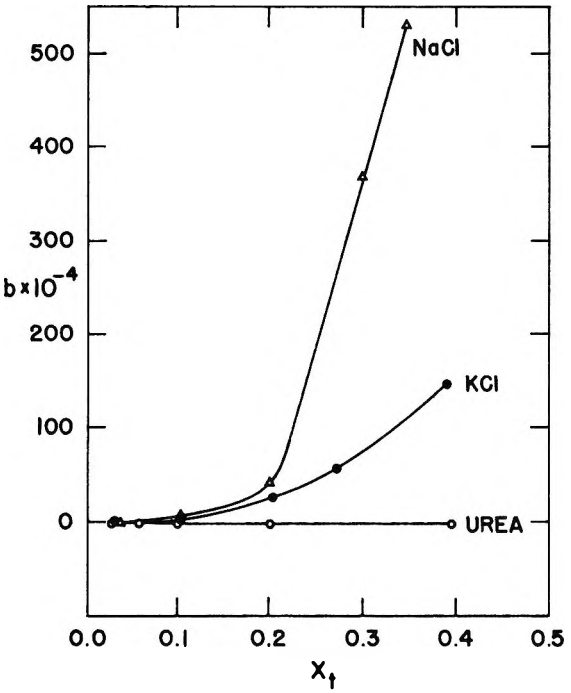

Figure 7. Deviations from linearity (eq 1) for water-soluble third components.

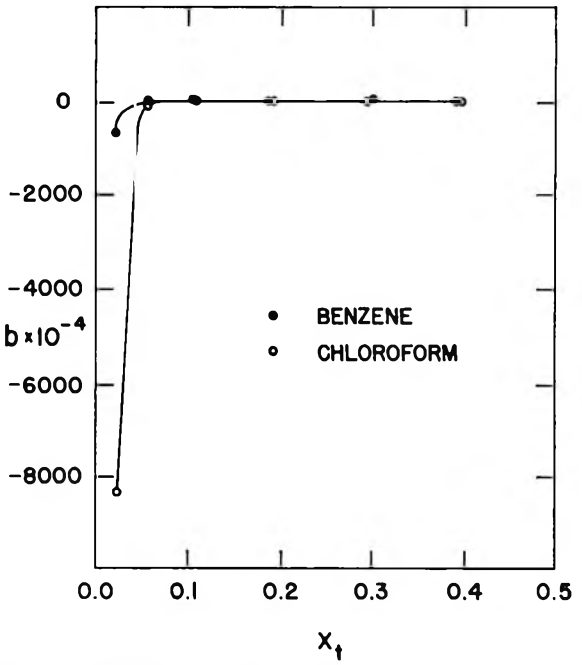

Figure 8. Deviations from linearity (eq 1) for triethylamine-soluble third components.

water–triethylamine systems with $X_t \cong 0.114$ (composition close to that of the LCST) are shown in Figure 2. These results support the generalization[1] that third components that are quite soluble in both water and triethylamine (ethyl and *t*-butyl alcohols) increase the mutual solubility (ΔT positive for change in temperature of phase separation) while third components that are appreciably soluble in only one of the "solvent" pair (urea and sodium chloride) decrease the mutual solubility (ΔT negative).

Since all the plots of ΔT *vs.* X_3 are nearly linear, we have represented the results by the equation

$$\Delta T = aX_3 + bX_3^2 \quad (1)$$

This equation may be rearranged to

$$\Delta T/X_3 = a + bX_3 \quad (2)$$

from which we see that the intercept and slope of a plot of $\Delta T/X_3$ *vs.* X_3 lead to values of the coefficients a and b. Values of the limiting slope a determined in this way are of particular relevance, since application[3] of regular solution theory has related this slope to parameters reflecting the properties of the various components, and it might be expected that similar methods could be applied to nonregular solutions.

Our a values for urea, KCl, NaCl, and K_2CO_3 are shown in Figure 3. In calculating X_3 values we have not made any allowance for possible dissociation of solutes. Each of these solutes is quite soluble in water and almost insoluble in triethylamine. Correspondingly, the a values are negative, signifying lowering the temperature of phase separation and the mutual solubility curve.

Our a values for benzene and chloroform are shown in Figure 4. Both of these solutes are completely miscible with triethylamine but only slightly soluble in water. The negative a values indicate the expected lowering of both the temperature of phase separation and the mutual solubility curve.

The absolute magnitude of the a values (all plotted as $a \times 10^{-2}$) is largest when the solvent mixture contains relatively little of the component in which the solute is quite soluble. That is, the effect of water-soluble solutes on the temperature of phase separation is greatest in water–triethylamine mixtures with relatively large X_t (Figure 3) and, conversely, the effect of triethylamine-soluble solutes is greatest in water–triethylamine mixtures with small X_t (Figure 4).

Methyl, ethyl, isopropyl, and *t*-butyl alcohols are all infinitely soluble in both water and triethylamine. In accord with Timmermans'[1] generalization, each of these solutes raises the temperature of phase separation and increases the mutual solubility of water and triethylamine as indicated by the positive a values shown in Figure 5. It should be noted that absolute magnitudes of these a values are small compared to those for solutes that are appreciably soluble in only one component of the solvent pair.

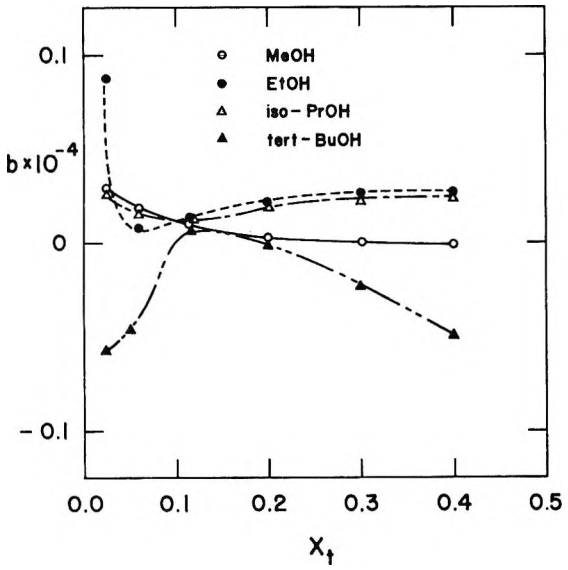

Figure 9. Deviations from linearity (eq 1) for alcohols which raise the temperature of phase separation (Figure 5).

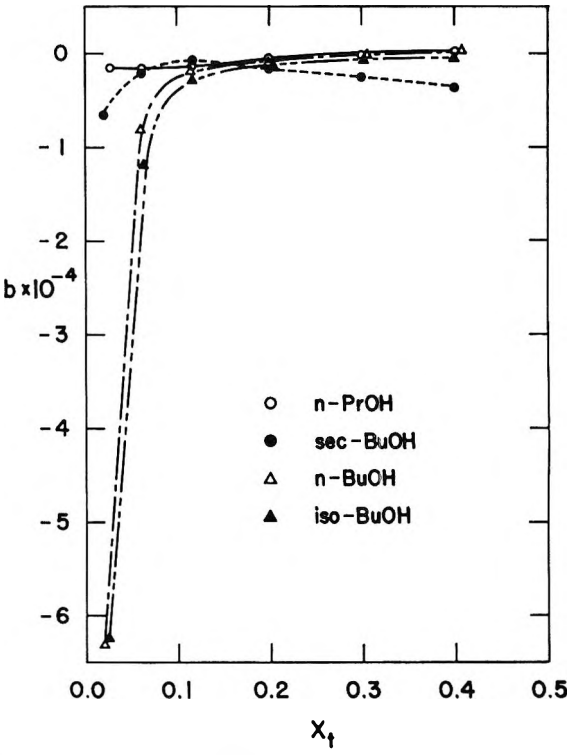

Figure 10. Deviations from linearity (eq 1) for alcohols which cross $a = 0$ line (Figure 6).

Since a values for all solutes so far mentioned depend at least slightly on solvent composition, it is possible that some solutes might have a values that cross the $a = 0$ line at some solvent composition. The results shown in Figure 5 suggest that higher alcohols might behave in this way, which corresponds to raising the temperature of phase separation for some solutions while lowering it for others. We have found four such solutes: *n*-propyl, isobutyl, *sec*-butyl, and *n*-butyl alcohols, for which a values are shown in Figure 6. In the water-rich region, each of these solutes lowers the temperature of phase separation and decreases mutual solubility of water and triethylamine. In mixtures containing more triethylamine, these solutes raise the temperature of phase separation and increase the mutual solubility of water and triethylamine.

Values of b for the various solutes in various water–triethylamine mixtures are shown in Figures 7–10.

Discussion

The most common way of presenting phase equilibrium data for three-component systems is by way of triangular phase diagrams. If our data for solutions (third components always present in small concentrations) were presented in this way, our results would take the form of short lines extending inward from the water–triethylamine side of the triangle. Our results for the water–triethylamine–propyl alcohol system are of particular interest in connection with the triangular diagram method of presenting phase equilibrium data. Each of these substances is completely miscible with each of the others in the temperature range of interest below the LCST for water–triethylamine. The a values for *n*-propyl alcohol shown in Figure 6 thus show that the triangular phase diagram for the water–triethylamine–propyl alcohol system must exhibit island curves[6] at temperatures below the LCST for water–triethylamine.

Detailed consideration of our results in terms of molecular properties or in terms of thermodynamic properties of binary mixtures would surely be interesting and useful. Lack of many of the relevant thermodynamic data for the binary systems and our inadequate knowledge of complicated molecular interactions combine to prevent such detailed interpretations at present. The results reported here are sufficient, however, to warrant drawing some conclusions.

Timmermans'[1] generalization that third components that are quite soluble in only water or triethylamine will lower the temperature of phase separation is supported by all of our relevant data. His further generalization that third components that are quite soluble in both water and triethylamine will raise the temperature of phase separation is supported by some of our results (Figure 5), but contradicted by some of our other re-

(6) A. W. Francis, "Liquid–Liquid Equilibriums," John Wiley and Sons, Inc., New York, N. Y., 1963.

sults (Figure 6). These contradictions are of special interest, partly because they include cases where addition of a third component has no effect on the temperature of phase separation.

Acknowledgments. We are grateful to the National Science Foundation for support of this research and to Mr. Robert Goldberg for his help with some of the measurements.

Nuclear Magnetic Resonance Dilution Shifts for Carboxylic Acids in Rigorously Dried Solvents. II. Benzoic Acid in Benzene

by Norbert Muller and O. Richard Hughes

Department of Chemistry, Purdue University, Lafayette, Indiana 47907 *(Received July 11, 1966)*

Proton magnetic resonance measurements are presented for solutions of benzoic acid in benzene prepared with special precautions to minimize contamination with water. Dilution shift curves for the carboxyl proton were obtained for several temperatures in the range 30 to 90° and analyzed assuming that the acid is an equilibrating mixture of monomeric and dimeric species and taking literature values for the enthalpy and free energy of dimerization. The previously reported, anomalously high value for the chemical shift for the monomeric species (δ_M) was not confirmed and is believed to be an effect of residual moisture. Instead, $\delta_M = 1.0 \pm 0.4$ ppm from benzene (solvent and internal reference) and for the dimeric acid, $\delta_D = -6.77 \pm 0.04$ ppm at 30°. Instead of the large displacement of δ_M to lower field with increasing temperature reported earlier for this and similar systems, a small shift in the opposite direction was observed. δ_D has a positive temperature coefficient similar in magnitude to values reported previously.

Introduction

The first paper of this series[1] is a report on nuclear magnetic resonance (nmr) studies on acetic acid in several basic solvents, showing that when traces of water are carefully excluded, the observed dilution shifts may be interpreted using a plausible set of spectroscopic and thermochemical parameters. We have now reinvestigated the dilution shifts of solutions of benzoic acid in benzene,[2,3] a typical carboxylic acid–inert solvent system.[4] Again we find that when great care is used in drying the materials, the results differ substantially from those reported earlier, and several anomalies encountered in the earlier work are now eliminated.

At first glance it would seem that adequate drying of an inert solvent should present little difficulty. Thus "purified" acetone may contain perhaps 0.2% water by weight, whereas benzene saturated with water at room temperature takes up only about one-third of this amount. However, the nature of the data obtained with inert solvents forces one to use a

(1) N. Muller and P. I. Rose, *J. Phys. Chem.*, 69, 2564 (1965). The Introduction to this paper contains the erroneous statement that dilute solutions of water in acetone have the OH signal at −2.3 ppm from tetramethylsilane; the value should be −2.8 ppm.

(2) J. C. Davis, Jr., and K. S. Pitzer, *ibid.*, 64, 886 (1960).

(3) P. I. Rose, Ph.D. Thesis, Purdue University, 1965.

(4) For brevity, we follow the tradition of using the word "inert" to refer to such solvents as benzene and carbon tetrachloride, which are at least an order of magnitude less basic than the common σ-electron donors, though much evidence exists which shows that these solvents are not absolutely inert.

method of analysis involving an algebraic extrapolation to infinite dilution, which magnifies the error due to a very small trace of water to an astonishing extent. This is illustrated by the following simplified calculation for a hypothetical system with parameters similar to those we eventually found for benzoic acid–benzene.

Chemical shifts are assigned the temperature-independent values, $\delta_M = 60$ Hz for the monomer, $\delta_D = -360$ Hz for the dimer, and $\delta_W = 380$ Hz for water. Using x_i to represent the mole fraction of the ith species, select an acid concentration so that $x_M = 1.0 \times 10^{-3}$ and $x_D = 5.25 \times 10^{-3}$ at 30°, corresponding to a dimerization constant $K_2 = x_D/x_M^2 = 5.25 \times 10^3$. The exchange-averaged chemical shift in the absence of water will be

$$\delta = (x_M\delta_M + 2x_D\delta_D)/(x_M + 2x_D) \quad (1)$$
$$= -323.5 \text{ Hz}$$

Now suppose that the solvent is benzene containing 0.005% water by weight so that $x_W = 0.213 \times 10^{-3}$. Since the water protons exchange with the carboxyl protons, the average hydroxyl-proton shift becomes

$$\delta' = (x_M\delta_M + 2x_D\delta_D + 2x_W\delta_W)/(x_M + 2x_D + 2x_W) \quad (2)$$
$$= -298 \text{ Hz}$$

Suppose that δ_D has been already evaluated from the spectrum of a concentrated solution and δ_M is to be found using (1) rearranged to give

$$\delta_M = \delta + (2x_D/x_M)(\delta - \delta_D) \quad (3)$$

If the presence of water is unsuspected and δ' is used in place of δ in eq 3, the result will be a spurious monomer shift, δ'_M, with

$$\delta'_M - \delta_M = \delta' - \delta + (2x_D/x_M)(\delta' - \delta) \quad (4)$$

Although $\delta' - \delta$ is only about 25 Hz, the error $\delta'_M - \delta_M$ is almost 300 Hz, because the factor $2x_D/x_M$ is 10.5 at 30°. Moreover, at a temperature near 80° where $K_2 = 720$ (corresponding to an enthalpy of dimerization of −8.4 kcal/mole), this factor becomes 3.6 and therefore δ'_M is reduced by nearly 200 Hz even though the true δ_M is temperature-independent by definition.

The actual workup of experimental data is more complex than this model calculation, since it involves combining data from a series of samples of different acid concentrations, but the effect of unsuspected water contamination is essentially the same. The apparent monomer shift is much larger than the true value at room temperature, and it appears to have a very large, negative temperature coefficient. This is precisely the sort of behavior found in previous studies of carboxylic acids in inert solvents.[2,5]

Preliminary work on this problem in this laboratory[3] involved attempts to prepare adequately dried samples of acetic acid and benzoic acid in benzene. Because of the rather low vapor pressure of benzoic acid, the benzoic acid samples were made in a drybox, while the acetic acid samples were prepared on the vacuum line. Analysis of the nmr dilution shifts indicated that the benzoic acid solutions, although more nearly anhydrous than those used in earlier work, still contained too much residual moisture to be acceptable. The acetic acid samples seemed to be much drier, but in this case interpretation of the data involved some uncertainties because the enthalpy and free energy of dimerization for acetic acid in benzene are not reliably known. Since our experience with acetic acid in basic solvents[1] also indicated that high-vacuum procedures are greatly superior to drybox procedures, we decided to reinvestigate the benzoic acid–benzene system using samples prepared on the vacuum line. The results are reported below.

Experimental Procedures and Results[6]

Baker's Analyzed reagent spectrophotometric grade thiophene-free benzene was refluxed over powdered lithium aluminum hydride for 18 hr and then fractionally distilled through a 6-in. glass helix-packed column. The middle fraction (bp 79.3° (746 mm)) was collected and stored on the vacuum line either over powdered $LiAlH_4$ or over P_2O_5.

About 30 g of Baker's Analyzed reagent benzoic acid was melted into a 40 × 1 cm glass tube which was then sealed under reduced pressure and placed in a Fisher zone refiner. The material was refined for 48 hr using two heating elements which made about 30 passes. The column was cut apart in a drybox and the material from the middle section was powdered and stored in a closed vial.

The nmr samples were prepared by two procedures, each involving use of a grease-free vacuum manifold onto which were sealed several precision nmr tubes. When the manifold and tubes had been evacuated and thoroughly flamed out, the apparatus was brought to atmospheric pressure by means of dry air. For the first procedure, the next step was to introduce an aluminum foil boat containing the benzoic acid. Again the air was pumped out and the glass was flamed except for the section immediately adjacent to the

(5) T. C. Chiang and R. M. Hammaker, *J. Mol. Spectry.*, 18, 110 (1965).

(6) For additional details, see O. R. Hughes, Ph.D. Thesis, Purdue University, 1966.

aluminum boat. The acid was then sublimed into the nmr tubes with the help of infrared heat lamps, the quantity transferred into each tube being roughly estimated visually. Then a previously provided glass breakoff seal was broken so as to connect the manifold with the storage bulb containing the solvent. Benzene was distilled in turn into each sample tube and cooled to liquid nitrogen temperature so that the tube could be sealed off.

The second procedure differed from the first only in that the time-consuming sublimation step was bypassed. A homemade long-handled spoon was used to drop an appropriate amount of the solid acid directly into each of several nmr tubes sealed onto a manifold and previously flamed out as above. The manifold was then pumped out and flamed, and the solvent was introduced as before. It was found later that data points representing samples made by either procedure fell on the same smooth dilution-shift curve.

To determine the concentrations of the solutions prepared as described it was necessary after completion of all spectroscopic work to analyze each sample. Each tube was weighed before and after removing its contents to determine the total amount of solution. The solution was poured into a beaker, and the sample tube was rinsed with benzene to assure complete transfer of the benzoic acid. After evaporating the benzene, the acid was dissolved in 10 ml of a neutralized water–ethanol mixture (50% by volume) and titrated with standardized aqueous sodium hydroxide under a nitrogen atmosphere.[7]

The nmr determinations were made with a Varian V-4311 spectrometer modified with a VK-3529 high-sensitivity kit, except that a dewar probe insert was used for all measurements in place of the high-sensitivity insert. The variable temperature accessory was also obtained from Varian Associates. For each sample the position of the hydroxyl proton resonance was determined at a spectrometer frequency of 56.445 MHz by means of side bands generated with an audiooscillator–frequency counter combination. The solvent peak provided the internal reference signal. The average of not less than five spectra, with mean deviations generally between 0.2 and 0.3 Hz, was used for each data point.

Temperature measurements were made with a copper–constantan thermocouple junction placed in the stream of hot air used to warm the samples. To evaluate the accuracy of these determinations, the apparatus was adjusted as though a spectrum were to be recorded and the sample was replaced by an unsealed "dummy" sample of ethylene glycol which had a second thermocouple junction immersed in the liquid. This made it possible to measure separately an "internal" and an "external" temperature, and also to determine by moving the internal junction whether there was a significant tendency for temperature gradients to occur within the tube. These experiments indicated that the error entailed by assuming that the internal and external temperatures are identical is smaller than the temperature fluctuations caused by variations in the rate of flow of the warm air stream. The total uncertainty of the temperature measurements was estimated to be within $\pm 1°$.

The results of chemical shift determinations as a function of temperature for each of eight samples, and the respective concentrations, are given in Table I. Each of these samples was made with benzene that had been dried over P_2O_5, and produced a sharp hydroxyl peak. Another set of samples, made with benzene dried over $LiAlH_4$, gave somewhat broadened peaks with chemical shift values lying 1 or 2 Hz to higher field than values obtained by interpolation from the data in Table I.

Table I: Carboxyl Proton Chemical Shifts for Solutions of Benzoic Acid in Benzene at Various Concentrations and Temperatures

x_a^0	T, °C	δ^a	x_a^0	T, °C	δ^a
0.0058	30.0	−328.5	0.0183	31.1	−350.2
	52.8	−287.4		52.8	−322.4
	69.2	−253.3		67.4	−297.6
	86.2	−211.7		85.0	−269.0
	95.7	−189.9		94.8	−250.5
0.0107	30.0	−341.3	0.0288	30.9	−355.5
	47.3	−316.6		50.2	−333.6
	57.0	−300.2		64.3	−314.9
	85.0	−244.0		85.2	−283.9
	95.3	−222.9		94.1	−270.8
	95.8	−223.0			
0.0159	30 5	−348.6	0.0443	30.8	−359.8
	52 2	−318.4		50.2	−340.0
	67 4	−293.3		64.4	−323.5
	84.1	−263.7		85.0	−297.5
	92.0	−249.9		94.2	−285.3
0.0178	31.2	−350.1	0.04935	30.8	−362.1
	52.4	−323.3		50.2	−341.8
	67.4	−298.1		65.9	−324.5
	85.7	−267.1		85.8	−298.2
	92.8	−253.9		95.1	−286.1

[a] Shifts are in Hz at 56.4 MHz and are to low field from benzene (internal reference).

(7) J. Grant, "Pregl's Quantitative Organic Microanalysis," J. and A. Churchill, Ltd., London, 1951, p 163.

Since benzene was used as the reference compound throughout, we determined the effects of temperature changes and of dissolved benzoic acid on the chemical shift difference between benzene and a trace of dissolved tetramethylsilane (TMS). For a sample of thiophene-free benzene with 1% TMS, the benzene peak is at −404 Hz from TMS at 56.4 MHz (or −7.17 ppm) at 30°, and this value changes by less than 1 Hz if benzoic acid is added or the sample is heated to 90°. If the benzene is saturated with water, the water peak is 6.68 ppm upfield from the benzene signal, or 0.48 ppm downfield from TMS.

Analysis of the Data

As a first step toward the quantitative interpretation of the data, we plotted the hydroxyl chemical shift for each sample against the temperature and obtained by interpolation shift values at 10° intervals over the range 30 to 90°. We could then plot the isothermal variation of shift with concentration at each temperature, as shown in Figure 1. From these dilution curves we calculated δ_M and δ_D at each temperature using a procedure modeled on that used by Davis and Pitzer,[2,8] whose notation also is adopted here wherever applicable.

Equation 1 may be rewritten in terms of f, the fraction of the benzoic acid which is in the dimeric form, giving

$$\delta = (1 - f)\delta_M + f\delta_D = \delta_M + f(\delta_D - \delta_M) \quad (5)$$

Moreover, if the solution contains a formula weights of acid in s moles of solvent and we define $x_a^0 = a/(a + s)$, it is readily shown that

$$f = \frac{4x_a^0K_2 + 1 - [4x_a^0K_2(2 - x_a^0) + 1]^{1/2}}{x_a^0(4K_2 + 1)} \quad (6)$$

Thus if K_2 may be assumed known from other sources, f and $(1 - f)$ can be evaluated numerically for each sample and used with the experimental value of δ to obtain a linear equation with δ_M and δ_D as the unknowns. Since there are more than two samples, the number of such equations is more than sufficient, and we elected to evaluate δ_M and δ_D by least squares, that is, by minimizing the sum of the squares of the residuals, R_i, defined for the ith sample as

$$R_i = \delta_i(\text{exptl}) - [\delta_M + f_i(\delta_D - \delta_M)] \quad (7)$$

Following Davis and Pitzer,[2] who reviewed the available data, we took $K_2 = 5.25 \times 10^3$ at 30° and for the heat of dimerization, the value $\Delta H = -8.4$ kcal/mole. Calculated values of K_2 at the other temperatures are given in Table II together with the best value of δ_M and δ_D at each temperature and the respective standard deviations. We used these values with eq 5 and 6 to calculate δ as a function of concentration at each temperature, the results being displayed as the solid curves in Figure 1.

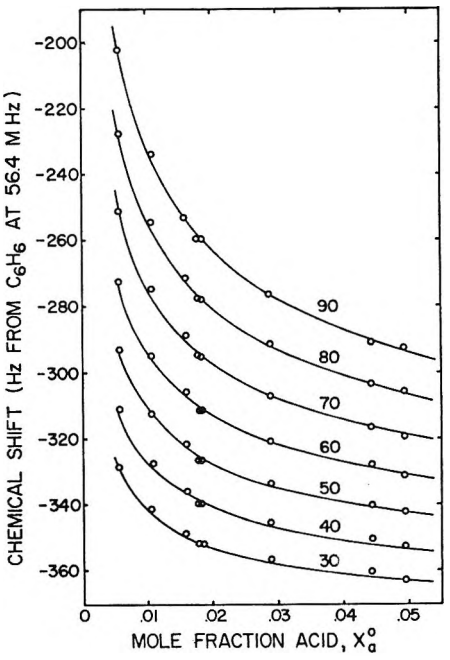

Figure 1. Hydroxyl proton chemical shift for benzoic acid in benzene as a function of concentration, at several temperatures. The solid curves were calculated using the least-squares values of δ_M and δ_D.

Neither δ_M nor δ_D is temperature independent. The dimer shift has a small, positive, approximately constant temperature coefficient, $\Delta\delta_D/\Delta T = 0.91 \times 10^{-2}$

Table II: Dimerization Constants and Calculated Chemical Shifts for Benzoic Acid in Benzene at Various Temperatures, Assuming $\Delta H = -8.4$ Kcal/Mole

T, °C	K_2, mf^{-1}	δ_M[a]	δ_D[a]
30	5250	55.7 ± 10.6	−381.5 ± 0.9
40	3364	59.3 ± 12.5	−376.4 ± 1.3
50	2219	59.1 ± 9.1	−370.2 ± 1.1
60	1499	64.4 ± 7.6	−364.3 ± 1.1
70	1036	77.3 ± 5.4	−359.4 ± 1.0
80	732	88.4 ± 5.2	−354.7 ± 1.2
90	527	99.3 ± 3.7	−350.6 ± 1.0

[a] Shifts are in Hz at 56.4 MHz from benzene, with the positive sign denoting a shift to higher field, and are given together with the standard deviation obtained from the least-squares procedure.

(8) See also C. Lussan, *J. Chim. Phys.*, **60**, 1100 (1963).

ppm/deg. The monomer shift also appears to *increase* as the temperature is raised, but not at a uniform rate, the total change being 0.77 ppm over the 60° temperature range.

Discussion

Effects of Residual Moisture. Figure 2 shows the dilution shift curve at 30° obtained in this study together with similar curves from references 2 and 3. It appears that when more and more stringent precautions are taken to avoid water contamination the curve obtained is progressively displaced to lower fields without any obvious change in its form. However, the above analysis shows that this movement downfield entails a large shift of the calculated δ_M and that the apparent temperature variation of δ_M is radically changed. This raises the question of whether still more rigorous drying would result in a continuation of these trends or whether indeed the present results represent the limit approached as the moisture content of the solutions is reduced toward zero.

We felt that it was not practicable to use conventional methods of trace water analysis because of the small total quantities involved and also because of the large probability that water would be picked up during the transfer of materials from the vacuum line to whatever analytical apparatus might be chosen. Therefore, our claim to have obtained true dilution curves must rest on several lines of indirect evidence.

Since each sample contains at least 95 mole % benzene, the dryness of the solvent is a much more critical factor than that of the solute. To estimate the effectiveness of P_2O_5 in drying inert solvents, one may use the fact that air in equilibrium with P_2O_5 at 25° contains less than 0.2 mg of water/l.[9] This corresponds to a partial pressure less than 2×10^{-5} torr. If Raoult's law holds approximately for very dilute solutions of water in benzene, this requires that a solution equilibrated with P_2O_5 must have $x_W < 1 \times 10^{-6}$. Thus if the residual moisture contained in the benzene is the only source of water in the samples, the difference between δ and δ' of eq 1 and 2 will be negligible.

It is difficult to set a limit on the amount of water that might be introduced with the benzoic acid or that might enter the solution by desorption from the surface of the sample tube. It is reassuring that the two methods described above for transferring the benzoic acid yielded samples with identical characteristics. Probably more significant is the fact that all the samples made with benzene dried over P_2O_5 yielded hydroxyl proton signals which were not detectably broadened. In work with donor solvents[1] it was found that at very low acid concentrations the effect of small traces of moisture is to broaden the signals without changing their position; additional moisture then causes them to shift upfield, and eventually, when the samples become quite wet, the signals again become sharp. Our observations (see above) with samples made with benzene dried over $LiAlH_4$ suggest that this drying agent is slightly less effective than P_2O_5, that for benzoic acid–benzene solutions there is again a range of values of x_W which leads to broadened signals, and that once x_W is below this range little if any additional shift occurs if x_W is still further reduced.

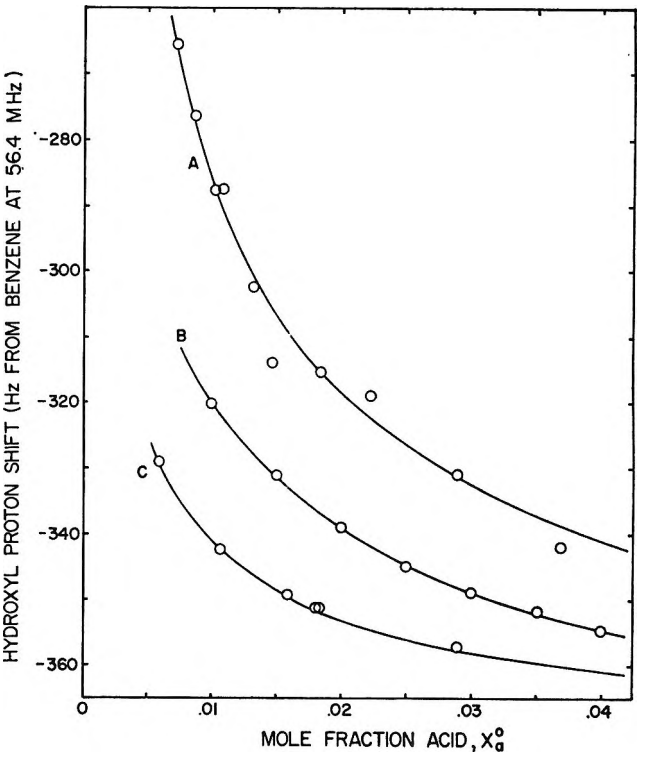

Figure 2. Comparison of dilution–shift curves at 30° obtained in three investigations of benzoic acid in benzene: A, ref 2; B, ref 3; C, this work.

Finally, it was shown in the Introduction that water contamination must lead to an apparent *downfield* shift of δ_M with rising temperature. This study produced the surprising observation that δ_M tends to shift to *higher* field as the temperature rises. If residual moisture were still making a negative contribution to the temperature coefficient of δ_M, one would be forced to the very unlikely conclusion that the true δ_M increases with rising temperature even faster than the data in Table II show.

The Monomer and Dimer Shifts and Their Variation

(9) I. M. Kolthoff and P. J. Elving, Ed., "Treatise on Analytical Chemistry," Vol. 1, Part II, Interscience Publishers, Inc., New York, N. Y., 1961, p 111.

with Temperature. Because of the relatively high degree of association of benzoic acid in the concentration range investigated, δ_D is much less subject to error from water contamination or other sources than δ_M, and indeed the δ_D values reported here are not very different from those given earlier. The value of δ_M at 30° is substantially lower than reported earlier, and the new value, as well as the new "hydrogen bond shift," $(\delta_M - \delta_D) \sim 7.8$ ppm, are much more nearly in line with data for alcohols,[10] amines,[11] and amides.[12] The actual value of δ_M of course depends directly on the choice of a value of K_2. We reanalyzed the 30° data using $K_2 = 5.00 \times 10^3$ and again using $K_2 = 5.50 \times 10^3$ and obtained δ_M values of 45.9 and 63.4 Hz, respectively. The value of δ_D is essentially unchanged in this range of K_2 values. Since it seems very probable that K_2 does indeed lie within this range[2,13] the total uncertainty in δ_M is probably no worse than ±20 Hz at 30°, while that in δ_D should be better than ±2 Hz.

The temperature coefficient of the dimer shift, $\Delta\delta_D/\Delta T$, lies between the two values reported earlier[2,3] for benzoic acid in benzene and very near the values found for neat decanoic acid[14] and for acetic acid in benzene.[2] It probably reflects a combination of two effects. First, the dimer concentration calculated from colligative properties is the sum of the concentrations of the cyclic and the acyclic dimer species. The concentration of acyclic or "open" dimers is probably small, but it will tend to increase as the temperature rises. Since the open dimer contains one free and one hydrogen-bonded proton, the exchange averaged chemical shift of open dimer must be in the neighborhood of $1/2(\delta_M + \delta_D)$, and therefore the average shift for the two dimeric species

$$\delta_D = (x_{cyclic}\delta_{cyclic} + x_{open}\delta_{open})/x_D \qquad (8)$$

will become less negative at higher temperatures. With reasonable estimates of the relevant thermodynamic functions, we found that this effect should yield $\Delta\delta_D/\Delta T \sim 0.7 \times 10^{-3}$ ppm/deg, about an order of magnitude less than the observed value. Hence most of the variation probably arises from the thermal excitation of low-lying vibrationally excited states of the cyclic dimers.[15] However, in view of the unexpected temperature variation of the monomer shift, it seems possible that a still unrecognized factor is also involved.

The temperature variation of δ_M is the least palatable result of this study, since our point of departure was the conviction that the true monomer shift should be essentially temperature independent. We have tried to rationalize this effect or to explain it away in a number of ways, briefly described in the following paragraphs, none of which seems entirely satisfactory.

Residual moisture cannot be the cause of the monomer shift variation, since we have already shown that it would lead to a negative rather than a positive temperature coefficient. The possibility that the effect results from hydrogen bonding with the benzene as a π-electron donor can be ruled out in a similar way, since Davis and Pitzer[2] showed that this should make a negative (though probably very small) contribution to $\Delta\delta_M/\Delta T$.

The calculated values of δ_M at the higher temperatures, of course, depend on the value adopted for the enthalpy of dimerization. Table III gives values of K_2, δ_M, and δ_D calculated at various temperatures with $K_2 = 5.25 \times 10^3$ at 30° and $\Delta H = -9.3$ kcal/mole. It is noteworthy that none of the δ_D values are much affected by this change of ΔH. The calculated monomer shift at 90° is now only slightly larger than at 30°, but the intermediate values show a pronounced "sag." Because of this and of the accumulation of evidence[2,13] favoring $\Delta H = -8.4$ kcal/mole we do not feel that this is a suitable way of reinterpreting the data.

Table III: Dimerization Constants and Chemical Shift Parameters Recalculated with $\Delta H = -9.3$ Kcal/Mole

T, °C	K_2, mf^{-1}	δ_M	δ_D
30	5250	55.7	−381.5
50	2023	42.3	−370.1
60	1311	41.3	−364.8
70	871	50.2	−360.8
80	593	54.5	−355.9
90	412	60.1	−352.7

A closely related procedure is to attempt to find a set of K_2 values that yield a constant δ_M even though this might require a somewhat temperature-dependent ΔH. Since the two choices tried for ΔH gave nearly the same set of values for δ_D, we took for this parameter the temperature-dependent value $\delta_D = -381.2 + 0.552 \cdot (T - 30)$ and for the monomer shift, $\delta_M = 55.7$. A set of K_2 values, derived from the observed shift at $x_a^0 = 0.0058$ at each temperature, is presented in Table IV, and a plot of log K_2 against $1/T$ is shown in Figure 3.

(10) J. C. Davis, Jr., K. S. Pitzer, and C. N. R. Rao, *J. Phys. Chem.*, **64**, 1744 (1960).

(11) C. S. Springer, Jr., and D. W. Meek, *ibid.*, **70**, 481 (1966).

(12) L. A. LaPlanche, H. B. Thompson, and M. T. Rogers, *ibid.*, **69**, 1482 (1965).

(13) G. Allen and E. F. Caldin, *Quart. Rev.* (London), **7**, 255 (1953), Table 6.

(14) L. W. Reeves, *Trans. Faraday Soc.*, **55**, 1684 (1959).

(15) N. Muller and R. C. Reiter, *J. Chem. Phys.*, **42**, 3265 (1965).

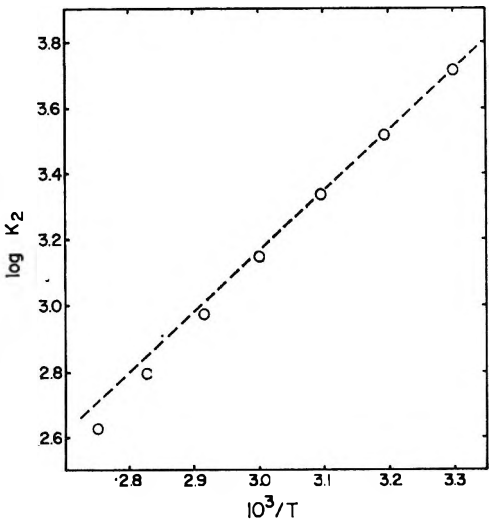

Figure 3. Plot of log K_2 against $10^3/T$ using values of K_2 calculated with a temperature-independent monomer shift. The dashed line has the theoretical slope predicted for $\Delta H = -8.4$ kcal/mole.

A smooth curve through the data points would be noticeably nonlinear, in contrast to the good straight line obtained in a similar plot[13] summarizing several studies of colligative properties. Again we are reluctant to claim that the temperature dependence of δ_M can be eliminated convincingly in this way.

Table IV: Dimerization Constant as a Function of Temperature Assuming $\delta_M = 55.7$ and $\delta_D = -381.2 + 0.552(T - 30)$

T, °C	K_2, mf^{-1}
30	5201
40	3273
50	2154
60	1411
70	944
80	627
90	426

Another possible line of argument involves the formation of a temperature-dependent quantity of water by the reaction

$$2C_6H_5COOH \rightleftarrows (C_6H_5CO)_2O + H_2O. \quad (9)$$

The equilibrium constant for this process has not been measured, but it has been shown[16] that at 130° the reverse rate is larger than the forward rate when the mole fraction of water and of benzoic anhydride are each 5×10^{-5} while that of benzoic acid is essentially unity. The equilibrium constant therefore cannot be greater than 2.5×10^{-9}, and the amounts of water formed in this way could have no significant effect on the chemical shift values.

Finally, it might be supposed that monomeric benzoic acid consists of a mixture of conformers and/or vibrationally excited species, with f_j being the fraction of the material existing in the jth form and having a hydroxyl proton chemical shift δ_j. Then

$$\delta_M = \sum_j f_j \delta_j \quad (10)$$

and

$$f_j = g_j e^{-E_j/kT} / \sum_j g_j e^{-E_j/kT} \quad (11)$$

where g_j is the statistical weight and E_j the energy of the jth species. A simple application of this idea is to consider only the two planar forms of the monomer

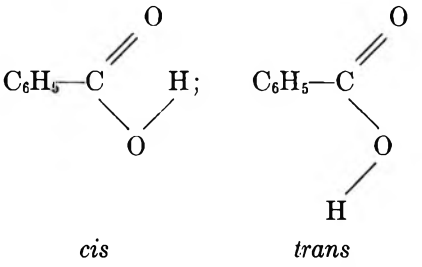

cis *trans*

Unfortunately, the *trans* form is 3 kcal/mole less stable than the *cis* form,[17] and hence it makes only a very small contribution in the range of temperatures of interest here. In fact, even to get $\Delta\delta_M/\Delta T = 0.3 \times 10^{-2}$ ppm/deg, it would be necessary to assume $\delta_{trans} - \delta_{cis} = 20$ ppm, which is out of the question. If the *cis–trans* energy difference is arbitrarily reduced to 1 kcal/mole the corresponding chemical shift difference still exceeds 4 ppm. In our opinion, this value is much too high; in the somewhat analogous case of formamide, there is only a very small difference in shift between the protons *cis* and *trans* to the C=O bond.[18] The possibility that vibrationally excited species, rather than the *trans* isomer, make a significant contribution seems remote because there is no evidence showing that any vibrational modes of the monomer have sufficiently low frequencies to be appreciably excited at fairly low temperatures.[19,20]

(16) F. W. Schwab and E. Wichers, *J. Res. Natl. Bur. Std.*, **25**, 747 (1940).

(17) M. Oki and M. Hirota, *J. Chem. Soc. Japan, Pure Chem. Sect.*, **86**, 115 (1965). See also ref 19 below.

(18) B. Sunners, L. H. Piette, and W. G. Schneider, *Can. J. Chem.*, **38**, 681 (1960).

(19) T. Migazawa and K. S. Pitzer, *J. Chem. Phys.*, **30**, 1076 (1959).

(20) K. Nakamoto and S. Kishida, *ibid.*, **41**, 1554 (1964).

We must conclude either that the unexpected temperature variation of δ_M reflects a systematic error, probably increasing in size as the temperature is raised, which we cannot track down, or that the effect is real and reflects a mode of behavior characteristic of carboxyl groups which is not yet understood. In this connection, it seems noteworthy that preliminary results[3] on acetic acid in benzene seemed to suggest a small, positive temperature coefficient of δ_M, which at the time was attributed to errors either in the temperature determinations or in the value chosen for the heat of dimerization.

Scope of the Nmr Method. We had hoped to be able to show that after taking suitable precautions to eliminate trace moisture the nmr results would be entirely consistent with enthalpies and free energies of dimerization obtained by other methods, and that eventually nmr determinations of these thermodynamic parameters for new acid–solvent systems might be made without a need for supplementary data. While we have made considerable progress toward the first of these goals, the outlook is not very encouraging with regard to the second. Each new system will involve at least the five unknown quantities, δ_M, δ_D, K_2, ΔH, and $\Delta\delta_D/\Delta T$, and perhaps, if the temperature dependence of the monomer shift proves to be real, also the sixth unknown, $\Delta\delta_M/\Delta T$. When solubility considerations allow it, work on concentrated solutions seems to make the evaluation of δ_D and its temperature coefficient fairly simple,[14] but it is not now feasible to determine all the remaining parameters accurately from nmr data alone. It may ultimately be possible to simplify the problem by showing that δ_M (and perhaps $\Delta\delta_M/\Delta T$) is the same for different acids, at least if the acids are closely related, but much painstaking work by both nmr and other methods would be required to establish any such hypothesis.

Conclusions

Carefully dried samples of benzoic acid in benzene yield nmr dilution shift curves at several temperatures which are qualitatively similar to those obtained earlier but displaced to lower fields. Least-squares analysis of the data by a procedure based on that of Davis and Pitzer indicates that at 30° $\delta_M = 1.0 \pm 0.4$ ppm from benzene (solvent and internal reference) and $\delta_D = -6.77 \pm 0.04$ ppm. The enormous negative shift of δ_M with increasing temperature, reported earlier, is now eliminated and seems to have been a result of water contamination. Instead, δ_M appears to become slightly more positive as the temperature is raised; no satisfactory explanation for this effect has been found. The temperature coefficient $\Delta\delta_D/\Delta T$ was found to be 0.91×10^{-2} ppm/deg in good agreement with other available data. The nmr method cannot at present replace nonspectroscopic methods as a means of characterizing dimerization equilibria in carboxylic acid–inert solvent systems, but the two types of experiment no longer give mutually incompatible results.

Radiolysis of Nitrous Oxide Saturated Solutions: Effect of Sodium Nitrate, 2-Propanol, and Sodium Formate[1]

by H. A. Mahlman

Chemistry Division, Oak Ridge National Laboratory, Oak Ridge, Tennessee *(Received July 13, 1966)*

The ^{60}Co γ radiolysis of aqueous N_2O-saturated $NaNO_3$ solutions has given the yield of reducing radicals not producing molecular hydrogen as 2.95 and $k(NO_3 + Red)/k(N_2O + Red)$ as 1.44. Hydrogen yields observed in the ^{60}Co γ radiolysis of aqueous N_2O-saturated 2-propanol solutions are interpreted as arising from (1) the G_{H_2} from the radiolysis of N_2O-saturated water and determined to be 0.34, (2) the H atom abstraction of hydrogen from the organic solute and evaluated as $G_H = 0.61$, and (3) a "direct effect" equal to 0.54[2-propanol]. Similar treatment of the sodium formate data evaluates $G_H = 0.57$ and the "direct effect" as 0.16[sodium formate]. The simultaneously measured nitrogen yields are constant, indicating that the H atoms are not reducing N_2O to N_2 in aqueous N_2O-saturated solutions.

Introduction

In the ^{60}Co γ radiolysis of neutral or basic aqueous solutions, chemical and physical evidence has identified the major reducing species as the solvated electron.[2] When aqueous solutions containing dissolved N_2O are irradiated, the hydrated electron has been shown to react rapidly with N_2O to produce N_2.[3] However, H atoms have also been shown to be produced in the radiolysis of aqueous solutions[4,5] and that they can react with N_2O in aqueous solution to form N_2.[6] It has been suggested that the $G(N_2)$ observed in the radiolysis of N_2O-saturated aqueous solutions may represent the sum of the solvated electron and the H atom yields.[7] The work reported in this paper was undertaken to determine the extent of the H atom reaction with N_2O dissolved in aqueous solution. Also reported is a redetermination of the data representing the competition between N_2O and NO_3^- for reducing radicals.[8]

The addition of 2-propanol or formate ions, which are good H atom scavengers,[9] to N_2O-saturated aqueous solutions would evaluate the question concerning the H atoms. In the course of this investigation, $G(H_2)$ was observed to increase as a function of the added organic solute concentration. The $G(H_2)$ was attributed to three sources: (1) the molecular hydrogen produced during the radiolysis of N_2O-saturated water, (2) the H atom abstraction of hydrogen from the organic solute, and (3) a "direct action effect" on the dissolved 2-propanol and formate ions that was directly proportional to the organic solute concentration.

Experimental Section

All $NaNO_3$ solutions were prepared from Baker and Adamson reagent grade $NaNO_3$ with triply distilled water. The pH of these solutions was 4.8–5.2. Baker and Adamson KBr and Na_2SO_4 were used without further purification. Appropriate amounts of Matheson Spectroquality reagent 2-propanol were added to N_2O-saturated water to obtain the desired alcohol concentrations. These solutions were in the pH range 5.8–6.5. The sodium formate solutions were prepared

(1) Research sponsored by the U. S. Atomic Energy Commission under contract with the Union Carbide Corp.

(2) E. J. Hart, *Ann. Rev. Nucl. Sci.*, **15** (1965); *Science*, **146**, 19 (1964).

(3) F. S. Dainton and D. B. Peterson, *Nature*, **186**, 878 (1960); *Proc. Roy. Soc.* (London), **A267**, 443 (1962).

(4) J. T. Allan and G. Scholes, *Nature*, **187**, 218 (1960).

(5) C. Lifshitz, *Can. J. Chem.*, **40**, 1903 (1962).

(6) G. Czapski and J. Jortner, *Nature*, **188**, 50 (1960).

(7) D. Head and D. C. Walker, *ibid.*, **207**, 517 (1965).

(8) A. M. Koulkes-Pujo and H. A. Mahlman, *Compt. Rend.*, **259**, 788 (1964).

(9) A. J. Swallow, "Radiation Chemistry of Organic Compounds," Pergamon Press Inc., New York, N. Y., 1960; M. Anbar and P. Neta, *Intern. J. Appl. Radiation Isotopes*, **16**, 227 (1965).

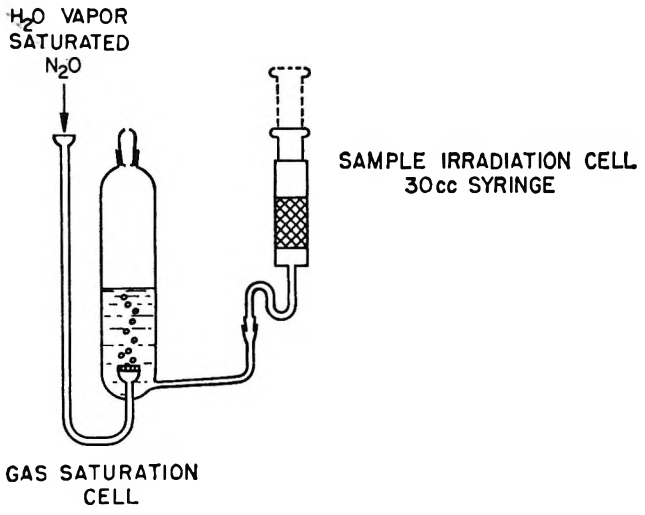

Figure 1. Gas saturation and irradiation cells.

with Baker's reagent grade crystals and were in the pH range 7.6–8.5.

Matheson reagent grade N_2O, especially low in nitrogen content, was used to deaerate and saturate each individual sample solution. The gas saturation cell and sample irradiation cell are illustrated in Figure 1. The irradiation cell, similar to that used by Hart and coworkers,[10] was a 30-cc B and D syringe with a capillary tube terminating with a $^5/_{20}$ ground-glass male joint. After thoroughly rinsing the syringe with N_2O-saturated solution, a 25-cc sample was withdrawn and the exit was capped. Upon completion of the irradiation the cap was removed and a 2-cc portion of sample was discarded. The irradiation cell was then placed on a vacuum line for analysis utilizing a $^5/_{20}$ female ground-glass joint with a mercury seal. A sample aliquot, about 20 cc, was introduced into the vacuum system followed successively by expansion of the gases to approximately a 500-cc volume, freezing the aqueous solution with CO_2 slush and the N_2O in a liquid N_2 trap. The permanent gases, N_2, H_2, and O_2, were then analyzed by the micro techniques previously described.[11] The exact amount of sample used in each analysis was determined by weight after the gas analysis.

The volume of N_2O dissolved in the $NaNO_3$ solutions was measured and the molarity was calculated to be 2.4×10^{-2} M at 24° and 750 mm pressure. This is in good agreement with the molarity calculated from Henry's constant.[12]

The ^{60}Co γ ray source used for the irradiations had a dose rate of 1.45×10^{18} ev ml^{-1} min^{-1} as determined by ferrous oxidation in an air-saturated 0.4 M H_2SO_4 solution assuming 15.60 molecules of ferrous are oxidized per 100 ev.[13] The ferric ion concentration was determined spectrophotometrically at 3050 A utilizing the molar extinction coefficient of 2240 at 25°.[13] All yields were calculated on the basis of total energy absorbed by the solution and the 100-ev yields are reported as G(product).

Results

Assuming that H atoms do not contribute to the $G(N_2)$ in N_2O-saturated aqueous solutions (which shall be proven later), the competition between N_2O and NO_3^- was considered to be for one type of reducing radical. The competitive reactions of N_2O and NO_3^- given by

$$N_2O + \text{Red} \longrightarrow N_2 + \ldots \quad (1)$$

$$NO_3^- + \text{Red} \longrightarrow \text{products other than } N_2 \quad (2)$$

may be kinetically expressed by

$$\frac{1}{G(N_2)} = \frac{1}{G_{\text{Red}}}\left[1 + \frac{k_2[NO_3^-]}{k_1[N_2O]}\right] \quad (I)$$

The straight line drawn through the data points in Figure 2 represents the least-squares fit and has a calculated intercept of 0.313 and a slope of 0.451. Thus the intercept corresponds to $G(N_2) = 3.19$ in N_2O-saturated water in agreement with other authors.[3,7,8,14-16] From the slope to intercept ratio, the ratio of reaction rate constants k_2/k_1 is calculated to be 1.44. Not plotted in Figure 2 is the $G(N_2) = 0.033$ determined at a NO_3^-/N_2O ratio of 52, which is in reasonable agreement with that calculated from the data at lower NO_3^-/N_2O ratios ($G(N_2) = 0.042$).

When 0.02 or 0.166 M Na_2SO_4 was added to a N_2O-saturated 0.02 M $NaNO_3$ aqueous solution, the observed nitrogen yields were 1.50 and 1.37, respectively. These nitrogen yields are much different from the $G(N_2)$ predicted if the rate constant is sensitive to changes in ionic strength.[17-20] A comparison of the

(10) E. J. Hart, S. Gordon, and D. A. Hutchison, *J. Am. Chem. Soc.*, 75, 6165 (1953).

(11) J. W. Boyle and H. A. Mahlman, *Nucl. Sci. Eng.*, 2, 492 (1957).

(12) "Handbook of Chemistry and Physics," 44th ed, Chemical Rubber Publishing Co., Cleveland, Ohio, 1962–1963, p 1709.

(13) C. J. Hochanadel and J. A. Ghormley, *J. Chem. Phys.*, 21, 880 (1953).

(14) J. T. Allan and C. M. Beck, *J. Am. Chem. Soc.*, 86, 1483 (1964).

(15) G. Scholes and M. Simic, *J. Phys. Chem.*, 68, 1731 (1964).

(16) G. V. Buxton and F. S. Dainton, *Proc. Roy. Soc.* (London), A287, 427 (1965).

(17) S. E. Benson, "The Foundations of Chemical Kinetics," McGraw-Hill Book Co., Inc., New York, N. Y., 1960, p 525.

(18) G. Czapski and H. A. Schwarz, *J. Phys. Chem.*, 66, 471 (1962).

(19) E. Collinson, F. S. Dainton, D. R., Smith, and S. Tazuke, *Proc. Chem. Soc.*, 140 (1962).

(20) P. J. Coyle, F. S. Dainton, and S. R. Logan, *ibid.*, 219 (1964).

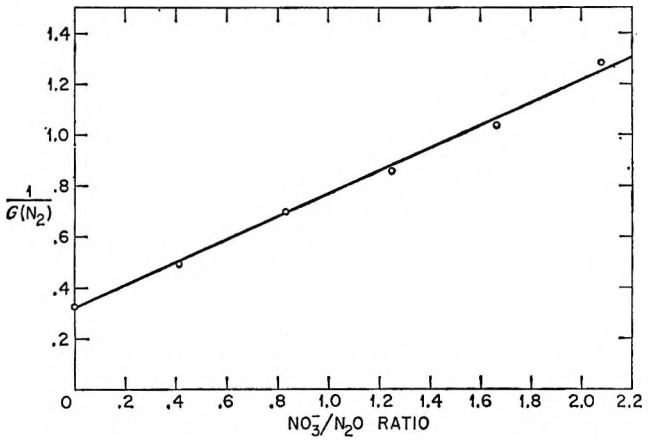

Figure 2. Variation of the $G(N_2)$ as a function of the NO_3^-/N_2O ratio in N_2O-saturated aqueous solution.

average $G(N_2) = 1.43$ observed in the presence of added Na_2SO_4 and the $G(N_2) = 1.42$ observed in the absence of Na_2SO_4 indicates that there is no significant effect attributable to increased ionic strength.

The nitrogen yields observed in the radiolysis of N_2O-saturated 2-propanol solutions are given in Table I. These nitrogen yields were calculated from the best values determined from a plot of doses *vs.* molecules of product and after correction of the data for nitrogen blanks. The constancy of the nitrogen yields is readily apparent, with excellent agreement shown between N_2O-saturated water, N_2O-saturated 10^{-3} *M* KBr solution, N_2O-saturated aqueous 2-propanol solutions, and with the calculated intercept of the N_2O–NO_3^-–H_2O solution data given in Figure 2.

The $G(N_2)$ observed from the N_2O-saturated aqueous sodium formate solutions (also given in Table I) are approximately constant but somewhat higher. Since these $G(N_2)$ are single determinations uncorrected for nitrogen blanks, attention was focused on the observation that no nitrogen yields were less than those observed for 2-propanol additions and, therefore, no significance was attached to the absolute magnitude of the yield. It has recently been suggested[21] that high nitrogen yields observed in N_2O-saturated aqueous formate solutions were due to the reduction of N_2O by formate radical. It was observed, however, that when N_2O gas containing an especially low N_2 content was used to saturate the sodium formate solutions, approximately the same nitrogen yields were observed as in the N_2O-saturated 2-propanol solutions.

The hydrogen yields, tabulated in Table I, are illustrated in Figure 3, where the linear dependency of $G(H_2)$ on the organic solute concentration is evident. A least-squares analysis of these data gave the equations

$$G(H_2) = 0.95 + 0.54[\text{2-propanol}] \quad \text{(II)}$$

$$G(H_2) = 0.91 + 0.16[\text{sodium formate}] \quad \text{(III)}$$

Table I: Nitrogen and Hydrogen Yields from N_2O-Saturated Solutions

H_2O–N_2O–$CH_3CHOHCH_3$–KBr			N_2O–H_2O–HCOONa–KBr		
[2-Propanol], *M*	$G(N_2)$[a]	$G(H_2)$	[HCOONa], *M*	$G(N_2)$	$G(H_2)$
0 (10^{-3} *M* KBr pH 5)	3.07	0.34	0.5	3.75[b]	1.00
0 (no KBr)	3.03	...	1.0	3.78[b]	1.05
0.0013	3.03	...	1.5	3.18[c]	1.16
0.013	3.06	...	2.0	3.49[b]	1.21
0.13	3.21	0.99	3.0	3.60[b]	1.45
0.50	3.17	1.20	4.0	3.06[c]	1.56
1.18	3.12	1.65	5.0	3.05[c]	1.69
3.08	2.95	2.59			
3.98	...	3.16			
5.00	3.04	3.62			
5.90	3.02	3.72			
Av	3.07				

[a] Corrected for N_2 blank. [b] Single determinations, uncorrected for N_2 blank. The $G(N_2)$ are greater than the $G(N_2)$ measured in the N_2O-saturated aqueous 2-propanol solutions. [c] New tank of N_2O with negligible N_2 content. The $G(N_2)$ are about equal to those measured in the N_2O-saturated aqueous 2-propanol solutions.

Discussion

Sodium Nitrate–Nitrous Oxide–Water Solutions. Baxendale, *et al.*,[22] and Gordon, *et al.*,[2,3] utilizing pulsed-radiolysis techniques, have determined the reaction rate constants for electrons reacting with various solutes. From their data, one can calculate the ratio of rate constants k_2/k_1 to be 1.46 and 1.27, respectively. Appleby, Scholes, and Simic[24] have obtained $k_2/k_1 = 1.17$ by a chemical method. These ratios are to be compared to the ratio $k_2/k_1 = 1.44$ calculated in this paper.

Some might consider fortuitous the excellent agreement between the pulsed-radiolysis experiments, which were determined at low ionic strength, and this work, where the ionic strength was allowed to vary from 0.01 to 0.05. Considering the Brønsted–Bjerrum theory of ionic reactions and the extended Debye–Hückel theory of electrolytes[17] one would predict that the ratio k_2/k_1 determined in this paper would be too large. Increas-

(21) G. Scholes and M. Simic, *J. Phys. Chem.*, 68, 1738 (1964).

(22) J. H. Baxendale, *et al.*, *Nature*, 201, 468 (1964).

(23) G. S. Gordon, E. J. Hart, M. S. Matheson, J. Rabani, and J. K. Thomas, *Discussions Faraday Soc.*, 36, 193 (1963).

(24) A. Appleby, G. Scholes, and M. Simic, *J. Am. Chem. Soc.*, 85, 3891 (1963).

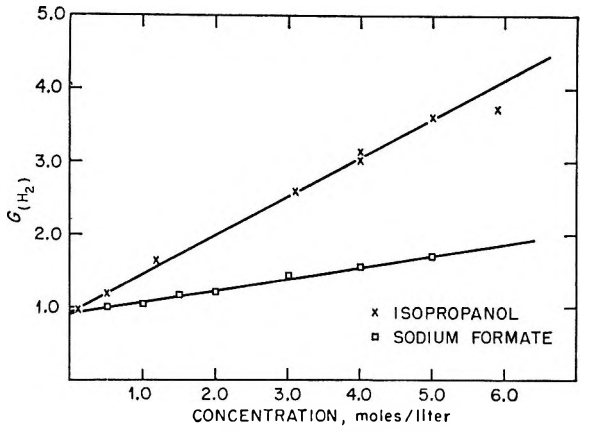

Figure 3. Hydrogen yields as a function of 2-propanol and sodium formate concentration in N_2O-saturated aqueous solution.

ing the ionic strength would favor the reaction of a negatively charged reducing radical with the negatively charged nitrate ion as given by

$$\log \frac{k}{k_0} = 1.02 Z_a Z_b \mu^{1/2}/(1 + \mu^{1/2}) \qquad \text{(IV)}$$

However, when the ionic strength of an N_2O-saturated 0.02 M $NaNO_3$ solution was altered by the addition of 0.02 or 0.166 M Na_2SO_4, no significant change in $G(N_2)$ was noted when compared with $G(N_2)$ observed in N_2O-saturated 0.02 M $NaNO_3$ solution. In fact, the average $G(N_2)$ determined in the solutions containing the Na_2SO_4 additions was 1.43 compared to 1.42 in the absence of Na_2SO_4.

The applicability of eq IV has been demonstrated in the radiolysis of dilute solutions;[18,19] however, at higher scavenging concentrations and ionic strengths the "constant" (1.02) has been observed to decrease.[20] Furthermore, the absence of an ionic strength effect has been reported[19] for a 0.01 M scavenging solute having a reaction rate constant about 10^{10} M^{-1} sec^{-1}. These variations in eq IV have been attributed to the reaction of the solvated electron in a time shorter than that necessary to establish an ionic atmosphere. Thus the absence of an ionic strength effect noted in the radiolysis of N_2O-saturated 0.02 M $NaNO_3$ solutions containing 0.02 or 0.166 M Na_2SO_4 may be attributed to the fast reaction of nitrate ions with solvated electrons, which also has a reaction rate constant about 10^{10} M^{-1} sec^{-1}. Consequently, agreement could be expected between the ratio k_2/k_1 determined in pulsed radiolysis studies at low ionic strengths and that determined in this work at much greater ionic strengths.

It should be emphasized that the $G(N_2) = 3.19$ reported in this paper represents the total number of species reacting with N_2O to produce N_2. Under no circumstances should it be construed to mean that the yield of reducing radicals in the bulk of the solution is 3.19. Three sources are considered to be contributing to the $G(N_2)$, namely: (1) the reducing radical yield in the bulk of the solution that reacts with N_2O; (2) an undetermined number of reducing radicals or other reducing species that "normally" are considered to disappear by back reactions to re-form water but in the presence of a high N_2O concentration now react with the solute; and (3) the reaction of molecular hydrogen precursors with N_2O.

In a deaerated aqueous 10^{-3} M KBr solution, the $G(H_2) = 0.46$,[25] while in an identical solution saturated with N_2O, the $G(H_2) = 0.34$. Thus the molecular hydrogen suppression by 2.4×10^{-2} M N_2O is 0.12. If it is assumed that for each hydrogen molecule suppressed, two molecules of N_2 are formed,[14] the contribution to the $G(N_2)$ manifested by suppression of the molecular hydrogen is 0.24. In the $NaNO_3$–N_2O–H_2O system, it may be concluded that exclusive of the molecular hydrogen suppression, the radicals reducing N_2O to N_2 have a yield of 2.95 in an aqueous solution of 2.4×10^{-2} M N_2O. From the average N_2 yields observed in the 2-propanol–nitrous oxide–water system (see Table I), the yield of radicals reducing N_2O to N_2 is 2.81 after correction for the molecular hydrogen suppression. Thus these two systems give reducing radical yields that are in good agreement with the $G_{e_{aq}^-} = 2.85$ determined by Czapski and Allen.[26]

A comparison of the data reported in this paper for aqueous N_2O-saturated $NaNO_3$ solutions with that previously reported[8] is reasonably good. The modified method employed herein for deaeration and N_2O saturation is considered to be more reliable and reproducible as reflected by the precision of Figure 2. Use of irradiation cells without free space above the solution may also be important.

2-Propanol–Nitrous Oxide–Water Solutions. In addition to solvated electrons, H atoms are a ^{60}Co γ-radiolysis product in aqueous solutions. Since H atoms can also react with N_2O to form N_2, the extent of this possible contribution to the observed $G(N_2)$ was investigated. When an aliphatic alcohol such as 2-propanol is irradiated in dilute aqueous solution, molecular hydrogen has been shown to be formed by hydrogen atoms abstracting hydrogen from the alcohol.[4,5,14,24,27–37] Therefore, in N_2O-saturated aqueous

(25) H. A. Mahlman and J. W. Boyle, *J. Chem. Phys.*, **27**, 1434 (1957).
(26) G. Czapski and A. O. Allen, *J. Phys. Chem.*, **66**, 262 (1962).
(27) P. Kelley and M. Smith, *J. Chem. Soc.*, 1487 (1961).
(28) J. Rabani and G. Stein, *J. Chem. Phys.*, **37**, 1865 (1962).

solutions containing 2-propanol, any competition between N_2O and 2-propanol for H atoms will be reflected by a decreasing N_2 yield and an increasing H_2 yield. As previously mentioned, the data in Table I show that $G(N_2)$ is unaltered even when the 2-propanol concentration is increased to 5.9 M. Thus it is concluded that the H atoms do not contribute to $G(N_2)$. $G(N_2)$ observed in the radiolysis of N_2O-saturated aqueous 2-propanol solutions is in excellent agreement with $G(N_2)$ determined in N_2O-saturated water and 10^{-3} M KBr and the intercept calculated in the NO_3^-–N_2O–H_2O system (Figure 2) and precludes an H atom contribution to the $G(N_2)$. The absence of an H atom contribution to $G(N_2)$ in N_2O-saturated water or solutions may be explained by the rapid reaction of the H atoms with the radiolysis products H_2O_2 and O_2.

The formation of molecular hydrogen in N_2O saturated aqueous solution of 2-propanol is illustrated in Figure 3 and is expressed by eq II. The $G(H_2)$ is considered to be a net yield from three sources: (1) the molecular hydrogen formed from the radiolysis of water, (2) the abstraction of hydrogen from the 2-propanol by H atoms, and (3) the "direct action" yield of hydrogen which appears to be linearly proportional to the 2-propanol concentration.

The intercept value, $G(H_2) = 0.95$, is calculated from the measured hydrogen yields in concentrated 2-propanol solutions, where all of the H atoms have reacted with the alcohol. Since the "direct effect" is zero at the intercept (zero 2-propanol concentration), the $G(H_2)$ at this point is assumed to be a composite of the molecular hydrogen formed by radiolysis of the water plus the molecular hydrogen formed by H atoms reacting with the alcohol. Since the G_{H_2} is determined to be 0.34 in an N_2O-saturated 10^{-3} M KBr solution, the G_H is calculated to be 0.61. The "direct effect" has a concentration dependency of 0.54 [2-propanol].

Nitrous Oxide–Sodium Formate–Water Solutions. In the ^{60}Co γ radiolysis of sodium formate or formic acid solutions, molecular hydrogen is also produced by H atom abstracting hydrogen from the organic solute.[4,5,21,24,27–45] The hydrogen yields produced during the radiolysis of N_2O-saturated aqueous sodium formate solutions are tabulated in Table I, illustrated in Figure 3, and represented by eq III. Using the same interpretation as employed for the 2-propanol solutions, the G_H is calculated to be 0.57 and the "direct effect" as 0.16 [sodium formate].

The H Atom Yield. These determinations of G_H are tabulated and compared in Table II with the determinations of other authors. Although the solutions used in this work contained two solutes, N_2O and 2-propanol or N_2O and formate ion, the G_H is not determined by competition between the solutes for the H atom. Thus a possible source of error was eliminated. If the reaction rate constants of two competitive solutes differ greatly, a high concentration of the solute with the lower rate constant may be required to obtain analytically significant differences in the monitored product. Thus a "direct effect" may insidiously enter to give results that are too large. For example, if the hydrogen yields observed in the competitive study of O_2-saturated aqueous sodium formate solutions[40] are corrected for the "direct effect" on the sodium formate, the calculated G_H is lowered about 20% and is then in excellent agreement with that determined in this work.

Table II: Yields of G_H in Aqueous Organic Solutions

Authors	System	G_H
Allan and Beck[14]	2-Propanol–nitrous oxide	0.60
Allan and Scholes[4]	2-Propanol–acetone	0.60
Allan[37]	Methanol–sodium nitrate	0.45
Anbar and Meyerstein[33]	2-Propanol–acetone	0.62
Hayon and Allen[40]	Chloroacetate	0.80
Kelley and Smith[27]	2-Propanol–N_3^-	0.30
Rabani and Stein[28]	2-Propanol–acetone	
	Sodium formate–acetone–ferricyanide	0.55
Scholes and Simic[41]	Sodium formate–oxygen	0.75
Scholes and Simic[21]	2-Propanol–nitrous oxide	0.74
	2-Propanol–Cu^{+2}–N_2O	0.66
This work	Concentrated 2-propanol–nitrous oxide	0.61
	Concentrated sodium formate–nitrous oxide	0.57

Acknowledgment. The author wishes to acknowledge discussions of this work with J. W. Boyle, C. J. Hochanadel, P. S. Rudolph, and T. J. Sworski.

(29) J. T. Allan, M. C. Robinson, and G. Scholes, *Proc. Chem. Soc.*, 381 (1962).
(30) J. Rabani, *J. Am. Chem. Soc.*, **84**, 868 (1962).
(31) J. Rabani, *J. Phys. Chem.*, **66**, 361 (1962).
(32) G. Czapski, J. Rabani, and G. Stein, *Trans. Faraday Soc.*, **58**, 2160 (1962).
(33) M. Anbar and D. Meyerstein, *Proc. Chem. Soc.*, 23 (1964).
(34) M. Anbar and D. Meyerstein, *J. Phys. Chem.*, **68**, 1713 (1964).
(35) M. Anbar and D. Meyerstein, *ibid.*, **68**, 3184 (1964).
(36) C. Lifshitz and G. Stein, *J. Chem. Soc.*, 3811 (1964).
(37) J. T. Allan, *J. Phys. Chem.*, **68**, 2697 (1964).
(38) H. Fricke, E. J. Hart, and H. P. Smith, *J. Chem. Phys.*, **6**, 229 (1938).
(39) D. Smithies and E. J. Hart, *J. Am. Chem. Soc.*, **82**, 4775 (1960).
(40) E. Hayon and A. O. Allen, *J. Phys. Chem.*, **65**, 2181 (1961).
(41) G. Scholes and M. Simic, *Nature*, **199**, 276 (1963).
(42) S. Nehari and J. Rabani, *J. Phys. Chem.*, **67**, 1609 (1963).
(43) G. Scholes and M. Simic, *ibid.*, **68**, 2697 (1964).
(44) E. J. Hart, *Radiation Res. Suppl.*, **4**, 74 (1964).
(45) E. Hayon, *Trans. Faraday Soc.*, **61**, 734 (1965).

Free Volume–Entropy Interpretation of the Electrical Conductance of Aqueous Electrolyte Solutions in the Concentration Range 2–20 N[1]

by C. A. Angell[2]

Chemistry Division, Argonne National Laboratory, Argonne, Illinois *(Received July 15, 1966)*

The electrical conductance of concentrated aqueous solutions of $Ca(NO_3)_2$ and $Mg(NO_3)_2$ has been studied at temperatures up to 180° and concentrations up to 9 M in order to test transport equations which recognize the liquid–glass transition phenomenon as a natural consequence of the dependence of particle packing density on temperature and cohesive energy. The data strongly suggest that on sufficient cooling or on sufficient concentration (*e.g.*, by isothermal evaporation of the solvent) at low enough temperatures, any supersaturated electrolyte solution would pass through a glass transition. The equivalent conductance of 7–8 M solutions has been followed as a function of temperature over three orders of magnitude and shown to conform to the equation $\Lambda = AT^{-1/2}\exp[-k/(T - T_0)]$ where T_0 is the theoretical glass transition temperature. The following new equation, derived from the above on the basis of a simple relation between T_0 and the electrostatic charge concentration, *i.e.*, equivalent concentration, N, is proposed to give a first approximation account of the isothermal composition dependence of conductance in the high concentration range $\Lambda_{(T)} = A\exp[-k'/(N_0 - N)]$ where N_0, conceptually akin to T_0, is the charge concentration at which T_0 equals the isothermal temperature T. Although the derivation oversimplifies the solution behavior, the form of this equation correctly describes the composition dependence of Λ for $Ca(NO_3)_2$ solutions over the concentration range 2–15 N despite changes in Λ amounting to three orders of magnitude. Equations of the same form will also be valid for solution *fluidities*. The results are also consistent with the existence of distinct hydrated cation species at the higher concentrations.

The transport properties of highly concentrated aqueous solutions on the whole have not received a great deal of attention and, despite the interesting program of Campbell and co-workers,[3] an explanation of the principal features of transport in this region remains to be given.

In the analysis of electrical conductance data of such solutions, the equation of Robinson and Stokes,[4] as modified and developed by Wishaw and Stokes,[5] has enjoyed considerable success for uni-univalent electrolytes at concentrations up to about 6 M.[3,5] This approach is expected to break down at concentrations where the water/salt ratio is too low for the "closest approach" concept, which is important to the Wishaw–Stokes model, to retain its full meaning. Indeed its success up to the high concentrations considered by Wishaw and Stokes is in part due to the arguable[1] introduction of a relative viscosity term. By using this term the theory avoids the basic problem of dealing with the cooperative mechanisms which must control *all* the mass transport processes at the molecular level. While it correctly relates solution conductance

(1) Based on work performed both at the Department of Metallurgy, Melbourne University, Australia, and under the auspices of the U. S. Atomic Energy Commission at Argonne National Laboratory, Argonne, Ill.

(2) To whom correspondence should be addressed at Department of Chemistry, Purdue University, Lafayette, Ind.

(3) (a) A. N. Campbell and D. F. Williams, *Can. J. Chem.*, **42**, 1778, 1984 (1964); (b) A. N. Campbell and G. H. Debus, *ibid.*, **34**, 1232 (1956); (c) A. N. Campbell and E. M. Kartzmark, *ibid.*, **33**, 887 (1955); (d) A. N. Campbell, E. M. Kartzmark, M. E. Bednas, and J. T. Herron, *ibid.*, **32**, 1051 (1954), and earlier references contained therein.

(4) R. A. Robinson and R. H. Stokes, *J. Am. Chem. Soc.*, **76**, 1991 (1954).

(5) B. F. Wishaw and R. H. Stokes, *ibid.*, **76**, 2065 (1954).

to solution viscosity, the Wishaw–Stokes equation thus provides little additional information on the factors which determine the absolute magnitude of the conductance of a solution of given concentration. This general limitation of the hydrodynamic approach, which has otherwise been so successful in the treatment of transport in dilute solutions, has recently been discussed in detail by Brummer and Hills.[6]

It has often been remarked that progress in the understanding of concentrated solution behavior must await a working theory of fused salts. While the latter seems far off the approach adopted in this paper to account for some salient features of transport in concentrated aqueous solutions has been suggested by an earlier treatment of transport behavior in anhydrous fused-salt systems.[7] As the approach is new in the treatment of electrolyte solutions, the main points will be outlined.

In the fused-salt work[7] it was found that in the "low-temperature region"[8] of the system the Arrhenius equation commonly used to represent the temperature dependence of fused-salt transport processes fails badly. In this region transport behavior, represented here by the equivalent conductance, Λ, is described by the following equation which is a simple modification of the Arrhenius equation

$$\Lambda = A_\Lambda T^{-1/2} \exp[-k/(T - T_0)] \qquad (1)$$

where A_Λ, k, and T_0 are constants. The equation implies that it is the temperature interval above the temperature T_0 rather than that above 0°K which is of importance to transport. Of the theoretical attempts to explain this equation[9,10] the available evidence[8] favors the theory of Adam and Gibbs.[10] This theory suggests, however, that eq 1 is only an approximate relation deriving form a more general expression

$$\Lambda = A_\Lambda \exp(-C/TS_c) \qquad (2)$$

where C is a constant containing a potential energy term and S_c is the macroscopic configurational entropy content of the liquid. S_c decreases with falling temperature and vanishes at the temperature T_0 of eq 1.

Successful applications of this simple equation have been described elsewhere.[10,11] In this paper we will deal only with its approximate form, eq 1, whose empirical basis both in the above form and particularly in the form of the equivalent[12] Williams, Landel, and Ferry equation is well established for different classes of liquids.[7,13,14] It is necessary to emphasize here, however, that when the configurational entropy, S_c, falls to zero, the material can no longer have fluid character since the successive rearrangements of particles necessary for fluid flow to occur are excluded. Provided crystallization does not occur, the properties of the material below T_0 must therefore be those of a glass. In practice the glass transition (at which the derivative properties, expansion coefficient, and heat capacity change discontinuously from liquidlike to crystallike values) occurs at a temperature ("glass temperature," T_g) which is somewhat higher than T_0, an amount of residual entropy which depends on the cooling rate, being "frozen in." The condition $S_c = 0$ is thus an ideal one, only to be realized in a cooling process of infinite time scale.[15]

For systems of simple particles this ideal state, which one recognizes as the thermodynamic low-temperature limit of the liquid state, may be taken as one of random close packing (*cf.* the molecular dynamics studies of Alder and Wainwright[16] and the work of Bernal[17] on dense random packing of hard spheres). Turnbull[18] has pointed out that although this minimum volume condition can evidently be realized in a rather large number of ways, the state of the system in each should be essentially the same and the entropy of the system should fulfill the third-law condition $S \to 0$ as $T \to 0$°K. Liquid volume in excess of that required for random close packing may be regarded as available for redistribution and with various qualifications[8,19] has been termed "free volume."

The application of these concepts and equations to the elucidation of the transport behavior of concentrated electrolyte solutions was suggested to us by the high viscosities of such solutions at ambient temperatures and their frequent ability to supersaturate and yield brittle glassy materials on cooling to lower temperatures. In at least one case—11 *M*

(6) S. B. Brummer and G. J. Hills, *Trans. Faraday Soc.*, **57**, 1816, 1823 (1961).

(7) C. A. Angell, *J. Phys. Chem.*, **68**, 218, 1917 (1964).

(8) (a) C. A. Angell, *ibid.*, **70**, 2793 (1966); (b) C. A. Angell, 17th CICTE Meeting, Tokyo, Sept 1966.

(9) M. H. Cohen and D. Turnbull, *J. Chem. Phys.*, **31**, 1164 (1959).

(10) G. Adam and J. H. Gibbs, *ibid.*, **43**, 139 (1965).

(11) R. Araujo, *ibid.*, **44**, 1299 (1966).

(12) A. A. Miller, *J. Polymer Sci.*, **A1**, 1857 (1963).

(13) G. S. Fulcher, *J. Am. Ceram. Soc.*, **8**, 339 (1925).

(14) M. L. Williams, R. F. Landel, and J. D. Ferry, *J. Am. Chem. Soc.*, **77**, 3701 (1955).

(15) The condition with respect to this ideal state of the vapor-deposited glasses, *e.g.*, vitreous ice [which apparently exhibit normal glass transition behavior during warmup (J. A. McMillan and S. C. Los, *Nature*, **206**, 806 (1965))], has not yet been clarified.

(16) B. J. Alder and T. E. Wainwright, *J. Chem. Phys.*, **31**, 459 (1959).

(17) J. D. Bernal and J. Mason, *Nature*, **188**, 910 (1960).

(18) D. Turnbull, "Physics of Non-Crystalline Solids," J. Prins, Ed., North-Holland Publishing Co., Amsterdam, Netherlands, 1965, p 41.

(19) D. Turnbull and M. H. Cohen, *J. Chem. Phys.*, **34**, 120 (1961).

$Na_2S_2O_3$ (molten $Na_2S_2O_3 \cdot 5H_2O$)—the glass transition has been studied in some detail, the transition being found to occur at $-42°$.[20]

In this paper we report on the aqueous solution behavior of the nitrates of magnesium and calcium at concentrations up to 9 *M* and temperatures up to 180°. Some preliminary observations on this behavior have been published previously[21] and the properties of mixtures of the molten hydrates with common molten salts have been discussed elsewhere.[22] Many of the measurements to be reported apply to solutions which are supersaturated. Although the ability to supersaturate is related to the properties of the liquid at the thermodynamic crystallization temperature, there are good general reasons,[8,23] abundantly supported by experimental data,[8,9,24,25] for regarding the circumstance of the liquid being metastable with respect to some crystalline phase as irrelevant to the observed liquid behavior *i.e.*, the liquid does not "know" it is metastable until a nucleus of a crystalline phase (not necessarily the most stable one) *chances* to form. This subject has been discussed elsewhere[8,18,23] and, apart from noting the points at which the liquids become metastable, we will not give further attention to it in this paper.

Results

(*i*) *Composition and Concentration Units.* The composition units which have been used in the tabulation and discussion of properties of aqueous solutions are the molality, weight, mole percentage, and recently the water/salt molar ratio, *R*.[26] The latter unit is particularly useful in discussing the composition region where there are insufficient water molecules to fill more than one or two hydration shells per cation. In this region the molality has lost its advantage of lying close to the molarity.

In dealing with the present results the mole percentage and *R* units will be used jointly for description. The normality, *N*, which defines the concentration of electrostatic charge in equivalents per liter, will be used for interpretation. In Table I the relation between the various units is given to three figures over the composition range encountered in this work using $Ca(NO_3)_2$ solutions as the example.

(*ii*) *Results.* The specific conductances, κ, of $Mg(NO_3)_2$ and $Ca(NO_3)_2$ solutions of compositions ranging from 14.3 to 25.9 mole % (*R* = 6–2.75) are shown as a function of temperature in Figure 1 in the form of an Arrhenius plot. It is clear that the temperature dependence of conductance is very poorly described by the Arrhenius equation.

Solution densities necessary to calculate equivalent conductances have only been measured for the 20 mole % (*R* = 4) compositions. They are described by the following linear equations in which *t* is the temperature

Table I: Relation between Composition and Concentration Units for $Ca(NO_3)_2$ Solutions

Mole %	*R*	Molality moles/kg of H_2O	Normality, g equiv $l.^{-1}$ 0°	Normality, g equiv $l.^{-1}$ 18°	Wt %
25	3.0	18.5	17.0	16.8	75.3
20.0	4.0	13.9	15.0	14.9	69.5
16.7	5.0	11.1	13.4	13.2	64.6
14.3	6.0	9.25	12.0	11.9	60.3
12.5	7.0	7.93	10.9	10.8	56.5
11.1	8.0	6.94	10.0	9.90	53.2
10.0	9.0	6.17	9.20	9.10	50.3
8.2	11.2	4.95	7.89	7.79	44.9
7.05	13.2	4.21	6.95	6.87	40.8
6.16	15.2	3.65	6.19	...	37.5
5.81	17.2	3.22	5.58	5.52	34.6

$Mg(NO_3)_2$ (*R* = 4):

$$\rho = 1.757_0 - 8.4 \times 10^{-4}t \pm 0.001 \text{ g cm}^{-3}$$

$Ca(NO_3)_2$ (*R* = 4):

$$\rho = 1.778_0 - 8.8 \times 10^{-4}t \pm 0.001 \text{ g cm}^{-3}$$

from which the expansion coefficients at 0 and 100° are

$Mg(NO_3)_2$ (*R* = 4):

$$\alpha = 4.7_8 \times 10^{-4}\ (0°);\ 5.0_2 \times 10^{-4}\ (100°)$$

$Ca(NO_3)_2$ (*R* = 4):

$$\alpha = 4.93 \times 10^{-4}\ (0°);\ 5.1_6 \times 10^{-4}\ (100°)$$

The errors quoted for the densities refer to the maximum departure of any experimental point from the linear plot. The standard deviation for the experimental points is much smaller. The absolute accuracy, however, is set by uncertainties in the compositions. The detailed measurements of Ewing and Mikovsky[24] place $\rho_{Ca(NO_3)_2\ (R\,=\,4,\ 25°)}$ 0.40% lower than the value found in the present work, suggesting the composition represented by the above equation may be 0.30 mole % richer in $Ca(NO_3)_2$ than the intended

(20) M. Samsoen, *Ann. Phys.*, 9, 35 (1928).

(21) C. A. Angell, *J. Phys. Chem.*, 69, 2137 (1965).

(22) C. A. Angell, *J. Electrochem. Soc.*, 112, 1224 (1965).

(23) D. Turnbull, *Trans. AIME*, 221, 422 (1961).

(24) W. W. Ewing and R. J. Mikovsky, *J. Phys. Chem.*, 57, 245 (1953); W. W. Ewing and R. J. Mikovsky, *J. Am. Chem. Soc.*, 72, 1390 (1950).

(25) R. H. Stokes, *Trans. Faraday Soc.*, 41, 637 (1945).

(26) C. A. Angell and D. M. Gruen, *J. Am. Chem. Soc.*, to be published.

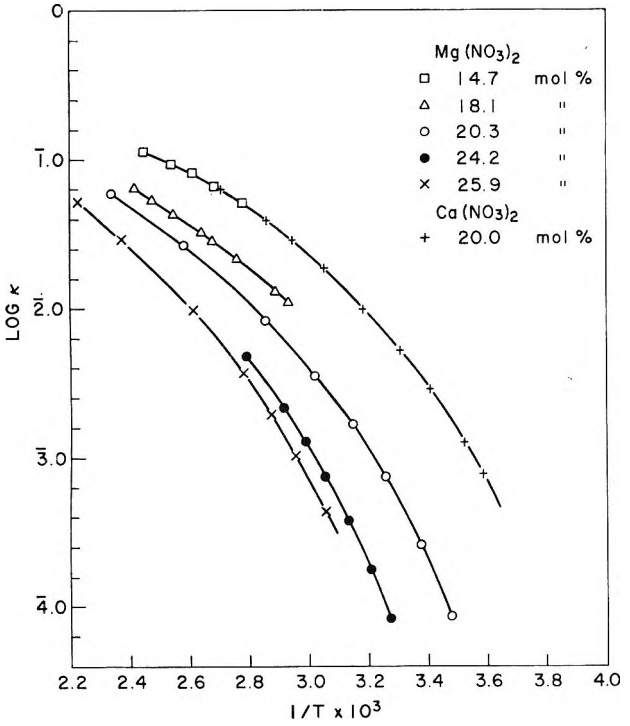

Figure 1. Arrhenius plot for specific conductance, κ, of $Ca(NO_3)_2$ and $Mg(NO_3)_2$ solutions.

figure of 20.0 mole %. Recent data by Moynihan[27] place $\rho_{Ca(NO_3)_2\ (R\ =\ 4,\ 25°)}$ 0.60% lower than the present value, *i.e.*, 0.20% less than that of Ewing and Mikovsky. It is worth noting that at $Ca(NO_3)_2$ contents less than about 6 mole % (R = 15) systematic departures from linearity in the density *vs.* temperature relations are indicated by Ewing and Mikovsky's data.

Equivalent conductances for the $Ca(NO_3)_2$ solution of nominal composition 20 mole % $Ca(NO_3)_2$ (R = 4), calculated using the above density data, are given in Table II as a function of temperature. The specific conductance values of Table II have previously[22] been reported under the composition 20.0 mole % $Ca(NO_3)_2$. In view of the discrepancy noted in the density data and the somewhat higher conductance values obtained by Moynihan,[27] it appears that some water was lost from the solution. On the basis of the density comparison, the composition of the solution has therefore been corrected to 20.30 mole % $Ca(NO_3)_2$ and the equivalent conductances calculated accordingly.

For $Mg(NO_3)_2$ the equivalent conductance at 20.30 mole % $Mg(NO_3)_2$ is given in Table III. To obtain Λ the density data obtained for the composition 20.0 mole % $Mg(NO_3)_2$ were increased uniformly by 0.29% to correspond to the composition at which the specific conductance was measured (determined by analysis to ±0.1 mole %). The uncertainty in Λ introduced by the density adjustment cannot be greater than 0.05%.

Table II: Conductance of 20 Mole % (Nominal) $Ca(NO_3)_2$ Solution (20.30 Mole % $Ca(NO_3)_2$, Corrected)[a]

Cell constant 61.85 cm^{-1}

T, °C	κ, ohms^{-1} cm^{-1}	Λ, ohm^{-1} cm^{-1} equiv^{-1}
96.4	0.06190	4.287
87.4	0.05057	3.487
76.4	0.03826	2.624
66.8	0.02871	1.959
54.8	0.01873	1.270
41.4	0.01038	0.6992
29.4	0.005356	0.3587
20.4	0.002899	0.1933
10.6	0.001256	0.0833
5.8	0.000774	0.0512

[a] Thermodynamic crystallization temperature, 43°.

Table III: Conductance of 20.3 Mole % $Mg(NO_3)_2$ Solutions[a]

Cell constant 36.40 cm^{-1}

T, °C	κ, ohms^{-1} cm^{-1}	Λ, ohms^{-1} cm^{-1} equiv^{-1}
155.2	0.06021	4.052
139.7	0.04569	3.052
139.6	0.04553	3.041
132.0	0.03920	2.608
126.4	0.03482	2.310
116.6	0.02800	1.848
114.2	0.02638	1.739
100.9	0.01867	1.223
91.0	0.01374	0.8953
77.3	0.008329	0.5390
65.6	0.005148	0.3312
55.7	0.003182	0.2038
44.7	0.001681	0.1071
	Cell constant 1.56 cm^{-1}	
34.3	0.000746	0.0473
23.4	0.000262	0.0165
14.6	0.000087	0.00546

[a] Thermodynamic crystallization temperature, 55.6°.

Plots showing the temperature dependence of the Arrhenius coefficients (so-called "activation energies") determined at short temperature intervals from the data of Tables II and III have been published elsewhere.[8] The coefficients increase rapidly with decreasing temperature in a manner which seems to be

(27) C. T. Moynihan, *J. Phys. Chem.*, **70**, 3399 (1966).

Table IV: Conductance of $Ca(NO_3)_2$ Solutions at 0.35 and 18.1°[a]

Wt %	R	N, equiv l.$^{-1}$		κ, ohm^{-1} cm^{-1}		Λ, ohms^{-1} cm^{-1} equiv^{-1}	
		0.35°	18.1°	0.35°	18.1°	0.35°	18.1°
				Cell constant 36.40			
69.51	4	15.01	14.88	0.000525		0.0350	0.208
67.05		14.18		0.001443		0.1018	
64.60	5	13.37	13.25	0.003033	0.009772	0.2269	0.7375
62.43		12.68	12.55	0.005116	0.01426	0.4035	1.136
60.28	6	12.04	11.91	0.008066	0.01975	0.6699	1.658
56.53	7	10.93	10.81	0.01380	0.03011	1.262	2.785
53.22	8	10.00	9.89	0.02027	0.04053	2.027	4.098
50.27	9	9.22		0.02653		2.877	
48.06	9.9	8.67		0.03156		3.640	
44.89	11.2	7.89		0.03791		4.805	
40.85	13.2	6.95		0.04677		6.730	
				Cell constant 630.8			
53.22	8	10.00		0.02024		2.024	
50.27	9	9.22	9.13	0.02649	0.04979	2.873	5.453
48.06	9.9	8.67	8.58	0.03143	0.05684	3.625	6.625
44.89	11.2	7.89	7.79	0.03795	0.06703	4.810	8.605
40.85	13.2	6.95	6.87	0.04693	0.07920	6.753	11.528
37.47	15.2	6.19		0.05378		8.688	
34.32	17.2	5.58	5.52	0.05830	0.09407	10.448	17.042

[a] Thermodynamic crystallization composition at 18°, 12.0 mole % $Ca(NO_3)_2$; 0°, 9.9 mole % $Ca(NO_3)_2$.

characteristic for liquids in their "low-temperature" regions.

The specific and equivalent conductances of $Ca(NO_3)_2$ solutions at 0.35 and 18.10° in the concentration range 5.5–15.0 *N* are recorded in Table IV. The density data of Ewing and Mikovsky[24] were used for the conversion. These results are plotted in Figure 2 together with earlier data of McGregory,[28a] Jones, and Getman[28c] and Jones and Pierce[28d] which cover the lower concentration region 0–6 *N*.

(*iii*) *Accuracy.* Errors in density measurements have been noted above. The uncertainties to be attributed to the reported conductance values arise almost entirely from the uncertainty in the composition of the liquid. In the high-concentration, low-temperature region the conductance changes by 5% per 0.1 mole % of composition [corresponding to, *e.g.*, an increase from 15.00 to 15.04 *N* (Table I)]. The correction of the nominally 20 mole % $Ca(NO_3)_2$ solution composition to 20.3 mole % removes most of the disagreement between the present Λ values and those reported by Moynihan[27] for this composition. The source of water loss was eliminated in the isothermal studies (Table IV), and the compositions are believed to be accurate to 0.1 mole % throughout. The present results at 18° are in agreement to 0.7% with early measurements by McGregory[28a] and Clausen[28b] in the region (4–6 *N*) common to each study. Adjusted to 0° our results at 5–8 *N* are 5% higher than those of Jones and Getman,[28c] whose results in the range 1–4 *N*, however, were found to be 2% low by Jones and Pierce[28d] and 7.5% low by Jones and Stine.[28e] The accuracy of the conductance measurements themselves is adequate to support the points of interpretation to be made in the following discussion. Data on $Ca(NO_3)_2$ solutions obtained using an Industrial Instruments Inc. Model RC 18 bridge are internally consistent to better than 0.1% to the lowest values reported. For the $Mg(NO_3)_2$ solutions studied earlier[1] using a Phillips PR 9500 bridge, the internal precision for the measurements above 45° (cell constant 36.40), Table II, was 0.2%. Balance points below 45° (cell constant 1.56) were less well defined, and the accuracy and precision are lower.

Discussion

It is first of all important to establish that the electrolyte solution behavior described here is not peculiar to the two nitrates investigated. In Figure 3 we sum-

(28) (a) A. C. McGregory, *Wiedemann's Ann.*, **51**, 126 (1894); (b) H. Clausen, *Heydweiller's Ann.*, **4**, 37, 51, 739 (1912); (c) H. C. Jones and F. H. Getman, *Am. Chem. J.*, **31**, 303 (1904); (d) H. C. Jones and J. N. Pierce, *ibid.*, **38**, 683 (1907); (e) H. C. Jones and C. M. Stine, *ibid.*, **39**, 313 (1908). The results of these workers are tabulated in J. Timmermans, "Physico Chemical Constants of Binary Systems," Interscience Publishers, Inc., New York, N. Y., 1960, p 783.

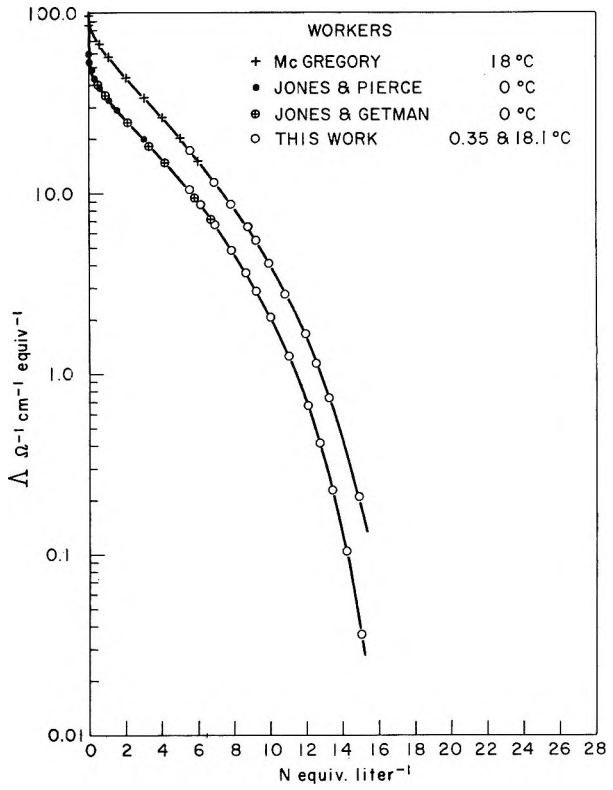

Figure 2. Dependence of equivalent conductance, Λ, of $Ca(NO_3)_2$ solutions on equivalent concentration, N, at 0.35 and 18.1°.

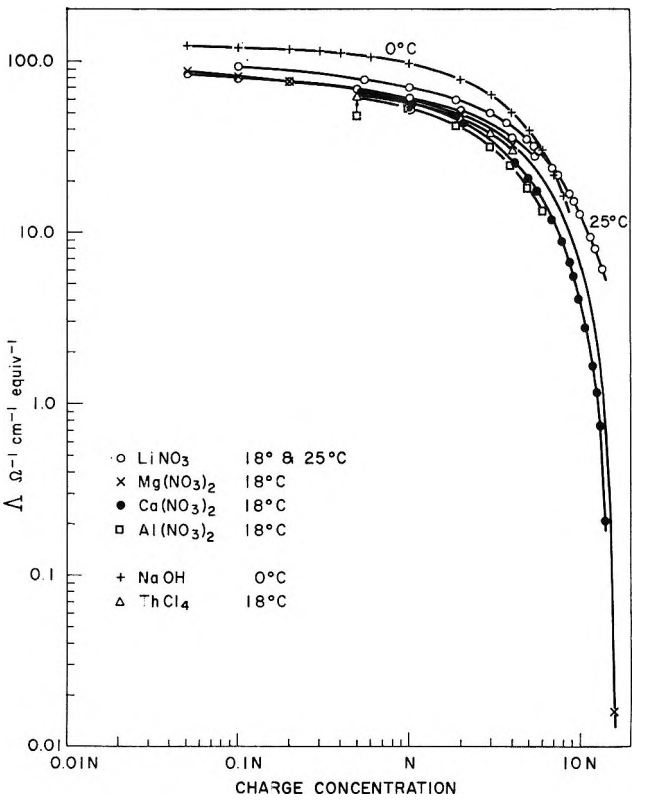

Figure 3. Equivalent conductance, Λ, of various solutions as a function of electrostatic charge concentration, N (equivalent concentration). Data for $LiNO_3$, $Ca(NO_3)_2$, $Mg(NO_3)_2$, $Al(NO_3)_3$, and $ThCl_4$ at 18° and NaOH at 0° taken from Timmermans, ref 28, and the present work. Data for $LiNO_3$ at 25° taken from ref 3.

marize on a log–log plot the conductance behavior of a number of electrolyte solutions[28] in the concentration range 0.01 to ~16 N. The plot emphasizes nitrate solutions but includes other salts to demonstrate the generality of the behavior. A plot of the same character may be drawn for electrolyte solution fluidities. On inclusion of the present results on $Ca(NO_3)_2$ and $Mg(NO_3)_2$ solutions it becomes apparent from Figure 3 that at 18° the mobility of the ionic species in any electrolyte solution tends rapidly to zero in the concentration region corresponding to 20–25 equiv $l.^{-1}$.

In principle, then, in the absence of crystallization *the fate of any electrolyte solution on sufficient concentration is to become a glass.* That this is not merely conjecture will be well known to anyone who has attempted to crystallize certain rare earth nitrates and halides by evaporation. The phenomenon of glass formation by evaporation of a solution is itself a familiar one, being the basis of the setting of most of the common household tube cements. In the general aqueous solution case, of course, crystallization will intercede before the glassy state can be realized; also it must be noted that solutions of most uni-univalent salts could never be obtained in the glassy state by concentration at room temperature because the glass transition temperature for the pure metastable liquid salt itself will lie below room temperature; *e.g.*, for KNO_3, $T_0 \approx 230°K$.[22] Owing to its importance in the later discussion, however, we wish to emphasize at this point that for the familiar salts of multivalent cations there exists a physically meaningful concentration for a given temperature at which the "solution" would lose its liquid character and become a glass. This concentration, which we will designate N_0, will be seen subsequently to fill a role in the interpretation of the isothermal composition dependence of electrolyte solution transport analogous to that of T_0 in the interpretation of the temperature dependence of transport for a given solution.

Because the interpretation will be based on the validity of eq 1 for the temperature dependence of conductance, it is first necessary to examine the application of this equation to the aqueous systems investigated in the present work.

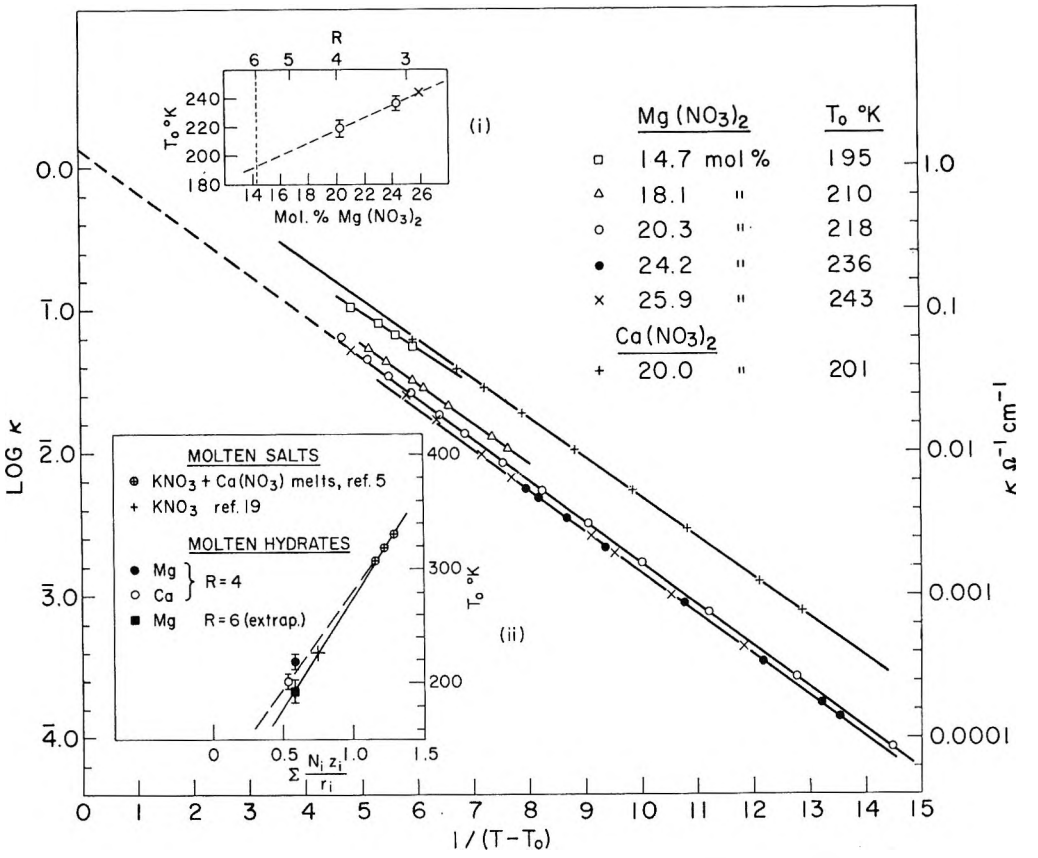

Figure 4. Plot of log κ *vs.* $1/(T - T_0)$ for $Mg(NO_3)_2$ and $Ca(NO_3)_2$ solutions. Inset i, plot of T_0 in relation to composition for $Mg(NO_3)_2$ solutions; inset ii, plot showing relation of T_0 to average cation potential for molten salts and salt solutions (compositions given in R units); dashed line taken from ref 7; solid line takes into account T_0 for KNO_3 obtained in ref 22.

Temperature Dependence of Conductance. According to eq 1 the curvilinear plots shown in Figure 1 should become straight lines when log κ is plotted against $1/(T - T_0)$ for the correct choice of T_0. Log κ *vs.* $1/(T - T_0)$ plots are shown in Figure 4, the choices of T_0 being given in the legend. Only for the compositions 20.3 and 24.9% $Mg(NO_3)_2$ (R = 3.9 and 3.0) and 20 mole % $Ca(NO_3)_2$ (R = 4) were the data extensive enough to obtain reliable values of T_0 by the fit to eq 1. These values are shown against composition in Figure 4, inset i: the remaining T_0 values employed were chosen to fall on this plot. The presence of the $T^{1/2}$ term in the preexponential of eq 1 could have been allowed for by plotting log $\kappa T^{1/2}$ *vs.* $1/(T - T_0)$. However the term has little influence on the linearity of the $1/(T - T_0)$ plots in the low-temperature region, and it has been ignored in Figure 4 in order to keep the comparison with Figure 1 as clear as possible. The Figure 4 plots are seen to be linear over the lower two and one-half orders of magnitude of κ, some deviation being apparent at high κ as observed previously for anhydrous molten nitrates.[7] For the compositions 20–25% $Mg(NO_3)_2$ (R = 4–3) where the data cover a wider temperature range the plots have the same slopes and almost coincide.

It must be recognized that this plot amounts to curve fitting by the introduction of a third adjustable parameter, and some success is therefore to be expected. To be convincing, not only is a theoretical justification required for the third parameter but some correlations resulting from its use need to be demonstrated. In the earlier investigation of pure fused-salt behavior[7] such a correlation was provided by the reduction of a mass of data covering a range of compositions and temperatures to virtually a single linear plot by the use of T_0 parameters which proved to be linearly related to composition and also to have the expected relation to the observed glass transition temperature. In the present case the results are not as satisfying since the adoption of T_0 values linearly related in mole % $Mg(NO_3)_2$ (within error also linearly related to equivalent concentration in the small composition range covered) does not reduce the data of Figure 1 to a single straight line.

On the positive side, however, besides the fact that data for the individual compositions spanning at least two orders of magnitude are consistent with eq 1, two additional observations may be made. (i) When allowance for the preexponential $T^{-1/2}$ is made, the slopes, k, of the linear plots are almost the same as the slope of the plot which correlated the anhydrous liquid nitrate conductance data.[7] The respective values of k are 670 and 690°K, the difference being within the uncertainty of the present determination. (ii) The T_0 values listed in the legend of Figure 4 are in the range to be expected from the anhydrous molten nitrate data if, as recent spectral studies[26] confirm, the water molecules are all bound to the dipositive cations. The basis for the latter point is the following. In the spectral studies the ligand field spectra of Ni^{2+} were used to show that Ni^{2+}, which normally hydrates strongly, is completely dehydrated in $MgCl_2$ solutions containing less than six H_2O molecules per Mg^{2+} ion. The water molecules in the composition region $R < 6$ are thus completely "tied up" by the Mg^{2+}. At $R = 6$ the coordination is undoubtedly octahedral (H_2O close packed) as in the crystalline hydrates, and a radius may therefore be assigned to the cation species $r_{Mg(H_2O)_6^{2+}} = r_{Mg^{2+}} + 2r_{H_2O} = 3.40$ A. Even if H_2O exchange among such cations is rapid, the properties of the liquid which depend on ionic potentials should be those of a molten nitrate. One therefore expects T_0, which has been correlated with cation potential (z_+/r_+) for anhydrous nitrates, to be predictable from z_+/r_+ of $Mg(H_2O)_6^{2+}$. According to Figure 4, inset i, T_0 at $R = 6$ is 193 ± 5°K, which does indeed fall squarely on the T_0 *vs.* cation potential plot for anhydrous molten nitrates (Figure 4, inset ii, solid line).[29] Since T_0, although obtained from the conductance data, is a constant of the material the above correlation does not necessarily mean that the mobile cation species is $Mg(H_2O)_6^{2+}$ but only means that the coulombic energy of the liquid is established by cations of this configuration.

Attempts to extend the interpretation in terms of distinct cation species to compositions with $R < 6$ meet with the unresolved difficulty of deciding how the water molecules are coordinated and how the effective cation potentials of different possible hydrated cation groups should be estimated. A more fruitful approach to describing the over-all transport behavior is outlined in the following section in which the concentration dependence of conductance is considered.

Concentration Dependence of Conductance. From the present data and those of Moynihan,[27] who has studied both viscosity and conductance, it appears that eq 1 gives a correct description of the temperature dependence of transport in molten hydrates. In view of its validity for other classes of liquids[12-14] it seems safe to assume its continuing validity for less concentrated aqueous solutions. Furthermore the constant k seems to be rather insensitive to the nature of the liquid being described; *e.g.*, for a variety of ionic liquids the value 680°K ± 5% seems to apply,[30] whereas for polymer[20] and hydrogen-bonded liquids reported values of k fall between 435 and 538°K.[10] The average value of 500 ± 25°K is only some 25% less than for ionic liquids. It appears then that large changes in transport properties as a function of composition should be attributable mainly to changes in T_0.

The magnitude of T_0 for liquids composed of simple particles is evidently some reflection of the cohesive energy of the liquid. This is implied by the correlation of T_0 with the cation potential for molten salts and also by the constancy on the reduced temperature scale of T_g for molecular liquids.[19,30a] For the case of solutions of nonassociating charged particles in a molecular solvent, the coulombic energy will be determined by the physical concentration of electrostatic charge so a correlation between T_0 and the conventional normality, N, of the solution might be anticipated. Sufficient data are not available at the moment to determine this dependence directly. We will therefore consider here only the simplest possible case.

Let it be supposed that k and A of eq 1 are composition invariant and T_0 is linearly dependent on the charge concentration, N. Then for a given concentration, N, T_0 of eq 1 is given by

$$T_{0(N)} = QN + T_{0(N=0)} \qquad (3)$$

where $T_{0(N=0)}$ is the value of T_0 at infinite dilution, *i.e.*, T_0 for the solvent. In the consideration of the *isothermal* composition dependence of Λ, T in eq 1 is constant. Recalling the initial discussion it is possible in principle to specify a limiting concentration, N_0, for which the value of T_0 becomes equal to the iso-

(29) In the original communication of these results,[21] before the detailed spectral information[26] or the independent estimate of T_0 for KNO_3[22] were available, we emphasized the $Mg(H_2O)_4^{2+}$ species. Although this was not as obvious a configuration to discuss as $Mg(H_2O)_6^{2+}$, not only could T_0 be obtained directly from the conductance data at the $R = 4$ composition (see Figure 4), but the T_0 values were in excellent agreement with the original extrapolation of the T_0 *vs.* cation potential plot (see Figure 4, inset ii, dashed plot).

(30) Moynihan's analysis for $Ca(NO_3)_2 \cdot 4H_2O$ indicates a value of k for conductance 8% lower than this figure. The lower value of k is not incompatible with the present result, however; it could be obtained by a change of only 2° in the value of T_0, which is within our uncertainty limits.

(30a) NOTE ADDED IN PROOF. It is not clear at the moment whether this is a result of a direct relation between T_0 and the cohesive energy or a consequence of changes in configurational freedom accompanying changes in cohesive energy.

thermal temperature T and the ionic mobility falls to zero. Using eq 3, T of eq 1 can therefore be replaced by $[QN_{0(T)} + T_{0(N=0)}]$.

Making these substitutions for T_0 and T in eq 1 one obtains the following expression for the isothermal conductance.

$$\Lambda_{(T)} = A_\Lambda \exp[-k/(QN_0 - QN)] = A_\Lambda \exp[(-k/Q)/(N_0 - N)] \quad (4)$$

Note that $T_{0(N=0)}$ of eq 3 drops out so that the question of alterations in specific solvent structure of low salt concentrations does not arise.

This simple treatment therefore suggests that the function $1/(N_0 - N)$ may serve to straighten out the log Λ *vs.* N plots of Figure 2 in the same way that the $1/(T - T_0)$ function straightened out the log Λ *vs.* $1/T$ plots (see Figures 1 and 4). The use of the function is subject to the same criticism noted before, *viz.*, that it employs an additional parameter (N_0) to eliminate the curvature present in the two-parameter plot. Again the use of a third parameter will only seem convincing if, besides an adequate theoretical justification, the parameter proves to have a reasonable numerical value and the treatment leads to useful, otherwise unobvious correlations.

In Figure 5 it is shown that the function $1/(N_0 - N)$ is indeed capable of yielding a linear relation between Λ and concentration. At 0° the linearity extends over about three orders of magnitude in Λ in the concentration range ~2–15 N. The value of N_0 giving the best linear plot at 0°, N_0 = 22.7 equiv/l., is quite reasonable since the anhydrous nitrate melt, 80% KNO_3–20% $Ca(NO_3)_2$, for which T_0 = 5°,[8] has a charge concentration $N \approx 22$ (if density data above 300°[31] may be extrapolated to low temperatures).[32] The slope of the 0° plot, 33.8 equiv^{-1} l., also seems very reasonable in that it leads to a value of Q in good agreement with that expected from the value of N_0 and the value of T_0 obtained at the composition R = 4 (see Figure 4). From the slope of the Figure 5 plot $Q = k/(2.303 \times 33.8)$ = 8.8° equiv^{-1} l. using k = 680°K. On the other hand, at the concentration N_0 = 22.7 equiv l.$^{-1}$, the derivation of eq 4 requires T_0 = 273°K; also T_0 = 201°K at R = 4 (where $N_{(201°K)}$ = 15.6 equiv l.$^{-1}$) whence $Q = (273 - 201)/(22.7 - 15.6)$ = 10.2° equiv^{-1} l. Both values of Q are close to the value of ~9° equiv^{-1} l. estimated for $Mg(NO_3)_2$ solutions from Figure 4, inset i using approximate interpolated values of N.

It would be remarkable indeed if such simple considerations could provide a complete account of the isothermal composition dependence of conductance in such concentrated solutions, and it is not too surprising to find, from the consideration of temperature effects, that the assumption of composition-invariant values of k, A, and Q cannot be wholly correct. For instance, if Q is 8.8° equiv^{-1} l.$^{-1}$, then according to eq 4 the $1/(N_0 - N)$ plot for the 18° isotherm of Figure 2 should coincide with the 0° plot if N_0 (18°) is taken 18/8.8 = 2.05 equiv l.$^{-1}$ greater than the value of N_0 used at 0°. This plot is shown as a dashed line in Figure 5 and it is seen that the plots do not superimpose, although the separation is not great. Thus the simple treatment, while obviously having qualitative merit, needs some refinement (as had to be expected, *e.g.*, from Figure 4). It is worth noting that if N_0 (18°) is taken as 24.1 instead of 24.75 equiv l.$^{-1}$, the plot coincides with the 0° plot over most of the composition range (Figure 5). The coincidence

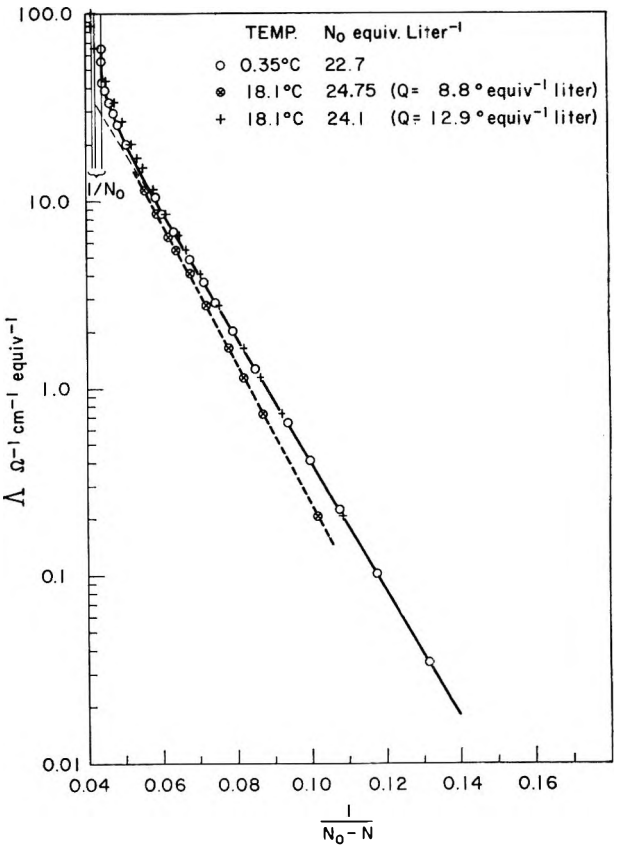

Figure 5. Dependence of equivalent conductance, Λ, of $Ca(NO_3)_2$ solutions on $1/(N_0 - N)$ at 0.35 and 18.1°.

(31) E. Rhodes, W. E. Smith, and A. R. Ubbelohde, *Proc. Roy. Soc.* (London), **A289**, 151 (1966).

(32) This statement is not meant to imply that T_0 values for pure fused salts are determined solely by charge concentration, although it is expected that this will be an important factor.

would not be affected noticeably (~3%) by the presence of a preexponential $T^{-1/2}$ term in eq 4.

Fortunately the assumptions leading to eq 4 can be checked in detail and modified by experimental measurements. $Ca(NO_3)_2$–H_2O solutions in a range of compositions from $R \sim 4$–10 can be readily supercooled so direct determination of the parameters k and T_0 by analysis of the transport temperature dependence should be possible and their concentration dependence determined. Beyond noting that k and Q probably remain proportional rather than constant with changing composition, we shall not attempt to anticipate the results of such studies. On the substitution of $\kappa = \Lambda N \times 10^{-3}$, eq 4 also directly predicts the maximum in specific conductance, κ, observed in aqueous solutions at 4–8 N.

To summarize, this paper presents a simple model for the conductance of concentrated electrolyte solutions in which both the composition and temperature dependence of the conductance process are considered to be determined mainly by changes in the configurational entropy content, S_c, or the related free volume of the liquid. By considering only the dependence of the zero entropy temperature on charge concentration a qualitative account of the transport behavior is possible in terms which are simpler in many ways than those employed in conventional hydrodynamic approaches. The approach has the additional advantage of interpreting the composition dependence of viscosities of concentrated solutions.[8a] Further development of the model must await more accurate and comprehensive studies on suitable systems.

Regardless of such refinements the treatment cannot achieve the status of a theory of concentrated aqueous solution transport without an adequate theory for k and T. The theories of Adam and Gibbs[10] and Gibbs and Dimarzio[33] supply this requirement for transport in liquid polymers, but while the Adam–Gibbs theory for k may be adopted essentially unchanged for ionic liquids, the theory for T_0 in which the molecular chain stiffness and chain length are the most important parameters[33] is not directly applicable.

For systems of essentially simple particles it may be observed that T_0 should be realized at the point where the continued thermal contraction of the liquid has brought the assembly of particles to a condition of random close packing of the Bernal[17] or Alder–Wainwright[16] type. However the problem of what determines T_0 is probably more usefully approached from the other side by asking the question: why should an amorphous but essentially close-packed system of particles commence to exchange vibrational for configurational degrees of freedom at T_0? The free volume model of Turnbull and Cohen suggests that the answer lies in the shape of the intermolecular potential function. A more complete answer may well emerge from a detailed examination of the glass-state vibrational frequency spectra of simply constituted amorphous systems, among which certain of the glasses derived from mixtures of simple fused salts may be the best examples.

As a final remark we consider such insight into concentrated solution behavior as may be provided by eq 1 and 4 to stand in support of the case recently argued[8] concerning the importance of information from the metastable supercooled liquid region to furthering understanding of general liquid behavior.

Experimental Section

The simplified techniques which have sufficed to obtain the accuracy required for these exploratory measurements have been described previously.[22] Most of the data were obtained using dip-type capillary cells of constants 630.8, 61.56, and 36.40. Some additional measurements at very low conductivity values were obtained using a standard-type cell of constant 1.56. In the measurements on $Mg(NO_3)_2$ solutions a Phillips PR 9500 conductance bridge was used to balance the cell resistance against an external resistance determined using precision decade boxes. Under these conditions the stated accuracy of the bridge is 0.2%. For $Ca(NO_3)_2$ solutions the resistance was measured directly using a 0.1% Industrial Instruments Inc. Model RC 18 bridge.

For the $Mg(NO_3)_2$ experiments the fused Analar grade hexahydrated salt (mp 89.9°) was used as starting material. To obtain the higher concentrations water was removed by ebullition under reduced pressure. Samples for analysis were taken at the end of each conductance *vs.* temperature run. A detectable amount of HNO_3 was lost in the production of the 25.9% $Mg(NO_3)_2$ composition.

For measurements on $Ca(NO_3)_2$ solutions the fused tetrahydrate, mp 43.5°, was used as starting material. Changes in compositions, in this case to lower water contents, were made by additions of doubly distilled water from a buret. Conductivity water is, of course, unnecessary at the high concentrations studied.

Acknowledgments. Much of the work reported here was performed while the author was at the Department of Metallurgy, University of Melbourne, Australia; thanks are due to Professors H. W. Worner and G. M.

(33) J. H. Gibbs and E. A. Dimarzio, *J. Chem. Phys.*, 28, 373 (1958).

Willis for their interest in the project and to Mr. B. D. Guerin for performing the analyses of the $Mg(NO_3)_2$ solutions. The author is also indebted to Dr. D. M. Gruen of the Chemistry Division, Argonne National Laboratory, in whose laboratory the necessary measurements were completed.

Transport Properties of the Tetraethanolammonium Ion in Nonaqueous Solvents at 10 and 25°

by G. P. Cunningham, D. F. Evans, and Robert L. Kay[1]

Mellon Institute, Pittsburgh, Pennsylvania 15213 *(Received July 18, 1966)*

Precise conductance measurements are presented for $(EtOH)_4NI$ in methanol and acetonitrile at 10 and 25°, $(EtOH)_4NBr$ in methanol at 25°, and tetraethanolammonium tetraphenylboride $[(EtOH)_4NBPh_4]$ in acetonitrile at 25°. $(EtOH)_4NI$ in aqueous solutions at 10° was also measured in order to extend the known temperature coefficient over a larger temperature range. The halides are only slightly associated in methanol but considerably associated in acetonitrile, owing to the difference in the acid–base properties of these two solvents and the possibility of hydrogen bonding of the $(EtOH)_4N^+$ ion to a halide anion. The small interaction of this large cation with acetonitrile as compared to that with methanol is reflected in the limiting ionic mobilities. A comparison of the limiting conductance–viscosity products for the $(EtOH)_4N^+$ ion in nonaqueous solvents with those for aqueous solution at different temperatures verifies the conclusion arrived at from previous measurements that this ion does not enforce water structure in aqueous solutions as is the case with its alkyl analog, the Pr_4N^+ ion. In contrast, there is some evidence that the $(EtOH)_4N^+$ ion has considerable structure-breaking powers in aqueous solution.

Introduction

Considerable interest has been generated in the properties of the tetraethanolammonium ion[2] owing to its normal behavior in aqueous solution in contrast to what has been considered abnormal behavior exhibited by its alkyl analog, the tetrapropylammonium ion.[3-6] The concentration dependence of partial molar volumes[3] heats of dilution,[4] and viscosity[6] for the tetraalkylammonium ions can only be explained by appealing to the effect of these large hydrophobic ions on water structure. The available evidence indicates that water structure enforcement occurs around the inert hydrocarbon side chains of these ions. However, the effects attributable to such water-structure enforcement are not observed in similar data for the $(EtOH)_4N^+$ ion, so that it would appear that the introduction of a terminal polar group into the otherwise inert side chains is sufficient to disrupt the increased degree of hydrogen bonding normally found around the alkyl analog of this ion.

(1) To whom all correspondence is to be addressed.

(2) (a) W. Y. Wen and S. Saito, *J. Phys. Chem.*, **69**, 3569 (1965); (b) D. F. Evans, G. P. Cunningham, and R. L. Kay, *ibid.*, **70**, 2974 (1966).

(3) W. Y. Wen and S. Saito, *ibid.*, **68**, 2631 (1964).

(4) S. Lindenbaum, *ibid.*, **70**, 814 (1966).

(5) R. L. Kay and D. F. Evans, *ibid.*, **70**, 2325 (1966).

(6) R. L. Kay, T. Vituccio, C. Zawoyski, and D. F. Evans, *ibid.*, **70**, 2336 (1966).

This result is particularly evident when the limiting mobilities and their temperature dependence for aqueous solutions of the tetraalkylammonium ions are compared to those for the $(EtOH)_4N^+$ ion.[2b] A further criterion that has been found useful in elucidating water-structural effects in the case of the tetraalkylammonium salts was the comparison of limiting mobilities in aqueous and nonaqueous solvents.[5] Here we report limiting ionic mobilities for the tetraethanolammonium halides in methanol and acetonitrile with the temperature dependence included for methanol solutions. The results support the conclusion already arrived at from a consideration of the data for aqueous solutions alone. Furthermore, the polyfunctional nature of the $(EtOH)_4N^+$ ion gives rise to a variety of possibilities as far as solute–solvent interactions are concerned, depending on the particular properties of the solvent. In solvents that can act as good acceptors and donors (water and methanol), this ion is strongly solvated, whereas in solvents with poor acid–base properties (acetonitrile) this ion is poorly solvated and is stabilized most readily by hydrogen bonding to the anion to form an ion pair.

Experimental Section

All electrical equipment, cells, salt cup dispensing device, and general techniques for the conductance measurements were the same as those previously described.[7,8] The method used to overcome the problems encountered in handling a salt as hygroscopic as $(EtOH)_4NBr$ has been outlined in detail.[2] The conductance baths were set at 10 and 25° within 0.003° with a calibrated platinum resistance thermometer. The change of cell constant with temperature was calculated to be less than 0.01% and therefore negligible.

The viscosity measurements were carried out using a suspended-level Ubbelhode-type viscometer[9] with a flow time of approximately 500 sec for H_2O at 25°. No kinetic energy correction was found necessary at either temperature. The experimental techniques were the same as previously described.[6]

The preparation and purification of $(EtOH)_4NBr$ and $(EtOH)_4NI$ have been described.[2b] The measurements described here were carried out at the same time as those for aqueous solution[2b] using the same salt samples, thereby introducing no new variable. $(EtOH)_4NBPh_4$ was prepared by mixing equimolar aqueous solutions of $(EtOH)_4NBr$ and $NaBPh_4$. The resulting precipitate was recrystallized only once with difficulty from acetone–water and finally dried in a vacuum oven at 50° for 12 hr. From previous experience, we have found this is not the best method for the preparation of a pure salt, owing to the possibility of coprecipitation. However, for the purpose for which this salt was used, the salt purity proved adequate.

The details describing the purification of the water,[10] methanol,[11] and acetonitrile[8] have been adequately covered in previous papers. Briefly, conductivity water was obtained by passing distilled water through a mixed-bed ion exchanger. Reagent grade methanol was passed through a water-free mixed-bed ion exchanger and fractionally distilled under nitrogen. Reagent grade acetonitrile was prepared by the Coetzee method.[12]

Results

The density increments for the volume concentrations and viscosity measurements were obtained by direct measurements on 0.1 M solutions of $(EtOH)_4NBr$ in methanol at 25 and 45°. The θ value in the density equation, $d = d_0 + \theta\bar{m}$, where $\bar{m}$ is the concentration in moles per kilogram of solution, was equal to 0.12 at both temperatures, as was the case with aqueous solutions.[5] The θ value for the iodide in methanol solution was assumed to be 0.13 in keeping with the I − Br difference found previously for the quaternary salts.[11] The θ values for acetonitrile solutions were assumed to be approximately the same as those for methanol in keeping with previous experience.[8,11] Cunningham has shown that the tetraphenylboride ion has about the same density increment as the iodide ion.[13]

The viscosity data for $(EtOH)_4NBr$ in methanol are plotted in Figure 1 and can be seen to conform to the Jones–Dole equation[14]

$$\psi/C^{1/2} = A + BC^{1/2} \qquad (1)$$

where $\psi = \eta/\eta_0 - 1$. A straight line through the points gives an intercept A in good agreement with the Falkenhagen theoretical value[15] of 0.02. It should be noted that $B = 0.98 \pm 0.05$ is the same at

(7) J. L. Hawes and R. L. Kay, *J. Phys. Chem.*, **69**, 2787 (1965).

(8) D. F. Evans, C. Zawoyski, and R. L. Kay, *ibid.*, **69**, 3878 (1965).

(9) Cannon Instrument Co., State College, Pa.

(10) D. F. Evans and R. L. Kay, *J. Phys. Chem.*, **70**, 366 (1966).

(11) R. L. Kay, C. Zawoyski, and D. F. Evans, *ibid.*, **69**, 4208 (1966).

(12) J. F. Coetzee, G. P. Cunningham, D. K. McGuire, and G. P. Padmanabhan, *Anal. Chem.*, **34**, 1139 (1962).

(13) G. P. Cunningham, Ph.D. Thesis, University of Pittsburgh, 1964.

(14) G. Jones and M. Dole, *J. Am. Chem. Soc.*, **51**, 2950 (1929).

(15) H. Harned and B. B. Owens, "The Physical Chemistry of Electrolyte Solutions," 3rd ed, Reinhold Publishing Corp., New York, N. Y., 1958, p 240.

Table I: Equivalent Conductances

10^4C	Λ	10^4C	Λ	10^4C	Λ
		CH_3OH			
$(EtOH)_4NI$, 10°		$(EtOH)_4NI$, 25°		$(EtOH)_4NBr$, 25°	
$10^8\kappa_0 = 1.1$		$10^8\kappa_0 = 2.6$		$10^8\kappa_0 = 2.7$	
5.971	75.56	5.853	93.15	6.769	87.21
10.168	73.95	10.607	91.16	13.775	84.16
14.564	72.60	16.574	88.92	22.013	81.61
20.710	71.05	21.794	87.34	29.243	79.82
25.938	69.94	25.569	86.32	34.394	78.72
30.614	69.06	30.195	85.21	41.074	77.43
35.462	68.23	34.402	84.28		
		40.005	83.15		
$10^8\kappa_0 = 1.0$		$10^8\kappa_0 = 2.1$		$10^8\kappa_0 = 2.6$	
4.205	76.58	5.213	93.79	7.544	86.78
8.336	74.71	10.607	91.08	14.457	83.95
13.696	72.95	15.472	89.20	21.844	81.67
19.258	71.49	19.815	87.81	28.830	79.92
22.911	70.67	23.974	86.64	35.865	78.45
28.519	69.54	29.017	85.37	45.256	76.71
32.575	68.79	34.518	84.15	52.369	75.56
		40.578	82.94	61.692	74.20
		CH_3CN		H_2O	
$(EtOH)_4NI$, 10°		$(EtOH)_4NI$, 25°		$(EtOH)_4NI$, 10°	
$10^8\kappa_0 = 3.4$		$10^8\kappa_0 = 1.7$		$10^7\kappa_0 = 0.80$	
7.091	124.18	5.110	148.75	5.005	72.40
12.570	116.66	9.581	140.34	11.833	71.62
18.080	110.80	14.319	133.42	17.941	71.12
23.391	106.15	19.691	127.13	23.687	70.70
28.809	102.11	23.937	122.91	29.749	70.31
34.196	98.66	29.709	117.95		
40.708	94.99	34.620	114.30		
		39.478	111.06		
$(EtOH)_4NI$, 25°		$(EtOH)_4NBPh_4$, 25°			
$10^8\kappa_0 = 1.9$		$10^8\kappa_0 = 1.7$			
4.879	149.65	4.632	115.52		
9.115	141.46	12.948	111.54		
14.282	133.86	17.461	110.04		
19.430	127.91	21.806	108.82		
24.385	123.03	26.528	107.66		
28.620	119.38	30.410	106.81		
33.754	115.47	34.932	105.91		
39.236	111.75				

both temperatures, as was the case with aqueous solutions of this salt.[2b]

The measured equivalent conductances and corresponding concentrations in moles per liter of solution are given in Table I along with κ_0, the solvent specific conductance.

The conductance parameters given in Table III were obtained from the Fuoss–Onsager conductance equation[16] for associated electrolytes

$$\Lambda = \Lambda_0 - S(C\gamma)^{1/2} + EC\gamma \log C\gamma + (J - B\Lambda_0)C\gamma - K_A C\gamma\Lambda f^2 \quad (2)$$

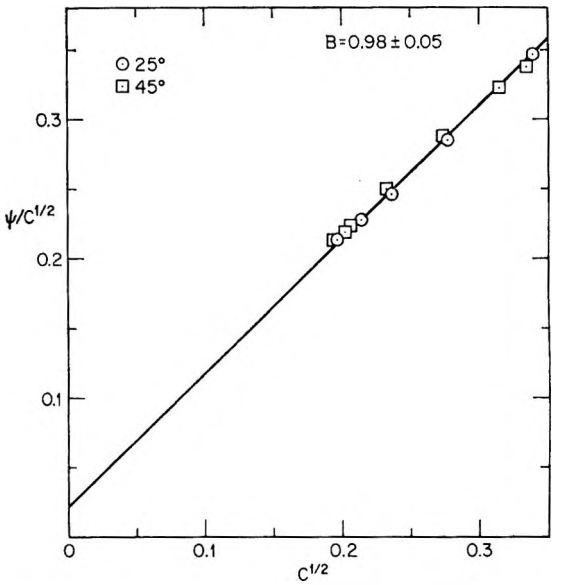

Figure 1. Plot of the Jones–Dole viscosity equation (eq 1) for $(EtOH)_4NBr$ in methanol at 25 and 45°.

using a least-squares computer analysis.[7] The dielectric constants, viscosities (poise) and densities (g ml^{-1}) of the solvents at the two temperatures are collected in Table II from the various sources cited. Only the data for acetonitrile at 10° were measured in this research using methods already described.[8]

Of the three parameters in eq 2, the value of the viscosity B coefficient used affects only the ion-size parameter $\mathring{a}$, and then only slightly. A 10% change in B changes $\mathring{a}$ by only 0.03 for both methanol and acetonitrile solutions. Consequently, $B = 0.98$ was

Table II: Solvent Properties

Solvent	Temp, °C	ϵ	$10^2\eta_0$	d_0
H_2O[5]	10	83.96	1.306	0.99973
CH_3OH[11]	10	35.70	0.672	0.80073
CH_3OH[11]	25	32.62	0.5445	0.78658
CH_3CN	10	38.34	0.397	0.7927
CH_3CN[8]	25	36.02	0.341[a]	0.7766

[a] This value of the viscosity was used in the calculation of limiting ionic conductance–viscosity products. However, in order to be consistent with previous calculations,[8] the somewhat higher value of 0.3448 cp was used in eq 2 for the evaluation of the conductance parameters. Separate calculations have shown that changes of this magnitude in the solvent viscosity result in negligible changes in the conductance parameters.

(16) R. M. Fuoss and F. Accascina, "Electrolytic Conductance," Interscience Publishers, Inc., New York, N. Y., 1959.

Table III: Conductance Parameters for Tetraethanolammonium Salts

Temp, °C	Salt	Λ_0	$\mathring{a}$	K_A	$\sigma\Lambda$	λ_0
			CH_3OH			
10	$(EtOH)_4NI$	80.64 ± 0.01	3.76 ± 0.09	9.9 ± 0.5	0.004	29.7
		80.88 ± 0.02	4.9 ± 0.3	16.4 ± 1.3	0.01	30.0
25	$(EtOH)_4NBr$	94.08 ± 0.04	4.5 ± 0.3	16 ± 2	0.02	37.6
		93.93 ± 0.04	3.7 ± 0.1	10 ± 1	0.02	37.5
25	$(EtOH)_4NI$	100.00 ± 0.02	4.1 ± 0.1	12.4 ± 0.8	0.01	37.2
		99.91 ± 0.01	4.0 ± 0.07	12.3 ± 0.4	0.006	37.1
			CH_3CN			
10	$(EtOH)_4I$	142.20 ± 0.04	1.61 ± 0.09	136.2 ± 0.9	0.01	
25	$(EtOH)_4I$	166.2 ± 0.1	1.9 ± 0.4	142 ± 3	0.07	63.5
		165.91 ± 0.03	1.6 ± 0.8	143 ± 0.7	0.01	63.2
25	$(EtOH)_4NBPh_4$	122.33 ± 0.05	5.26 ± 0.07	0.0	0.05	64.2
			H_2O			
10	$(EtOH)_4NI$	73.74 ± 0.008	(0.30 ± 0.04)		0.006	18.35

used for both salts in methanol and the somewhat lower value $B = 0.8$, for acetonitrile solutions.[8]

Since eq 2 gave small negative association constants for $(EtOH)_4NBPh_4$, this salt was considered completely dissociated. The conductance parameters were obtained by setting $\gamma = 1$ and $K_A = 0$ in eq 2.

Included in Table III are data for $(EtOH)_4NI$ in aqueous solution at 10° that complement the previous results[2] for this salt in H_2O at 25 and 45°.

The anion limiting conductances required for the cation values given in the last column of Table III were obtained in various ways. The values for methanol at 25° were taken from a compilation by Kay and Evans[5] that is based on precise transference data.[17] The value $\lambda_0(I^-) = 50.9$ for methanol solution at 10° is based on transference and conductance data recently obtained in this laboratory.[18] For acetonitrile at 25°, the value of $\lambda_0(I^-) = 102.7$ is based[5] on the assumption that both ions of i-$Am_3BuNBPh_4$ have the same limiting conductance.[19] Neither transference numbers nor conductance data on a salt of two large ions are available at the present time for acetonitrile at 10°.

The value of $\lambda_0[(EtOH)_4N^+] = 37.3 \pm 0.2$ for methanol at 25° as obtained from the bromides and iodides shows the typically lower precision to be expected if one salt is highly hygroscopic. For acetonitrile solutions, the agreement in the value of $\lambda_0[(EtOH)_4N^+] = 63.3$ as obtained from the iodide is in poor agreement with the value 64.2 obtained from the tetraphenylboride, a result we attribute to the difficulty encountered in the preparation and purification of the tetraphenylboride salt.

Discussion

The ion-size parameters, $\mathring{a}$, given in Table II for the tetraethanolammonium salts in methanol are in good agreement with the value 3.8 obtained for the tetraalkylammonium halides in methanol[11] at 10 and 25°, acetonitrile[8] and nitromethane[20] at 25°. The small departures from this value could be attributed to the difficulty of splitting the last two terms of eq 2 in obtaining $\mathring{a}$ and K_A. We do not consider the magnitude of the association constants for $(EtOH)_4N$ halides in methanol to be significantly different from those obtained for the tetrapropylammonium halides[11] in the same solvent (K_A = 5–17). Association constants of the magnitude obtained here correspond to about 3% association into pairs at 5×10^{-3} M. Large uncertainties are to be expected in the absolute value of association constants of this magnitude since these salts do not have the stability of the quaternary ammonium or alkali metal halides, and furthermore they are hygroscopic. From these results we have concluded that the tetraethanolammonium salts in methanol at 10 and 25° have the same concentration dependence to a first approximation as the quaternary ammonium salts.

In contrast to methanol, these halides are considerably associated in acetonitrile. The iodide has

(17) J. A. Davies, R. L. Kay, and A. R. Gordon, *J. Chem. Phys.*, **19**, 749 (1951).

(18) G. A. Vidulich, G. P. Cunningham, and R. L. Kay, to be published.

(19) M. A. Coplan and R. M. Fuoss, *J. Phys. Chem.*, **68**, 1181 (1964).

(20) R. L. Kay, S. C. Blum, and H. I. Schiff, *ibid.*, **67**, 1223 (1963).

an association constant of about 140 with little dependence on temperature. Measurements were carried out on $(EtOH)_4NBr$ in acetonitrile at 25°, but the rate of solution of this salt was so slow that data at only three concentrations could be obtained, and those were of limited precision. Although it was not possible to obtain an accurate value of Λ_0, a good estimate of $K_A = 1 \times 10^3 \pm 10\%$ was obtained from a Shedlovsky plot. On a size basis, the association of the bromide should be no greater than 10% above that of the iodide rather than almost seven times greater as is the case in acetonitrile. In contrast, the alkyl analogs of these salts, namely, Pr_4NI and Pr_4NBr, are essentially unassociated in acetonitrile (K_A = 3–5).[8] Since ions of the same size as the tetraethanolammonium halides are not significantly associated, the large association of the tetraethanolammonium halides is not entirely coulombic in origin. Furthermore, if at all, solvation would tend to stabilize the $(EtOH)_4N^+$ ion rather than the tetraalkylammonium ions. It is clear that a different effect is stabilizing the tetraethanolammonium ion pairs in acetonitrile solution. The most likely explanation is a stabilization of the ion pairs by an acid–base interaction between the protons of the hydroxyl groups on the cation and the unsolvated anion to form a hydrogen bond. This type of ion pairing was used by Taylor and Kraus[21] to explain the high degree of association of the picrates of hydroxyl-substituted quaternary ammonium cations, $K_A[(CH_3)_3(OH)NPi] = 6 \times 10^4$ and $K_A[(CH_3)_3(EtOH)NPi] = 140$, compared to the symmetrical tetraalkylammonium cation, $K_A[(CH_3)_4NPi] = 24$, in nitrobenzene, a solvent comparable to acetonitrile in dielectric constant and acid–base properties. Acetonitrile is an exceedingly weak acid and base,[22] and consequently only weakly solvates the anions and the terminal hydroxyl groups of the cation. Ionic charge–solvent dipole interaction is also weak because of the relatively large sizes of these ions. On the other hand, methanol has much stronger acid and base properties and solvates both the anions and the terminal hydroxyl groups of the tetraethanolammonium ion readily. Consequently, this stabilization of the free ions by solvation in methanol solution accounts for the low degree of association found here for the tetraethanolammonium halides in that solvent. The high degree of solvation of $(EtOH)_4NBr$ by methanol is also reflected in the high-viscosity B coefficient of 0.98 compared to 0.67 for its alkyl analog, Pr_4NBr, in methanol.[6] Furthermore, it is likely that the poor base properties of the tetraphenylboride ion as well as its large size contribute to the complete dissociation of $(EtOH)_4NBPh_4$ in acetonitrile.

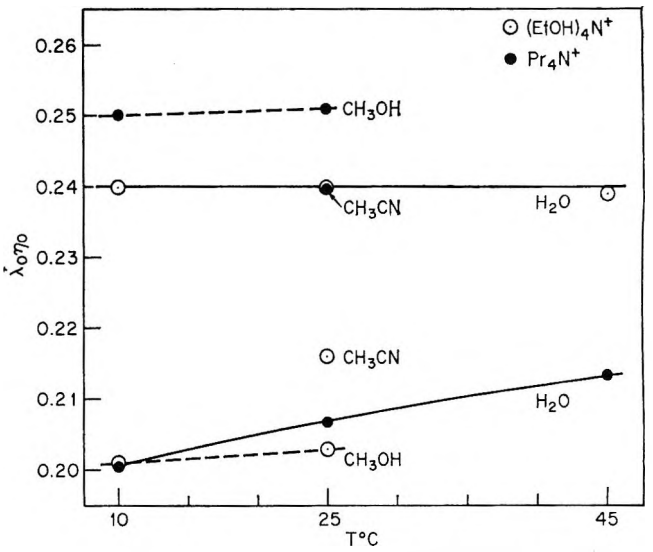

Figure 2. Limiting conductance–viscosity products for the $(EtOH)_4N^+$ ion (⊙) and its alkyl analog, the Pr_4N^+ ion (●) in aqueous, ———, and methanol, - - - -, solutions as a function of temperature. Data for acetonitrile are also included at 25°.

The $\lambda_0\eta_0$ product for the $(EtOH)_4N^+$ ion in these nonaqueous solvents substantiates these conclusions as well as those that have been made concerning the properties of this ion in aqueous solutions.[2b] The data for this ion as well as those for its alkyl analog, the Pr_4N^+ ion, are collected from various sources in Table IV and are shown in Figure 2 as a function of temperature. The point reported here for aqueous solutions at 10° is in good agreement with the near-zero temperature coefficient found previously for this ion.[2b]

The much lower values of $\lambda_0\eta_0$ for the Pr_4N^+ ion in water compared to those for that ion in methanol

Table IV: Limiting Ionic Conductance–Solvent Viscosity Products

Solvent	Temp, °C	$(EtOH)_4N^+$ $\lambda_0\eta_0$	Pr_4N^+ $\lambda_0\eta_0$
H_2O	10	0.240	0.2005
	25	0.240	0.2067
	45	0.239	0.2134
CH_3OH	10	0.201	0.2500
	25	0.203	0.2509
CH_3CN	25	0.216	0.240

(21) E. G. Taylor and C. A. Kraus, *J. Am. Chem. Soc.*, 69, 1731 (1947).

(22) J. Coetzee in "Progress in Physical Organic Chemistry," A. Streitwieser and R. Taft, Ed., Interscience Publishers, Inc., New York, N. Y., 1966.

have been interpreted as indicating a considerable amount of water-structure enforcement around that ion in aqueous solution.[5] Furthermore, the relatively large positive temperature coefficient of $\lambda_0\eta_0$ for the Pr_4N^+ ion in aqueous solutions as compared to that for methanol solutions has been shown to be added evidence for water-structure enforcement about the hydrocarbon side chains of this hydrophobic ion.[5] By inserting a dipole moment into the side chains by the replacement of a terminal methyl by a hydroxyl group to form the $(EtOH)_4N^+$ ion, the mobility in aqueous solution increases and becomes comparable to that for its analog, the Pr_4N^+ ion, in both methanol and acetonitrile, solvents in which three-dimensional structures are not possible. In other words, the inclusion of the hydroxyl group in the side chain has sufficient orienting influence on the water dipoles so as to interfere with the enforcement of water structure around this ion. In methanol, however, the $(EtOH)_4N^+$ ion appears to be considerably solvated, and slower as seen by the low value of $\lambda_0\eta_0$ as compared to that for aqueous solution and by its slightly positive temperature coefficient. This is in agreement with the predictions made above from the association behavior of this ion in methanol. Also, in acetonitrile, the mobility is higher, indicating less solvation, a conclusion also in agreement with the association behavior. It would be interesting to verify this conclusion by the temperature coefficient of the $\lambda_0\eta_0$ product for this ion in acetonitrile, but lack of transference data does not permit this. However, the $\Lambda_0\eta_0$ for the iodide salt gives 0.565 and 0.566 at 10 and 25°, respectively, indicating very little temperature dependence.

It would appear that one inconsistency remains. The $\lambda_0\eta_0$ product for the $(EtOH)_4N^+$ ion in aqueous solutions is higher than in acetonitrile although this ion must be solvated to a greater extent in water than in acetonitrile. This problem can be resolved by assuming this large ion to be a good structure-breaker in aqueous solution and therefore exhibits some excess mobility in aqueous solution owing to its ability to break water structure in its cosphere. The lack of a pronounced temperature dependence for the $(EtOH)_4N^+$ ion in aqueous solution could then be the result of the negative temperature coefficient characteristic of structure breakers and a positive component due to the tendency of the hydroxyl groups to be solvated more extensively with water molecules at lower temperatures.

The results obtained here add considerably to the reliance to be placed on the criteria we have developed[5] for the detection of the effect of solvent structure on the transport properties of electrolytes. These criteria are based on a comparison of both the magnitude of the transport properties and their temperature coefficients in aqueous and nonaqueous solvents. In particular, the use of the limiting ionic conductance–viscosity product has in many cases been quite conclusive and certainly refutes the claims made in a recent discussion[23] concerning the usefulness of Stokes' law.

Acknowledgment. This work was supported by Contract 14-01-0001-359 with the Office of Saline Water, U. S. Department of the Interior.

(23) B. E. Conway and R. G. Barrados, Ed., "Chemical Physics of Ionic Solutions," John Wiley and Sons, Inc., New York, N. Y., 1966 p 576.

Molecular Characterization of Polychloroprene in a θ Solvent

by K. Hanafusa,[1] A. Teramoto, and H. Fujita

Department of Polymer Science, Osaka University, Toyonaka, Japan *(Received July 18, 1966)*

From light-scattering and osmotic-pressure measurements, it was found that methyl ethyl ketone (MEK) is capable of bringing M-40 polychloroprene (equivalent to the familiar Neoprene W) to the unperturbed state at 25°. This is a first record of the θ solvent for polychloroprene. The temperature dependence of A_2 (second virial coefficient) near the θ point was as small as $\pm 1 \times 10^{-6}$ mole ml g^{-2} deg^{-1} or less, giving about 0.05 for the entropy parameter ψ_1 in the Flory theory of polymer solutions. This small value of ψ_1 is shown to explain the observation that MEK solutions of polychloroprene caused no phase separation even in a freezer (−20°). Measurements of limiting viscosity numbers $[\eta]$ of M-40 polychloroprene fractions covering the range of weight-average molecular weight $\bar{M}_w$ from 6 to 70 $\times 10^4$ yielded the following relation: $[\eta]^{25}_{MEK} = (1.16 \times 10^{-3})\bar{M}_w^{0.5}$, where $[\eta]$ is expressed in dl/g. Relations between $[\eta]$ and $\bar{M}_w$ were also obtained in benzene at 25° and in cyclohexane at 45.5°. The latter solvent was found from phase-separation experiments to act as another θ solvent for the polymer concerned. In MEK at 25° the limiting sedimentation coefficient s_0 (in seconds) varied with $\bar{M}_w$ following the relation: $s_0 = (3.10 \times 10^{-15})\bar{M}_w^{0.5}$.

Introduction

In previous papers[2-4] we have reported dilute solution properties of two typical synthetic rubbers, *i.e.*, styrene–butadiene copolymer (SBR) and *cis*-polybutadiene, in a θ solvent relevant to each. The present paper is concerned with a similar study on type M-40 polychloroprene in a θ solvent methyl ethyl ketone (MEK) at 25°. As far as we have surveyed, mainly based on a table recently compiled by Kurata, *et al.*,[5] this is a first record of the θ solvent for polychloroprene. Our results, however, contradict the recent study of Curchod and Ve,[6] who determined a relation between limiting viscosity number and molecular weight for Neoprene W, equivalent to our type M-40 polychloroprene, in MEK at 25° and concluded that this solvent medium acts as a good solvent for polychloroprene.

Experimental Section

Polymer Sample. Two samples of type M-40 polychloroprene, designated f and F, were specially prepared for the present study at the Aomi Plant of Denkikagaku Kogyo Co. The conversion ratios were controlled below 10% in order to obtain samples with a minimum of branching. These samples were purified by reprecipitation into methanol from a benzene solution and then freeze-dried. Appropriate amounts of an antioxidant, phenyl-β-naphthylamine, were added to both benzene and methanol, and all operations were effected with a minimum exposure of the solution to light. The samples so purified are designated f-0 and F-0, respectively.

Sample f-0 was separated into 14 fractions (designated f-1, f-2, ···, f-14 in the presentation below) by the usual method of fractional precipitation with benzene as solvent and methanol as nonsolvent.[7-9]

(1) Research Fellow from the Aomi Plant of Denkikagaku Kogyo, Co., Aomi, Japan.

(2) T. Homma, K. Kawahara, and H. Fujita, *J. Appl. Polymer Sci.*, 8, 2835 (1964).

(3) T. Homma and H. Fujita, *ibid.*, 9, 1701 (1965).

(4) M. Abe, Y. Murakami, and H. Fujita, *ibid.*, 9, 2549 (1965).

(5) M. Kurata, M. Iwama, and K. Kamada in "Polymer Handbook." J. Brandrup and E. H. Immergut, Ed., Interscience Publishers, Inc., New York, N. Y., 1966, Section IV.

(6) J. Curchod and T. Ve, *J. Appl. Polymer Sci.*, 9, 3541 (1965).

(7) W. E. Mochel and J. B. Nichols, *J. Am. Chem. Soc.*, 71, 3435 (1949).

(8) W. E. Mochel, J. B. Nichols, and C. J. Mighton, *ibid.*, 70, 2185 (1948).

(9) W. E. Mochel and J. B. Nichols, *Ind. Eng. Chem.*, 43, 154 (1951).

Similarly, sample F-0 was divided into six fractions (F-1, F-2, ···, F-6). All operations were performed in the dark with a constant stream of argon bubbling through the fractionation vessel. Each fraction was purified in the same manner as described above, freeze-dried from a benzene solution (containing no antioxidant), sealed in a nitrogen-filled brown bottle, and stored at −20° until used.

For the physical measurements we chose six fractions from the f series and four fractions from the F series.

Osmometry. Except for two fractions (f-2 and F-6), osmotic pressures of these fractions in MEK at 25° were measured, using a Mechrolab 502 high-speed membrane osmometer fitted with an adequately conditioned gel cellophane. By the reason which will be explained below, we performed similar measurements on one fraction (F-2) at three temperatures above and below 25°.

Light Scattering. A Shimazu light-scattering photometer fitted with a cylindrical cell was used. Data were obtained on nine fractions (excepting F-6) in MEK at 25° for the unpolarized light of wavelength 4360 A. The photometer was calibrated with pure benzene, taking a value of 49.5×10^{-6} for the Rayleigh ratio, R_{90}, at this wavelength.[10] Test solutions were made up with antioxidant-free MEK, centrifuged for 1 hr at 15,000 rpm in a Marusan refrigerated centrifuge and then directly pipetted into the cell. Additional measurements were made on one fraction (F-2) at two temperatures other than 25°.

The specific refractive index increments for this polymer in MEK at 25° were 0.162 and 0.156 (ml/g), respectively, for the wavelengths of 4360 and 5460 A. when determined by means of a Brice–Phoenix differential refractometer. The refractive indexes of MEK at 25° for these two wavelengths, measured with a Bausch & Lomb precision sugar refractometer, were 1.38497 and 1.37803, respectively. Curchod and Ve[6] reported a value of 0.152 (ml/g) for the specific refractive index increment of Neoprene W in MEK for light of wavelength 5460 A.

Viscometry. A capillary viscometer of the Ubbelohde suspended-level type was used; its efflux time for benzene at 25° was 181.3 sec, and its upper bulb had a capacity of about 2 ml. Data were taken for all fractions in benzene at 25° in MEK at 25°, and in cyclohexane at 45.5°. As will be explained below, this last solvent medium also acts as a Θ solvent for polychloroprene. In all the cases examined, neither the kinetic energy correction nor the shear-rate correction was needed. The limiting viscosity number $[\eta]$ and the Huggins slope parameter k' were evaluated, using the method of Ibrahim,[11] as well as the customary procedure.

Ultracentrifugation. For six fractions the limiting sedimentation coefficients, s_0, in MEK at 25° were determined, using a Spinco Model E ultracentrifuge and a 12-mm double-sector cell. Rotor speeds were varied in the range from 24,630 to 44,770 rpm, depending on the sample's molecular weight and the initial concentration of a particular experiment. Thanks to the large difference in density between polymer and solvent, these relatively low speeds were enough to cause the movement of sedimentation boundaries which can be measured with high precision. The sedimentation coefficient s for each initial concentration c_0 was evaluated by the usual peak method. In all cases examined, the boundary gradient curves were quite symmetrical about their centroid. The desired value of s_0 was determined by linear extrapolation of a plot for s *vs.* c_0 to infinite dilution. The correction of this s_0 value for pressure effects seemed unnecessary, because, as mentioned above, the present data were all taken at relatively low speeds of rotation.

A preliminary viscosity measurement suggested that the molecular weight of fraction F-6 would be too low to be measured with precision by light scattering or by osmometry. We therefore utilized the sedimentation equilibrium method for the evaluation of its $\bar{M}_w$. The solvent used was MEK at 25°. Data were taken at one initial concentration of about 0.16 g/dl and at a rotor speed of 6166 rpm, using the Rayleigh interference optical system. The short-column technique as suggested by Van Holde and Baldwin[12] was employed to speed the attainment of sedimentation equilibrium. Pycnometric measurements gave 0.773 ml/g for the partial specific volume $\bar{v}$ of fraction F-6 in MEK at 25° and 0.7994 g/ml for the density, ρ_0, of this solvent medium. These values were substituted into the usual formula for the calculation of $\bar{M}_w$.

Results and Discussion

Determination of Θ Solvents. In the hope that a Θ solvent relevant for the study of polychloroprene could be found by the familiar Flory procedure utilizing phase separation, we began with solubility tests, taking the whole polymer f-0 as sample. In total, 99 organic liquids were examined, which included 12 kinds of hydrocarbons, 12 kinds of ketones, 27 kinds of esters, 12 kinds of amines, and 36 others, but, after all the examinations, the ones which seemed promising for our

(10) C. I. Carr and B. H. Zimm, *J. Chem. Phys.*, **18**, 1616 (1950).

(11) F. W. Ibrahim, *J. Polymer Sci.*, **A3**, 469 (1965).

(12) K. E. Van Holde and R. L. Baldwin, *J. Phys. Chem.*, **62**, 734 (1958).

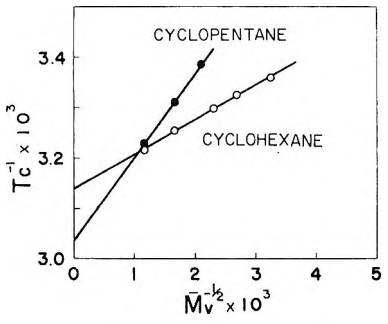

Figure 1. Plots for T_c^{-1} (°K^{-1}) *vs.* $\bar{M}_v^{1/2}$ on solutions of polychloroprene.

purpose were only cyclohexane and cyclopentane. So we proceeded to determine the Θ temperatures for these solvents using the procedure of Shultz and Flory.[13] The results obtained are shown in the form of $1/T_c$ plotted against $1/\bar{M}_v^{1/2}$ in Figure 1. Here T_c is the critical miscibility temperature, and $\bar{M}_v$ has been evaluated from the limiting viscosity number in benzene at 25° by making use of the relation of Mochel and Nichols:[9] $[\eta] = (1.55 \times 10^{-4})\bar{M}_n^{0.71}$. Analysis of the data shown in Figure 1 according to Flory's formalism[14] gives the following results: the Θ temperatures and the mixing entropy parameters, ψ_1, are 45.5° and 0.412 for cyclohexane, and 56.3° and 0.143 for cyclopentane. Unfortunately, these Θ points lie too high above room temperature and thus cannot be regarded as suitable for practical purposes.

Solubility tests with MEK had indicated that the presence of polychloroprene caused no phase separation even in a freezer (*ca.* −20°), and so we naturally had not conceived that this solvent could be a Θ solvent for this polymer at room temperature. However, now that it became almost hopeless to find relevant Θ solvent for the polymer concerned, it appeared suitable to use MEK for measurements of sample molecular weights, since it was anticipated that the system polychloroprene–MEK may have a relatively large refractive index increment so as to make light-scattering measurements easier.

We began the study on this system with viscosity measurements, choosing 25° as the working temperature by an entirely practical reason. When the measurements proceeded to several fractions, we noticed that the measured $[\eta]$ all nearly coincided with the corresponding values which had already been determined in a Θ solvent (cyclohexane) at 45.5°. This rather unexpected fact caused us to predict that the polychloroprene molecule would be brought to the unperturbed state in MEK at or near 25°. We therefore chose fraction F-2 as the sample and conducted light-

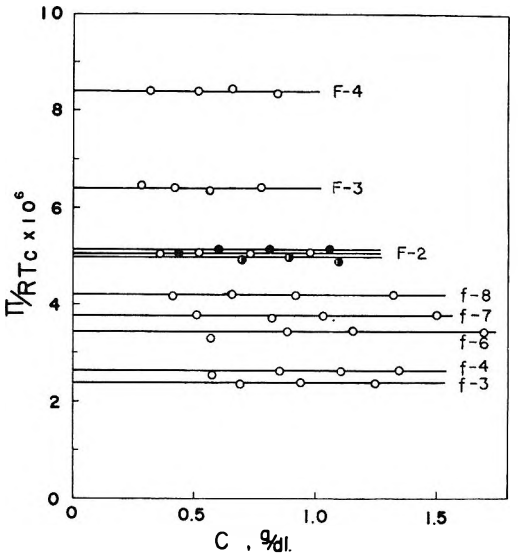

Figure 2. Osmotic pressure data for polychloroprene in methyl ethyl ketone at 17.5° (◑), 25° (○), and 35° (●).

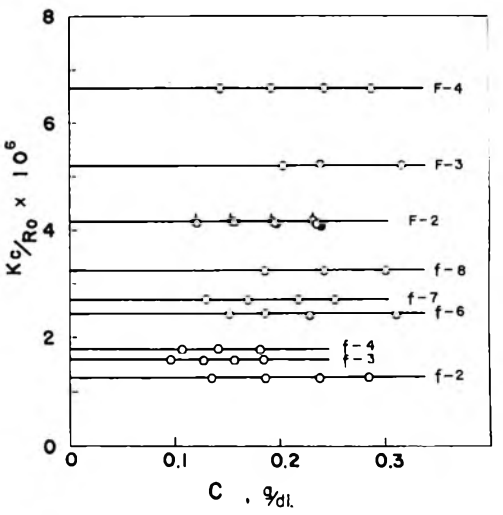

Figure 3. Light-scattering data for polychloroprene in methyl ethyl ketone at 15° (●), 25° (○), and 35° (○).

scattering and osmotic-pressure measurements in this solvent medium at 25°. The expectation was right; both measurements gave zero for the second virial coefficient A_2. Encouraged, we effected similar measurements at two other temperatures above and below 25° and confirmed, as shown below, that polychloroprene in MEK really realizes the unperturbed state at or quite close to 25°. As far as we are aware, this is a first record of the Θ condition for polychloroprene.[5]

(13) A. R. Shultz and P. J. Flory, *J. Am. Chem. Soc.*, **74**, 4760 (1952).

(14) P. J. Flory, "Principles of Polymer Chemistry," Cornell University Press, Ithaca, N. Y., 1953.

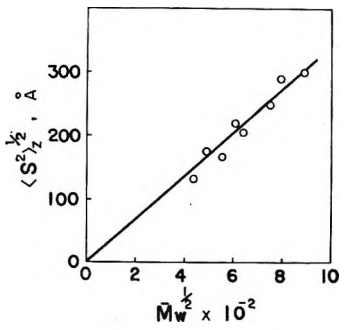

Figure 4. Plot for $\langle S^2 \rangle_z^{1/2}$ of polychloroprene in methyl ethyl ketone at 25° against $\bar{M}_w^{1/2}$.

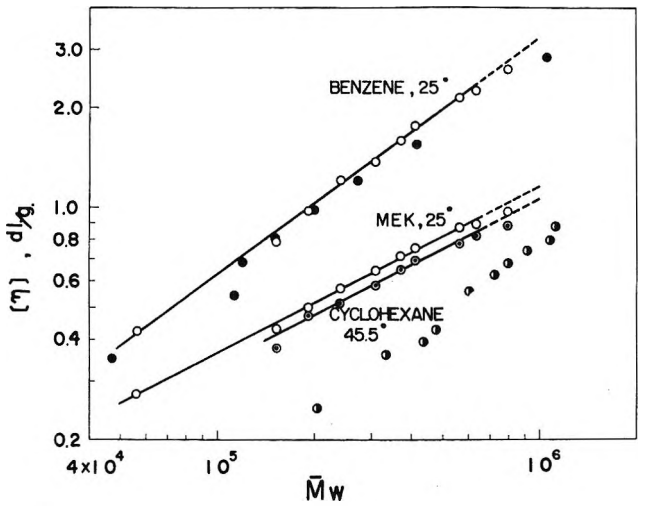

Figure 5. Double logarithmic plots for $[\eta]$ of polychloroprene *vs.* $\bar{M}_w$. Solvents: MEK at 25°, present data (○), Curchod and Ve[6] (◑); benzene at 25°, present data (○), Mochel and Nichols[9] (●) (based on $\bar{M}_n$); cyclohexane at 45.5° (⊙).

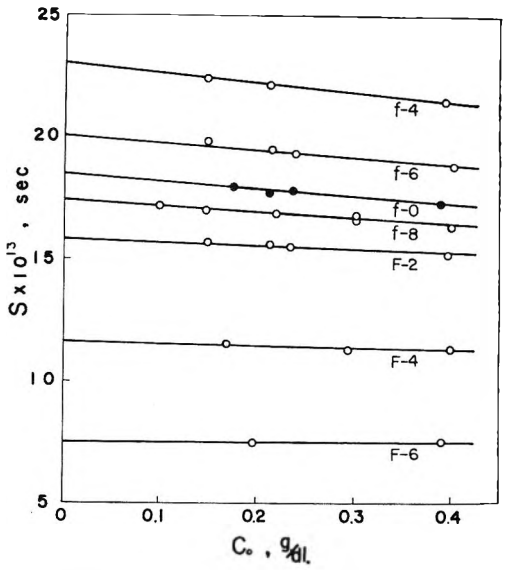

Figure 6. Sedimentation coefficient s as a function of initial concentration c_0 for polychloroprene in methyl ethyl ketone at 25°.

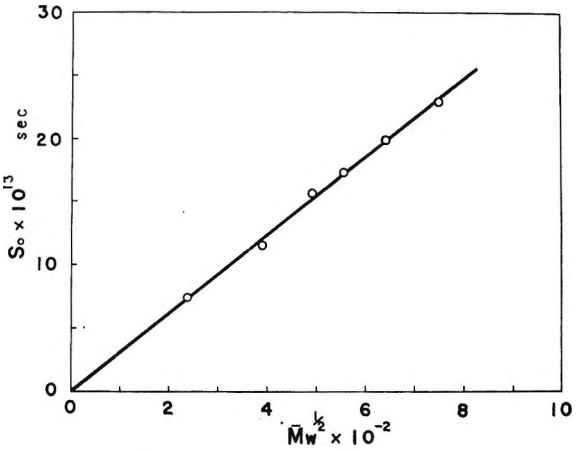

Figure 7. Plot for s_0 of polychloroprene in methyl ethyl ketone at 25° *vs.* $\bar{M}_w^{1/2}$.

Results from Equilibrium Experiments. Figure 2 shows osmotic pressure data for eight polychloroprene fractions in MEK at 25° and those for one fraction at two other temperatures. The corresponding data from light-scattering experiments are shown in Figure 3. These results indicate that MEK brings polychloroprene to the Θ state not at a specific temperature but over a range of temperature. However, close examination of the data reveals a trend that A_2 changes its sign from negative to positive at 25 ± 1° as the temperature is raised. From this fact we tentatively assign 25.0° to the Θ temperature for our polychloroprene in MEK. Since the measured A_2 at 10° above and below 25° were as small as $\pm 1.0 \times 10^{-5}$ mole ml g^{-2} or less, only a rough evaluation of the trend of A_2 near the Θ point is possible. For example, application of the Flory formalism[14] gives 298.2°K and 0.05 for Θ and ψ_1, respectively. These numerical values, taken literally, yield about 200°K for the critical miscibility temperature of a polychloroprene fraction of $\bar{M}_w = 70 \times 10^4$ in MEK. This is consistent with our solubility test in which MEK failed to cause phase separation even in a freezer (*ca.* −20°).

The values of the number-average molecular weight $\bar{M}_n$ and the weight-average molecular weight $\bar{M}_w$ calculated from the ordinate intercepts of the horizontal lines drawn in Figures 2 and 3 are summarized in Table I. This table also lists the value of $\bar{M}_w$ for fraction F-6 determined from the sedimentation equilibrium experiment, the values of $\langle S^2 \rangle_z^{1/2}$ deduced from the Zimm plots (here $\langle S^2 \rangle_z$ represents the z-average mean-square

Table I: Results from Osmotic Pressure and Light-Scattering Measurements on Polychloroprene Fractions in Methyl Ethyl Ketone at 25°

Fraction no.	$\bar{M}_n \times 10^{-4}$	$\bar{M}_w \times 10^{-4}$	$\langle S^2 \rangle_z^{1/2}$, A	$\bar{M}_w/\bar{M}_n$
f-2	...	79.4	300	...
f-3	42.0	63.3	290	1.50
f-4	38.0	56.2	248	1.45
f-6	29.1	41.0	204	1.40
f-7	26.7	37.0	220	1.39
f-8	23.8	30.9	166	1.30
F-2	19.8	24.1	175	1.22
F-3	15.6	19.2	132	1.23
F-4	11.9	15.3	...	1.29
F-6	...	5.6[a]	...	...

[a] Determined by sedimentation equilibrium experiment in methyl ethyl ketone at 25°.

radius of gyration), and the values of the polydispersity parameter $\bar{M}_w/\bar{M}_n$.

In this study, no attempt was made to evaluate the microstructure of the samples. Our samples were prepared by emulsion polymerization of the monomer at 40°. Thus we believe that their molecules are almost of 1–4 addition type and that the configuration of the chain around the double bond is largely of *trans* type.

Figure 4 shows that the values for $\langle S^2 \rangle_z$ vary linearly with $\bar{M}_w^{1/2}$, in agreement with the expectation that this direct proportionality should be obtained under Θ conditions. The scatter of the plotted points is attributed in part to the experimental difficulty of precise measurement of polymer dimensions under Θ conditions and in part to the variation of molecular heterogeneity from fraction to fraction.

Viscosity vs. Molecular Weight Relationships. In Table II are summarized the viscosity data in MEK at 25°, cyclohexane at 45.5°, and benzene at 25°. The conventional double logarithmic plots of these data for $[\eta]$ against $\bar{M}_w$ are given in Figure 5. In this graph, the data of Mochel and Nichols[9] for Neoprene W in benzene at 25° and those of Curchod and Ve[6] for the same rubber in MEK at 25° are also shown for comparison.

Each set of our data is fitted by a straight line, except in the region of $\bar{M}_w$ above 6×10^5, where the plotted points deviate slightly downward from the indicated line. This deviation may be attributed to molecular branching. The solid lines drawn in the figure are represented by the following Mark–Houwink–Sakurada equations

$$[\eta] = (1.16 \times 10^{-3})\bar{M}_w^{0.50} \text{ (in MEK at 25°)} \quad (1)$$

$$[\eta] = (1.07 \times 10^{-3})\bar{M}_w^{0.50} \text{ (in cyclohexane at 45.5°)} \quad (2)$$

$$[\eta] = (1.55 \times 10^{-4})\bar{M}_w^{0.72} \text{ (in benzene at 25°)} \quad (3)$$

The exponent 0.50 in eq 1 and 2 is consistent with the conclusion from evidences that polychloroprene comes to the Θ state in MEK at 25° and also in cyclohexane at 45.5°.

Figure 5 shows a remarkably good agreement of our data for the benzene system with the rather old data of Mochel and Nichols for the same system. However, this agreement may be somewhat accidental, since ours are plotted against $\bar{M}_w$, whereas those of the latter authors are against $\bar{M}_n$. As regards the MEK system, an appreciable discrepancy exists between the data of Curchod and Ve and ours. Both are divergent not only in the absolute magnitude but also in the dependence on molecular weight. Actually, Curchod and Ve have reported a value of 0.74 for the exponent in the Mark–Houwink–Sakurada equation. This relatively high exponent implies that MEK at 25° acted as a good solvent for their polymer samples and doubtlessly contradicts our observation with type M-40 polychloroprene in this solvent medium. No further comment on this discrepancy can be made until the equivalence in microstructure of the polychloroprene samples used by us and by Curchod and Ve is checked experimentally.

The slope of the straight line drawn in Figure 4 together with the coefficient in eq 1 may be utilized to evaluate the familiar constant Φ in Flory's formalism of dilute polymer solutions.[14] The result is $2.0_1 \times 10^{21}$. An appropriate correction for polydispersity will raise this to a value which is closer to the often-assumed value 2.5×10^{21}.

Table II: Results from Viscosity and Sedimentation Measurements on Polychloroprene Fractions

Fraction no.	$[\eta]$, dl/g MEK[a] at 25°	Benzene at 25°	Cyclohexane at 45.5°	s_0, MEK at 25°
f-2	0.975	2.61	0.885	...
f-2	0.895	2.26	0.820	...
f-4	0.870	2.14	0.779	23.0
f-6	0.754	1.77	0.698	20.0
f-7	0.715	1.58	0.650	...
f-8	0.646	1.37	0.583	17.4
F-2	0.571	1.21	0.515	15.8
F-3	0.500	0.975	0.475	...
F-4	0.430	0.786	0.376	11.6
F-6	0.274	0.426	...	7.5
f-0[b]	0.714	1.57	0.620	18.5

[a] Methyl ethyl ketone. [b] Unfractionated sample.

Sedimentation Coefficient vs. Molecular Weight Relationship. Figure 6 shows the results from sedimentation velocity measurements in MEK at 25°. The data for each fraction are reasonably well fitted by the empirical equation $s = s_0(1 - k_s c_0)$, where c_0 is the initial concentration of particular experiment. The slope constant k_s is quite small but shows a trend increasing linearly with the limiting sedimentation coefficient s_0. The values of s_0 read off the intercepts of the indicated lines are listed in Table II and are plotted against $\bar{M}_w^{1/2}$ in Figure 7. As should be expected under Θ conditions, the plotted points follow a straight line passing through the coordinate origin. This straight line is represented by

$$s_0 = (3.1_0 \times 10^{-15})\bar{M}_w^{1/2} \quad (s_0 \text{ in seconds}) \qquad (4)$$

Substituting eq 1 and 4, together with the experimentally determined values for ρ_0, $\bar{v}$, and solvent viscosity η_0 (0.384×10^{-3} poise), into the well-known Flory–Mandelkern equation, we obtain a value of 2.0×10^6 for the constant $\Phi^{1/3}P^{-1}$. This value is closer to the value 2.5×10^6 widely assumed for flexible polymers than those which we have obtained for *cis*-polybutadiene (1.74×10^6)[4] and styrene–butadiene copolymer rubber (1.70×10^6)[3]. Substituting $2.0_1 \times 10^{21}$ for Φ, we have $P = 6.3_1$, which is about 20% larger than the value expected for impermeable polymer coils from the theory of Kirkwood and Riseman. We shall not too much mind these discrepancies about Φ and P, since at least from the experimental point of view, it is still unresolved whether these quantities are really universal constants or not.

Acknowledgment. This study was made possible by a grant from the Denkikagaku Kogyo Co., Ltd. One of the authors (K. H.) thanks the company for having allowed him to leave his position at the Aomi Plant during the period 1965–1966.

Calorimetric Heats of Adsorption of Nitrogen, Carbon Monoxide, and Argon on Graphon at −70°

by R. A. Beebe, R. L. Gale, and T. C. W. Kleinsteuber

Department of Chemistry, Amherst College, Amherst, Massachusetts 01002 *(Received July 25, 1966)*

The heats of adsorption of N_2, CO, and Ar on Graphon have been measured calorimetrically in the low coverage region and over the temperature range from −52 to −81°. The calorimeter described by Gale, Haber, and Stone has been adapted and somewhat modified to meet the conditions of the present research. The observed heats are compared with recently reported isosteric heats which were chromatographically determined at similar coverages and temperatures. The heat of adsorption was found to be independent of temperature in the range from −196 to −60°, and no change in the heats with coverage was observed for these three gases on Graphon.

Introduction

A number of recent papers have been addressed to the possibility of obtaining data on heats of adsorption by means of gas–solid chromatography.[1] In this laboratory, studies have been made on gas–solid systems consisting of the elementary gases N_2, O_2, and Ar, as well as certain compound gases such as CO and C_2F_6 as adsorbates, on graphitized carbon blacks, and on bone mineral as adsorbent column materials. In this work both the pulse method[2] and the continuous flow (frontal analysis) method[3] of chromatography were employed. In both it was possible to obtain values for the heats of adsorption at low coverages in the temperature range from −80° to room temperature by application of the Clapeyron–Clausius equation. The results of the two methods agree when the isotherms at low coverage follow Henry's law. When the isotherms were nonlinear, however, it was found that the heat values obtained by the pulse method deviated from the presumably correct values obtained by the continuous flow method in the direction predicted previously.[3]

Having obtained these differential heat values by means of chromatography, it is of interest to compare them with the calorimetrically measured values. There were no prior calorimetric data in the literature for the range of temperature and of coverage studied in the chromatographic work. Data were available from our earlier calorimetric work at a much lower temperature (−196°) and at considerably higher coverage.[4,5] In order to compare these data with the chromatographically determined values, it is necessary to extrapolate them to higher temperatures and lower coverages. These twice extrapolated values are open to the criticism that they involve the assumption that the heats vary only very little with either temperature or coverage. To fill in the logical gap, we have now undertaken to measure the calorimetric heats under conditions of temperature and coverage which duplicate as nearly as possible those of the chromatographic work. It was decided to develop a calorimeter to use in the temperature range from −80 to −50° (where most of our gas–solid chromatography had been done) with a sensitivity high enough to permit us to use it down to the low coverages involved in the chromatographic measurements. For this purpose we have modified the calorimeter described by Gale, Haber, and Stone,[6] and we have made a thorough study of the

(1) An extensive bibliography is given by H. W. Habgood in "The Solid–Gas Interface," E. A. Flood, Ed., Marcel Dekker, New York, N. Y., to be published. See also references given in ref 2 and 3 of this paper.

(2) R. L. Gale and R. A. Beebe, *J. Phys. Chem.*, **68**, 555 (1964).

(3) R. A. Beebe, P. L. Evans, T. C. W. Kleinsteuber, and L. W. Richards, *ibid.*, **70**, 1009 (1966).

(4) R. A. Beebe, J. Biscoe, W. R. Smith, and C. B. Wendell, *J. Am. Chem. Soc.*, **69**, 95 (1947).

(5) R. A. Beebe, B. Millard, and J. Cynarski, *ibid.*, **75**, 839 (1953).

(6) R. L. Gale, J. Haber, and F. S. Stone, *J. Catalysis*, **1**, 32 (1962).

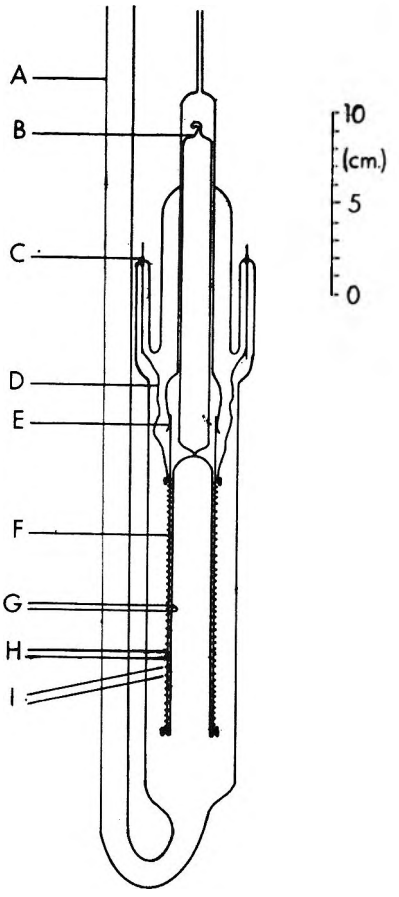

Figure 1. Cross section of the calorimeter (drawn to scale): A, connecting tube for evacuating the vacuum jacket; B, glass filler to reduce the dead space; C, Kovar glass seal; D, lead wires to thermometer and heater coil; E, glass–platinum seal; F, adsorbate; G, platinum walls; H, heater coil; I, thermometer coil.

behavior of this calorimeter, paying particular attention to the determination of the heat capacity. The calorimeter was then applied to the measurement of the heats of adsorption of Ar, CO, and N_2 on Graphon.

Experimental Section

Apparatus and Procedure. The modified calorimeter is shown in Figure 1. In order to improve the heat distribution, the two concentric tubes G were made out of platinum 0.15 mm thick instead of glass, and they are joined at their common base by vacuum-tight silver soldering. The adsorbent was placed in the annular space between the platinum tubes. Two identical coils of 0.0508-mm diameter nickel wire of high temperature coefficient were interwound noninductively upon the outer platinum tube. In order to secure the wires and at the same time insulate them electrically from the platinum, a thin layer of Dow Corning 935 silicone varnish was painted on the platinum tube before winding the wires onto it. After curing for approximately 30 min at 250°, the wires were found to be well secured and insulated and the varnish film withstood repeated heating and cooling between −80 and 250°. The coils had a resistance of 168 ohms at 0°. One coil was connected to a Müller bridge and served as a resistance thermometer which was calibrated by comparison with a platinum resistance thermometer standard. The other coil was used as a heater in the determination of the heat capacity of the calorimeter. The whole assembly was immersed in a 15-l. dewar flask filled with methanol which served as a cryostat. Its temperature was controlled by the device described by Smith[7] and by Graham.[7]

The temperature change of the calorimeter was observed by means of a sensitive Leeds & Northrup galvanometer which recorded the out-of-balance current of the Müller bridge. The response of the calorimeter was extremely rapid and hence a slight drift of the bath temperature could be tolerated. The maximum temperature reading was generally reached in less than 20 sec, and it was therefore found sufficient to record the time–temperature curve for 400 sec after the generation of heat. Figure 2 shows a typical response curve from an adsorption measurement. We determined the temperature rise ΔT, due to the heat of adsorption, graphically from the time–temperature curve. The product of ΔT times the heat capacity is then the adiabatic heat of adsorption. We measured heats varying from 0.03 to 0.3 cal.

An excessively high rate of admission of the gas to the calorimeter was avoided by sending the initial major part of any gas increment through a by-pass tube of very small (0.1 mm) diameter.

Materials. Because of its high specific surface area (89 m^2/g) in comparison with the other graphitized carbon blacks,[2] we have chosen to use Graphon in the present calorimetric work. This material has been used as one of the adsorbents in our gas chromatographic columns and is described in an earlier publication.[4] A 6.8-g sample of the Graphon was used in the calorimeter. All gases used were of prepurified grade supplied by the Matheson Co.

Determination of the Heat Capacity. The calorimeter used in the present research was designed to be calibrated by the equilibrium method as described by Wahba and Kemball,[8] Klemperer and Stone,[9] and Gale, Haber, and Stone.[6] Unfortunately, this method

(7) F. W. Smith, Ph.D. Thesis, St. Andrews University, Great Britain, 1952; D. Graham, *J. Phys. Chem.*, **66**, 1815 (1962).

(8) M. Wahba and C. Kemball, *Trans. Faraday Soc.*, **49**, 1351 (1953).

(9) D. F. Klemperer and F. S. Stone, *Proc. Roy. Soc.* (London), **A243**, 375 (1957).

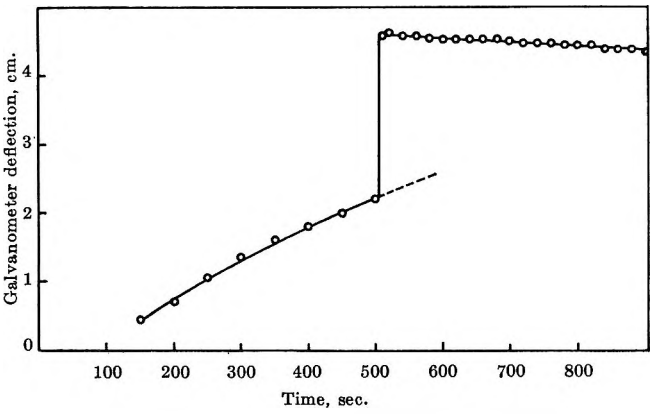

Figure 2. Typical response curve of an adsorption experiment. N_2 on Graphon; heat observed, 0.089 cal.

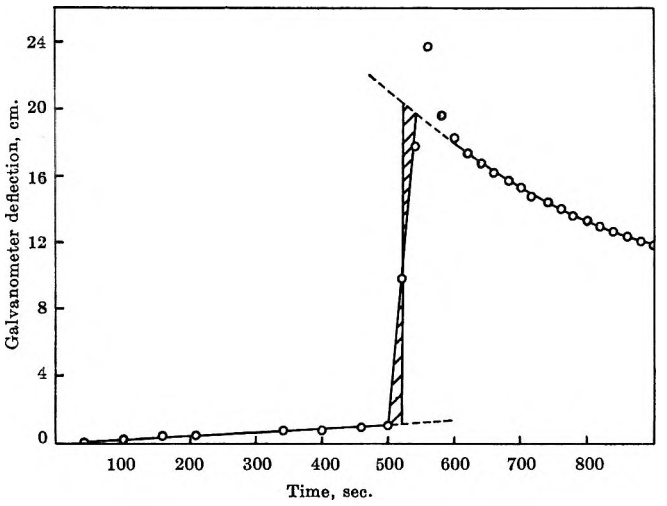

Figure 3. Typical response curve of a calibration experiment. Temperature, −67°; heat input, 0.95 cal.

requires a steadier base line than we have been able to achieve in our cryostat in the low-temperature range from −80 to −50°. It therefore seemed to us preferable to inject measured quantities of energy in the form of electrical pulses of short duration, thus simulating more closely the actual adsorption experiments (see Figures 2 and 3). We measured the potential drop across the heater coil with a precision voltmeter, the time of heat input with an accurate stopwatch, and the electrical resistance value by means of the Müller bridge. The electrical energy input was determined to ±0.6%. It is of course desirable to distribute the heat quickly and uniformly throughout the whole mass of the calorimeter. In order to assist the heat distribution during the calibration, a low pressure of helium (1–5 mm) was included in the annular space containing the adsorbent.

By an extensive series of calibration experiments, especially at −67°, we showed that the observed value for the heat capacity of the calorimeter was independent of the size of the energy pulse inserted over the range from 0.008 to 8 cal. The observed heat capacity was likewise independent of the rate of energy input over the range 0.0057 to 0.086 cal/sec.

Figure 3 gives a typical response curve of a calibration measurement. The excessively high readings between 550 and 600 sec are due to an emf induced in the thermometer coil in switching off the heater current. We extrapolated the cooling curve to the time at which the two shaded areas are equal, as is common practice in calorimetry.[10,11]

A rough estimate was made of the amount of heat radiated directly from the heater coil to the vacuum jacket during calibration. The estimated heat loss was less than 1% of the total heat input and could therefore be neglected.

The data for the heat capacity measurements are given in Table I.

Table I: Heat Capacities of Calorimeter Filled with Graphon

Temp, °C	No. of measurements	Mean value in cal/deg
−55	16	3.51 ± 1.2%
−67	50	3.52 ± 0.9%
−75	14	3.49 ± 1.2%
−80	18	3.50 ± 1.2%

Correction for the Heat of Compression. It is well known that the heat of adsorption observed in an adiabatic calorimeter contains a term which is due to the compression of the gas phase in the dead space of the calorimeter. This effect was first observed and considered by Ward.[12] The detailed discussion of the thermodynamics of gas adsorption by Hill[13] accounts for this term implicitly; it has since been discussed in greater detail by Kington and Aston[14] and by Young and Crowell.[15] The heat of compression is of im-

(10) M. Braun and R. Kohlhaas, *Z. Angew. Phys.*, **14**, 91 (1962).

(11) In order to check our method of determining the heat capacity, we plotted log $(T_c - T_b)$ *vs.* time, where T_c is the temperature of the calorimeter and T_b is the temperature of the bath. If the heat distribution through the calorimeter is sufficiently rapid, this plot should give a straight line. A linear plot was indeed obtained and this justifies our practice of limiting the observation of the cooling curve to 400 sec (see Figures 2 and 3).

(12) A. F. H. Ward, *Proc. Roy. Soc.* (London), **A133**, 506 (1931).

(13) T. L. Hill, *J. Chem. Phys.*, **17**, 520 (1949).

(14) G. L. Kington and J. G. Aston, *J. Am. Chem. Soc.*, **73**, 1929 (1951).

(15) D. M. Young and A. D. Crowell, "Physical Adsorption of Gases," Butterworth and Co. Ltd., London, 1962, p 74.

Table II: Heats of Adsorption, q_{st}, of N_2, CO, and Ar on Graphon

(1) System	(2) Coverage in % of monolayer, this paper	(3) No. of measurements, this paper	(4) Temp range, this paper	(5) q_{st} by calorimetry, this paper	(6) q_{st} by calorimetry, −196°	(7) q_{st} by chromatography, pulse	(8) q_{st} by chromatography, frontal
N_2–Graphon	0.4–1.0	16	−81 to −65°	2.9 ± 0.1	3.0[4]	2.7[2]	3.0 ± 0.2[3]
CO–Graphon	0.5–2.6	8	−81 to −52°	2.9 ± 0.1	...	...	...
Ar–Graphon	1.0–1.2	4	−81 to −65°	2.7 ± 0.2	2.6[5]	2.7[2]	2.9 ± 0.2[3]

portance if calorimetric and isosteric heats of adsorption are to be compared with each other. The following relationship is given by Young and Crowell

$$q_{cal} = q_{st} + V_g\left(\frac{\partial p}{\partial n_s}\right)_{ad} \quad (1)$$

where q_{cal} is the differential heat calorimetrically measured under adiabatic conditions, q_{st} is the heat derived from isosteres by the Clapeyron–Clausius relationship, V_g is the volume of the gas phase in the calorimeter vessel, and $(\partial p/\partial n_s)_{ad}$ is the change of pressure due to the adsorption of ∂n_s moles if the total entropy is kept constant. We are dealing with a reversible adsorption process and measuring under adiabatic conditions. Furthermore, the ideal gas law is valid in our systems. Therefore, the correction for the heat of compression for a small increment is made as follows

$$\Delta n_s q_{cal} - V_g(p_f - p_i) = \Delta n_s q_{st} \quad (2)$$

where Δn_s is the amount adsorbed, and p_i and p_f are, respectively, the pressures before and after the addition of an increment. This is the same correction term as Ward[12] gave. Frequently, the heat of compression, $V_g(p_f - p_i)$, is very small compared to the heat of adsorption, $\Delta n_s q_{cal}$. In our measurements, however, this term amounted to a significant correction, approximately 10 to 20%. Therefore, we tested this relation by admitting helium into the calorimeter. Since helium is presumably not adsorbed at the temperatures used, we are measuring the heat of compression only. The results are shown in Figure 4. As predicted, the observed heat values are directly proportional to the pressure changes. In a recent publication, Smith and Ford[16] have reported an experimentally observed linear relationship between pressure change and the heats of compression as well as the heats of expansion. Using the dimensions of the platinum vessel of our calorimeter and the weight and density of the Graphon in the vessel, we have estimated the volume of the gas phase V_g. The calculated values for

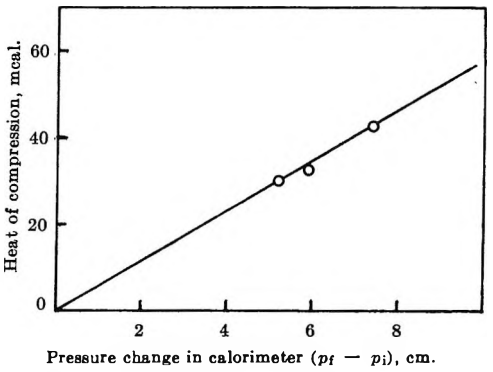

Figure 4. Observed heat of compression *vs.* pressure change in calorimeter at −67°.

$V_g(p_f - p_i)$ and the experimentally observed heats of compression are in satisfactory agreement.

All the heats of adsorption reported in this paper have been corrected for the heat of compression and can therefore be compared to the isosteric heats of adsorption as obtained by gas chromatography.

Results and Discussion

The results of our present calorimetric work with N_2, CO, and Ar on Graphon are presented in column 5 of Table II. As indicated above, these data are corrected for heat of compression. The conditions of the experiments in the present research are given in columns 1–4. All but five measurements referred to in column 3 were made on the admission of measured small quantities to the previously evacuated calorimeter. Four of the measurements with N_2–Graphon and one with CO–Graphon were taken for second increments added without pumping out the gas of the initial increment. Although there was some scattering of the data, this effect was to a great extent offset by conducting a substantial number of determinations. As a result, the average deviation of the mean value was no more than 3% for the N_2–Graphon and CO–Graphon systems, and 6% for Ar–Graphon.

(16) W. R. Smith and D. G. Ford, *J. Phys. Chem.*, 69, 3587 (1965).

For comparison with the data of the present work, we list in column 6 earlier calorimetric measurements at −196°.[4,5] It was estimated that at −196° the correction for the heat of compression was negligible. Thus all the values of columns 5–8 are comparable in that they represent isosteric heats. Joyner and Emmett[17] have measured the isotherms for the system N_2–Graphon over the temperature range from −183 to −205°. The isosteric heats they derived are in excellent agreement with the calorimetrically determined values[4] at −196°. In columns 7 and 8 the data are given for the heats of adsorption obtained by chromatography by the pulse method[2] and by the frontal analysis method,[3] respectively. All the data of Table II are drawn from work done in this laboratory. It is difficult to put an exact error value on the data of columns 6 and 7; however, we estimate the error here to be roughly ±0.2 kcal/mole.

From the data of Table II, within the limits of the inherent experimental errors, we may draw the following conclusions for the adsorption of N_2, CO, and Ar on the Graphon adsorbent. (1) There is no evidence for any temperature dependence of the heats of adsorption in any of the three systems studied in the region from −50 to −196°. (2) There is no evidence for any change in the heats of adsorption with coverage in the range up to 1.0 to 2.0% of a monolayer.

The above conclusions are perhaps not unduly surprising when we remember that Graphon presents an essentially nonpolarizing surface.[2,3] As a result, even with molecules of a polarizable gas like CO, which also have a small permanent dipole, the forces involved in adsorption are essentially van der Waals in nature and there is probably small change in their nature over the ranges of temperature and coverage in question.

For polarizing surfaces such as dry bone mineral[2,3] and TiO_2,[16] there is definite evidence for a decrease in the heats of adsorption of N_2 and CO with increasing coverage in the region of low coverage. At the present time we know of no definitive data to test the temperature dependence of the heat of adsorption on these strongly polarizing surfaces. It is felt that it will be very worthwhile to obtain such data.

Acknowledgments. Our gratitude is due to the National Institutes of Health and the National Science Foundation for financial support of this work.

(17) L. G. Joyner and P. H. Emmett, *J. Am. Chem. Soc.*, **70**, 2356 (1948).

Thermodynamics of Calcium Sulfate Dihydrate in Aqueous Sodium Chloride Solutions, 0–110°[1,2]

by William L. Marshall and Ruth Slusher

Reactor Chemistry Division, Oak Ridge National Laboratory, Oak Ridge, Tennessee *(Received June 13, 1966)*

An evaluation of the extensive solubility measurements of calcium sulfate dihydrate in aqueous sodium chloride solutions obtained in this study further confirmed that the variation of the ion solubility product could be described to high ionic strengths (2 *m*) at temperatures from 0 to 110° by only one parameter, commonly referred to as the "ion-size parameter," $\mathring{a}$, in the extended Debye–Hückel expression. This evaluation yielded a constant value of 4.5 A for $\mathring{a}$ over the entire range of temperature. At ionic strengths above 2 *m* and at low temperatures, the ion solubility products showed negative deviations from the one-parameter expression in contradiction to the expected behavior for the association of Ca^{2+} or SO_4^{2-} with Na^+ or Cl^- ions. The negative deviation could be described by the inclusion of two additional terms which essentially approach zero at the higher temperatures. This behavior may suggest a decrease in the structure of water as the temperature rises and thus an increase in the simplicity of aqueous solutions at high temperatures compared to their behavior at 25°. From the derived solubility product constants, values for $\Delta G°$, $\Delta H°$, $\Delta S°$, and $\Delta C_p°$ were determined along with the variation of thermodynamic functions with the ionic strength and temperature. At temperatures of 70–95° and at high concentrations of NaCl, a double salt of $CaSO_4$ and Na_2SO_4, in addition to $CaSO_4 \cdot 2H_2O$, saturated the solution phase.

Introduction

In a previous study at this laboratory,[3] it was shown that the variation of the ion solubility product for $CaSO_4$ and its hydrates could be expressed to high ionic strengths (2 *m*) at temperatures to 200° by only one parameter, A, in the extended Debye–Hückel expression, $\sqrt{I}/(1 + A\sqrt{I})$, where I is the ionic strength, $A = b\mathring{a}$, b is a function of the absolute temperature and dielectric constant, and $\mathring{a}$ is the parameter commonly called the "ion-size" parameter. The questions not entirely answered were (1) whether the assumption that calcium sulfate is essentially dissociated in aqueous media is valid, (2) whether additional terms to express the ion solubility products at ionic strengths approaching 6 *m* did smoothly drop out as the temperature rose above 25°, (3) whether either A or $\mathring{a}$ is a constant or varies with the temperature, a subject of much controversy but with little or no experimental data for support, (4) whether the standard heat of solution, $\Delta H°$, did indeed become zero at ~30°, and (5) whether sufficiently accurate data for extrapolation could be obtained over a very wide temperature range to allow the calculation of meaningful values not only for $\Delta G°$, $\Delta H°$, and $\Delta S°$ but also for $\Delta C_p°$ for the dissolution of $CaSO_4 \cdot 2H_2O$ into water solution. In view of the very few comprehensive studies originating at low temperatures and extending to temperatures above 100°, definite answers to some of the above questions would give further insight into the particular system under study, the general nature of the electrolyte solutions in the virgin high-temperature region, and the nature of the solvent, water. Therefore, in the present extensive

(1) Work sponsored by the Office of Saline Water, U. S. Department of the Interior, and performed at the Oak Ridge National Laboratory which is operated by the Union Carbide Corporation for the U. S. Atomic Energy Commission. Presented before the Division of Physical Chemistry at the 151st National Meeting of the American Chemical Society, Pittsburgh, Pa., March 22–31, 1966.

(2) Paper No. XVI in a series, "Aqueous Systems at High Temperatures." Previous paper, W. L. Marshall and R. Slusher, *J. Chem. Eng. Data*, **10**, 353 (1965).

(3) W. L. Marshall, E. V. Jones, and R. Slusher, *ibid.*, **9**, 187 (1964).

study many additional solubilities of calcium sulfate dihydrate were measured at temperatures from 0 to 110° and to sufficiently high concentrations of sodium chloride (~6 *m*), where either NaCl or another solid phase was found to saturate the solutions. From these results the thermodynamic behavior of this system at saturation vapor pressure is described over its entire range of stability.

Values for the solubility product constants and the variation of the ion solubility product with the ionic strength and temperature are obtained at the several temperatures from which the thermodynamic functions at zero and high ionic strengths are calculated. The interpretation of these results by means of the extended Debye–Hückel expression with the one $\dot{A}$ parameter shows that very good agreement can be obtained by assuming that $CaSO_4$ in solution completely dissociates to Ca^{2+} and SO_4^{2-} ions, within the limits of detection of our method. Additional terms to express the ion solubility products were essentially unnecessary at temperatures somewhat above 25°, thus strongly suggesting the assumed breakdown in the structure of water at the high temperatures. A constant value for the ion size, $\dot{a}$, of 4.5 A was observed over the entire range of temperature. The value for $\Delta H°$ did reach zero at 30°, and the over-all data were found to be sufficiently accurate to obtain estimates for $\Delta C_p°$ in reasonable agreement with other independent estimates.

The thermodynamic functions are compared with analogous values for $CaSO_4$ (anhydrite) from which the change in the transition temperature with ionic strength, $CaSO_4 \cdot 2H_2O(s) \rightarrow CaSO_4(s) + 2H_2O$, was calculated and compared with some literature values. The thermodynamic functions for this reaction over a range of the ionic strength and temperature were also obtained.

Experimental Section

The reagents used and their methods of purification have been stated previously.[3] Experimental procedures have been described before[3] except that a refrigeration unit was added to the thermostat bath for use between 0 and 25°. Most experimental runs at 70–110° were made in the high-pressure vessels described elsewhere.[4] Samples of the liquid phase were removed periodically for calcium analysis by EDTA potentiometric titration.[5] For analyses for NaCl, liquid samples were either dried and weighed, or poured through a cation-exchange resin to remove Na and Ca, and subsequently titrated for the remaining HCl and H_2SO_4. With either method the analyzed quantity of $CaSO_4$ was subtracted from the total quantity of $CaSO_4$ and NaCl. In one set of experiments at 70°, where various weighed quantities of Na_2SO_4 were added to a NaCl solution saturated with both $CaSO_4 \cdot 2H_2O$ and a second solid, the solution–solid mixtures were heated in a flask that was connected to a reflux condenser. A magnetic stirrer–hot plate unit was used; by adjustment of the heat output, the temperature could be held constant to ±2°. Solid phases were removed initially and periodically and dried rapidly by the vacuum filtration of the excess liquid phase. The solids were examined with a petrographic microscope and were identified by the comparison of the properties with those of known compounds.[6]

Results and Discussion

Specific. The solubility equilibrium under study

$$CaSO_4 \cdot 2H_2O(s) \rightleftharpoons Ca^{2+} + SO_4^{2-} + 2H_2O$$

can be expressed by a solubility product constant

$$K_{sp}° = a_{Ca^{2+}} a_{SO_4^{2-}} a_{H_2O}^2 \quad (1)$$

$$= m_{Ca^{2+}} m_{SO_4^{2-}} \gamma_{Ca^{2+}} \gamma_{SO_4^{2-}} a_{H_2O}^2 \quad (2)$$

$$= K_{sp}(P) \gamma_{Ca^{2+}} \gamma_{SO_4^{2-}} a_{H_2O}^2 \quad (3)$$

where $K_{sp}°$ is the solubility product constant for $CaSO_4 \cdot 2H_2O$ at zero ionic strength, $a_{Ca^{2+}}$, $a_{SO_4^{2-}}$, and a_{H_2O} are the activities of the several species, $m_{Ca^{2+}}$ and $m_{SO_4^{2-}}$ are the analytical molalities of the ions, $\gamma_{Ca^{2+}}$ and $\gamma_{SO_4^{2-}}$ are their respective activity coefficients, and $K_{sp}(P)$ is a practical ion solubility product ($= [Ca^{2+}][SO_4^{2-}]$). The ion solubility product that includes the activity of water will be considered the "true" product and therefore we shall let $K_{sp}(T) = K_{sp}(P) a_{H_2O}^2$ where $K_{sp}(T) \rightarrow K_{sp}(P) \rightarrow K_{sp}°$ as the ionic strength approaches zero and a_{H_2O} approaches unity. From an extended Debye–Hückel relationship and the addition of linear and quadratic terms, the ion solubility products can be expressed by

$$\log K_{sp}(T) = \log K_{sp}° + 8S\sqrt{I}/(1 + A_{sp}\sqrt{I}) + BI - CI^2 \quad (4)$$

and

$$\log K_{sp}(P) = \log K_{sp}° + 8S\sqrt{I}/(1 + A_{sp}\sqrt{I}) + B'I - C'I^2 \quad (5)$$

where S is the Debye–Hückel limiting slope $\times \sqrt{d_{H_2O}}$, I is the ionic strength ($= 4 \times$ molal solubility of $CaSO_4$ + molality of NaCl), and A_{sp}, B, B', C, and C' are adjust-

(4) J. S. Gill and W. L. Marshall, *Rev. Sci. Instr.*, **32**, 1060 (1961).
(5) H. A. Flaschka, "EDTA Titrations," Pergamon Press Ltd., London, 1959.
(6) A. E. Hill and J. H. Wills, *J. Am. Chem. Soc.*, **60**, 1647 (1938).

able parameters, where B' and C' account also for the variation of $a_{H_2O}^2$ with I. Since in our experiments $m_{Ca^{2+}} = m_{SO_4^{2-}}$, eq 5 for $\log K_{sp}(P)$ reduces to

$$\log s = \log s^\circ + 4S\sqrt{I}/(1 + A_{sp}\sqrt{I}) + \frac{B'}{2}I - \frac{C'}{2}I^2 \quad (6)$$

where s is the molal solubility of $CaSO_4 \cdot 2H_2O$ and s° is the (hypothetical) solubility at $I = 0$.

Our new, experimentally attained values for the molal solubility of $CaSO_4 \cdot 2H_2O$ in NaCl–H_2O solutions are given in Table I. The times for equilibration varied from 16 to 96 hr. [Unfortunately some of our original data at 40° after 20 hr rocking time (Table I, ref 3) were published in error and those particular $CaSO_4$ molalities should be corrected from 0.0227, 0.0290, 0.0455, 0.0530, 0.0519, 0.0477, and 0.0436 to 0.0228, 0.0292, 0.0463, 0.0558, 0.0552, 0.0519, and 0.0483, respectively. Footnote *c* in Table II of ref 3 refers to the correct values after 20 hr, which at concentrations of NaCl above 1 *m* are only 2% lower than the reported values after 68 hr.]

From the previous study it was found that the solubilities could be expressed to moderately high ionic strengths (2 *m*) by the use of eq 6 with only two terms, s° and $\sqrt{I}/(1 + A_{sp}\sqrt{I})$. In this present study all the data of Table I, previous values at 40 and 60°,[3] and available literature data are shown in Figures 1 and 2 plotted as the logarithm of the analyzed calcium concentration (molal solubility of $CaSO_4 \cdot 2H_2O$ where no additional solid other than NaCl is present) *vs.* $\sqrt{I}/(1 + A_{sp}\sqrt{I})$. Values of A_{sp} were obtained from a least-squares treatment described below. Literature data included in Figures 1 and 2 are the solubilities of Cameron,[7] Denman,[8] Bock,[9] Shternina,[10] Power, Fabuss, and Satterfield.[11,12] Not plotted but evaluated also are the data of Langelier, Caldwell, and Lawrence[13] at 100°

Table I: The Molal Solubility of $CaSO_4 \cdot 2H_2O$ (Gypsum) in NaCl–H_2O Solutions at 0–110° [a]

NaCl (m)	$CaSO_4$ (m)[b]											
T = 0.5°C		2.871	0.0560	0.402	0.0328	0.548	0.0371	0.3905	0.0310			
0.0000	0.0128	3.954	0.0551	0.701	0.0400	0.834	0.0429	0.984	0.0442			
0.0136	0.0139	6.08	0.0437[c]	1.050	0.0464	1.005	0.0457	1.955	0.0548			
0.0277	0.0150	T = 10°C		2.050	0.0551	T = 40°C		2.044	0.0542			
0.0357	0.0156	0.0000	0.0140	2.866	0.0571	0.0000	0.0156	2.907	0.0603			
0.0560	0.0168	0.0372	0.0173	3.969	0.0559	0.0118	0.0165	3.075	0.0583			
0.1020	0.0193	0.1066	0.0211	6.12	0.0452[c]	0.0256	0.0178	(3.53)	(0.0712)[d]			
0.1228	0.0200	0.2117	0.0256	T = 25°C		0.0516	0.0195	(4.05)	(0.1015)			
0.2043	0.0233	0.3965	0.0315	0.0000	0.0151	0.1148	0.0238	(3.72)	(0.0825)			
0.2066	0.0237	0.695	0.0386	0.0117	0.0162	0.1923	0.0270	(4.56)	(0.0983)			
0.2459	0.0248	1.045	0.0450	0.0257	0.0175	0.2321	0.0282	(4.70)	(0.0680)			
0.401	0.0299	2.051	0.0546	0.0513	0.0194	0.548	0.0371	(5.14)	(0.0960)			
0.579	0.0339	2.844	0.0568	0.1147	0.0231	0.834	0.0427	(6.36)	(0.1215)			
0.703	0.0374	3.961	0.0551	0.1921	0.0266	1.005	0.0462	T = 95°C				
0.878	0.0403	6.08	0.0444[c]	0.2319	0.0281	6.24	0.0480[c]	0.0000	0.0123			
1.053	0.0442	T = 15°C		0.548	0.0372	T = 60°C		0.1045	0.0194			
1.055	0.0437	0.0000	0.0145	0.689	0.0388	0.0000	0.0148	0.3892	0.0286			
2.053	0.0545	0.0392	0.0179	0.834	0.0430	6.39	0.0523[c]	0.973	0.0427			
2.875	0.0571	0.1083	0.0220	1.005	0.0457	T = 70°C		2.043	0.0538			
3.978	0.0553	0.2156	0.0267	1.024	0.0452	0.0441	0.0176	(2.94)	(0.0749)[d]			
6.10	0.0442	0.401	0.0325	2.024	0.0540	0.3887	0.0317	(3.46)	(0.0848)			
6.08	0.0437[c]	0.701	0.0395	2.870	0.0560	2.048	0.0546	(4.06)	(0.0957)			
T = 5°C		1.050	0.0461	4.125	0.0560	3.092	0.0578	(4.56)	(0.0927)			
0.0000	0.0133	2.056	0.0548	6.13	0.0489	3.637	0.0583	(5.16)	(0.0920)			
0.0360	0.0164	2.866	0.0576	6.22	0.0481[c]	4.29	0.0575	T = 110°C				
0.1043	0.0201	3.982	0.0559	T = 30°C		4.78	0.0567	0.0000	0.0100			
0.2075	0.0245	6.14	0.0471[c]	0.0000	0.0152	(5.30)	(0.0746)[d]	0.1011	0.0161			
0.3865	0.0303	T = 20°C		0.0118	0.0165	(6.40)	(0.1050)	0.3642	0.0308			
0.689	0.0373	0.0000	0.0149	0.0259	0.0176	T = 80°C		3.500	0.0619			
1.037	0.0437	0.0407	0.0183	0.0512	0.0197	0.0000	0.0135	4.10	0.0719			
2.028	0.0533	0.1101	0.0224	0.1148	0.0231	0.0369	0.0164	4.62	0.0672			
		0.2169	0.0271	0.1921	0.0265	0.1040	0.0208	5.18	0.0734			
				0.2320	0.0287							

[a] Times of equilibration vary from 16 to 96 hr. [b] Solution concentration is expressed as molality of $CaSO_4$. [c] Solution saturated with two solid phases, $CaSO_4 \cdot 2H_2O$ and NaCl. [d] Values in parentheses are for solutions saturated with $CaSO_4 \cdot 2H_2O$ and a double salt of $CaSO_4$ and Na_2SO_4 (at the highest molality, NaCl(s) also is present). Thus these concentrations for NaCl are only approximate, and those for $CaSO_4$ represent only the concentrations of calcium and not of $CaSO_4$.

Table II: The Solubility Product Constant of $CaSO_4 \cdot 2H_2O$ and Parameters for the Variation of the Solubility Product with Ionic Strength (in NaCl Solution)

T, °C	$K_{sp}^\circ \times 10^6$	A_{sp}	B'[a]	C'[b]	Data evaluated (no. of data points)[c]
0.5	34.31	1.450	0.0880	0.0234	a (22)
5	36.85	1.458	0.0620	0.0202	a (11)
10	39.22	1.468	0.0474	0.0182	a (11)
15	40.94	1.479	0.0360	0.0164	a (11), b (7)
20	41.73	1.490	0.0272	0.0148	a (11), c (1)
23	41.88	1.495	0.0224	0.0142	b (11)
25	42.31	1.500	0.0194	0.0134	a (16), b (8), d (17), e (3), f (12)
30	42.50	1.510	0.0124	0.0130	a (10), b (7), d (7)
35	42.27	1.520	0.0060	0.0124	c (1), e (3)
40	41.49	1.530	0.0022	0.0120	a (19), c (1), e (7)
45	40.33	1.537	0.0011	0.0114	c (1), e (3)
50	38.57	1.544	0	0.0108	b (9), c (1), d (7)
60	35.88	1.558	0	0.0096	a (9), c (1)
65	34.41	1.564	0	0.0090	c (1), e (3)
70	32.40	1.570	0	0.0082	d (7), b (6), c (1)
80	28.50	1.580	0	0.0064	a (9), c (1)
82	28.20	1.581	0	0.0060	b (9), c (4)
85	27.57	1.584	0	0.0054	c (1), e (3)
90	25.67	1.588	0	0.0042	c (4)
95	24.04	1.591	0	0.0030	a (5), e (3)
100	23.60	1.594	0	0.0020	g (6)
110	19.50	1.595	0	0.0008	a (7)

[a] $B = B' - 0.020$. [b] $C = C' + 0.0030$. [c] a, present data; b, Cameron; c, Denman; d, Bock; e, Power, *et al.*; f, Shternina; g, Langelier.

(7) F. K. Cameron, *J. Phys. Chem.*, **5**, 556 (1901).

(8) W. L. Denman, *Ind. Eng. Chem.*, **53**, 817 (1961).

(9) E. Bock, *Can. J. Chem.*, 39, 1746 (1961).

(10) E. B. Shternina and E. V. Frolova, *Izv. Sektora Fiz-Khim Analiza, Inst. Obshch. Neorgan. Khim., Akad. Nauk SSSR*, 21, 271 (1952); E. B. Shternina, *ibid.*, 17, 351 (1949); E. B. Shternina, *Dokl. Akad. Nauk SSSR*, 60, 247 (1948).

(11) W. H. Power, B. M. Fabuss, and C. N. Satterfield, *J. Chem. Eng. Data*, 9, 437 (1964).

(12) W. H. Power, B. M. Fabuss, and C. N. Satterfield, *ibid.*, 11, 149 (1966).

(13) W. F. Langelier, D. H. Caldwell, and W. B. Lawrence, *Ind. Eng. Chem.*, 42, 126 (1950).

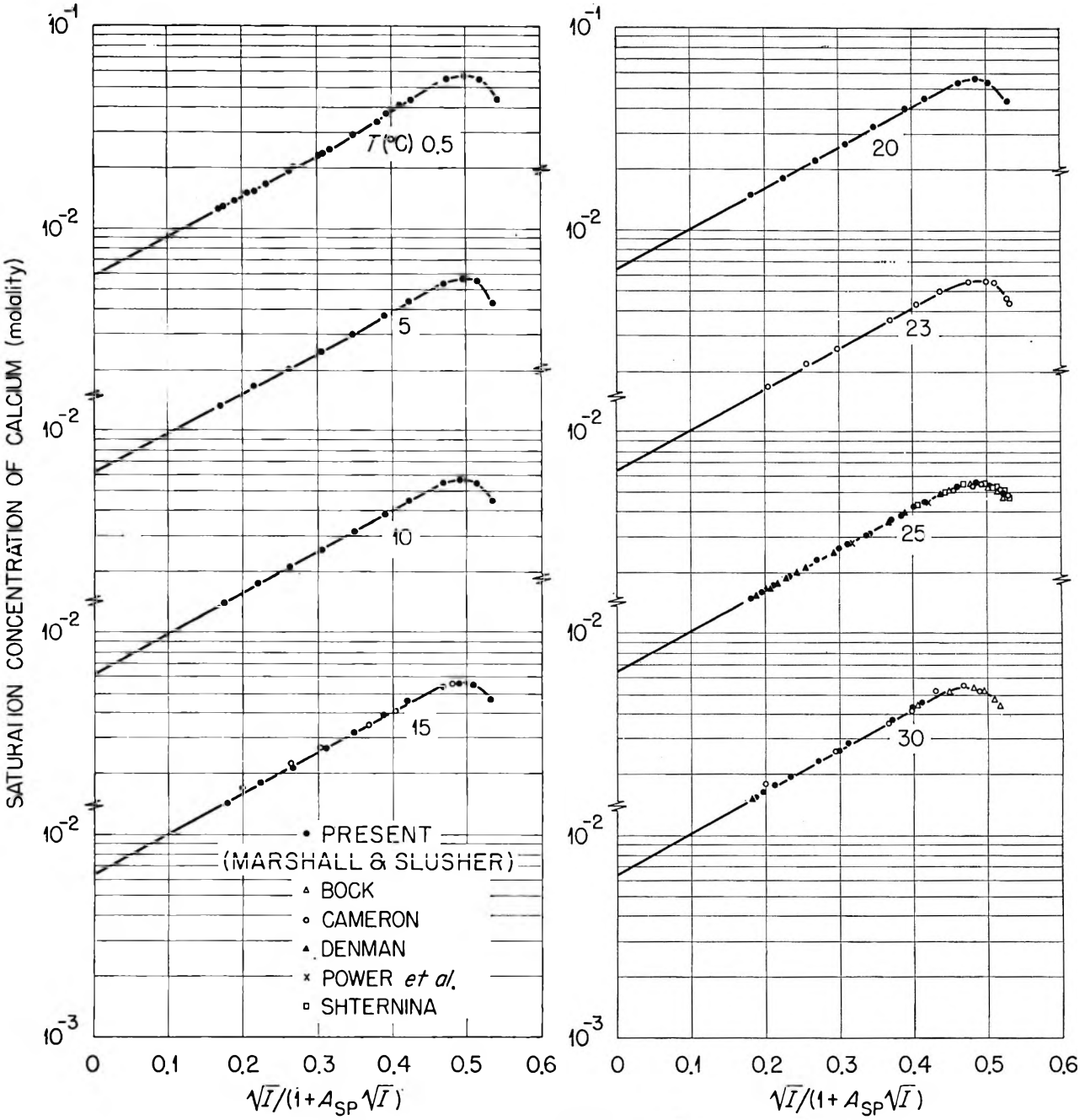

Figure 1. The solubility of $CaSO_4 \cdot 2H_2O$ (gypsum) in NaCl–H_2O solutions *vs.* $\sqrt{I}/(1 + A_{sp}\sqrt{I})$ at 0.5–30°.

in sea water concentrates; the evaluated results are included in Table II. The recent results of Zen[14] agree well with the over-all evaluation.

The limiting slopes drawn in Figures 1 and 2 correspond to the theoretical slope, $4S$, of eq 6 with the extrapolated value at zero ionic strength corresponding to $s°$. The deviations from linearity at high ionic strengths can be fitted by the two additional terms, $(B'/2)I$ and $(C'/2)I^2$. At temperatures up to 60° the solution at the highest ionic strength is saturated by the two solids, $CaSO_4 \cdot 2H_2O$ and NaCl. At 70–95°, however, a new saturating solid in addition to $CaSO_4 \cdot 2H_2O$ was found and will be discussed below. The evidence in Figure 2 shows that the new solid removes sulfate from solution and thereby allows the analytical concentration of calcium to increase sharply to satisfy the ion solubility

(14) E-an Zen, *J. Petrol.*, 6, 124 (1965).

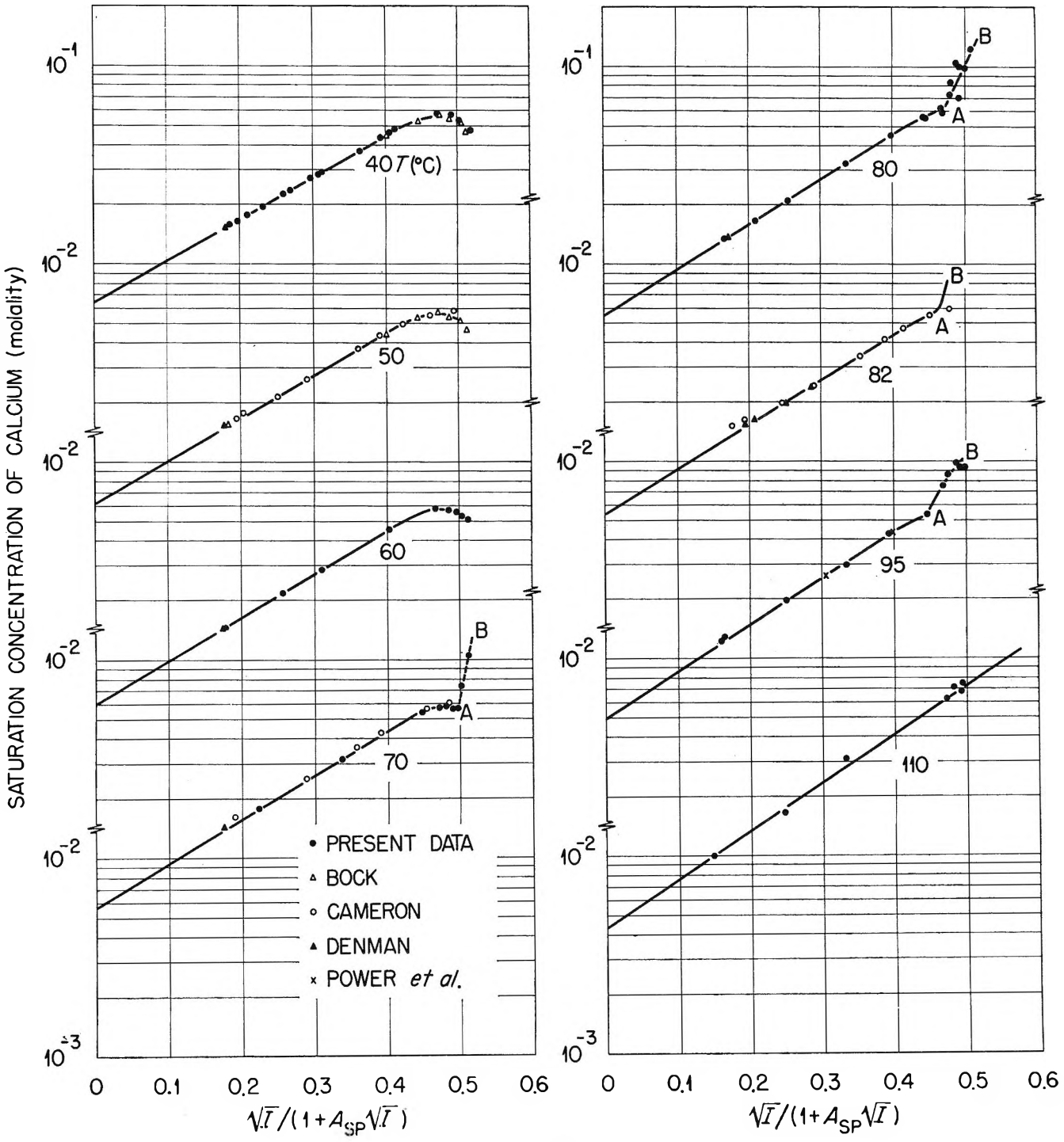

Figure 2. The solubility of $CaSO_4 \cdot 2H_2O$ (gypsum) in NaCl–H_2O solutions *vs.* $\sqrt{I}/(1 + A_{sp}\sqrt{I})$ at 40–110°; appearance of a new solid phase.

product ($[Ca^{2+}][SO_4^{2-}]$) of $CaSO_4 \cdot 2H_2O$. At these temperatures (70–95°) and at the highest ionic strength there appear to be three saturating solids, $CaSO_4 \cdot 2H_2O$, NaCl, and the third solid.

In preliminary steps to evaluate the four parameters, $s°$, A_{sp}, B', and C', of eq 6, the parameters were determined simultaneously at each temperature from the data shown in Figures 1 and 2 by a method of least

squares.[15] With smoothed values of A_{sp} *vs.* temperature, the data were reevaluated for $s°$, B', and C'. Smoothed values of $s°$ together with those for A_{sp} were then used to reevaluate B' and C'. Finally, smoothed values of B' *vs.* temperature were used to obtain C' values. The final values of C' were smoothed to obtain B' but with no further improvement in the curve of B' *vs.* temperature.

For evaluating the B and C parameters of eq 4, separate values of $K_{sp}(T) = (sa_{H_2O})^2$ were calculated from the experimental solubilities and the activity of water as a function of NaCl concentration and temperature. Equations 1–6 of Stoughton and Lietzke's paper,[16] derived from literature data, were used to obtain the activity of water (and also the Debye–Hückel slope used in this and the previous evaluation). By using the smoothed values of both $K_{sp}° = (s°)^2$ and A_{sp}, values of B and C were determined in the same manner described for B' and C'.

A plot of the values of A_{sp} at each temperature obtained by the above procedures is given in Figure 3. The smoothed curve through the values was strongly weighted for the A_{sp} values obtained from our present study and from most of the other studies depending upon the number of data available and the estimated reliability. In our previous paper,[3] A_{sp} was arbitrarily selected as 1.5 to be used at temperatures from 25 to 200°. In reevaluating the previous solubilities of $CaSO_4$ in NaCl–H_2O, 125–200°, we have obtained best-fit values of A_{sp} in the vicinity of 1.6 ± 0.1 and therefore have drawn the smoothed curve of Figure 1 to approach 1.6 at temperatures above 110°. The corresponding plot of log $K_{sp}°$, determined separately at each temperature, *vs.* $1/T(°K)$ is given in Figure 4. Those individual values for the B, B', C, and C' parameters are shown in Figure 5.

The separately determined values of $K_{sp}°$ and

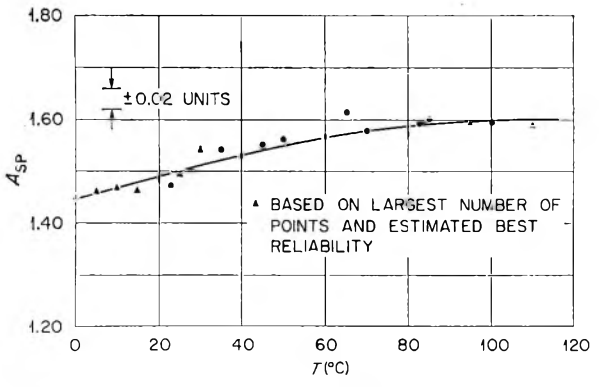

Figure 3. Variation of the A_{sp} parameter with temperature for the description of the solubility product of $CaSO_4 \cdot 2H_2O$ in NaCl–H_2O solutions.

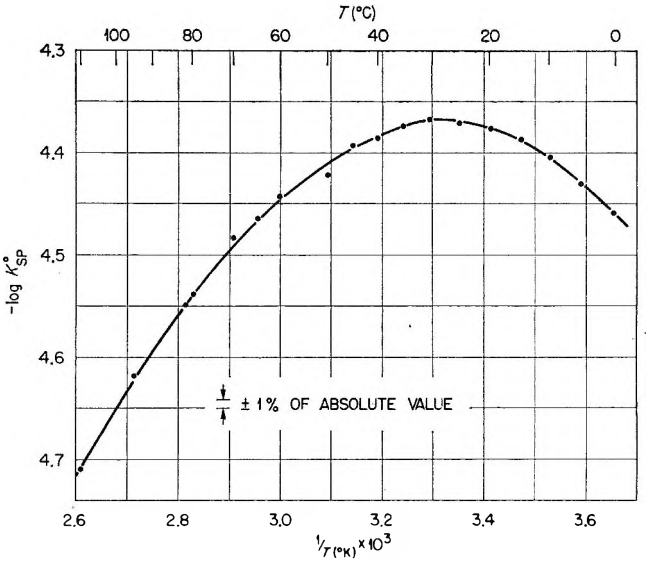

Figure 4. Negative logarithm of $K_{sp}°$ *vs.* $1/T(°K)$ for $CaSO_4 \cdot 2H_2O$ (gypsum) at 0–110°.

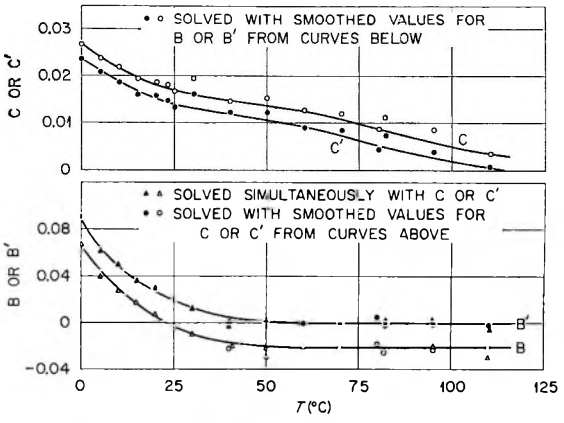

Figure 5. The B, C [for $K_{sp}(T)$] and B', C' [for $K_{sp}(P)$] parameters obtained from the solubility products of $CaSO_4 \cdot 2H_2O$ in NaCl–H_2O solutions.

smoothed values of A_{sp}, B', and C' together with the sources of data and the number of points evaluated at each temperature are given in Table II. Within the limits of precision and according to the curves of Figure 5

$$B = B' - 0.020 \quad (7)$$

$$C = C' + 0.0030 \quad (8)$$

With the parameters of Table II and the use of eq 6, all experimental solubilities of $CaSO_4 \cdot 2H_2O$ from 0 to 95° shown in Figures 1 and 2 (where $CaSO_4 \cdot 2H_2O$ is

(15) M. H. Lietzke, "A Generalized Least-Squares Program for the IBM 7090 Computer," U. S. AEC Report ORNL-3259, April 1962.

(16) R. W. Stoughton and M. H. Lietzke, *J. Chem. Eng. Data*, **10**, 254 (1965).

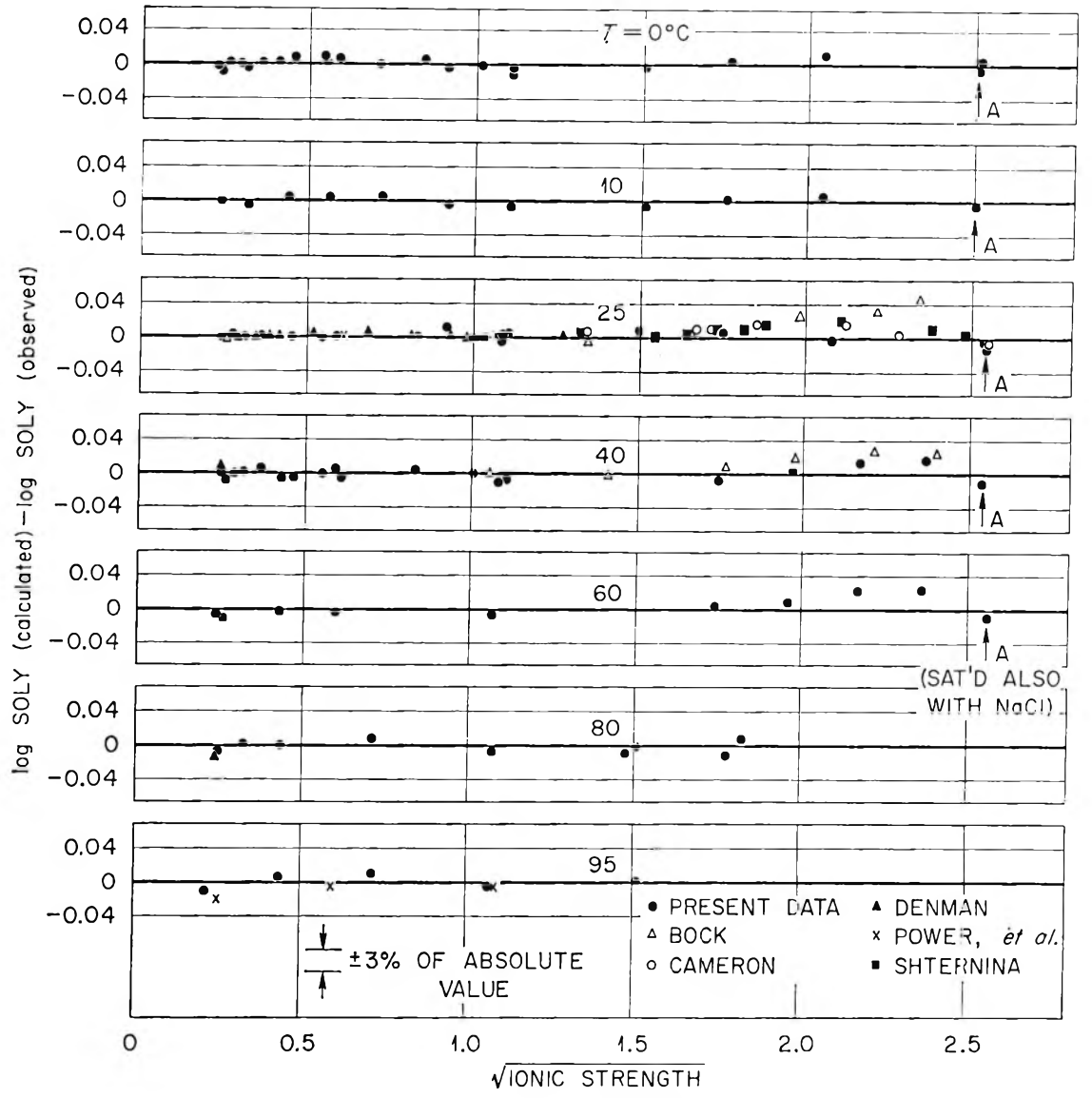

Figure 6. A representative comparison of the calculated values of the log solubility minus the observed log solubility for $CaSO_4 \cdot 2H_2O$ (gypsum) in NaCl–H_2O solutions from 0 to saturation at 0–95°.

the only solid phase) were calculated to within about ±0.5–3%. Those few calculations at 110° showed a wider spread (6%). Representative values of log solubility (calcd) − log solubility (obsd) are shown in Figure 6 plotted against the square root of the ionic strength in order to spread out the individual points. The literature values and the present results are in good agreement at all temperatures and ionic strengths.

General Significance. Published values for the dissociation constants (in aqueous solution at 25°) of 2–2 sulfate salts are in the vicinity of 10^{-2}.[17] A value for $CaSO_4$ of $10^{-2.31}$, derived from the deviation of some solubilities from the Davies equation, has been published by Bell and George,[18] who state that the value is based on the validity of the Davies equation and must

(17) J. Bjerrum, G. Schwarzenbach, and L. G. Sillén, Compilers, "Stability Constants, Part II, Inorganic Ligands," The Chemical Society, Burlington House, London, 1958.

(18) R. P. Bell and J. H. B. George, *Trans. Faraday Soc.*, **49**, 619 (1953).

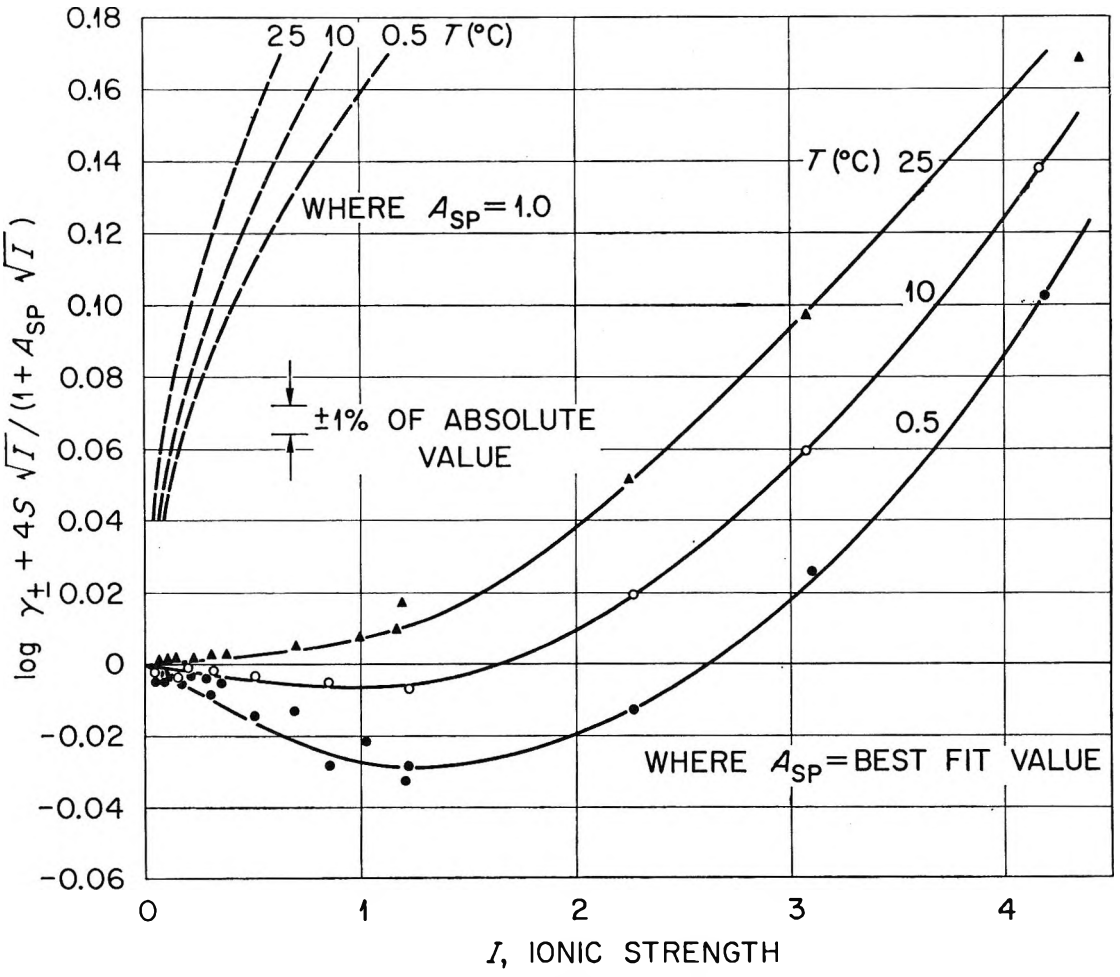

Figure 7. A deviation function to show the contribution of the BI and CI^2 terms to the calculated mean activity coefficient of $CaSO_4$ in NaCl–H_2O solutions.

be considered an estimate. In our present work, by assuming both equilibria

$$CaSO_4 \cdot 2H_2O(s) \overset{K_{sp}^\circ}{\rightleftharpoons} Ca^{2+} + SO_4^{2-} + 2H_2O$$

$$CaSO_4^0 \overset{K_d^\circ}{\rightleftharpoons} Ca^{2+} + SO_4^{2-}$$

and by assuming that the activity coefficient of the neutral species, $CaSO_4^0$, is unity and invariant with ionic strength, the following equation can be obtained

$$\log (s - K_{sp}^\circ/K_d^\circ) = {}^1/_2 \log K_{sp}^\circ + 4S\sqrt{I'}/(1 + A_{sp}\sqrt{I'}) + (B'/2)I' - (C'/2)(I')^2 \quad (9)$$

where K_d° is the dissociation constant for $CaSO_4^0$ and $I' = I - 4K_{sp}^\circ/K_d^\circ$. With this expression, differing by the terms K_{sp}°/K_d° and I' from eq 6, we obtained essentially the same variance of fit to our data (shown in Figures 1 and 2 and given in ref 3 to 200°) as with eq 6, and obtained values of K_d° in the vicinity of 10^{-2} to 10^{-4}, but with standard errors of 50–400%. For this comparison the last two terms both of eq 6 and 9 were not included (they are significant only at very high ionic strengths), and only the solubilities at ionic strengths to 1 were evaluated. A curve of K_d° *vs.* temperature gave smoothed values of $-\log K_d^\circ$ of 1.8 ± 0.4, 1.9 ± 0.4, 2.5 ± 0.4, and 3.5 ± 0.6 at 0, 25, 100, and 200°, respectively. This study therefore provides support for the association of $CaSO_4$ in rather good agreement with published values at low temperatures, but it shows for these measurements that its assumption is unnecessary. This proposition may also be valid for many other 2–2 sulfate salts.

The A_{sp} in the extended Debye–Hückel expression is expressed by $b\mathring{a}$ where b is a function of the temperature and dielectric constant and $\mathring{a}$ is the commonly called "ion-size parameter" presumably related to an average ion radius in angstrom units. Although at present this extended theory is subject to considerable controversy,

it is of interest to obtain the values of $\mathring{a}$ as a function of temperature from the values of A_{sp} given in Figure 3. Within the limits of uncertainty $\mathring{a}$ was found to be essentially constant at 4.5 A from 0 to 110°, thus perhaps indicating an invariant hydration sphere radius with changing temperature.

The general purpose of this present study is based on the propositions (1) that water is much less structured or hydrogen-bonded at temperatures above 100°, (2) that this simplicity may be indirectly observed by solubility studies, and (3) that ultimately a suitable aqueous solution theory may be obtained for direct use at very high ionic strengths at high temperatures or for application to an ideal state at low temperatures. The effect of water structure at low temperatures may be preventing the attainment of a satisfactory theory applicable at high ionic strengths. This effect might be resolved from the proposed "ideal" behavior at temperatures above 100°. In the present study, the decrease with temperature of the contribution of the terms $B'I$ (approaches zero at 45°) and $C'I^2$ (approaches zero at 100°) certainly provides much greater simplicity at high temperatures in the representation of the variation of solubility products or activity coefficients with ionic strength, and may revive interest in the possible theoretical significance of an A_{sp} parameter, the solutions at high temperatures being less encumbered by hydrogen bonding.

Deviation Functions. The mean activity coefficient, $\gamma_{\pm}(CaSO_4)$, can be expressed by $s^\circ/(sa_{H_2O})$. By substituting this value into eq 4 [where $\sqrt{K_{sp}^\circ/K_{sp}(T)} = s^\circ/(sa_{H_2O})$] and rearranging

$$\log \gamma_{\pm} + 4S\sqrt{I}/(1 + A_{sp}\sqrt{I}) = -\frac{B}{2}I + \frac{C}{2}I^2 \quad (10)$$

The quantity on the left side of eq 10 is plotted against the ionic strength in Figures 7 and 8. This type of plot provides a stringent test for the correctness of A_{sp} and s° (or K_{sp}°) necessary to fit the data; differences of 3% in A_{sp} give sharp divergencies in the plots of Figure 7 as $I \rightarrow 0$. Incorrect values of s° displace equally all points with respect to the ordinate and do not allow the extrapolation to zero for the deviation function. The negative deviation at low ionic strengths is attributed to the term $-(B/2)I$, where the slope, as $I \rightarrow 0$, corresponds to $-B/2$. The $(C/2)I^2$ term gives the positive deviation at very high ionic strengths, thus masking the effect of the $-(B/2)I$ term. The plots show well the diminishing value of B with rising temperature. For comparison, the dashed curves on Figures 7 and 8 show a similar deviation function when A_{sp} = unity; thus the relative contribution of the extra terms under this condition is large.

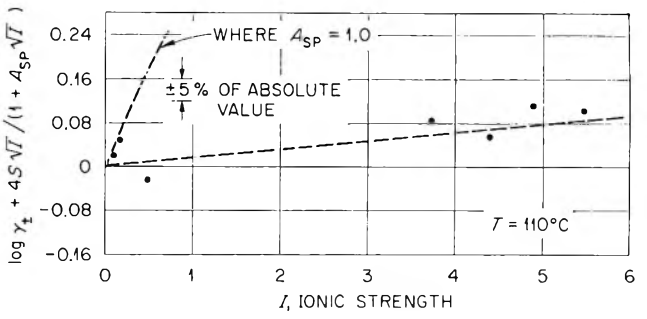

Figure 8. A deviation function to show the contribution of the BI term to the calculated mean activity coefficient of calcium sulfate in NaCl–H_2O solutions at 110°.

For describing the variation of activity coefficients with ionic strength, Pitzer and Brewer,[19] following an earlier suggestion of Guggenheim,[20] have proposed the use of A_{sp} = unity with the addition of a second term, $B \cdot I$, where $B \cdot$ is given as a deviation parameter. By following this procedure, values of $B \cdot$ have been calculated for all the solubility data. Representative plots at the several temperatures are given in Figure 9 of the $B \cdot$ parameter in the equation

$$\log s^\circ/(sa_{H_2O}) = \log \gamma_{\pm} = -4S\sqrt{I}/(1 + \sqrt{I}) + B \cdot I \quad (11)$$

It is seen that whereas for this system $B \cdot$ can be represented in graphical or tabular form, it is not a constant for this 2–2 salt but is very dependent on ionic strength. These $B \cdot$ values may be useful for comparing with the many $B \cdot$ values tabulated elsewhere but for 1–1 electrolytes.[21]

Standard Thermodynamic Values for $CaSO_4 \cdot 2H_2O$. The standard heat of solution, ΔH°, is given by

$$\Delta H^\circ = E + \int_0^T \Delta C_p^\circ dT \quad (12)$$

where E is a parameter. For use of eq 12 the assumption was made that the standard change in the heat capacity at constant pressure, ΔC_p°, could be given by

$$\Delta C_p^\circ = F + GT \quad (13)$$

where F and G are parameters. The resulting expression for ΔH° was substituted into the van't Hoff equation

$$d \ln K_{sp}^\circ/d(1/T) = -\Delta H^\circ/R \quad (14)$$

(19) G. N. Lewis and M. Randall, "Thermodynamics," 2nd ed, revised by K. S. Pitzer and L. Brewer, McGraw-Hill Book Co., New York, N. Y., 1961, Chapter 22, p 326.

(20) E. A. Guggenheim, *Phil. Mag.*, **19**, 588 (1935).

(21) G. N. Lewis and M. Randall, ref 19, Appendix 4.

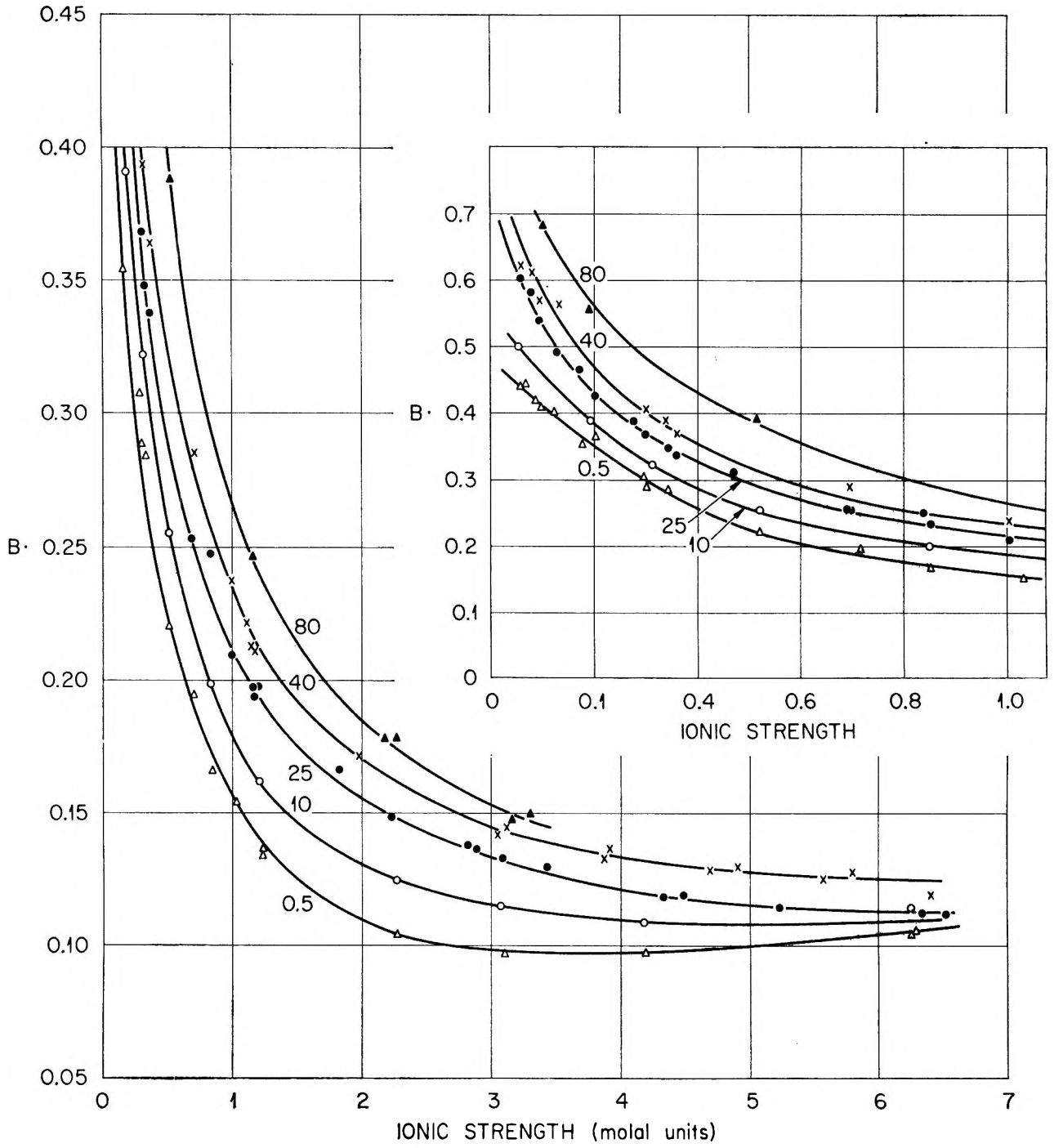

Figure 9. The Guggenheim–Pitzer–Brewer deviation parameter ($B\cdot$) *vs.* the ionic strength for the mean activity coefficient of calcium sulfate in NaCl–H_2O solutions at 0–80°.

which was then integrated over all values of $K_{sp}°$ and T(°K) to obtain a four-parameter equation. With the separately determined values of $K_{sp}°$ (unsmoothed but obtained using smoothed values of A_{sp}) from Table II, the four parameters were evaluated by the method of least squares to obtain eq 15.

$$\log K_{sp}° = 390.9619 - 152.6246 \log T - 12545.62/T + 0.0818493T \quad (15)$$

The average deviation from this equation of the experimental values shown in Figure 4 was ±0.6%. Values of $\Delta H°$ at each temperature were obtained by

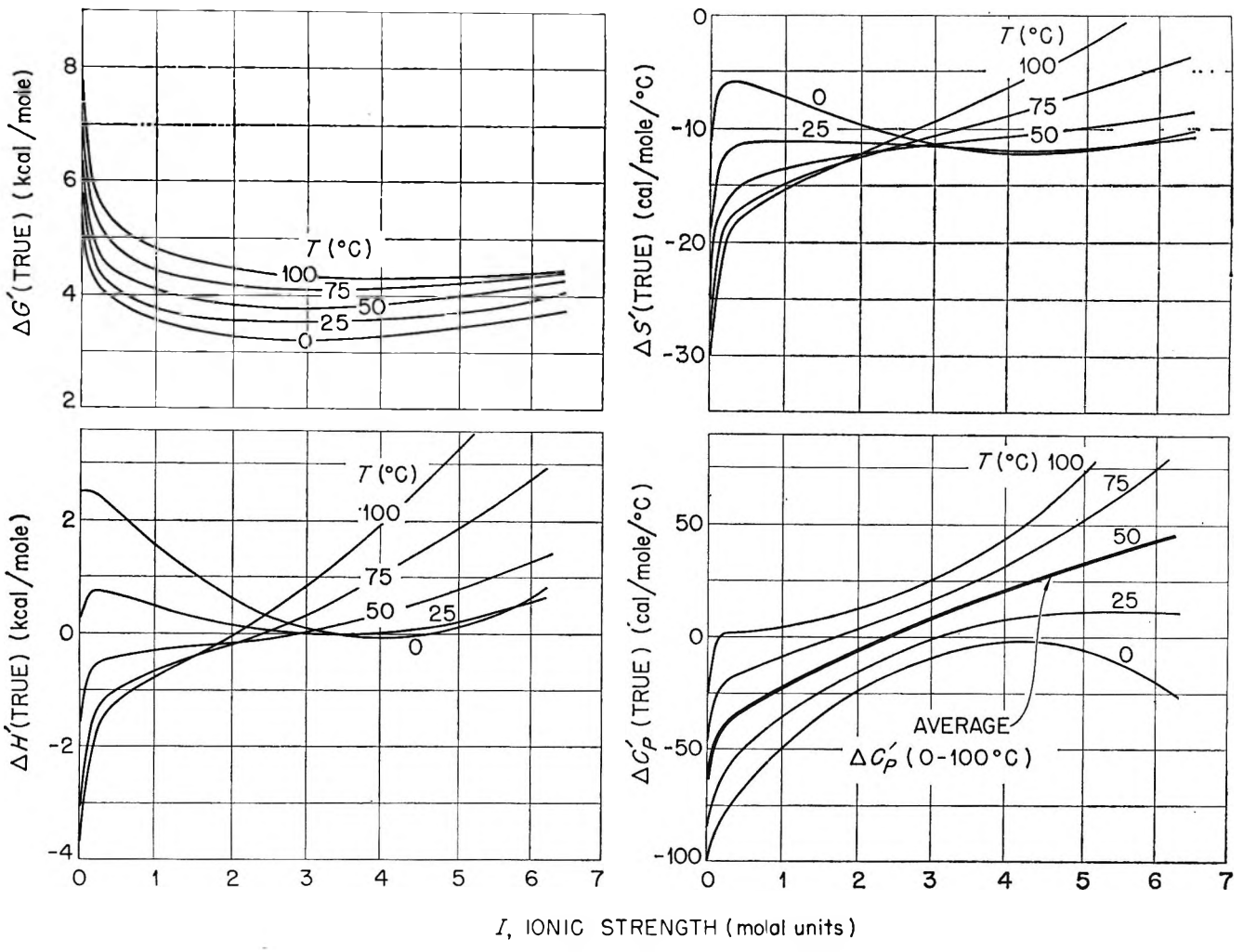

Figure 10. Thermodynamic quantities for the solubility of $CaSO_4 \cdot 2H_2O$ (gypsum) in NaCl–H_2O solutions; 0–6 *m* at 0–100°.

differentiating eq 15 with respect to $1/T$(°K) and substituting the result into the van't Hoff equation (14), while those values of $\Delta C_p°$ were obtained by differentiating with respect to T the resulting expression for $\Delta H°$. Values of $\Delta G°$ were calculated by using eq 15, where $\Delta G° = -2.303\,RT \log K_{sp}°$, and thus $\Delta S°$ was obtained from eq 16. Representative calculated thermodynamic

$$\Delta S° = (\Delta H° - \Delta G°)/T \qquad (16)$$

values obtained by these procedures are given in Table III. It is seen that $\Delta H° = 0$ at $T = 29°$. Although it is not surprising that $\Delta H°$ would pass through zero, we know of no dissolution process in water that exhibits this behavior at this low temperature.

At 25° in Table III the value for $\Delta C_p°$ of −80 cal/(mole deg) agrees well with that of −75 calculated from a value of $C_p°$ for gypsum obtained from Kelley's compilations[22] and the ionic heat capacities for Ca^{2+} and SO_4^{2-} presented by Criss and Cobble.[23] The average value from 0 to 110° is −58 cal/(mole deg), compared with a value of −57 when $\Delta C_p°$ is assumed to be a constant and the data are fitted with a three-parameter equation. A much better fit of log $K_{sp}°$ was obtained, however, with the four-parameter equation.

Thermodynamic Values for $CaSO_4 \cdot 2H_2O$ in NaCl–H_2O Solutions. With the use of eq 4, 5, and 15, values for K_{sp}(T) and K_{sp}(P) were calculated at several ionic strengths and at 5° temperature intervals from 0 to 110°. The parameters for the eq 15 type for the variation of K_{sp}(T) and K_{sp}(P) at the several constant ionic strengths were evaluated from which, by subsequent treatment like that for the standard values, the thermodynamic quantities, $\Delta G'$(T), $\Delta H'$(T), $\Delta S'$(T), $\Delta C_p'$(T), and their analogous "practical" values were obtained. In Figure 10 representative isotherms for the "true"

(22) K. K. Kelley, "The Data on Theoretical Metallurgy," Part XIII, Bulletin 584, U. S. Bureau of Mines, U. S. Government Printing Office, Washington, D. C., 1960, p 46.

(23) C. M. Criss and J. W. Cobble, *J. Am. Chem. Soc.*, **86**, 5390 (1964).

Table III: Standard Thermodynamic Functions for $CaSO_4 \cdot 2H_2O$ at 0–110°

T °C	$K_{sp}^\circ \times 10^5$ [a]	ΔG° [b]	ΔH° [b]	ΔS° [c]	ΔC_p° [c]
0	3.42	5.58	+2.50	−11.3	−99
10	3.90	5.71	+1.55	−14.7	−91
20	4.17	5.87	+0.68	−17.7	−84
25	4.23	5.96	+0.27	−19.1	−80
30	4.24	6.06	−0.12	−20.4	−76
40	4.13	6.28	−0.85	−22.8	−69
50	3.90	6.52	−1.50	−24.8	−61
60	3.59	6.77	−2.07	−26.5	−54
70	3.24	7.05	−2.57	−28.0	−46
80	2.88	7.33	−3.00	−29.2	−39
90	2.55	7.63	−3.35	−30.2	−31
100	2.24	7.94	−3.62	−31.0	−24
110	1.96	8.25	−3.82	−31.5	−16

[a] Use of eq 15. [b] In kcal/mole. [c] In cal/(mole deg).

values are plotted *vs.* the ionic strength. The calculated "practical" values at 25° for $\Delta G'(P)$ are approximately 0.1, 0.2, and 0.4 kcal/mole lower than $\Delta G'(T)$, and for $\Delta S'(P)$ are 0.2, 0.5, and 1.2 cal/(mole deg) higher than $\Delta S'(T)$ at ionic strengths of 2, 4, and 6 *m*, respectively. The differences between the "true" and "practical" values of $\Delta H'$ and $\Delta C_p'$ are insignificant; they are dependent only on the very small change at constant I of a_{H_2O} with temperature. The parallel curves of $\Delta G'(T)$ *vs.* I at the various temperatures appear significant, with a minimum in $\Delta G'(T)$ occurring at an ionic strength near 3 *m* at all temperatures.

Comparative Thermodynamic Behavior of $CaSO_4 \cdot 2H_2O$ and $CaSO_4$; Transition Temperatures. The values for the solubility product constant of $CaSO_4$ [K_{sp}° (A)] from our own results[3] and those of Power, *et al.*,[12] given at temperatures from 25 to 200°, were evaluated according to the above method for $CaSO_4 \cdot 2H_2O$ to yield the following equation (like eq 15)

$$\log K_{sp}^\circ(A) = -7.084 + 6.6489 \log T - 1200.9/T - 0.032057T \quad (17)$$

With this eq 17 and the fact that $K_{sp}(A)$ should behave like $K_{sp}(T)$ with changing solution ionic strength, the variation of $K_{sp}(A)$ can be expressed by

$$\log K_{sp}(A) = \log K_{sp}^\circ(A) + \frac{8S\sqrt{I}}{(1 + A_{sp}\sqrt{I})} + BI - CI^2 \quad (18)$$

Therefore the differences between the thermodynamic quantities for $CaSO_4 \cdot 2H_2O$ and $CaSO_4$ are independent of the ionic strength; for example, $\Delta(\Delta G') = \Delta G'(T) - \Delta G'(A)$ and is equivalent to $\Delta G^\circ - \Delta G^\circ(A)$. The

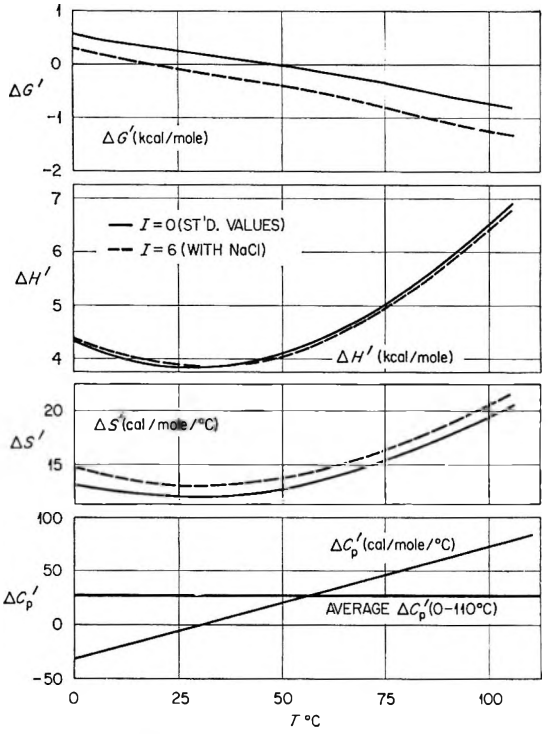

Figure 11. Thermodynamic values for the reaction $CaSO_4 \cdot 2H_2O(s) \rightleftharpoons CaSO_4(s) + 2H_2O(liq)$.

thermodynamic values for $CaSO_4$ obtained by the use of eq 17 and the analogous values for $CaSO_4 \cdot 2H_2O$ (Table III) were used to obtain these differences. Representative values are shown in Figure 11 and give the changes in free energy, heat content, entropy, and heat capacity according to eq 19 when 2 moles of H_2O from $CaSO_4 \cdot 2H_2O(s)$ are liberated to a solution phase where water has an activity of unity, the values being independent of ionic strength.

$$CaSO_4 \cdot 2H_2O(s) \rightleftharpoons CaSO_4(s) + 2H_2O(liq) \quad (19)$$

Similarly, the "practical" changes at high ionic strengths were calculated by the use of eq 5 and 18. These values depend only slightly on ionic strength and represent the changes for the liberation of water (eq 19) into a solution where $a_{H_2O} \neq$ unity. The dashed curves in Figure 11 show their behavior at $I = 6$.

The transition of $CaSO_4 \cdot 2H_2O$ to $CaSO_4$ occurs when the value for $K_{sp}(P)$ reaches the equivalent value for $K_{sp}(A)$. Thus by allowing $K_{sp}(P)$ and $K_{sp}(A)$ to be equal and combining eq 5 and 18, the following quadratic equation is obtained

$$0.0030I^2 + 0.020I + \log [K_{sp}^\circ/K_{sp}^\circ(A)] = 0 \quad (20)$$

Values for K_{sp}° and $K_{sp}^\circ(A)$ at several temperatures were calculated with eq 15 and 17; eq 20 was then solved for I. The curve of Figure 12 represents these cal-

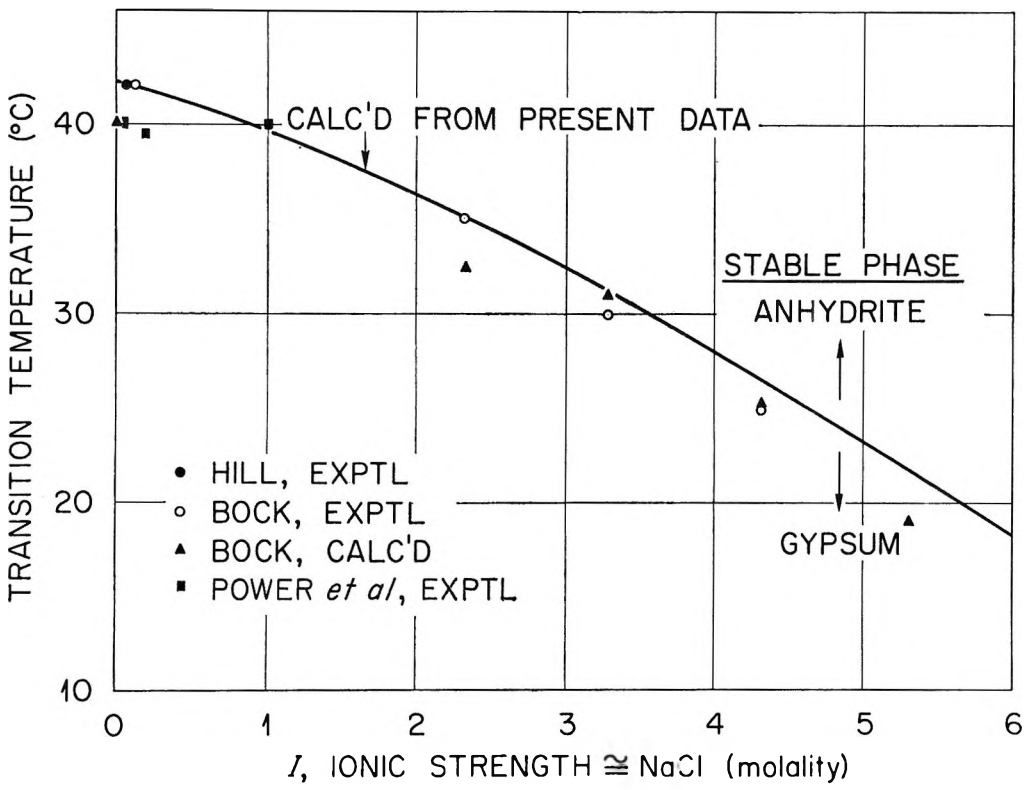

Figure 12. Transition temperatures for gypsum–anhydrite conversion in NaCl–H_2O solutions.

culated values *vs.* temperature, read as the variation of transition temperature with ionic strength. Experimentally derived (with some calculated) values of Bock,[9] Power, *et al.*,[12] and Hill[24] in H_2O and in NaCl–H_2O solutions are shown for comparison. The agreement is good.

The Additional Solid Phase. The curves shown in Figures 1 and 2 give the solubility behavior of $CaSO_4 \cdot 2H_2O$ from that in pure water to that in solutions containing sufficient NaCl to be saturated with a second solid phase. For all temperatures from 0 to 60° this second solid phase is NaCl. Thus only the solids $CaSO_4 \cdot 2H_2O$ [excluding anhydrous $CaSO_4$ as either a stable (above 42°) or metastable (below 42°) phase] and NaCl are the two saturating phases. However, above 60 and below 110° a second solid phase was found. The regions of stability (curves *AB*) of these solids ($CaSO_4 \cdot 2H_2O$ and the additional phase) are shown in Figure 2 at 70, 80, 82, and 95°, where point A represents the upper extent of the region of saturation by $CaSO_4 \cdot 2H_2O$ alone. At higher concentrations of NaCl the additional solid appears. In special experiments at 70° (see Experimental Section), this second saturating solid phase was identified by petrographic examination as $Na_2SO_4 \cdot 5CaSO_4 \cdot 3H_2O$ found previously in the system NaCl–Na_2SO_4–H_2O.[6] It was found also at 70° in larger quantities when Na_2SO_4 was added in small increments to a solution of calcium concentration lying midway on curve AB of Figure 2, thus further establishing its identity. By the formation of $Na_2SO_4 \cdot 5CaSO_4 \cdot 3H_2O$ from solutions initially only of NaCl and $CaSO_4$, the system becomes a five-component system rather than three and must be defined by the components $CaSO_4$, Na_2SO_4, NaCl, $CaCl_2$, and H_2O.

Acknowledgments. The authors wish to thank Emily Johnson (ORAU Summer Student Trainee from Winthrop College, Rock Hill, S. C., 1964) for obtaining some of the results at 25–40°. It is a pleasure to acknowledge many helpful discussions on this work with Professors George Scatchard, Massachusetts Institute of Technology, and John E. Ricci, New York University.

(24) A. E. Hill, *J. Am. Chem. Soc.*, 59, 2242 (1937).

Second Dissociation Constant of Sulfuric Acid from 25 to 350° Evaluated from Solubilities of Calcium Sulfate in Sulfuric Acid Solutions[1,2]

by William L. Marshall and Ernest V. Jones

Reactor Chemistry Division, Oak Ridge National Laboratory, Oak Ridge, Tennessee *(Received June 13, 1966)*

Values for second dissociation quotients and constants of H_2SO_4 were determined from extensive solubility measurements of $CaSO_4$ and its hydrates in aqueous sulfuric acid from 0 to 1.0 *m* (4.8 *m* below 50°) at temperatures from 25 to 350°. It was shown that the dissociation quotients could be described over the entire range of temperature to very high ionic strengths by the use of the one extended Debye–Hückel term, $\sqrt{I}/(1 + b\mathring{a}\sqrt{I})$, which contained only the "ion-size" parameter, $\mathring{a}$. The ion size varied from 2.8 A at 25° to a maximum of 4.2 A at 200°. The pK value for the second dissociation constant increased from 1.99 at 25° to 6.42 at 350°. This study is believed to be one of the first comprehensive investigations of this type to obtain an acid constant over such an extreme range of temperature and ionic strength. Whereas additional parameters were necessary to describe the dissociation quotients at 25–43° at the highest ionic strengths (0.5–4.8 *m*), these terms were unnecessary at higher temperatures, thus further supporting the contention that aqueous electrolyte solutions in general behave more simply at temperatures above 100°.

The solubility behavior of $CaSO_4$ in high-temperature aqueous electrolyte solutions is of particular interest since this salt has a sufficiently low solubility for relatively easy extrapolation of solubilities to zero ionic strength, and it appears not to hydrolytically precipitate oxysulfates at moderately high temperatures as do $NiSO_4$ and $MgSO_4$.[3,4] By using previously determined values and estimates for the solubility product constant of $CaSO_4$ at temperatures from 25 to 350° and the variation in solubility of $CaSO_4$ in sulfuric acid solutions over the same temperature range, values for the second dissociation quotient of H_2SO_4, $K_2 = [H^+][SO_4^{2-}]/[HSO_4^-]$, could be determined as a function both of temperature and ionic strength. Since this work is believed to be one of the first extensive studies and evaluations over the extreme range of temperature and ionic strength, aside from obtaining the standard state thermodynamic functions it was of very much interest to determine (1) whether the Debye–Hückel theory would be applicable at extreme temperatures; (2) whether the variation in the dissociation quotient with ionic strength could be expressed to very high ionic strengths by the single extended Debye–Hückel term, $\sqrt{I}(1 + A_K\sqrt{I})$, where A_K is the only adjustable parameter; (3) whether A_K would have a common value with A_{sp}, the parameter used previously[2] to express the variation in the ion solubility product of $CaSO_4$; and (4) whether any additional simplicity in representation might be observed at temperatures above 100° to substantiate previous suggestions that water solutions exhibit greater simplicity at high temperatures. With these unanswered questions the solubilities of $CaSO_4$ (or its hydrates) in H_2SO_4 solutions varying from 0 to 1 *m* (to 4.8 *m* below 50°) were measured at temperatures from 25 to 350° and are presented. From the results it was found that the calculated dissociation quotients could be described very well by the

(1) Work sponsored jointly by the U. S. Atomic Energy Commission and the Office of Saline Water, U. S. Department of the Interior, and performed at the Oak Ridge National Laboratory, which is operated by the Union Carbide Corporation. Presented before the Division of Physical Chemistry at the 149th National Meeting of the American Chemical Society, Detroit, Mich., April 4–9, 1965.

(2) Paper XVII in a series "Aqueous Systems at High Temperature." Previous paper: W. L. Marshall and R. Slusher, *J. Phys. Chem.*, **70**, 4015 (1966).

(3) W. L. Marshall, J. S. Gill, and R. Slusher, *J. Inorg. Nucl. Chem.*, **24**, 889 (1962).

(4) W. L. Marshall and R. Slusher, *J. Chem. Eng. Data*, **10**, 353 (1965).

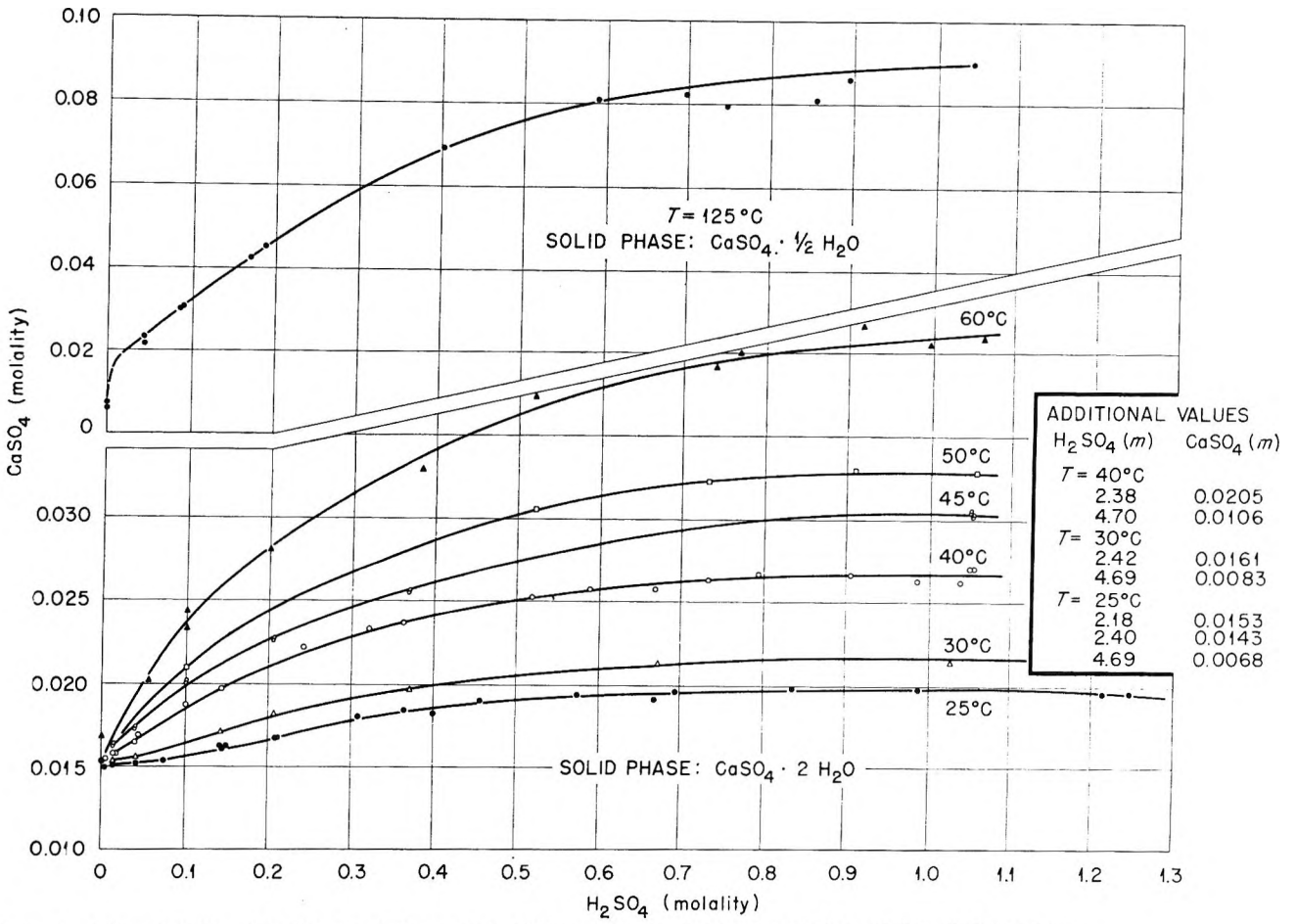

Figure 1. The solubility of $CaSO_4 \cdot 2H_2O$ (from 25 to 60°) and $CaSO_4 \cdot {}^1/_2H_2O$ (at 125°) in H_2SO_4–H_2O solutions.

single Debye–Hückel term to the highest temperature, but that two separate values for the A parameters (A_K, A_{sp}) were necessary for description. It therefore is believed that this study may substantiate the use of separate values of A parameters in general to describe separate equilibria not only at low temperatures but also to the very high temperatures. While the controversy of the theoretical significance of the A parameter, which equals $b\mathring{a}$ where b is a function of temperature and the dielectric constant and $\mathring{a}$ is the commonly called "ion-size" parameter, currently exists—most consider it to be strictly an empirical parameter—the evaluation presented herein may provide further insight into the true significance (if any) of these parameters. Although at 25 to 43° there was a positive divergence for K_2 from the single-term Debye–Hückel expression (Figure 4), this divergence was nonexistent at the higher temperatures. Thus the system shows greater simplicity at higher temperatures, suggesting further that this behavior may arise from the breakdown in the structure of water. From the additional evaluation of the results, the standard-state second dissociation constant of sulfuric acid, $K_2°$, and the related thermodynamic functions were obtained over the entire range of temperature, thus extending these values to 350° from those of Lietzke, Stoughton, and Young to 225°.

Experimental Section

Reagent grade $CaSO_4 \cdot 2H_2O$ (both Mallinckrodt and Baker and Adamson Co.) was used. The solid used in most of the experimental runs was washed several times with distilled water by heating the mixture, with stirring, at 100° for 4–24 hr and then decanting the supernate. By allowing this washed solid to remain in contact with water at 25°, any hemihydrate that may have formed was converted back to the dihydrate. When unwashed solid was used in comparative runs there was no perceptible difference in the solubilities.

Sulfuric acid (J. T. Baker Co.) stock solutions were prepared, analyzed, and diluted to the concentrations required for the experiments. Although only analyzed values are reported, those for H_2SO_4 were checked against the initial concentrations to avoid errors. (At high temperatures and high pressures the analyzed

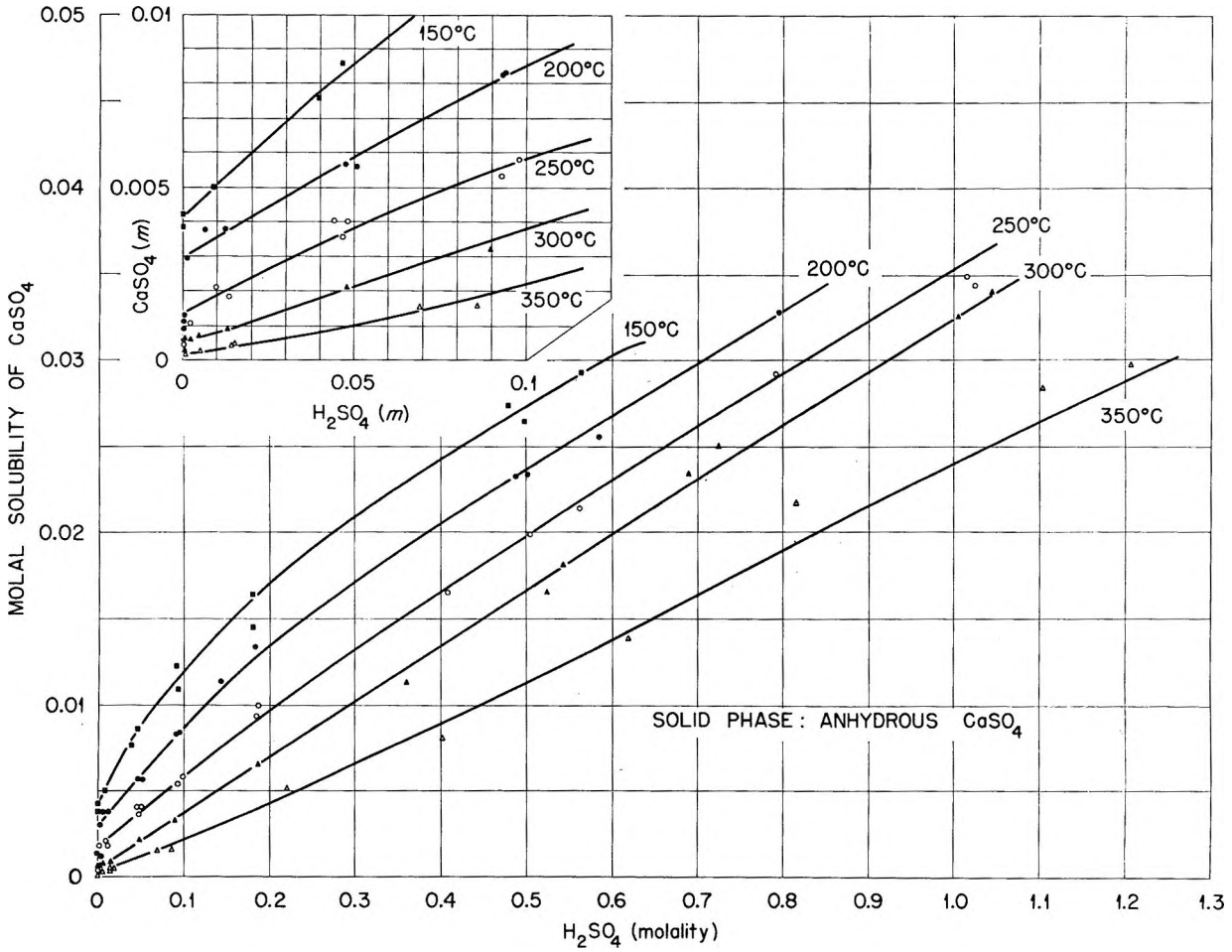

Figure 2. The solubility of $CaSO_4$ in H_2SO_4–H_2O solutions at 150–350°.

concentration will not agree exactly with the initial concentration—neglecting density changes by dissolution of $CaSO_4$—because of the loss of H_2O and H_2SO_4 to the vapor phase. Also, at times the high-pressure vessels may leak.)

All analytical and experimental procedures were followed chiefly as described previously[2-5] but with the use of modified high-pressure vessels and sampling techniques. Previously, a solution sample was decanted through a capillary sampling tube that was connected to the head of the bomb and reached below the solution level. In the present study, solution samples were filtered through a porous Teflon disk (Pall Corp.) that fitted into a recess in each head and was held by a retaining ring. For example, the vessels were placed in inverted positions by turning the heating block, and the liquid phase was filtered directly through the solid that now lay on top of the porous Teflon. The Teflon filter was used successfully at temperatures to 375°. However, above 327° a new disk was inserted after each run since the large expansion (at the Teflon transition temperature of about 327°) and subsequent contraction upon cooling prevented repeated use. The times necessary for the attainment of equilibrium were approximately the same (1.5–5 hr depending on the temperature and solid phase transition) as for the solubility of $CaSO_4$ in NaCl–H_2O solutions.[5] Samplings and analyses of the solution phases were all performed on a volumetric basis. Free acid was determined by standard acid–base titrations (with a recording titrimeter) and calcium by recorded potentiometric (rather than colorimetric) titrations with the use of EDTA as a complexing agent.[5] The results were converted to molal units by using literature values for the densities of aqueous H_2SO_4 solutions at 25°[6] and assuming that the contribution to the density by dissolved $CaSO_4$ was negligible compared with that of the H_2SO_4. The solid phases were isolated after each run

(5) W. L. Marshall, R. Slusher, and E. V. Jones, *J. Chem. Eng. Data*, 9, 187 (1964).

(6) "International Critical Tables," 1st ed, E. W. Washburn, Ed., McGraw-Hill Book Co., New York, N. Y., 1928, Vol. 3, p 56.

Table I: The Molal Solubility of $CaSO_4$ and Its Hydrates in H_2SO_4–H_2O Solutions at 25–350°

H_2SO_4 (m)	$CaSO_4$ (m)	H_2SO_4 (m)	$CaSO_4$ (m)	H_2SO_4 (m)	$CaSO_4$ (m)	H_2SO_4 (m)	$CaSO_4$ (m)	H_2SO_4 (m)	$CaSO_4$ (m)	H_2SO_4 (m)	$CaSO_4$ (m)	H_2SO_4 (m)	$CaSO_4$ (m)
T = 25°C $CaSO_4 \cdot 2H_2O$[a]		T = 40°C $CaSO_4 \cdot 2H_2O$[a]		T = 50°C $CaSO_4 \cdot 2H_2O$[a]		(16)[b]		0.790	0.0319[d]	(1.5)[b]		0.00178	0.00108	0.725	0.0250
(24)[b,c]		(24)[b,c]		(16)[b,c]		0.0000	0.0069	0.984	0.0354[d]	0.0588	0.00428	0.01324	0.00182	1.045	0.0339
0.1472	0.0160	0.0141	0.0156	0.1021	0.0209	0.0451	0.0218	(16)[b]		0.0965	0.00707	0.0442	0.00404	T = 325°C $CaSO_4$[a]	
0.2101	0.0167	0.0407	0.0168	0.520	0.0304	0.0885	0.0302	0.0005	0.00086	0.1817	0.0104	T = 275°C $CaSO_4$[a]		(5)[b]	
0.402	0.0182	0.1021	0.0187	0.728	0.0321	$CaSO_4$[a]		0.00085	0.00140	0.402	0.0177	(1.5)[b]		0.0000	0.00002
0.691	0.0196	1.048	0.0269	0.908	0.0329	(1.5)[b]		0.00189	0.00208	0.569	0.0236	0.0505	0.00268	0.000181	0.000162
1.243	0.0195	(24)[b,c]		1.054	0.0327	0.0180	0.0076	0.00230	0.00243	0.782	0.0298	0.1039	0.00494	0.000201	0.000221
(68)[b,c]		0.516	0.0253	T = 60°C $CaSO_4 \cdot 2H_2O$[a]		(16)[b]		0.0122	0.00434	0.992	0.0346[d]	0.428	0.0164	0.00484	0.000411
0.00482	0.0149	0.729	0.0263	(16)[b,c]		0.372	0.0268	0.0267	0.00636	(6)[b]		0.601	0.0207	0.01464	0.000692
0.01347	0.0152	0.903	0.0266	0.1021	0.0232	0.523	0.0295	0.0419	0.00689	0.0000	0.0003	0.848	0.0294		
0.0401	0.0152	1.048	0.0271	0.517	0.0372	0.721	0.0318	T = 200°C $CaSO_4$[a]		0.00016	0.00039	(2.5)[b]		(5)[b]	
0.1443	0.0161	(42)[b,c]		0.737	0.0390	T = 150°C $CaSO_4$[a]		(1.5)[b]		0.00035	0.00079	0.0486	0.00276	0.0549	0.00142
0.2080	0.0167	0.00511	0.0155	0.913	0.0415	(1.5)[b]		0.0000	0.0006	0.00124	0.00176	0.0941	0.00453	0.0667	0.00204
0.364	0.0184	0.01424	0.0158	1.060	0.0408	0.0000	0.0015	0.0000	0.0005	0.00180	0.00178	0.1889	0.00764	0.195	0.00611
0.667	0.0190	0.0400	0.0165	(72)[b]		0.0000	0.0016	0.0005	0.0013	0.00392	0.00178	0.511	0.0185	0.370	0.0093
2.403	0.0143	0.1433	0.0197	0.0000	0.0149	0.0088	0.0050	0.0471	0.00565	(16)[b]		0.802	0.0276	0.594	0.0152
4.69	0.0068	0.363	0.0237	0.0565	0.0202	0.0393	0.0076	0.0509	0.00560	0.00888	0.00309	1.040	0.0351	0.760	0.0217
(72)[b,c]		0.667	0.0252	0.1006	0.0243	0.0459	0.0086	0.0935	0.00828	0.0456	0.00433	(5)[b]		1.040	0.0293
0.0000	0.0152	1.039	0.0262	0.2016	0.0281	0.0912	0.0122	0.0940	0.00830	0.0875	0.00645	0.0000	0.00009	1.047	0.0292
0.0744	0.0152	2.384	0.0205	0.385	0.0329	0.0926	0.0108	0.1431	0.0113	0.1763	0.0107	0.00065	0.00028	(-)[b]	
0.1492	0.0162	4.70	0.0106	0.769	0.0399	0.1782	0.0145	0.1833	0.0133	0.500	0.0212	0.01284	0.00114	0.431	0.0120
0.3078	0.0179	(72)[b]		1.002	0.0404	0.1800	0.0164	0.488	0.0232	0.796	0.0290	0.0475	0.00252		
0.455	0.0189	0.242	0.0222	T = 125°C $CaSO_4 \cdot \frac{1}{2}H_2O$[a]		0.476	0.0273	0.501	0.0233	0.998	0.0351	T = 300°C $CaSO_4$[a]		T = 350°C $CaSO_4$[a]	
0.573	0.0193	0.321	0.0233			0.493	0.0262	0.585	0.0255	T = 250°C $CaSO_4$[a]		(3)[b]		(5)[b]	
0.833	0.0197	0.587	0.0258	(1.5)[b]		0.564	0.0293	0.796	0.0327	(1.5)[b]		0.00453	0.0007	0.00040	0.000172
0.987	0.0197	0.792	0.0266	0.0000	0.0070	0.863	0.0344[d]	0.998	0.0360[d]	0.0479	0.00402	0.0895	0.00323	0.00503	0.000295
1.210	0.0194	0.986	0.0262	0.1733	0.0426	0.972	0.0359[d]	(16)[b]		0.0981	0.00577	1.005	0.0325	0.01426	0.000422
2.180	0.0153	T = 45°C $CaSO_4 \cdot 2H_2O$[a]		0.592	0.0805	T = 175°C $CaSO_4$[a]		0.0000	0.0005	0.1848	0.00993	(16)[b]		0.01494	0.000479
T = 30°C $CaSO_4 \cdot 2H_2O$[a]		(7)[b,c]		0.700	0.0821	(1.5)[b]		0.00014	0.00063	0.407	0.0165	0.000511	0.000645	(16)[b]	
(52)[b,c]		0.0142	0.0162	0.858	0.0802	0.0000	0.0009	0.00035	0.00113	0.562	0.0213	0.000830	0.000305	0.220	0.00511
0.01420	0.0153	0.0406	0.0172	1.045	0.0898	0.0006	0.0030	0.00095	0.00297	0.792	0.0292	0.00199	0.000613	0.403	0.00794
0.0404	0.0156	0.1021	0.0200	(2)[b]		0.0463	0.0071	0.00652	0.00378	1.017	0.0348	0.01280	0.000877	0.619	0.0137
0.1426	0.0173	0.2067	0.0226	0.0000	0.0068	0.0548	0.0078	0.01214	0.00380	(3)[b]		(16)[b]		0.815	0.0217
0.2057	0.0182	0.368	0.0255	0.0453	0.0239	0.0909	0.0100	T = 225°C $CaSO_4$[a]		0.00934	0.00212	0.0478	0.00210	1.106	0.0284
0.370	0.0196	1.050	0.0302	0.0885	0.0302	0.0917	0.0093	(1)[b]		0.0466	0.00358	0.185	0.00650	(-)[b]	
0.672	0.0211	(20)[b,c]		0.1891	0.0454	0.1787	0.0131	0.398	0.0176	0.0929	0.00534	0.359	0.0112	0.0688	0.00153
1.027	0.0213	0.1021	0.0200	0.405	0.0691	0.1836	0.0145	0.574	0.0235	0.1835	0.00926	0.523	0.0165	0.0856	0.00156
2.416	0.0161	1.049	0.0304	0.749	0.0790	0.481	0.0244	0.776	0.0298	0.504	0.0198	0.541	0.0181	1.209	0.0297
4.69	0.0083			0.896	0.0855	0.489	0.0244	1.011	0.0346[d]	1.026	0.0343	0.690	0.0234		
						0.578	0.0276			(16)[b]					
										0.0000	0.00016				

[a] Saturating solid phase. [b] Stirring time (hr). [c] Data of R. Slusher. [d] Values may be about 10% low. Used for K_2 calculations but not shown in Figure 2.

by the method described previously[2–5] and identified by comparison of their X-ray diffraction patterns with known patterns.

Results and Discussion

General. The experimentally determined molal solubilities of $CaSO_4$ and its two hydrates in sulfuric acid solutions at temperatures from 25 to 350° are given in Table I. Included also are the times of equilibration for various separate sets of results. In Figures 1 and 2 these data are plotted against the molal concentrations of H_2SO_4. Some published solubilities of $CaSO_4 \cdot 2H_2O$ in H_2SO_4–H_2O are those of Cameron and Breazeale at 25, 35, and 43°,[7] of Van Veldhuizen at 25°[8] (twice as high as our present values—probably for the solubility of anhydrous $CaSO_4$), and of Castagnou and Larcebau[9] at 10° (only in very concentrated H_2SO_4 solutions). In Figure 3 are plotted smoothed solubilities of $CaSO_4 \cdot 2H_2O$ from the data in Table I as a function of temperature (25–60°) at several constant concentrations of H_2SO_4. Included for comparison are values similarly obtained from those data of Cameron and Breazeale. We are unable to account for the approximately 10% difference between our values and those of Cameron and Breazeale. Cameron's values in H_2O and in NaCl–H_2O from 25 to 55°,[10] however, agree within 1% with some recent confirmatory values of our own and with recent literature values.[2,11,12]

(7) F. K. Cameron and J. F. Breazeale, *J. Phys. Chem.*, **7**, 571 (1903).

(8) H. Van Veldhuizen, Thesis, Utrecht, 1929; A. Siedell and W. F. Linke, "Solubilities of Inorganic and Metal-Organic Compounds," 4th ed, D. Van Nostrand Co., New York, N. Y., 1958, Vol. I, p 663.

(9) R. Castagnou and S. Larcebau, *Bull. Soc. Pharm. Bordeaux*, **89**, 187 (1951); A. Seidell and W. F. Linke, "Solubilities of Inorganic and Metal-Organic Compounds," 4th ed, D. Van Nostrand Co., New York, N. Y., 1958, Vol. I, p 662.

(10) F. K. Cameron, *J. Phys. Chem.*, **5**, 556 (1901).

(11) W. L. Denman, *Ind. Eng. Chem.*, **53**, 817 (1961).

(12) W. H. Power, B. M. Fabuss, and C. N. Satterfield, *J. Chem. Eng. Data*, **9**, 437 (1964).

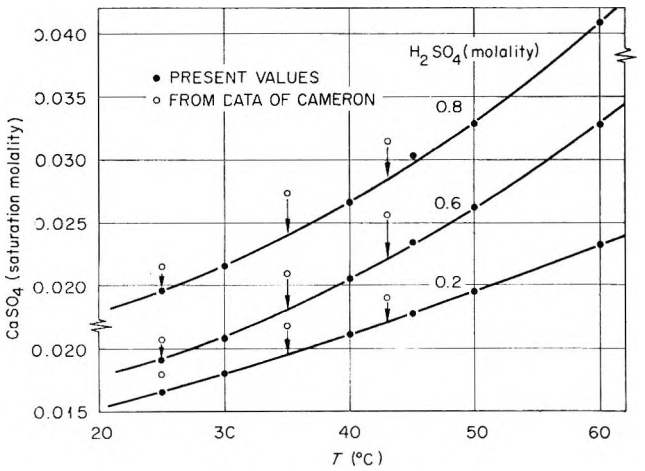

Figure 3. The comparison of the smoothed solubilities of $CaSO_4 \cdot 2H_2O$ at several constant molalities of H_2SO_4 at 25–60°.

In accordance with Figures 1 and 2, at low temperatures (25–60°) the addition of H_2SO_4 moderately increases the solubility of $CaSO_4 \cdot 2H_2O$, but at very high concentrations of H_2SO_4 the solubility is decreased. However, at higher temperatures the solubility increases strongly with increasing H_2SO_4 concentration. This behavior to moderately high concentrations of H_2SO_4 is certainly due to the sharply decreasing second dissociation constant of H_2SO_4 with rising temperature, which upon the addition of H_2SO_4 to saturated $CaSO_4$–H_2O solutions reduces the concentrations of SO_4^{2-} and allows an increase in the solubility of $CaSO_4$ to satisfy the solubility product. This increase is due also to the increase in the ionic strength upon addition of acid. Superimposed on these effects is the change in the solubility caused by the decreasing (with increasing temperature) solubility product of $CaSO_4$ (or its hydrates), in conformance with the solubility behavior of most sulfate salts at high temperatures.

The Second Dissociation Constant of H_2SO_4. The second dissociation constant of H_2SO_4 ($K_2°$) from 25 to 350° was calculated by using the experimental solubilities both in H_2SO_4 and NaCl solutions by the following procedure. An extended Debye–Hückel equation was used and assumptions were made that (1) the calcium ion was unassociated, (2) the first dissociation constant of H_2SO_4 was infinite, *i.e.*, there were no H_2SO_4 neutral species, and (3) the solubility product (K_{sp}) and the second dissociation quotient of H_2SO_4 (K_2) were the only equilibrium values in effect and described the following two equilibria

$$CaSO_4 \cdot xH_2O(s) \overset{K_{sp}}{\rightleftharpoons} Ca^{2+} + SO_4^{2-} + xH_2O$$

$$HSO_4^- \overset{K_2}{\rightleftharpoons} H^+ + SO_4^{2-}$$

at an ionic strength, I. If s = the molal solubility of $CaSO_4$, m = the formal molality of H_2SO_4, and y = the increase in the molality of H^+ or SO_4^{2-} caused by the dissociation of HSO_4^-, then $[Ca^{2+}] = s$, $[SO_4^{2-}] = s + y$, $[HSO_4^-] = m - y$, $[H^+] = m + y$, and $[a_{H_2O}]$ = the activity of H_2O. By neglecting the activity of H_2O (for anhydrous $CaSO_4$, $x = 0$ and the term drops out; otherwise it is nearly unity at moderately low molalities) and allowing K_{sp} to be equal to the ionic solubility product, by obtaining a value for y ($y = K_{sp}/s - s$), and by substituting the above quantities and the value for y into the relationship for K_2, eq 1 is obtained

$$K_2 = \frac{K_{sp}}{s}\left(\frac{m - s + K_{sp}/s}{m + s - K_{sp}/s}\right) \quad (1)$$

For the ionic strength = $\frac{1}{2}\Sigma(mz^2)$ on a molal basis, where z = charge on ion, eq 2 is derived

$$I = 2s + m + 2K_{sp}/s \quad (2)$$

The solubility product constant is given by

$$K_{sp}° = [Ca^{2+}][SO_4^{2-}]\gamma_{Ca^{2+}}\gamma_{SO_4^{2-}}a_{H_2O}^{x} \quad (3)$$

where $\gamma_{Ca^{2+}}$ and $\gamma_{SO_4^{2-}}$ are the activity coefficients of the respective ions, and a_{H_2O} is the activity of H_2O. According to an extended Debye–Hückel equation, $\gamma_{Ca^{2+}}$ and $\gamma_{SO_4^{2-}}$ may be expressed by

$$\log \gamma_{Ca^{2+}} = \log \gamma_{SO_4^{2-}} = -4S\sqrt{I}/(1 + A\sqrt{I}) - (B/2)I + (C/2)I^2 \quad (4)$$

where S is the Debye–Hückel limiting slope for a 1–1 electrolyte, in our case at each temperature always corrected for the use of molal units [$S(m) = S(M) \times \sqrt{d_{H_2O}}$], and A, B, and C are adjustable parameters.[2] With these relationships, values of log K_{sp} [$K_{sp}(P)$ of ref 2] were calculated by the equation

$$\log K_{sp} = \log K_{sp}° + 8S\frac{\sqrt{I}}{(1 + A_{sp}\sqrt{I})} + B'I - C'I^2 \quad (5)$$

where $K_{sp}°$ is the thermodynamic solubility product at $I = 0$, A_{sp} is a parameter that is assumed to be independent of the uncommon ions in the solvent medium, and B' and C' are parameters that account also for the variation of the activity of water when gypsum is the saturating phase.[2] Values for $K_{sp}°$, A_{sp}, B', and C' were obtained and reported from the solubilities of $CaSO_4$ in NaCl–H_2O solutions at temperatures up to 200°;[2,5] above 200° values of $K_{sp}°$ and A_{sp} (B' and C' = 0) were estimated both from our recent values for the solubilities of $CaSO_4$ in aqueous NaCl, $NaNO_3$, and Li-

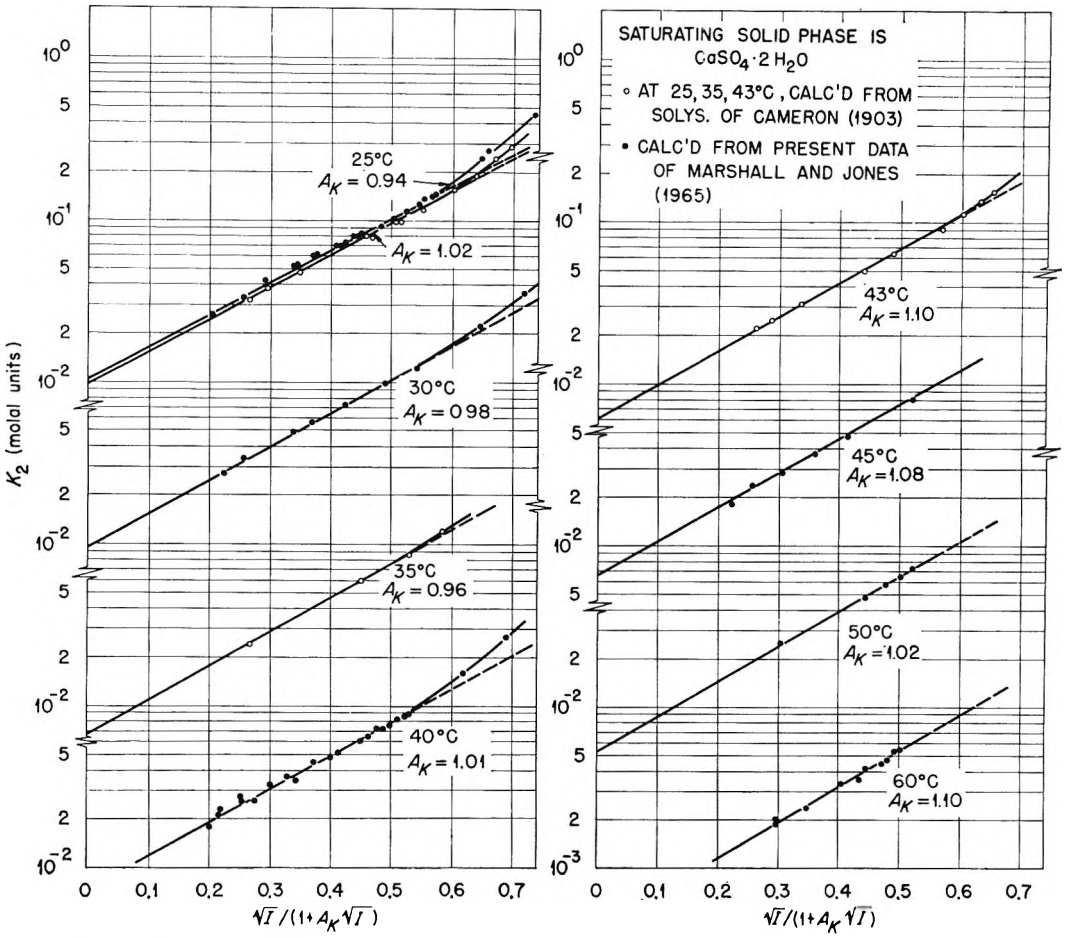

Figure 4. The variation of the second dissociation constant of H_2SO_4, K_2, with a function of the ionic strength, I (from solubilities of $CaSO_4 \cdot 2H_2O$ in H_2SO_4–H_2O) at 25–60°.

NO_3 solutions to 350°[13] and by extrapolation from the values at lower temperatures (25–200°).

A computer program was written that evaluated (by an iterative process) K_{sp}, I, and K_2 from the solubilities of $CaSO_4$ in H_2SO_4–H_2O. However, as the molality of sulfuric acid approached zero, the calculation failed due to the inability to obtain sufficient accuracy of measurement. Therefore, those values of K_2 at a very low molality (usually below about 0.01 m H_2SO_4) plotted preliminarily *vs.* $\sqrt{I}/(1 + 1.5\sqrt{I})$ and showing scatter greater than about ±5% were ignored. Also, those values at temperatures of 25–43° calculated from solubilities in H_2SO_4 solutions greater than about 1.0 m were not used since they showed a marked, systematic deviation from linearity on the preliminary plots. The remaining values of K_2 were evaluated by a generalized method of least squares[14] to obtain simultaneously the best values of $K_2°$ and A_K according to the equation

$$\log K_2 = \log K_2° + 4S\frac{\sqrt{I}}{(1 + A_K\sqrt{I})} \qquad (6)$$

The values of S at temperatures to 300° were the Debye–Hückel limiting slopes; at 325 and 350° the best observed slopes were about 10% greater than the Debye–Hückel slopes.

It will be mentioned in a later section that by selecting arbitrarily values of A_{sp} within a close approximation the best fit was obtained with the same values as derived from studies in NaCl–H_2O. Values of B' and C' obtained from the solubilities of $CaSO_4$ in NaCl–H_2O may certainly be arbitrary for use in evaluating the variation of K_2; however, they contribute significantly only at ionic strengths above about 0.5 m and thus have a negligible effect on the extrapolated value for $K_2°$.

Plots of log K_2 *vs.* $\sqrt{I}/(1 + A_K\sqrt{I})$ are shown in Figures 4 and 5 at the several temperatures (25–350°)

(13) W. L. Marshall and R. Slusher, to be submitted for publication.

(14) M. H. Lietzke, Oak Ridge National Laboratory Report ORNL-3259, 1962.

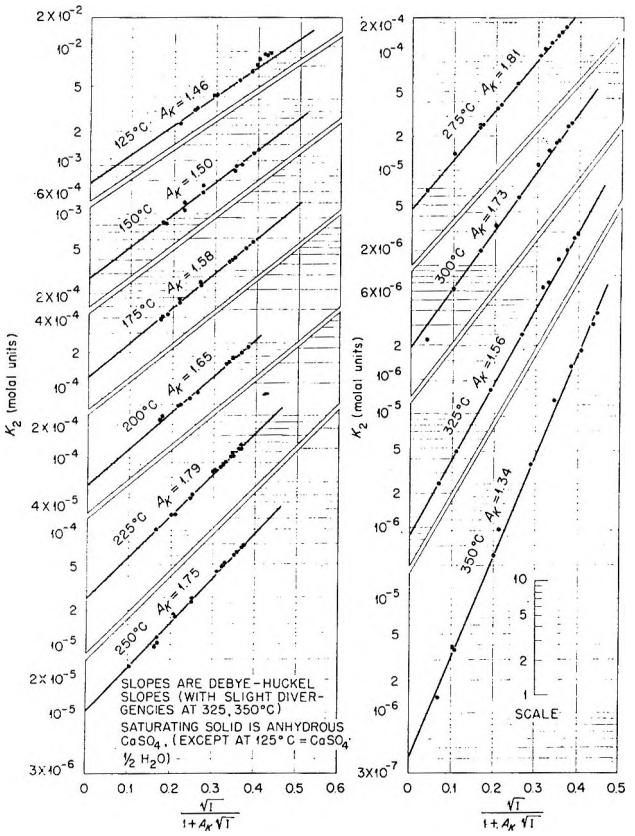

Figure 5. The variation of the second dissociation constant of H_2SO_4, K_2, with a function of the ionic strength, I (from solubilities of $CaSO_4$ in H_2SO_4–H_2O at 125–350°).

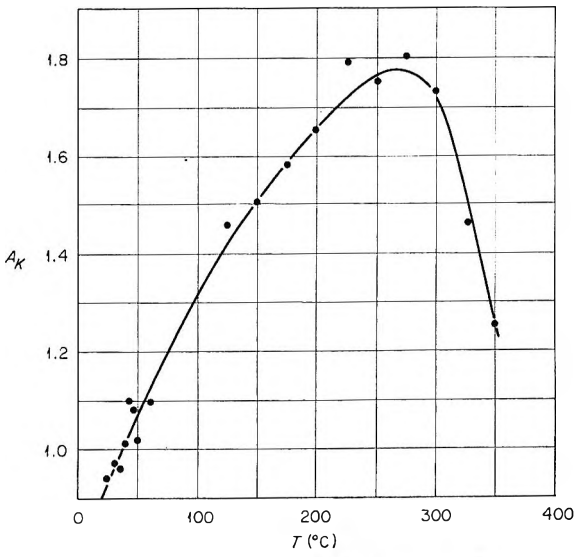

Figure 6. The A_K parameter in $\sqrt{I}/(1 + A_K\sqrt{I})$ experimentally determined for a variation of K_2 (for H_2SO_4) with ionic strength, I at 25–350°.

where the straight lines drawn through the data correspond to $4S$. The values of A_K, separately determined for each temperature, are given. The relative position of the lines drawn through the data correspond to the simultaneous least-square treatment for the intercept, K_2^c, at $I = 0$.

The separate values for the A_K parameters are plotted against the temperature in Figure 6. The standard error for each value was about 0.04 unit. In contrast to an expected near constancy for this parameter over small changes in temperature and even over a large span of temperature (*e.g.*, A_{sp} changes only from 1.5 to 1.6 as the temperature rises from 25 to 350°, see Table II) it changes markedly from 0.94 at 25° to 1.77 at 275°. The observed decrease from 1.77 to 1.34 at 350° was unexpected. Although the slopes used at the two highest temperatures were about 10% greater than the Debye–Hückel limiting slopes, use of the theoretical slopes for best fitting the data would have given even lower values for A_K.

Values of $K_2°$, determined independently at each temperature, and smoothed values for A_K are included in Table II. The values of $K_{sp}°$ and the corresponding values of A_{sp} that were used in eq 5 are included also.[2,5,13] The standard error (in parentheses) for each value of $K_2°$ is given together with the number of data points used for the simultaneous determination of $K_2°$ and A_K.

A product of the activity coefficients, $\Gamma_{HSO_4^-} = \gamma_{H^+}\gamma_{SO_4^{2-}}/\gamma_{HSO_4^-}$, can be expressed by

$$-\log \Gamma_{HSO_4^-} = -\log K_2°/K_2 = 4S\sqrt{I}/(1 + A_K\sqrt{I}) \quad (7)$$

The slope of log $\Gamma_{HSO_4^-}$ *vs.* $\sqrt{I}/(1 + A_K\sqrt{I})$ at each temperature can be normalized to the slope, $4S_{25}$, at 25° by multiplying log $\Gamma_{HSO_4^-}$ by $(4S_{25})/(4S_T)$ where $4S_T$ is the slope at the particular temperature T. A plot of all calculated values of $-\log \Gamma_{HSO_4^-}$ at *all* temperatures, normalized in this manner, against $\sqrt{I}/(1 + A_K\sqrt{I})$, where the A_K parameters used are the smoothed values given in Table II, is shown in Figure 7. We have therefore condensed a description of the variation of $\Gamma_{HSO_4^-}$ (and accordingly K_2) both with ionic strength (to about 1 m) and temperature to one linear relationship.

In Figure 8 our calculated values of $K_2°$ at low temperatures are plotted against $1/T$ (°K) and are compared to many literature values found between 0 and 60.°[15–19] Dunsmore and Nancollas recently have

(15) C. R. Singleterry and I. M. Klotz, Theses, University of Chicago, 1940; quoted by R. A. Robinson and R. H. Stokes, "Electrolyte Solutions," Butterworth and Co. Ltd., London, 1959, pp 385–387.

(16) C. W. Davies, H. W. Jones, and C. B. Monk, *Trans. Faraday Soc.*, **48**, 921 (1952).

Table II: Calculated Values for the Second Dissociation Constant of H_2SO_4 and Related Values Used in the Calculations

T, °C	$K_2°$	No. data points	A_K[a]	$K_{sp}°$	A_{sp}[a]	DHS[b]
25	$1.028\ (\pm 0.02) \times 10^{-2}$	18	0.94	4.24×10^{-5}[d]	1.49	0.5080
25	$9.76\ (\pm 0.08) \times 10^{-3}$[c]	5	0.94	4.24×10^{-5}[d]	1.49	0.5080
30	$9.42\ (\pm 0.22) \times 10^{-3}$	7	0.96	4.25×10^{-5}[d]	1.51	0.5125
35	$6.75\ (\pm 0.04) \times 10^{-3}$[c]	3	0.98	4.21×10^{-5}[d]	1.52	0.5176
40	$7.25\ (\pm 0.16) \times 10^{-3}$	22	1.01	4.10×10^{-5}[d]	1.53	0.5229
43	$6.09\ (\pm 0.05) \times 10^{-3}$[c]	4	1.02	4.02×10^{-5}[d]	1.53	0.5262
45	$6.66\ (\pm 0.01) \times 10^{-3}$	6	1.03	3.97×10^{-5}[d]	1.53	0.5282
50	$5.31\ (\pm 0.04) \times 10^{-3}$	5	1.07	3.83×10^{-5}[d]	1.54	0.5337
60	$4.32\ (\pm 0.18) \times 10^{-3}$	11	1.12	3.57×10^{-5}[d]	1.55	0.5449
125	$7.07\ (\pm 0.20) \times 10^{-4}$	7	1.42	9.49×10^{-6}[e]	1.60	0.6422
150	$2.75\ (\pm 0.11) \times 10^{-4}$	11	1.51	1.00×10^{-6}[f]	1.60	0.6899
175	$1.25\ (\pm 0.03) \times 10^{-4}$	12	1.58	3.36×10^{-7}[f]	1.60	0.7451
200	$5.69\ (\pm 0.14) \times 10^{-5}$	13	1.65	1.14×10^{-7}[f]	1.60	0.8097
225	$2.65\ (\pm 0.05) \times 10^{-5}$	16	1.71	3.31×10^{-8}[f]	1.60	0.8880
250	$1.05\ (\pm 0.03) \times 10^{-5}$	15	1.77	9.12×10^{-9}[f]	1.60	0.9848
275	$4.59\ (\pm 0.13) \times 10^{-6}$	14	1.77	2.29×10^{-9}[f]	1.60	1.112
300	1.94×10^{-6}	11	1.73	6.03×10^{-10}[f]	1.60	1.287
325	8.74×10^{-7}	10	1.56	1.66×10^{-10}[f]	1.60	1.69[g]
350	3.85×10^{-7}	11	1.34	4.27×10^{-11}[f]	1.60	2.18[g]

[a] Smoothed values. [b] Calculated Debye–Hückel limiting slope $\times \sqrt{d_{H_2O}} = S$. [c] Calculated from data of Cameron. [d–f] Saturating solid phase: *d*, $CaSO_4 \cdot 2H_2O$; *e*, $CaSO_4 \cdot {}^1/_2H_2O$; *f*, $CaSO_4$ (anhydrous). [g] Best observed slope—used in calculations at 325 and 350°; Debye–Hückel slopes, $S = 1.548$ and 1.984, respectively.

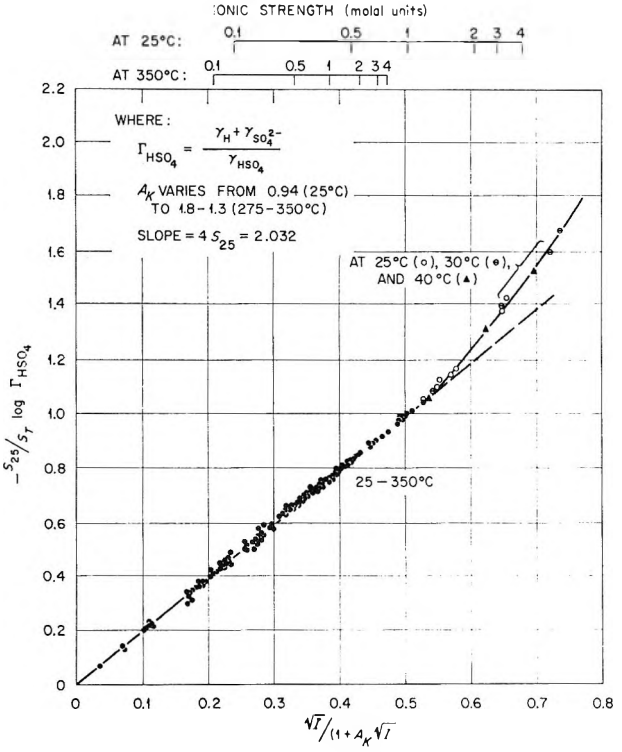

Figure 7. The variation of log Γ_{HSO_4} (the product of the activity coefficients for the dissociation of HSO_4^-) with a function of the ionic strength, *I*, from 25 to 350°; slopes normalized to Debye–Hückel slope at 25°.

published a review of values of $K_2°$ with some additional treatment[20] and have concluded that the best value at 25° is 0.0103 mole kg^{-1}. Young and Irish[18] in an earlier review accepted a value of 0.0102. In another very recent paper,[21] Covington, Dobson, and Wynne-Jones, from their own additional emf measurements and from a further reanalysis of previous values, have proposed a revised value of 0.0106 ± 0.0009 mole kg^{-1}. Our own value at 25° of 0.0103 ± 0.0002 mole kg^{-1} agrees well with the earlier "accepted" values and is within the stated limits of uncertainty of the value of Covington, *et al.* Also, our present values from 25 to 60° fit well within the limits of agreement of the various sets of data.

In Figure 9 the values of $K_2°$ from this paper are plotted as a function of temperature to 350°. The curve drawn through these values extends from the curve on Figure 8. Lietzke, Stoughton, and Young's

(17) W. J. Hamer in "The Structure of Electrolyte Solutions," W. J. Hamer, Ed., John Wiley and Sons, Inc., New York, N. Y., 1959, p 236.

(18) T. F. Young and D. E. Irish, *Ann. Rev. Phys. Chem.*, 13, 448 (1962).

(19) M. H. Lietzke, R. W. Stoughton, and T. F. Young, *J. Phys. Chem.*, 65, 2247 (1961).

(20) H. S. Dunsmore and G. H. Nancollas, *ibid.*, 68, 1579 (1964).

(21) A. K. Covington, J. V. Dobson, and W. F. K. Wynne-Jones, *Trans. Faraday Soc.*, 61, 2057 (1965).

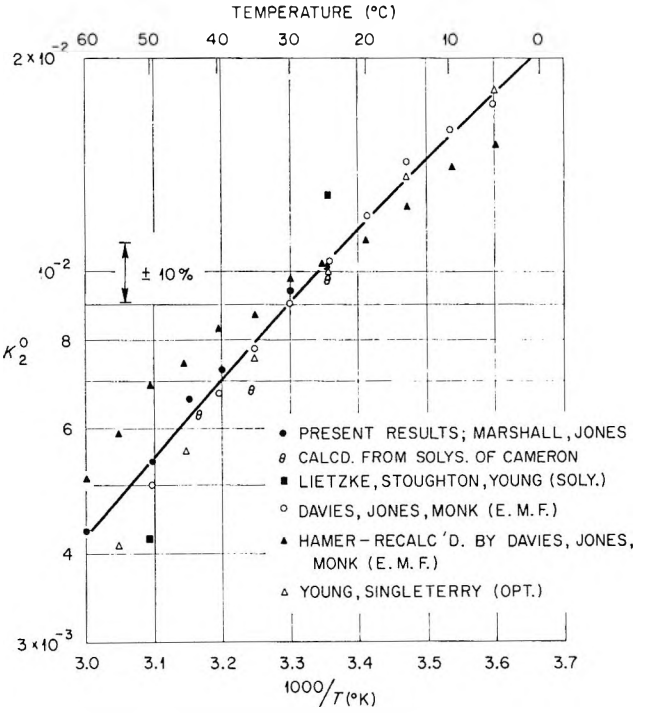

Figure 8. The comparison of $K_2°$ for H_2SO_4 obtained by various investigators at 0–60°.

individual results obtained from their solubility measurements on Ag_2SO_4 in H_2SO_4–H_2O solutions from 25 to 225°[19] are included for comparison. The difference (about 20%) between the two sets is well outside the standard error (usually varying between 1 and 4% (Table II)) of the extrapolated results shown in Figures 4 and 5. However, separate salts (Ag_2SO_4 *vs.* $CaSO_4$) were studied, and somewhat different methods were used to obtain $K_2°$ values. For the Ag_2SO_4 solubilities, values of the two separate A parameters for the variation of K_{sp} and K_2 were kept constant with temperature but were varied to obtain the best fit to the ionic strength function of K_2, whereas for $CaSO_4$ the A_{sp} parameter for the K_{sp} variation with ionic strength was either determined by arbitrarily selecting values of A_{sp} to give the best fit for $K_2°$ and A_K, or determined separately[2,5] and then used to determine $K_2°$ and A_K simultaneously. Essentially the same value of A_{sp} was obtained by either method. The fact that a 2–2 salt according to theory is considerably more complicated to describe than a 1–1 or 1–2 salt may be used to question the validity of extrapolation of the present data. In the present study, however, the equilibrium expressed by K_2 is that for the equilibrium behavior between 1+ and 2+ ions. Nevertheless, K_{sp} for the 2–2 salt is involved also. An adjustment of 20% in our present values of $K_{sp}°$ to account for the differences in $K_2°$ does not seem justifiable in view of the measurements.[2,5]

In one attempt to account for the differences in the values of $K_2°$, the values for a dissociation constant, $K_d°$, for the equilibrium, $CaSO_4°$ (soln) $\rightleftarrows$ $Ca^{2+} + SO_4^{2-}$, of 10^{-2} at 25° to 10^{-4} at 200°[2] were used in a modified equation 1 together with somewhat lower values of $K_{sp}°$ and A_{sp} obtained simultaneously with $K_d°$. Values of $K_2°$ derived by this procedure, when plotted *vs.* the temperature and read from the smoothed curve (the individual points showed greater scatter), were essentially unchanged due to a canceling-out effect between $K_d°$ and the revised values of $K_{sp}°$ and A_{sp}. The variance of fit at most temperatures was nearly the same or slightly better without the assumption of the association of $CaSO_4$.

Another constant

$$K_R° = K_{sp}°/K_2° = \frac{[Ca^{2+}][HSO_4^-]}{[H^+][CaSO_4(s)]} \qquad (8)$$

is plotted also as a function of temperature in Figure 9. Because $K_2°$ is obtained from an extrapolation of values of K_2 calculated from eq 1, for very low values of $K_{sp}°$ (above 150°) the constant, $K_R°$, is essentially independent of $K_{sp}°$.

The Sensitivity of K_2 (Eq 1) to Experimentally Derived (or Assigned) $K_{sp}°$ Values. At temperatures below 100° where $K_{sp}°$ is moderately large, eq 6 appears to fit the calculated K_2 values to low ionic strengths only if a unique value of $K_{sp}°$ is used for calculating K_2 values. With an incorrect $K_{sp}°$ value a divergence may be caused by the effect of the calculated K_{sp} within the parentheses of eq 1, observed only at low ionic strengths and for moderately large values of $K_{sp}°$, and by the equal percentage displacement of all the K_2 values from the first-order effect of K_{sp} outside the parentheses (of eq 1). Figure 10 shows several plots of calculated K_2 values at 40° using several arbitrary values of $K_{sp}°$ for $CaSO_4 \cdot 2H_2O$. It is seen at this temperature that both the extrapolated value of $K_2°$ and the adherence at low ionic strengths of calculated K_2 values to eq 6 are very sensitive to small changes (2–5%) in the assigned value of $K_{sp}°$. With this observation all data at low temperature for the solubility of $CaSO_4 \cdot 2H_2O$ in H_2O and in NaCl–H_2O solutions, combined with additional results at this laboratory, were reevaluated.[2]

The Evaluation of Thermodynamic Functions. Equation 9 for the standard heat of reaction, $\Delta H°$, and an assumed eq 10 for the standard change in heat capacity at constant pressure, $\Delta C_p°$

$$\Delta H° = E + \int_0^T \Delta C_p° dT \qquad (9)$$

$$\Delta C_p° = F + GT \qquad (10)$$

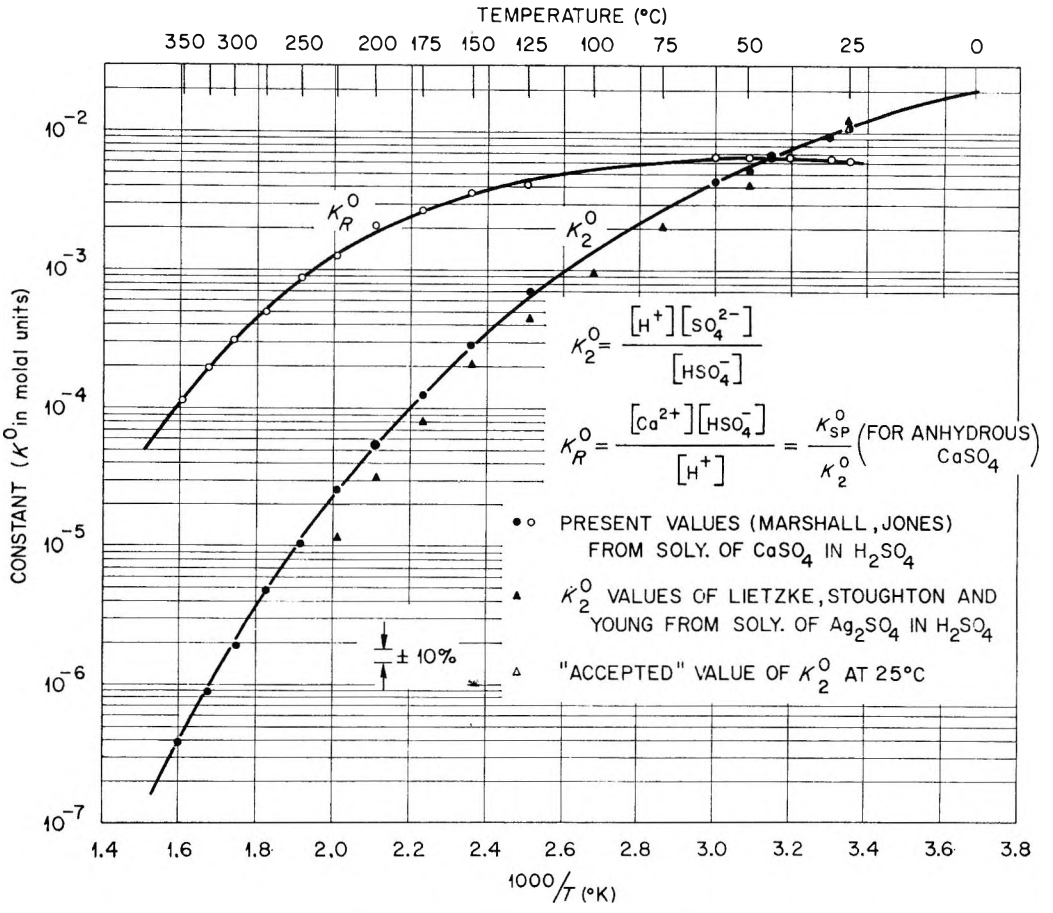

Figure 9. The second dissociation constant of H_2SO_4 and the related constant derived from the solubilities of $CaSO_4$ and its hydrates in H_2SO_4–H_2O at 0–350°.

where E, F, and G are constants and T is the temperature in °K, were substituted into the van't Hoff equation

$$\mathrm{d} \ln K_2^\circ/\mathrm{d}(1/T) = -\Delta H^\circ/R \qquad (11)$$

which was then integrated over all values of K_2° and T to obtain a four-parameter equation. With the experimental values of K_2° from 25 to 350° given in Table II (except those from Cameron's data at 25, 35, and 43°), the four parameters were evaluated by the generalized method of least squares[14] to obtain the equation

$$\log K_2^\circ = 56.889 - 19.8858 \log T - 2307.9/T - 0.006473T \qquad (12)$$

The average fit from 25 to 350° of the experimental values of $\log K_2^\circ$ to this equation was ±0.013 logarithmic unit. Values of ΔH° at each temperature were obtained by differentiating eq 12 with respect to $1/T$ (°K) and substituting the result into the van't Hoff equation (eq 11), while those values of ΔC_p° were obtained by differentiating with respect to T the resulting expression for ΔH°. Values of ΔS° and ΔG° were obtained from the standard thermodynamic equation

$$\Delta G^\circ = -RT \ln K_2^\circ = \Delta H^\circ - T\Delta S^\circ \qquad (13)$$

Some calculated thermodynamic values from 0 to 350° obtained by these procedures are included in Table III. The values at 25° of $\Delta H^\circ = -3.85$ kcal mole^{-1} and of $\Delta S^\circ = -22.0$ eu are considerably different from those of -5.3,[20] -5.2,[22] and -4.9[19] kcal mole^{-1} for ΔH°, and -27.0,[20] -26.3,[22] and -25.6[19] eu for ΔS° reported by others. However, they agree very well with those values of -4.02 kcal mole^{-1} for ΔH° and -22.5 eu for ΔS° obtained from Criss and Cobble's assignments of ionic entropies[23] and based on their recent calorimetric studies.

From Cobble's assigned values for average heat capacities, $\bar{C}_p^\circ$, over the temperature ranges 25–60, 25–100, 25–150, and 25–200°, the average values for

(22) K. S. Pitzer, *J. Am. Chem. Soc.*, 59, 2365 (1937).
(23) C. M. Criss and J. W. Cobble, *ibid.*, 86, 5385 (1964).

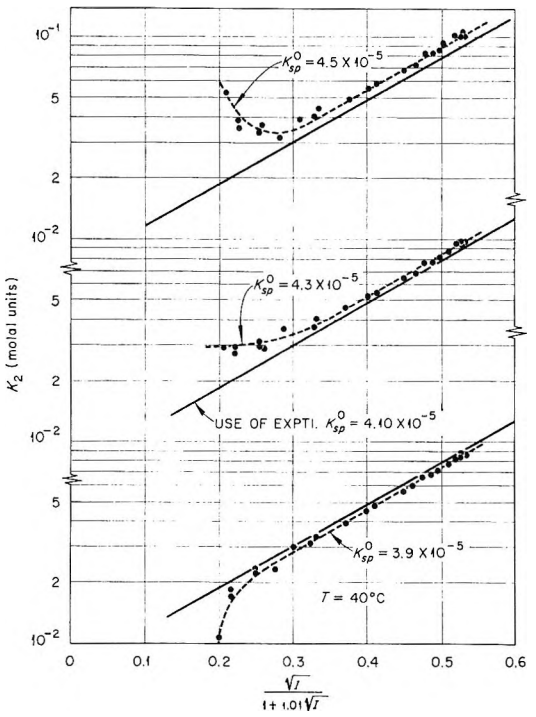

Figure 10. The effect of arbitrary small variations of $K_{sp}°$ used in the calculation of K_2 as a function of ionic strength.

Table III: Thermodynamic Values for the Dissociation of the Bisulfate Ion in Aqueous Solution

(Use of Equation 12 for $K_2°$)

T, °C	log $K_2°$	$\Delta G°$, kcal mole^{-1}	$\Delta H°$, kcal mole^{-1}	$\Delta S°$, cal mole^{-1} deg^{-1}	$\Delta C_p°$, cal mole^{-1} deg^{-1}
0	−1.778[a]	2.222	−2.44	−17.1	−56
25	−1.988	2.711	−3.85	−22.0	−57
50	−2.246	3.320	−5.30	−26.7	−59
75	−2.539	4.04	−6.79	−31.1	−60
100	−2.855	4.87	−8.31	−35.3	−62
150	−3.534	6.84	−11.5	−43.3	−65
200	−4.246	9.19	−14.8	−50.6	−67
250	−4.971	11.90	−18.2	−57.6	−70
300	−5.698	14.94	−21.8	−64.1	−73
350	−6.421	18.30	−25.6	−70.4	−76
370	−6.708[a]	19.74	−27.1	−72.8	−78

[a] Calculated values at 0 and 370° exceed the experimental range of 25–350° and therefore are extrapolated.

$\Delta C_p°$ ($= \overline{\Delta C}_p°]_{25}^t$) can be obtained.[24] From our calculated values of $\Delta C_p°$ at 5° intervals from 25 to 350° with the use of the differentiated form of eq 13, we have obtained values for $\overline{\Delta C}_p°]_{25}^t$ of −58, −59, −61, −62, −64, −65, and −67 cal mole^{-1} deg^{-1} over the temperature ranges from 25 to 60, 100, 150, 200, 250, 300, and 350°, respectively. These values are in good agreement with those of −62, −67, −54, and −61 cal mole^{-1} deg^{-1} over the ranges 25 to 60, 100, 150 and 200°, respectively, obtained from Cobble's table of $\overline{C}_p°]_{25}^t$ values.

When ΔC_p was expressed as a constant or single average value, $\overline{\Delta C}_p°]_{25}^{350}$, the resulting three-parameter equation was obtained by the least-square treatment of the values of $K_2°$

$$\log K_2° = 91.471 - 33.0024 \log T - 3520.3/T \quad (14)$$

This equation provided an average fit to the experimental log $K_2°$ values of ±0.014 unit, giving calculated values at 25° of $K_2° = 0.0100$, $\Delta G° = -2.727$ kcal mole^{-1}, $\Delta H° = -3.44$ kcal mole^{-1}, $\Delta S° = 20.7$ eu, and $\overline{\Delta C}_p°]_{25}^{350} = -66$ cal deg^{-1} mole^{-1}. Equation 3 of Cobble's paper,[24] given previously by Criss and Cobble[23]

$$\Delta G°_{t_2} - \Delta G°_{25} = \overline{\Delta C}_p°\Delta T - \Delta S°_{25}\Delta T - T_2\overline{\Delta C}_p° \ln (T_2/T_1) \quad (15)$$

where $\Delta T = (t_2 - 25°)$ and T_2 and T_1 are values of temperature (°K) at t_2 and $t = 25°$, respectively, reduces to eq 14 when all values at the reference temperature are incorporated into the three parameters. However, since our experimental values for $K_2°$ cover a very wide range of temperature, we believe that the four-parameter eq 12 should be used to describe the variation of $K_2°$ with temperature and thereby to obtain also an estimate of the variation of $\Delta C_p°$ with temperature.

Comments on the A Parameters. In the extended Debye–Hückel theory the A parameter corresponds to a term $50.29\mathring{a}/(DT)^{1/2}$, where D is the macroscopic dielectric constant of the solvent, T is the absolute temperature, and $\mathring{a}$ in angstrom units is the "distance" of closest approach of neighboring ions.[25,26] There is considerable controversy over the theoretical significance of this quantity in part due to an inability to correlate it with specific mean activity coefficients. A value of A adjusted between 0.5 and 2.0 with no additional term seems to fit most experimental determinations of activity coefficients at moderately low ionic strengths. A particular value of 1.5 for A gives good fits with the eq 4 type (excluding the $(B/2)I$ and

(24) J. W. Cobble, *J. Am. Chem. Soc.*, 86, 5394 (1964).

(25) H. S. Harned and B. B. Owen, "The Physical Chemistry of Electrolytic Solutions," 3rd ed, Reinhold Publishing Corp., New York, N. Y., 1958, pp 64–66, 164–166.

(26) G. N. Lewis and M. Randall, "Thermodynamics," 2nd ed, revised by K. S. Pitzer and L. Brewer, McGraw-Hill Book Co., New York, N. Y., 1961, Chapter 23.

$(C/2)I^2$ terms) for many experimentally determined activity coefficients at ionic strengths up to about 0.2 m and accordingly has been suggested by Scatchard and others for use as a constant in expressing the variation of many activity coefficients, with deviations placed in additional terms. Pitzer and Brewer,[27] following an earlier comment of Guggenheim,[28] have suggested the use of A = unity and the inclusion of one additional term with a deviation parameter, $B\cdot$ (whereby $\log \gamma_{\pm} = -4S\sqrt{I}/(1 + \sqrt{I}) + B\cdot I$), but then $B\cdot$ many times is dependent on ionic strength.

For the dissociation of HSO_4^-, several values of A_K have been obtained from various experimental studies. Baes[29] found that a value of 0.4 at 25° described the dissociation quotients (their variation with ionic strength) of Young, *et al.*,[15] obtained from H_2SO_4 and NH_4HSO_4 solutions (spectrophotometric measurements) and those of Sherrill and Noyes[30] obtained from H_2SO_4 and $NaHSO_4$ solutions (conductance measurements). Also, Lietzke's best value of 0.4[31] from the solubilities of Ag_2SO_4 in H_2SO_4–H_2O solutions was kept constant with temperature.[19] After an evaluation of existing determinations of $K_2°$ from electromotive force data with either aqueous HCl–K_2SO_4 or HCl–Na_2SO_4 as electrolyte solutions, including the discussions by Hamer,[17] Dunsmore and Nancollas obtained A_K = 1.60 at 25°.[20] In a most recent paper by Covington, *et al.*,[21] on emf measurements, a value for A_K as high as 1.9 has been proposed. In Figure 11, calculated values of log $K_2°$ (from the present solubilities) by the use of eq 6 with various arbitrary values of A_K are plotted at 25° against ionic strength. The calculated values according to classical theory ($A_K = \infty$) and the limiting law (A_K = 0) are shown also. A maximum ionic strength of 0.02 shown by Dunsmore and Nancollas[20] in a similar figure is hardly perceptible or of 0.3 by Covington, *et al.*,[21] is small on Figure 11. It is clear from these plots, extended to very high ionic strengths, that our own value of 0.94 for A_K at 25° does not agree with previously reported values, and that a difference in A_K greater than about ±5% cannot be tolerated for the results of our present study with the interpretation that was used.

If the A parameters are not dependent on the particular ions of an equilibrium but on *all* ions in solution, then for calculations of equilibrium behavior in

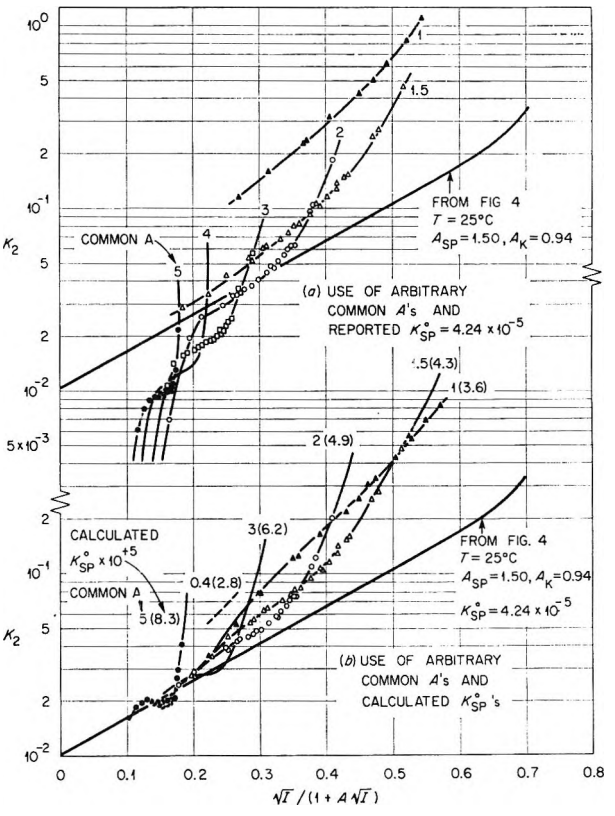

Figure 12. Fits of K_2 values at 25° calculated by using arbitrary common A values compared with that obtained from a separate A_{sp} and A_K.

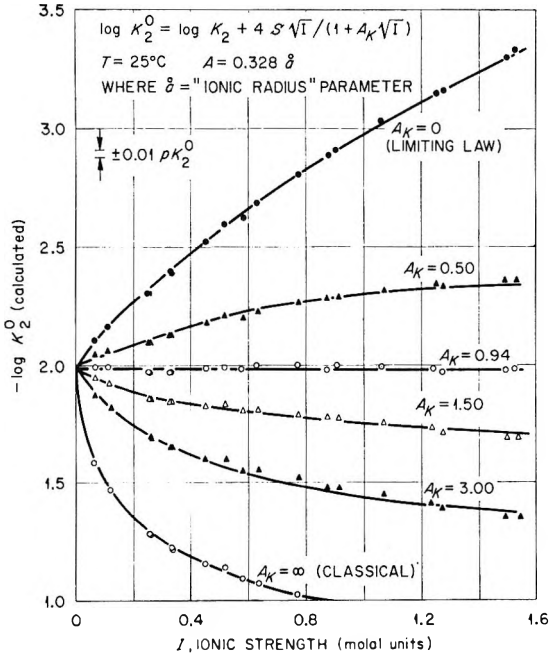

Figure 11. The effect of varying the A_K parameter on the calculation of $K_2°$ for H_2SO_4 at 25° (from solubilities of $CaSO_4 \cdot 2H_2O$ in H_2SO_4–H_2O).

(27) Reference 26, pp 318, 326–330.
(28) E. A. Guggenheim, *Phil. Mag.*, **19**, 588 (1935).
(29) C. F. Baes, *J. Am. Chem. Soc.*, **79**, 5611 (1957).
(30) M. S. Sherrill and A. A. Noyes, *ibid.*, **48**, 1861 (1926).
(31) M. H. Lietzke, personal communication, 1966.

the $CaSO_4$–H_2SO_4–H_2O media A_{sp} should equal A_K. In order to test this proposition at 25°, values from 0.4 to 5.0 for a common A were used in calculations of K_2. With a common A other than 1.50, it was necessary to recalculate a value of $K_{sp}°$ in order to satisfy the requirement that when $m_{H_2SO_4} \rightarrow 0$, the calculated K_{sp} of $CaSO_4$ must approach the true value in water (see eq 5). With this procedure, and by using as the criteria for acceptance (a) a fit to high ionic strengths of K_2 comparable with that shown in Figure 4, (b) an adherence to the theoretical limiting slope, (c) an attainment of $K_2°$ at 25° = 0.0103, and (d) a reasonable calculated value for $K_{sp}°$ (which really limits the common A to values near 1.5), we were unable to obtain agreement with that obtained by the separate use of A_{sp} and A_K. Even by accepting a 100% divergency from the reported $K_{sp}°$ value of 4.24×10^{-5}, agreement with the other criteria was not attained. For common A values from 0.4 to 0.6, the iteration process failed at high ionic strengths. Figure 12 shows representative plots of log K_2 obtained by the use of several arbitrary common A values with (a) the reported $K_{sp}°$ value of 4.24×10^{-5} and (b) a recalculated $K_{sp}°$ value for each A. These values are plotted against $\sqrt{I}/(1 + A\sqrt{I})$ and can be compared to the line from the similar plot at 25° in Figure 4 where both A_K and $K_{sp}°$ = the reported values are used for calculation and representation.

In other calculations A_K and A_{sp} were arbitrarily and independently varied from 0.4 to 5.0. As judged by the above criteria, the best fit was obtained when A_{sp} and A_K approached 0.94 and 1.50, respectively. Similar treatment was performed at all other temperatures with the result that two separate A parameters were always necessary, the best value of A_{sp} corresponding essentially to that found and used to describe the variation of K_{sp} in NaCl–H_2O solutions. It would appear that each A parameter relates only to the specific reaction equilibrium. However, this conclusion is certainly paradoxical to the attainment by different investigators of different values of A_K for the variation of the same equilibrium constant, depending upon the method of attainment and the type and concentrations of ions within the various solution media.

If one accepts the dependency of A on a specific reaction equilibrium, then the increase in A_K from 0.94 at 25° to 1.77 at 275° may reflect the abnormal behavior of the hydrogen ion at low temperature, which approaches "normal behavior" at high temperatures, a value in the vicinity of 1.60 to 1.80 assumed to represent this "normal behavior." A value of 1.60 for A_{sp} was estimated to express the variation of K_{sp} (of $CaSO_4$) with ionic strength in NaCl–H_2O solutions from 125 to 350°.

Acknowledgments. The authors wish to thank Ruth Slusher, ORNL, and Emily Johnson (ORAU Summer Student Trainee from Winthrop College, Rock Hill, S. C., 1964) for making some of the solubility determinations at 25–60°. The many helpful and critical discussions of this work with Professor John E. Ricci, New York University, are gratefully acknowledged.

Bond Lengths and Atomic Orbital Radii in the Diatomic Hydrides[1]

by Peter Politzer[2]

Department of Chemistry, Indiana University, Bloomington, Indiana *(Received June 13, 1966)*

It has been found that the gaseous diatomic hydrides, AH, show certain trends in the values of the quantity $(R_e - r)$, the difference between the equilibrium bond length and the radius of the outermost occupied orbital of atom A. These trends have been interpreted as reflecting the penetration, to various extents, of the outer shell of A by the hydrogen atom. Consistent with this hypothesis is the fact that the quantities $(R_e - r)$, which are taken to be a measure of this penetration, can be correlated to the widths of the outer shells. Using these correlations it was possible to predict the bond lengths of diatomic hydrides for which R_e values have not been observed experimentally and seemingly good results were obtained.

It has been found that there exists a definite pattern in the bond lengths of the gaseous diatomic hydrides when these are compared to the theoretical radii of the atoms involved.[3] Certain features of this pattern are suggestive and have been used as the bases for some inferences concerning the natures of the interactions in these molecules. However, even apart from any new insight which may have been gained, it is most encouraging to observe that atomic radii obtained by purely theoretical *ab initio* calculations are meaningful and consistent with experimentally determined bond lengths.[4,5]

The procedure followed in this work was simply to subtract from the experimental equilibrium bond length of each diatomic hydride, AH, the "radius" of the outermost occupied orbital of the atom A. By the "radius" of an atomic orbital φ_i is meant the distance to the maximum of the radial probability distribution function, $4\pi r^2 \varphi_i^* \varphi_i$. The orbital radii for all of the atoms are available, computed from self-consistent Dirac–Slater wave functions.[6] The internuclear distances were taken from published tables.[7]

The results are presented in Table I.[8] Some general trends are apparent. In group I, the alkali metal hydrides, the quantities $(R_e - r)$ are very small (except for NaH). They increase as one moves horizontally across the periodic table; there is a sharp rise in the next two or three groups, which seem to be an intermediate region, and then there is a very slow increase in the remaining groups, almost as though limiting values were being approached. For the first horizontal row, moreover, this apparent limiting value is very nearly equal to the radius of the hydrogen atom, 0.529

(1) This work was supported by grants from the National Science Foundation and the U. S. Air Force Office of Scientific Research.

(2) To whom correspondence should be addressed at: Department of Chemistry, Louisiana State University in New Orleans, Lake Front, New Orleans, La. 70122.

(3) A somewhat similar comparison of bond lengths and (semi-empirical) orbital radii was carried out for a few hydrides by R. S. Mulliken, *J. Am. Chem. Soc.*, **72**, 4493 (1950). Mulliken's primary concern, however, was with the relationship between overlap integrals and the properties of chemical bonds; the bond length data for the hydrides were listed but only briefly mentioned.

(4) A very interesting analysis of the diatomic hydrides, based on spectroscopic data, which has certain ideas in common with the interpretation to be presented here, was given by R. S. Mulliken, *Phys. Rev.*, **33**, 730 (1929); *Rev. Mod. Phys.*, **4**, 1 (1932).

(5) For discussions of other trends and periodicities among the diatomic hydrides, see R. Mecke, *Z. Physik*, **42**, 390 (1927); G. W. King, *J. Chem. Phys.*, **6**, 378 (1938); R. K. Sheline, *ibid.*, **18**, 927 (1950); J. R. Platt, *ibid.*, **18**, 932 (1950); C. E. Jentelson and S. M. Blinder, *ibid.*, **42**, 4306 (1965); K. Fajans, *ibid.*, **43**, 2159 (1965).

(6) J. T. Waber and Don T. Cromer, *ibid.*, **42**, 4116 (1965).

(7) T. L. Cottrell, "The Strengths of Chemical Bonds," 2nd ed, Butterworth and Co. Ltd., London, 1958, Table 11.5.1; "Tables of Interatomic Distances and Configuration in Molecules and Ions," Main Volume and Supplement, The Chemical Society, London, Special Publications No. 11 (1958) and No. 18 (1965).

(8) The subtracting of the free atoms' orbital radii is given some support by Mulliken's conclusion[4] that the orbitals of the atoms A are essentially unchanged, only slightly perturbed, by the interactions with hydrogen atoms. The fact that it is the 2s orbital radii which, being outermost, are subtracted from R_e in CH through FH (in boron the 2p orbital has a very slightly larger radius than the 2s) is consistent with King's inference from energetic considerations that the bond lengths (but not the dissociation energies) in the hydrides BH to FH are predominantly determined by interactions between the hydrogen atoms and the 2s electrons of the atoms A.[5]

Table I: Relationship between Bond Lengths and Orbital Radii in the Gaseous Diatomic Hydrides

	Group I	II	III	IV	V	VI	VII
Hydride	LiH	BeH	BH	CH	NH	OH	FH
$(R_e - r)$, A	0.009	0.303	0.457	0.500	0.517	0.520	0.521
Hydride	NaH	MgH	AlH	SiH	PH[a]	SH	ClH
$(R_e - r)$, A	0.174	0.452	0.334	0.453	0.501	0.53	0.549
Hydride	KH	CaH	GaH	GeH	AsH	SeH	BrH
$(R_e - r)$, A	0.082	0.312	0.42	0.501			0.557
Hydride	RbH	SrH	InH	SnH[a]	SbH	TeH	IH
$(R_e - r)$, A	0.080	0.310	0.463	0.532			0.565
Hydride	CsH	BaH	TlH	PbH	BiH	PoH	AtH
$(R_e - r)$, A	−0.024	0.172	0.551	0.624	0.514		
			Transition Metal Hydrides				
Hydride		MnH	CoH[a]	NiH	CuH	ZnH	
$(R_e - r)$, A		0.453	0.350	0.335	0.272	0.529	
Hydride					AgH	CdH	
$(R_e - r)$, A					0.331	0.577	
Hydride					AuH	HgH	
$(R_e - r)$, A					0.337	0.614	

[a] No values could be found for the equilibrium internuclear distances, R_e, of PH, SnH, and CoH. However the average internuclear distance, R_0, is known for each, and since the difference $R_0 - R_e$ averages about 0.012 A for the second-row hydrides, 0.013 A for the fourth row, and 0.011 A for the first transition series hydrides, R_e was taken to be $R_0 - 0.012 = 1.420$ A for PH, $R_0 - 0.013 = 1.772$ A for SnH, and $R_0 - 0.011 = 1.531$ A for CoH.

A; it increases somewhat for subsequent rows as one goes to larger and more complex systems.

The transition metal hydrides are listed separately; they do not seem to fit into the picture at this point, although the $(R_e - r)$ values for ZnH, CdH, and, to a lesser extent, HgH—in all of which the atom A again has completely filled inner shells—are once more in the neighborhood of the hydrogen atom radius.

There are some apparent deviations from these regularities. $(R_e - r)$ is too large for NaH, while the values for MgH and AlH are just the reverse of what one would expect. And the trio TlH, PbH, and BiH do not appear to fit in properly. However, the existence of an over-all pattern seems clear.

In an attempt to explain these trends, at least in a general manner, the following hypothesis has been formulated. The atoms of the alkali metals have large, diffuse outer shells containing only one electron. In the formation of the hydrides, then, it is suggested that an approaching hydrogen atom enters this diffuse outer shell and penetrates it until the hydrogen nucleus is just short of the region of maximum charge density.[9] As one moves horizontally across the periodic table, however, the outer shells of the atoms become smaller in size and also contain an increasing number of electrons. Accordingly, it is to be expected that penetration by the hydrogen atom will be more difficult and the quantity $(R_e - r)$ will increase. This is observed in groups II to IV. After groups IV or V, little, if any, penetration occurs;[10] the total bond length can now be quite closely approximated as the sum of the orbital radius of the atom A and the hydrogen atom.

Of the two factors mentioned above—the decreasing size of the valence shell and the increase in the number of valence electrons—it appears that the former is the more important. In fact, and somewhat surprisingly, considerations of size alone are sufficient to explain, at least roughly, the observed trends and even to account for the deviations. Figures 1 and 2 show plots of $(R_e - r)$ *vs.* log $(r - r_c)$, where r is again the radius of the outermost orbital of atom A, either an ns or

(9) This model of the alkali metal hydrides has previously been mentioned by P. Politzer and R. E. Brown, *J. Chem. Phys.*, **45**, 451 (1966), in connection with a study of the electronic density distribution in lithium hydride. However, nothing was said of the other diatomic hydrides (groups II–VII).

(10) The term "penetration" is being used in this article to denote the situation where the maximum of the radial probability distribution function of the hydrogen atom is within that of the outermost orbital of atom A. From the standpoint of quantum theory, of course, there is some overlap or "penetration" of the atoms' electron clouds even at large interatomic distances.

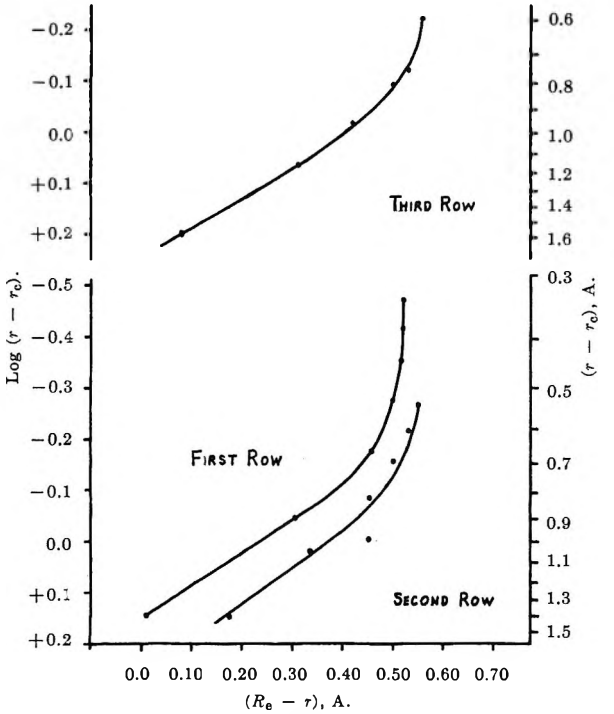

Figure 1. Relationship between the width of the outer shell of atom A, $(r - r_c)$, and the extent of penetration by the hydrogen nucleus, $(R_e - r)$, for the diatomic hydrides AH of the first three rows of the periodic table. Of the transition metal hydrides, only ZnH is included.

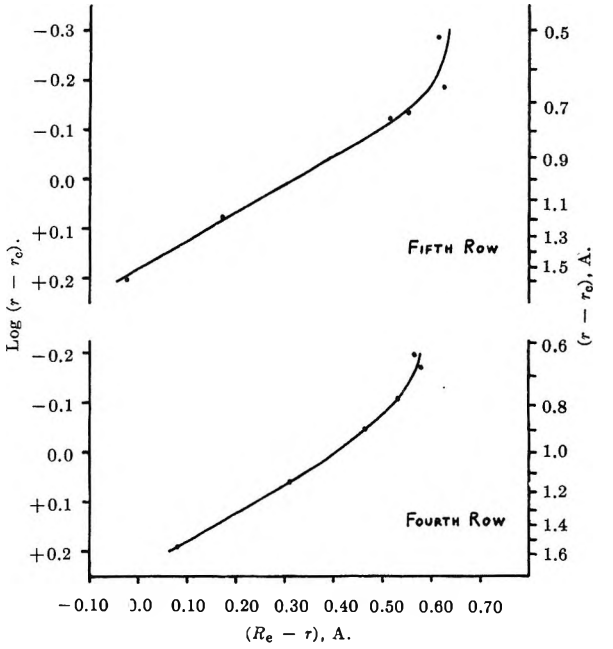

Figure 2. Relationship between the width of the outer shell of atom A, $(r - r_c)$, and the extent of penetration by the hydrogen nucleus, $(R_e - r)$, for the diatomic hydrides AH of the fourth and fifth rows of the periodic table. Only CdH and HgH are included from the transition metal hydrides.

np orbital, and r_c is the radius of the largest $(n - 1)$ orbital.[11] The logarithm of $(r - r_c)$ is used because otherwise the range of ordinate values would be too great.

The curves fit the data quite well, on the whole, implying that there does exist a correlation.[12] The apparent approach of $(R_e - r)$ toward a limiting value as the outer shell decreases in size is clearly seen. Of particular interest is the fact that $(r - r_c)$ is anomalously large for Al and Bi. This provides at least a partial explanation, if one accepts the above hypothesis, of the unexpectedly small values of $(R_e - r)$ for the corresponding hydrides—a most gratifying development! It is further seen that ZnH, CdH, and HgH fit the curves nicely.

It should be pointed out that nearly as good curves are obtained if the penetration is supposed to be a volume rather than a linear effect and $(R_e - r)$ is plotted against log $(r^3 - r_c^3)$, and the same explanation of the deviations is applicable. This is not the case, however, if one considers log $[(r^3 - r_c^3)/N]$, N being the total number of ns and np electrons. Although this quantity varies generally in the same direction as $(R_e - r)$ and did seem originally the most appropriate, since it takes account of both the volume of the outer shell and the number of electrons that this shell contains, it turns out that the process of dividing by N removes the anomalies at Al and Bi in the values of $(r^3 - r_c^3)$ [and also $(r - r_c)$] and thus renders inapplicable the proposed explanation of the deviations in $(R_e - r)$ for the corresponding hydrides.

In any case, the important point is that the $(R_e - r)$ values, which are believed to indicate the extent of penetration by the hydrogen nucleus, can definitely be related to the size of the outer shell. There are certainly other factors involved as well, but this is apparently a particularly important one—a conclusion which reinforces the hypothesis presented earlier.[13]

(11) For the second-row atoms, Na to Cl, r_c should be the radius of the 2s orbital; however these numbers are not listed in ref 6. They were taken, therefore, from the Hartree–Fock–Slater calculations of F. Herman and S. Skillman, "Atomic Structure Calculations," Prentice-Hall, Inc., Englewood Cliffs, N. J., 1963. Although there is a slight discrepancy between radii coming from the two sources, it is essentially insignificant as far as the curve in Figure 1 is concerned.

(12) Note that the second-row hydrides would satisfy a smooth curve nearly perfectly if the point for MgH [log $(r - r_c) = -0.0052$, $(R_e - r) = 0.452$ A] were neglected.

(13) There is of course some uncertainty in the data which have been used. The SCF Dirac–Slater functions are only approximations to the true wave functions, after all (see, for example, I. Lindgren, *Phys. Letters*, **19**, 382 (1965)). Furthermore, the maxima in the radial probability distribution functions may be very broad, as is shown to be the case for the 3s orbital of magnesium (ref 6, Figure 1), making the precise values assigned to the orbital radii less meaningful.

The curves in Figures 1 and 2 also permit the prediction of the bond lengths, R_e, of the six hydrides listed in Table I for which no experimental values were found. These are: AsH, 1.53 A; SeH, 1.47 A; SbH, 1.74 A; TeH, 1.67 A; PoH, 1.79 A; and AtH, 1.75 A. It is to be expected that the first two will be the most accurate, since the curve for the third row fits the data better than do those for the fourth and fifth rows.[14]

It must be stressed that the model which has been proposed in this paper is a rough one, intended only to describe some general features of the A–H interactions. Nothing has been said of the small-scale distortions of the electron clouds from which come the binding forces. Clearly it is not being suggested that hydrogen fluoride, for example, is made up of two spherical charge distributions side by side. However, this model does provide, it is believed, some physical insight into the structures of these molecules.

Acknowledgment. The author wishes to thank Professor Harrison Shull for his kind support and encouragement and Dr. Norman T. Huff for his comments about this paper.

(14) A good idea of the accuracy of these predictions can be obtained by comparing them to the observed A–H bond lengths in the corresponding polyatomic hydrides. These are: AsH_3, R_0 = 1.519 ± 0.005 A; SeH_2, R_0 = 1.46 ± 0.01; SbH_3, R_0 = 1.707 ± 0.005 A; and TeH_2, R_0 = 1.7 A. ("Interatomic Distances—Supplement," ref 7.) The results of this comparison are most encouraging, especially when one takes into account the fact that bond lengths in diatomic hydrides are generally slightly larger than in the corresponding polyatomic hydrides.

Sorption of Deuterium at Very Low Pressures by Molybdenum Films[1a]

by R. A. Pasternak[1b] and N. Endow

Stanford Research Institute, Menlo Park, California *(Received July 11, 1966)*

The thermodynamics and the kinetics of deuterium adsorption by porous molybdenum films have been studied at very low pressure over a temperature range of 77–373°K. The isobars and isotherms, and isosteric heats derived from them, indicate the existence of at least two adsorption states, one of which is stable only at temperatures below 200°K. The rate curves show a corresponding change in character. At all temperatures the sticking probability on the exposed surfaces is high, about 0.5; however, at low temperatures the internal surfaces are reached by flow through the pores and at high temperatures by fast surface diffusion. Consideration of the interrelation between binding energy and activation energy of diffusion strongly suggests that deuterium is adsorbed atomically even in the low-temperature state.

Introduction

The sorption kinetics of gases on porous metal films is undoubtedly more complex than on filaments because, in addition to the surface process itself, transport of the adsorbate from the exposed to internal surfaces may be the rate-determining step. For this reason the study of films provides significant information on surface mobility and the state of binding of the adsorbed species. This paper describes the kinetics and thermodynamics of deuterium sorption by porous molybdenum films; a similar study of nitrogen sorption has recently been published.[2]

(1) (a) This research was supported by the Research Division of the U. S. Atomic Energy Commission; (b) Sardar Patel University, Vallabh Vidyanagar, Gujarat State, India.

(2) R. A. Pasternak, N. Endow, and B. Bergsnov-Hansen, *J. Phys. Chem.*, **70**, 1304 (1966).

Experimental Section

The apparatus and the experimental procedure have been described in detail previously.[2] Base pressures in the 10^{-10}-torr range were obtained routinely, and pressures of about 1×10^{-9} torr could be maintained during the deposition of the films by electron-beam evaporation. In order to minimize the production of carbon monoxide by the ion gauges in the presence of hydrogen or deuterium (which has been generally observed in ultrahigh-vacuum studies), thorium oxide coated iridium filaments were employed at emission currents at 0.2 ma. Tests in a similar system containing a mass spectrometer had indicated that under such operating conditions both carbon monoxide production and hydrogen pumping were negligible.

Deuterium from a lecture bottle (99.5% D_2) was admitted to the gas reservoir through a silver–palladium leak. The adsorption characteristics of deuterium and hydrogen on molybdenum had been found to be identical within the precision of the present technique.[3a] Deuterium was used in preference to hydrogen because ion gauge sensitivity and pumping could be determined by passing the gas stream from the unit through a helium leak detector.[3b] For the experimental conditions employed, ion gauge pumping was negligible.

Four films were studied; they were deposited at liquid nitrogen temperature and annealed at 100° for about 5 min. The temperature dependence of saturation coverage and of the adsorption kinetics was studied primarily by the constant-pressure technique.[2,4] Flash desorption was employed only for qualitative checks, because of the difficulty of establishing a definite final temperature (which critically determines the coverage). For films 1 and 2, the adsorption kinetics and saturation amounts were observed first at film temperatures of 300 and 373°K, respectively; the temperature was then lowered in steps to 77°K, and at each step the adsorption rates and the increment in coverage were determined. After desorbing part of the deuterium (by raising the temperature of the film), the adsorption experiments were repeated. Both the detailed kinetics and the increments in coverage were well reproducible (see Table I); contamination effects became noticeable only about 1 day after film deposition. The same experimental procedure was employed for films 3 and 4, except that they were held at 77°K during the first exposure to deuterium and then warmed to 330°K.

The pressure dependence of coverage was investigated by a dynamic approach. The film was saturated with deuterium at a specific, steady-state pressure, defined by constant flow through a small conductance (0.6 l. sec^{-1} of D_2) out of the cell. The gas supply was then cut off suddenly, and the pressure in the cell was recorded continuously. The amount desorbed was evaluated as a function of pressure by integrating the pumpout curves and correcting them for deuterium originally in the cell volume.

Table I: Sorption of Deuterium on Molybdenum Films at a Nominal Pressure of 2.5×10^{-8} Torr[a]

1	2	3	4	5
	Temp, °K			Amount
Expt no.	Initial	Adsorption	Initial sticking probability	sorbed, 10^{14} molecules/cm²
1	Clean film	300	0.49	81.0
2	300	273	0.20	7.0
3	273	195	0.27	18.7
4	195	77	0.41	16.0
5	298	255	0.22	7.4
6	255	233	0.18	5.4
7	233	213	0.15	4.0
8	213	195	0.15	2.4
9	195	171	0.13	3.8
10	171	133	0.14	3.4
11	133	87	0.32	8.7
12	87	77	0.27	2.7
13	301	195	0.39	25.2
14	298	77	0.49	19.1

[a] The amounts refer to unit geometric areas. Film 1: weight, 50 $\mu g/cm^2$; true surface area, 36 cm^2.

Except for room-temperature experiments, the gas and film temperatures were not identical, because only the film substrate was thermostated. The data reported here are not corrected for the temperature difference. The error introduced in the thermodynamic function is small; moreover, it has generally been found that the gas temperature has little effect on the kinetics of adsorption on metals.

At the end of the runs the true film areas were determined by xenon physisorption as described previously[5] and the film weights by chemical analysis (Table II).

Results

Adsorption Kinetics. In Table I the initial sticking probabilities and the amounts of deuterium sorbed are listed for the sorption experiments with film 1, at a pressure of about 2.5×10^{-8} torr. Column 1 is the se-

(3) (a) B. Bergsnov-Hansen and R. A. Pasternak, *J. Chem. Phys.*, **45**, 1199 (1966); (b) B. Bergsnov-Hansen, N. Endow, and R. A. Pasternak, *J. Vacuum Sci. Tech.*, **1**, 7 (1964).

(4) R. Gibson, B. Bergsnov-Hansen, N. Endow, and R. Pasternak, Transactions, 10th National Symposium, American Vacuum Society, Boston, Mass., 1963, p 88.

(5) N. Endow and R. A. Pasternak, *J. Vacuum Sci. Tech.*, **3**, 196 (1966).

Table II: Summary of Deuterium Sorption Data on Molybdenum Films[a]

1	2	3	4	5	6	7	8
Film no.	W,[b] μg	A,[c] cm²	A/W, cm² μg⁻¹	ΔM,[d] 10^{14} molecules	M,[e] 10^{14} molecules	$\Delta M/A$, 10^{14} molecules cm⁻²	$M/\Delta M$
1	52	36	0.69	42	123	1.1	2.9
2		32[f]		41	109	1.1[f]	2.7
3	26	20	0.77	22	41	1.1	1.9
4	82	58	0.71	88	160	1.5	1.8

[a] The data refer to 1 cm² of the geometric area. [b] W = film weight. [c] A = true area as determined by xenon adsorption. [d] ΔM = increment in coverage between 300 and 77°K. [e] M = deuterium coverage at 77°K. [f] Derived by comparison with film 1. No experimental data were obtained.

quence number of the experiment; column 2 the temperature at which the film was equilibrated prior to the run; column 3 the adsorption temperature; column 4 the initial sticking probability; and column 5 the amount sorbed per unit geometric area of the film. The reproducibility in repeat series is within the precision of the experimental technique.

In Figure 1, four adsorption curves are shown; the logarithm of the sticking probability is plotted *vs.* the amount adsorbed per unit geometric area. Two kinetic patterns were observed; curves a and b represent one type, c and d the other. Curve a was obtained when fresh film 1 was exposed to deuterium at 300°K, and curve b when the same film, after equilibration with deuterium at 273°K, was cooled to 195°K. These two curves have the same character and differ only in the amounts adsorbed during the run; the sticking probability is high, and declines very little with coverage to near-saturation. Curve c represents an adsorption run with the fresh film 3 at 77°K, and curve d, a run with film 1 at 77°K, after equilibration at 195°K. These two curves also have similar characteristics except that the amounts sorbed differ. The sticking probability is initially high and remains so until an amount is adsorbed comparable to a monolayer on the exposed surface; it then decreases pronouncedly, passes through a flat range, and finally drops rapidly to zero.

Sticking probability curves of type a were observed at temperatures of 195°K and higher, and those of type c at 77 and 87°K, irrespective of the initial coverage of the surface. The initial sticking probability is high at all temperatures but is somewhat lower for small increment in coverage (Table I); it is of the magnitude found for hydrogen adsorption on a molybdenum ribbon.[6]

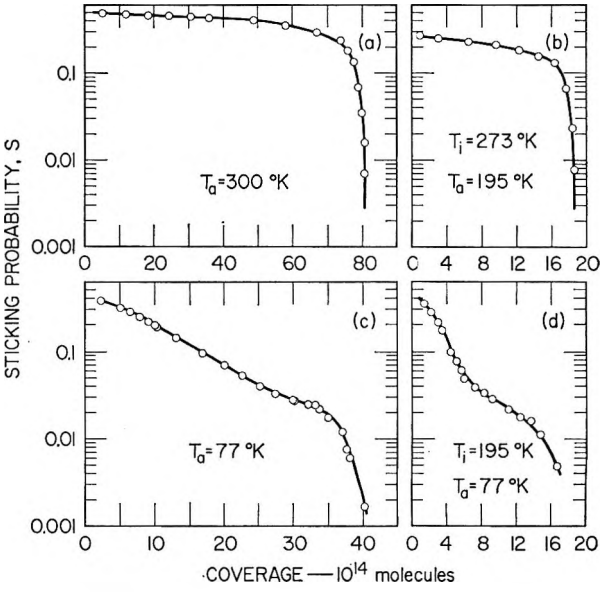

Figure 1. Sticking probability curves of deuterium on molybdenum films, nominal pressure 2.5 × 10^{-8} torr. The abscissa represents the amount per unit geometric area absorbed during the particular experiment: (a) film 1, adsorption at 300°K on clean film; (b) film 1, adsorption at 195°K after equilibration at 273°K; (c) film 3, adsorption at 77°K on clean film; (d) film 1, adsorption at 77°K after equilibration at 195°K.

Isobar. The steady-state coverages for film 1 are listed in Table I; they are in principle smaller than the true saturation amounts, since in the technique employed a sticking probability of 0.002 cannot be distinguished from zero. The deviation may be significant for thick films and particularly at the lowest temperatures where the sticking probability curves flatten out (Figure 1). With this limitation, adsorption is reversible in respect to temperature, and the data represent an isobar.

In Figure 2a, curve a, the averaged isobar for film 1, is plotted in terms of coverage per square centimeter of the true surface; the data for film 2 are shown also, normalized so that the two isobars coincide at 300°K (Table II). Close agreement is found over the entire temperature range. The coverage increases with decreasing temperature and approaches a constant value, but increases again at about 150°K. Apparently a second adsorption state for deuterium becomes significant at the lowest temperatures.

In the temperature range of 300–77°K, films 3 and 4, which were initially exposed to deuterium at 77°K, show the same characteristics as films 1 and 2. Quanti-

(6) R. A. Pasternak and H. U. D. Wiesendanger, *J. Chem. Phys.*, **34**, 2062 (1961).

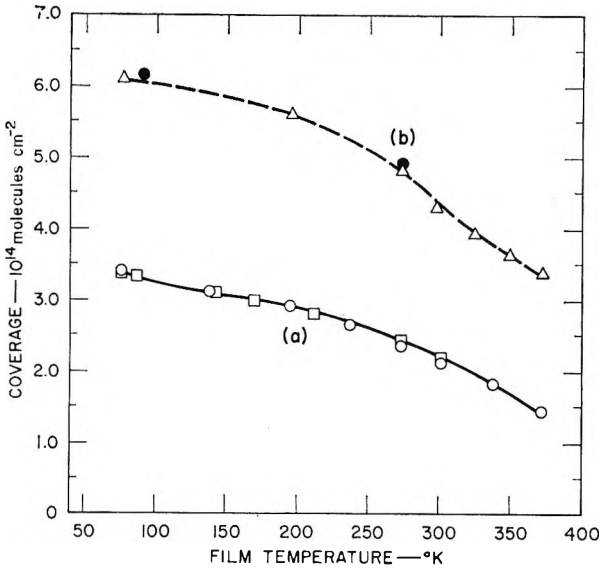

Figure 2. (a) Isobars of deuterium on molybdenum films, nominal pressure 2.5×10^{-8} torr: (□) film 1, (○) film 2. (b) Isobar of hydrogen on tungsten filaments (△) (Hickmott[8]), $p = 2.5 \times 10^{-8}$ torr; hydrogen on tungsten films (●) (Brennan and Hayes[9]), $p = 10^{-5}$ torr.

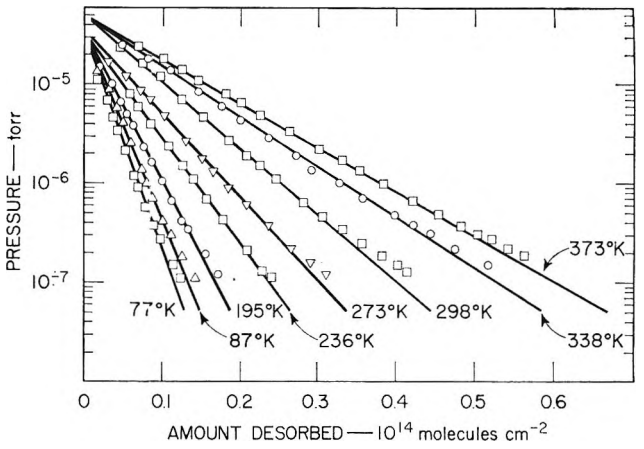

Figure 3. Isothermal desorption of deuterium from molybdenum, film 2. The amounts desorbed refer to the true surface area.

tative data for the four films are summarized in Table II. The film weights (column 2) vary by a factor of about 3, but the true surface areas (A) per unit weight (column 4) are the same within the precision of the measurements, about 70 m^2 g^{-1}. (For film 2 no such data could be obtained because of system failure, but the true area is derived by comparison with film 1.) Between 300 and 77°K, the increment of deuterium coverage (ΔM) per square centimeter of the true surface area is identical for films 1 and 3 (column 7). It is somewhat higher for film 4; we suspect that this difference is due to experimental uncertainties.

For films 1 and 2 the coverage, M, at 77°K (column 6) is the sum of the increments adsorbed in the temperature series. For films 3 and 4 it is the total amount adsorbed during the initial adsorption at 77°K. The ratio $M/\Delta M$ (column 8) is significantly lower for films 3 and 4. Either equilibrium is approximated extremely slowly when the entire amount of deuterium is adsorbed in one step at 77°K, or else the film structure opens up on interaction with the gas at higher temperatures. A qualitative observation supports either interpretation. When thick film 4 was warmed rapidly to about 200°K after initial adsorption at 77°K, no significant amount of deuterium was released. However, on repeating the desorption experiment after readsorbing deuterium at 77°K, an amount was evolved comparable to that taken up. Knor and Ponec,[7] in a study of hydrogen sorption by annealed, porous nickel films, made similar observations: at low temperature, the quantity of hydrogen sorbed by a fresh film *increased* with increasing temperature. However, on subsequent temperature cycling, the same film exhibited a (reversible) isobar which *decreased* with increasing temperature, as observed in this study.

The temperature dependence of deuterium coverage is very similar to that found previously for hydrogen-on-tungsten filaments; the coverages reported by Hickmott[8] (extrapolated to our experimental pressures) are shown in Figure 2 (curve b). The two isobars can be brought to approximate coincidence by introducing a scale factor of about 2 for the coverage. This factor may be due to different crystallographic orientations and to uncertainties in ion gauge calibration and in the estimated true surface areas of the films. Coverages for hydrogen on tungsten films at 273 and 90°K and a pressure of 10^{-5} torr, reported by Brennan and Hayes,[9] are also marked in Figure 2; they are of the same magnitude as the present data.

Isotherms and Isosteric Heats. A series of experimental degassing curves for film 2 at constant temperature are plotted in Figure 3 as log p *vs.* $\Delta\sigma$, the amount leaving the film during the runs. The data fit straight lines except at the very beginning, and at pressures in the low 10^{-7}-torr range. The former deviation is due to the finite time required to stop the gas flow; the latter is due to degassing of the walls of the cell, as was shown in blank runs. At any given temperature, parallel curves

(7) Z. Knor and V. Ponec, *Collection Czech. Chem. Commun.*, **26**, 37 (1961).

(8) T. W. Hickmott, *J. Chem. Phys.*, **32**, 810 (1960).

(9) D. Brennan and F. H. Hayes, *Trans. Faraday Soc.*, **60**, 589 (1964).

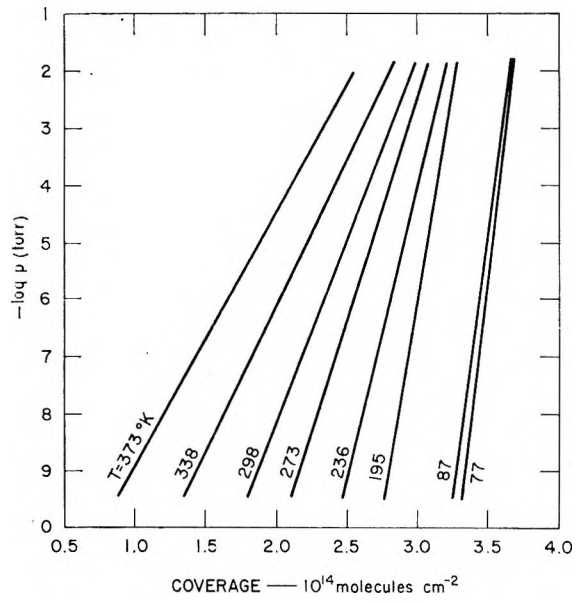

Figure 4. Isotherms for deuterium on molybdenum, film 2. The coverage refers to the true surface area.

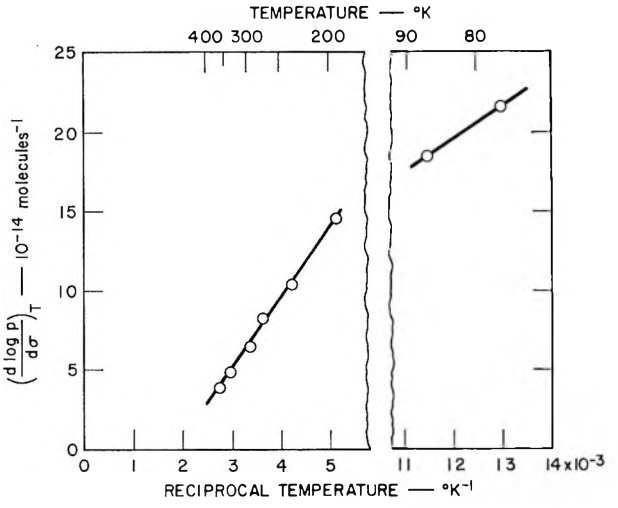

Figure 5. Slope of the isotherms plotted *vs.* reciprocal temperature.

were obtained irrespective of the initial steady-state pressures which were varied by a factor of up to 100.

In the degassing experiments, the geometric area of the film was about 300 times the area of the conductance; thus the rate of removal of gas was slow. Furthermore, the adsorption kinetics indicates fast surface diffusion at temperatures of 195°K and higher; thus, virtually uniform surface coverage was probably maintained. We therefore assume that the system passed through quasi-equilibrium states (this is also supported by the independence of the slopes on the initial pressure); consequently the degassing curves represent segments of isotherms. By adding to them the appropriate surface coverages obtained from the isobar (Figure 2), the Temkin isotherms[10] shown in Figure 4 are obtained. Their slopes are plotted *vs.* the reciprocal temperature in Figure 5. For temperatures to 195°K they fit a straight line which does not go through the origin. It is doubtful whether this empirical relationship is of fundamental significance; however, the slopes at 77 and 87°K do not fit the pattern; a change in adsorption mechanism between 195 and 87°K is again indicated. In his flash filament study of hydrogen on tungsten filaments, Hickmott[8] has obtained data which also fit Temkin isotherms. He assumes, in accordance with a theoretical treatment by Brunauer, *et al.*,[11] that the slopes are inversely proportional to temperature.

In the present study the isotherms were determined experimentally over a pressure range of about two powers of ten; a linear extrapolation over the same interval was assumed to be justified. A series of isosteres was derived from the isotherms within these pressure limits; they are plotted in Figure 6 as log p *vs.* $1/T$. (The isosteres derived from the isotherms at 77 and 87°K are not shown.) The isosteres are, with two exceptions, determined by at least three points and cover a temperature range of up to 100°K. They can be approximated by straight lines, the slopes of which are proportional to the isosteric heats. The linearity of the isosteres shows that the binding energy is a function of surface coverage only and does not depend on temperature.

The isosteric heats are plotted in Figure 7 (curve a) as function of relative coverage, which is expressed as fraction θ of the coverage at 195°K and a pressure of 2.5×10^{-8} torr. At $\theta = 1$, the isosteric heat is about 15 kcal; it increases gradually with decrease in coverage. At $\theta = 1.2$, representative for the temperatures of 77 and 87°K, the isosteric heat is only 3 kcal mole^{-1}. The pronounced change in slope of the heat curve between 87 and 195°K again indicates a change in the state of binding.

Heats of adsorption of hydrogen on tungsten films as a function of coverage have been measured by calorimetry.[9,12] They are approximately differential heats, which in turn differ only by RT cal mole^{-1} from isosteric heats. The heats measured by Brennan and Hayes[9] at a temperature of 195°K are also plotted in Figure 7 (curve b); the saturation coverage is taken as unity. The agreement between the two heat curves is

(10) M. I. Temkin, *Russ. J. Phys. Chem.*, **15**, 296 (1941).

(11) S. Brunauer, K. S. Love, and R. G. Keenan, *J. Am. Chem. Soc.*, **64**, 751 (1942).

(12) O. Beeck, *Advan. Catalysis*, **2**, 151 (1959).

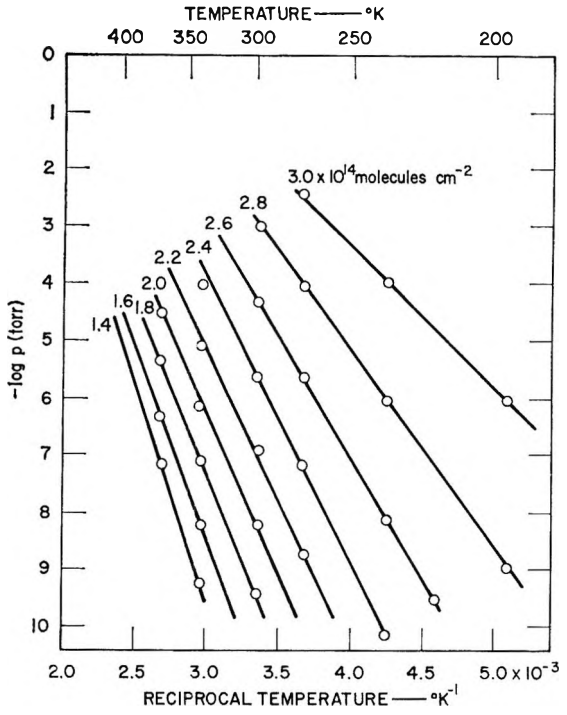

Figure 6. Isosteric of deuterium derived from isotherms.

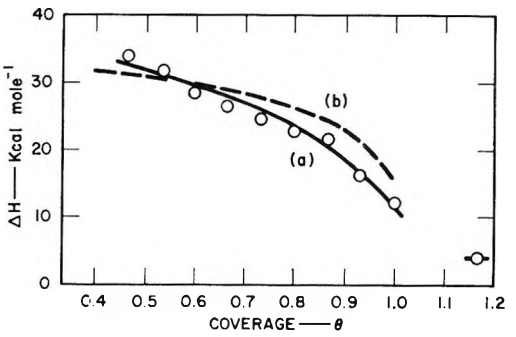

Figure 7. Heats of adsorption as a function of coverage: (a) isosteric heats of deuterium on molybdenum film (present investigation); (b) calorimetric heats of hydrogen on tungsten films (Brennan and Hayes[9]).

rather satisfactory in view of the widely different approaches employed in the two studies. It again indicates that the heat of adsorption is a function of surface coverage only and does not depend on temperature or pressure.

Discussion

Both the thermodynamic and the kinetic data presented here indicate the existence of at least two binding states for deuterium, one of which is populated only at low temperatures. This is in agreement with flash filament studies of hydrogen on tungsten;[8] moreover, the high-energy state for hydrogen on molybdenum[6] and on tungsten[13–16] has been resolved into at least two additional states; since these states differ very little in energy, they undoubtedly cannot be observed on films because of their crystallographic heterogeneity.

The change in adsorption kinetics with temperature also suggests two modes of binding. Irrespective of the temperature, deuterium is adsorbed on the exposed surfaces at a rate which declines little with coverage (as has been observed for both molybdenum and tungsten filaments). At the higher temperatures, a significant fraction of the adsorbate has a high mobility and is removed continuously to the internal surfaces by surface diffusion; thus, the sticking probability remains high almost to saturation of the entire surface. In contrast, at 77 and 87°K the adsorbate is immobile. Therefore, the internal surface can be reached only by those gas molecules that hit a pore entrance, the area of which represents only a small fraction of the total geometric area. The observed drop in sticking probability is due to this geometric factor; the gas flow through the pores themselves is rapid.[17] A transition from high to insignificant surface mobility at about 180°K has been found in a field emission microscopy study of hydrogen on tungsten.[18] This observation supports our interpretation of the adsorption kinetics.

A comparison of estimated activation energies of diffusion with the observed heats of adsorption indicates that deuterium is adsorbed atomically at all the temperatures studied. The average number of surface jumps, n, made by an adsorbed particle between impacts of gas molecules on the same adsorption site is approximately $n = 10^6 p^{-1} \exp[-(\Delta H/RT)]$ where ΔH is the activation energy of diffusion and p the pressure.[2] If we postulate somewhat arbitrarily that the adsorption step is rate determining for n larger than 100, the limiting value of ΔH at $p = 10^{-7}$ torr is approximately $55T$ kcal mole^{-1}. Moreover, the ratio of the activation energy of diffusion to the binding energy is of the magnitude of 1:5 to 1:3.[19]

At temperatures of 77, 195, and 300°K, the highest activation energies still allowing fast surface diffusion

(13) E. W. Müller, *Ergeb. Exakt. Naturw.*, **27**, 290 (1953).

(14) P. A. Redhead, *Proc. Symp. Electron Vacuum Phys., Balatonfoldvar, Hung., 1962*, 89 (1963).

(15) L. J. Rigby, *Can. J. Phys.*, **42**, 1256 (1964).

(16) F. Ricca, R. T. Medana, and G. Saini, *Trans. Faraday Soc.*, **61**, 1492 (1965).

(17) J. H. de Boer, "The Dynamic Character of Adsorption," The Clarendon Press, New York, N. Y., 1953.

(18) R. Gomer, R. Wortman, and R. Lundi, *J. Chem. Phys.*, **26**, 1147 (1957).

(19) G. Ehrlich in "Structure and Properties of Thin Films," John Wiley and Sons, Inc., New York, N. Y., 1959, pp 425–475.

are 4, 11, and 16.5 kcal mole^{-1}, and the upper limit for the associated binding energies assuming a ratio of 1:5 are 20, 55, and 82 kcal mole^{-1}, respectively. Thus, the low surface mobility of deuterium at 77°K implies that its binding energy is significantly larger than 20 kcal mole^{-1}. deuterium is therefore bound in atomic form, since molecular adsorption cannot be associated with such a high energy.

There is little doubt that also at higher temperatures deuterium is adsorbed in atomic form. The binding energies, $1/2(103 + \Delta H_{st})$ kcal (g-atom)$^{-1}$, can be calculated from the isosteric heats ΔH_{st} shown in Figure 7. They are 53, 60, and 70 kcal (g-atom)$^{-1}$ at 77, 195, and 300°K, respectively, much larger, close to, or smaller than the values estimated as upper limits for fast surface diffusion at these temperatures. Thus, the proposed model for the adsorption kinetics is at all temperatures consistent with atomic adsorption.

In an unsaturated layer deuterium exhibits less, if any, surface mobility since the isosteric heat, and therefore the binding energy, is higher. Thus, during the adsorption process deuterium cannot spread uniformly over the entire surface but penetrates the film progressively, since it can move fast only over those surface areas which are already close to saturation. This picture for the adsorption process implies that the calorimetric heats of adsorption measured on films are not truly differential heats but represent some weighted average. This averaging process should be particularly pronounced at low coverages and/or low temperature and result in experimental heats with a smaller coverage dependence than the true differential heats. Such an effect is noticeable in the data of Brennan and Hayes;[9] the heat curve at 273°K is steeper than that at 195°K. At 90°K, when surface diffusion is negligible, the heat is constant over the entire coverage range.

Concluding Remarks

After conclusion of this study the preprint of a paper by Hayward, *et al.*,[20] became available; these authors investigated the sorption of hydrogen by evaporated molybdenum films at low temperatures and pressures. Although the techniques employed and the logic of their approach differ appreciably from the present study, close agreement is obtained in overlapping areas. In particular, the kinetic curves at 77°K and the interpretation of the data in terms of surface diffusion are very similar.

(20) D. O. Hayward, N. Taylor, and F. C. Tomkins, private communication.

The Extrinsic Cotton Effect of Acridine Orange Bound to Native DNA and Helical Poly-α,L-glutamic Acid[1]

by K. Yamaoka and R. A. Resnik

Laboratory of Physical Biology, National Institute of Arthritis and Metabolic Diseases, National Institutes of Health, Bethesda, Maryland 20014 (Received July 11, 1966)

The absorption spectra and optical rotatory dispersion (ORD) curves of acridine orange (AO) plus native deoxyribonucleic acid (DNA) and helical sodium poly-α,L-glutamate have been measured at several ratios of dye to polymer sites (D/P) between 350 and 600 mμ, where the bound dye shows intense absorption bands. Induced extrinsic optical activity was observed even at very low values of D/P for both systems. The bearing that these results have on the applicability of exciton theory to the system AO–DNA is discussed. An analysis of the ORD data, using a modified form of the Kronig–Kramers transform, revealed that at least four partial Cotton effects are required to reconstruct the experimental ORD curves. The resultant circular dichroism (CD) curves computed from these partial Cotton effects were compared with the experimental CD curves previously reported for the two systems by Mason's laboratory. These results reveal that the α band of the absorption spectrum of AO–DNA complexes is composed of at least two electronic transitions. It is concluded on this basis that the dye stacking hypothesis based on changes in the α band needs to be reevaluated. The wavelength assignments of the partial Cotton effects for both AO–DNA and AO–NaPLG are compared with the spectral data for free AO obtained by Zanker and co-workers.

Introduction

Drastic changes in the absorption spectra of cationic acridine orange (AO) have been found when AO is bound to synthetic[2,3] and natural[2] polymers in aqueous media. Michaelis first suggested that interaction between bound dye molecules is the basis for this metachromasy.[4] Zanker observed similar changes in the absorption spectra of unbound AO as a function of dye concentration. By analyzing the data in terms of an equilibrium between the monomer and dimer he showed that the aggregation of dye molecules accounts for the observations.[5]

Bradley and co-workers[2b,6,7] have formulated an extension of the aggregation hypothesis to explain apparent inconsistencies that occur when a dye forms complexes with different polymers, a point that Michaelis could not resolve.[8] The experimental basis of the "stacking theory"[2b] is the observation that the absorption maximum of unbound AO at 492 mμ shifts to 504 mμ in the presence of DNA at concentrations of the polymer such that the number of anionic sites greatly exceeds the number of AO molecules and that the absorption maximum at 504 mμ decreases as the polymer becomes more saturated with the dye. In AO–DNA, as in the findings of Zanker, a maximum appears at shorter wavelengths, around 465 mμ.

A full understanding of both the α band, or complex,

(1) The following abbreviations will be used: NaPLG, sodium poly-α,L-glutamate; DNA, deoxyribonucleic acid; AO, cationic acridine orange; ORD optical rotatory dispersion; CD, circular dichroism; D/P, ratio of concentration of dye to anionic polymer sites.

(2) (a) R. F. Beers, D. D. Hendley, and R. F. Steiner, *Nature*, **182**, 242 (1958); (b) D. F. Bradley and M. K. Wolfe, *Proc. Natl. Acad. Sci. U. S.*, **45**, 944 (1959).

(3) G. Blauer, *J. Phys. Chem.*, **65**, 2457 (1961).

(4) L. Michaelis, *Cold Spring Harbor Symp. Quant. Biol.*, **12**, 131 (1947).

(5) V. Zanker, *Z. Physik. Chem.*, **199**, 225 (1952).

(6) D. F. Bradley and G. Felsenfeld, *Nature*, **185**, 1920 (1959).

(7) A. L. Stone and D. F. Bradley, *J. Am. Chem. Soc.*, **83**, 3627 (1961).

(8) L. Michaelis, *J. Phys. Colloid Chem.*, **54**, 1 (1950).

II band, at 504 mμ and the β band, or complex I band, at 466 mμ is needed to justify the application of the stacking concept to dye–polymer interactions. If these bands belong to purely monomerically bound AO (complex II) and dimerically bound AO (complex I), respectively, and if each band originates from a single electronic transition, an unequivocal application of the stacking theory is possible. If, however, either of the absorption bands has some degree of multiplicity, then further investigation is needed. It is apparent from the previous studies that conventional techniques of absorption spectroscopy cannot resolve these questions.

Blout and Stryer[9] studied the optical rotatory properties of dyes bound to polypeptides. They made the interesting observation that an extrinsic Cotton effect in the wavelength region corresponding to the absorption band of bound AO was obtained only when the dye combined with the helical form of poly-α,L-glutamic acid.[10] They also pointed out that the extrinsic Cotton effect was a double one having inflection points well correlated with the absorption maxima of the complex. They explained their results in a manner consistent with the aggregation concept. The view that interaction between bound dye molecules is a necessary condition for the appearance of the extrinsic Cotton effect was favored even though the alternative, that configurationally induced optical rotatory power could arise from the interaction of unaggregated bound dye with a binding site, was discussed.[10]

Neville and Bradley[11] carried out a more detailed investigation of the induced Cotton effect as a function of D/P in the AO–DNA system. They considered the induced ORD to be a composite of two partial Cotton effects—one at 503 mμ and the other at 464 mμ. From the observations that no measurable rotation was detected either for AO bound to heat-denatured DNA or for AO bound to DNA at D/P 0.018, they apparently assumed, in order to explain the 504-mμ Cotton effect, that sufficiently weak coupling of bound monomeric AO molecules was strong enough to cause optical activity.[11] The 464-mμ Cotton effect, which was maximal at D/P 1, was said to be clearly due to strongly coupled dyes.

In this paper we present some results of the measurement of the induced Cotton effects and absorption spectra resulting from the interaction of AO with native DNA and helical NaPLG, with the thought that a systematic study of dye–polymer complexes at low D/P is indispensable for an understanding of the phenomena of the extrinsic Cotton effect and metachromasy. Recent improvements in commercially available spectropolarimeters have made it possible to obtain the detailed ORD curves, which have revealed some unexpected complexities. We also present the results of the analysis of the experimental ORD curves. The resolution of such curves into components is essential for the interpretation of dye–polymer interactions. Finally we show that discussions based upon the gross appearance of absorption spectra and ORD curves can lead to incorrect conclusions.[12]

Experimental Section

Materials. A highly polymerized calf thymus DNA preparation was purchased from Worthington Biochemical Corp., Freehold, N. J. A concentrated stock solution (2 mg/ml) in 1×10^{-3} M NaCl was stored in the cold and diluted just prior to use. In all work with the DNA plus AO the final salt concentration was 1×10^{-3} M. The concentration of DNA was determined photometrically with a molar extinction coefficient at 260 mμ of 6400. As a result concentrations of DNA were expressed in terms of phosphate residues. A 35% increase in optical density at 260 mμ was noted after heating an aliquot of dilute DNA at 100° for 15 min and then cooling rapidly in an iced water bath for an equal period. On this basis the DNA used was native. A sample of sodium poly-α,L-glutamate was purchased from Pilot Chemicals, Inc., Watertown, Mass. The degree of polymerization was 610. To calculate the molecular weight of the polymer a value of 169 was used for the mean residue weight of monosodium glutamate monohydrate. Acridine orange (Allied Chemical and Dye Corp., New York, N. Y.) was first converted to the neutral form with 0.1 N NaOH.[7] The neutral dye was dried and then extracted with anhydrous benzene in a Soxhlet tube to remove metallic impurities. The neutral dye was crystallized by means of the dropwise addition of anhydrous n-hexane. Tiny crystals were filtered and then recrystallized from hot benzene five times. The purified neutral form of AO was dissolved in benzene and converted to the hydrochloride by introducing hydrogen chloride gas into the solution until the supernatant was faintly colored. The red precipitate was crystallized from methanol by the dropwise addition of ethyl ether. Excess acid was removed by washing repeatedly with ethyl ether. This crystallization cycle was repeated five times. The dark red, needlelike crystals, after drying *in vacuo* at 45–50°, had a melting point of 289–290° (uncorrected). The

(9) E. R. Blout and L. Stryer, *Proc. Natl. Acad. Sci. U. S.*, **45**, 1591 (1959).

(10) L. Stryer and E. R. Blout, *J. Am. Chem. Soc.*, **83**, 1411 (1961).

(11) D. M. Neville, Jr., and D. F. Bradley, *Biochim. Biophys. Acta*, **50**, 397 (1961).

(12) K. Yamaoka and R. A. Resnik, *Nature*, in press.

maximum molar extinction coefficient in Spectrograde chloroform was 65,000 at 494 mμ in the concentration range of 1×10^{-4}–1×10^{-5} *M*. A value of 301.6 was used for the molecular weight of the AO monohydrochloride.

Procedures. To investigate the ORD of dye–polymer complexes as a function of *D/P* it is desirable to keep one of the components at a constant concentration. In this study the polymer concentration was held constant unless otherwise stated. This is preferred since, if the dye is held constant, the variation of polymer concentration often introduces effects due to shifts in the ionization of the anionic sites.

No buffers were used. The pH was adjusted by the addition of dilute HCl and NaOH. In the case of NaPLG and AO–NaPLG the pH was at 4.5. The final concentration of NaPLG was always 1.6 mg/ml. DNA and AO–DNA solutions were all at a pH of 6.5. The final concentration of DNA was 1×10^{-4} *M* for *D/P* values from 0.02 to 0.2. Beyond this point the DNA concentration had to be reduced to 5×10^{-5} *M* to avoid the precipitation of the AO–DNA complex. In both systems studied, the component solutions were adjusted to the desired pH separately and dye solution was added slowly to the polymer solution with continuous stirring. In the case of AO–NaPLG some precipitate appeared and as a result these solutions had to be filtered just prior to measuring the ORD. The decrease in solubility of NaPLG with AO added has previously been noted.[10] While it results in some uncertainty with regard to the absolute magnitude of the measured molar rotations, the general shape of the curves should remain unaltered. In fact, as will be noted later, the observed rotations in this work are in good agreement with those of Stryer and Blout.[10]

Absorption spectra were obtained with a Cary Model 14 spectrophotometer at 23–24°. ORD measurements were carried out in a Cary 60 spectropolarimeter. The temperature in the cell compartment of this instrument was 27°. Checks were made for instrumental artifacts using cells of several different path lengths. The specific rotation of a sample solution remained constant up to an optical density of about 3 in the visible spectral region, although the noise-to-signal ratio increased. The cells were rinsed with sample to minimize the effect of adsorption of dye. For both the absorption and ORD measurements the appropriate polymer solution served as the reference or blank. Repeated scanning of the absorption spectrum and ORD curve for a particular sample assured the absence of any serious changes within the period of time required to complete a full scan.

All observed optical rotations of the dye–polymer complex were expressed in terms of the net molar rotation, $[R]^{D}_{C}$, as calculated from the following relationship

$$[R]^{D}_{C} = (10/M_D)[(\theta_C/l_C) - (\theta_P/l_P)] \quad (1)$$

where θ_C and θ_P are the net rotations in degrees, *i.e.*, the rotation of the solution minus that of the solvent, for solutions of the complex and polymer, respectively. M_D is the molarity of the dye in the complex (this is taken to be the total concentration of dye in the solution in the present study; thus the net molar rotation theoretically gives the lower limit). l_C and l_P are the path lengths in decimeters of the solutions of the complex and polymer, respectively. Equation 1 holds only when the concentration of polymer is equal in both solutions.

Analysis of ORD Data. The observed ORD curves were analyzed into partial rotations using a semiempirical formula, eq 2, developed by Moscowitz and Moffitt on the basis of the Kronig–Kramers transform.[13,14] In the form of the equation used it is assumed that each circular dichroic (CD) band can be represented by a Gaussian distribution as a function of wavelength[15] rather than of wavenumber[16] as given by eq 3.

$$[R] = \Sigma[R]_k = \frac{96N}{hc}\Sigma\left\{\left(\frac{R_k\lambda_k}{\Delta_k}\right) \times \left[e^{-[(\lambda-\lambda_k)/\Delta_k]^2}\int_0^{(\lambda-\lambda_k)/\Delta_k} e^{x^2}\,dx - \frac{\Delta_k}{2(\lambda+\lambda_k)}\right]\right\} + \frac{m_i}{\lambda^2 - \lambda_i^2} \quad (2)$$

$$(\epsilon_l - \epsilon_r) = (\epsilon_l - \epsilon_r)_{max} e^{-[(\lambda-\lambda_k)/\Delta_k]^2} \quad (3)$$

The symbols are defined as $[R]$, the net molar rotation; $[R]_k$, the k'th partial molar rotation; *N*, Avogadro's number; *h*, Planck's constant; c, the velocity of light; λ, wavelength; λ_k, the wavelength of the transition giving rise to the kth CD band; R_k, the rotational strength of the kth CD band; Δ_k, the half band width of the k'th CD band where the intensity is $1/e$ times its maximum value; and $(\epsilon_l - \epsilon_r)$, circular dichroism. The last term in eq 2, with m_i and λ_i constants, is a one-term Drude expression which may be used to compensate for any monotonic background rotation when

(13) W. Moffitt and A. Moscowitz, *J. Chem. Phys.*, **30**, 648 (1959).

(14) A. Moscowitz in "Optical Rotatory Dispersion," C. Djerassi, Ed., McGraw-Hill Book Co., Inc., New York, N. Y., 1960, p 150.

(15) T. M. Lowry and H. Hudson, *Phil. Trans. Roy. Soc. London*, **A232**, 117 (1933).

(16) W. Kuhn and E. Braun, *Z. Physik. Chem.* (Leipzig), **B8**, 281 (1930).

Table I: Summary of Absorption and ORD Data for AO–DNA and AO–NaPLG

	AO, pH 4.5	AO–DNA, pH 6.5			AO–NaPLG, pH 4.5		
D/P	...	0.02	0.2	0.5	0.0001	0.002	0.004
Concn of AO, M	2.07×10^{-6}	2.07×10^{-6}	2.07×10^{-6}	2.5×10^{-5}	1.035×10^{-6}	2.07×10^{-5}	4.14×10^{-5}
Absorption peaks,[a] shoulders,[b] and molar extinction coefficients	492 mμ[p] (57,200); ~470 mμ[s] (48,000)	502.5 mμ[p] (52,500); ~475 mμ[s] (27,000)	497.5 mμ[p] (41,800); ~475 mμ[s] (28,500)	495 mμ[p] (27,400); ~472 mμ[s] (28,200)	495 mμ[p] (36,000); ~470 mμ[s] (28,500)	~522 mμ[s] (5400); ~500 mμ[s] (9700); 453 mμ[p] (23,000)	~527 mμ[s] (5200); ~500 mμ[s] (12,600); 461 mμ[p] (21,800)
ORD peaks,[a] troughs,[c] shoulders,[b] and net molar rotations	None	509 mμ[t] (−17,500); ~480 mμ[s] (3500); ~458 mμ[p] (9500)	520 mμ[p] (50,500); 498 mμ[t] (−106,000); ~475 mμ[s] (−41,600); ~453 mμ[p] (12,500); ~440 mμ[s] (11,000)	520 mμ[p] (53,000); 495 mμ[t] (−81,000); 475 mμ[t] (−71,000); 435 mμ[p] (4000)	525 mμ[p] (35,000); 496 mμ[t] (−98,000); ~482 mμ[s] (−80,000); 450 mμ[p] (50,000), corrected values	~552 mμ[t] (−13,000); ~537 mμ[t] (−5000); ~495 mμ[s] (−86,000); 486 mμ[t] (−95,200); 450.5 mμ[p] (239,000); ~415 mμ[t] (−14,200)	~557 mμ[t] (2700); 532.5 mμ[p] (12,300); ~515 mμ[s] (−22,600); 487 mμ[t] (−132,500); 450 mμ[p] (175,000); ~413 mμ[t] (−13,700)
ORD crossover points	None	491 mμ	510.5 mμ; 463.5 mμ	507.5 mμ; 447 mμ	512 mμ; 465 mμ	470 mμ; 426 mμ	546.5 mμ; 523.5 mμ; 468 mμ; 426 mμ

[a] p, peak. [b] s, shoulder. [c] t, trough.

such a correction is needed. The first term in the brackets in eq 2 is Dawson's integral, the values of which are obtained from a table.[17] In eq 3 $(\epsilon_l - \epsilon_r)_{max}$, the maximum intensity at λ_k of the k'th CD band, is equal to $(2.687 \times 10^{-4})(a_k)$. a_k is in turn equal to $(96N/hc)(R_k\lambda_k/\Delta_k)$ and is called the intensity factor of the k'th partial Cotton effect in this study.

The computations required an initial assumption of the number of partial Cotton effects, **N**, necessary to reproduce an observed ORD curve. An inspection of the curve then led to the selection of initial values of parameters, λ_k and Δ_k, for each partial Cotton effect. From this information plus experimentally obtained molar rotations, the intensity factors were obtained with a computer program. The resultant ORD curve composed of **N** partial Cotton effects was constructed, and if the agreement with the observed ORD was unsatisfactory changes were made in the selection of λ_k and Δ_k. If serious discrepancies remained in certain areas **N** was increased. An approximate relationship, $\lambda_{extremes} = \lambda_k \pm 0.92\Delta_k$, was used to locate the positions of the peak and trough with respect to the inflection point, λ_k.[18]

Results

Induced ORD of AO–DNA and AO–NaPLG. Figure 1 shows some representative curves depicting changes of the induced optical activity of complexes of AO–DNA as D/P is varied. The variations in the ORD profiles are strikingly systematic. At D/P 0.02 the induced ORD is negative down to the crossover point at 491 mμ, having a trough at 509 mμ, followed by a positive plateau between 490 and 470 mμ, and a weak peak at 460 mμ. As D/P increases, a positive peak develops in the region of 520 mμ. Simultaneously the trough around 510 mμ increases in magnitude, moving toward shorter wavelengths, and the plateau region becomes negative and develops into a discrete shoulder. With a further increase in D/P the peak at 520 mμ and the trough at 497 mμ reach maximum magnitudes. This occurs around D/P 0.3 and agrees with the observation reported previously.[11] There also appears a definite depression in the positive lobe between 450 and 440 mμ in the D/P range 0.1–0.3. At the highest D/P in Figure 1 the shoulder develops into a trough at 475 mμ, while the longer wavelength trough and the peak at 520 mμ diminish in size. The second crossover point is displaced further toward the blue (447 mμ) and there is a very weak peak at 435 mμ. This family of observed ORD curves may be divided into three groups with the curves at D/P 0.02, 0.2, and 0.5 taken as

(17) National Bureau of Standards, AMS No. 55, U. S. Government Printing Office, Washington, D. C., 1964.

(18) Upon completion of this work a new computer program for reiteration employing a least-square method became available. With use of this program the uniqueness of the decomposition into components of an observed ORD curve for AO–DNA was tested. The number, position, intensity, and band width of the components agreed quite well with those reported here.

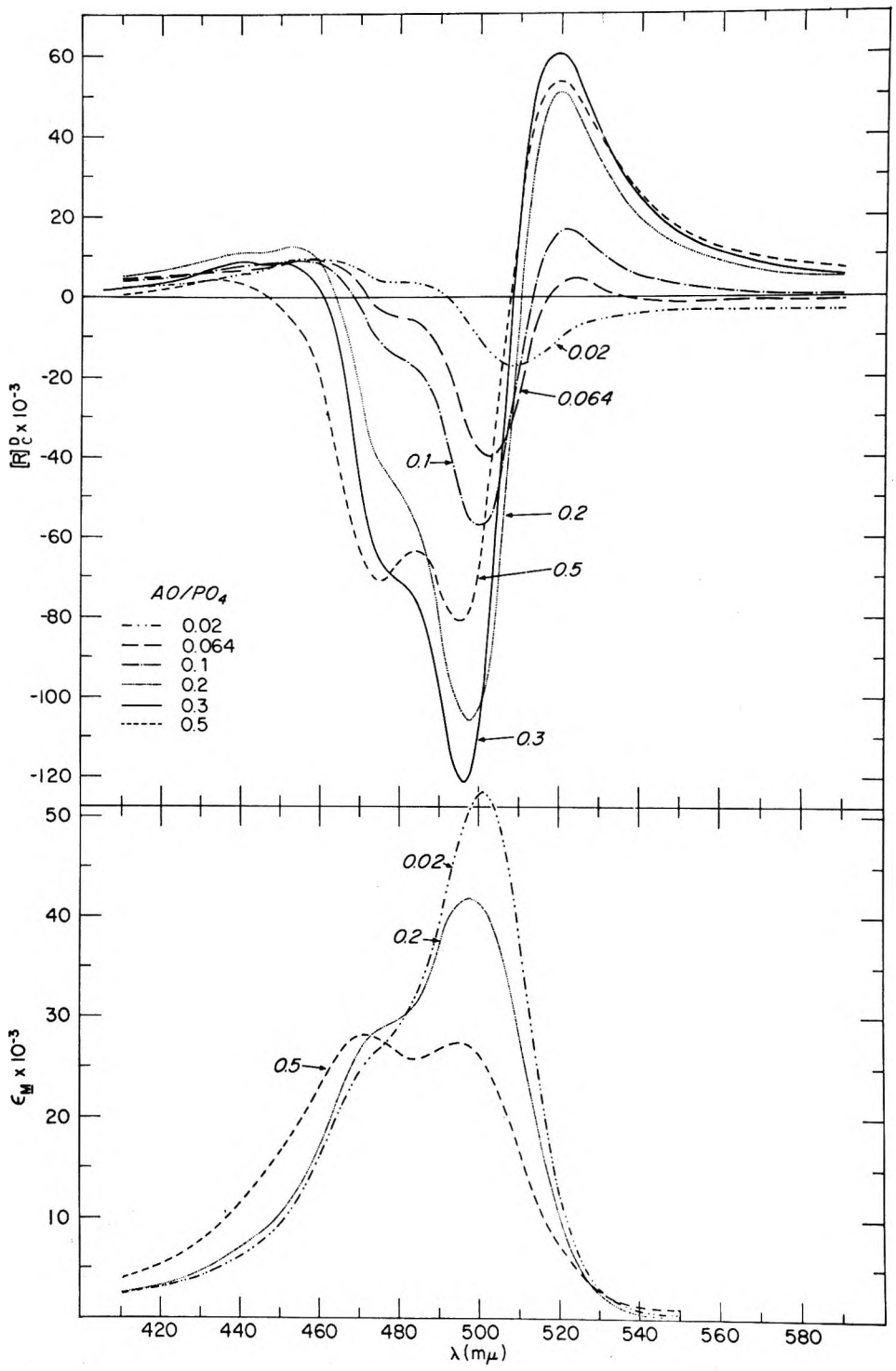

Figure 1. The ORD curves (upper) and the absorption spectra (lower) of the AO–DNA system with a variation of D/P.

representative ones. The experimental data are given in Table I.

The extrinsic Cotton effects of AO–NaPLG complexes at various D/P are shown in Figure 2. At the lowest ratio, D/P 0.0001, a broad positive peak is located at 525 mμ and a steep negative trough with a distinctive shoulder around 480 mμ. A second peak is situated at 450 mμ. As D/P increases, the longest wavelength peak shifts to the red and its magnitude continuously diminishes. In the region of 490 mμ the

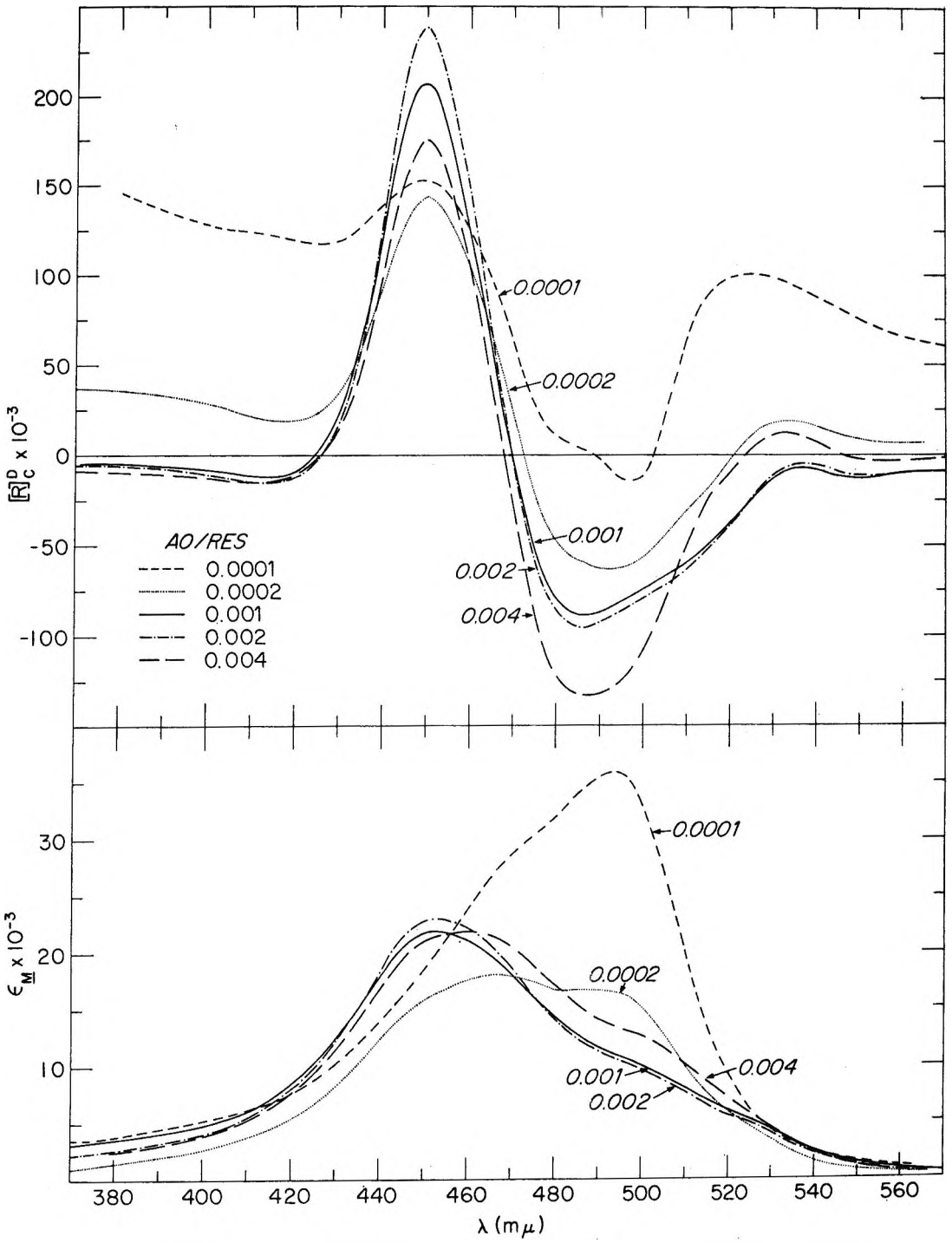

Figure 2. The ORD curves (upper) and the absorption spectra (lower) of the AO–NaPLG system with a variation of D/P.

broad trough increases in magnitude with a shoulder developing in the long-wavelength side (500–520 mμ). The position of the major peak remains remarkably constant at 450 mμ even though its magnitude does not bear any simple relation to D/P. A striking feature is the symmetric shape of this peak, which is not the case for the positive lobe of any single Cotton effect. At D/P 0.004 the trend of the longest wavelength peak shifting to the red is reversed. Together with the blue shift there occurs an increase in magnitude of the trough at 487 mμ and a decrease in magnitude of the peak at 450 mμ. A shallow trough is present in all

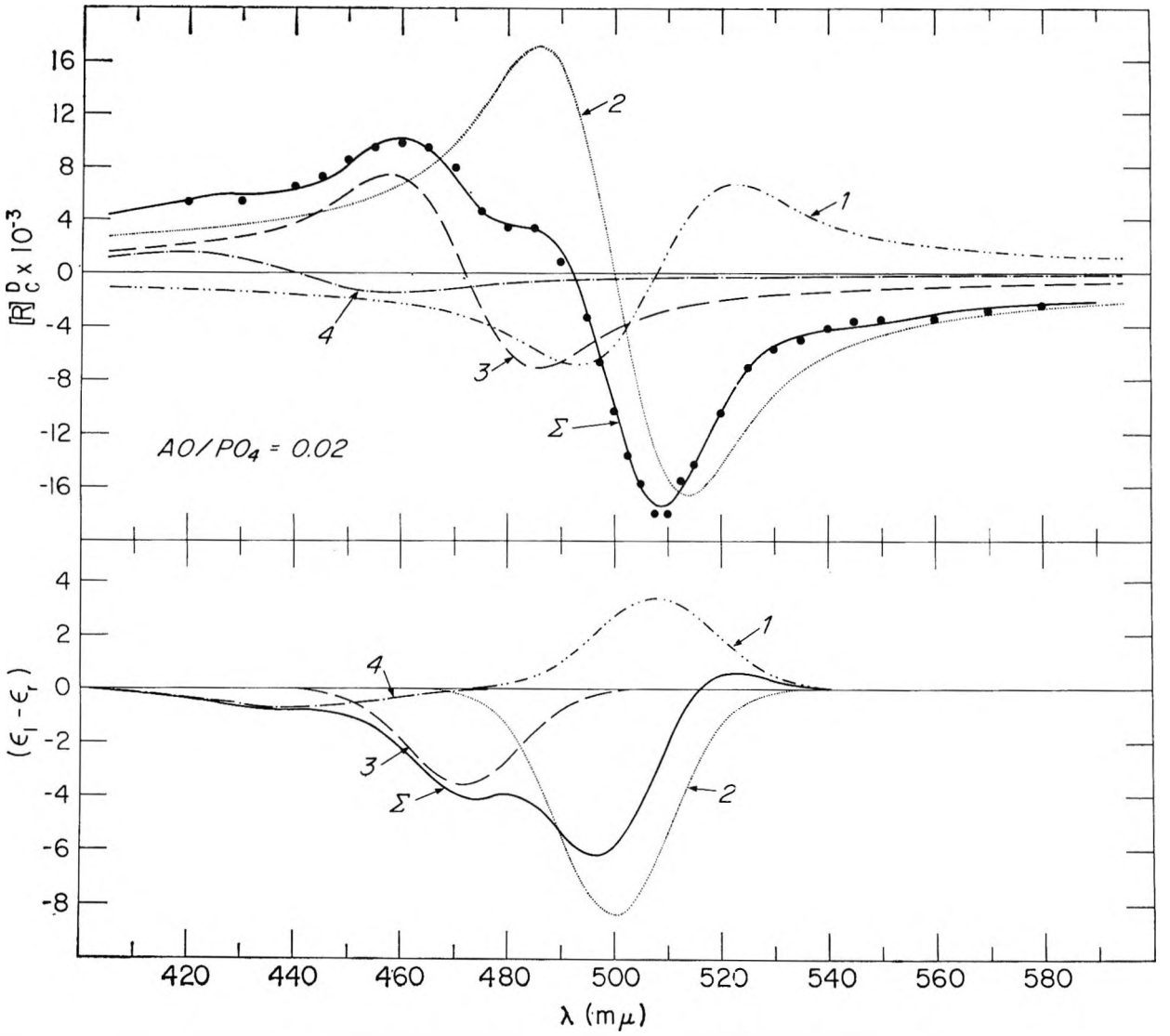

Figure 3. The resultant and component ORD curves (upper) and the resultant and component CD curves (lower) of the representative AO–DNA complex: ●, experimental points; numbers correspond to those of the k'th transition in Table II; curves 1–4, component Cotton effects; Σ, sum of curves 1–4. $AO/PO_4 = 0.02$.

curves between 415 and 425 mμ. The details of this system are summarized in Table I. It is convenient to regard the ORD curves at D/P 0.0001, 0.002, and 0.004 as representative ones for this system.

Absorption Spectra of AO, AO–DNA, and AO–NaPLG. The molar extinction coefficient of AO, ϵ_M, at 492 mμ, determined at a dye concentration of 2.07×10^{-6} M, was 57,000 at pH 4.5 (55,300 at pH 6.5). In the range of concentrations between 4×10^{-5} and 2×10^{-6} M two isosbestic points were observed at pH 4.5: one at 474 mμ (ϵ_M 41,000) and the other at 518 mμ (ϵ_M 8700). Similar results were obtained by Zanker,[5] who found isosbestic points at 472–473 and 518 mμ for AO in high salt concentration at pH 6.

The absorption spectra obtained for AO–DNA (Figure 1 and Table I) have been so extensively studied in the past, *vide supra*, that only specific points will be noted. At D/P 0.02 the absorption maximum was observed at 502.5 mμ,[2a] not at 504 mμ,[7,11] with a molar extinction coefficient of 53,000. The absorption spectra at D/P 0.2 and 0.5 are qualitatively in agreement with the findings of Stone and Bradley (see Figure 4 in ref 7).

Compared with the AO–DNA system, the AO–NaPLG spectra have more detail (Figure 2 and Table I). At D/P 0.0001 the general shape of the absorption spectrum is very different from the others. It resembles that of unbound AO except for the broadening of the longer wavelength limb. As D/P increases,

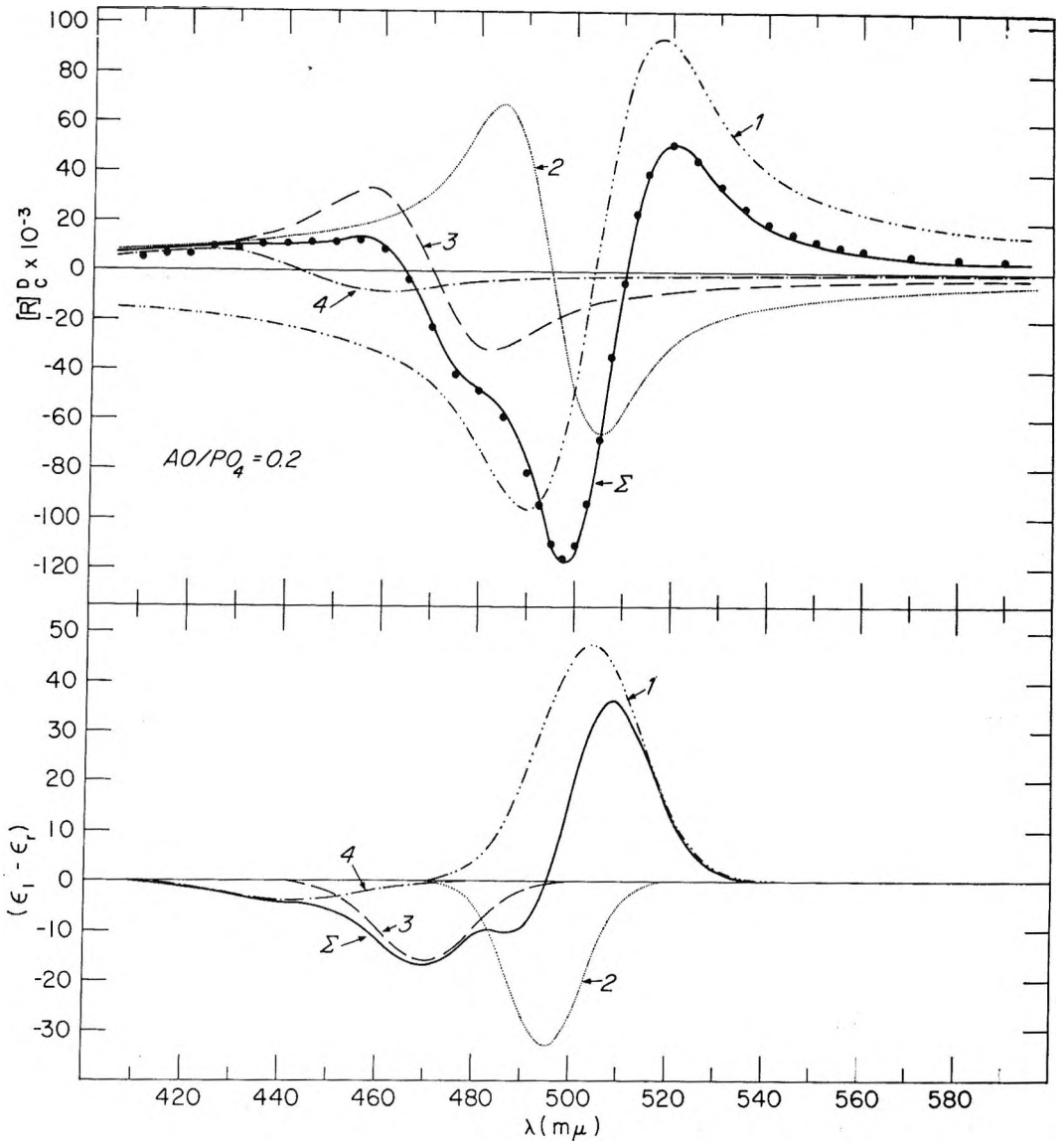

Figure 4. Same as Figure 3, except $AO/PO_4 = 0.2$.

a new band appears, as revealed by a distinctive shoulder at 520–530 mμ. This band has not been reported previously. The maximum at 494 mμ is drastically diminished in intensity and appears as a shoulder in this region. Simultaneously a broad band centered at 453 mμ appears (D/P 0.001–0.002). This band has also been found by others.[9] The shape of the absorption spectra at these D/P values is very similar to that observed by Zanker at high concentrations of unbound AO.[5] At further increased D/P this band diminishes slightly and is displaced to the red (461 mμ) while the absorption band at 500 mμ increases.

Analysis of the Induced ORD Curves. Figures 3–8 contain the results of the analyses of the representative ORD curves whereby the individual partial Cotton effects were identified with respect to both position and magnitude. The experimental data, represented by the filled circles, are quite well reproduced by the resultant ORD curves in all cases. The resultant CD curves constructed from the partial CD bands are also included in the lower portions of these figures. In the two diverse systems studied a minimum of four partial Cotton effects is required to reproduce all the features found in the observed data. Whenever the number was reduced to three, at least one region of the resultant ORD curve showed poor agreement with the experimental one. This is not to be construed as implying that four partial Cotton effects are necessarily the actual

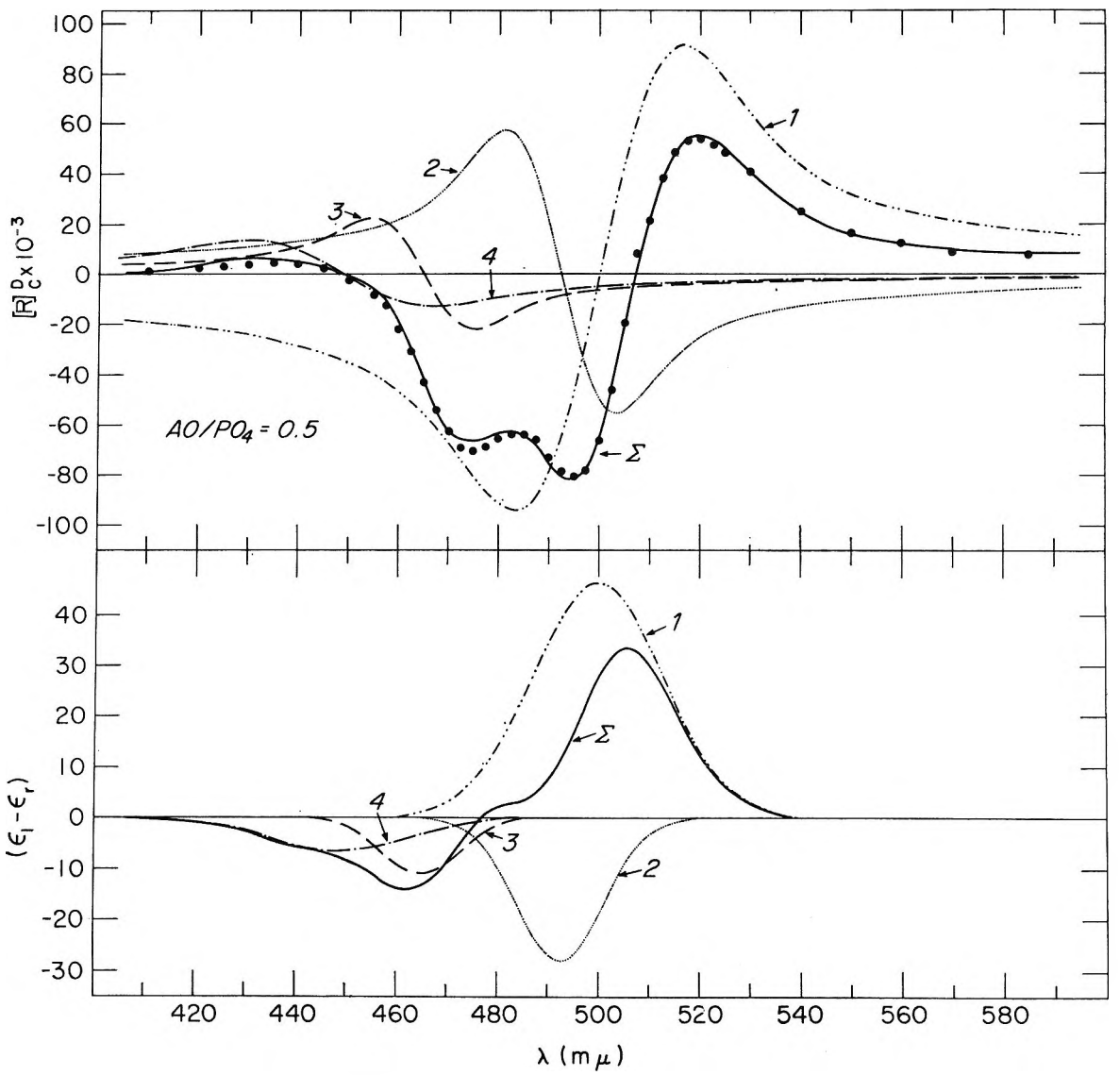

Figure 5. Same as Figure 3, except AO/PO_4 = 0.5.

number involved, but it is considered to be the minimum number of components required. The parameters for each of the component Cotton effects are summarized in Table II.

In all three of the AO–DNA curves analyzed the first (longest wavelength) component is always positive and the other three are negative. The presence of a positive partial Cotton effect for D/P 0.02 is not readily apparent by visual inspection. In the course of increasing D/P the increase in rotational strength of this component results in the appearance of a peak around 520 (λ_k 508 and 504 mμ, see Figures 3 and 4). This positive rotational strength either reaches a plateau or starts diminishing at D/P above 0.5. The three negative partial Cotton effects interact destructively in the ORD, giving rise to a weak net positive rotation at shorter wavelengths, and additively in the CD, forming a broad negative CD band (Figures 3–5). Finally it should be noted that the relationship between the positions of the transitions giving rise to the partial Cotton effects and the maxima and shoulders of the absorption spectra is not a simple one (compare Tables I and II).

The three representative ORD curves of AO–NaPLG, resolved into partial Cotton effects, are shown in Figures 6–8. At the lowest D/P (Figure 6) the experimental curve and the first three partial Cotton effects identified are similar to those for AO–DNA at D/P 0.5. For the purpose of analysis the experimental data for AO–NaPLG at D/P 0.0001 were corrected for the large background rotation using the last term in eq 2. This

Table II: Summary of the Analysis of Representative ORD Curves for AO–DNA and AO–NaPLG

	AO–DNA, pH 6.5				AO–NaPLG, pH 4.5			
	D/P 0.02				*D*/Residue 0.0001			
k	1	2	3	4	1	2	3	4
λ_k, mμ	508	500	472	440	505	494.5	468	441
Δ_k, mμ	16	15	15	24	18	10	18	11
$a \times 10^{-3}$	12.52	−31.12	−13.38	−2.68	118.3	−56.0	−99.5	20.0
$R_k \times 10^{39}$	0.432	−1.02	−0.464	−0.147	4.61	−1.24	−4.18	0.55
$(\epsilon_l - \epsilon_r)_{max}$	3.37	−8.37	−3.57	−0.721	31.8	−15.0	−26.7	5.4
	D/P 0.2				*D*/Residue 0.002			
k	1	2	3	4	1	2	3	4
λ_k, mμ	504	495	470	443	522	470	464	445
Δ_k, mμ	15	11	14	20	12	14	20	22
$a \times 10^{-3}$	175.8	−122.8	−59.9	−15.0	33.8	95.7	−431.0	238.1
$R_k \times 10^{39}$	5.71	−2.98	−1.95	−0.742	0.85	3.1	−20.3	12.9
$(\epsilon_l - \epsilon_r)_{max}$	47.25	−33.0	−16.1	−4.03	9.08	25.7	−115.8	64.0
	D/P 0.5				*D*/Residue 0.004			
k	1	2	3	4	1	2	3	4
λ_k, mμ	500	492.5	465	449	522	506	463	449
Δ_k, mμ	18	12	11	20	12	10	19	24
$a \times 10^{-3}$	171.8	−103.8	−41.0	−24.4	46.3	67.1	−351.3	188.9
$R_k \times 10^{39}$	6.77	−2.77	1.06	−1.19	1.16	1.45	−15.8	11.0
$(\epsilon_l - \epsilon_r)_{max}$	46.15	−27.9	−11.0	−6.56	12.4	18.0	−94.4	50.7

was necessitated by the fact that a slight difference in the concentration of the polymer in the complex and control solutions caused a huge change in the background rotation in a 10-cm cell. A value of 212 was used for λ_i since it has been used to represent the plain dispersion of proteins and polypeptides in the visible region of the ORD curve.[19] A value of 1.64×10^{-4} was assigned to m_i on the basis that at 600 mμ the influence of the induced Cotton effect is negligible; therefore the rotation of the complex should be virtually identical with that of NaPLG at the same pH. As *D/P* increases (Figures 7 and 8) the effects of the third and fourth components become very pronounced. It is at once apparent that the symmetrical shape of the virtual peak in the ORD curve at 450 mμ is in all cases a result of the mutual cancellation of the negative lobe of the fourth partial Cotton effect by the positive lobe of the third partial Cotton effect. In contrast to the AO–DNA system, changes in the first two components in the AO–NaPLG system are less systematic (Table II). The longest wavelength partial Cotton effect at higher *D/P* (522 mμ) is probably associated with the absorption shoulder appearing at around 525 mμ (Figure 2). This positive component was not resolved at *D/P* 0.0001 (Figure 6). A positive component at 505 mμ was found at *D/P* 0.0001 and 0.004 but not at *D/P* 0.002.

When the position and sign of each of the partial Cotton effects are plotted at various ratios of dye to residue (Figure 9), some of the correlations become apparent. It is at once evident that the changes of λ_k in the AO–DNA system are quite systematic, whereas in the AO–NaPLG system some of the transitions are missing. This may be due to the limitations of the experimental and computational techniques.

Discussion

Extrinsic Cotton Effects in AO–DNA and AO–NaPLG. When available sites greatly exceed the number of dye molecules Bradley and Felsenfeld[6] noted that at sufficiently low *D/P*, about 0.01, the extinction at 504 mμ reaches a plateau and that this indicates complete dye unstacking. Accordingly only the monomeric form of bound AO would exist under such conditions. The absorption spectra currently obtained for AO–DNA with *D/P* lower than 0.04 agree with those previously reported.[2a,6] Consequently the present experimental data indicate that there is no mutual interaction between bound dyes at *D/P* 0.02 (Figure 1). The view that weak coupling of bound AO molecules is an obligatory requirement for

(19) W. Moffitt and J. T. Yang, *Proc. Natl. Acad. Sci. U. S.*, **42**, 596 (1956).

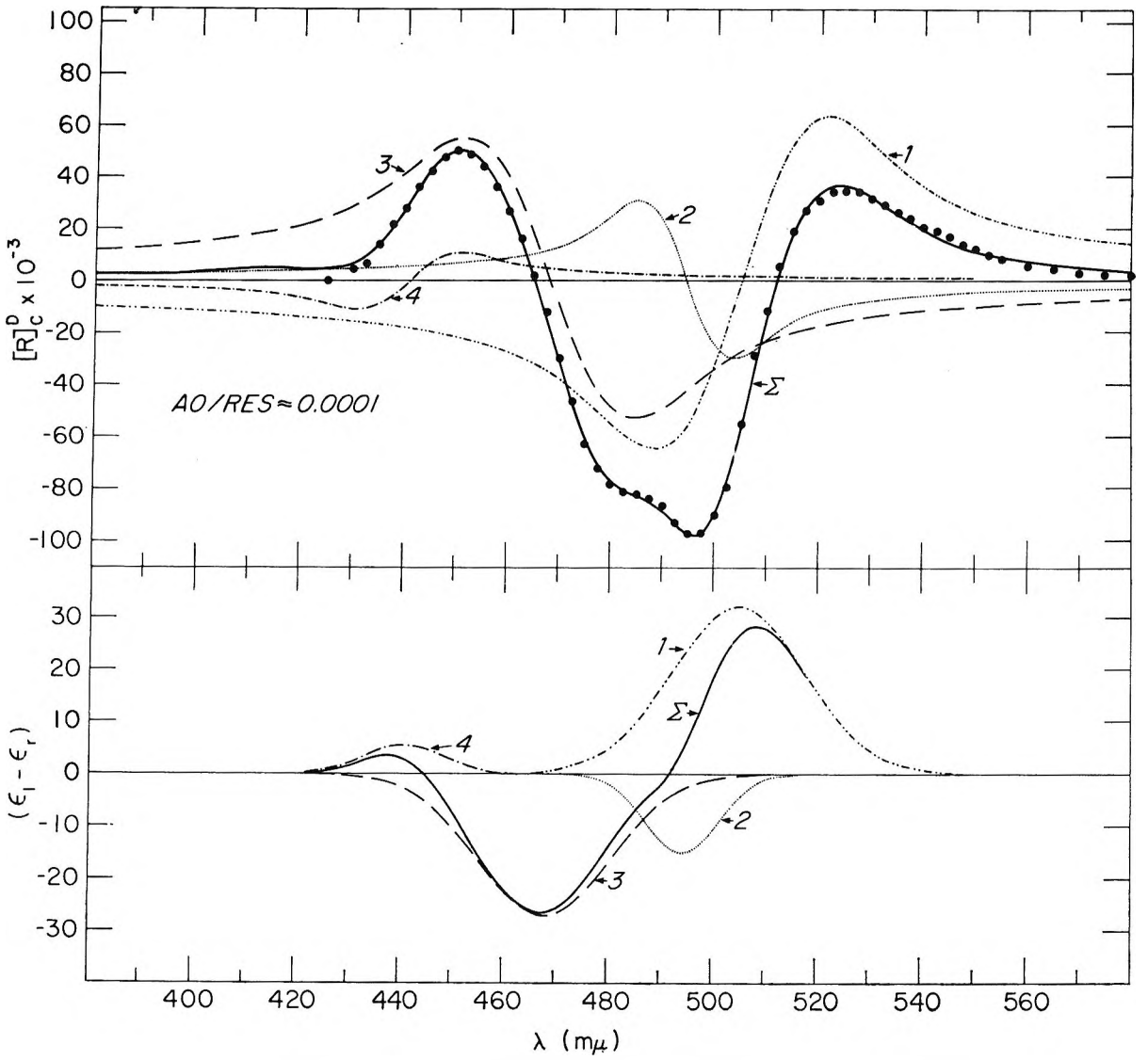

Figure 6. The resultant and component ORD curves (upper) and the resultant and component CD curves (lower) of the representative AO–NaPLG complex. Symbols are all the same as Figures 3–5. AO/(residue) = 0.0001 Correction for background rotation was made (see text).

optical activity induced in the AO–DNA system[11] is not supported by the current experimental results. The shape of the induced Cotton effect is essentially unchanged up to D/P 0.04.[20] The fact that an extrinsic Cotton effect is induced by a monomeric chromophore bound to DNA (as an average, at D/P 0.02 there are only two dye molecules per five turns of the double-stranded DNA helix with a separation of 84 A) obviates the necessity for invoking either weak or strong coupling exciton theory to explain the observed results at low D/P.[11] Analysis of the ORD curve for D/P 0.02 (Figure 3) shows that there are *at least* two partial Cotton effects of opposite signs involved in the region of the bound monomeric AO absorption band (Figure 1), which has been designated as the α band by Michaelis[4] and as the complex II band by Beers, *et al.*[2a] The fact that two partial Cotton effects were resolved in the region of the α band indicates that this band does not represent the intrinsic absorption of monomeric bound AO (the maximum of the monomeric AO absorption band is located at 492 mμ in the absence of polymers) and that it really consists of two electronic transitions. The salient point, that this 502-mμ absorption band is

(20) Recently, using a differential cell holder, induced optical activity could be detected at D/P 0.0018, an order of magnitude lower than any previous case. The shape and magnitude of the extrinsic Cotton effect are practically identical with those reported for D/P 0.02 in this paper.

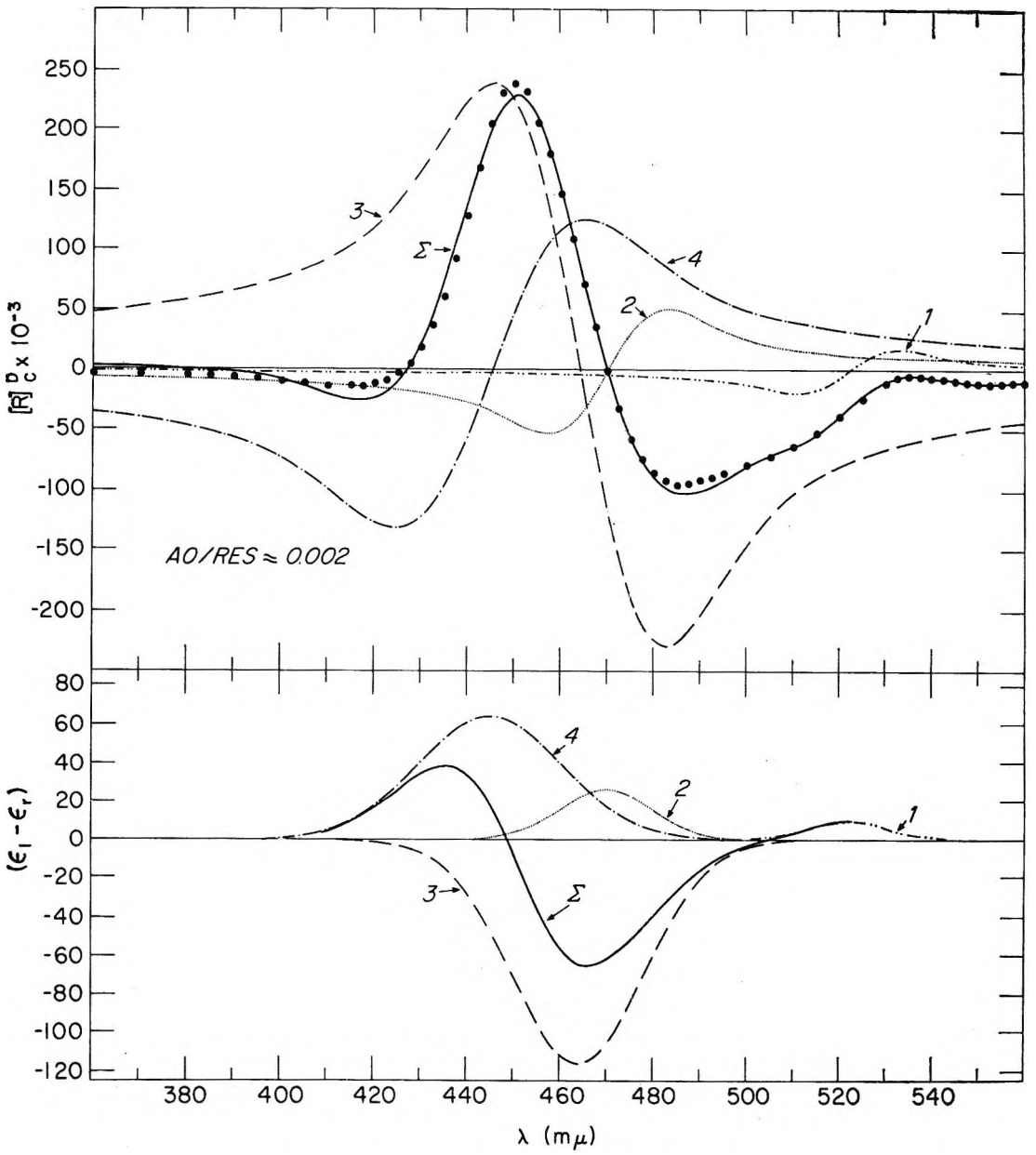

Figure 7. Same as Figure 6, except AO/(residue) = 0.002.

heterogeneous, is consistent with the experimental observation that the stacking coefficient of the AO–DNA system varies with the wavelength at which it is computed (*i.e.*, 504, 510, and 515 mμ).[7]

Considering now the data for the AO–DNA system, it is seen that the sum of the first two rotational strengths in the three cases (Table II) is never zero. This does not support the idea that these partial Cotton effects arise from dye–dye interactions based on exciton theory.[21] The model used to explain the induced Cotton effect by strong coupling exciton theory does not represent the mode of binding of AO to DNA sites.[22] Therefore it is quite natural that the gross appearance of the theoretically calculated ORD curves (see Figure 3 of ref 21) does not resemble those obtained in this study. The findings that a positive Cotton effect is counterpoised by three successive negative ones in each case (Figures 3–5) and that their relative positions remain unchanged (Figure 9) indicate that

(21) I. Tinoco, Jr., R. W. Woody, and D. F. Bradley, *J. Chem. Phys.*, **38**, 1317 (1963).

(22) (a) S. F. Mason and A. J. McCaffery, *Nature*, **204**, 468 (1964); (b) L. S. Lerman, *Proc. Natl. Acad. Sci. U. S.*, **49**, 94 (1963); (c) R. A. Resnik and K. Yamaoka, to be published.

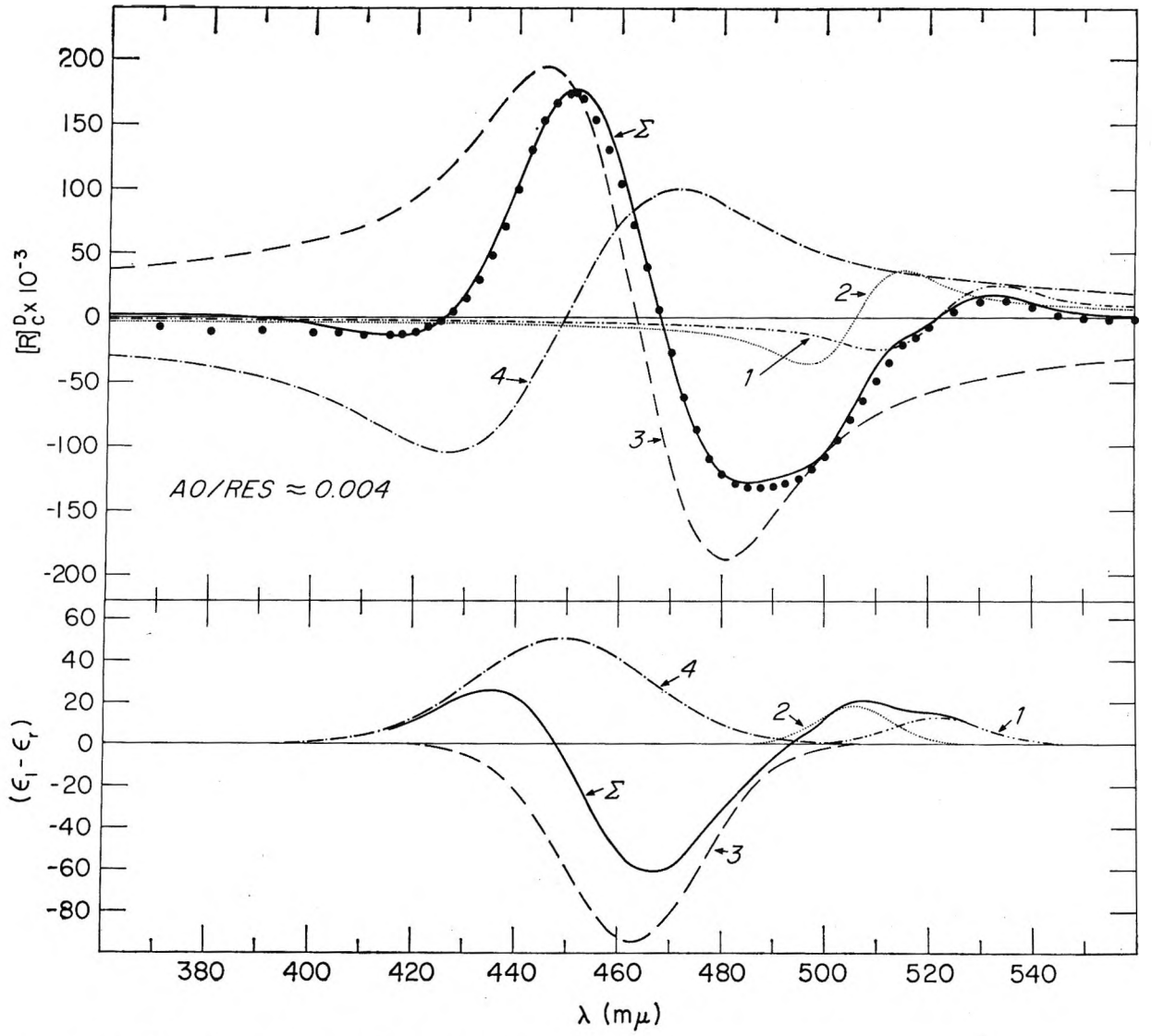

Figure 8. Same as Figure 6, except AO/(residue) = 0.004.

strong dye–dye interaction is not operative in this system. Therefore the AO–DNA system may not be the most suitable one to prove the applicability of strong coupling exciton theory.[21]

The choice of a peak at 515–520 mμ and a trough at 490–500 mμ in the ORD curves as indications of a single Cotton effect[11] does not appear to be valid. The present results (Table II and Figure 1) indicate that although the molar rotation at 515 mμ decreases with further increase in D/P after reaching a maximum at around 0.3, the rotational strength of the positive Cotton effect either increases or levels off by D/P 0.5.

Turning now to the AO–NaPLG system, the experimental ORD curves in this report (Figure 2) are in good agreement with those reported by Stryer and Blout.[10] These workers also held the view that the aggregation of bound AO molecules is necessary for induced optical activity and proposed three models to explain their results with AO–NaPLG.[10] Two models were considered as being consistent with the experimental results: model II, in which dye molecules form a super helix of a single screw sense, and model III, in which dye molecules form a tangential helix. Model I, having monomeric dye bound near the asymmetric environment of the α-carbon atom, was not accepted because of the lack of experimental evidence in support of it. It should be noted that at least two AO molecules are required to approach close enough to form a segment of one of the proposed helical structures. On the contrary, Stryer and Blout's data show that the long-wavelength portion of the induced Cotton effect,

corresponding to the α band of the absorption spectrum, is maximal when there exists on the average less than one AO molecule per polymer molecule.

Of course the binding of AO does not have to be random. In fact Ballard, *et al.*,[23] explained their finding that optical activity was induced in the AO–NaPLG complex with D/P 0.001 (approximately two AO molecules per three polymer molecules) by assuming that AO bound to NaPLG has a high stacking tendency. This is a point which has not been proven quantitatively as yet. The stacking coefficient, moreover, has been related to the conformation of a polymer with more highly ordered polymers having a lower coefficient.[2b] The stacking theory was originally derived for a single, infinitely long polymer molecule.[24] NaPLG is much smaller than DNA; accordingly, end effects are more influential. The situation is further complicated because the carboxyl (α and γ) groups, which are the most probable binding sites of this polymer, are mostly un-ionized at pH 4.5.[25] The effective number of polymer molecules or sites capable of binding dye is therefore only a small fraction if an ionized site is needed for an AO molecule to form a dye–polymer complex. On this basis it is understandable why the absorption spectrum for D/P 0.001 (Figure 2), or one AO molecule per two polymer molecules, appears similar to that of AO at very high concentrations in the absence of polymer.[5] Whether this is due to bound dye–bound dye or bound dye–free dye interaction will not be discussed at present.

In the current study optical activity was detected in the AO–NaPLG complex at D/P one order of magnitude lower, D/P 0.0001, where there would be on the average one AO molecule per twenty polymer molecules. Aggregation of dye on the polymer does not seem likely to occur under these conditions. This is reflected in the absorption spectrum and the ORD (Figure 2). Furthermore, analysis of the ORD curve for D/P 0.0001 reveals the same situation as in the AO–DNA system. At least two optically active transitions contribute to the α band at 495 mμ. It may therefore be concluded that in the AO–NaPLG system at D/P 0.0001 a majority of the bound dye population is monomeric with no appreciable dye–dye interaction.

Our analysis gives support to model I, proposed and rejected by Stryer and Blout,[10] as a necessary condition for induced optical activity in the two systems studied. In general then, monomeric bound dye does not have to be located, as originally thought, near the asymmetric α carbon atom. Vicinal disymmetry is sufficient for induced optical activity. This condition would be fulfilled when isolated dyes are rigidly bound to sites and are in proper orientation. Thus induced optical activity would not necessarily disappear even if the extended helical conformation of polymers is destroyed by such factors as heat or pH.[26,27] Needless to say, aggregated dyes constitute sufficient conditions for induced optical activity, as in the models proposed by Stryer and Blout,[10] and in the helical array of stacked dyes considered by Tinoco, *et al.*[21]

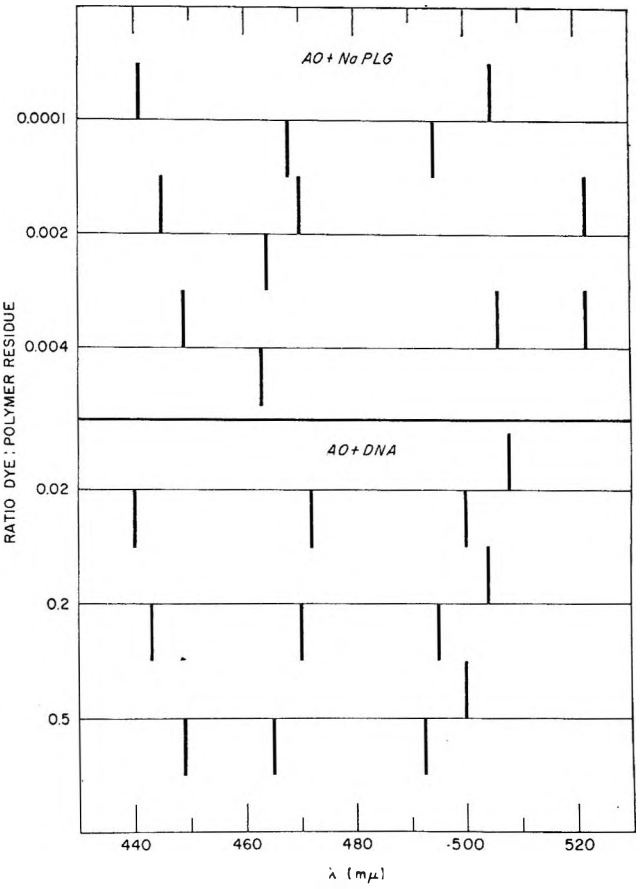

Figure 9. The position of optically active transitions of AO–NaPLG and AO–DNA systems at representative D/P. The signs of the vertical lines, which indicate the position, are positive if they are above the horizontal line.

Comparison of Resultant CD Curves with Experimental Ones. Throughout this study the assumption has been made that the Kronig–Kramers transform (eq 2 and 3) can adequately describe the observed ORD curves. Thus it is desirable to test the validity of the premise by comparing the resultant CD curves computed from

(23) R. E. Ballard, A. J. McCaffery, and S. F. Mason, *Biopolymers*, **4**, 97 (1966).

(24) S. Geisser and D. F. Bradley, *Bull. Inst. Intern. Statist.*, **39**, 269 (1962).

(25) (a) A. Wada, *Mol. Phys.*, **3**, 409 (1960); (b) M. Nagasawa and A. Holtzer, *J. Am. Chem. Soc.*, **86**, 538 (1964).

(26) A. Blake and A. R. Peacocke, *Nature*, **206**, 1009 (1965).

(27) R. A. Resnik and K. Yamaoka, unpublished observations.

the partial Cotton effects with experimental ones. CD measurements for AO–DNA have been reported by Mason and McCaffery.[22a] Judging from the absorption spectrum of their sample, D/P appears to be between 0.3 and 0.5 (compare Figure 1 of the current work and Figure 2 in ref 7 with Figure 2 in ref 22a). Their CD curve resembles rather well the resultant curve shown in Figure 4, with the qualification that the shoulder around 490 mμ should be slightly less negative.

Mason and McCaffery considered the observed CD curve to be composed of only two bands; one at 505 mμ polarized perpendicular to and one at 467 mμ polarized parallel to the axis of the DNA helix. They ignored the details around 490 mμ. This shoulder cannot be overlooked because it may arise from a completely canceled positive component or a partially canceled negative component. A little scrutiny of the resultant and the component CD bands in Figure 4 shows that the shoulder at 490 mμ is indeed caused by the destructive interaction between a strong positive component centered at 504 mμ and a negative one at 495 mμ. The broad negative band that Mason and McCaffery found at 467 mμ is in reality composed of three components of like sign (Figure 4). The strongest of these, at 495 mμ, is barely discernible. The extent to which interplay among components markedly affects the shape and sign of the resultant curve is clearly evident from all the CD curves for the AO–DNA system (Figures 3–5).

During the preparation of this paper, CD results for the system of AO–NaPLG appeared.[23] Since the results were presented in an abbreviated form, only a qualitative comparison can be made here. The observed CD data by Ballard, *et al.*, at D/P 0.0025 (see Table I, ref 23) are compared with the resultant CD curve at D/P 0.002 of this work (Figure 7) in Table III. The positions and signs of all three extremes are in good agreement. The positions of these extremes in the table, however, appear to be virtual when compared with the locations of the individual CD bands (Figures 6–8). When the rotational strengths are calculated from the positions of the observed CD extremes the magnitudes are for the most part underestimated, as illustrated by Figures 7 and 8.

Table III: Summary of Experimental and Resultant CD Curves for AO-NaPLG

Ballard, *et al.*, ref 23		Present work	
λ, mμ	$(\epsilon_l - \epsilon_r)$	λ, mμ	$(\epsilon_l - \epsilon_r)$
522	+7.2	522	+9
465	−25	466	−65.5
438	+11	436	+37

Assignment of Optically Active Absorption Bands. An unequivocal determination of the origin of the individual CD bands certainly requires much more work. However some relationships between the results of the present analysis of extrinsic Cotton effects and data on unbound AO are worthy of note.

In a recent analysis of the absorption spectra of AO in the absence of polymers, two models representing the monomer–dimer equilibrium are discussed.[28] While there is some correlation between the positions of the partial Cotton effects found for the AO–NaPLG system (Table II and Figure 9) and the positions of the absorption bands of dimeric and monomeric AO (see Figure 6, ref 28), certain inconsistencies exist. It should be recalled, as noted earlier, that there are two, not just one, isosbestic points in the absorption spectra of AO. As a result the possibility that three different species coexist in equilibrium cannot be ruled out, and the extrapolated spectra for these species must be refined.

Zanker and his assocates[5,29–31] have reported that the absorption spectrum of AO in the visible region shows three absorption bands in very dilute solution. They considered these bands at 495, 470, and 446 mμ as representing respectively the $0 \rightarrow 0$, $0 \rightarrow 1$, and $0 \rightarrow 2$ vibrational levels of a single electronic transition. The relative intensities of these bands vary as the concentration increases and the 446-mμ ($0 \rightarrow 2$) band becomes the most intense one above 10^{-1} M, possibly because of changes in Franck–Condon allowedness as a result of dye interaction. This electronic transition was assigned to the ^1L_b band, according to Platt's nomenclature.[30] The existence of another electronic transition, the ^1L_a band, at longer wavelengths was predicted.[31] In fact a discrete shoulder, or vorband, was observed above 500 mμ and assigned to the ^1L_a band.[30]

The current results for both AO–DNA and AO–NaPLG appear to be explained in terms of Zanker's observations. As AO binds to the sites of polymers (phosphates and/or nucleotide bases for DNA; α and/or γ carboxyl groups for NaPLG), the molecular symmetry of unbound AO would be modified and the forbiddeness of the ^1L_a transition of unbound AO in

(28) M. E. Lamm and D. M. Neville, Jr., *J. Phys. Chem.*, **69**, 3872 (1965).

(29) V. Zanker, *Z. Physik. Chem.*, **200**, 250 (1952).

(30) V. Zanker, M. Held, and H. Rammensee, *Z. Naturforsch.*, **11B**, 789 (1959).

(31) A. Wittwer and V. Zanker, *Z. Physik. Chem.* (Frankfurt), **22**, 417 (1959).

turn becomes less restrictive.[31] Thus the enhanced intensity at the longest wavelength transition shifts the apparent absorption maximum to 502 mμ for AO–DNA, while for AO–NaPLG the absorption maximum is displaced to 495 mμ with a broadened, longer wavelength limb (Figures 1 and 2). It should be noted that the position of the maximum intensity of the α band has been shown to vary with different polymers.[2b] The changes in rotational strengths with D/P of three negative partial Cotton effects in the AO–DNA system (Table II) are what would be expected from the spectroscopic studies of AO.[5] At D/P 0.02, the strongest is the negative Cotton effect at 500 mμ which would correspond to the 0 → 0 vibrational level of the ^1L_b band of unbound AO. The rotational strength of this component becomes overshadowed by the positive one at longer wavelengths as D/P increases. It appears reasonable, therefore, to conclude that for AO–DNA the positive partial Cotton effect is associated with the ^1L_a band, and the three negative partial Cotton effects, whose positions agree quite well with those found by Zanker, *et al.*,[5,30] for free AO, are related to the vibrational levels of the ^1L_b transition.

The less orderly variation of the partial Cotton effects with D/P for AO–NaPLG makes an interpretation of the origin of its optically active transitions more difficult. For AO–NaPLG at D/P 0.0001 the same argument used for AO–DNA may be applied to all but the fourth partial Cotton effect (Table II and Figure 9). This transition could be assigned to one of the higher order vibrational levels of the ^1L_a band,[30] with the qualification that some of the intermediate levels were not resolved in the present work. Alternatively, the positive Cotton effect at 441 mμ may be attributed to a transition of AO dimer, since a small fraction of bound dye could exist as aggregates. At higher D/P ratios the situation is complicated. Whether or not the positive partial Cotton effect at 522 mμ (Figures 7 and 8) belongs to the ^1L_a transition of monomeric bound AO is uncertain. Since AO can bind to NaPLG in a number of ways the dye, being bound in different environments, could give rise to partial Cotton effects at different wavelengths.

Finally, we wish to point out that the role of water has been ignored for the present. Also the problem of whether the ground-state interaction between bound monoprotonated AO and polymer sites modifies the electronic configuration of the dye remains unresolved.

Acknowledgment. The authors are indebted to Dr. E. Charney of this laboratory for useful discussions and wish to acknowledge the assistance of Mr. R. Shrager of the Computation and Data Processing Branch.

NOTES

The Reaction of Sulfur Dioxide with Active Nitrogen

by A. Jacob,[1a] R. A. Westbury,[1b] and C. A. Winkler[1a]

Departments of Chemistry, McGill University, Montreal, Quebec, Canada, and Marianopolis College, Montreal, Quebec, Canada
(Received May 13, 1966)

Since the reactions of active nitrogen with hydrogen sulfide and with sulfur have been studied previously,[2] it was of interest to investigate the corresponding reaction with sulfur dioxide, in which sulfur possesses a formal positive charge. Previous studies have indicated that SO_2 was not decomposed by active nitrogen.[3,4]

The apparatus and methods were essentially similar to those used in many earlier studies from this laboratory.[5,6] The system was of the conventional fast-flow type in which active nitrogen was formed by using either a condensed electrode or a microwave discharge. The discharge was operated for at least 60 min in the "poisoned" system and for 2 hr in the "unpoisoned"

(1) (a) McGill University; (b) Marianopolis College.

(2) (a) R. A. Westbury and C. A. Winkler, *Can. J. Chem.*, **38**, 334 (1960); (b) J. A. S. Bett and C. A. Winkler, *J. Phys. Chem.*, **59**, 371 (1955).

(3) K. D. Bayes, D. Kivelson, and S. C. Wong, *J. Chem. Phys.*, **37**, 1217 (1962).

(4) J. J. Smith and W. J. Jolly, *Inorg. Chem.*, **4**, 1006 (1965).

(5) P. A. Gartaganis and C. A. Winkler, *Can. J. Chem.*, **34**, 1457 (1956).

(6) E. M. Levy and C. A. Winkler, *ibid.*, **40**, 686 (1962).

system before each experiment of 100-sec duration. The reaction vessel was a straight, Pyrex-glass tube of 32-mm i.d., with a fixed reactant jet 17 cm below the discharge. The pressure in the system was 2 torr with a flow rate of molecular nitrogen of 190 $\times$ 10^{-6} mole sec^{-1}. Nitrogen (Linde "bond dry") was used after it had passed through a copper furnace at 420° to remove possible traces of oxygen. During experiments in the "unpoisoned" system, a liquid-air trap was used to remove traces of moisture from the gas. Commercial NO of 99% purity (Matheson Co.) was frozen at liquid-nitrogen temperature and freed from nitrogen by evacuation; NO_2 and N_2O_3 were removed by distillation of NO through a silica-gel column at −78°. Anhydrous ammonia and sulfur dioxide (Matheson Co.) were used after three bulb-to-bulb distillations during which only the middle fraction was retained. Excess NH_3 or SO_2 was trapped at liquid-air temperature. A Kjeldahl distillation was used to follow destruction of NH_3, and iodimetry was used to follow SO_2 destruction.

Experiments were first made in an "unpoisoned" system, using either a condensed electrode or a microwave discharge. The active-nitrogen flow rates, estimated by the gas-phase NO "titration,"[7] were 2.35 $\times$ 10^{-6} and 1.83 $\times$ 10^{-6} mole sec^{-1}, respectively. No destruction of SO_2 was detectable. Neither was it possible to detect any destruction of NH_3 by active nitrogen under these conditions.

In a system "poisoned" with water vapor ($\sim$5 $\times$ 10^{-6} mole sec^{-1}) in the nitrogen stream through the *microwave* discharge, the active-nitrogen flow rate was increased only slightly (15%), and neither SO_2 nor NH_3 was detectably decomposed. When the nitrogen stream through the *condensed* discharge contained a similar relatively large amount of water vapor, the active-nitrogen flow rate was increased to 21 $\times$ 10^{-6} mole sec^{-1}. The SO_2 reaction was then accompanied by the familiar blue glow, associated with the reaction, $N + O \rightarrow NO^*$. The glow extended from the sulfur dioxide inlet jet to the cold trap. The amount of SO_2 decomposed increased markedly with SO_2 flow rate (Table I) and a pale yellow solid collected in the cold trap. When this was warmed to room temperature, an oily film remained. This residue was acidic and was probably sulfuric acid. Ammonia was also decomposed with the same experimental conditions (Table I), but the maximum extent of its decomposition never exceeded about one-fifth the N atom flow rate.

When the water vapor supply was reduced to 0.1 $\times$ 10^{-6} mole sec^{-1}, with a concomitant decrease in the active-nitrogen flow rate, the decomposition of SO_2 did not give rise to the blue glow, nor was the yellow afterglow extinguished, even at high SO_2 flow rates. Almost no yellow solid was collected. The data are shown in Table II, together with corresponding results for the reaction of NH_3 under the same conditions. (A blank experiment in the absence of ammonia indicated that no NH_3 was formed by reaction of active nitrogen with the trace of H_2O present.)

Table I: Reactions of SO_2 and NH_3 with Active Nitrogen[a]

SO_2 flow	SO_2 reacted	NH_3 flow	NH_3 reacted
9.0	7.5	3.8	3.8
9.5	9.2	3.9	3.9
14.0	11.8	5.4	4.1
17.0	13.2	5.5	4.1
47.5	16.2	11.3	4.1

[a] System "poisoned" with H_2O vapor. N atom flow rate 21 $\times$ 10^{-6} mole sec^{-1}, by NO "titration"; ratio of this value to maximum HCN yield from C_2H_4 reaction was 1.4. All quantities are (moles sec^{-1}) $\times$ 10^{-6}.

Table II: Reactions of SO_2 and NH_3 with Active Nitrogen[a]

Active-nitrogen flow	SO_2 flow	SO_2 reacted	Active-nitrogen flow	NH_3 flow	NH_3 reacted
10.5	9.0	1.9	7.9	10.4	1.5
10.5	11.3	1.7	10.5	7.5	1.7
10.5	14.8	1.8	11.8	22.6	2.0
11.8	7.0	2.0	13.5	8.0	2.2
11.8	23.4	2.0	13.5	5.6	2.5

[a] System "poisoned" with H_2O vapor. All quantities are (moles sec^{-1}) $\times$ 10^{-6} N atom flow rate by NO "titration." Ratio of this value to maximum HCN yield from C_2H_4 reaction was 1.4.

The relative behavior of SO_2 and NH_3, in their reactions with active nitrogen, was studied independently with a second apparatus, in which the active nitrogen was formed in a condensed discharge. The observations reported above were fully confirmed. It was also found that an increase of reaction temperature to 200° had no effect on the limiting extents to which either NH_3 or SO_2 reacted (*cf.* a similar earlier observation for the NH_3 reaction, ref 8).

With a small amount of H_2 ($\sim$0.5 $\times$ 10^{-6} mole sec^{-1}), instead of H_2O vapor, in the nitrogen flow before it entered the condensed discharge, the active-nitrogen

(7) F. Kaufman and J. R. Kelso, *J. Chem. Phys.*, **27**, 1209 (1957).

(8) G. R. Freeman and C. A. Winkler, *J. Phys. Chem.*, **59**, 371 (1955).

flow rate was 13.3 × 10^{-6} mole sec^{-1}. (Under these conditions the active-nitrogen flow rate obtained with the microwave discharge was 2.43 × 10^{-6} mole sec^{-1}.) The SO_2 reaction occurred with the formation of little solid, with the results shown in Table III. Also included in the table are data for the NH_3 reaction under similar experimental conditions.

Table III: Reactions of SO_2 and NH_3 with Active Nitrogen[a]

SO_2 flow	SO_2 reacted	NH_3 flow	NH_3 reacted
6.8	1.3	11.3	1.1
10.4	1.1	16.2	1.3
11.3	1.6	20.0	1.2
18.8	1.4	22.5	1.2

[a] System "poisoned" with H_2. N atom flow rate 13.3 × 10^{-6} mole sec^{-1}. All quantities are (moles sec^{-1}) × 10^{-6}.

It is evident from the data that ammonia and sulfur dioxide are decomposed to approximately the same extent by active nitrogen from a condensed discharge. Failure to decompose either SO_2 or NH_3 by active nitrogen from the microwave discharge might be due simply to the low N atom concentration produced. Alternatively, there might be a qualitative difference in the active nitrogen produced by the two methods. The relatively larger extents of SO_2 and NH_3 reactions in the system "poisoned" with water vapor, compared with the system "poisoned" with H_2, might also be due to a larger concentration of active species, although it is possible that it reflects some interference from oxygen atom reactions.

The persistence of the yellow nitrogen afterglow during the SO_2 and the NH_3 reactions, even for very high reactant flow rates (much above the value corresponding to the maximum destruction of either SO_2 or NH_3), indicates that these reactions involve a species other than N atoms in the ^4S state. Previous work has indicated that an excited nitrogen molecule, either N_2 ($^3\Sigma_u^+$)[9-11] or N_2 ($^5\Sigma_g^+$),[12] might be responsible for the ammonia reaction. It seems likely that the same species is also responsible for the SO_2 reaction.

Attempts to study the reaction of active nitrogen with mixtures of SO_2 and NH_3 were unsuccessful. When the two gases were mixed, a very rapid gas-phase reaction occurred and a yellow-brown water-soluble solid was formed. It was probably $H_2NSO_2NH_4$[13] or $(NH_4)_2S_2O_5$.[14] (Sulfur dioxide is a strong electron acceptor and forms a variety of molecular complexes with electron donors.)

Acknowledgment. Acknowledgment is gratefully made to the American Sulfur Institute for financial assistance during this investigation.

(9) A. N. Wright and C. A. Winkler, *Can. J. Chem.*, **20**, 5 (1962).

(10) A. N. Wright, R. L. Nelson, and C. A. Winkler, *ibid.*, **40**, 5 (1962).

(11) H. B. Dunford, *J. Phys. Chem.*, **67**, 258 (1963).

(12) K. D. Bayes and G. B. Kistiakowsky, *J. Chem. Phys.*, **32**, 992 (1960).

(13) K. A. Hofmann and U. R. Hofmann, "Anorganische Chemie," 11th ed, Frieder, Vieweg, and Sohn, Braunschweig, Germany, 1945, p 176.

(14) T. Hata and S. Kinumaki, *Nature*, **203**, 1378 (1964).

Homogeneous Chemical Kinetics with the Rotating Disk Electrode

by P. A. Malachesky, L. S. Marcoux, and R. N. Adams

Department of Chemistry, University of Kansas, Lawrence, Kansas 66044 *(Received June 13, 1966)*

Homogeneous chemical reactions coupled to electron transfers are of great importance in studies of organic electrode processes.[1,2] The rotating disk electrode (RDE) and the rotating ring-disk electrode have been shown to be of value in investigations of electrode reactions.[3,4] However, the capabilities of the RDE have not been fully exploited.

Theoretical treatments, with experimental verification, have appeared for the ECE electrolysis mechanism (1) for chronopotentiometry,[5] chronoamperometry,[6] cyclic voltammetry,[7] cyclic chronopotentiometry,[8] and polarography.[9] We wish to present an approximate treatment of the ECE mechanism for the RDE which appears applicable to first-order rate constants

(1) T. Mizoguchi and R. N. Adams, *J. Am. Chem. Soc.*, **84**, 2058 (1962).

(2) D. Hawley and R. N. Adams, *J. Electroanal. Chem.*, **8**, 163 (1964).

(3) Z. Galus and R. N. Adams, *J. Am. Chem. Soc.*, **84**, 2061 (1962).

(4) V. G. Levich, "Physicochemical Hydrodynamics," Prentice-Hall, Inc., Englewood Cliffs, N. J., 1962.

(5) A. C. Testa and W. H. Reinmuth, *J. Am. Chem. Soc.*, **83**, 784 (1961).

(6) G. S. Alberts and I. Shain, *Anal. Chem.*, **35**, 1859 (1963).

(7) R. S. Nicholson and I. Shain, *ibid.*, **37**, 178 (1965).

(8) H. B. Herman and A. J. Bard, *J. Phys. Chem.*, **70**, 396 (1966).

(9) R. S. Nicholson, J. M. Wilson, and M. L. Olmstead, *Anal. Chem.*, **38**, 542 (1966).

not easily measured by the previous techniques. Preliminary experimental results are also reported.

$$A \xrightarrow{\pm n_1 e} B \xrightarrow{k} C \xrightarrow{\pm n_2 e} D \qquad (1)$$

We will assume the following: laminar flow; equality of diffusion coefficients; $n_1 = n_2 = n$; and that C is reduced (oxidized) more easily than A. Under steady-state conditions, the total limiting current i_T, may be expressed as

$$i_T = nFAD[(\partial C_A/\partial x)_{x=0} + (\partial C_C/\partial x)_{x=0}] \qquad (2)$$

At the limiting current, $(\partial C_A/\partial x)_{x=0}$ can be written according to Levich as[4]

$$(\partial C_A/\partial x)_{x=0} = C_A^b/\delta \qquad (3)$$

where C_A^b is the bulk concentration of A and δ is the thickness of the diffusion layer given by

$$\delta = 1.62D^{1/3}\gamma^{1/6}\omega^{-1/2} \qquad (4)$$

γ is the kinematic viscosity and ω is the angular velocity which is equal to $2\pi N$ (N is the number of rotations per second). However, $(\partial C_C/\partial x)_{x=0}$ is not easily arrived at since the mass-transfer rate and the chemical reaction rate must be treated simultaneously. $(\partial C_C/\partial x)_{x=0}$ can be obtained in the following fashion.

In the chronoamperometric treatment, the flux of C is given by[6]

$$D(\partial C_C/\partial x)_{x=0} = \sqrt{D}C_A^b\left[\frac{1}{\sqrt{\pi t}} - \frac{1}{\sqrt{\pi t}}\exp(-kt)\right] \qquad (5)$$

However, in RDE studies, steady-state conditions prevail and no time dependence of the flux is normally observed. We can relate t and ω, the independent variable in RDE methodology, by means of the diffusion layer thickness.

If we assume that, on the average, a molecule diffuses $\sqrt{\pi Dt}$ centimeters, the time necessary for it to diffuse from the electrode surface, $x = 0$, to $x = \delta$ is $\delta^2/\pi D$ seconds. Substitution of $t = \delta^2/\pi D$ in (5) and the use of (3), (4), and (5) in (2) gives the total limiting current for an ECE process

$$i_T = 0.62nFAC_A^b D^{2/3}\gamma^{-1/6}\omega^{1/2}[2 - \exp(-0.834\gamma^{1/3}k/D^{1/3}\omega)] \qquad (6)$$

For a fast chemical reaction, $k >> \omega$, the exponential term in (6) becomes zero and therefore the observed limiting current is that corresponding to $2n$ electrons. If $k << \omega$ (slow chemical reaction), a limiting current due to a process involving n electrons is obtained.

In practice, (6) can be applied by measuring $(i_{LIM}/\omega^{1/2}C_A^b)_{k=0}$ for solution conditions under which no control by the chemical reaction is evident or at an ω value corresponding to a n value of n or $2n$. A ratio of $(i_{LIM}/\omega^{1/2}C_A^b)$ for a limiting current controlled by the rate of the chemical reaction to $(i_{LIM}/\omega^{1/2}C_A^b)_{k=0}$ gives an apparent n value, n_{app}. In terms of n_{app}/n, (6) becomes

$$\frac{n_{app}}{n} = \frac{(i_{LIM}/\omega^{1/2}C_A^b)}{(i_{LIM}/\omega^{1/2}C_A^b)_{k=0}} = 2 - \exp(-0.834\gamma^{1/3}k/D^{1/3}\omega) \qquad (7)$$

From (7), knowing D and γ, a plot of k/ω *vs.* $1/\omega$ can be constructed and the resulting straight line has a slope equal to k. This is analogous to a plot of kt *vs.* t for other electrochemical techniques.[10]

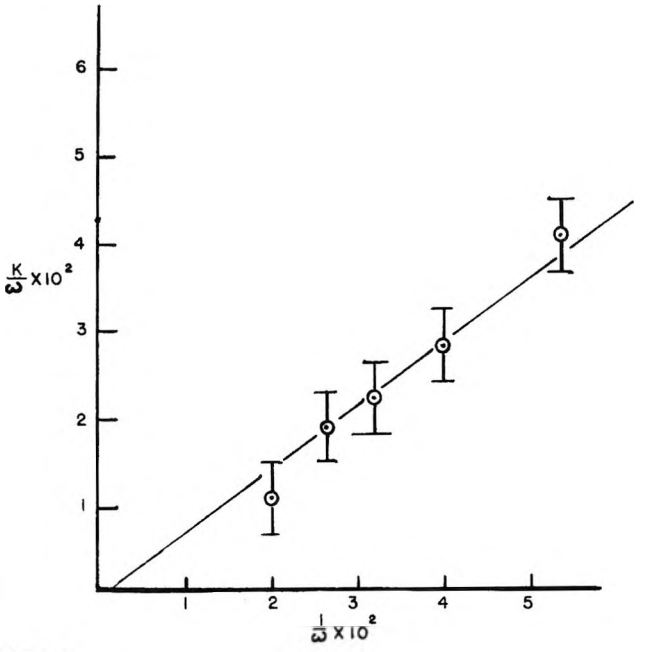

Figure 1.

The reduction of *p*-nitrosophenol was chosen for the verification of (7) since this oxidation–reduction system had been evaluated previously by a variety of techniques.[6-9] Figure 1 shows a plot of k/ω *vs.* $1/\omega$ for the dehydration of the *p*-hydroxylaminophenol formed by the two-electron reduction of *p*-nitrosophenol at pH 2.3 (Britton and Robinson buffer, 20% v/v ethanol and 0.2 *M* Na_2SO_4). $(i_{LIM}/\omega^{1/2}C_A^b)_{k=0}$ was determined by variation of ω. Least-squares analysis of the slope yields $k = 0.7 \pm 0.1$ sec^{-1} compared to the average value of $k = 0.5 \pm 0.1$ sec^{-1} at comparable solvent compositions reported in the literature.

(10) Professor S. Bruckenstein has suggested that (6) could be rearranged and a plot made of ln $[2 - (i_T/0.62nFAC_A^b D^{2/3}\gamma^{-1/6}\omega^{1/2})]$ *vs.* $1/\omega$, which has a slope equal to $-0.834\omega^{1/3}D^{-1/3}k$. This would eliminate the need to know $(i_{LIM}/\omega^{1/2}C_A^b)_{k=0}$, although n values would have to be assumed if they were not known.

Further studies, on the cyclization of the open-chain quinone of adrenalin, have also yielded encouraging results. Ball and Chen have measured, by means of a flow technique and chemical oxidation, the cyclization rate constant of the adrenalin quinone as being independent of pH at pH >6 and equal to *approximately* 10 sec^{-1}.[11] The values of k measured by the RDE at pH 6.3 and 7.15 are 19 ± 6 sec^{-1} and 20 ± 4 sec^{-1}, respectively. $(i_{LIM}/\omega^{1/2}C_A{}^b)_{k=0}$ was obtained from runs at pH 2.75, where k is effectively zero. In the electrochemical study of Hawley, *et al.*,[12] k's at pH >5 were too fast to be measured by the chronoamperometric technique since this technique and the others mentioned previously are not easily applied for $k > 1.0$ sec^{-1}.

The rotating disk electrode appears to be a very valuable tool in studying the kinetics of homogeneous chemical reactions of electrochemically generated intermediates. Using the limits of ω as 5 and 300 radians/sec, first-order rate constants in the range of 0.3–100 sec^{-1} may easily be measured. Studies are now in progress with the RDE on the kinetics of other homogeneous chemical reactions coupled to electrochemical charge transfer. The effects of such chemical reactions on diffusion coefficient measurements and on correlations of electrochemical parameters with molecular orbital theory are also under investigation using the RDE.

Acknowledgments. This work was supported by the National Science Foundation through Grant GP-5079 and this support is gratefully acknowledged. The authors wish to express their appreciation to the University of Kansas Computation Center and to Donald W. Leedy for technical assistance.

(11) E. G. Ball and T. Chen, *J. Biol. Chem.*, **102**, 691 (1933).
(12) M. D. Hawley, S. Tatwawadi, S. Piekarski, and R. N. Adams, submitted for publication.

Studies on Solutions of High Dielectric Constant. IX. Cationic Transport Numbers of KBr in N-Methylpropionamide at Different Temperatures and Concentrations[1]

by Ram Gopal and O. N. Bhatnagar[2]

Chemistry Department, Lucknow University, Lucknow, India
(Received June 24, 1966)

In continuation with our previous work on the cationic transport numbers in solvents of high dielectric constant like formamide,[3] N-methylacetamide[4] (NMA), and N-methylformamide[5] (NMF), studies have now been extended to N-methylpropionamide (NMP), which has a dielectric constant of 164.3[6] at 30°. Despite its stability, it does not appear to have received adequate attention from the workers in this field. Dawson and co-workers[7] have reported the limiting equivalent conductivities of the halides of sodium and potassium from 30 to 60°, at 10° intervals. Hoover[8] reported the limiting equivalent conductance of KCl in this solvent from 20 to 40°. However, in the absence of limiting ionic conductance data, our understanding of the ion–solvent interaction in this solvent would be more limited. It is, therefore, desirable to have accurate ionic transport number data in order to evaluate the ionic mobilities. Strangely enough, no one appears to have attempted even the usual indirect method, used by Dawson and co-workers[9] for evaluating the ionic conductances in some solvents in which the transport number data have not been available.

The present note reports the measurements of the cationic transport numbers of potassium bromide in NMP at 30, 40, and 50°, at different concentrations by the Hittorf method. From the data obtained, the limiting ionic conductivities have been evaluated from the available electrolytic conductance data at infinite dilution.

Experimental Section

Eastman Kodak N-methylpropionamide (specific conductivity ≈ 10^{-5} mho) was first dried over freshly ignited quicklime and the supernatant liquid was distilled under reduced pressure. The process was repeated until the distillate was found to have a specific conductivity of (6–8) × 10^{-7} mho. It was stored in dark amber bottles in the drybox. The conductivity of the purified samples was checked from time to time. Changes in conductivity were found to

(1) Work supported by the Council of Scientific and Industrial Research (CSIR), India.
(2) Junior Research Fellow, CSIR, India.
(3) R. Gopal and O. N. Bhatnagar, *J. Phys. Chem.*, **68**, 3892 (1964).
(4) (a) R. Gopal and O. N. Bhatnagar, *ibid.*, **69**, 2382 (1965); (b) Tewari and Jauhari (*J. Phys. Chem.*, **70**, 197 (1966)) have recently reported transport numbers of KCl in formamide (25°) and in N-methylacetamide at 40° without referring to our work already published in this journal. There appears to be a deliberate attempt to suppress information already available in the literature.
(5) R. Gopal and O. N. Bhatnagar, *ibid.*, **70**, 3007 (1966).
(6) G. R. Leader and J. I. Gormley, *J. Am. Chem. Soc.*, **73**, 5731 (1951).
(7) L. R. Dawson, *et al.*, *ibid.*, **79**, 298 (1957).
(8) T. B. Hoover, *J. Phys. Chem.*, **68**, 876 (1964).
(9) L. R. Dawson, *et al.*, *J. Am. Chem. Soc.*, **79**, 3004, 5906 (1957).

be negligible and the solvent appeared to be quite stable. AR grade potassium bromide was recrystallized from conductivity water, thoroughly dried, and stored in a vacuum desiccator. It was subsequently used for preparing solutions. The transport number cell and the electrodes, used in the experiments, were similar to those used for solutions in NMA.[4a] Solutions of KBr were prepared in freshly distilled samples of NMP. The experimental procedure, including the precautions to avoid atmospheric moisture while preparing solutions and during the course of experiments, were the same as described previously.[3,4] The transport numbers, thus obtained at different temperatures and concentrations, are summarized in Table I.

Table I: Transport Numbers of K^+ in KBr, Dissolved in NMP, at Different Temperatures and Concentrations

Concn. M	Transport number at 30°	40°	50°
0.000	0.4320	0.4370	0.4425[a]
0.075	0.4200	0.4249	0.4313
0.100	0.4182	0.4221	0.4286
0.150	0.4132	0.4195	0.4236
0.200	0.4104	0.4143	0.4202
0.250	0.4076	0.4113	0.4179

[a] From the graph.

From the values of transport numbers, given in Table I, the limiting transport numbers, t_+^0, of K^+, at different temperatures, have been obtained by the Longsworth procedure,[10] as followed in the cases of the solutions in formamide,[3] NMF,[5] and NMA,[4a] reported earlier. The values of viscosity, dielectric constant, and the limiting equivalent conductance at different temperatures needed to calculate the Longsworth function were as follows: viscosity (in poise): $\eta_{30°} = 0.04568$, $\eta_{40°} = 0.03451$, $\eta_{50°} = 0.02825$; dielectric constant: $\epsilon_{30°} = 164.3$, $\epsilon_{40°} = 148.9$, $\epsilon_{50°} = 133.4$; limiting conductance: $\lambda°_{30°} = 12.40$, $\lambda°_{40°} = 15.90$, $\lambda°_{50°} = 19.80$ (as given by Dawson and coworkers[11]). The values of the limiting transport numbers of K^+, thus obtained, are also given in Table I.

Results and Discussion

It is evident from Table I that the cationic transport number, t_+, at any temperature, decreases with increase in concentration, C, and increases with increase in temperature, a behavior similar to that found in formamide,[3] N-methylformamide,[5] and in N-methylacetamide.[4a] Potassium ion, K^+, with a transport number less than 0.5, has a positive temperature coefficient for t_+. The ion–solvent interaction in NMP should, therefore, be similar to that in formamide, NMF, and NMA. It is not possible to calculate the solvation of ions in NMP since the conductance of tetraalkylammonium ions, needed for this purpose,[4a] are not available in this solvent.

Ionic Mobilities. The values of the limiting transport numbers, $t_+°$, at 30, 40, and 50°, have been used to calculate the ionic conductivities from the appropriate available electrolytic conductance data at infinite dilution.[7] In order to evaluate the ionic conductance at 60°, at which some electrolytic conductance data are available in the literature, the required limiting transport number, $t_+°$, was obtained from the extrapolation of the $t_+°$ *vs.* t (temperature) curve to 60°. The curve was found to be almost a straight line. The value of $t_+°$, corresponding to 60°, was found to be 0.4475. The ionic mobilities of some ions, thus obtained, are given in Table II.

Table II: Mobilities of Some Ions at Different Temperatures

Ion	Ionic mobility at 30°	40°	50°	60°
Na^+	5.06	6.45	8.06	10.01
K^+	5.36	6.95	8.76	10.91
Cl^-	6.24	7.95	9.94	11.99
Br^-	7.06	8.95	11.04	13.49
I^-	8.34	10.45	12.94	15.69

It may be noticed from Table II that the ionic mobilities are very low indeed and are similar to those in formamide, NMF, and NMA. The temperature coefficient of conductance is about 2.7%/deg which appears to be slightly higher than those in formamide, NMF, and NMA. The conductivities of Na^+ and K^+ are almost the same, as in the other solvents of this family, indicating no abnormal ion–solvent interaction which occurs in water in which the structure-breaking effect of K^+ enhances its mobility abnormally.

Acknowledgment. The authors' thanks are due to the Council of Scientific and Industrial Research, India, and to the American Society of Sigma Xi, for financial assistance.

(10) L. G. Longsworth, *J. Am. Chem. Soc.*, **57**, 1185 (1935).
(11) L. R. Dawson, *et al.*, *ibid.*, **79**, 298 (1957).

Reaction of the Hydrated Electron with Carbon Monoxide as Studied by Pulse Radiolysis

by Y. Raef and A. J. Swallow

Paterson Laboratories, Christie Hospital, and Holt Radium Institute, Withington, Manchester 20, England *(Received August 17, 1966)*

Studies with γ radiation have shown that hydrated electrons react readily with carbon monoxide.[1,2] An absorption attributed to the hydrated electron has been seen in the pulse radiolysis of aqueous solutions of carbon monoxide, and from its rate of disappearance under appropriate conditions, presumed to be by reaction with CO, the rate constant for the reaction of hydrated electrons with carbon monoxide has been calculated to be 10^9 M^{-1} sec^{-1} at pH 7 or 13.[3-5] It had been suggested that the reaction might produce a hydrated formyl radical in an ionized or neutral form[6]

$$(H_2O)^- + CO \longrightarrow H\dot{C}(OH)O^- \quad (1a)$$

$$\xrightarrow{+H^+} \dot{C}H(OH)_2 \quad (1b)$$

or the formyl radical itself in an ionized or neutral form.[1]

$$(H_2O)^- + CO \longrightarrow \dot{C}O^- + H_2O \quad (2a)$$

$$\longrightarrow H\dot{C}O + OH^- \quad (2b)$$

Another suggestion is that the reaction might lead to the formation of the formate ion and the hydrogen atom.[7]

$$(H_2O)^- + CO \longrightarrow HCOO^- + H \quad (3)$$

We now present evidence from pulse radiolysis which indicates that the reaction should be represented as eq 1a or 1b.

Experimental Section

Pulse radiolysis experiments were conducted using the 4-Mev electron linear accelerator at AEI, using the equipment described by Keene.[8] Carbon monoxide, stated to be 99.5% pure, was obtained from Matheson. Water was distilled from alkaline permanganate. Other chemicals were of Analar grade or the best available laboratory grade.

Results and Discussion

If reaction 3 were occurring, then in alkaline solutions of carbon monoxide (pH 13) electrons would be regenerated according to

$$H + OH^- \xrightarrow{k = 2 \times 10^7} (H_2O)^- \quad (4)$$

and would therefore decay at a different rate from in neutral solutions. By irradiating carbon monoxide at two different concentrations (10^{-4} and 10^{-3} M) and two pH values (pH 7 and 13), we have confirmed the earlier result,[3-5] that the rate of decay of the transient absorbing at ~7000 A is in fact independent of pH. At low doses, the decay follows first-order kinetics under all conditions studied, and leads to the same rate constant as previously observed. Further evidence relating to reaction 3 was obtained by comparing the pulse radiolysis of formate (10^{-1} M) saturated with CO_2 on the one hand and with CO on the other. In the solutions containing formate and CO_2, OH radicals, H atoms, and hydrated electrons all give rise to CO_2^-.[9] In solutions containing formate and CO, if reaction 3 took place, the solvated electrons should produce H atoms which together with OH radicals should give rise to the same yield of CO_2^- as in the system containing formate and CO_2. In fact, we find that the optical density at 2500 A, attributed to CO_2^- (ϵ 2250 M^{-1} cm^{-1})[9] is twice as great in the system containing CO_2 as in the system with CO, confirming that reaction 3 does not occur.

In an attempt to obtain the absorption spectrum of the hydrated formyl radical, we have irradiated solutions containing sulfuric acid (10^{-1} N) and formaldehyde (10^{-1} M). Formaldehyde exists predominantly as the hydrate in dilute aqueous solution,[10] so that it might be expected that the following reactions would occur.

$$OH + H_2C(OH)_2 \longrightarrow \dot{C}H(OH)_2 + H_2O \quad (5)$$

$$(H_2O)^- + H^+ \longrightarrow H + H_2O \quad (6)$$

$$H + H_2C(OH)_2 \longrightarrow \dot{C}H(OH)_2 + H_2 \quad (7)$$

(1) J. Holian, G. Scholes, and J. J. Weiss, *Nature*, **191**, 1386 (1961).

(2) Y. Raef and A. J. Swallow in "Radiation Effects in Physics, Chemistry and Biology," M. Ebert and A. Howard, Ed., North-Holland Publishing Co., Amsterdam, 1963, p 47.

(3) D. Bradley in British Empire Cancer Campaign Report 41, Part II, 1963, p 491.

(4) E. J. Hart, J. K. Thomas, and S. Gordon, *Radiation Res. Suppl.*, **4**, 74 (1964).

(5) J. H. Baxendale, E. M. Fielden, C. Capellos, J. M. Francis, J. V. Davies, M. Ebert, C. W. Gilbert, J. P. Keene, E. J. Land, A. J. Swallow, and J. M. Nosworthy, *Nature*, **201**, 468 (1964).

(6) Y. Raef and A. J. Swallow, *Trans. Faraday Soc.*, **59**, 1631 (1963).

(7) J. J. Weiss, *Radiation Res. Suppl.*, **4**, 141 (1964).

(8) J. P. Keene, *J. Sci. Instr.*, **41**, 493 (1964).

(9) J. P. Keene, Y. Raef, and A. J. Swallow in "Pulse Radiolysis," M. Ebert, J. P. Keene, A. J. Swallow, and J. H. Baxendale, Ed., Academic Press Inc., New York, N. Y., 1965, p 99.

(10) R. Bieber and G. Trümpler, *Helv. Chim. Acta*, **30**, 1860 (1947).

A species was seen in this system which absorbed weakly in the ultraviolet ($\epsilon \sim 2 \times 10^2\ M^{-1}\ cm^{-1}$ at 2400 A). There was no absorption in the visible region of the spectrum. We have also irradiated a solution of formaldehyde ($10^{-1}\ M$) saturated with CO at atmospheric pressure (pH 5). A similar low absorption was seen with almost the same optical density for a given dose as in the acid formaldehyde system. Again no absorption was seen in the visible. In order to establish the charge of the species absorbing in this system, we have measured the rate of decay at three different concentrations of added salt. The salt used was sodium formate. It should be noted that at the relative concentrations of formaldehyde and formate used it would not be expected that there would be any significant attack of OH radicals on the formate, and indeed the initial optical density was the same in the presence of formate as in its absence, confirming that CO_2^-, which has a relatively high extinction at 2400 A, was playing no part in this system. The experimental points which are accurate to within 10% are shown in Figure 1 and show that the rate of decay of the species is independent of the presence of salt.

To account for the fact that the absorption produced after reaction of the electrons with CO and the OH radicals with formaldehyde is the same as the absorption in the acid formaldehyde system, we conclude that reaction 1 is taking place. To account for the lack of an effect of added salt, the species must be neutral, so that at pH 5 the reaction would be (1b). The rate constant for disappearance of the species attributed to $\dot{C}H(OH)_2$ is calculated from Figure 1 to be $2k = 5 \times 10^8\ M^{-1}\ sec^{-1}$.

The formulation of the reaction of the electron with CO as (1) implies the hydration of CO^- or $H\dot{C}O$ in aqueous solution, either because CO^- or $H\dot{C}O$ are intermediates which are hydrated very rapidly, or because the reaction of the electron with CO proceeds directly to the hydrate. Infrared analysis has shown that the force constants and structural parameters of the formyl radical are close to those of formaldehyde,[11] so it seems quite likely that $H\dot{C}O$ will behave similarly to HCHO with respect to hydration. The $H\dot{C}O$ radical is known to absorb in the visible,[12] probably to a greater extent than in the ultraviolet,[13] and CO^- might be expected to absorb in the same region. However, we have seen no trace of any absorption which could be attributed to $H\dot{C}O$ or CO^-. If these species are formed at all, then from the rapid rate at which the absorption at 2400 A is formed in our experiments, the pseudo-unimolecular rate constant for the hydration would appear to be greater than $k \sim 10^4\ sec^{-1}$.

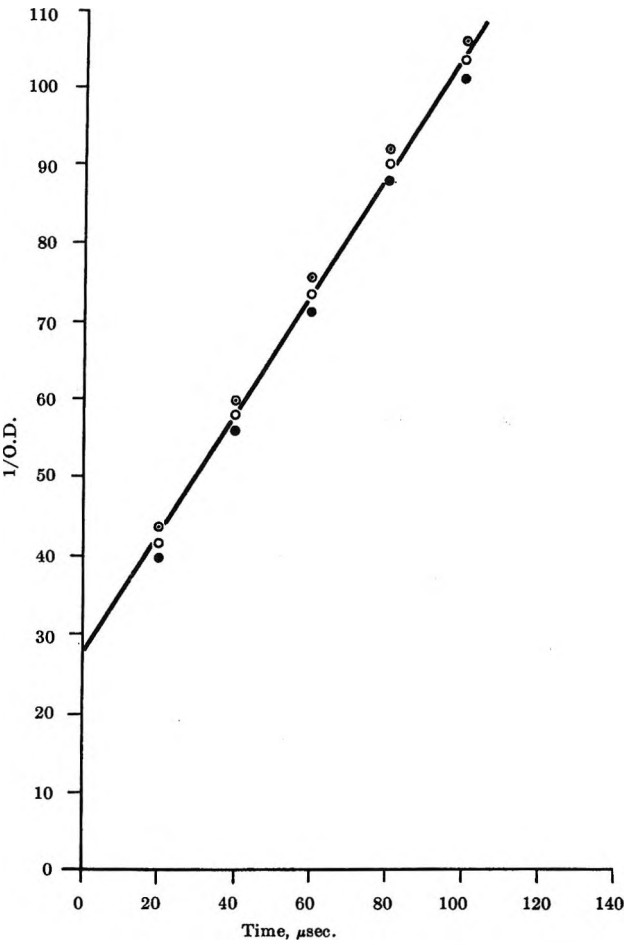

Figure 1. Second-order rate of decay of transient at 2400 A in solutions of $5 \times 10^{-1} M$ HCHO saturated with CO, pH 5, at different sodium formate concentrations: ⊙, $2 \times 10^{-3}\ M$; ○, $10^{-2}\ M$; ●, $2 \times 10^{-2}\ M$; dose 6700 rads/2-μsec pulse.

The chain-propagating steps in the production of formate in the γ radiolysis of alkaline carbon monoxide[6] can now be formulated as reaction 1 followed by reaction of the hydrated formyl radical with OH^- to give the hydrated electron. Since electrons are not regenerated in the pulse radiolysis of alkaline carbon monoxide, this latter reaction must be slow and cannot have a rate constant greater than about $10^5\ M^{-1}\ sec^{-1}$. The slow occurrence of this reaction is consistent with the low yield ($G = 44$ under the conditions employed by us[6]) for the chain hydration of CO.

(11) G. E. Ewing, W. E. Thompson, and G. C. Pimental, *J. Chem. Phys.*, **32**, 927 (1960).

(12) G. Herzberg and D. A. Ramsay, *Proc. Roy. Soc.* (London), **A233**, 34 (1955).

(13) A. Thomas, *Trans. Faraday Soc.*, **57**, 1679 (1961).

Shock Waves in Chemical Kinetics. Further Studies in the Dissociation of Fluorine[1]

by Daniel J. Seery and Doyle Britton

Department of Chemistry University of Minnesota, Minneapolis, Minnesota 55455 *(Received November 16, 1965)*

The dissociation of F_2 in the presence of argon has been reported previously.[2,3] We report here the results of some exploratory experiments on the effect of added krypton and xenon on the dissociation of F_2. This work was prompted, of course, by the recent discovery of xenon and krypton fluorides.[4] We did not expect that stable inert gas fluorides would be formed at the high temperatures which occur in the shock-wave experiments, but we did expect that the stability of the intermediate XeF (or KrF) would be relatively large, which would lead to the path

$$Xe + F_2 \longrightarrow XeF + F$$

$$XeF + M \longrightarrow Xe + F + M$$

being considerably more rapid than the usual reaction with Ar as third body for dissociation of F_2. At the time the work was done there were no data available for making estimates of the stability of the various Xe–F species at the temperatures of these experiments. Although, as will be described, we found anomalous results with xenon present, we plan no further work on this problem and therefore report these somewhat inconclusive results.[5]

The rate constants for the simple dissociation processes are defined by

$$F_2 + M \underset{k_R}{\overset{k_D}{\rightleftharpoons}} F + F + M$$

$$\frac{d(F_2)}{dt} = -k_D(M)(F_2) + k_R(M)(F)^2$$

All concentrations will be in moles per liter. All times in the rate expressions will be in seconds.

Experimental Section

[illegible] have been described previously. The xenon and krypton were research grade (stated to be 99.99% pure) supplied by the Matheson Co. and were used without purification or analysis.

The data consist of a set of oscilloscope traces representing transmitted light as a function of time. The shape of these oscillograms for the dissociation of a colored species is well known: a level trace during the period before the shock wave reaches the observation station; a fast decrease in the transmitted light intensity corresponding to the increase in concentration as the shock front passes the observation station; a slow increase in transmitted light intensity as the dissociation proceeds; a level trace again corresponding to the amount of light transmitted by the equilibrium mixture (the oscillogram may not be continued long enough for the equilibrium position to be recorded, however). In principle then, three measurements are possible: first, the abrupt change at the shock front may be used to measure the concentration or the extinction coefficient of the colored species, provided one or the other is known; second, the shape of the curve after the shock front may be used to determine the rate of the reaction provided that the transmitted light is due to only one species and there is no emission; third, the equilibrium light intensity may be used to measure the equilibrium constant for the reaction, provided equilibrium is attained in a reasonable time. We shall discuss the experiments below in terms of these three possible measurements.

Results

F_2–Ar Mixtures. Four shock waves were run in 5% F_2–95% Ar mixtures. The results appeared normal in all respects. The extinction coefficients and the rate constants for the dissociation of F_2 agreed with those from previous work.[2] The equilibrium constants for the dissociation of F_2 estimated from the equilibrium positions of the curves showed considerable scatter but agreed within the scatter with those given in the "JANAF Tables."[6]

A least-squares straight line through all of the data for 5% F_2–95% Ar results, including those of ref 2, gives the following equation.

(1) Presented in part at the U. S. Army Research Office, Durham, Symposium on Chemical Reactions in Shock Tubes, Durham, N. C., April 1964.

(2) C. D. Johnson and D. Britton, *J. Phys. Chem.*, **68**, 3032 (1964).

(3) R. W. Diesen, *J. Chem. Phys.*, **44**, 3662 (1966), has studied the dissociation of F_2 in the presence of neon, argon, and krypton, but was preparing to leave. There was not time to interpret the results as the data were collected; therefore, a number of obvious further experiments were not made. At the conclusion of the experimental work the apparatus was dismantled, and for safety's sake the components for handling fluorine were discarded. We do not plan to resume working with fluorine in shock waves.

(6) "JANAF Thermochemical Tables," The Dow Chemical Co., Midland, Mich., Sept 1964.

$$\log k_D = 9.49 - 5970/T$$

(mole^{-1} l. sec^{-1}) for the temperature dependence of the rate constants. This corresponds to an apparent activation energy of 27.3 ± 2.5 kcal/mole. We regard this number as the best estimate for the rate constant for F_2 in the presence of argon that can be made from the available data.

F_2–Kr–Ar Mixtures. Six shock waves were run in 5% F_2–20% Kr–75% Ar mixtures and ten in 10% F_2–20% Kr–70% Ar mixtures. Pure Kr (and later Xe) was not used for the inert gas because of the high cost and the large amounts required. It was felt that if any unusual behavior were to occur it would probably be detectable with the proportions used. The extinction coefficients, the dissociation rate constants, and the final equilibrium positions appear more or less normal. The extinction coefficients in the 10% F_2 mixtures perhaps appear somewhat low, but those in the 5% mixtures do not, and we would expect a greater effect when the Kr/F_2 ratio is 4:1, as in the 5% mixtures, than when this ratio is 2:1 as in the 10% F_2 mixtures. The rate constants (mole^{-1} l sec^{-1}) appear normal and can be summarized by

$$5\% \text{ mixtures: } \log k_D = 10.15 - 6800/T$$

$$10\% \text{ mixtures: } \log k_D = 8.57 - 4280/T$$

The rate constants for both the 5% and 10% F_2–20% Kr mixtures are a trifle higher than in the mixtures with only Ar, which suggests that the Kr is slightly more efficient than Ar in the dissociation reaction, but the spread in the data is so great that no quantitative conclusion can be drawn. The equilibrium positions in the oscillograms correspond to those expected for F_2 in equilibrium with F atoms. The scatter is large and two points are quite far off, but in general the results appear normal. In some of the oscillograms there is a slow rise in the apparent F_2 concentration after 200–300 μsec of observational time. However, this slow rise is neither systematically nor reproducibly present, and it also occurs occasionally in F_2–Ar shocks. Generally, we are inclined to ignore anything after the first 200 μsec, so our conclusion would be that nothing unusual is occurring in the shocks with Kr present.

F_2–Xe–Ar Mixtures. A series of six shocks was run in 5% Fe_2–20% Xe–75% Ar mixtures and a series of seven in 10% F_2–20% Xe–70% Ar. Qualitatively, the 5% F_2 series appeared to be normal, but closer inspection showed the apparent extinction coefficients to be low, the rate constants to be apparently normal, and the apparent equilibrium constants to be low. The 10% F_2 series was abnormal even to a qualitative inspection; the traces were nearly flat with apparently little or no dissociation. In a few cases the transmitted light decreased slightly after the shock front. The only measurements that were possible were the apparent extinction coefficients, which again appeared consistently low. The apparent rate constants and equilibrium constants would have been near zero in most cases.

There was no evidence that Xe and F_2 had reacted in the mixing bulbs at room temperature, nor has there been any report of reaction at room temperature,[4] so the apparently low values of the extinction coefficient estimated from the change in transmitted light at the shock front are most likely due to the occurrence of a reaction in the shock front. Any reaction with a mean life of less than about 20 μsec would behave this way. It should be noted that the amount of F_2 that seems to be used up does not correspond to the establishment of dissociative equilibrium but is considerably less. If some colored species (at 313 mμ) were formed, then it is conceivable that F_2 does reach equilibrium with respect to F atoms in the shock front, but the existence of a reasonable amount of this other absorbing species obscures the true F_2 concentration.

The apparent equilibrium with too little dissociation makes it clear that some other stable absorbing species is formed. The formation of any Xe–F species could only lower the final equilibrium F_2 concentration, since they would remove F_2 from the system and also raise the final equilibrium temperature. Since the bulk of the mixture is Ar, the reaction Ar + F_2 = Ar + 2F must go on at its normal rate and could not be inhibited in any way, so that the F_2 must be gone in 50–200 μsec of observational time, as it was in the F_2–Ar mixtures, or sooner if some other reaction takes place. Since F_2 must be used up, but the transmitted light intensity does not increase, some other colored species must be formed at about the same rate F_2 is actually disappearing.

The process taking place in the 5% F_2 mixture at about the rate of the usual dissociation reaction must be more complex than would appear at first glance since there must be other species present from the fast reaction in the shock front; if only dissociation occurred, there is no reason why it should stop short of equilibrium.

The above arguments show why we are sure something unusual is taking place in the F_2–Xe–Ar mixtures. However, when we try to be explicit about what is going on, we find we cannot fit our observations to the previously reported data. The stable species formed seems most likely to be XeF_2, and the transient species inferred from the behavior of the absorption at

the shock front is probably XeF, but no detailed kinetic system that we could find is consistent with all of the observations.[7]

Conclusions

The dissociation of F_2 molecules proceeds more slowly in the presence of Ar as a third body than would be expected by comparison with other halogens.[2,8] The addition of Kr does not appear to greatly affect the rate in Ar, so we conclude the bond energy in KrF is not especially large (certainly less than 10 kcal/mole). The addition of Xe affects not only the rate but the course of the reaction. At least one stable, colored Xe–F species is formed between 1100 and 1600°K; probably this is XeF_2. This one species, however, is not sufficient to account for the initial differences in the apparent rate of change of the F_2 concentration, and it would appear that XeF is an important intermediate.

Acknowledgment. We thank the U. S. Army Research Office (Durham) for support of this work.

(7) Since no detailed conclusions are given, we will omit the detailed discussion of the possibilities. This is available from the authors if desired.

(8) D. J. Seery, *J. Phys. Chem.*, **70**, 1684 (1966).

Hydrogen Atom Yield from Benzene Photolyzed at 1849 A[1]

by Frank Mellows and Sanford Lipsky

Department of Chemistry, University of Minnesota, Minneapolis, Minnesota *(Received May 26, 1966)*

The quantum yield for the disappearance of benzene vapor at 1849 A has been recently determined to be 0.25 ± 0.02 at 1 torr and to extrapolate to 1.0 at zero pressure.[2] The present study was undertaken to determine the contribution to the disappearance yield from process 1.

$$C_6H_6 \xrightarrow{h\nu} C_6H_5 + H \qquad (1)$$

Previous studies by Wilson and Noyes[3] using a group of Al lines between 1855 and 2000 A have indicated that process 1 is not an important primary process in view of a low H_2 quantum yield and no evidence for production of deuterated benzenes in the presence of D_2. Our results confirm this conclusion.

The technique employed involved the measurement of H_2 yields in the presence and absence of saturated hydrocarbons (RH). The H atom quantum yield, $\phi(H)$, from (1) is related to the measured H_2 quantum yield, $\phi(H_2)$, as

$$\phi(H) = [\phi(H_2) - \phi_0(H_2)]\left(1 + \frac{k_3[C_6H_6]}{k_4[RH]}\right) \qquad (2)$$

where $\phi_0(H_2)$ is the H_2 yield from pure benzene and k_3 and k_4 are rate constants for reactions 3 and 4.

$$H + C_6H_6 \longrightarrow C_6H_7 \qquad (3)$$

$$H + RH \longrightarrow R + H_2 \qquad (4)[4]$$

All photolyses were carried out in Pyrex cells to which were sealed 1-mm thick Suprasil quartz windows. Cell volumes for liquid and gas phase photolyses were 10 and 200 ml, respectively. An electrodeless lamp was employed containing Hg + 2 torr of Ar. Power was supplied from a Raytheon 2450-Mc microwave generator. For improved stability the lamp was air cooled during operation. The emission spectrum of the lamp, determined with a 0.5-m Seya-Namioka grating monochromator, was found to contain below 2600 A only two lines at 2537 and 1849 A. No attempt was made to remove the 2537-A line. A lamp output of 1.7×10^{16} quanta sec^{-1} was determined using NH_3 at 100 torr as actinometer.[5] This value compares well with a value of 2.0×10^{16} quanta sec^{-1} obtained with an ethanol–water actinometer.[6] To keep conversions low, irradiation times ranged from 10 to 100 sec. H_2 was determined by gas–solid chromatography using Ar as the carrier gas. Complete separation of H_2, O_2, and N_2 was achieved with a 1-m column of Molecular Sieve 5A. With a thermistor detecting unit, H_2 yields as low as 5×10^{-10} mole could be determined. Matheson Coleman and Bell Spectrograde benzene was purified by recrystallization from the melt three times. Spectrograde isooctane was purified by repeated passage through silica gel columns. Spectrograde cyclohexane was used without further purification. Optical densities of 1 cm of pure deoxygenated liquid cyclohexane and isooctane at 1850 A were 0.75 and 0.5, respectively.[7] Instrument grade propane and ammonia were further purified by bulb-to-bulb distillations. The propane had an extinction coefficient at 1850 and 1750 A of 0.015

(1) Research supported by U. S. Atomic Energy Commission COO-913-7.

(2) K. Shindo and S. Lipsky, *J. Chem. Phys.*, **45**, 2292 (1966).

(3) J. E. Wilson and W. A. Noyes, Jr., *J. Am. Chem. Soc.*, **63**, 3025 (1941).

(4) In the derivation of 2 it is assumed that the reaction of H with C_6H_6 to produce H_2 is of negligible importance compared to reaction 3.

(5) W. Groth and H. Rommel, *Z. Physik. Chem.* (Frankfurt), **45**, 96 (1965).

(6) J. Barrett, M. F. Fox, and A. L. Monsell, *J. Phys. Chem.*, **69**, 2996 (1965).

and 0.025 atm^{-1} cm^{-1}, respectively.[7] The extinction coefficient of benzene was determined to be 707 atm^{-1} cm^{-1} for the 1849-A line as emitted by our lamp. All substances were deoxygenated prior to photolysis. The temperature was 27 ± 2°.

Photolysis of both 1 and 2 torr of benzene gave an H_2 quantum yield of 2.5 ± 0.5 × 10^{-3}. This value is in good agreement with a value of 3 × 10^{-3} reported in the earlier work over the pressure range from 200 to 760 torr.[3] In Table I are presented the results of all experiments with added hydrocarbons.

Table I: Quantum Yields of H_2 and H from Benzene–Hydrocarbon Mixtures at 1849 A

Alkane	Partial vol. % C_6H_6	$\phi(H_2) - \phi_0(H_2)$	$\phi(H)$
550 torr of propane	0.027	0.010	0.010
500 torr of propane	0.25	0.015	0.020
10 torr of propane	2.0	0.005	0.015
4 torr of propane	5.0	0.002	0.010
40 torr of isooctane	2.5	0.003	0.006
100 torr of cyclohexane	1.0	0.007	0.009
Liquid cyclohexane	0.0025	0.006	0.006
Liquid cyclohexane	0.025	0.006	0.006

The H atom quantum yields presented in Table I for benzene–propane mixtures were calculated with the value of $k_3/k_4 = 100$ as determined by Yang.[8] For both cyclohexane and isooctane, a value of $k_3/k_4 = 33$ was used based on a ratio of collision yields for H atom abstraction from propane and cyclohexane of[9] $k_4(C_6H_{12})/k_4(C_3H_8) = 3$.

The low value of *ca.* 0.01–0.02 for $\phi(H)$ indicates clearly that processes other than C–H bond rupture are mainly responsible for benzene disappearance at 1849 A. This is further confirmed by the fact that no biphenyl has been detected in the vapor-phase photolysis,[2,3] whereas it has been demonstrated, at least in solution, that reaction of phenyl radicals with benzene produces biphenyl and dihydrobiphenyl as major products.[10]

Owing to some H_2 production from polymer buildup on the photolysis window (and this was kept minimal by virtue of the low conversions), we feel that little significance can be placed upon the variation between individual yields in Table I. Within our uncertainties, therefore, there does not appear to be evidence for any important effect of total gas pressure on $\phi(H)$. This contrasts markedly with a very high sensitivity to foreign gas pressure exhibited by $\phi(-C_6H_6)$[2] and tends to support an early suggestion of Nordheim, Sponer, and Teller[11] that H atoms may arise from benzene owing to absorption into a repulsive state underlying the $\pi-\pi^*$ $E_{1u} \leftarrow A_{1g}$ transition. However, the major benzene disappearance route appears to be predissociative.

(7) For an extremely wide range of olefins, Jones and Taylor (*Anal. Chem.*, **27**, 228 (1958)) report extinction coefficients at 1850 A of *ca.* 7500–10,000 l./mole cm. If we therefore assume that all of the alkane optical absorption is due to olefin, we obtain upper bounds to the olefin concentration of *ca.* 0.001% in cyclohexane and isooctane and of *ca.* 0.005% in propane. With the exception of one of our measurements at 0.0025% benzene, these olefin levels are considered sufficiently low to be neglected.

(8) K. Yang, *J. Am. Chem. Soc.*, **84**, 3795 (1962).

(9) H. Schiff and E. Steacie, *Can. J. Chem.*, **29**, 1 (1951).

(10) D. F. DeTar and R. A. J. Long, *J. Am. Chem. Soc.*, **80**, 4742 (1958).

(11) G. Nordheim, H. Sponer, and E. Teller, *J. Chem. Phys.*, **8**, 455 (1940).

An Interpretation of the Concentration Dependence of Mobilities in Fused Alkali Carbonate Mixtures

by R. Mills and P. L. Spedding

Diffusion Research Unit, Research School of Physical Sciences, Australian National University, Canberra, Australia
(Received May 31, 1966)

In a recently reported study from this laboratory[1] which was concerned primarily with the temperature dependence of tracer diffusion in alkali metal carbonates and their eutectic mixtures, we observed that diffusion coefficients at the eutectic compositions were considerably higher than in the component pure salts. With a view to exploring this behavior further, we have now made a more detailed study of the concentration and temperature dependence of the tracer-diffusion coefficients of Na^+ and CO_3^{2-} ions in Li_2CO_3–Na_2CO_3 mixtures.

The experimental techniques used in this study have been described fully elsewhere.[1,2] The data are tabulated in abbreviated form in Table I and for completeness we have included also the preliminary data obtained previously.[1,2]

With these data we have calculated sets of isothermal diffusion coefficients and graphed them against composition as shown in Figure 1. Two notable features of the graph which invite interpretation are the marked

(1) P. L. Spedding and R. Mills, *J. Electrochem. Soc.*, **113**, 599 (1966).

(2) P. L. Spedding and R. Mills, *ibid.*, **112**, 594 (1965).

Table I: Tracer Diffusion in Li_2CO_3–Na_2CO_3 Mixtures

Medium	Trace species	Temp range, °C	$D^* \times 10^2$, cm²/sec
Li_2CO_3	Na^+	809–905	$(1.32 \pm 0.44) \exp[-(9630 \pm 370)/RT]$
	CO_3^{2-}	849–991	$(1.35 \pm 0.06) \exp[-(9740 \pm 40)/RT]$
75:25 mole % Li_2CO_3–Na_2CO_3	Na^+	757–938	$(4.42 \pm 0.15) \exp[-(10,060 \pm 90)/RT]$
	CO_3^{2-}	757–938	$(3.57 \pm 0.33) \exp[-(10,920 \pm 100)/RT]$
53.3:46.7 mole % Li_2CO_3–Na_2CO_3	Na^+	580–863	$(9.81 \pm 0.14) \exp[-(10,990 \pm 140)/RT]$
	CO_3^{2-}	569–842	$(7.36 \pm 0.02) \exp[-(11,560 \pm 120)/RT]$
25:75 mole % Li_2CO_3–Na_2CO_3	Na^+	778–932	$(9.40 \pm 2.08) \exp[-(11,910 \pm 240)/RT]$
	CO_3^{2-}	778–932	$(4.26 \pm 0.33) \exp[-(11,130 \pm 90)/RT]$
Na_2CO_3	Na^+	910–1043	$(10.0 \pm 0.05) \exp[-(12,170 \pm 130)/RT]$
	CO_3^{2-}	901–1062	$(2.86 \pm 0.10) \exp[-(10,620 \pm 180)/RT]$

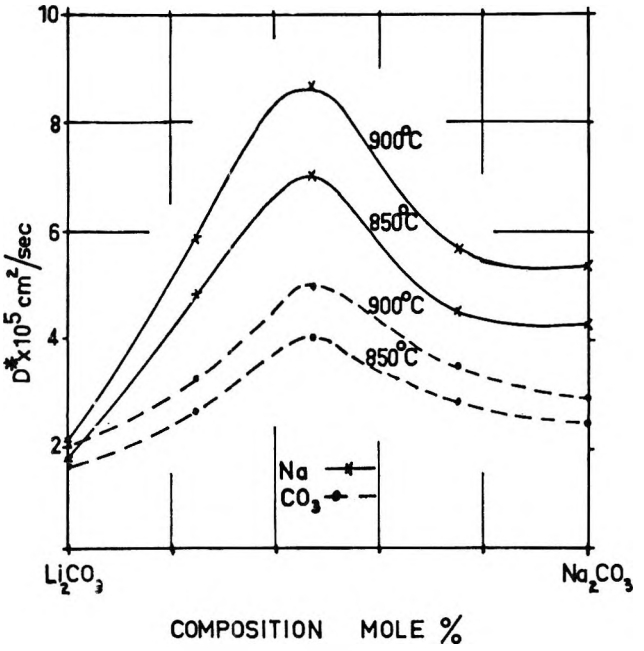

Figure 1. Tracer-diffusion coefficient *vs.* composition isotherms for labeled Na^+ and CO_3^{2-} in Li_2CO_3–Na_2CO_3 mixtures.

positive deviations from linearity for each set of coefficients and the apparent maxima at the eutectic composition.

It has been found that when the equivalent conductances of Li_2CO_3–Na_2CO_3 mixtures are graphed against composition, the curves show negative deviations from linearity.[3,4] Moynihan and Laity[5] have interpreted similar deviations for the LiCl–KCl system by invoking polarization effects. They implied also that in diffusion the presence of associated ions or groups of ions would tend to nullify the factors affecting the conductance and produce a more nearly linear dependence of the tracer-diffusion coefficients with composition. Instead, as Figure 1 shows, there is a large positive deviation for the two species investigated.

The Nernst–Einstein equation is often used in molten salts to compare conductance and diffusional mobilities. The substantial deviations from this equation which usually result can be interpreted in at least two ways. Thus, on the one hand, Angell[6] has presented evidence to support the contention that mutual ionic interference causes the breakdown of the equation in these systems. On the other hand, Bockris and Hooper[7] have interpreted these deviations as being due to a paired vacancy process which allows diffusion to proceed by two mechanisms. More recently, Lantelme and Chemla[8] in their extensive work on the alkali metal nitrates have used the latter general approach and attributed their deviations to the presence of free ions and polyionic groups[9] in the melts, so allowing differing conduction and diffusion modes. They were able to give quantitative expression to this concept and to calculate the percentages of free ions and associated species in their melts, the former usually being quite appreciable (>30%.)

We have not been able to apply the Nernst–Einstein equation to the Li_2CO_3–Na_2CO_3 systems as neither the tracer diffusion of Li^+ ion nor transport numbers for the ions have been measured. However, the deviations for the pure Na_2CO_3 melt have been calculated and shown to be appreciable in the temperature range of this study.[1] If the presence of free ions and ionic aggregates is assumed in the Li_2CO_3–Na_2CO_3 system, then

(3) G. V. Vorobev, S. V. Karpachev, and S. F. Palguev, AEC-tr-5948, 1963, p 167.

(4) P. L. Spedding, unpublished work.

(5) C. T. Moynihan and R. W. Laity, *J. Phys. Chem.*, **68**, 3312 (1964).

(6) C. A. Angell, *ibid.*, **69**, 399 (1965).

(7) J. O. Bockris and G. W. Hooper, *Discussions Faraday Soc.*, **32**, 218 (1962).

(8) F. Lantelme and M. Chemla, *Electrochim. Acta*, **10**, 663 (1965).

(9) By "free ions" are meant single ions such as Na^+ or CO_3^{2-}. The polyionic groups include ion pairs of the type $[M^+CO_3^{2-}]^-$, neutral groups such as M_2CO_3, and possibly larger aggregates.

from consideration of all the data now available we put forward the following suggestions regarding transport in these melts. The ideas which we outline give a feasible qualitative explanation for the behavior of these data which is otherwise rather puzzling.

We postulate that conduction proceeds *predominantly* by movements of free ions and tracer diffusion *predominantly* by groups of ions either neutral or charged. A corollary of this is that the concentration of free ions is very low since diffusion can proceed by both species. This first postulate asserting that essentially separate species are involved in conduction and diffusion is in accord with most of the known facts. Thus, we have shown previously[1] that the activation energy for tracer diffusion for several ions in the alkali carbonates is about 11 kcal, whereas that for conductance is in the range 6–8 kcal. This can be explained in terms of the large activation energy needed for an aggregate of ions to diffuse and the small activation energy needed for free ions to migrate. Again, the equivalence of cation and anion activation energies in diffusion is strong evidence for an associated act such as aggregate movement. One can also explain why the equivalent conductance of Li_2CO_3 is much higher than that of Na_2CO_3, whereas tracer-diffusion mobilities are in the reverse order, being higher in pure Na_2CO_3. With the small size of the cation and its associated high polarizing power, Li_2CO_3 can be visualized as a structured melt[10] with an essentially anionic lattice which would allow Li^+ ion migration but inhibit aggregate movement.

We next postulate that if the above picture of the two transport mechanisms is accepted, the positive deviations for diffusion shown in Figure 1 can be explained by some kind of structural breakdown as Na_2CO_3 is progressively added to the Li_2CO_3 melt. This loosening of the structure can be attributed basically to the differing sizes of the cations which have the effect of providing asymmetry either by reason of differing polarizing power or from purely geometrical considerations. Structural breakdown is also reflected in the negative deviation of the viscosity for many binary salt systems. In any event, the ion aggregates are able to diffuse faster in the looser melt reaching an apparent maximum at the eutectic composition. By analogy with other electrolyte systems,[11] the migration of free ions in the conduction process would be much less affected by structural changes.

There is some controversy about the nature of the entities in melts at their eutectic composition, and this has recently been discussed by Antipin.[12] In particular, the behavior of eutectic mixtures under pressure points to the fact that they should be regarded as the most loosely packed combinations of the ions or atoms which constitute them. It is also noteworthy that Janz and Saegusa[13] found that the activation energy for viscous flow in a ternary eutectic of the alkali carbonates was 10 kcal, whereas that for the pure salts was of the order of 25 kcal. To explain the diffusion maxima one might postulate further, then, that there is maximal structural looseness at the eutectic composition.

The measurement of the tracer-diffusion coefficients of Li^+ ion in the above system is of course necessary to confirm the picture here presented. At the moment we do not have the facilities for mass spectrometric analysis. If our assumptions are correct, the lithium ion coefficients should show a positive deviation of the same type as Na^+ and CO_3^{2-} ions. These data would also allow a comparison of conductance and diffusion mobilities *via* the Nernst–Einstein equation and the extent of the deviations should then permit a quantitative test of the above ideas.

Finally, it should be remarked that the positive deviations in the tracer-diffusion data appear to be most marked when the cations in the binary mixtures are fairly different in size, when the lithium ion is present, and when the anion is highly polarizable. Thus studies in the alkali nitrates show some evidence of the effects described but are not very definite. Similarly, our data for the K_2CO_3–Na_2CO_3 system,[2] though incomplete, indicate a more nearly linear relationship.

Acknowledgment. We wish to thank Dr. C. A. Angell for helpful discussions on this subject.

(10) The use of the term "structure" here and below should perhaps be qualified. Many models of molten salts assume the existence of interpenetrating anion and cation lattices which do not have the long-range order of the crystalline state yet are sufficiently real to the extent that each ion has, on the average, more nearest neighbors of opposite charge than of its own charge. This departure from a purely random state is what we imply by the term structure.

(11) R. H. Stokes and R. Mills, "Viscosity of Electrolyte Solutions," Pergamon Press Ltd., London, 1965, p 56.

(12) L. N. Antipin, AEC-tr-5948, 1963, p. 123.

(13) G. J. Janz and F. Saegusa, *J. Electrochem. Soc.*, 110, 452 (1963).

Deactivation in the Photolysis of Hexafluoroacetone at Low Pressure

by Gerald B. Porter and Kengo Uchida[1]

Department of Chemistry, University of British Columbia, Vancouver, Canada *(Received June 13, 1966)*

In the gas phase, the dissociation of the vibrationally excited molecules in an upper electronic state

competes with the collisional deactivation by other molecules in their ground state. In the latter process, two mechanisms have been considered:[2] (i) weak (multistage) collisional deactivation and (ii) strong collision deactivation.

If case i is operative, it has been shown that at low pressures a point of inflection should appear in a plot of the reciprocal of the primary quantum yield of dissociation against pressure and that the plot should lead to zero slope at zero pressure. On the other hand, if case ii is operative, the plot should be a straight line. Porter, *et al.*,[2,3] have examined the photolysis of ketene and have supported case ii. However, Strachan, Boyd, and Kutschke[4] have suggested other treatments of the experimental data and demonstrated that the literature data on the quantum yield for the decomposition of hexafluoroacetone is better interpreted in terms of a multistage deactivation (case i). According to their method, very precise measurements of the absolute quantum yield are required. Moreover, Bowers and Porter[5] have recently studied the photolysis of hexafluoroacetone in detail at pressures above 1 mm and have assumed that the reaction occurs through case ii, since the reciprocals of the primary quantum yields extrapolate to unity at all wavelengths of excitation. However, some doubt still remains about the primary process of deactivation, since the accurate measurement of the absolute quantum yield is difficult and the extrapolated value might deviate slightly from unity. All results studied previously have been obtained at relatively high pressures.

One of the best methods to confirm directly which case is operative is to examine quantum yields carefully at lower pressures than 1 mm, where the curvature could be readily seen if it occurs. In this paper, the simple photolysis of hexafluoroacetone was extended to 0.1 mm.

A special reaction cell was used to photolyze hexafluoroacetone at low pressure. It is about 80 cm long and 3 cm in diameter, and is divided at the center by a quartz window into two parts, one of which is a reference filled with hexafluoroacetone at constant low pressure and is used as a monitor of the light intensity. The exciting light at 3130 A from a mercury lamp (Model PEK-200) was focused to a parallel beam by a quartz lens and was isolated by a Corning filter 9863 and an interference filter (Jena PIL, λ_{max} 3090 A). Since it has been observed[6] that products of the photolysis are simply carbon monoxide and hexafluoroethane near room temperature and the quantum yield of the dissociation has the same value as that of the formation of carbon monoxide, the product gas, after the irradiation, was passed through a trap cooled by liquid nitrogen, and only noncondensable carbon monoxide was collected and measured by using an automatic Toepler–McLeod gauge. All photolyses were performed at 35°.

The results are shown in Table I. Previously the following primary processes have been presented and the rate constants and some energies of activation have been determined[5,6]

$$A \xrightarrow{h\nu} {}^1A^* \quad (1)$$

$${}^1A^* \longrightarrow CO + 2CF_3 \quad (2)$$

$${}^1A^* + A \longrightarrow {}^1A^0 + A \quad (3)$$

$${}^1A^0 \longrightarrow {}^3A^0 \quad (4)$$

$${}^1A^0 \longrightarrow A\ (+h\nu_{fluo}) \quad (5), (6)$$

$${}^3A^0 \longrightarrow A\ (+h\nu_{phos}) \quad (7), (9)$$

$${}^3A^0 \longrightarrow CO + 2CF_3 \quad (8)$$

Table I: Quantum Yields at Low Pressure

Pressure, mm	ϕ	ϕ_s
1.040	0.832	0.787
1.037	0.823	0.779
1.030	0.823	0.779
1.020	0.820	0.776
1.018	0.819	0.775
0.837	0.844	0.807
0.815	0.838	0.802
0.621	0.880	0.851
0.618	0.874	0.845
0.424	0.908	0.887
0.419	0.918	0.897
0.404	0.919	0.899
0.209	0.948	0.937
0.208	0.960	0.949
0.203	0.979	0.968
0.197	0.980	0.969
0.106	0.974	0.968
0.104	1.02	1.01
0.100	0.936	0.931

(1) On leave from Hirosaki University, Japan.

(2) G. B. Porter and B. T. Connelly, *J. Chem. Phys.*, **33**, 81 (1960).

(3) G. A. Taylor and G. B. Porter, *ibid.*, **36**, 1353 (1962).

(4) A. N. Strachan, R. K. Boyd, and K. O. Kutschke, *Can. J. Chem.*, **42**, 1345 (1964).

(5) P. G. Bowers and G. B. Porter, *J. Phys. Chem.*, **70**, 1622 (1966).

(6) P. B. Ayscough and E. W. R. Steacie, *Proc. Roy. Soc.* (London), **A234**, 476 (1956).

where the superscripts 1 and 3 represent the multiplicity of the excited electronic state, while an asterisk denotes a molecule with more vibrational energy than a vibrationally equilibrated molecule with superscript zero. The quantum yields obtained here are relative values only. For the purpose of investigating the linearity of $1/\phi$ *vs.* [A], relative quantum yields are adequate. However, in order to represent these data, we have corrected them so that $\phi = 1$ at zero pressure. The fraction of the light absorbed in each cell was always less than 4%; therefore it could be taken as strictly proportional to the pressure in the cell. It is evident that a few per cent of the dissociation takes place by process 8, the dissociation *via* the triplet state, even below 1 mm. Thus, the quantum yield of dissociation from the singlet excited state directly is obtained by subtracting that *via* the triplet from the over-all quantum yield, with $\phi^{\infty} = 0.29$. The corrected results are shown in Table I and in Figure 1, where reciprocals of quantum

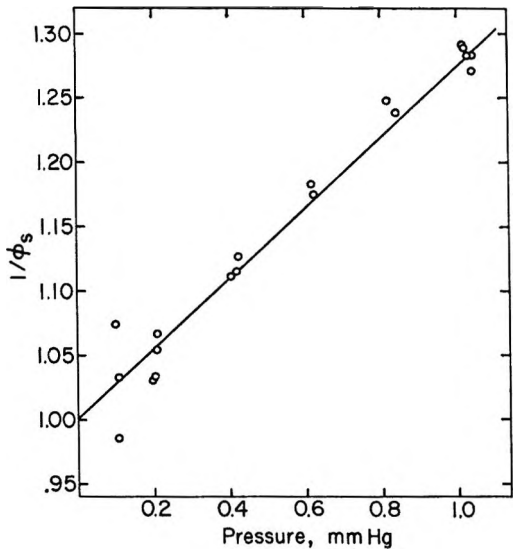

Figure 1.

yields of dissociation *via* only singlet state are plotted against the pressure. The straight line is drawn by a method of least squares. The experimental error is large at the lowest pressure, but there is no tendency to concavity upward. Therefore, the strong collision deactivation, case ii, is undoubtedly supported in this system.

Acknowledgment. This work was supported by a grant from the National Research Council of Canada.

The Isomerization of *n*-Pentyl and 4-Oxo-1-pentyl Radicals in the Gas Phase

by L. Endrenyi and D. J. Le Roy

Lash Miller Chemical Laboratories, University of Toronto, Toronto, Canada *(Received June 13, 1966)*

Some years ago Kossiakoff and Rice[1] suggested that in many cases the activation energy for the isomerization of a long-chain free radical may be much less than the activation energy for its decomposition, and they were able to explain the products of the decomposition of hydrocarbons in terms of intramolecular hydrogen migration in alkyl radicals. Somewhat later, Sefton and Le Roy,[2] in studying the polymerization of ethylene initiated by ethyl radicals labeled in the methylene group with C^{14}, obtained evidence for radical isomerizations involving 1–5 and 1–6 intramolecular hydrogen migration. They showed that most of the product olefins were formed by the decomposition of alkyl radicals and that the molar activity of these was comparable to that of the ethyl radicals which initiated the polymerization. Since a simple decomposition of the long-chain alkyl radicals would have yielded inactive biradicals, and hence inactive olefins, they concluded that the radicals had undergone intramolecular hydrogen migration before decomposition. A number of additional examples have been reported more recently,[3] although quantitative kinetic data are lacking.

In the course of a study of the kinetics of the addition of methyl radicals to ethylene it became necessary to follow, in a quantitative way, all of the subsequent reactions of the propyl radicals formed by the addition of methyl radicals (from the photolysis of acetone) to ethylene. From the nature and amounts of certain of the products we were able to obtain kinetic parameters for 1–4 intramolecular hydrogen migration in *n*-pentyl radicals and somewhat less conclusive data for 1–5 intramolecular hydrogen migration in 4-oxo-1-pentyl radicals.

Experimental Section

Acetone at a concentration of 3.60×10^{-6} mole cm^{-3} was photolyzed in the presence of 0.240×10^{-6} mole cm^{-3} of ethylene (0.300×10^{-6} mole cm^{-3} was

(1) A. Kossiakoff and F. O. Rice, *J. Am. Chem. Soc.*, **65**, 590 (1943).
(2) V. B. Sefton and D. J. Le Roy, *Can. J. Chem.*, **34**, 41 (1956).
(3) E.-A. I. Heiba and R. M. Dessau, *J. Am. Chem. Soc.*, **88**, 1589 (1966).

used in one of the experiments) using the radiation isolated from a 250-w medium-pressure mercury arc by means of a Corning 9700 filter. The effective radiation consisted mostly of 3130 A. The reaction vessel was a quartz cylinder 6 cm long and 5 cm in diameter with plane windows.

After the removal of CO and CH_4 at liquid nitrogen temperature the remaining products were separated into two fractions by pumping the more volatile products through a trap at −120°. Each fraction was analyzed by gas chromatography. Quantitative determinations were based on calibrated relative molar responses using certain reference substances added to the system in accurately measured amounts: one of these, CO_2, was added before reaction; the other, isopropyl ether, was added after reaction.

Ethane and butane were determined on a 13-ft, 0.25-in. column containing 35–100 mesh activated silica gel, using elution temperatures of 80 and 130°, respectively. The less volatile fraction was analyzed using a 20-ft column containing tri-*m*-tolyl phosphate (31% by weight on 30–60 mesh firebrick). A more detailed description of the qualitative and quantitative analysis will be presented in a forthcoming publication.

The duration of the irradiation ranged from 6 to 21 min, depending on the temperature. The amount of acetone consumed ranged from 4 to 6.3% and the amount of ethylene consumed from 17 to 19%. No studies of the time dependence of the product ratios was made. While the extent of reaction is somewhat greater than one might wish, this was a compromise.

Results and Discussion

The portion of the over-all reaction scheme which is relevant to the problem of radical isomerization is shown in Figure 1.

Isomerization of n-Pentyl Radicals. If k_7 is the rate constant for the isomerization and k_{-7} is that for the reverse reaction, then in the steady-state

$$0 = \frac{d}{dt}(sec\text{-}C_5H_{11}) = k_7(n\text{-}C_5H_{11}) - k_{-7}(sec\text{-}C_5H_{11}) - k_8(sec\text{-}C_5H_{11})(CH_3) \quad (1)$$

or

$$\frac{k_8}{k_7}(CH_3) = \frac{(n\text{-}C_5H_{11})}{(sec\text{-}C_5H_{11})} - \frac{k_{-7}}{k_7} \quad (2)$$

It seems reasonable to assume that $k_6 \simeq k_8$ and hence

$$\frac{(n\text{-}C_5H_{11})}{(sec\text{-}C_5H_{11})} = \frac{k_6(n\text{-}C_5H_{11})(CH_3)}{k_8(sec\text{-}C_5H_{11})(CH_3)} = \frac{R_6{}^4}{R_f[i\text{-}C_6H_{14}]} \quad (3)$$

Also

$$R_6 = R_f[n\text{-}C_6H_{14}] - k_4(C_3H_7)^2 = R_f[n\text{-}C_6H_{14}] - \frac{k_3k_4}{k_2^2}\frac{\{R_f[C_4H_{10}]\}^2}{R_f[C_2H_6]} \quad (4)$$

Thus

$$\frac{k_8}{k_7}(CH_3) = \frac{k_8}{k_3^{1/2}k_7}\{R_f[C_2H_6]\}^{1/2} = \frac{R_f[n\text{-}C_6H_{14}] - \frac{k_3k_4}{k_2^2}\frac{\{R_f[C_4H_{10}]\}^2}{R_f[C_2H_6]}}{R_f[i\text{-}C_6H_{14}]} - \frac{k_{-7}}{k_7} \quad (5)$$

In this development it has been assumed that reactions 7 and 8 are the only ones undergone by *sec*-C_5H_{11} radicals. Since (CH_3) was larger than any other radical concentration, the main additional reaction would be to form C_5H_{10} by disproportionation. This product was formed, but only in quantities ranging from 0.01 to 0.06 × 10^{-12} mole cm^{-3} sec^{-1}. It has not been taken into account because it could not be measured with very great accuracy. It could be included in eq 5 by multiplying k_8 by a factor slightly greater than unity.

The rates of formation of the various products are given in Table I. Most of the available data on the combination and cross-combination of methyl and *n*-propyl radicals are in substantial agreement with the approximate theoretical estimate that k_3k_4/k_2^2 should be equal to $^1/_4$, and we have assumed this value in using eq 5.[5,6]

Table I: Isomerization of n-C_5H_{11}[a]

T, °K	n-C_6H_{14}	i-C_6H_{14}	C_4H_{10}	C_2H_6	$\frac{k_3^{1/2}k_7}{k_8} \times 10^6$
502.5	3.10	1.49	19.4	41.9	12.88
502.9	2.62	1.27	22.4	63.8	15.60
479.8	2.54	0.864	22.1	79.7	7.71
457.5	1.97	0.401	20.5	94.2	4.52
438.5	1.31	0.203	15.6	91.8	2.99

[a] Rates of formation of products are in moles cm^{-3} sec^{-1} × 10^{12}.

(4) We use the terminology R_6 to indicate the rate of reaction 6 and $R_f[i\text{-}C_6H_{14}]$ to indicate the rate of formation of 2-methylpentane.

(5) J. A. Kerr and A. F. Trotman-Dickenson, *Progr. Reaction Kinetics*, 1, 107 (1961).

(6) S. W. Benson and W. B. DeMore, *Ann. Rev. Phys. Chem.*, 16, 397 (1965).

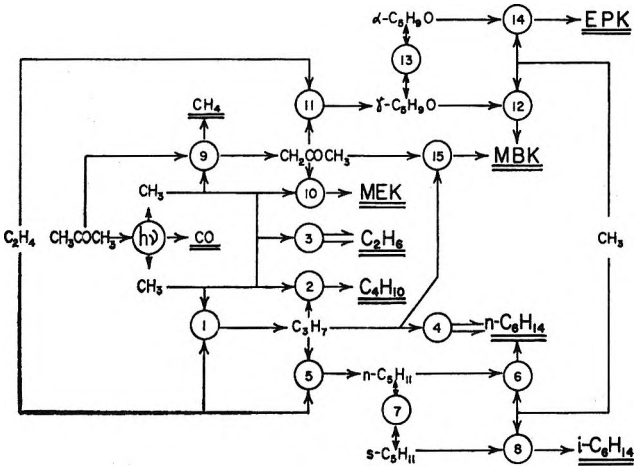

Figure 1. Reaction scheme for formation and isomerization of *n*-pentyl and 4-oxo-1-pentyl radicals. γ-C_5H_9O and α-C_5H_9O refer to 4-oxo-1-pentyl and 2-oxo-1-pentyl, respectively, and EPK, MBK, and MEK refer to ethyl propyl ketone, methyl butyl ketone, and methyl ethyl ketone.

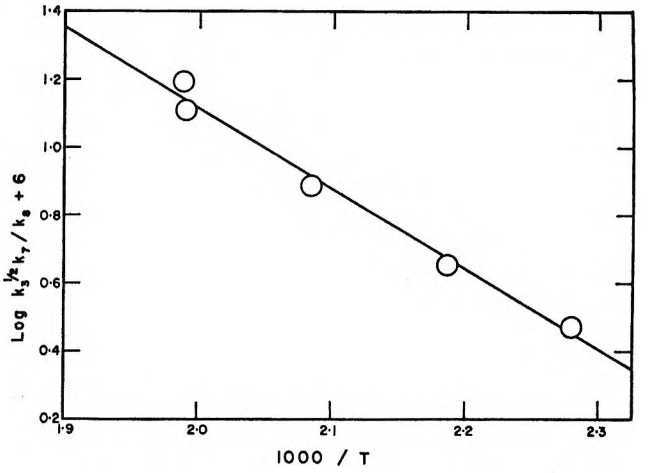

Figure 2. Arrhenius plot for the isomerization of *n*-pentyl radicals.

Values for k_{-7}/k_7 are not available but a reasonably accurate estimate can be made. Thus

$$\frac{k_{-7}}{k_7} = \frac{1}{K_7} \simeq e^{\Delta E^\circ/RT} \qquad (6)$$

where K_7 is the equilibrium constant for reaction 7 and ΔE° is the standard increase in internal energy for the isomerization.[7] From bond dissociation energy data for the removal of primary and secondary H atoms from normal paraffins ΔE° can be estimated to be of the order of -5 kcal mole^{-1}, and hence in the temperature range used in these experiments k_{-7}/k_7 will be of the order of 3×10^{-3} to 7×10^{-3}. By contrast, the first term on the right of 5 ranges from 0.51 to 3.2. The quantity k_{-7}/k_7 in eq 5 will therefore be neglected. The values of $k_3^{1/2}k_7/k_8$ obtained in this way are given in Table I and in Arrhenius form in Figure 2.

A least-squares calculation gave $E_7 + {}^1/_2E_3 - E_8 = 10.8 \pm 0.8$ kcal mole^{-1} and $\log A_7A_3^{1/2}/A_8 = 1.58 \pm 0.35$. Assuming A factors of $10^{13.34}$ for reaction 3 and 10^{14} for reaction 8,[5] and neglecting their activation energies

$$k_7 = 1.4 \times 10^7 \exp(-10.8 \times 10^3/RT) \qquad (7)$$

Isomerization of 4-Oxo-1-pentyl Radicals. The steady-state treatment of the reaction scheme for this isomerization, shown at the top of Figure 1, is analogous to that which has been given for the isomerization of *n*-pentyl radicals.

$$\frac{k_{14}}{k_{13}}(CH_3) = \frac{R_{12}}{R_f[EPK]} - \frac{k_{-13}}{k_{13}} \qquad (8)$$

where

$$R_{12} = R_f[MBK] - k_{15}(CH_2COCH_3)(C_3H_7)$$
$$= R_f[MBK] - \frac{k_3k_{15}}{k_2k_{10}} \frac{R_f[MEK]R_f[C_4H_{10}]}{R_f[C_2H_6]} \qquad (9)$$

The rates of formation of the various products are given in Table II.

The estimation of R_{12} is subject to error arising from the uncertainty in the value of k_3k_{15}/k_2k_{10}. A reasonable assumption would be that $k_{15} \simeq k_{10}$; if we accept the values $k_3k_4/k_2^2 = {}^1/_4$,[5,6] $k_3 = 10^{13.34}$,[5] and $k_4 = 10^{14}$,[5] it follows that $k_3k_{15}/k_2k_{10} = k_3/k_2 = 0.23$. These values were used in obtaining the values of $R_{12}/R_f[EPK]$ given in Table II. The relative constancy of $R_f[EPK]\{R_f[C_2H_6]\}^{1/2}/R_{12}$ suggests that this quantity cannot be equated to $k_{13}k_3^{1/2}/k_{14}$, *i.e.*, that k_{-13}/k_{13} in eq 8 cannot be neglected.

Rewriting eq 8 and expressing (CH_3) as $\{R_f[C_2H_6]\}^{1/2}/k_3^{1/2}$

$$\frac{R_{12}}{R_f[EPK]\{R_f[C_2H_6]\}^{1/2}} = \frac{k_{14}}{k_{13}k_3^{1/2}} + \frac{k_{-13}}{k_{13}} \frac{1}{R_f[C_2H_6]^{1/2}} \qquad (10)$$

The first term on the right of eq 10 will decrease with increasing temperature while the second term will increase, so that the quantity on the left of eq 10 may be relatively independent of temperature under condi-

(7) Rigorously, $1/K_7 = e^{\Delta H^\circ/RT}e^{-\Delta S^\circ/R}$. However, the number of moles does not change in the reaction $\Delta H^\circ = \Delta E^\circ$, and the entropies of the two radicals would be expected to differ by very little, so that $\Delta S^\circ \approx 0$. This is supported by the data for *n*- and *sec*-C_4H_9 (J. E. Calvert and J. N. Pitts, Jr., "Photochemistry," John Wiley and Sons, Inc., New York, N. Y., 1966, p 819).

Table II: Isomerization of 4-Oxo-1-pentyl[a]

T, °K	MBK	MEK	EPK	C_4H_{10}	C_2H_6	$\frac{R_{12}}{R_f[EPK]}$	$\frac{R_f[EPK]\{R_f[C_2H_6]\}^{1/2}}{R_{12}} \times 10^6$
502.5	10.77	36.6	8.27	19.4	41.9	0.831	7.8
502.9	11.29	47.5	9.89	22.4	63.8	0.754	10.6
479.8	8.27	42.9	6.58	22.1	79.7	0.840	10.6
457.5	5.07	34.1	4.38	20.5	94.2	0.767	12.6
438.5	3.21	23.8	2.38	15.6	91.8	0.958	10.0

[a] Rates of formation of products are in moles cm^{-3} $sec^{-1} \times 10^{12}$.

tions where k_{-13} is of the order of magnitude $k_{14}\{R_f[C_2H_6]\}^{1/2}/k_3^{1/2}$. This suggests that, in the temperature range used, k_{-13} is of the order of $10^{14} \times 8 \times 10^{-6}/10^{6.7} = 170\ sec^{-1}$.

Discussion

Reaction 7 is an intramolecular analog of the reaction

$$R + R'H = RH + \textit{sec}\text{-}R'$$

Most of the available data when R'H is a paraffin are for R = CH_3 and indicate that A is of the order of 10^{11} cm^3 $mole^{-1}$ sec^{-1} and E of the order 8.3 kcal $mole^{-1}$,[5] in comparison with $A_7 = 1.4 \times 10^7$ and $E_7 = 10.8$.

The low value of A_7 cannot be attributed solely to the loss of the entropy of rotation about the three C–C bonds which are incorporated into the cyclic activated complex. The A factor of a unimolecular reaction can be written, in terms of transition-state theory, in the form

$$A = \kappa e \frac{kT}{h} e^{\Delta S^+/R} \qquad (11)$$

If the transmission coefficient κ is assumed to be unity, then $\Delta S^+ = -31$ eu at the mean temperature of 470°K.

Kemp and Egan[8] have estimated an entropy for the restricted rotation of the two methyl groups in propane of 3.84 eu at 298.2°K, and Aston and Messerly[9] have estimated an entropy of 1.44 eu for the restricted rotation of the ethyl group in *n*-butane at 272.66°K. It is evident, therefore, that the removal of internal rotation alone cannot account for an entropy of activation of −31 eu if $\kappa \simeq 1$. In order to treat the results in terms of transition-state theory it is necessary to assume that $\kappa << 1$.

Reaction 7 appears to be the only example of a homogeneous gas-phase intramolecular hydrogen shift for which Arrhenius parameters have been determined. It is to be hoped that additional examples will be forthcoming so that this type of reaction might serve to test the various theories of unimolecular reactions.

The increase of *ca.* 2.5 kcal $mole^{-1}$ in activation energy above that for an intermolecular hydrogen abstraction can probably be accounted for by the strain energy on forming the cyclic complex. Kaarsemaker and Coops[10] have estimated a strain energy of 6.5 kcal $mole^{-1}$ for cyclopentane, in contrast to the strain-free configuration in cyclohexane. A quantitative comparison of inter- and intramolecular hydrogen abstraction is probably not justified since the dynamics of the two processes are quite different.

Acknowledgments. The authors wish to express their appreciation of the assistance of Mr. Frank Safian. The financial assistance of the National Research Council of Canada is gratefully acknowledged.

(8) J. D. Kemp and C. J. Egan, *J. Am. Chem. Soc.*, **60**, 1521 (1938).
(9) J. G. Aston and G. H. Messerly, *ibid.*, **62**, 1917 (1940).
(10) S. Kaarsemaker and J. Coops, *Rec. Trav. Chim.*, **71**, 125 (1952).

Evidence for the Influence of Resonance-Contributing Structures on Proton Coupling Constants in Certain Aromatic Systems

by William B. Smith and Thomas J. Kmet

Department of Chemistry, Texas Christian University, Fort Worth, Texas *(Received June 27, 1966)*

Chemists have long found it convenient to discuss certain chemical and physical properties of aromatic systems in terms of the various contributing forms used to describe the resonance hybrid structure of the molecule in question. Thus, the acidity of *p*-nitrophenol and the relatively weak base strength of *p*-nitroaniline have been explained as being in part due to the more significant contributions of the quinoid

Table I: Nmr Parameters[a]

Compound	τ_A	τ_B	J_{ortho}	J_{para}	J_{meta}	J_{meta}'
p-Nitrophenol	1.88	3.08	8.89	0.23	2.96	2.64
p-Nitrophenolate	1.98	3.52	9.45	0.06	3.30	2.50
p-Bromophenol	2.74	3.27	8.71	0.26	3.05	2.56
p-Bromophenolate	2.77	3.47	8.77	0.25	3.24	2.57
p-Cyanophenol	2.46	3.11	8.50	0.36	2.54	2.27
p-Cyanophenolate	2.68	3.37	8.54	0.30	2.51	2.40
p-Nitroaniline	1.99	3.25	8.97	0.14	2.86	2.39
p-Nitroanilinium	1.47	2.07	8.59	0.31	2.84	2.37
Fuchsone	2.33	3.29	10.55	0.07	3.02	1.98
4-Methyl-4-trichloromethyl-2,5-cyclohexadienone	2.73	3.59	10.48	0.12	3.39	1.92

[a] Coupling constants in cps.

structures I and II to the phenolate and free amine

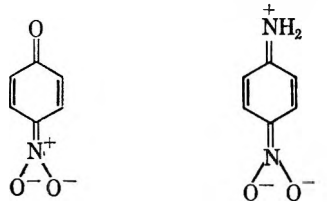

I II

in comparison to the phenol and anilinium ion, respectively.[1]

The postulation of such structures as contributing to the form of the hybrid implies certain consequences on the proton coupling constants in these systems, for, as the quinoid character becomes more pronounced, one would reasonably expect the π-electron contribution to the coupling constants to enhance J_{ortho}, to decrease J_{meta}, and probably to decrease J_{para}. Recent evidence supporting this contention has been provided by Hutton and Schaeffer,[2] who studied the spectra of *p*-nitroanisole in a series of solvents of increasing polarity where the dipolar quinoid structure would be expected to become increasingly important.

According to the Ramsey formulation of spin coupling, the value of the coupling constant depends on the excitation energy to triplet states.[3] The assumption is made here that that value will not change in going from phenol to phenolate or from aniline to anilinium. In general, it would be expected that the value would not vary significantly in going from one aromatic compound to another.[4]

The nmr parameters for a series of phenols and their corresponding phenolates in methanol are given in Table I as are the parameters for *p*-nitroaniline and its conjugate acid. In order to compare the values of these aromatic systems with a typical cross-conjugated quinoid structure, the parameters for fuchsone and 4-methyl-4-trichloromethyl-2,5-cyclohexadienone were also determined and included in Table I.

As expected, both cross-conjugated dienones show an enhanced value of J_{ortho} and decreased value of J_{para} compared to most of the aromatic compounds in Table I. The values of J_{meta} span the range found in aromatic compounds.

The value of J_{ortho} shows a marked increase (0.5 cps) in going from *p*-nitrophenol to phenolate. Similarly, J_{ortho} decreases by 0.4 cps in going from *p*-nitroaniline to the anilinium ion. The changes in J_{para} in both cases are seen to parallel our expectations of enhanced quinoid contributions to the phenolate ion and the free amine, respectively.

The results for *p*-cyanophenol and *p*-bromophenol and their phenolates support the contention that the above alterations are not due to the changes in the charge densities on the aromatic proton coupling constants. In these two systems, the contribution of the quinoid structure to the phenolate hybrid is not perceptible.

The analysis of the AA'BB' spectra in this study does not allow one to differentiate the two values of J_{meta} in each. Martin and Dailey[5] have found values of J_{meta} to be enhanced by intervening substituents of electron-donating character. Thus, one might expect

(1) For a recent survey see L. N. Ferguson, "The Modern Structural Theory of Organic Chemistry," Prentice-Hall, Inc., Englewood Cliffs, N. J., 1963, p 308.

(2) H. M. Hutton and T. Schaeffer, *Can. J. Chem.*, **43**, 3116 (1965).

(3) N. F. Ramsey, *Phys. Rev.*, **91**, 303 (1953).

(4) The nmr coupling constants of *para*-disubstituted benzenes are well known to vary only slightly with different substituents. When the substituent is directly bonded to the site of the proton in question this assumption may fail (N. Muller, *J. Chem. Phys.*, **42**, 4309 (1965)).

(5) J. S. Martin and B. P. Dailey, *ibid.*, **39**, 1722 (1963).

the change from phenol to phenolate to increase J_{meta} while affecting J_{meta}' only slightly. This behavior is noted in all three phenol systems in Table I, and it is reasonable to assume that the values listed as J_{meta} are for protons adjacent to the phenolic hydroxyl.

A reverse behavior would be expected for the coupling between the protons *ortho* to the amine group in going to the conjugate acid. The values for the sets J_{meta}–J_{meta}' for *p*-nitroaniline and its conjugate acid, as listed in Table I, either indicate no change in these values or else an increase in J_{meta}' upon protonation. No such change in J_{meta}' was noted in the phenol–phenolate series.

In view of the wide range of solvent conditions necessitated in this study, no conclusions regarding changes in chemical shifts seem warranted.

Experimental Section

Spectra were determined on a Varian A-60 operating at ambient temperature. Six or more sweeps were made on each compound, and the line positions were averaged. Typically, the standard deviations of the line positions were 0.04–0.07 cps, and often lower values were obtained. The spectra were typical AA'BB' spectra and were analyzed according to the procedure of Grant, Hirst, and Gutowsky.[6] Values of the spectral parameters were refined with the aid of the FREQINT IV A 1620 program until all lines fit to better than 0.1 cps. Empirically, we noted that variation in any of the coupling constants by 0.1 cps from the optimum values determined by this procedure resulted in perceptibly poorer fit of the observed and calculated lines. It was felt that the coupling constants so determined were, therefore, good to ±0.1 cps.

The aromatic compounds were all commercially available samples. The 4-methyl-4-trichloromethyl-2,5-cyclohexadienone was kindly supplied by Dr. M. G. Reinecke of these laboratories. Fuchsone was synthesized by the method of Bistrzycki and Herbst.[7]

The phenols were determined in 10% solutions of methanol, and the phenolates were run in the same solvent containing about 10% excess dissolved potassium hydroxide. *p*-Nitroaniline was run as a 20% solution in acetone as was the cyclohexadienone. A 16% solution of *p*-nitroaniline in trifluoroacetic acid served as the source of the anilinium spectrum. Fuchsone was determined as a 20% solution in deuteriochloroform. Tetramethylsilane was used as an internal standard in each case.

(6) D. M. Grant, R. C. Hirst, and H. S. Gutowsky, *J. Chem. Phys.*, 38, 470 (1963).

(7) A. Bistrzycki and C. Herbst, *Ber.*, 36, 2333 (1903).

Acknowledgment. We wish to express our gratitude to the Robert A. Welch Foundation for its generous support of this work.

Dependence of Contact Angles on Temperature: Polar Liquids on Polypropylene

by Harold Schonhorn

Bell Telephone Laboratories, Incorporated, Murray Hill, New Jersey *(Received June 17, 1966)*

Recently, experimental results for the temperature dependence of the contact angle of liquids on nonpolar solids have been presented by Phillips and Riddiford,[1] Johnson and Dettre,[2] Brewis,[3] and this author.[4]

In this note we shall present the results for the polar liquid–polypropylene (melt crystallized film) systems based on the reported surface tension measurements for polypropylene.[5]

Assuming that $\gamma_{SV}^{d} = (\gamma_{LV})_P^{d}$, Fowkes' modification[6] of the Young equation yields

$$\cos\theta = \frac{2[(\gamma_{LV})_P^{d}\gamma_{LV}^{d}]^{1/2}}{\gamma_{LV}} - 1 \qquad (1)$$

where subscript P refers to polymer and superscript d refers to the dispersion component of the surface tension. For polypropylene, where only dispersion forces are assumed operative, $\gamma_{SV}^{d} = (\gamma_{LV})_P$. Further, assuming the ratio $\gamma_{LV}^{d}/\gamma_{LV}$ to be temperature invariant, we obtain

$$\cos\theta = 2\left[\frac{k(\gamma_{LV})_P}{\gamma_{LV}}\right]^{1/2} - 1 \qquad (2)$$

where $k = \gamma_{LV}^{d}/\gamma_{LV}$. The calculated and experimental results are shown in Table I. Experimental details are given elsewhere.[4] As has been observed in the polar liquid–polyethylene systems,[4] the contact angles of these liquids on polypropylene appear to be in-

(1) M. C. Phillips and A. C. Riddiford, *Nature*, 205, 1005 (1965).

(2) R. E. Johnson, Jr., and R. H. Dettre, *J. Colloid Sci.*, 20, 173 (1965).

(3) D. M. Brewis, presented at the 22nd Annual Technical Conference, S.P.E., March 1966.

(4) H. Schonhorn, *Nature*, 210, 896 (1966).

(5) H. Schonhorn and L. H. Sharpe, *J. Polymer Sci.*, B3, 235 (1965).

(6) F. M. Fowkes, *J. Phys. Chem.*, 66, 1863 (1962); 67, 2538 (1963); Advances in Chemistry Series, No. 43, American Chemical Society, Washington, D. C., 1964, p 99.

Table I: The Temperature Dependence of the Wettability of Polypropylene by Water, Glycerol, and Formamide

T, °C	$(\gamma_{LV})_F$, dynes/cm	γ_{LV}, dynes/cm	k	γ_{LV}^d, dynes/cm	cos θ	θ, deg	θ_{exptl}, deg	θ,[a] deg
				Water–Polypropylene				
0	29.2	75.60	0.300	22.7	−0.3302	109	...	...
10	28.8	74.22		22.2	−0.3283	108	...	...
20	28.4	72.75		21.8	−0.3155	108	95	...
30	28.0	71.18		21.3	−0.3144	108	...	...
40	27.6	69.56		20.8	−0.3099	108	...	...
50	27.2	67.91		20.3	−0.3079	108	...	...
60	26.8	66.18		19.8	−0.3049	108	...	...
70	26.4	64.40		19.3	−0.2981	107	...	...
80	26.0	62.60		18.7	−0.2971	107	...	...
100	25.2	58.90		17.6	−0.2869	107	...	...
				Glycerol–Polypropylene				
20	28.4	63.4	0.584	37.0	0.0221	89	91–92	87
90	25.6	58.6		34.2	0.0102	89	90–91	...
				Formamide–Polypropylene				
0	29.2	59.9	0.679	40.7	0.1519	81	...	...
20	28.4	58.2		39.5	0.1512	81	83	...
50	27.2	55.7		37.8	0.1526	81	...	...

[a] E. Wolfram, *Kolloid-Z.*, **182**, 75 (1962).

sensitive to temperature. Again, as observed for the polar liquid–polyethylene systems, the experimental and calculated contact angles agree well except for the results with water. It is possible that the choice of 21.8 dynes/cm for $(\gamma_{LV}^d)_{H_2O}$ at 20° needs some revision to obtain better agreement with the experimental contact angle.

The apparent insensitivity of the contact angle to temperature is related to the relative constancy of $[(\gamma_{LV})_P/\gamma_{LV}]^{1/2}$ in eq 2. However, this is probably not general with respect to all liquids in contact with low energy polymers. Since the test liquid and polymer probably have different critical temperatures (T_c), the temperature where $\gamma_{LV} = 0$, there should be an intermediate temperature where $(\gamma_{LV})_P = \gamma_{LV}$. When this condition is fulfilled, $\theta = 0$.

From the critical temperatures of low molecular weight n-hydrocarbons, it was estimated[7] that T_c of polyethylene is 1031°K, considerably higher than any of the polar liquids included in this study. A similar value of T_c is expected for polypropylene based on the work of Frisch and Rogers.[8] Therefore, at some temperature below the T_c of the polymer, assuming no polymer degradation, $\theta = 0$. However, wettability studies have been confined generally to low temperatures, well below the T_c of both liquid and polymer, but, as shown in Table I, there is a general trend to a lower value of θ as T increases.

(7) H. Schonhorn, *Makromol. Chem.*, **93**, 262 (1966).

(8) H. L. Frisch and C. E. Rogers, Jr., *J. Polymer Sci.*, **C12**, 297 (1966).

Solvent Effects in the Proton Chemical Shifts of Acetonitrile and Malononitrile[1]

by Taku Matsuo and Yasushi Kodera

Department of Organic Synthesis, Faculty of Engineering, Kyushu University, Hakozaki, Fukuoka-Shi, Japan

(Received July 18, 1966)

Since the original suggestion of the "reaction field theory"[2] and its experimental application to the proton chemical shifts of acetonitrile in various solvents,[3] the Buckingham formula has been widely used in the investigation of the polar effect of solvent on the chemical shift of solute molecule. Buckingham's formula gives the change in nuclear screening constant of a proton held by an X–H bond in terms of the reaction field R of the media in the form

(1) Contribution No. 111 from the Department of Organic Synthesis, Faculty of Engineering, Kyushu University.

(2) A. D. Buckingham, *Can. J. Chem.*, **38**, 300 (1960).

(3) A. D. Buckingham, T. Schaefer, and W. G. Schneider, *J. Chem. Phys.*, **32**, 1227 (1960).

$$\Delta\sigma = -2 \times 10^{-12}R \cos\theta - 10^{-18}R^2 \qquad (1)$$

where θ is the angle between the X–H bond and the reaction field vector $\bar{R}$. However, a number of examples have been known not to follow the above equation. Many criticisms have been made in this connection, as summarized in the paper by Becconsall and Hampson.[4] Some of the most important problems involved are (1) the point-dipole approximation for the solute molecule and (2) the assumption of homogeneous continuum of dielectric media as the model of solution.

In the present experiment, the solvent effects on the proton chemical shifts of acetonitrile and malononitrile are compared, and the appropriateness of the above two assumptions was examined.

Experimental Section

Acetonitrile and other various solvents of reagent grade were purchased from Wako Pure Chemical Industry Ltd. and were purified by the standard procedure for each. Extreme care was taken to prevent contamination by any impurities that would disturb the experiment. *n*-Hexane, carbon tetrachloride, chloroform, and benzene were easily purified to various spectroscopic qualifications. Acetonitrile, dioxane, acetone, and dimethyl sulfoxide (DMSO) were also free from any impurities except a trace of water (much less than the solute used in the experiment). However, since the data in these polar solvents were hardly affected by the further addition of a small amount of water, the initial values were concluded to represent the true status in the respective solvents. Malononitrile was either purchased from Tokyo Kasei Chemical Industry Ltd. or synthesized from ethyl cyanoethanoate and were purified by vacuum distillation before use. The chemical shifts were measured by the use of a Varian A-60 spectrometer with TMS signals as the internal reference. The concentrations of the solutions were approximately 0.5 *M*, except for malononitrile in carbon tetrachloride and benzene, where the solute was hardly soluble and the saturated solutions (less than 0.1 *M*) were used in the experiments.

Results and Discussion

The chemical shifts of acetonitrile and malononitrile thus obtained are summarized in Table I where the dielectric constants of the solvents are also included.

On the basis of dipole moments of acetonitrile (3.94 D.) and malononitrile (3.56 D.), the reaction field for the proton of the former is expected to be almost the same as that for the latter when the value is estimated from the Onsager model

$$R = \frac{(2\epsilon - 1)(n^2 - 1)}{3(2\epsilon + n^2)} \frac{M}{\alpha} \qquad (2)$$

Table I: The Chemical Shifts of Acetonitrile and Malononitrile in Various Solvents (cps)[a]

Solvent	Dielectric constant (20°)	Aceto-nitrile	Malono-nitrile
n-Hexane	(1.89)	109.5	...
Carbon tetrachloride	(2.24)	119.6	209.2
Chloroform	(4.81)	119.7	215.5
Acetonitrile	(38.8)	118.1	226.7
Dioxane	(2.21)	118.2	228.1
Acetone	(21.4)	123.1	253.8
DMSO	(45)	126.3	264.4
Benzene	(2.28)	47.3	85.5

[a] The shifts are measured from the internal TMS signal taking the low-field shift as the positive value. The accuracy of measurement is 0.5 cps.

In this expression, n, M, α, and ϵ represent the refractive index, the electric dipole moment, the polarizability of the solute, and the dielectric constant of medium, respectively. Then the point-dipole approximation combined with eq 1 indicates that the proton chemical shift of malononitrile should be affected by the use of polar solvent to almost the same extent as that of acetonitrile. The data in Table I show, however, that the chemical shift of malononitrile is much more strongly dependent on the polarity of solvent than that of acetonitrile. The difference in the chemical shift of malononitrile between the solutions in carbon tetrachloride and in DMSO amounts to 55 cps in comparison with 7 cps in the case of acetonitrile. Clearly, the situation cannot be explained by the simple reaction field theory as described above. The largest difference between acetonitrile and malononitrile is the number of cyano groups which are highly electronegative in nature. Then a better understanding may be made by considering the specific solvation in the close neighborhood of the solute molecule.

In a microscopic model, the lone-pair electrons of polar solvent molecules are considered to be weakly associated with the effectively positive carbon atom of the cyano group to avoid the electron-rich nitrogen atom. Such specific solvation brings about a considerable change in the electromagnetic environment of the proton closer to the cyano group than otherwise. On the other hand, however, neither preferential association nor repulsion is expected between any parts of a polar solvent and TMS molecules. Then the data in Table I should be taken as the difference in the solvent shifts between TMS and the solute molecule caused by

(4) J. K. Becconsall and P. Hampson, *Mol. Phys.*, **10**, 21 (1965).

the respective mode of solvation as above. The larger the number of cyano groups or the amount of positive charge around the nearby proton, the larger the effect of the solvation on the chemical shift of the proton. The relation between acetonitrile and malononitrile in Table I is in good agreement with this expectation. As to the solvent molecules, DMSO is found to give the highest degree of solvation effect among those in Table I. To be compared with this observation, DMSO is known to afford a very powerful hydrogen bonding site to the hydroxyl group of organosilanols.[5] Formation of charge-transfer complex with iodine was also reported on DMSO as a strong n donor.[6] Furthermore, Stewart, *et al.*, found the presence of strong charge-transfer interaction between DMSO and tetracyanoethylene, a typical π acceptor.[7] All of these works ascribe the strong basicity to the lone-pair electrons of oxygen of the sulfinyl group. Then it may be reasonable to suggest a kind of specific interaction between the oxygen lone-pair electrons of DMSO and the positive part of the solute molecule. This association introduces a new electric field and magnetic anisotropy due to the sulfinyl group and also causes a change in the polarization of the cyano group. In addition to that, the dispersion interaction between the proton and the surrounding solvent becomes larger under such circumstances than otherwise. Quantitative estimation of each effect cannot be made easily. However, all of these factors result in a low-field shift of the proton signals as shown in Table I. The fact that the effect of acetone is a little less than that of DMSO is interpreted as due to the less polar nature of the former in comparison with the latter. Drago and his co-workers also came to a similar conclusion from the complex behavior of the same compounds with iodine and phenol.[6] In this connection, much less solvent shift in acetonitrile solution seems odd, since both the dipole moment and the dielectric constant of this solvent are larger than those of acetone. The situation may be that the diamagnetic field along the axis of the cyano group has some compensating effect on the low-field shift caused by the association.

The effect of dioxane, carbon tetrachloride, and chloroform is not explained by the simple reaction field theory, as is obvious from the inspection of the data in Table I. The compounds of this group are characterized by the presence of easily polarizable lone-pair electrons and the absence of the unsaturated, polar functional group in the molecular structure. Then the solvent shift may be caused by the weak intermolecular interactions due to the dispersion force and others of similar nature. Attention should also be paid, in the case of dioxane, to the small but noticeable amounts of the basicity due to the lone-pair electrons. As to the effect of polar solvent on the proton chemical shift, the most important factor may be thus concluded to be the microscopic nature of polar functional groups that participated in the solvation rather than the dipole moment or the dielectric constant of the molecule as a whole.

The large diamagnetic shifts of acetonitrile and malononitrile in the benzene solutions are interpreted as the result of complex formation between the solute and the solvent molecules, in analogy to the similar study on the proton chemical shift of acetonitrile in toluene solutions.[8] Carbon tetrachloride may be chosen as the reference solvent because of both its inertness and the closeness of its dielectric constant to that of benzene. The trends for complex formation are evaluated by the differences between the shifts in benzene and in carbon tetrachloride solutions: acetonitrile (72.3 cps) and malonitrile (123.7 cps). Then the ease for malononitrile to form such a complex is found to be much higher than that for acetonitrile. Thus the cause of complex formation between benzene and the polar solutes under investigation also is anticipated to be correlated with the amounts of positive charge induced by the cyano group.

(5) J. F. Hampton, C. W. Lacefield, and J. F. Hyde, *Inorg. Chem.*, **4**, 1659 (1965).

(6) R. S. Drago, B. Wayland, and R. L. Carlson, *J. Am. Chem. Soc.*, **85**, 3125 (1963).

(7) F. E. Stewart, M. Eisner, and W. R. Carper, *J. Chem. Phys.*, **44**, 2866 (1966).

(8) J. V. Hatton and W. G. Schneider, *Can. J. Chem.*, **40**, 1285 (1962).

Diffusion of the Solutes at Trace Concentrations in the Ternary System Water–Sucrose–Mannitol at 25°

by R. Mills and H. David Ellerton[1]

Diffusion Research Unit, Research School of Physical Sciences, Australian National University, Canberra, Australia
(Received July 18, 1966)

Diffusion data have been obtained recently[2] using a Gouy diffusiometer for the ternary system water–

(1) Visiting Fellow from Department of Physical and Inorganic Chemistry, University of Adelaide, Adelaide, South Australia.

(2) H. D. Ellerton, Ph.D. Thesis, University of Adelaide, Adelaide, South Australia, 1966.

sucrose–mannitol at 25°. The diffusion equations for this system can be written in the form

$$(J_1)_v = -(D_{11})_v\frac{\partial c_1}{\partial x} - (D_{12})_v\frac{\partial c_2}{\partial x} \quad (1)$$

$$(J_2)_v = -(D_{21})_v\frac{\partial c_1}{\partial x} - (D_{22})_v\frac{\partial c_2}{\partial x} \quad (2)$$

where J_i is the flow of component i in moles/(cm² sec), D_{ii} and D_{ij}, respectively, are the main-term and cross-term diffusion coefficients with dimensions cm²/sec and c_i is the concentration of component i in moles/1000 ml. The subscript v refers to the volume-fixed frame of reference and subscripts 1 and 2 to the components sucrose and mannitol, respectively. Although the above study[2] was designed primarily to measure the cross-term diffusion coefficients, D_{ij}, which can be used to test the Onsager reciprocal relations, subsidiary information became available with regard to the main-term coefficients D_{ii}. In particular, the concentration dependence of $(D_{11})_v$ at a fixed concentration c_2 can be studied as c_1 is varied, and similarly for $(D_{22})_v$. However, the Gouy method cannot be used effectively when the concentrations of the diffusing species are very low. For example, in the former case we would like to measure the value of $(D_{11})_v$ at some concentration c_2 when c_1 is very close to zero. To supplement the Gouy data, we have therefore resorted to the diaphragm-cell method and used radiotracers to follow the diffusing species.

In addition to completing the picture of diffusion in this ternary system, these measurements, the first of their kind, serve also as a check on the accuracy of extrapolations which are often made from data at higher concentrations. Some measurements have also been made of binary diffusion in the water–sucrose and water–mannitol systems again at very low solute concentrations for comparison with extrapolations from other Gouy data.

Experimental Section

Materials. Analar grade sucrose and mannitol were obtained from the Colonial Sugar Refining Co. Ltd. of Australia and from By-Products and Chemicals Pty Ltd., Australia, respectively, and were used without further purification. Sucrose and mannitol each labeled with carbon-14 were obtained from the Radiochemical Centre, Amersham, England. The radioactive compounds were purified by adding to them carrier solutions of the inactive B.D.H. Micro-AR materials and then inducing recrystallization by the addition of ethanol and cooling. The purified crystals were separated from the mother liquid by centrifugal drainage and dried in a desiccator.

Since the Gouy experiments were run at concentrations of 0.25 and 0.50 *M* for both sucrose and mannitol, it was thought desirable to perform the tracer experiments at these same concentrations. Use was made of analytical expressions relating the density separately to the concentration and weight percentages of the solutes.[2] The solutions were then made up as exactly as possible gravimetrically with the appropriate vacuum corrections made to the weights.

Apparatus and Procedure. The apparatus and procedures for diffusion and for analysis by conductance and radioactive counting have been described in previous papers.[3-5] Two modifications should be mentioned, however. The diaphragm cell had a platinum sinter in place of the usual glass one. This sinter had a porosity about midway between M and F grade glass sinters as measured with pressure tests. It had the advantage of a high cell constant which was convenient for the measurement of slowly diffusing molecules such as sucrose and mannitol. The other change was to use a scintillator solution containing in addition to the usual constituents a small amount of methanol and ethylene glycol. The recipe for this solution has been given by Bray[6] and was used here because of greater compatibility with the higher concentrations of sucrose and mannitol.

Results

In Tables I and II, we reproduce the diffusion coefficients measured in this work together with other relevant information.[7] The reproducibility of the data

Table I: Integral Diffusion Coefficients for Water–Sucrose and Water–Mannitol at 25°

Labeled component	Concn, mole/1000 ml	$\bar{D}_v \times 10^5$, cm²/sec (obsd)	$D_v^\circ \times 10^5$, cm²/sec (from Gouy extrapolation)	Dev, %
Sucrose	0.00285	0.5250	0.5226[a]	0.45
Mannitol	0.00159	0.6703	0.6662[b]	0.6

[a] See ref 7a. [b] See ref 7b.

(3) R. Mills, *J. Phys. Chem.*, **67**, 600 (1963).
(4) J. G. Albright and R. Mills, *ibid.*, **69**, 3120 (1965).
(5) J. G. Albright, *ibid.*, **70**, 2299 (1966).
(6) G. A. Bray, *Anal. Biochem.*, **1**, 279 (1960).
(7) (a) L. J. Gosting and J. M. Morris, *J. Am. Chem. Soc.*, **71**, 1998 (1949); (b) P. J. Dunlop, *J. Phys. Chem.*, **69**, 4276 (1965).

Table II: Values of $(D_{ii})_v$ in the System Water–Sucrose–Mannitol at 25°

Labeled component	Concn of tracer, mole/1000 ml	Concn of medium, mole/1000 ml	$(D_{ii})_v \times 10^5$, cm²/sec (obsd)	$(D_{ii})_v \times 10^6$, cm²/sec (from Gouy extrapolation)	Dev, %
Sucrose	0.00281	0.25002 mannitol	0.4759	0.455[a]	4.6
Sucrose	0.00286	0.25002 mannitol	0.4751	0.455[a]	4.4
Sucrose	0.000786	0.50000 mannitol	0.4161	0.409[a]	1.7
Mannitol	0.000347	0.25003 sucrose	0.5295	0.530[a]	−0.2
Mannitol	0.000345	0.50118 sucrose	0.4461	0.427[a]	4.4

[a] See ref 2.

has a precision of order ±0.2%. The absolute accuracy is discussed in the next section.

It will be noted that the measured diffusion coefficients in Table I ($\bar{D}_v$) are not tracer-diffusion coefficients as ordinarily defined[4] but integral binary coefficients referred to a volume-fixed frame of reference. They would correspond to differential coefficients at approximately half the concentrations given in column 2. Since this concentration is very low, it is possible, therefore, to make a direct comparison with the limiting binary coefficient D_v^0.

In Table II, the measured diffusion coefficients are equated with the $(D_{ii})_v$ of eq 1 and 2. This is possible because referring to eq 1, as $c_1 \to 0$, then $D_{12} \to 0$ so that at trace concentration levels

$$(J_1)_v = -(D_{11})_v \frac{\partial c_1}{\partial x} \qquad (3)$$

In this instance $(D_{11})_v$ can be identified with the tracer-diffusion coefficient D_1^* for these systems.

Discussion

Before discussing the results for the ternary systems, it is instructive to look at the data for the binary systems water–sucrose and water–mannitol as given in Table I. It will be observed that for the sucrose case, the diaphragm-cell value is 0.45% above the Gouy limiting value, and for mannitol, it is 0.6% above. Albright and Mills[4] and Albright[5] have recently reported limiting values, derived by extrapolations of tracer-diffusion data, for the systems water–urea, water–α-alanine, and water–β-alanine. These limiting values were, respectively, 0.3, 1.3, and 0.5% above those from extrapolated Gouy data. The consistency of this positive deviation indicates either that the Gouy extrapolations are incorrect or that there is some systematic error in the diaphragm-cell measurements at these concentrations. A possible explanation for the latter eventuality may be related to surface transport. It is well known that for very dilute aqueous electrolytes

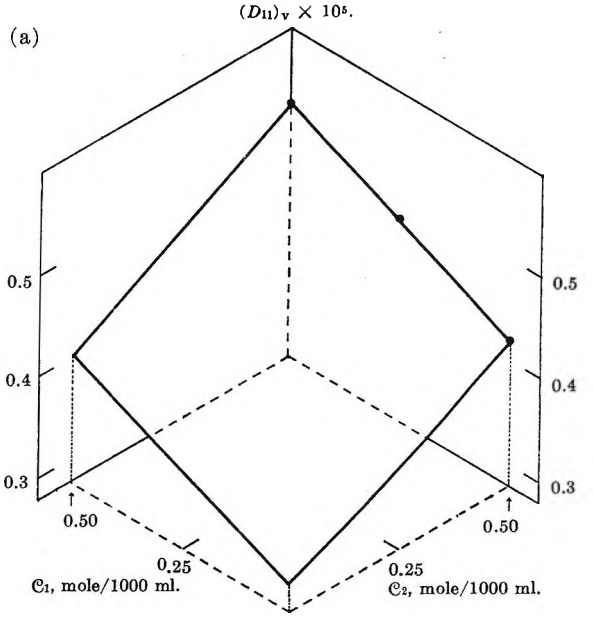

Figure 1a. Three-dimensional diagram of the $(D_{11})_v$ as functions of c_1 and c_2. Solid lines are derived from Gouy data;[2] ●, this work.

the diaphragm cell gives extrapolated coefficients up to 15% higher than the Nernst limiting values and this anomaly is commonly attributed to the formation of ionic double layers at the diaphragm surface which therefore allows another diffusion mode. It is perhaps not unreasonable to suppose that dipolar molecules are also subject to a weak adherence to the surface and the effect, which is only $^1/_{40}$ as large, seems to be about of the right order. It is also noteworthy that the effect is not evidenced with nonpolar molecules.

For the description of diffusion in ternary systems, it is convenient to use three-dimensional diagrams. Such diagrams for the $(D_{ii})_v$ coefficients in the water–sucrose–mannitol system are shown in Figure 1 (a and b). The data measured in this work are represented by the filled circles in the $(D_{11})_v$–c_2 and $(D_{22})_v$–c_1 planes.

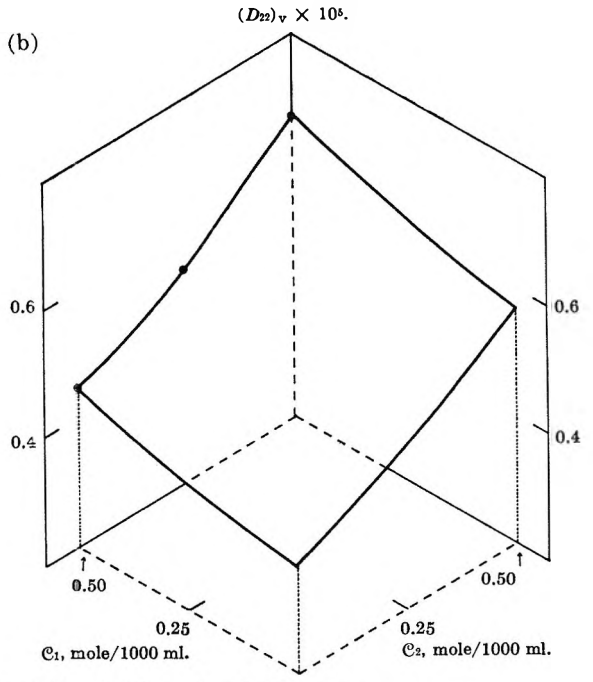

Figure 1b. $(D_{22})_v$, and as in Figure 1a.

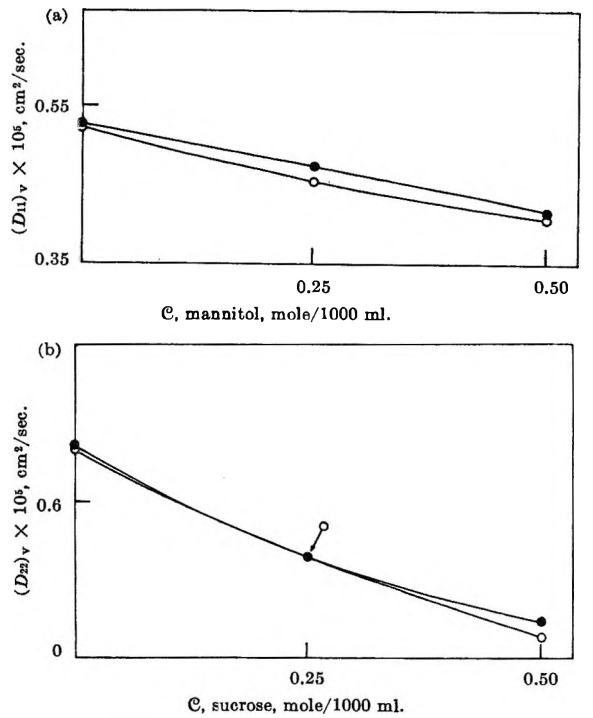

Figure 2. Details of $(D_{ii})_v$–c_j planes from Figures 1a and b: O, extrapolated Gouy data;[2] ●, this work.

In effect, the lines joining these points represent the intersections of the $(D_{ii})_v$ surfaces with these two planes. The other diffusion data represented by the solid curves in these diagrams are from ref 2 and will be published in detail shortly. Strictly speaking, the tracer values will not fall exactly in these $(D_{ii})_v$–c_j planes because, as shown in Table II, the trace solutes have very small but nevertheless finite concentrations and the coefficients have not been extrapolated to zero concentration. However, the error in using these data in the planes is quite negligible.

To compare our values with those obtained from Gouy extrapolations, we show also in Figure 2 the $(D_{11})_v$–c_2 and $(D_{22})_v$–c_1 planes in which both sets of data are graphed. In all but one case, the tracer coefficients are higher than the extrapolated ones. A fairly large discrepancy (4.5%) between the tracer value and the extrapolated Gouy value occurs for trace sucrose in a 0.25 *M* mannitol solution and for mannitol in a 0.5 *M* sucrose solution. However, reasonable agreement is found for trace sucrose in 0.5 *M* mannitol and for mannitol in a 0.25 *M* sucrose solution. In this regard, it should be emphasized that extrapolations of Gouy data of the type considered here are very approximate in nature. Only two points are available in each case; these are at relatively high concentrations and a simple linear extrapolation is used. Evidently, there is some curvature in the $(D_{ii})_v$ surfaces which is more pronounced in some regions than others. This would account for the variation in the deviations discussed above.

Gaseous Alkali–Nitrogen–Oxygen and Alkali–Phosphorus–Oxygen Compounds[1]

by Alfred Büchler and James L. Stauffer

Arthur D. Little, Inc., Cambridge, Massachusetts
(Received July 29, 1966)

The vaporization of alkali nitrates and nitrites has been recently reported by Hardy and Field.[2] On the basis of the low volatility of these compounds, Hardy and Field suggested that they should be ionic rather than covalent. This conclusion contrasts with that of Butkov and Tschassowenny,[3] who found that the electronic spectrum of gaseous KNO_3 resembled that of covalent nitrato compounds (such as methyl nitrate)

(1) This work was supported by the U. S. Army Research Office, Contract No. DA-19-020-ORD-5584, ARPA Order No. 40-62, with funds provided by the Advanced Research Projects Agency.

(2) C. J. Hardy and B. O. Field, *J. Chem. Soc.*, 5130 (1963).

(3) K. Butkov and V. Tschassowenny, *Acta Physicochim. URSS*, 5, 137 (1936).

rather than that of the nitrate ion. A tendency to form dimers and higher polymers is characteristic of gaseous compounds such as the alkali halides and hydroxides,[4] which are commonly considered ionic. We therefore undertook a mass-spectrometric examination of lithium and sodium nitrate and nitrite vapors to find whether polymers are present in these systems also. In an extension of this work, the mass spectrum of the vapor in equilibrium with lithium phosphate was also examined.

Experimental Section

The mass spectrometer used in this work was a Nuclide Associates 12-in. radius, 60°-sector magnetic deflection, high-temperature instrument. Commercial samples of the various compounds were used, lithium nitrite being obtained from A. D. Mackay, New York, N. Y. All samples were dried under vacuum for 1 week at 100°. The dried samples were placed in nickel effusion cells which were heated by radiation. A movable shutter discriminated between gaseous species entering the mass spectrometer directly from the effusion cell and those present as background gases. Temperatures were measured with platinum—platinum–10% rhodium thermocouples.

Results

Typical mass spectra for the four systems are shown in Table I. In each case large amounts of permanent gases were given off. For the nitrates the principal gaseous decomposition product was O_2, whereas in the case of the nitrites roughly equal amounts of NO and N_2 were given off. In addition, each of the mass spectra contains ions of the type M^+, MX^+, and M_2X^+, where M = Li or Na and X = NO_3 or NO_2. Such mass spectra are typical of the alkali halides and pseudohalides, and immediately indicate the presence of the dimers $Li_2(NO_3)_2$, $Na_2(NO_3)_2$, $Li_2(NO_2)_2$, and $Na_2(NO_2)_2$. For the two nitrates and sodium nitrite, the ratio MX^+/MX_2^+ varied with temperature, thus indicating that the monomers $LiNO_3$, $NaNO_3$, and $NaNO_2$ were also present. Because of the high pressure in the crucible and the changing composition of the sample, it was, however, impossible to obtain heats of vaporization from log (partial pressure) *vs.* reciprocal temperature plots for these species. In the case of the two nitrates, monomer and dimer appear to be present in approximately equal amounts. In the case of sodium nitrite, the dimer is the principal species. For lithium nitrite, the ratio $LiNO_2^+/Li_2NO_2^+$ was independent of temperature, indicating that $LiNO_2^+$ is largely the result of the dissociative ionization of $Li_2(NO_2)_2$. If we assume an $Li_2(NO_2)_2$ pressure between 10^{-6} and 10^{-8} atm, a dimerization entropy of 40 eu,[5] and a monomer:dimer ratio of 1:100 at 700°K, one obtains a dimerization energy ranging from 61 to 67 kcal/mole for $Li_2(NO_2)_2$. These values compare well with the dimerization energies of LiF (61.3 kcal)[6,7] and $LiBO_2$ (67 kcal).[8]

Table I: Mass Spectra of Vapor above Lithium and Sodium Nitrate and Nitrite (I^+ = Ion Intensity in Arbitrary Units)

$LiNO_3$, 670°K			$NaNO_3$, 750°K		
Ion	I^+(shutter)	I^+(total)	Ion	I^+(shutter)	I^+(total)
O_2^+	16	75	O_2^+	300	1200
NO^+	11	90	NO^+	15	1000
N_2^+	...	20	N_2^+	...	240
NO_2^+	8		NO_2^+	0.6	
Li^+	1.3		Na^+	4.6	
$LiNO_3^+$	0.4		$NaNO_3^+$	0.18	
$Li_2NO_3^+$	0.11		$Na_2NO_3^+$	0.11	
$LiNO_2^+$	0.05		$NaNO_2^+$	0.06	
$Li_2NO_2^+$	0.008		$Na_2NO_2^+$	0.06	
$LiNO_2$, 695°K			$NaNO_2^+$, 690°K		
Ion	I^+(shutter)	I^+(total)	Ion	I^+(shutter)	I^+(total)
NO^+	400	3000	NO^+	~50	3000
N_2^+	...	2760	N_2^+	~50	2300
O_2^+	1.5	90	O_2^+	...	Small
NO_2^+	8.6		Na^+	5.2	
Li^+	3.6		$NaNO_2^+$	0.1	
$LiNO_2^+$	0.06		$Na_2NO_2^+$	0.3	
$Li_2NO_2^+$	0.28				

The existence of gaseous nitrates and nitrites suggested the possible existence of the corresponding metaphosphates and metaphosphites. The mass spectrum of the vapor above liquid Li_3PO_4 was therefore examined. The result is shown in Table II. In addition to decomposition products such as $P_2(g)$ and $Li_2O(g)$, a significant amount of lithium metaphosphite, $LiPO_2(g)$, was found, together with a much smaller amount of lithium metaphosphate, $LiPO_3(g)$.

Discussion

The gaseous nitrate and nitrite species reported here

(4) S. H. Bauer and R. F. Porter in "Molten Salt Chemistry," M. Blander, Ed., Interscience Publishers, Inc., New York, N. Y., 1964, p 607.

(5) For $LiBO_2$, a dimerization entropy of 37 eu may be calculated from the experimental data of D. L. Hildenbrand, W. F. Hall, and N. D. Potter, *J. Chem. Phys.*, **39**, 296 (1963), and A. Büchler and J. B. Berkowitz-Mattuck, *ibid.*, **39**, 286 (1963). For a nonlinear LiOH, a dimerization entropy of 39 eu was estimated by J. Berkowitz, D. J. Meschi, and W. A. Chupka, *ibid.*, **33**, 533 (1960).

(6) J. Berkowitz, H. A. Tasman, and W. A. Chupka, *ibid.*, **36**, 2170 (1962).

(7) A. Büchler and J. L. Stauffer in "Thermodynamics," Proceedings of a Symposium, Vienna, 1965, Vol. I, International Atomic Energy Agency, Vienna, 1966, p 271.

(8) A. Büchler and J. B. Berkowitz-Mattuck, *J. Chem. Phys.*, **39**, 286 (1963).

Table II: Mass Spectrum of Vapor above Li_3PO_4 at 1400°K

Ion	Rel intensity
P_2^+	100
$LiPO_2^+$	12
Li^+	12
P^+	7
PO^+	1.7
Li_2O^+	0.7
$LiPO_3^+$	0.3

—$LiNO_3$, $Li_2(NO_3)_2$, $Li_2(NO_2)_2$, $NaNO_3$, $Na_2(NO_3)_2$, $NaNO_2$, and $Na_2(NO_2)_2$—are typical of the vapor species associated with the vaporization behavior of halides and pseudohalides; the dimerization energy of $LiNO_2$ derived above also is typical of such compounds. To that extent, the present work supports Hardy and Field's suggestion[2] as to the ionic nature of the gaseous alkali nitrates and nitrites. Against this must be placed the results of Butkov and Tschassowenny[3] and the recent electron-diffraction work of Khodchenkov, Spiridonov, and Akishin,[9] which suggest a covalent structure. Further work would seem to be necessary to classify the nature of bonding in the alkali nitrates and nitrites. In particular, vibrational spectra, which permit a clear differentiation between ionic nitrate and covalent nitrato groups,[10] would be highly desirable.

(9) A. N. Khodchenkov, V. P. Spiridonov, and P. A. Akishin, *Zh. Strukt. Khim.*, 6, 765 (1965).

(10) C. C. Addison and N. Logan, *Advan. Inorg. Chem. Radiochem.*, 6, 72 (1964).

The Chain Decomposition of Propane Initiated by Vacuum Ultraviolet Photolysis

by A. H. Laufer and J. R. McNesby

Institute for Basic Standards, National Bureau of Standards, Washington, D. C. *(Received June 20, 1966)*

One of the more striking features of the photolysis of mixtures of C_3H_8 and C_3D_8 at 1470 A and 25° is that the methane product is more than 90% $CH_4 + CD_4$.[1] This certainly signifies that the dominant mode of methane formation is molecular elimination from excited propane rather than abstraction of hydrogen from propane by methyl radicals. At 25°, a minor contribution of methyl radicals to methane formation is demonstrated by the appearance of CD_3H. The reactions leading to methane formation are

$$C_3H_8 \longrightarrow CH_4 + C_2H_4 \quad (1)$$

$$C_3D_8 \longrightarrow CD_4 + C_2D_4 \quad (2)$$

$$CD_3 + C_3H_8 \longrightarrow CD_3H + C_3H_7 \quad (3)$$

$$CD_3 + C_3D_8 \longrightarrow CD_4 + C_3D_7 \quad (4)$$

$$CH_3 + C_3H_8 \longrightarrow CH_4 + C_3H_7 \quad (5)$$

$$CH_3 + C_3D_8 \longrightarrow CH_3D + C_3D_7 \quad (6)$$

where C_3D_7 and C_3H_7 may be *n*-propyl or isopropyl. It will be seen in the Results section that about 80% of the methanes formed by mechanisms other than molecular elimination come from abstraction reactions 3–6 and only 20% from disproportionation of methyl and ethyl. The latter mechanism has, therefore, been neglected. The ratios CH_4'/CH_3D' and CD_3H'/CD_4', where the prime signifies the rate of formation, are given by

$$\frac{CH_4'}{CH_3D'} = \frac{\Phi_1 I_1}{k_6[CH_3][C_3D_8]} + \frac{k_5[C_3H_8]}{k_6[C_3D_8]} \quad (7)$$

$$\frac{CD_3H'}{CD_4'} = \frac{\dfrac{k_3[C_3H_8]}{k_4[C_3D_8]}}{\dfrac{\Phi_2 I_2}{k_4[CD_3][C_3D_8]} + 1} \quad (8)$$

where I_1 and I_2 are the rates at which light is absorbed by C_3H_8 and C_3D_8, respectively, and Φ_1 and Φ_2 are the quantum yields for molecular elimination of methane and methane-d_4. Under conditions where $k_6[CH_3]\cdot[C_3D_8] \gg \Phi_1 I_1$ and $k_4[CD_3][C_3D_8] \gg \Phi_2 I_2$, eq 7 and 8 become

$$\frac{CH_4'}{CH_3D'} = \frac{k_5[C_3H_8]}{k_6[C_3D_8]} \quad (9)$$

$$\frac{CD_3H'}{CD_4'} = \frac{k_3[C_3H_8]}{k_4[C_3D_8]} \quad (10)$$

It is known that the activation energies corresponding to k_4 and k_6 are in the range 11.1–12.5 kcal/mole depending upon whether the secondary or primary D atom is abstracted.[2] If the quantities $\Phi_1 I_1$ and $\Phi_2 I_2$ are assumed to be essentially independent of temperature, the conditions required for eq 9 and 10 to be valid will be approached by increasing the temperature. The chain is propagated by the decomposition of *n*-propyl formed in reactions 3–6.

(1) H. Okabe and J. R. McNesby, *J. Chem. Phys.*, 37, 1340 (1962).

(2) W. M. Jackson, J. R. McNesby, and B. deB. Darwent, *ibid.*, 37, 1610 (1962).

$$n\text{-}C_3H_7 \longrightarrow CH_3 + C_2H_4 \qquad (11)$$

The objective of this work is to estimate the chain length of propane decomposition well below pyrolysis temperatures.

Experimental Section

The vacuum system was of the conventional type with the exception that all valves in the gas-handling system were of Viton and Pyrex and no absorption of hydrocarbon products or reactants was experienced. The Xe resonance lamp was ring-sealed into the reaction cell and the LiF window was sealed onto the lamp envelope by means of a silver–silver chloride graded seal as previously described.[3] Absorbed light intensities were about 10^{14} quanta cc^{-1} sec^{-1} at 1470 A. The reaction mixture was circulated continuously to prevent accumulation of reaction products near the window. After photolysis the reaction mixture was sampled for chromatographic analysis (10 m of 30% Squalane on Celite and flame ionization detection), and finally the condensibles were frozen out and the volatile methane–hydrogen fraction was allowed to expand into an evacuated sample flask. This fraction was analyzed by mass spectrometry. Control experiments were done to ensure the absence of any mechanism in the procedure for fractionating reaction products. Cracking patterns of authentic samples of the isotopic methanes were measured in separate experiments. The maximum impurity in the propane and in the C_3D_8 was 0.02% and no detectable methane or hydrogen was present. Photolysis of C_3D_8 alone was done at all temperatures to assess the contribution to CD_3H of incompletely deuterated propane impurities. Corrections were made for this contribution prior to entering the data in Table I. Temperatures were controlled automatically to ±3°.

Results and Discussion

It has been shown[2] that within experimental error CH_3 and CD_3 abstraction reactions exhibit the same kinetic parameters and $k_5/k_6 = k_3/k_4 = 1.04 \exp(1400/RT)$. It follows that when the conditions for the validity of eq 9 and 10 are met

$$CH_4'/CH_3D' = CD_3H'/CD_4' = 1.04 \exp(1400/RT) \qquad (12)$$

Thus, the Arrhenius plot of eq 12 should be approached asymptotically both by CH_4'/CH_3D' and CD_3H'/CD_4' as the temperature is raised. Temperatures sufficiently high to demonstrate this point were not achieved because of failure of the LiF–Ag–AgCl seals around 400°. However, Figure 1 shows the experimental points approaching the expected straight line defined by eq 12.

Table I: Product Analysis in the Photolysis of 1:1 Mixtures[a] of Propane and Propane-d_8

	Analysis			
	25°	150°	248°	320°
H_2	100.0	100.0	100.0	100.0
HD	20.4	30.3	34.2	31.0
D_2	57.5	42.0	38.6	28.6
CH_4	10.40	9.68	24.3	54.0
CH_3D	0.11	0.82	3.07	15.0
CH_2D_2	0.62	0.13	1.56	0.05
CD_3H	1.33	3.14	8.06	17.5
CD_4	6.32	4.92	8.86	9.95
Ethane	14.5	...	15.3	14.5
Ethylene	30.5	...	51.0	96.9
Acetylene	7.4	...	5.1	0
Propylene	61.0	...	...	...

[a] Total pressure, 22.0 torr.

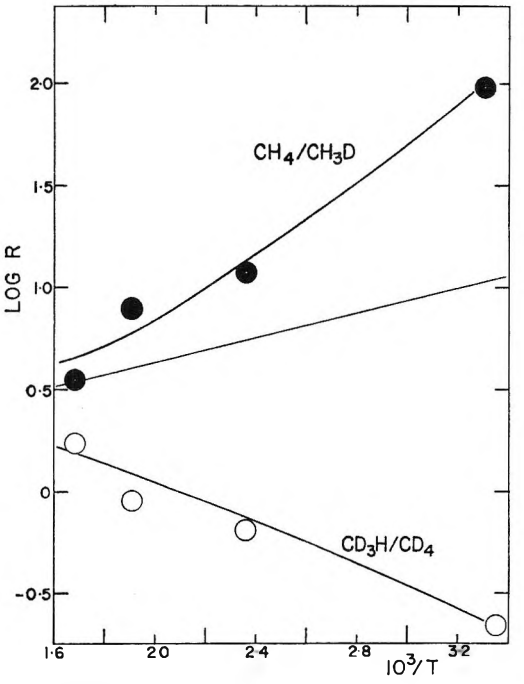

Figure 1. Variation of methane isotope analysis with temperature (below the figure). The straight line is the relationship predicted for a pure methyl radical mechanism.

The assumptions made in the following argument result in a lower limit for the chain length. The figures used are relative numbers of molecules. From experiments on the photolysis of $CH_3CD_2CH_3$ at room temperature and 1470 A, it can be estimated that an

3) R. F. Hampson, Jr., and J. R. McNesby, *J. Chem. Phys.*, **42**, (2200 (1965).

upper limit of one-third of the ethane is formed by association of methyl radicals.[1] Thus, reference to Table I (25° run) shows that of the 14.5 ethanes formed, a maximum of 5 ethanes arises from association of 10 methyl radicals. Since equal amounts of methyl and ethyl are formed in primary processes 13 and 14 and assuming the ethyl radical does not decompose (up to 350°, hydrogen atom formation from ethyl radical decomposition has been shown[3,4] to be

$$C_3H_8 \longrightarrow CH_3 + C_2H_5 \quad (13)$$

$$C_3D_8 \longrightarrow CD_3 + C_2D_5 \quad (14)$$

a relatively minor process), random association of methyl and ethyl requires that 10 additional methyl radicals must have disappeared by association with ethyl. Thus 20 methyl radicals disappear by association. Disproportionation of methyl and ethyl is only 6% as important as association[5,6] and only 0.6 methane is formed by disproportionation and 2.4 methanes are formed by abstraction of H and D. This includes CD_3H and CH_3D as well as that part of the CH_4 and CD_4 arising from methyl radical abstraction (obtained from eq 12). Thus a total of 23 methyl radicals must have been formed. Since D atom formation up to 350° is relatively unimportant,[3,4] it is safe to assume that at 320° the D_2 product is still almost entirely attributable to molecular elimination.

The D_2 is chosen as the monitor rather than H_2 since the fraction of D_2 arising from D atom abstraction reactions must be much smaller than the fraction of H_2 arising from H atom reactions because of the kinetic isotope effect. The number of methyl radicals (based on $D_2 = 57.5$) equals $(57.5/28.6) \times 90 \cong 181$. In this calculation it is estimated (again on the basis of eq 12) that 90 of the 96 methane molecules arise from methyl radicals. If the average chain length is defined as the number of methyl radicals that form methane divided by the number formed in the primary process, the result is that the average chain length is 181/23 = 7.9 at 320°.

The chain lengths at 25, 150, 248, and 320° are approximately 0.07, 0.54, 2.2, and 7.9. Since the chain termination is effected by free-radical association reactions, the chain length is a function of the light intensity, and the present conclusions are valid for light intensity of about 10^{14} quanta/cc^{-1} sec^{-1}.

(4) S. Bywater and E. W. R. Steacie, *J. Chem. Phys.*, 19, 326 (1951).
(5) P. Ausloos and E. W. R. Steacie, *Can. J. Chem.*, 33, 1062 (1955).
(6) C. A. Heller, *J. Chem. Phys.*, 28, 1255 (1958).

Electron-Acceptor Properties of Mellitic Trianhydride

by H. M. Rosenberg, E. Eimutis, and D. Hale

Air Force Materials Laboratory, Research and Technology Division, Wright-Patterson Air Force Base, Ohio *(Received July 25, 1966)*

The following equation, proposed by McConnell, Ham, and Platt,[1] is generally applicable for describing

$$E_\pi = I_D - E_A - W \quad (1)$$

the energy of the charge-transfer (CT) transition of π complexes as a function of the ionization potential of the donor (I_D) and electron affinity of the acceptor (E_A). W is a collective term which includes all other energy interactions arising principally from solvation and coulombic attraction and is essentially constant for a similar series of π complexes.

Electron affinities are directly proportional to the Hammett σ_p of the substituents of *p*-benzoquinone.[2] Increasing the number of electron-withdrawing substituents enhances the electron affinity, although this effect does not appear to be simply additive but is dependent on the positions of substitution.[3]

It has been noted that substituents with $\sigma_p > 0.60$ (CN, 0.66; NO_2, 0.78) are particularly effective in CT acceptors.[3] Since σ constants for disubstituents, in general, have not been evaluated, the properties of functional groups such as cyclic anhydrides must be determined experimentally. A comparison of the electron affinities of pyromellitic dianhydride and 1,2,4,-5-tetracyanobenzene reveals that the cyclic anhydride group is more effective than two adjacent cyano groups.[3] It is therefore not surprising that pyromellitic dianhydride complexes have been actively investigated,[4] although the complexes of mellitic trianhydride have been neglected since their initial observation by Mustafin.[5]

All complexes were prepared by adding appropriate amounts of donor to saturated solutions of mellitic trianhydride in chloroform. Spectroscopic data were obtained on a Cary Model 11 recording spectrophotom-

(1) H. McConnell, J. S. Ham, and J. R. Platt, *J. Chem. Phys.*, 21, 66 (1953).
(2) P. R. Hammond, *J. Chem. Soc.*, 471 (1964).
(3) A. R. Lepley and J. R. Thelman, *Tetrahedron*, 22, 101 (1966).
(4) L. I. Ferstandig, W. G. Toland, and C. D. Heaton, *J. Am. Chem. Soc.*, 83, 1151 (1961); Y. Nakayama, Y. Ichikaw, and T. Matsuo, *Bull. Chem. Soc. Japan*, 38, 1674 (1965); T. Matsuo, *ibid.*, 38, 2110 (1965).
(5) I. S. Mustafin, *J. Gen. Chem. USSR*, 17, 560 (1947).

Table I: Charge-Transfer Energies of Pyromellitic Dianhydride and Mellitic Trianhydride with Aromatic Hydrocarbon Donors[a]

Donor	E_π, ev PMDA	E_π, ev MTA	ΔE_π,[b] ev
Naphthalene	3.01	2.74	0.27
Anthracene	2.40	2.10	0.30
Phenanthrene	3.07	2.74	0.33
Acenaphthene	2.66	2.35	0.31
Pyrene	2.46	2.10	0.36
Fluorene	2.91	2.56	0.35
2-Methylnaphthalene	2.91	2.63	0.28
1,8-Dimethylnaphthalene	2.70	2.46	0.24
1-Chloronaphthalene	3.07	2.71	0.36
1-Bromonaphthalene	3.05	2.70	0.35
2-Methylanthracene	2.33	2.08	0.25
		Av	0.31 ± 0.04

[a] In chloroform solution. [b] $E_\pi^{PMDA} - E_\pi^{MTA}$.

eter, equipped with a four-place digital voltmeter. The wavelength maxima were determined to a precision of ±2 mμ using 5-cm matched silica cells with solvent as reference. All complexes gave typical broad structureless charge-transfer absorption bands.

We report in Table I the charge-transfer energy at wavelength of maximum absorption for a series of mellitic trianhydride–aromatic hydrocarbon complexes. These are compared with pyromellitic dianhydride complexes having the same donors and the differences in charge-transfer energy for both series shown in the table.

From eq 1, assuming W to be constant for complexes having the same donor, we get

$$E_\pi^{PMDA} - E_\pi^{MTA} = E_A^{MTA} - E_A^{PMDA} \quad (2)$$

The electron affinity of mellitic trianhydride is shown to be 0.31 ± 0.04 ev higher than that of pyromellitic dianhydride. Hence, its electron affinity is 1.17 based on the reported value of 0.86 ev for pyromellitic dianhydride.[6] Since the electron affinity of phthalic anhydride is 0.1,[6] it is seen that consecutive addition of cyclic anhydride substituents to phthalic anhydride does not yield a uniform increase in electron affinity, the first addition being considerably more effective than the second addition.

(6) G. Briegleb, *Angew. Chem.*, **76**, 326 (1964).

COMMUNICATIONS TO THE EDITOR

The Ultraviolet Spectrum of Trimethylborane and the Ethylene Problem

Sir: The spectra of small molecules are of considerable interest as they provide a testing ground for theoretical and empirical calculations of spectroscopic properties.

Attempts[1] have been made to obtain the ultraviolet spectrum of trimethylborane, and the observation of rising end absorption in the 225-mμ region has been interpreted as indicating an absorption maximum in the region of 220–230 mμ. We have previously suggested[2] that the 220–230-mμ transition observed[1b] in the spectra of tributylboranes was a charge-transfer transition from a delocalized σ orbital to boron, whose transition energy should be proportional to the ionization potential of the hydrocarbon. We would therefore expect this charge-transfer transition of alkylboranes to move to higher energies with increasing hydrocarbon ionization potential.

We have recently measured the ultraviolet spectrum of trimethylborane between 4000 and 1770 A (Figure 1). There are clearly two different band systems, at energies substantially lower than the Rydberg transitions observed for methane, which cannot therefore be assigned to analogous transitions in the methyl group. At 1770 A we see the beginning of the transition reported in earlier qualitative unpublished results by Goodman and Love.[3] This transition, $\lambda_{max} \approx 1750$ A, 7.1 ev, log $\epsilon \approx 2.9$, we have previously assigned to

(1) (a) J. Rosenbaum and M. Symons, *Proc. Chem. Soc.*, 92 (1959); (b) A. G. Davies, D. Hare, and L. Larkworthy, *Chem. Ind.* (London), 1519 (1959); (c) H. Jaffe and M. Orchin, "Theory and Applications of Ultraviolet Spectroscopy," John Wiley and Sons, Inc., New York, N. Y., 1962, p 455.

(2) B. G. Ramsey, *J. Phys. Chem.*, **70**, 611 (1966).

the hyperconjugative $n_B \leftarrow \pi_{CH}$ transition in which an electron is promoted from a C–H σ bond to the empty p_z orbital of boron. Previous calculations[2] using a charge-transfer model predicted an energy of 7 ev for this transition. A simple Hückel calculation using the empirical heteroatom model[4,5] of the methyl group as an electron pair donor and a spectroscopic resonance integral of 2.37 ev also suggests a transition energy of some 7 ev for the $n_B \leftarrow \pi_{CH}$ transition. Comparison of the molar extinction coefficients for the 225-mμ transitions of the tributylboranes (log ϵ = 2.4) with that of trimethylborane also supports the correlation of these bands.[6]

Figure 1. The ultraviolet spectrum of $(CH_3)_3B$ at 33 and 6 mm pressure; 5-cm path length CaF_2 cells.

In addition, however, to the $n_B \leftarrow \pi_{CH}$ charge-transfer transition there are the possible transitions from the B–C filled σ orbitals to the boron p_z orbital which must be considered; under D_{3h} symmetry, these are the allowed $A_2'' \leftarrow A_1$ and the forbidden $E'' \leftarrow A_1$ transitions.[7] We believe the weak bands found in the trimethylborane spectrum between 2250 and 1950 A (log $\epsilon \approx 1.7$) may be assigned to the $n_B \leftarrow \sigma_{B-C}$ transitions.

The importance of the above assignment with respect to the weak 2000-A region absorption characteristic of alkenes is obvious. This alkene absorption, which has received a variety of assignments, has most recently been ascribed to either[8] a $\sigma^* \leftarrow \pi$ or a $\pi^* \leftarrow \sigma$ transition[9] analogous to the $\pi^* \leftarrow$ n transition of the carbonyl group.

It should be recognized the boron empty p_z orbital is an excellent model both in symmetry and energy[5] for the antibonding π^* orbital of an alkene. The observation, therefore, of a weak transition in the trimethylborane spectrum which may be correlated with similar transitions in the spectra of alkenes and carbonyls we feel provides strong support for the Berry[9] $\pi^* \leftarrow \sigma_{C-R}$ assignment in alkene spectra rather than the $\sigma^* \leftarrow \pi$ assignment[8] which is necessarily absent in trimethylborane.

Additional consequences of these results are the possible assignment of the observed very weak transitions at 2140 and 2160 A in the spectrum of the methyl radical[9,10] to an $n_C \leftarrow \sigma_{CH}$ transition and the expectation of such a transition in the spectra of the isoelectronic carbonium ions. The $n_C \leftarrow \sigma_{C-C}$ transition of a carbonium ion is expected in the near-infrared or visible region of the spectrum, depending on assumptions made about the columb integral of the C^+ empty p_z carbon atomic orbital.

Spectra were taken using CaF_2 5-cm gas cells on a Model 350 Perkin-Elmer spectrometer after several hours of flushing with dry nitrogen. Spectra were recorded at slow scanning speeds and are not reported beyond the wavelength at which maximum slit opening occurs. We therefore feel certain that we are not observing a false maximum at 1770 A.

Acknowledgment. We wish to acknowledge the support of the Research Corp. and to thank Dr. Peter Love[3] for providing the trimethylborane used in this research.

(3) Several years ago, L. Goodman and P. Love (private communication, Pennsylvania State University) obtained a preliminary spectrum of $(CH_3)_3B$ to wavelengths below 1700 A. They recorded no absorption above 2100 A and the center of gravity of a broad featureless band near 1750 A. Unfortunately the original spectrum itself has been misplaced and is unavailable for comparison. For method of synthesis and purification of $(CH_3)_3B$, see P. Love, *J. Chem. Phys.*, 39, 3044 (1963).

(4) F. A. Matsen, *J. Am. Chem. Soc.*, 72, 5243 (1950).

(5) A. Streitwieser, Jr., "Molecular Orbital Theory for Organic Chemist," John Wiley and Sons, Inc., New York, N. Y., 1961, p 133.

(6) Preliminary spectra of triisopropylborane lend additional support for the CT nature of the more intense transition, in that the onset of the transition is found at 192 mμ, a red shift in keeping with the lower ionization potential of propane compared with that of methane. The weaker transition remains in the 200–220-mμ region.

(7) A. D. Walsh, *J. Chem. Soc.*, 2296 (1953).

(8) M. B. Robin, R. R. Hart, and N. A. Kuebler, *J. Chem. Phys.*, 44, 1803, 2664 (1966).

(9) R. S. Berry, *ibid.*, 38, 1934 (1963).

(10) G. Herzberg and J. Shoosmith, *Can. J. Phys.*, 34, 523 (1956).

DEPARTMENT OF CHEMISTRY
UNIVERSITY OF AKRON
AKRON, OHIO 44304
B. G. RAMSEY

RECEIVED SEPTEMBER 6, 1966

The Θ Condition for Random and Block Copolymers of Styrene and Methyl Methacrylate

Sir: The concepts of the Θ condition for (homo)-polymer solutions have been fully established by Flory.[1] In short, the Θ condition is that at which excess chemical potential is zero and deviations from ideality vanish. Consequently, the osmotic second virial coefficient A_2 becomes zero, and the polymer chain assumes a random flight configuration, its dimension being determined solely by the short-range interactions. Our primary concern in this study is to find out whether these concepts may stand valid for solutions of random and block copolymers as well.

For the present purpose, we selected random and block copolymers of styrene (ST) and methyl methacrylate (MMA); the former is a low conversion product by free-radical polymerization method, while the latter is of (PMMA–PST–PMMA) type prepared by an anionic polymerization technique.[2] To answer the above questions, first we have to find Θ solvents, preferably pure ones, for the ST–MMA copolymers, to which, as far as we are aware, only cyclohexanol has been reported as a pure Θ solvent.[3] Varieties of other solvents were examined and a few of them have been found to be promising. They are (i) cyclohexanol (CHL) and methyl cyclohexanols which have similar solvent power toward both of the parent homopolymers[3] and (ii) alcohol ethers[4] which are nonsolvent for polystyrene (PST) and rather poor solvents for poly(methyl methacrylate) (PMMA). For some of these systems, we have examined the temperature dependence of A_2 by osmotic pressure measurements and determined the temperatures at which $A_2 = 0$, as shown in Table I.

Table I: Θ Temperatures and $(\partial A_2/\partial T)_\Theta$ for ST–MMA Copolymers

	ST mole %	$10^{-4}M_n$	2-Ethoxyethanol —Θ (°C) and $10^5(\partial A_2/\partial T)_\Theta$ [a]—	Cyclohexanol
PMMA	0		Soluble	77.6[b]
		Random Copolymers		
SM3-7	29.3	35.4	40.0 (0.46)	68.0 (2.3)
SM5-6	56.2	35.0	58.4 (0.52)	61.3 (1.3)
SM7-3	70.2	34.2	72.8 (0.70)	63.0 (1.3)
		Block Copolymers		
15B	49.6	31.7	81.0 (0.33)	81.3 (1.8)
16B	73.2	39.2	Insoluble	84.0 (...)
11B	85.1	19.3	Insoluble	84.0 (1.8)
PST	100	20.6	Insoluble	81.8[c] (1.7)

[a] Values in parentheses. [b] Reported by Froelich and Benoit.[3] [c] Reported by Froelich and Benoit[3] as Θ = 83.5°.

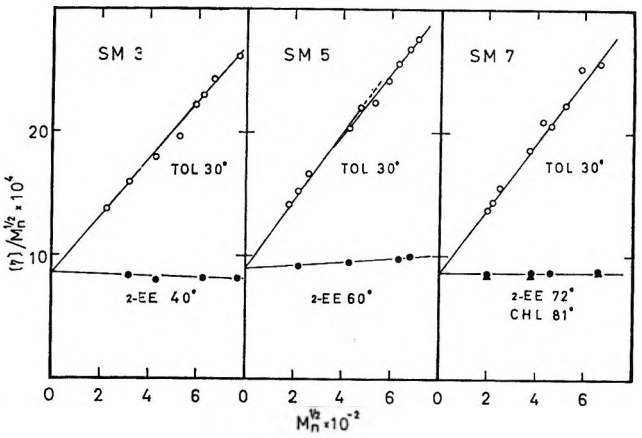

Figure 1. Plots of $[\eta]/M_n^{1/2}$ *vs.* $M_n^{1/2}$ for the ST–MMA random copolymers. For abbreviations, see text.

Then we proceeded to examine the molecular weight dependence of the intrinsic viscosity $[\eta]$ of these Θ-solvent systems together with some good solvent systems. Figure 1 shows the results for three series of the random copolymers coded as SM3, SM5, and SM7, by using now familiar plots of $[\eta]/M^{1/2}$ *vs.* $M^{1/2}$ (for M we employed the number-average molecular weight M_n). The good solvent (toluene, 30°) data give slightly downward concave curves, particularly in higher molecular weight ranges. On the other hand, the Θ-solvent data give straight lines with zero or nearly zero slopes, which are approximately expressed as ($[\eta]$ in units of 100 ml/g): for SM3 (average composition = 29.8 ST mole %; $10^{-4}M_n$ = 4.7–59.2)

$$[\eta]/M_n^{1/2} = 8.6 \times 10^{-4} - 0.04 \times 10^{-6}M_n^{1/2}$$

(2-ethoxyethanol, 40.0°)

for SM5 (56.7 ST mole %; $10^{-4}M_n$ = 3.4–50.0)

$$[\eta]/M_n^{1/2} = 9.0 \times 10^{-4} + 0.12 \times 10^{-6}M_n^{1/2}$$

(2-ethoxyethanol, 60.0°)

for SM7 (70.4 ST mole %; $10^{-4}M_n$ = 4.0–43.0)

$$[\eta]/M_n^{1/2} = (8.75 \pm 0.05) \times 10^{-4}$$

(2-ethoxyethanol, 72.0°)

(1) P. J. Flory, "Principles of Polymer Chemistry," Cornell University Press, Ithaca, N. Y., 1953.

(2) See, for example, M. Szwarc and A. Rembaum, *J. Polymer Sci.*, **22**, 189 (1956).

(3) D. Froelich and H. Benoit, *Makromol. Chem.*, **92**, 224 (1966). Reported Θ temperatures are 77.6° for PMMA, 83.5° for PST, 68.6° for azeotropic ST-MMA random copolymer, and 81.6° for (PST–PMMA) type block copolymer (50 ST mole %).

(4) H. Ohnuma first noticed them as Θ solvents for this copolymer.

$$[\eta]/M_n^{1/2} = (8.6 \pm 0.2) \times 10^{-4}$$

(cyclohexanol, 64.0°)

Although the evidence available at the moment is somewhat indirect, we may say that the random copolymers behave just as ordinary flexible chain polymers do in Θ solvents. The K_Θ ($= [\eta]_\Theta/M_n^{1/2}$) values and presumably the so-called unperturbed dimensions are dependent on the composition. In this particular case, they appear to be slightly larger than the linear averages of those of the parent homopolymers.[5]

For the block copolymers, more work is necessary before reaching any definite conclusion. Nevertheless, the presently available data, shown in Table II, are suggestive and interesting. In toluene, $[\eta]$ values are smaller than those of the corresponding random copolymers. In cyclohexanol, the block copolymers of about 50 ST mole % appear to have an almost equal K_Θ value, which is smaller than that of the corresponding random copolymer and seems to be closer to the linear average of those of the parent homopolymers. On the other hand, in ethoxyethanol, their K_Θ values are quite different from one another and also from those in cyclohexanol. However, since 2-ethoxyethanol is a nonsolvent for PST, it is quite likely that the PST portion of the block copolymer collapses and each molecule as a whole is barely dispersed in the solvent, presumably by being protected by PMMA portions. In such a peculiar case, the polymer molecule would not assume a random flight configuration even at the condition at which $A_2 = 0$. The anomalies in viscosity may not be surprising at all.

Acknowledgment. The authors wish to thank Professor Hiroshi Inagaki for his valuable discussion and Mr. Nobuo Donkai for his competent help in carrying out the experiments.

Table II: Viscosity Data for the (PMMA–PST–PMMA) Block Copolymers: $[\eta]$ (in 100 ml/g) and $10^4[\eta]/M_n^{1/2}$ [a]

Sample code (ST mole %) $10^{-4}M_n$	Toluene, 25.0°	Cyclohexanol, 81.0°	2-Ethoxyethanol, 81.0°
15B			
(49.6)	0.915	0.418	0.348
31.7	(16.2)	(7.4)	(6.15)
10B			
(48.2)	1.54	0.526	0.677
53.0	(21.1)	(7.2)	(9.27)
19B			
(43.1)	1.465	0.500	0.808
50.9	(20.5)	(7.02)	(11.3)
MSM-III[b]			
(46.1)	0.207		
3.6	(10.9)		

[a] Values in parentheses. [b] Prepared by coupling method; see H. Inagaki and T. Miyamoto, *Makromol. Chem.*, **87**, 166 (1965).

(5) Currently accepted $K\Theta$ values are $10^4K\Theta = 8.0 \pm 0.5$ for PST and 5.0 ± 0.5 for PMMA: see, for example, M. Kurata, M. Iwama, and K. Kamada in "Polymer Handbook," J. Brandrup and E. H. Immergut, Ed., Interscience Publishers, Inc., New York, N. Y., 1966, Chapter IV-1.

INSTITUTE FOR CHEMICAL RESEARCH — TADAO KOTAKA
KYOTO UNIVERSITY — HIROSHI OHNUMA
TAKATSUKI, OSAKA, JAPAN — YOJI MURAKAMI

RECEIVED SEPTEMBER 27, 1966

ADDITIONS AND CORRECTIONS

1960, Volume 64

Robert L. Scott: Thermodynamic Functions for Mixing at Constant Volume.

Page 1242. Equation 2 should read

$$x_1(\bar{V}_1'' - \bar{V}_1') + x_2(\bar{V}_2'' - V_2') = \tilde{V}_m' - x_1\bar{V}_1' - x_2\bar{V}_2' = \tilde{V}^E$$

Page 1242. Equation 9 should read $\Delta\tilde{S}_{IIA} = \ldots$.

Page 1244. The unnumbered equation preceding eq 25 should read

$$\left(\frac{\partial^2 P}{\partial T^2}\right)_V = \frac{1}{\kappa}\left(\frac{\partial \alpha}{\partial T}\right)_P - \frac{2\alpha}{\kappa^2}\left(\frac{\partial \kappa}{\partial T}\right)_P - \frac{\alpha^2}{\kappa^3}\left(\frac{\partial \kappa}{\partial P}\right)_T \cong 0$$

Page 1245. In Table VIII, column IIA, $T\tilde{S}^{VE} = -23$ cal (not -60), and $\tilde{E}^{VE} = 295$ cal (not 258).

Page 1245. In Table IX, column IIA, $T\tilde{S}^{VE} = -23$ cal (not -59), and $\tilde{E}^{VE} = 293$ cal (not 257).

Page 1247. Equation 31 should read

$$\tilde{S}^{VE}(T,\tilde{V}_u^\circ) - \tilde{S}^E(T,P^\circ) = \left(\frac{V_T^\circ}{V_P^\circ}\right)_m \tilde{V}^E - \ldots.$$

Page 1247. In column 1, the second paragraph (starting, "The differences between ...") line 9 should read $T(\tilde{S}_{IIB}{}^{VE} - \tilde{S}_{IIA}{}^{VE}) = -25$ cal (not $+42$), ..." The fourth and fifth (last) sentences should be stricken.—Robert L. Scott.

1965, Volume 69

Leonard S. Silbert, B. F. Daubert, and Leo S. Mason: The Heats of Combustion, Formation, and Isomerization of Isomeric Monoglycerides.

Page 2891. In column 1, line 6, "ΔE_w, the Washburn Corrections" should read: ΔE_w, the summation $\xi_I(T_{25^\circ} - T_1) + \xi_F(T_2 - T_{25^\circ})$, in accordance with the Washburn reduction of the bomb calorimetric data to 25° (ref 34, pp 550–551).

Page 2891. In column 1, line 10, add the following sentence: Washburn corrections for the aliphatic monoglycerides were in the range of 0.0375–0.0490% and averaged 0.0750% for the aromatic derivatives.

Page 2891. In Table III, change $\Delta E_c^\circ/M$ to read $-\Delta E_c/M$.

Page 2891. In column 2, line 2, ΔE_R should read ΔE_R°.—Leonard S. Silbert.

I. Unger: Triplet State of Fluorobenzene.

Page 4285. In column 1, line 13, the value for the reciprocal linear dispersion of the monochromator should be 16 A/mm, not 6.6.—Israel Unger.

1966, Volume 70

Richard Payne: Structure of the Electrical Double Layer at A Mercury Electrode in the Presence of Adsorbed Perchlorate Ions.

Page 204. Owing to an error in calculation, the values of the specifically adsorbed chage (q^1) given in this paper are systematically low by a factor of 0.5916. The ordinate axis in Figure 2 and the abscissa in Figures 3, 5, and 9 should therefore be multiplied by a factor of 1/0.5916. Although this error is carried through the subsequent analysis, its effect is not serious and does not significantly alter the conclusions. Experimental data are available to interested persons on request.—Richard Payne.

Julian Heicklen: The Reactions of Ozone with Perfluoroolefins.

Page 480. Because of a computational error, the rate constants reported in molar units are incorrect. The corrected values are

Olefin	k_1, M^{-1} sec^{-1}	k_1k_3/k_2, M^{-2} sec^{-1}
C_2F_4	300	$>28 \times 10^6$
C_3F_6	46	$>4.2 \times 10^6$
C_4F_8	4.1	0.066×10^6

Julian Heicklen

Jan Hermans, Jr.: Experimental Free Energy and Enthalpy of Formation of the α Helix.

Page 514. A serious mistake was made in the article, in that it mentions experimental results and conclusions which are improperly attributed to Dr. Gerald Fasman. As a consequence, the paragraph on p 514 concerning these data ("An interesting ..... our extrapolation.") should be disregarded, since it does not represent the viewpoints on this matter of either Dr. Fasman or the author. Recent results obtained by Fasman and coworkers regarding the formation of the β conformation in poly-L-lysine solutions have been described elsewhere (B. Davidson, N. Tooney, and G. Fasman, *Biochem. Biophys. Res. Commun.*, **23**, 156 (1966)).—Jan Hermans, Jr.

B. E. Conway and R. E. Verrall: Ion–Solvent Size Ratio as a Factor in the Thermodynamics of Electrolytes.

Page 1476. In the four equations summarizing the partial molal volume behavior of a series of symmetrical tetraalkylammonium salts, the equation printed for the $(n\text{-Pr})_4NCl$ salt in fact referred to the $(n\text{-Pr})_3NHCl$ salt which had also been studied. The data for the $(n\text{-Pr})_4NCl$ salt correctly referred to elsewhere [B. E. Conway, R. E. Verrall, and J. E. Desnoyers, *Z. Physik. Chem.* (Leipzig), **230**, 157 (1965)] are expressed by the equation

$$\bar{V} = 232.9 + 2.792c^{1/2} - 38c$$

[Also see B. E. Conway, R. E. Verrall, and J. E. Desnoyers, *Trans. Faraday Soc.*, **62**, 2738 (1966)].—B. E. Conway.

Thomas H. Donnelly: The Direct Estimation of Continuous Molecular Weight Distributions by Equilibrium Ultracentrifugation.

Page 1863. In eq 21, the E^t in the denominator should be e^t.

Page 1864. In eq 28 and 29, a slash should appear above P in the exponential terms.

Page 1870. In the denominator of eq A10a, the first term in the denominator in the second parentheses should be n (not Σn). Also, the first term in the denominator of the third parentheses should be Σu (not n).—T. H. Donnelly.

John A. Larkin, David V. Fenby, Theodore S. Gilman, and Robert L. Scott: Heats of Mixing of Nonelectrolyte Solutions. III. Solutions of the Five Hexane Isomers with Hexadecane.

Page 1959. In the data reported for the system n-hexane + n-hexadecane, one measurement (at $x_2 = 0.7004$) was included in the figure and in the calculations leading to numbers reported in the abstract but not in the tables. The differences all lie within experimental error, but for consistency the following corrections must be reported.

Page 1961. In Table III, add an eleventh line: 0.7004, 94.8.

The excesses, θ, in the third column correspond to a revised least-squares fit and should now read -0.4, 0.2, 0.3, 0.4, 0.0, -0.5 -0.2, 0.8, -0.3, 3.4, -0.8 (from the additional measurement). The inclusion of this result yields $\bar{H}^{E}_{max}$ = 113.7 joules mole^{-1} (p 1961 and Table X) as reported correctly in the abstract.

Page 1962. In Table VIII, the first line (n-hexane + n-$C_{16}H_{34}$) should be revised to read 454.8, -2.5, 0.9, 108.7, -0.6, 0.2.—ROBERT L. SCOTT.

AUTHOR INDEX *to Volume 70, 1966*

SUBJECT INDEX *to Volume 70, 1966*[1]

(1) Index prepared by Mrs. P. Cunniff, College Park, Md.